frontiers | Research Topics

Identification and characterization of contrasting genotypes/cultivars to discover novel players in crop responses to abiotic/biotic stresses, volume II

Edited by
Raul Antonio Sperotto, Elizabeth R. Waters, Magdalena Arasimowicz-Jelonek, Felipe Klein Ricachenevsky and Guihua Bai

Published in
Frontiers in Plant Science

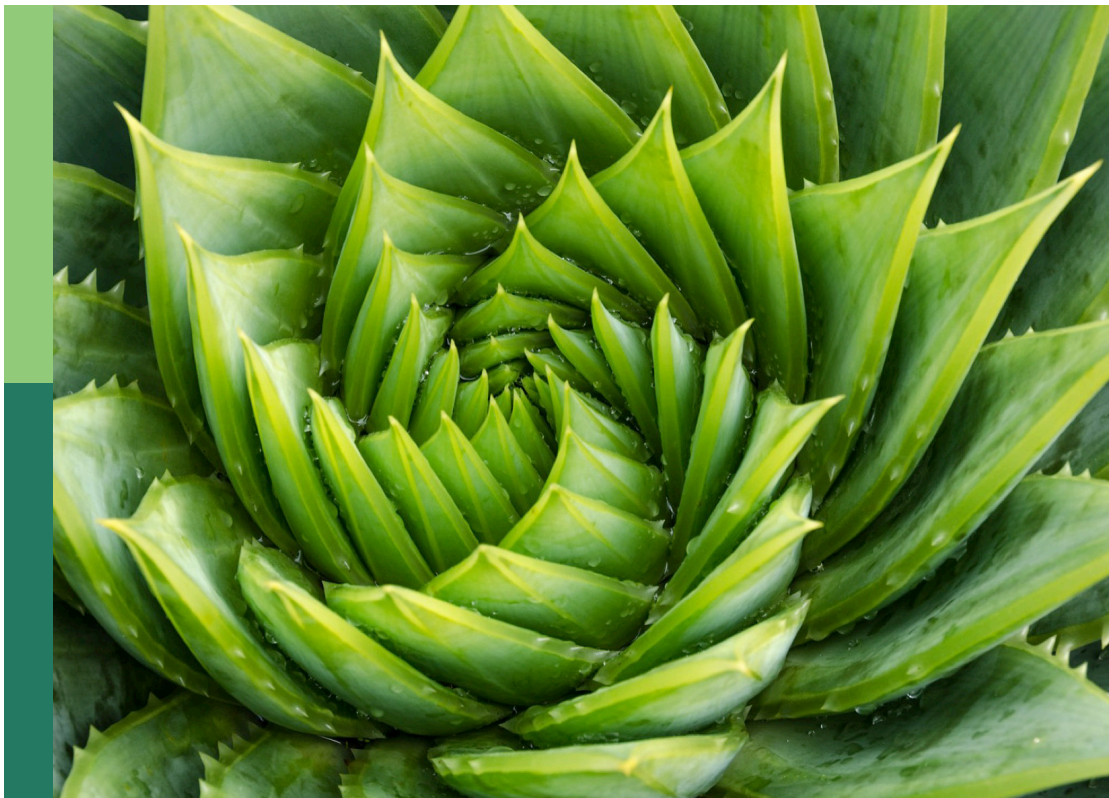

FRONTIERS EBOOK COPYRIGHT STATEMENT

The copyright in the text of individual articles in this ebook is the property of their respective authors or their respective institutions or funders. The copyright in graphics and images within each article may be subject to copyright of other parties. In both cases this is subject to a license granted to Frontiers.

The compilation of articles constituting this ebook is the property of Frontiers.

Each article within this ebook, and the ebook itself, are published under the most recent version of the Creative Commons CC-BY licence. The version current at the date of publication of this ebook is CC-BY 4.0. If the CC-BY licence is updated, the licence granted by Frontiers is automatically updated to the new version.

When exercising any right under the CC-BY licence, Frontiers must be attributed as the original publisher of the article or ebook, as applicable.

Authors have the responsibility of ensuring that any graphics or other materials which are the property of others may be included in the CC-BY licence, but this should be checked before relying on the CC-BY licence to reproduce those materials. Any copyright notices relating to those materials must be complied with.

Copyright and source acknowledgement notices may not be removed and must be displayed in any copy, derivative work or partial copy which includes the elements in question.

All copyright, and all rights therein, are protected by national and international copyright laws. The above represents a summary only. For further information please read Frontiers' Conditions for Website Use and Copyright Statement, and the applicable CC-BY licence.

ISSN 1664-8714
ISBN 978-2-83251-264-7
DOI 10.3389/978-2-83251-264-7

About Frontiers

Frontiers is more than just an open access publisher of scholarly articles: it is a pioneering approach to the world of academia, radically improving the way scholarly research is managed. The grand vision of Frontiers is a world where all people have an equal opportunity to seek, share and generate knowledge. Frontiers provides immediate and permanent online open access to all its publications, but this alone is not enough to realize our grand goals.

Frontiers journal series

The Frontiers journal series is a multi-tier and interdisciplinary set of open-access, online journals, promising a paradigm shift from the current review, selection and dissemination processes in academic publishing. All Frontiers journals are driven by researchers for researchers; therefore, they constitute a service to the scholarly community. At the same time, the *Frontiers journal series* operates on a revolutionary invention, the tiered publishing system, initially addressing specific communities of scholars, and gradually climbing up to broader public understanding, thus serving the interests of the lay society, too.

Dedication to quality

Each Frontiers article is a landmark of the highest quality, thanks to genuinely collaborative interactions between authors and review editors, who include some of the world's best academicians. Research must be certified by peers before entering a stream of knowledge that may eventually reach the public - and shape society; therefore, Frontiers only applies the most rigorous and unbiased reviews. Frontiers revolutionizes research publishing by freely delivering the most outstanding research, evaluated with no bias from both the academic and social point of view. By applying the most advanced information technologies, Frontiers is catapulting scholarly publishing into a new generation.

What are Frontiers Research Topics?

Frontiers Research Topics are very popular trademarks of the *Frontiers journals series*: they are collections of at least ten articles, all centered on a particular subject. With their unique mix of varied contributions from Original Research to Review Articles, Frontiers Research Topics unify the most influential researchers, the latest key findings and historical advances in a hot research area.

Find out more on how to host your own Frontiers Research Topic or contribute to one as an author by contacting the Frontiers editorial office: frontiersin.org/about/contact

Identification and characterization of contrasting genotypes/cultivars to discover novel players in crop responses to abiotic/biotic stresses, volume II

Topic editors

Raul Antonio Sperotto — Universidade do Vale do Taquari - Univates, Brazil
Elizabeth R. Waters — San Diego State University, United States
Magdalena Arasimowicz-Jelonek — Adam Mickiewicz University, Poland
Felipe Klein Ricachenevsky — Federal University of Rio Grande do Sul, Brazil
Guihua Bai — Independent researcher, USDA-ARS Hard Winter Wheat Genetics Research Unit, Manhattan KS 66506, United States

Citation

Sperotto, R. A., Waters, E. R., Arasimowicz-Jelonek, M., Ricachenevsky, F. K., Bai, G., eds. (2023). *Identification and characterization of contrasting genotypes/cultivars to discover novel players in crop responses to abiotic/biotic stresses, volume II*. Lausanne: Frontiers Media SA. doi: 10.3389/978-2-83251-264-7

The authors declare that the research was conducted in the absence of any commercial or financial relationships that could be construed as a potential conflict of interest.

Table of contents

frontiers | Frontiers in Plant Science

TYPE Editorial
PUBLISHED 20 December 2022
DOI 10.3389/fpls.2022.1105598

Check for updates

OPEN ACCESS

EDITED AND REVIEWED BY
Leo Marcelis,
Wageningen University and Research, Netherlands

*CORRESPONDENCE
Raul A. Sperotto
rasperotto@univates.br
Felipe K. Ricachenevsky
felipecruzalta@gmail.com
Elizabeth R. Waters
ewaters@sdsu.edu
Guihua Bai
guihua.bai@usda.gov
Magdalena Arasimowicz-Jelonek
arasim@amu.edu.pl

SPECIALTY SECTION
This article was submitted to Crop and Product Physiology, a section of the journal Frontiers in Plant Science

RECEIVED 22 November 2022
ACCEPTED 12 December 2022
PUBLISHED 20 December 2022

CITATION
Sperotto RA, Ricachenevsky FK, Waters ER, Bai G and Arasimowicz-Jelonek M (2022) Editorial: Identification and characterization of contrasting genotypes/cultivars to discover novel players in crop responses to abiotic/biotic stresses, volume II. *Front. Plant Sci.* 13:1105598. doi: 10.3389/fpls.2022.1105598

COPYRIGHT
© 2022 Sperotto, Ricachenevsky, Waters, Bai and Arasimowicz-Jelonek. This is an open-access article distributed under the terms of the Creative Commons Attribution License (CC BY). The use, distribution or reproduction in other forums is permitted, provided the original author(s) and the copyright owner(s) are credited and that the original publication in this journal is cited, in accordance with accepted academic practice. No use, distribution or reproduction is permitted which does not comply with these terms.

Editorial: Identification and characterization of contrasting genotypes/cultivars to discover novel players in crop responses to abiotic/biotic stresses, volume II

Raul A. Sperotto[1,2]*, Felipe K. Ricachenevsky[3]*, Elizabeth R. Waters[4]*, Guihua Bai[5]* and Magdalena Arasimowicz-Jelonek[6]*

[1]Graduate Program in Biotechnology, Life Sciences Area, University of Taquari Valley - Univates, Lajeado, Brazil, [2]Graduate Program in Plant Physiology, Federal University of Pelotas, Pelotas, Brazil, [3]Graduate Program in Cell and Molecular Biology, Botany Department, Federal University of Rio Grande do Sul, Porto Alegre, Brazil, [4]Department of Biology, San Diego State University, San Diego, CA, United States, [5]USDA-ARS Hard Winter Wheat Genetics Research Unit, Manhattan, KS, United States, [6]Department of Plant Ecophysiology, Faculty of Biology, Adam Mickiewicz University, Poznań, Poland

KEYWORDS

biotic factors, drought, heat, nutrition, salinity, shade

Editorial on the Research Topic
Identification and characterization of contrasting genotypes/cultivars to discover novel players in crop responses to abiotic/biotic stresses, volume II

Securing global food supply in an increasingly volatile climate and rapidly growing population is one of the greatest challenges facing humanity in the current century (Yan et al., 2022). Increased frequency and intensity of abiotic and biotic stress will demand a sustainable increase in food productivity with more efficient and diversified agricultural management (Farooq et al., 2022). One recurrent strategy used by plant scientists is to identify and characterize plant genotypes/cultivars with contrasting responses to these stressful conditions (Sperotto et al., 2021; Habibpourmehraban et al., 2022; Somaddar et al., 2022; Yu et al., 2022; Zhao et al., 2022), allowing the identification of molecular, biochemical, and physiological mechanisms involved in crop response and stress tolerance. This improved knowledge can be used to boost crop growth and productivity even under non-optimal conditions (Zhang H. et al., 2022). Therefore, this Research Topic presents an update on the advances to understanding plant responses to stressful conditions and provides an overview of different approaches used for

improving crop tolerance/resistance. Here we highlight the major points arising from these reports.

Heat-related

Global warming due to climate change affects plant growth and development throughout its life cycle. In addition, the increasing occurrence of heat waves is drastically reducing the global crop yield (Haider et al., 2022). Due to accelerating climate change, there is an urgent need across all crop species to identify heat tolerant varieties and to understand the genetic and physiological traits that provide resilience to heat stress. Tomás et al. evaluated whole transcriptomic profiles of wheat developing grains of commercial genotypes and landraces submitted to heatwave-like treatments during grain filling. Landraces showed more differentially expressed genes and presented more similar responses than commercial genotypes, showing that landraces are more affected by the high temperature treatment. Only six upregulated genes were detected in all four evaluated genotypes: three small heat shock proteins HSP20, one adenylate kinase (essential for cellular homeostasis), a BAG domain protein (responsible for the modulation of chaperones activity), and a ferritin (recently related with increased tolerance to several abiotic stresses in Arabidopsis - Zang et al., 2017). Additionaly, the commercial variety Bancal seems to be a promising genotype to cope with high temperatures.

Li et al. reported on a detailed study of two alfalfa (*Medicago sativa*) varieties that differ in their ability to tolerate heat stress. Plants were exposed to continuously rising temperatures up to a maximum of 43°C. It was reported that the heat-tolerant variety (MS30) was able to maintain higher chlorophyll fluorescence rates and had lower rates of electrolyte leakage during heat stress. In addition, the antioxidant defense system was also higher in MS30 compared to the heat-sensitive (MS37) variety. Proteomic analysis revealed that in both varieties photosynthesis-related genes were differentially regulated, as were the heat shock proteins. It is interesting that the sensitive variety MS37 had a higher number of differentially regulated proteins, suggesting that the tolerant MS30 has a higher ability to buffer plant metabolism during heat stress.

Abro et al. reported on a study of fifty-eight cotton genotypes. These authors utilized a heat-susceptibility index (HSI) that evaluates yield during control conditions compared to yield under heat stress. In addition, they examined electrolyte leakage as well as stomata and trichome size. Seventeen of the varieties examined were found to be heat-tolerant based on HSI and low electrolyte leakage. There was no clear relationship between the size of trichomes and heat tolerance, but there was a clear relationship between stomata size and heat tolerance. This study indicates that stomata size and electrolyte leakage will be useful in future studies of cotton heat-tolerance.

Devi et al. examined 39 field-grown genotypes of *Cicer arietinum* (chickpea) for evidence of genetic variation in responses to heat stress. From this original analysis, they identified ten heat-sensitive and ten heat-tolerant varieties for more detailed characterization. Heat-tolerant varieties displayed higher chlorophyll content, chlorophyll fluorescence, lower electrolyte leakage, higher stomatal conductance, higher pollen germination and viability. The heat-tolerant chickpea varieties identified in this study can now be utilized for crop improvement to generate varieties that will maintain higher yield as the climate warms and heat stress becomes more prevalent.

Drought-related

Among the abiotic stresses that affect plants, drought is one of the main factors which reduces growth and yield, with an estimated third of the total cultivated area affected by water deficit. Therefore, we need to improve our knowledge of the molecular mechanisms underlying drought tolerance in order to develop new drought tolerant genotypes (Fadoul et al., 2021). In light of ever increasing climate change and the new agricultural challenges this brings, Álvarez-Maldini et al. emphasized the importance of identifying and selecting anisohydric woody plants that are able to withstand cavitation better than isohydric plants. Based on pot desiccation experiment, the authors described anisohydric and isohydric behavior of the selected almond (*Prunus dulcis*) cultivars and indicated that anisohydric ones, Soleta and Isabelona, are characterized by maximum stomatal conductance, lower water potentials for stomatal closure and turgor loss, and lower vulnerability to xylem cavitation. They found that almond can avoid cavitation by closing stomata during the early stages of drought. In addition, they reported that root system architecture (RSA) plays a vital role in plant productivity under water stress.

Abdirad et al. compared the transcriptomic responses of root tips to water stress between a shallow-rooting drought-susceptible rice cultivar IR64 and a drought-tolerant and deep-rooting cultivar Azucena. They found that Azucena avoided water stress through enhancing growth and exploration of roots to access water from deep soil, whereas IR64 relied on cell insulation to maintain water and antioxidant system to withstand stress. Many putative candidate genes were identified as associated with RSA and drought tolerance, some of which may have the potential to be used to enhance drought adaptation in rice.

Shade-related

Depending on the strategy adopted to cope with vegetative shade, plants can be classified into two groups: shade avoiding or shade-tolerant species. Species typically found in forest

understories exhibit shade tolerance responses, which allows them to maintain adequate growth under shade conditions (Xu et al., 2021). Cheng et al. presented new aspects of the lodging resistance mechanism of soybean in the strip intercropping system, which is especially important in areas with low solar radiation. Using a shade-tolerant soybean in the strip intercropping system could reduce yield loss by regulating its spatial canopy structure and stem characteristics. In the field, Tianlong No. 1 cultivar showed increased light energy capture and photosynthesis that favor morphological and physiological development of the stem. Parameters characterizing the canopy spatial structure such as high transmission coefficient (TC) and low leaf area index (LAI) and mean leaf angle (MLA) could be used in the future as indicators for screening soybean cultivars with shade and lodging tolerance.

Salt-related

Salt stress is a widespread problem in both agriculture and natural environments. It is predicted that 50% of today's arable land will be lost to salinization in the future (Goyal et al., 2016), making the identification of salt tolerant species and genotypes and the understanding of salt-tolerance mechanisms a priority. Currently, breeding salinity-tolerant cultivars is the most promising solution for salinity tolerance in high-yielding crops (Zhang J. et al., 2022). Wheat is one of the most important crops worldwide, but it is sensitive to salt stress. Another grass from the Triticeae tribe, *Thinopyrum elongatum*, is a halophyte that can generate hybrids when crossed with the common wheat variety 'Chinese spring'. Peng et al. performed biochemical, physiological, and molecular comparisons between common wheat and wheat/*T. elongatum* hybrids, named *Tritipyrum*, which are highly salt-tolerant, exposed to NaCl. Tolerance was associated with increased antioxidant enzyme activity, proline and soluble sugar levels, and lower detrimental effects on photosynthesis in *Tritipyrum* compared to wheat. Transcriptomic analyses suggested a quantitative effect, rather than qualitative, of known salt tolerance mechanisms. This work provides interesting new information in an important breeding material for generating salt-tolerant wheat genotypes.

Hou et al. demonstrated that wild soybean (*Glycine soja*) is more salt-tolerant than cultivated soybean, and associated the natural sequence variation in dehydration responsive element-binding (DREB) family transcription factor genes (*DREB3a* and *DREB3b*) with salt tolerance in soybean. Soybean plants carrying the wild soybean *DREB3b* allele (*DREB3b39Del*) were more salt-tolerant than those containing the reference genome allele (*DREB3bRef*). Domestication of cultivated soybean that lost the *DREB3b39Del* allele may be associated with a reduction in salt tolerance.

Zhang et al. treated two sorghum species, *LRNK1* (salt-tolerant (ST)) and *LR2381* (salt-sensitive (SS)) with 180 mM NaCl salt solution, and combined transcriptomic, metabolomic, and physiological analyses to elucidate key biological pathways in sorghum response to salinity stress. Under salt stress, the ST species presented higher plant height, leaf area, and chlorophyll contents than the SS one, besides accumulating higher levels of salicylic acid and betaine. Additionally, the expression of *SbNPR1*, a salicylic acid receptor, was positively correlated with salt tolerance. This study will play an important role in identifying salt-tolerant varieties that can be used in sorghum breeding programs.

Zhang et al. compared three rice genotypes under different NaCl concentrations. They showed that panicle number, grain number per panicle, and 1,000 grains weight were reduced at high NaCl concentration. However, salt-sensitive genotypes in fact increased yield components when exposed to low NaCl concentration, whereas tolerant genotypes did not. A similar trend was observed in grain quality, in which salt tended to decrease product quality, but low NaCl level could improve important properties for the consumers. The study should be followed up by more extensive works with other rice varieties, which could lead to increased rice production in salt-containing areas such as mudflats.

Nutrient-related

Plants require both macro and micro nutirents to complete their life cycles. Plant growth and productivity can be severely affected by disbalanced nutrient availability, and different adaptations have enabled plants to cope with inappropriate nutrient levels (Pita-Barbosa et al., 2019; Islam et al., 2022). Adequate plant nutrition is a key problem that needs to be tackled to maintain our food security quality in the future when the human population will reach more than 9 billion people. Yam (*Dioscorea* spp.) is a key crop, especially in West Africa. Using six white Guinea yam (*Dioscorea rotundata*) genotypes, Matsumoto et al. tested how NPK (Nitrogen, Phosphorus, Potassium) fertilization affects biomass production and nutrient use efficiency in field trials. The varieties responded differently to fertilization with NPK. The authors identified the varieties that increase tuber dry matter, nutrient efficiency, and recovery, and those susceptible to variation in soil fertility. This work will help farmers identify genotypes more suitable to each condition, especially those that can produce quality biomass when soil fertility is low and nutrient input is not adequate.

Biotic stress-related

Biotic stresses are crucial constraints to the productivity of crop plants, especially under climate change conditions (Parihar et al., 2022), and lead to more than 20% crop yield losses (Savignac et al., 2022). Galewski et al. identified specific genomic features associated with seedling rhizoctonia resistance by whole genome sequencing of selected and unselected bulk derived from a synthetic outcrossing

sugar beet population and the genome-wide variation resulting from the selection. An increased level of allele fixation in the resistant bulk indicated that a greater selection pressure was applied. Using population genetics and statistics approaches, and the EL10.2 physical map, a list of enriched candidate genes was identified with the functions in cell wall metabolism and plant disease resistance, including pathogen perception, signal transduction, and pathogen response.

The brown planthopper (*Nilaparvata lugens* Stål, BPH) belongs to the most devastating pest of rice that causes significant yield loss. By the application of bulked segregant RNA sequencing, Guan et al. identified candidate genes involved in BPH virulence. Comparison of virulent and avirulent BPH extreme bulks after feeding on YHY15 rice plants carrying the *Bph15* resistance gene allowed to identify 751 differentially expressed genes (DEGs). Functional analysis of 418 DEGs with upregulated expression in the avirulent insects revealed that BPH induces carbohydrate, amino acid, and nucleotide metabolism, endocrine system, and signal transduction pathways in response to feeding on YHY15 rice. Moreover, authors identified 24 polymorphic SNPs related to BPH virulence and 21 genes potentially engaged in virulence mechanisms.

Final comment

In summary, the studies presented here documents how contrasting genotypes differently cope with abiotic and biotic stress conditions. The identification of these tolerance/resistance mechanisms can be used in the future to enhance plant abilities to respond to unfavorable environmental conditions.

Author contributions

All authors listed have made a substantial, direct, and intellectual contribution to the work and approved it for publication.

Conflict of interest

The authors declare that the research was conducted in the absence of any commercial or financial relationships that could be construed as a potential conflict of interest.

Publisher's note

All claims expressed in this article are solely those of the authors and do not necessarily represent those of their affiliated organizations, or those of the publisher, the editors and the reviewers. Any product that may be evaluated in this article, or claim that may be made by its manufacturer, is not guaranteed or endorsed by the publisher.

References

Fadoul, H. E., Martínez Rivas, F. J., Neumann, K., Balazadeh, S., Fernie, A. R., and Alseekh, S. (2021). Comparative molecular and metabolic profiling of two contrasting wheat cultivars under drought stress. *Int. J. Mol. Sci.* 22, 13287. doi: 10.3390/ijms222413287

Farooq, M. S., Uzair, M., Raza, A., Habib, M., Xu, Y., Yousuf, M., et al. (2022). Uncovering the research gaps to alleviate the negative impacts of climate change on food security: A review. *Front. Plant Sci.* 13, 927535. doi: 10.3389/fpls.2022.927535

Goyal, E., Amit, S. K., Singh, R. S., Mahato, A. K., Chand, S., and Kanika, K. (2016). Transcriptome profiling of the salt-stress response in *Triticum aestivum* cv. kharchia local. *Sci. Rep.* 6, 27752. doi: 10.1038/srep27752

Habibpourmehraban, F., Wu, Y., Wu, J. X., Hamzelou, S., Masoomi-Aladizgeh, F., Kamath, K. S., et al. (2022). Multiple abiotic stresses applied simultaneously elicit distinct responses in two contrasting rice cultivars. *Int. J. Mol. Sci.* 23, 1739. doi: 10.3390/ijms23031739

Haider, S., Iqbal, J., Naseer, S., Shaukat, M., Abbasi, B. A., Yaseen, T., et al. (2022). Unfolding molecular switches in plant heat stress resistance: a comprehensive review. *Plant Cell Rep.* 41, 775–798. doi: 10.1007/s00299-021-02754-w

Islam, W., Tauqeer, A., Waheed, A., and Zeng, F. (2022). MicroRNA mediated plant responses to nutrient stress. *Int. J. Mol. Sci.* 23, 2562. doi: 10.3390/ijms23052562

Parihar, A. K., Kumar, J., Gupta, D. S., Lamichaney, A., Naik Sj, S., Singh, A. K., et al. (2022). Genomics enabled breeding strategies for major biotic stresses in pea (*Pisum sativum* L.). *Front. Plant Sci.* 13, 861191. doi: 10.3389/fpls.2022.861191

Pita-Barbosa, A., Ricachenevsky, F. K., and Flis, P. M. (2019). One "OMICS" to integrate them all: Ionomics as a result of plant genetics, physiology and evolution. *Theor. Exp. Plant Physiol.* 31, 71–89. doi: 10.1007/s40626-019-00144-y

Savignac, J. M., Atanasova, V., Chéreau, S., Ortéga, V., and Richard-Forget, F. (2022). Role of tocochromanols in tolerance of cereals to biotic stresses: Specific focus on pathogenic and toxigenic fungal species. *Int. J. Mol. Sci.* 23, 9303. doi: 10.3390/ijms23169303

Somaddar, U., Dey, H. C., Mim, S. K., Sarker, U. K., Uddin, M. R., Ahmed, N. U., et al. (2022). Assessing silicon-mediated growth performances in contrasting rice cultivars under salt stress. *Plants (Basel)* 11, 1831. doi: 10.3390/plants11141831

Sperotto, R. A., Ricachenevsky, F. K., Waters, E. R., Bai, G., and Arasimowicz-Jelonek, M. (2021). Identification and characterization of contrasting Genotypes/Cultivars to discover novel players in crop responses to Abiotic/Biotic stresses. *Front. Plant Sci.* 12, 784874. doi: 10.3389/fpls.2021.784874

Xu, H., Chen, P., and Tao, Y. (2021). Understanding the shade tolerance responses through hints from phytochrome a-mediated negative feedback regulation in shade avoiding plants. *Front. Plant Sci.* 12, 813092. doi: 10.3389/fpls.2021.813092

Yan, H., Harrison, M. T., Liu, K., Wang, B., Feng, P., Fahad, S., et al. (2022). Crop traits enabling yield gains under more frequent extreme climatic events. *Sci. Total Environ.* 808, 152170. doi: 10.1016/j.scitotenv.2021.152170

Yu, T., Zhang, J., Cao, J., Li, X., Li, S., Liu, C., et al. (2022). Metabolic insight into cold stress response in two contrasting maize lines. *Life (Basel)* 12, 282. doi: 10.3390/life12020282

Zang, X., Geng, X., Wang, F., Liu, Z., Zhang, L., Zhao, Y., et al. (2017). Overexpression of wheat ferritin gene *TaFER-5B* enhances tolerance to heat stress and other abiotic stresses associated with the ROS scavenging. *BMC Plant Biol.* 17, 14. doi: 10.1186/s12870-016-0958-2

Zhang, J., Xu, T., Liu, Y., Chen, T., Zhang, Q., Li, W., et al. (2022). Molecular insights into salinity responsiveness in contrasting genotypes of rice at the seedling stage. *Int. J. Mol. Sci.* 23, 1624. doi: 10.3390/ijms23031624

Zhang, H., Zhu, J., Gong, Z., and Zhu, J. K. (2022). Abiotic stress responses in plants. *Nat. Rev. Genet.* 23, 104–119. doi: 10.1038/s41576-021-00413-0

Zhao, P., Ma, B., Cai, C., and Xu, J. (2022). Transcriptome and methylome changes in two contrasting mungbean genotypes in response to drought stress. *BMC Genomics* 23, 80. doi: 10.1186/s12864-022-08315-z

frontiers in Plant Science

ORIGINAL RESEARCH
published: 09 December 2021
doi: 10.3389/fpls.2021.753011

Physiological and Proteomic Responses of Contrasting Alfalfa (*Medicago sativa* L.) Varieties to High Temperature Stress

Yingzhu Li[1†], Xinrui Li[1,2†], Jin Zhang[1†], Daxu Li[1], Lijun Yan[1], Minghong You[1], Jianbo Zhang[1], Xiong Lei[1,2], Dan Chang[1], Xiaofei Ji[1], Jinchan An[1,3], Mingfeng Li[1,3], Shiqie Bai[1] and Jiajun Yan[1]**

[1] Institute of Herbaceous Plants, Sichuan Academy of Grassland Science, Chengdu, China, [2] College of Grassland Science and Technology, Sichuan Agricultural University, Chengdu, China, [3] Institute of Qinghai-Tibetan Plateau, Southwest Minzu University, Chengdu, China

OPEN ACCESS

Edited by:
Marouane Baslam,
Niigata University, Japan

Reviewed by:
Mohammed Mouradi,
Université Sultan Moulay Slimane, Morocco
Iker Aranjuelo,
Superior Council of Scientific Investigations, Spain

***Correspondence:**
Shiqie Bai
baishiqie@126.com
Jiajun Yan
51037529@qq.com

[†] These authors have contributed equally to this work and share first authorship

Specialty section:
This article was submitted to Plant Abiotic Stress, a section of the journal Frontiers in Plant Science

Received: 04 August 2021
Accepted: 11 November 2021
Published: 09 December 2021

Citation:
Li Y, Li X, Zhang J, Li D, Yan L, You M, Zhang J, Lei X, Chang D, Ji X, An J, Li M, Bai S and Yan J (2021) Physiological and Proteomic Responses of Contrasting Alfalfa (Medicago sativa L.) Varieties to High Temperature Stress. Front. Plant Sci. 12:753011. doi: 10.3389/fpls.2021.753011

High temperature (HT) is an important factor for limiting global plant distribution and agricultural production. As the global temperature continues to rise, it is essential to clarify the physiological and molecular mechanisms of alfalfa responding the high temperature, which will contribute to the improvement of heat resistance in leguminous crops. In this study, the physiological and proteomic responses of two alfalfa (*Medicago sativa* L.) varieties contrasting in heat tolerance, MS30 (heat-tolerant) and MS37 (heat-sensitive), were comparatively analyzed under the treatments of continuously rising temperatures for 42 days. The results showed that under the HT stress, the chlorophyll content and the chlorophyll fluorescence parameter (Fv/Fm) of alfalfa were significant reduced and some key photosynthesis-related proteins showed a down-regulated trend. Moreover, the content of Malondialdehyde (MDA) and the electrolyte leakage (EL) of alfalfa showed an upward trend, which indicates both alfalfa varieties were damaged under HT stress. However, because the antioxidation-reduction and osmotic adjustment ability of MS30 were significantly stronger than MS37, the damage degree of the photosynthetic system and membrane system of MS30 is significantly lower than that of MS37. On this basis, the global proteomics analysis was undertaken by tandem mass tags (TMT) technique, a total of 6,704 proteins were identified and quantified. Gene Ontology (GO) analysis and Kyoto Encyclopedia of Genes and Genomes (KEGG) analysis indicated that a series of key pathways including photosynthesis, metabolism, adjustment and repair were affected by HT stress. Through analyzing Venn diagrams of two alfalfa varieties, 160 and 213 differentially expressed proteins (DEPs) that had dynamic changes under HT stress were identified from MS30 and MS37, respectively. Among these DEPs, we screened out some key DEPs, such as ATP-dependent zinc metalloprotease FTSH protein, vitamin K epoxide reductase family protein, ClpB3, etc., which plays important functions in response to HT stress. In conclusion, the stronger heat-tolerance of MS30 was attributed to its higher adjustment and repair ability, which

could cause the metabolic process of MS30 is more conducive to maintaining its survival and growth than MS37, especially at the later period of HT stress. This study provides a useful catalog of the *Medicago sativa* L. proteomes with the insight into its future genetic improvement of heat-resistance.

Keywords: alfalfa, high temperature stress, physiological changes, isobaric tandem mass tag labeling (TMT), photosynthesis-responsive protein, metabolism-responsive protein, heat shock protein

INTRODUCTION

In recent years, the greenhouse effect has led to an upward trend in the global climate. Global warming predictions indicate that temperatures will increase another 2–6°C by the end of this century (Li et al., 2013; Sévellec and Drijfhout, 2018). Excessive temperature has a certain effect on plant growth and development, nutritional quality, yield and distribution range (Hinojosa et al., 2019; Kumar, 2020). Some studies have shown that the high temperature could greatly damage the potato yield and lead to the physiological defects of tuber (Rykaczewska, 2015). Therefore, it is very essential to study the impact of high temperatures (HT) on plant growth and development to maximize agricultural production and food security in the future (Li B. et al., 2018).

Heat stress caused by HT could cause damage to the plant growth. Such damage can be specifically divided into morphological, physiological and biochemical damage, which is interrelated and influence each other (Chen et al., 2016; Faiz et al., 2020). Under the condition of HT, the growth rate of plants is slow, the leaves are withered and yellow and the fruit of plants is often not full and abnormal (Krauss and Marschner, 1984; Guilioni et al., 2003; Shen et al., 2016). These phenotypic characteristics are closely related to the physiological changes of plants. Many types of environmental stresses both biotic and abiotic produce characteristic changes in physiology and metabolic processes of higher plants (Miteva et al., 2005). And under the HT stress, the metabolic process will change to maintain the homeostasis of plant. Some studies have indicated that the physiological and biochemical responses of plants to HT stress mainly consist of four systems that are membrane system, osmotic regulation system, antioxidant defense system and photosynthetic system (Ibrahim and Quick, 2001; Jia et al., 2016; Djanaguiraman et al., 2018; Pu et al., 2019). Biological membranes are highly ordered structures consisting of mosaics of lipids and protein, excessive temperatures can directly and effectively change the properties of these membranes, including their fluidity and permeability, which could lead to changes in the type and concentration of material exchange on both sides of the membrane (Zheng et al., 2011; Niu and Xiang, 2018). These changes act as a signal that can be transmitted to other systems and pathways. Osmotic regulating system is one of the main systems responding to these changes. The osmotic regulating system is mainly composed of some osmotic regulating substances, which are easy to dissolve and have small molecular weight, such as soluble proteins, proline, betaine and their derivatives (Guo, 2010; Liu et al., 2013). When cells need to be maintained or regulated, such substances can be rapidly generated and accumulated in large quantities, so as to improve the ability of water retention and acquisition, which is beneficial for maintaining the normal growth of plants (Wang et al., 2001). As a matter of fact, the main cause of damage to plants under stress is excessive reactive oxygen species (ROS), which is a class of substances that can react with macromolecules, such as lipids, DNA, RNA, and proteins, thereby destroying the structure and function of the cell (Kundu et al., 2020). Therefore, in order to prevent the excessive accumulation of ROS, plant cells have evolved a variety of antioxidant mechanisms to eliminate the toxicity caused by ROS, which is mainly divided into antioxidant enzymatic and non-enzymatic system (Navrot et al., 2007; Junmatong et al., 2015). Antioxidant enzymatic system mainly includes superoxide dismutase (SOD), peroxidase (POD), catalase (CAT) and non-enzymatic system is mainly some organic matter with small relative molecular mass, such as proline, ascorbic acid (ASA) and glutathione (GSH) (Ban et al., 2012; Chetty, 2017; Kolupaev et al., 2020). Compared with other systems, high temperature stress has more effect on photosynthetic system. Some studies have shown that under HT stress, thylakoid membrane was easy to be destroyed, the activity of photosynthesis-related enzymes was decreased or lost and the stomatal activity was drastically affected, which eventually leads to the decrease of net photosynthetic rate and the hindrance of the substances synthesis in plants (Schrader et al., 2004; Djanaguiraman et al., 2018; Sharma, 2020). It is worth noting that under the HT stress, the changes of phenotypic characteristics, physiological and biochemical processes in plants are regulated by complex genes networks (Wilkins et al., 2016; Li B. et al., 2018; Miguel et al., 2020). Proteomics has been a promising tool to reveal the dynamic response mechanism of proteins in plants under the biotic and abiotic stress (Hashiguchi et al., 2010; Sergeant and Renaut, 2010). Through comparative proteomic analysis, Mohammadi et al. (2014) found that proteins involved in cellular traffic, energy and metabolism, disease and defense, protein synthesis and signal transduction play an important role in the physiological and morphological responses of canola to HT stress. By studying the proteome of rice seeds, Liu et al. (2015) reported that high temperature could decrease

Abbreviations: 2-DE, two-dimensional gel electrophoresis; APX, ascorbate peroxidase; CAT, catalase; EL, electrolyte leakage; DEPs, differentially expressed proteins; Fv, variable fluorescence; Fm, maximal fluorescence; Fv/Fm, the chlorophyll fluorescence parameter; GO, gene ontology; GSH-Px, glutathione peroxidase; H2O2, hydrogen peroxide; Hsps, heat shock proteins; KEGG, Kyoto Encyclopedia of Genes and Genomes; LC-MS/MS, liquid chromatography-tandem mass spectrometry; MDA, malondialdehyde; POD, peroxidase; PRM, parallel reaction monitoring; Pro, Proline; ROS, reactive oxygen species; RuBisCO, Ribulose-1,5-bisphosphate carboxylase/oxygenase; SOD, superoxide dismutase; SSC, soluble sugar content; TMT, tandem mass tags.

the abundance of proteins involved in methionine metabolism, amino acid biosynthesis, energy metabolism, reserve degradation and protein folding and stress responses, which eventually inhibits seed germination. These studies will provide valuable information for understanding of HT-tolerant mechanisms in crops and pave the way for genetic engineering to improve crop resistance.

Medicago sativa L. is a high-quality forage due to its characteristics of high yield and excellent nutritional quality, which has the longest planting history and the largest planting area in the world (Chen et al., 2020). In China, alfalfa is one of the main herbages for animal husbandry and industrial feed production, it plays an important role in the industrialization of forage, the construction of artificial grassland and ecological environmental management (Li et al., 2015; Wang, 2020). In recent years, with the transformation and development of animal husbandry, the demand for forage with high yield and quality has increased year by year, which has led to an intense increase in the demand for alfalfa. In China, the planting area of alfalfa is mainly in the north, the introduced varieties in the south have the phenomena of decreasing yield, serious diseases and pests and quality deterioration, which is due to the high temperature climate affecting the normal growth of alfalfa (Lin et al., 2007; Xu et al., 2017; Anley, 2020). In fact, the damage of high temperature stress to alfalfa is one of the main factors limiting its popularization. And with global warming, high temperature weather in summer will be more frequent in China, which will seriously limit the production and utilization of alfalfa (Gao et al., 2019). Therefore, it is essential to study the heat tolerance mechanism of alfalfa and develop alfalfa cultivars that could cope better with stressful temperature events. In addition, with the development of liquid chromatography coupled to tandem mass spectrometry (LC-MS/MS), two popular quantitative proteomic approaches have been developed including label-free quantification (LFQ) and isobaric labeling strategy such as Tandem Mass Tags (TMT) and isobaric Tags for Relative and Absolute Quantitation (iTRAQ) (Ulsen et al., 2009; Nogueira et al., 2012; Kawashima et al., 2019). Compared with conventional 2-DE technique, Tandem Mass Tags (TMT) based quantitative proteomics could more efficiently and accurately analyze more numerous proteins (Pagel et al., 2015). However, the current research studies on alfalfa stress resistance mainly focus on cold resistance, drought resistance and salt-alkaline resistance (Zhang et al., 2017, 2018; Liu et al., 2020). And reports on heat resistance of alfalfa are relatively scattered, and quantitative proteomics studies on heat-stressed alfalfa leaves based on TMT analysis have not been reported. Based on the above, in the present study, TMT is performed to identify the global changes in protein expression under HT treatment in MS30 and MS37, which is screened according to our previous experimental results (**Supplementary Table 1**) and respectively represent HT-tolerant and HT-sensitive alfalfa varieties. Furthermore, we comprehensively compare the physiology and proteomic changes of these two alfalfa varieties under continuously increasing HT stress, characterize the HT-responsive proteins, and analyzed the functions of these differentially expressed proteins (DEPs) in order to clarify differential physiological and proteomic responses of two different heat resistant alfalfa varieties to HT stress. The results of this study could enhance the current understanding of the protein changes underlying HT stress-related cellular and physiological responses between HT-resistant and HT-sensitive alfalfa varieties, and provide basic data and technical theoretical support for the genetic improvement of high-quality and heat-resistant alfalfa varieties.

MATERIALS AND METHODS

Plant Growth Conditions and Stress Treatments

Two alfalfa varieties contrasting in heat tolerance, MS30 and MS37, were used for this experiment, and their seeds were provided by Sichuan Academy of Grassland Sciences. HT-tolerant MS30 and HT-sensitive MS37 were screened according to our previous experimental results (**Supplementary Table 1**), and the specific experimental methods and the selection of experimental indicators are based on Zhang et al. (2010), Liu et al. (2014), and Li (2015). The seeds of two alfalfa varieties were surface sterilized with 10% sodium hypochlorite solution and repeated washes with sterilized distilled water. The washed seeds were sown in a nutritional bowl (20 cm in diameter and 18 cm in height) filled with natural soil 0.45 kg (30%), nutrient soil 0.6 kg (40%), perlite 0.225 kg (15%) and vermiculite 0.225 kg (15%). Natural soil, nutrient soil, perlite and vermiculite were disinfected by the corresponding methods to reduce the influence of bacteria and worm eggs on alfalfa growth. Seeds of each alfalfa variety were sown in three pots as three biological repeats. The nutritional bowls were placed in a growth chamber with controlled conditions (day/night cycle: 16/8 h, 20/15°C, 60 ± 5% relative humidity, 400 $\mu E \cdot m^{-2} \cdot s^{-1}$ PPFD). After 2 months of growth, all alfalfa varieties grow into adult-plants. Select 10–15 healthy plants with consistent growth to remain in each nutritional bowl. All materials are transferred to artificial climate boxes (day/night cycle: 16/8 h, 60 ± 5% relative humidity, 400 $\mu E \cdot m^{-2} \cdot s^{-1}$ PPFD) for high temperature stress treatment. According to the results of a prior experiment and the relevant report, the treatment temperature was set to 20, 25, 30, 35, 40, and 43°C, which is a gradient upward trend. Among them, alfalfa growing at 20°C were used as the control (non-HT stress). All alfalfa varieties were treated at each temperature gradient for 7 days and the leaves was collected for the determination of physiological indicators. Moreover, the physiological conditions of the plants and the humidity of the climate box were observed at any time. Water the plants properly once a day to ensure the water demand of the plants. Based on the results of the above experiment, some key physiological responses demonstrated that both alfalfa varieties showed the most significant variation at 20, 35, and 43°C. Therefore, leaf samples collected from plants after exposure to 20, 35, and 43°C for 7 days, respectively, were harvested for further TMT quantitative proteomic analysis.

Physiological Measurements

The indicators of membrane system, osmotic regulation system, antioxidant defense system and photosynthetic system were

measured in each treatment group. About the photosynthetic system, the chlorophyll content of the leaves was measured by a chlorophyll meter (SPAD-502; Konica Minolta Sensing, Inc., Osaka, Japan). The measurements were made on the axial surface of 10 different green leaves taken from each nutritional bowl (Sharma et al., 2015). Chlorophyll fluorescence was measured by a Chlorophyll Fluorescence Imager (CF Imager; Technologica, Inc., United Kingdom). The plants were dark adapted for 30 min, then the five measured leaves were illuminated with a 2 s saturating light flash at 3,000 μmol photons m^{-2} s^{-1} for CF Imager. The fluorescence data were analyzed and Fv/Fm ratio was calculated using the CF Imager software (version 1.10) (Sharma et al., 2012). About the membrane system, Malondialdehyde (MDA) content was measured by the thiobarbituric acid (TBA) reaction using the method described by Chołuj et al. (2014). Briefly, the leaves (0.1 g) were grinded, homogenized in 10 mL 10% trichloroacetic acid (TCA), and centrifuged at 1,500 × *g* for 10 min. Then 2 ml supernatant was isovolumetric mixed with 0.6% TBA and boiled at 100°C for 10 min. The absorbance values at 532 nm and 600 nm were used to calculate the MDA content. Each sample has three biological repeats. Electrolyte leakage (EL) was detected by using a conductivity meter (YSI Model 32, Yellow Spring, OH, United States) and calculated as the percentage of initial conductivity (Cinitial) and maximum conductance (Cmax) (Blum and Ebercon, 1981). About the osmotic regulation system, the soluble protein content was measured using bovine serum albumin as described by Bradford (1976). The soluble sugar content was measured according to Buysse and Merckx (1993). The leaves (0.1 g) were grinded and added into 10 mL 80% ethanol and then extracted in boiled water (100°C) for 15 min. After centrifugation at 3600 g_n for 10 min, supernatants were collected for further analysis. The reaction mixture contained 1 mL of supernatant, 1 mL of 18% phenol solution, and 5 mL concentrated sulfuric acid. The mixture was shaken, and absorbance was read at 490 nm using a spectrophotometer (Spectronic Instruments). The free proline content was determined using the acid ninhydrin method (Bates et al., 1973). The leaves (0.1 g) were grinded and immerged in 5 mL 3% aqueous sulfosalicylic acid and then heated in a water bath (100°C) for20 min. After centrifugation at 12,000 g_n, the supernatant was used for the estimation of the proline concentration. The reaction mixture consisted of 1 mL of supernatant, 1.5 mL of 2.5% acid ninhydrin, and 1 mL of glacial acetic acid, which was heated at 100°C for 40 min. The reaction mixture was immediately cooled down in an ice bath, and extracted with 2.5 mL of toluene then absorbance was read at 520 nm.

About the antioxidant defense system, the extraction procedure of the enzymes was carried out at 4°C (Chao et al., 2010). The leaves were homogenized (1:10 w/v) in an ice cold mortar using 50 mM sodium phosphate buffer pH 7.0 containing 0.5 M NaCl, 1 mM EDTA and 1 mM sodium ascorbate. After centrifugation (20,000 × *g*, 20 min) the supernatant was used for the determination of SOD, POD, CAT, APX and GSH-Px activities. The SOD activity was measured at 560 nm according to Giannopolitis and Ries (1977). An amount of 50 μl of crude extract was added in a 1.5-ml reaction solution containing 195 mM methionine, 3 μM EDTA, 1.125 mM NBT, 60 μM riboflavin, and 50 mM PBS buffer (pH 7.8). The reduction of absorbance was recorded at 560 nm with a spectrophotometer. The POD activity was assayed at 470 nm as described by Chance and Maehly (Machly and Chance, 1955). The assay mixture contained 50 mM sodium acetate buffer pH 5.6, 5.4 mM guaiacol, 15 mM H_2O_2 and enzyme extract. The increase in absorbance due to the oxidation of guaiacol to tetraguaiacol was monitored at 470 nm. The activities of CAT and APX were assayed by the method of Nakano and Asada (1981). Briefly, the assay mixture contained 50 mM sodium phosphate buffer pH 7.0, 15 mM H_2O_2 and enzyme extract. Decomposition of H_2O_2 was measured at 240 nm. The assay mixture consisted of 50 mM sodium phosphate buffer pH 7.0 containing 1 mM EDTA, 0.25 mM sodium ascorbate, 25 μM H_2O_2 and enzyme extract. Addition of H_2O_2 started the reaction. Rates were corrected for the non-enzymatic oxidation of ascorbate by the inclusion of reaction mixture without enzyme extract. The GSH-Px activity was assayed at 470 nm as described by Wheeler et al. (1990). The mixture contained 50 mM potassium phosphate buffer pH 7.0, 2 mM EDTA, 150 mM GSH, 4.2 mM NADPH, 0.5 unit of glutatione reductase and 2.2 mM *t*-butyl peroxide, which started the reaction. The absorbance of the reacted solution at 340 nm was determined with a spectrophotometer. The levels of the above physiological parameters were all calculated based on fresh weight.

Protein Extraction

The sample was grinded by liquid nitrogen into cell powder and then transferred to a 5-mL centrifuge tube. After that, four volumes of lysis buffer (8 M urea, 1% Triton-100, 10 mM dithiothreitol, and 1% Protease Inhibitor Cocktail) was added to the cell powder, followed by sonication three times on ice using a high intensity ultrasonic processor (Scientz) (Note: For PTM experiments, inhibitors were also added to the lysis buffer, e.g., 3 μM TSA and 50 mM NAM for acetylation). The remaining debris was removed by centrifugation at 20,000 *g* at 4°C for 10 min. Finally, the protein was precipitated with cold 20% TCA for 2 h at −20°C. After centrifugation at 12,000 *g* 4°C for 10 min, the supernatant was discarded. The remaining precipitate was washed with cold acetone for three times. The protein was redissolved in 8 M urea and the protein concentration was determined with BCA kit according to the manufacturer's instructions.

Trypsin Digestion and Tandem Mass Tags Labeling

For digestion, the protein solution was reduced with 5 mM dithiothreitol for 30 min at 56°C and alkylated with 11 mM iodoacetamide for 15 min at room temperature in darkness. The protein sample was then diluted by adding 100 mM TEAB to urea concentration less than 2 M. Finally, trypsin was added at 1:50 trypsin-to-protein mass ratio for the first digestion overnight and 1:100 trypsin-to-protein mass ratio for a second 4 h-digestion. After trypsin digestion, peptide was desalted by Strata × C18 SPE column (Phenomenex) and

vacuum-dried. Peptide was reconstituted in 0.5 M TEAB and processed according to the manufacturer's protocol for TMT kit. Briefly, one unit of TMT reagent were thawed and reconstituted in acetonitrile. The peptide mixtures were then incubated for 2 h at room temperature and pooled, desalted and dried by vacuum centrifugation.

Liquid Chromatography-Tandem Mass Spectrometry Analysis and Database Search

The tryptic peptides were dissolved in 0.1% formic acid (solvent A), directly loaded onto a home-made reversed-phase analytical column (15-cm length, 75 μm i.d.). The gradient was comprised of an increase from 6 to 23% solvent B (0.1% formic acid in 98% acetonitrile) over 26 min, 23 to 35% in 8 min and climbing to 80% in 3 min then holding at 80% for the last 3 min, all at a constant flow rate of 400 nL/min on an EASY-nLC 1000 UPLC system.

The peptides were subjected to NSI source followed by tandem mass spectrometry (MS/MS) in Q ExactiveTM Plus (Thermo) coupled online to the UPLC. The electrospray voltage applied was 2.0 kV. The m/z scan range was 350 to 1800 for full scan, and intact peptides were detected in the Orbitrap at a resolution of 70,000. Peptides were then selected for MS/MS using NCE setting as 28 and the fragments were detected in the Orbitrap at a resolution of 17,500. A data-dependent procedure that alternated between one MS scan followed by 20 MS/MS scans with 15.0 s dynamic exclusion. Automatic gain control (AGC) was set at 5E4. Fixed first mass was set as 100 m/z.

The resulting MS/MS data were processed using Maxquant search engine (v.1.5.2.8). Tandem mass spectra were searched against human uniprot database concatenated with reverse decoy database. Trypsin/P was specified as cleavage enzyme allowing up to 4 missing cleavages. The mass tolerance for precursor ions was set as 20 ppm in First search and 5 ppm in Main search, and the mass tolerance for fragment ions was set as 0.02 Da. Carbamidomethyl on Cys was specified as fixed modification and acetylation modification and oxidation on Met were specified as variable modifications. FDR was adjusted to <1% and minimum score for modified peptides was set >40. The mass spectrometry proteomics data have been deposited to the ProteomeXchange Consortium via the PRIDE partner repository with the dataset identifier PXD025642.

Parallel Reaction Monitoring Validations

To verify the protein expression levels obtained by TMT analysis, 14 DEPs (unique peptides ≥ 2, fold change > 1.2) were randomly chosen based on the TMT results and further quantified by the parallel reaction monitoring (PRM) assay according to Xu's method (Xu et al., 2018) at Jingjie PTM-Biolab Co., Ltd. (Hangzhou, China). Briefly, peptides were prepared as above described for TMT assay. These obtained peptide mixtures were subjected to NSI source followed by tandem mass spectrometry (MS/MS) in Q ExactiveTM Plus (Thermo) coupled online to the UPLC. A full MS was performed in the Orbitrap at a resolution of 70,000 (AGC target at 3E6; the maximum injection time at 50 ms and the m/z range was 350–1200), followed by 20 MS/MS scans on the Orbitrap at a resolution of 17,500 (AGC target was 1E5, and the maximum injection time was 100 ms). Mass window for precursor ion selection was 1.6 m/z. The isolation window for MS/MS was set at 2.0 m/z. The NCE was 27% with HCD. The FDR was set to 0.01 for the proteins and peptides. The resulting MS data were processed using Skyline (v.3.6) program as described before (Kim et al., 2016).

Statistical Analysis

All physiological data analyses were performed using the SPSS Statistical Software (version 19.0; SPSS Institute Ltd., United States), and the significance of differences were tested using Fisher's protected least significant difference test (LSD) with a P-value ≤ 0.05 set as statistically significant.

RESULTS

Effect of High Temperature Stress on Physiological Level of Alfalfa

Effect of High Temperature Stress on Photosynthetic System

Under the HT stress, the variation trend of chlorophyll content in the two alfalfa varieties was different (**Figure 1A** and **Supplementary Table 2**). The heat resistant alfalfa variety (MS30) had the highest chlorophyll content at 35°C, and then significant decreased with the increasing of temperature. In the condition of 43°C, the chlorophyll content of MS30 is significantly lower than that of the CK by 32.19 SPAD ($p < 0.05$). But for MS37, the chlorophyll content was no significant change under 20 and 25°C, and with the increase of temperature, the chlorophyll content decreased obviously. At the condition of 43°C, the chlorophyll content was only 25.06 SPAD, which is similar to MS30. During the period of HT stress, the chlorophyll fluorescence parameter Fv/Fm in the two alfalfa varieties showed a gradual declining trend with the increased temperature (**Figure 1B** and **Supplementary Table 2**). As the temperature increased from 20 to 43°C, the decreased range of Fv/Fm in MS37 is obviously higher than that of MS30. The Fv/Fm value of MS37 was only 0.33 under the 43°C, which was significantly lower than that of MS30 under this condition ($p < 0.05$).

Effect of High Temperature Stress on Membrane System

Under the condition of the HT stress, the membrane system of two alfalfa varieties were all effected to certain degrees (**Figures 1C,D** and **Supplementary Table 2**). As the temperature gradually increases, the content of Malondialdehyde (MDA) in the two alfalfa varieties were significantly higher than that in control ($p < 0.05$). Under the condition of 43°C, the content of MDA in the two alfalfa varieties were highest, which of MDA in MS30 was significantly lower than that in MS37 ($p < 0.05$). And with the increase of temperature, the electrolyte leakage (EL) of the two alfalfa varieties showed an upward trend. But it is worth noting that the varied degree of EL in MS37 were significantly greater than those of MS30 under the HT stress. The EL of MS30

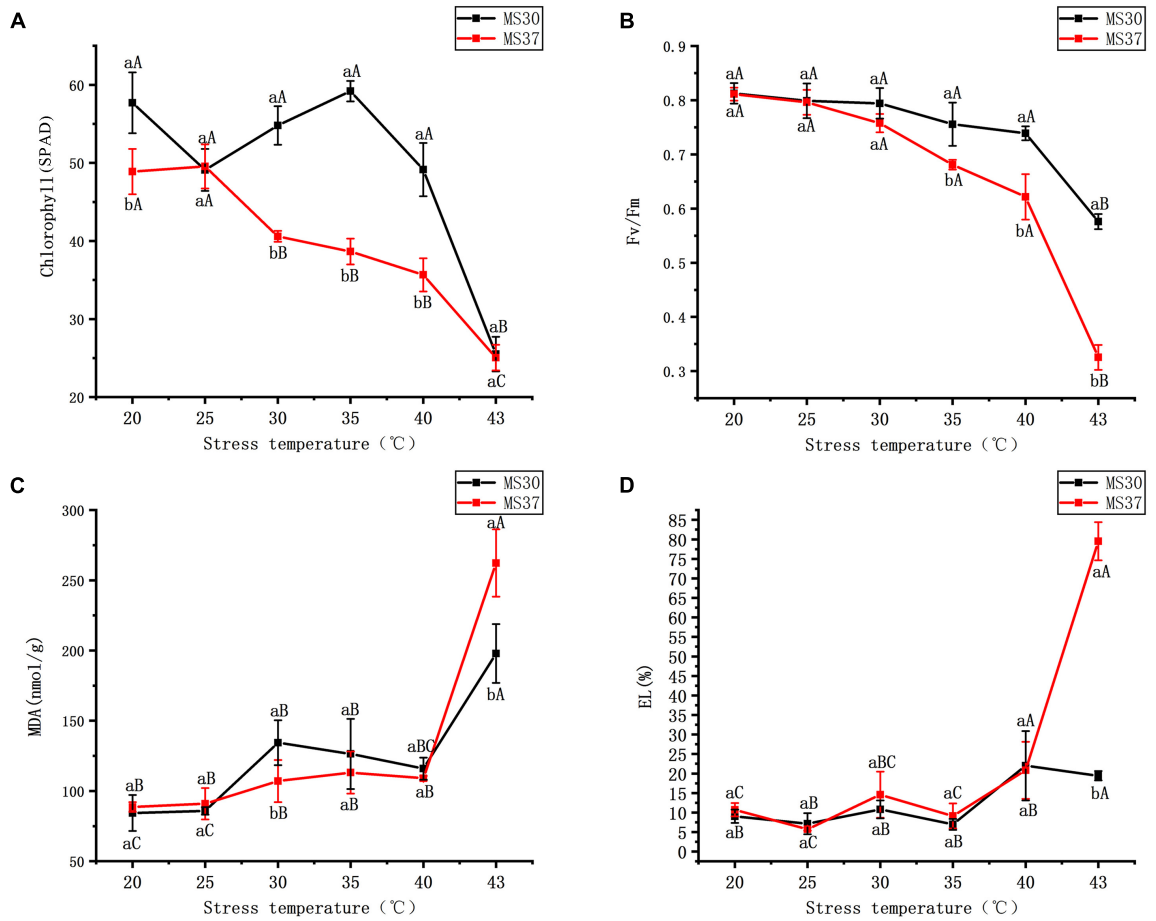

FIGURE 1 | The changes of photosynthetic system and membrane system in MS30 and MS37 under HT stress. **(A)** Total chlorophyll content. **(B)** The chlorophyll fluorescence parameter (Fv/Fm). **(C)** MDA content. **(D)** Electrolyte leakage. Different capital letters above line graphs indicate significant difference among various temperature treatments within the same alfalfa varieties ($p < 0.05$), different little letters above line graphs indicate significant difference among two alfalfa varieties under the same temperature ($p < 0.05$). Data are means ± SE from measurements of three replicate experiments.

peaked at the condition of 43°C, which is significantly higher than MS37 ($p < 0.05$).

Effect of High Temperature Stress on Osmotic Regulation System

With the increased intensity of high temperature stress, the osmotic regulation system in both alfalfa varieties showed an apparent change (**Figures 2A–C** and **Supplementary Table 2**). The two alfalfa varieties content of proline peaked at the condition of 43°C. And compared with the proline content under the control, the proline content of MS30 and MS37 increased by 667.49 and 223.68 μg/g, respectively. It is noteworthy that the proline content of MS30 had increased to 754.82 μg/g at the 43°C, which was significantly higher than this of MS37 by 577.64 μg/g ($p < 0.05$). This result indicates that under the HT stress, the response of osmotic adjustment substances in heat-resistant alfalfa variety, MS30, are better than those of heat sensitive alfalfa variety, MS37. The changes of soluble sugar content (SSC) in the two alfalfa varieties under HT stress also prove this result. The SSC in MS30 peaked at the condition of 43°C, which is significantly greater than this of MS37 ($p < 0.05$). Under HT stress, the content of soluble protein in the two alfalfa varieties generally showed an increasing trend, and the soluble protein content of MS37 Peaked at the condition of 40°C. However, at the 43°C, the soluble protein content of MS30 was similar to this of MS37, which is 45.07 and 42.62 mg/g, respectively.

Effect of High Temperature Stress on Antioxidant Defense System

According to the results of **Figure 2**, the superoxide dismutase (SOD) and catalase (CAT) activities of MS30 were higher than that of MS37 in all the treatments except for 30°C (**Figures 2D,E** and **Supplementary Table 2**). The maximum and minimum values of SOD and CAT activities in the two alfalfa varieties were both detected at 25 and 43°C. The activities of peroxidase (POD) in the two alfalfa varieties peaked at 25°C, and the POD activity of MS37 was significantly higher than that of MS30 ($p < 0.05$) (**Figure 2F**). But when the temperature gradually increases to 43°C, the POD activity of MS30 was 1515 U/g, which

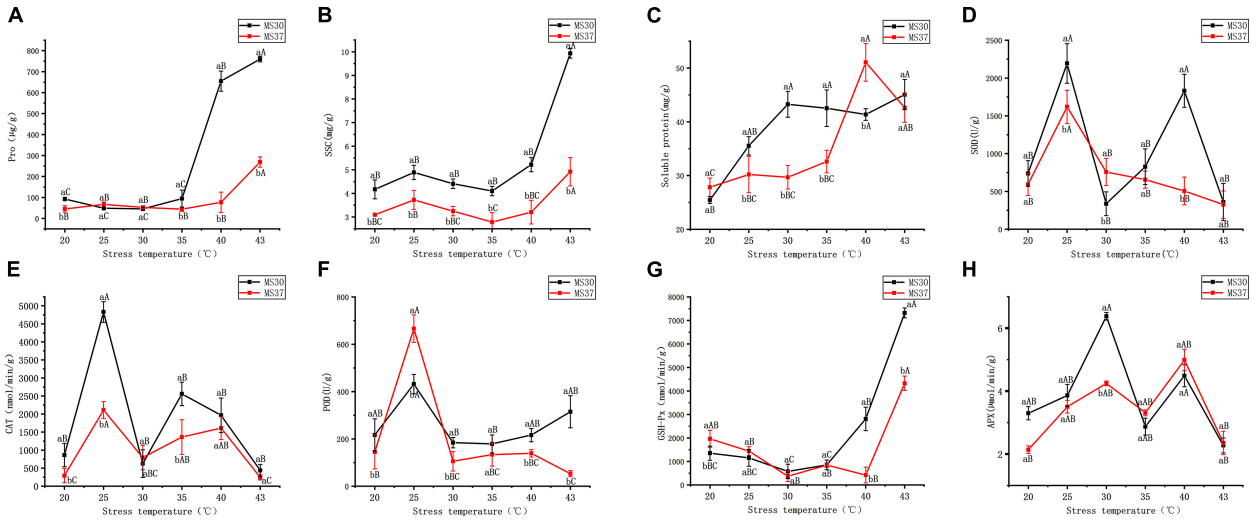

FIGURE 2 | The changes of Osmotic Regulation System and Antioxidant Defense System in MS30 and MS37 under HT stress. **(A)** Pro content. **(B)** Soluble sugar content (SSC). **(C)** Soluble protein content. **(D)** The activity of superoxide dismutase (SOD). **(E)** The activity of catalase (CAT). **(F)** The activity of peroxidase (POD). **(G)** The activity of glutathione peroxidase (GSH-Px). **(H)** The activity of ascorbate peroxidase (APX). Different capital letters above line graphs indicate significant difference among various temperature treatments within the same alfalfa varieties ($p < 0.05$), different little letters above line graphs indicate significant difference among two alfalfa varieties under the same temperature ($p < 0.05$). Data are means ± SE from measurements of three replicate experiments.

was significantly greater than that of MS37 ($p < 0.05$). In the early stage of HT stress, the glutathione peroxidase (GSH-Px) activities of the two alfalfa varieties all declined (**Figure 2G**). But in the later stage of HT stress, the GSH-Px activities of the two alfalfa varieties both showed an upward trend, and the GSH-Px activities in MS30 were significantly greater than that of MS37 at 43°C ($p < 0.05$). Under the HT stress, the ascorbate peroxidase (APX) variation trends of the two alfalfa varieties were consistent (**Figure 2H**). And the APX activities of MS30 and MS37 are both decreased at 43°C, which was respectively 2.27 and 2.35 μmol/min/g.

Effect of High Temperature Stress on Proteome of Alfalfa

According to the trend of physiological indicators of two alfalfa varieties, it's apparent to find that both of alfalfa varieties had notable changes under 35 and 43°C compared with 20°C. Therefore, the proteomic information of two alfalfa varieties exposed to 20, 35, and 43°C were analyzed by using TMT-LC/MS-MS. In this experiment, a total of 1,575,487 spectrum were generated through the TMA analysis. After searching the database of protein, the number of match spectrum was 184,025, which shows the utilization ratio of spectrum was 11.7%. A total of 93,785 peptides were identified at 95% confidence level through spectral analysis, in which has 88,958 unique peptides. A total of 7,300 proteins were identified, which has 6,704 quantifiable proteins (**Supplementary Table 3**). In order to analyze the differentially expressed proteins (DEPs) of two alfalfa varieties under HT stress, we compared the DEPs of MS30 and MS37 under different and same temperature respectively (**Figure 3** and **Supplementary Table 4**). For MS30 and MS37, the number of DEPs were the most in the 43/35°C comparison group, with 1,235 and 1,355 respectively (**Figures 3A,B**). Under the same temperature comparison, the number of DEPs is the largest in the MS3035/MS3735 comparison group, which has a total of 575 DEPs and the up-regulated DEPs accounted for 71.3% (**Figure 3C**).

Information-Identification and Trend Analysis of Differentially Expressed Proteins

Gene Ontology Analyses of Differentially Expressed Proteins in Response to High Temperature

The GO database[1] was used to annotate the DEPs. The result indicated that all identified DEPs were classified to different biological processes (BP) in which the major categories were response to organic substance metabolic process, cellular metabolic process, primary metabolic process and nitrogen compound metabolic process (**Figures 4A–G**). Among cellular components (CC), intracellular, intracellular organelle and membrane-bounded organelle were the most abundant groups. Additionally, in terms of molecular functions (MF), most of the DEPs were classified to the following categories: organic cyclic compound binding, heterocyclic compound binding, hydrolase activity and protein binding. In order to find the more specific GO items that play an important role under heat stress, the DEPs enrichment of the BP, CC and MF were analyzed in the GO classification, respectively (**Supplementary Table 5**). According to the results of the DEPs in the GO classification, we found that for MS30 and MS37, GO terms related to energy metabolism and photosynthetic processes appeared in 35/20 and 43/35°C comparison groups, such as cellular response to blue

[1]http://www.ebi.ac.uk/GOA/

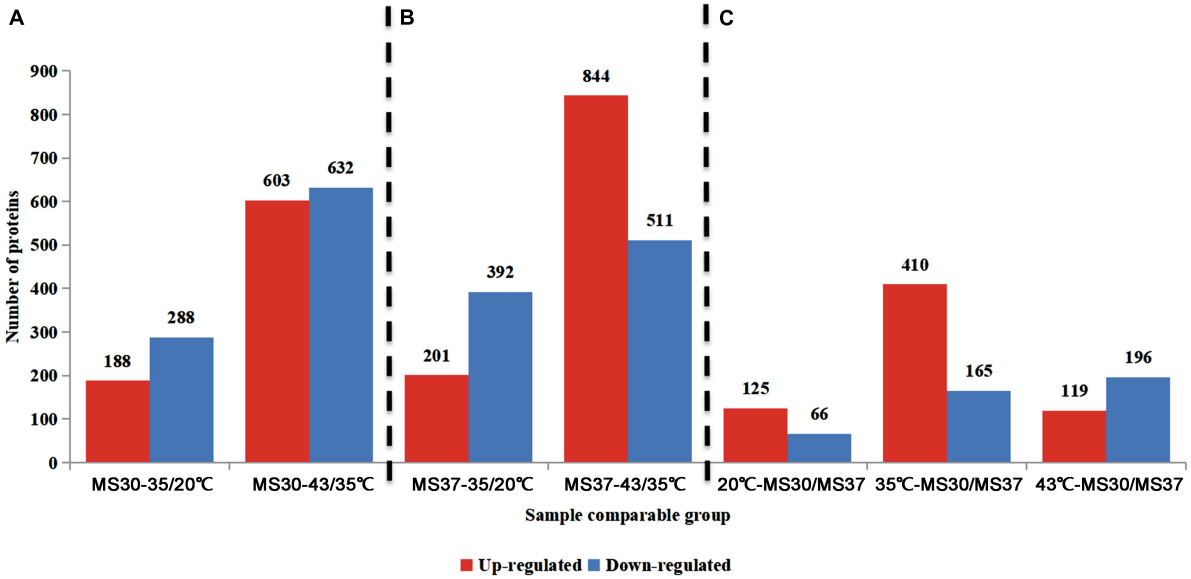

FIGURE 3 | The number of DEPs in different comparison groups. **(A)** The comparison groups of MS30. MS30-35/20°C stands for the proteome of MS30 at 35°C compared with that of MS30 at 20°C. MS30-43/35°C stands for the proteome of MS30 at 43°C compared with that of MS30 at 35°C. **(B)** The comparison groups of MS37. MS37-35/20°C stands for the proteome of MS37 at 35°C compared with that of MS37 at 20°C. MS37-43/35°C stands for the proteome of MS37 at 43°C compared with that of MS37 at 35°C. **(C)** The comparison groups of MS30 and MS37 under the same temperature. The data on the columns indicate the number of up- or down-regulated expressed DEPs.

light, chloroplast inner membrane and acetyl-CoA biosynthetic process. In addition, we also discovered the dynamic changes of the DEPs in GO enrichment. For MS30, the DEPs were significantly enriched to the GO terms related to the cell wall in the 35/20°C comparison group, while in the 43/35°C comparison group, the DEPs were significantly enriched to GO term associated with PS II repair and chaperone repair. These results indicate that the photosynthetic processes and the repair process play an important role in the resistance of alfalfa to HT stress, especially under the stress of 43°C. We further compared the GO terms of the MS30/MS37 comparison group under 20, 35, and 43°C, and found that the synthesis of flavonoids and the process of RNA modification may be also related to the heat tolerance of plants.

Kyoto Encyclopedia of Genes and Genomes Analyses of Differentially Expressed Proteins in Response to High Temperature

The result of KEGG analysis[2] show that for the MS30, most up-regulated DEPs in the 35/20°C comparison group enriched in pathways of Steroid biosynthesis, Circadian rhythm-plant, Protein processing in endoplasmic reticulum and Plant-pathogen interaction, whereas proteins involved in Porphyrin and chlorophyll metabolism were down-regulated (**Supplementary Table 6**). Most of DEPs related to Protein processing in endoplasmic reticulum and Carotenoid biosynthesis were increased, while DEPs associated with Biosynthesis of secondary metabolites-other antibiotics, Photosynthesis-antenna proteins, Photosynthesis and Ribosome were decreased in the 43/35°C comparison group. For the material MS37, the DEPs of the 35/20°C comparison group involved in the pathways of Photosynthesis-antenna proteins, Linoleic acid metabolism, alpha-Linolenic acid metabolism and Photosynthesis were up-regulated, whereas DEPs in Zeatin biosynthesis were down-regulated. In the 43/35°C comparison group, the up-regulated DEPs were significantly enriched in pathways of Monobactam biosynthesis and Protein processing in endoplasmic reticulum, while down-regulated DEPs were significantly enriched in Photosynthesis-antenna proteins, Photosynthesis-antenna proteins and Linoleic acid metabolism. We further analyzed the KEGG enrichment of DEPs in the MS30/MS37 comparison group under 20, 35, 43°C, respectively, and also found pathways related to Glucosinolate biosynthesis, alpha-Linolenic acid metabolism and Diterpenoid biosynthesis. In addition, pathways such as Ribosome, Porphyrin and chlorophyll metabolism, Lysine biosynthesis and Thiamine metabolism also appeared in each comparison group of MS30/MS37. The dynamic changes of these pathways reflect the response mode of two alfalfa varieties under high temperature stress and are related to their heat tolerance.

Key Proteins Among Differentially Expressed Proteins in Response to High Temperature Stress

According to the results of GO and KEGG enrichment, we found that the DEPs were mainly enriched in the processes of photosynthesis, energy, damage and repair. Therefore, we

[2]http://www.genome.jp/kegg/

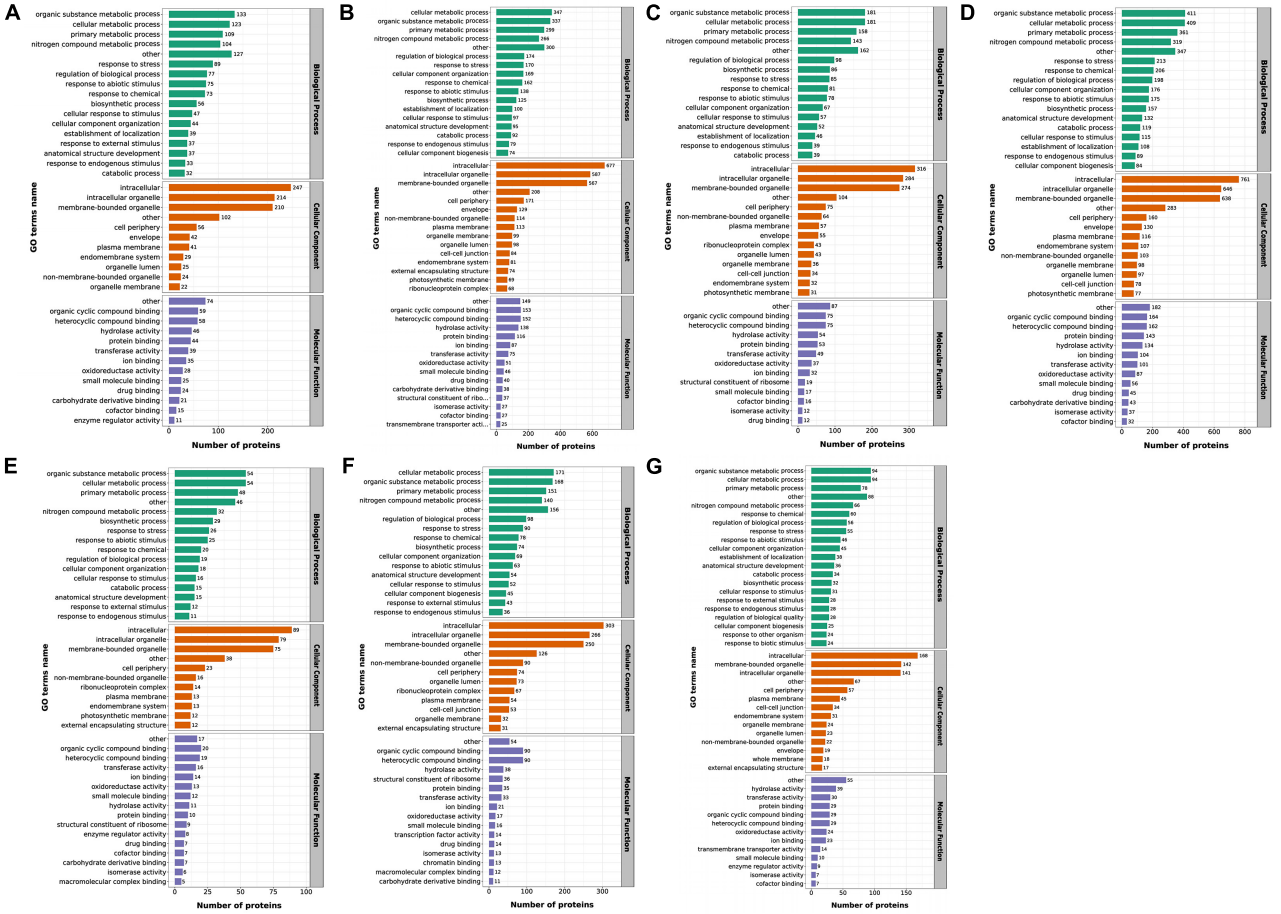

FIGURE 4 | The functional distribution of DEPs in response to HT stress by GO level 2. The *x*-axis represents the number of enriched DEPs by GO annotation and the note number mean protein number. **(A)** The DEPs of MS3035/MS3020 by GO. **(B)** The DEPs of MS3043/MS3035 by GO. **(C)** The DEPs of MS3735/MS3720 by GO. **(D)** The DEPs of MS3743/MS3735 by GO. **(E)** The DEPs of MS3020/MS3720 by GO. **(F)** The DEPs of MS3035/MS3735 by GO. **(G)** The DEPs of MS3043/MS3743 by GO.

constructed the Venn diagrams of MS30 and MS37 under HT stress, respectively (**Figure 5**). And the DEPs associated with photosynthesis, regulation, repair and metabolism were selected in the overlapping regions of the Venn diagrams to analyze their dynamic changes under HT stress.

Photosynthesis-Related Differentially Expressed Proteins

Venn diagram analysis was illustrated the numbers of common DEPs in both comparison groups of MS30 is 160 (**Figure 5A**). Among these 160 DEPs, a total of 10 DEPs are involved in the photosynthetic process under high temperature stress, including those related to photosynthetic system II, chlorophyll, calvin cycle and light photoreceptor (**Supplementary Table 7A**). Among these DEPs, there are four DEPs showing an up-regulated trend and two DEPs showing a down-regulated trend as the temperature rises. For the material MS37, the Venn diagram analysis was illustrated that 213 DEPs were located in the repeated regions of the two comparison groups (**Figure 5B**). Among them, there are a total of 15 DEPs related to photosynthesis (**Supplementary Table 7B**). We observed that four DEPs related to photosynthesis co-exist in MS30 and MS37, and their accumulation trends in these two varieties were consistent, which indicates that these DEPs play an important role in alfalfa response to HT stress (**Figure 6**). It is noteworthy that among these four DEPs, three DEPs have been always up-regulated under the HT stress, and their increased accumulation in MS30 was significantly higher than that in MS37. Considering the difference in heat resistance of two varieties, we infer that these three DEPs could be one of the key factors that determine the heat resistance of alfalfa.

Antioxidant-Related Differentially Expressed Proteins

Here, we observed that HT stress altered the abundance of five DAPs in the both comparable groups of MS30, and six DAPs in the both comparable groups of MS37, which is mainly related to glutathione (**Supplementary Tables 8A,B**). Among these DEPs, two DEPs related to glutathione S-transferase co-exist in MS30 and MS37, and have always been up-regulated under the HT stress (**Figure 6**). In addition, we also found two other DEPs

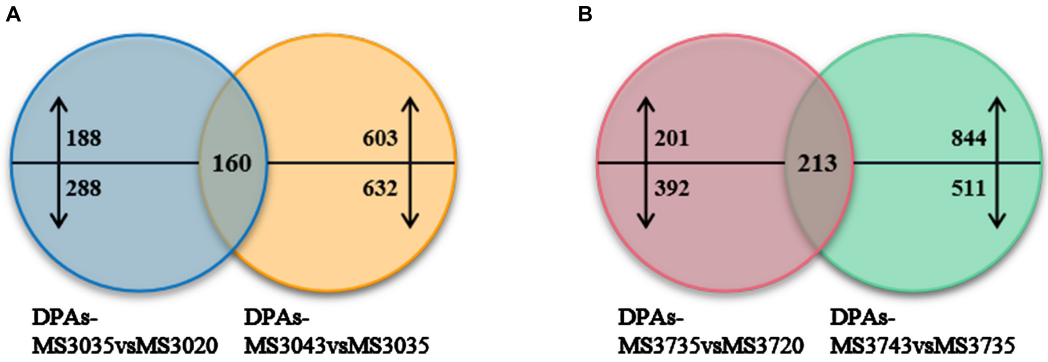

FIGURE 5 | Venn diagrams of two alfalfa varieties. **(A)** Venn diagrams of MS30. **(B)** Venn diagrams of MS30. Venn diagrams show the number of common, significantly up-regulated and down-regulated proteins in two alfalfa varieties under high temperature stress, up- and downward arrows represent up-regulated and down-regulated proteins, respectively.

related to glutathione S-transferase in MS37, and they were also up-regulated during the whole process of high temperature stress. These results indicate that glutathione S-transferase could play a positive role in alfalfa response to HT stress.

Different Expressed Heat Shock Proteins

The number of different expressed heat shock proteins (DEHSPs) that were found in both comparison groups of MS30 is thirty-six, which is more than the number of DEHSPs that were found in both comparison groups of MS37 (**Supplementary Tables 9A,B**). In additional, we found the DEHSPs in MS30 includes all classes of heat shock proteins, but the DEHSPs in MS37 only includes five classes of heat shock proteins, sHSP, HSP70, HSP90, HSP100, and FKBP. Comparing the accumulation trends of the DEHSPs shared by MS30 and MS37, we found that almost all DEHSPs were up-regulated with increasing temperature, only ATP-dependent Clp protease ATP-binding subunit (TRINITY_DN17376_c2_g3_Gene_31004) has been changed in a fluctuating way, which is down-regulated in the 35/20°C comparable group and up-regulated in the 43/35°C comparable group (**Figure 6**). Moreover, the accumulations of the DEHSPs that has always been up-regulated in MS30 are higher than that in MS37 at 35°C. These results indicate that under the HT stress, the difference in HSPs between the two varieties largely affects their heat resistance.

Metabolism-Related Differentially Expressed Proteins

There are twenty-three metabolism-related DEPs in both comparison groups of MS30 (**Supplementary Table 10A**). Among these DEPs, sixteen DEPs are related to primary metabolism and seven DEPs are related to secondary metabolism (**Figure 7A**). In both comparison groups of MS37, we found thirty-seven metabolism-related DEPs, including twenty-eight DEPs related to primary metabolism and nine DEPs related to secondary metabolism (**Figure 7B** and **Supplementary Table 10B**). Analyzing the DEPs shared by MS30 and MS37, we found that under the HT stress, the accumulation trends of these DEPs in the two alfalfa varieties are exactly the same (**Figure 6**). All these results indicated that HT stress had an effect on the metabolism of the two alfalfa varieties, but from the number of metabolism-related DEPs and the metabolic pathways involved in these DEPs, the HT stress has a greater impact on the MS37.

Validation of Candidate Functional Protein Selections by Parallel Reaction Monitoring

Among the DEPs in MS30 and MS37, those having predicted annotations related to "photosynthesis," "regulation," "repair," and "metabolism" are most likely to be responsive to HT stress. Therefore, we annotated the DEPs that shared by the two alfalfa varieties, MS30 and MS37. In order to validate the TMT results, 14 DEPs were randomly selected for targeted parallel reaction monitoring (PRM) assay, of which 11 proteins had quantitative information and showed a good consistency with TMT results, including one DEP related to oxidation-reduction, two DEPs related to photosynthesis, four DEPs related to heat shock proteins and four DEPs related to metabolism in both MS30 and MS37 (**Table 1**).

DISCUSSION

The Change of Photosynthesis Under Heat Stress

Photosynthesis is a process by which plants use light energy to assimilate carbon dioxide (CO_2) and water (H_2O) to produce organic substances and release oxygen, which is closely related to plant growth and productivity (Yamamoto, 2001; Foyer et al., 2017). However, when plants are exposed to heat stress, photosynthesis is the most sensitive physiological process (Wahid et al., 2007). In this study, we exposed alfalfa plants to periodically increasing high temperature treatment as heat stress. Our data showed that the photosynthetic system of both alfalfa materials was affected, which was reflected in physiological level and protein level. In terms of physiological changes, although the Fv/Fm shows a downward trend in both materials, the decrease of Fv/Fm in MS37 is significantly stronger than that in MS30.

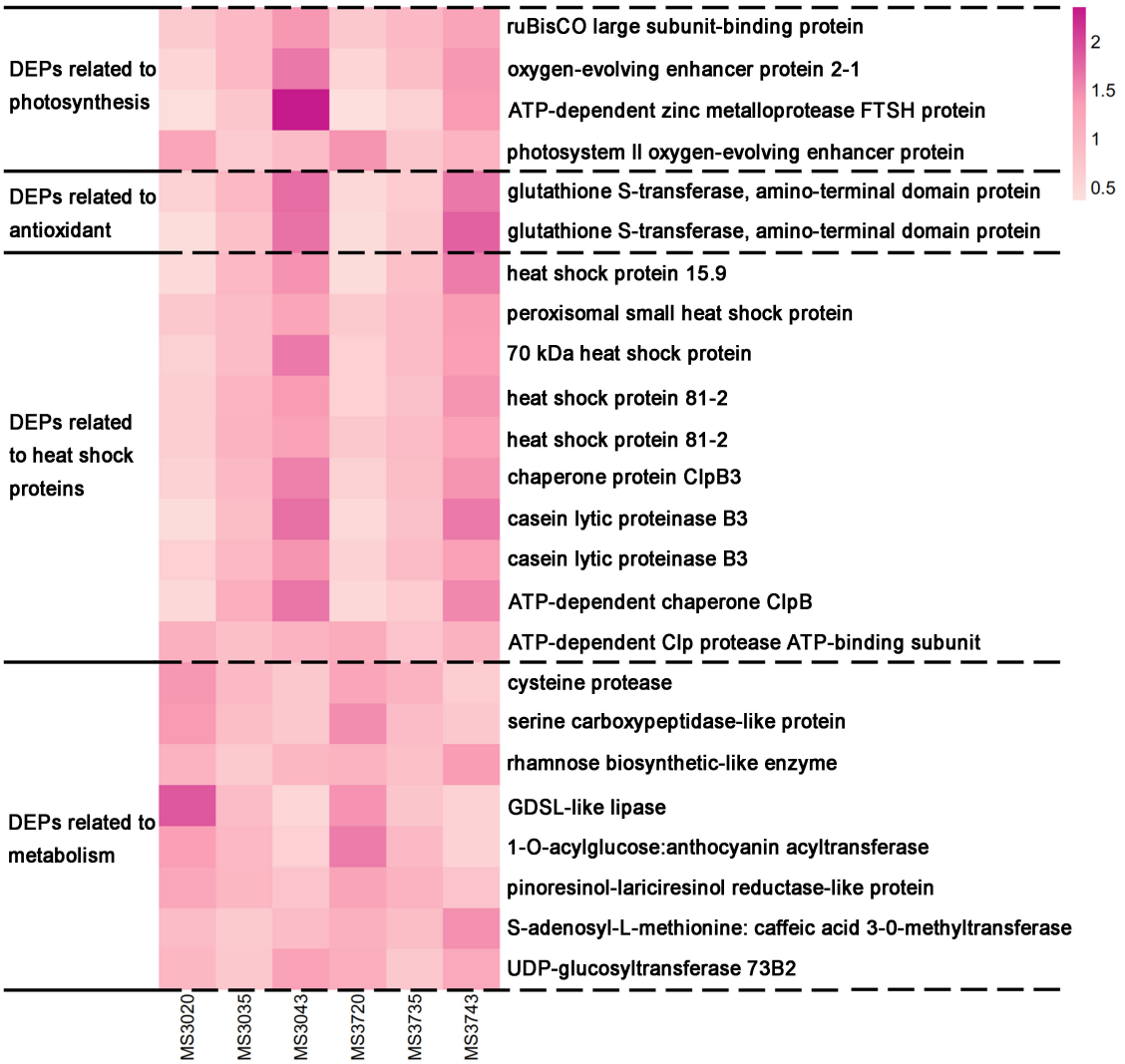

FIGURE 6 | The heatmap of key DEPs co-existed by both alfalfa varieties in response to HT stress. Heat map based on the expression leave of each protein in each sample. The darker the color, the higher the protein expression, and the lighter the color, the lower the protein expression. Each row in the heat map represents the levels of a DEP under different conditions. The DEP name were listed on the right side of the heat map.

And the chlorophyll content of MS37 also showed a decrease trend with the increase of temperature, but that of MS30 showed fluctuating changes. These results revealed that the photosynthesis of the MS37 was significantly stronger affected than that of MS30 under the heat stress. Similar conclusions have been reported in the study of heat resistance of wheat (Sharma et al., 2015).

In terms of protein expression, our data found that heat stress altered the abundance of ten proteins in MS30 and fifteen proteins in MS37 related to photosynthesis. Of these, there are four DEPs co-existing in MS30 and MS37, which is RuBisCO large subunit-binding protein (TRINITY_DN17135_c0_g1_Gene_34667), oxygen-evolving enhancer protein 2-1 (TRINITY_DN16844_c0_g3_Gene_8166), ATP-dependent zinc metalloprotease FTSH protein (TRI NITY_DN21254_c0_g1_Gene_19039) and magnesium-chelatase subunit ChlI (TRINITY_DN12545_c0_g1_Gene_9459). The RuBisCO large subunit-binding protein has two different types of subunit, termed alpha and beta, and some studies suggest this protein is implicated in the assembly of Rubisco in higher plant chloroplasts (Musgrove and Ellis, 1986). Rubisco plays an important role in plant growth, which catalyzes the photosynthetic assimilation of CO_2 into organic compounds (Carmo-Silva et al., 2015). In this experiment, the RuBisCO large subunit-binding protein has been up-regulated in the two alfalfa materials, which could contribute to enhance heat tolerance of alfalfa. Oxygen-evolving enhancer protein 2-1 reported in Arabidopsis thaliana and *Nicotiana tabacum* may be involved in the regulation of photosystem II[3]. More specifically, the function of oxygen-evolving enhancer protein

[3]https://www.uniprot.org/

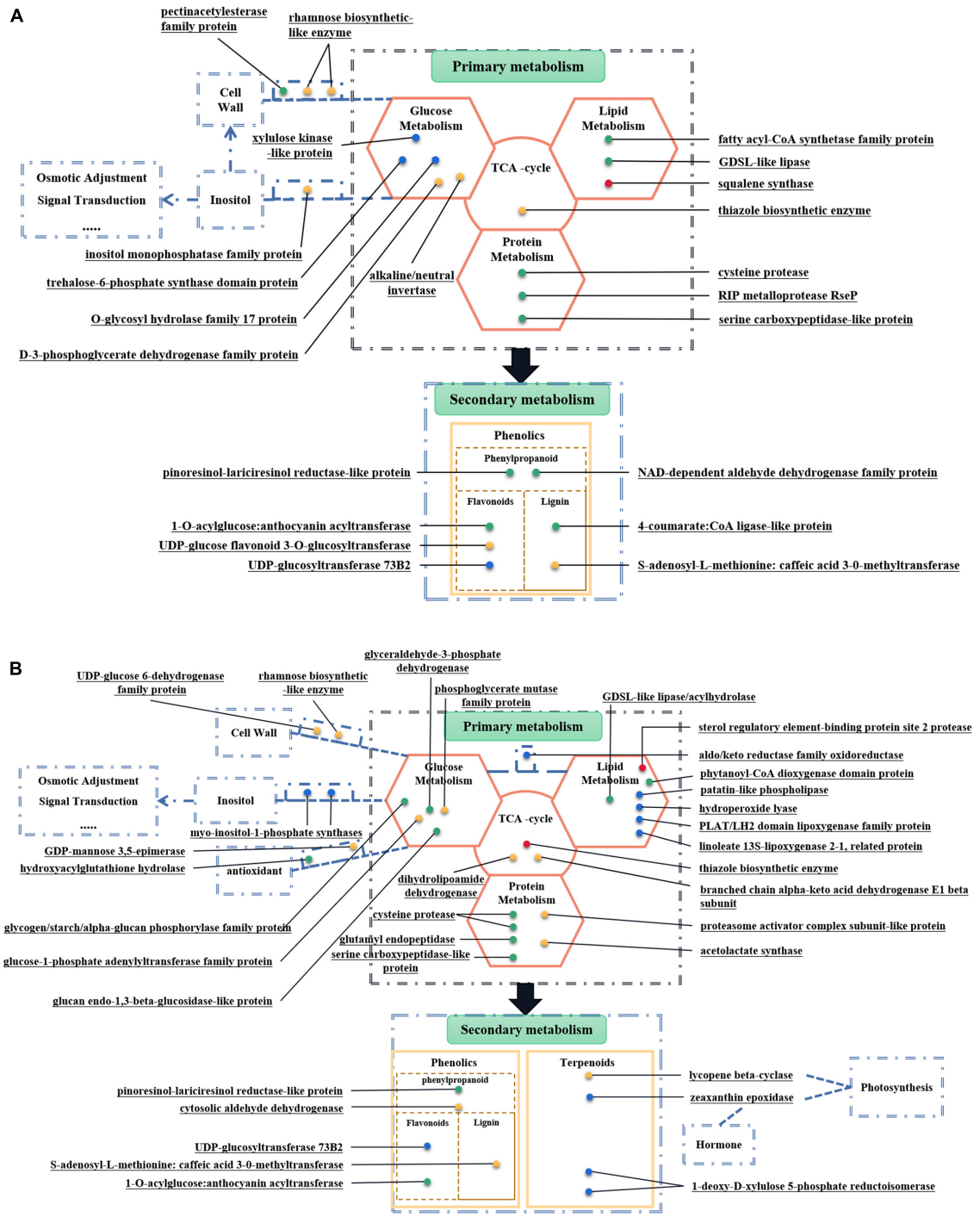

FIGURE 7 | Metabolism-Related DEPs of two alfalfa varieties. **(A)** Metabolism-Related DEPs in MS30. **(B)** Metabolism-Related DEPs in MS37. These figures can be divided into two parts, including primary metabolism and secondary metabolism. Each dot represents a protein, which plays a role in the corresponding metabolic process. The green dots indicate proteins that have been down-regulated throughout the process of HT stress. The red dots indicate proteins that have been up-regulated throughout the process of HT stress. The blue dots indicate the protein whose expression level rises first and then falls during the entire process of HT stress. The yellow dots indicate proteins whose expression levels first decrease and then increase during the entire process of high temperature stress.

is related to photosynthetic oxygen evolution and it is thought to optimize the manganese cluster during water oxidation (Heide et al., 2004). Moreover, the oxygen evolution enhancer protein could respond to heat stress and protects the reaction center D1 protein (Yamamoto, 2001). Therefore, this protein was up-regulated in two alfalfa materials could contribute

TABLE 1 | Comparison between the isobaric tandem mass tag labeling (TMT) for relative quantitation and parallel reaction monitoring (PRM).

Pathway	Protein Accession	Protein description	MS3035/ MS3020 Ratio	MS3043/ MS3035 Ratio	MS3035/ MS3020 Ratio (TMT)	MS3043/ MS3035 Ratio (TMT)	MS3735/ MS3720 Ratio	MS3743/ MS3735 Ratio	MS3735/ MS3720 Ratio (TMT)	MS3743/ MS3735 Ratio (TMT)
Photosynthesis	TRINITY_DN12545_ c0_g1_Gene_9459	magnesium-chelatase subunit ChlI	0.15	4.29	0.56	1.31	0.22	2.63	0.52	1.38
	TRINITY_DN16844_ c0_g3_Gene_8166	oxygen-evolving enhancer protein 2-1	3.07	2.54	1.82	1.68	3.30	2.11	1.68	1.59
Antioxidant activities	TRINITY_DN18935_ c0_g3_Gene_24344	glutathione S-transferase, amino-terminal domain protein	3.69	2.53	2.11	1.95	2.28	3.08	1.67	2.44
Heat shock proteins	TRINITY_DN10929_c0 _g1_Gene_4083	heat shock protein 81-2	2.97	1.85	1.65	1.34	1.88	2.71	1.36	1.69
	TRINITY_DN21025_ c0_g2_Gene_8907	70 kDa heat shock protein	1.57	2.08	1.56	1.77	1.56	2.42	1.47	1.48
	TRINITY_DN17376_ c2_g3_Gene_31004	ATP-dependent Clp protease ATP-binding subunit	0.65	2.39	0.79	1.22	0.63	2.08	0.67	1.36
	TRINITY_DN14499_ c0_g1_Gene_14445	peroxisomal small heat shock protein	1.44	2.38	1.27	1.34	1.90	2.11	1.27	1.49
Metabolism	TRINITY_DN14955 _c2_g1_Gene_12704	cysteine protease	0.53	0.78	0.67	0.79	0.70	0.52	0.83	0.63
	TRINITY_DN14760_c0 _g2_Gene_11432	rhamnose biosynthetic-like enzyme	0.45	3.28	0.68	1.40	0.66	3.07	0.80	1.60
	TRINITY_DN22711_c0 _g1_Gene_33078	1-O-acylglucose: anthocyanin acyltransferase	0.55	0.52	0.72	0.63	0.38	0.60	0.59	0.61
	TRINITY_DN10050_c0 _g2_Gene_32110	S-adenosyl-L-methionine: caffeic acid 3-0-methyltransferase	0.50	2.20	0.78	1.30	0.64	2.79	0.83	1.63

to enhance heat tolerance of alfalfa. ATP-dependent zinc metalloprotease FTSH protein has been reported to play an important role in plant heat resistance (Chen et al., 2006). That is because FtsH plays a critical role in the biogenesis of thylakoid membranes, quality control in the photosystem II repair cycle and photosynthetic electron-transport pathways (Kato and Sakamoto, 2018). In this experiment, the expression and up-regulation trend of this protein in MS30 were significantly higher than that of MS37, especially under the HT stress of 43°C. And it is noteworthy that in the MS30 we found another ATP-dependent zinc metalloprotease FTSH protein (TRINITY_DN21254_c0_g1_Gene_19039) has also been up-regulated under the HT stress of 43°C. Therefore, this DEP may be one of the factors for the difference in heat resistance between the two alfalfa varieties.

In MS37, we find the DEPs related to light-harvesting complex I and photosystem I reaction center, which has been up-regulated under the HT stress of 35°C and down-regulated under 43°C. This result indicates that the MS37 has a certain heat resistance ability under the high temperature stress of 35°C, but under 43°C, the heat resistance ability is obviously reduced, and the structure and function of photosystem I are destroyed. In addition, photosystem II reaction center PsbP family protein (TRINITY_DN21665_c0_g1_Gene_23571) had always been down-regulated during heat stress. PsbP protein could stabilize and coordinate supramolecular organization and function of PSII, which plays an important role in the dynamic life cycle of PSII (Ifuku et al., 2011). And the expression of PsbP protein is beneficial to the oxygen-evolving activity and photoautotrophic growth of plants (Nishimura et al., 2017). The other DEP related PSII is vitamin K epoxide reductase family protein (TRINITY_DN17556_c0_g3_Gene_31603) in MS37. Studies have shown that the deletion of vitamin K epoxide reductase (VKOR) gene will reduce the photosynthetic efficiency of plants and affect the stability of PSII assembly (Du, 2015). In this experiment, VKOR protein was up-regulated under the heat stress of 35°C, but down-regulated under 43°C, indicating that the protein could respond to a certain intensity of heat stress. At the same time, we infer that the Change in expression of photosystem II reaction center PsbP family protein (TRINITY_DN21665_c0_g1_Gene_23571) and vitamin K epoxide reductase family protein (TRINITY_DN17556_c0_g3_Gene_31603) may be associated with the significant decrease of Fv/Fm in MS37. Taken together, the above results indicated that the effect made by HT stress to Photosynthesis in MS37 is stronger than that in MS30. And the physiological and proteomic data indicate that MS37 has a certain degree of heat resistance under 35°C heat stress, but MS37 is severely affected by 43°C heat stress, which explains the difference in heat resistance of the two varieties.

The Change of Substance Metabolism Under High Temperature Stress

It has been reported that heat stress, drought stress, salt stress, etc., can cause damage to plant growth, and at the same time induce the production of substances related to anti-oxidation and osmotic adjustment to maintain the homeostasis in plants (He et al., 2012; Rivero et al., 2014; Soltabayeva et al., 2021). In this experiment, the results of MDA and EL indicate under HT stress, the membrane systems of the two alfalfa varieties were damaged, especially under 43°C HT stress. And the membrane system of MS37 is more severely damaged than that of MS30. In terms of osmotic regulators substances, induced by HT stress, the contents of proline, soluble protein and soluble sugar of the two alfalfa varieties have all changed. But on the whole, the osmotic adjustment substance of MS30 is significantly more responsive to HT stress than that of MS37. In terms of antioxidant systems, we get the same result that the activity of antioxidants in both alfalfa varieties were affected by HT stress. Therefore, the physiological results indicate heat stress affected the substance content and activity in both alfalfa varieties, which involves changes of the substances metabolism in alfalfa and is related to the heat resistance of alfalfa.

The Change of Primary Metabolism Under High Temperature Stress

We found that HT stress respectively altered the abundance of twenty-three and thirty-eight proteins related to metabolism in MS30 and MS37. There are sixteen DEPs related to primary metabolism in MS30, of which DEPs related to carbohydrate metabolism are the most numerous. It is noteworthy that we found that carbohydrate metabolism involves the metabolism of inositol. Inositol has important biological functions in plants, which not only participates in the formation of cell walls and cell membranes, but also plays an important role in various life activities such as osmotic regulation, signal transduction, and stress regulation (Zhang et al., 2013; Johnen, 2021). Inositol monophosphatase (IMPase) is a catalytic enzyme for the final step of inositol biosynthesis (Goswami et al., 2018). Studies have shown that abiotic stresses such as low temperature, drought and high salinity can affect the activity of IMPase (Nourbakhsh et al., 2015). In this experiment, inositol monophosphatase family protein (TRINITY_DN9184_c0_g3_Gene_30850) is up-regulated under 43°C HT stress, indicating that MS30 could promote the inositol synthesis through carbohydrate metabolism pathway, which could contribute to enhance heat tolerance of MS30. We have also found DEPs, myo-inositol 1-phosphate synthase (TRINITY_DN18700_c1_g2_Gene_12271) and myo-inositol-1-phosphate synthases (TRINITY_DN21940_c0_g2_Gene_13532), associated with inositol synthesis in MS37. Myo-inositol 1-phosphate synthase (MIPS) is a key enzyme that catalyzes D-Glucose-6-phosphate to form Myo-inositol-1-phosphate (Yang et al., 2017). Studies have shown that MIPS genes from different species play an important role in plant stress resistance (Majee et al., 2004; Das-Chatterjee et al., 2006; Guo et al., 2017). In this experiment, the DEPs related to inositol synthesis in MS37 are up-regulated under 35°C HT stress, but down-regulated under 43°C, indicating that MIPS contribute to the heat resistance of alfalfa under a certain degree of heat stress. Therefore, the results of MS30 and MS37 show that HT stress can cause changes in inositol metabolism in alfalfa, thereby affecting the heat resistance of alfalfa. In addition, among DEPs

related to carbohydrate metabolism, we also found DEPs related to plant cell walls. Rhamnose is an important component in the cell wall and participates in many metabolic processes in plants (Liu et al., 2019; Jiang et al., 2020). Rhamnose synthase catalyze the initial step of the synthesis of rhamnose (Han, 2014). In this experiment, we found that rhamnose biosynthetic-like enzyme (TRINITY_DN14760_c0_g2_Gene_11432) coexisted in two alfalfa varieties, both were down-regulated at 35°C high temperature stress, and up-regulated at 43°C. Moreover, there is another rhamnose biosynthetic-like enzyme (TRINITY_DN17882_c0_g1_Gene_10641) showed the same change trend in MS30, which indicates that high temperature stress may affect the structure and function of alfalfa cell wall through rhamnose metabolism pathway.

In this experiment, we also found that high temperature stress affected the TCA cycle of MS30 and MS37. Thiazole biosynthetic enzyme is not only related to plants growth and development, but also plays an important role in stress resistance. This is because thiazole biosynthetic enzyme is involved in plant thiamine biosynthesis (Sun et al., 2018). Plant thiamine could be response to oxidative stress by scavenging free radical and involve in TCA cycle, pyruvate carboxylase, pyruvate oxidase as an essential coenzyme (Zhou et al., 2012; Sun et al., 2018). In this experiment, thiazole biosynthetic enzyme as a DEP co-existed in both alfalfa varieties. In MS30, thiazole biosynthetic enzyme (TRINITY_DN20649_c0_g2_Gene_9792) was up-regulated at 43°C, and its expression was significantly higher than that at 20°C. In MS37, thiazole biosynthetic enzyme (TRINITY_DN11811_c1_g1_Gene_35054) has been always up-regulated under high temperature stress. These results indicate that high temperature stress can affect the TCA cycle and heat resistance of alfalfa by affecting the expression of thiazole biosynthetic enzyme.

The Change of Secondary Metabolism Under High Temperature Stress

Plant secondary metabolites play important roles for plants to improve defensive and competitive abilities as well as correspond to the environments (Yan et al., 2007). In this experiment, our data found that HT stress altered the abundance of seven and nine proteins related to secondary metabolism in MS30 and MS37, respectively. In MS30, the seven DEPs are all involved in the biosynthesis of phenolic compounds in plant secondary metabolites. But in MS37, except for five DEPs involved in the biosynthesis of phenolic compounds, there are four DEPs involved in the biosynthesis of terpenoids. In the biosynthesis of phenolic compounds, there are four DEPs coexist in both alfalfa varieties. Of these, 1-O-acylglucose: anthocyanin acyltransferase (TRINITY_DN22711_c0_g1_Gene_33078) and pinoresinol-lariciresinol reductase-like protein (TRINITY_DN16684_c0_g2_Gene_19375) have always been down-regulated under the high temperature stress. 1-O-acylglucose: anthocyanin acyltransferase has the function of acyltransferase, which can catalyze the conversion of glycosylated anthocyanins into acylated anthocyanins. Studies have shown that acylated anthocyanins have higher thermal stability and can enhance the antioxidant properties of purple cabbage (Yuan, 2018). Pinoresinol-lariciresinol reductase (PLR) are enzymes involved in the lignan biosynthesis after the initial dimerization of two monolignols (Xiao et al., 2021). Some studies have also shown lignans play a role in defense against oxidative stress (Li et al., 2006; Markulin et al., 2019). In this experiment, the accumulations of these two proteins were down-regulated under the HT stress, indicating that the metabolic pathways of anthocyanin and lignan were affected. Therefore, we speculate that HT stress may cause damage to alfalfa by reducing the effects of anthocyanins and lignan in plants. In addition, the enzyme involved in the metabolism of lignin, S-adenosyl-L-methionine: caffeic acid 3-0-methyltransferase (TRINITY_DN10050_c0_g2_Gene_32110), has been down-regulated at 35°C and up-regulated at 43°C in both alfalfa varieties. S-adenosyl-L-methionine: caffeic acid 3-0-methyltransferase (COMT) is involved in S lignin biosynthesis. It is worth noting that 4-coumarate: CoA ligase-like protein (TRINITY_DN17517_c0_g1_Gene_20937) in MS30 has been down-regulated under HT stress. 4-coumarate: coenzyme A ligase (4CL) converts 4-coumaric acid and its hydroxylated derivatives into the CoA thiol esters, directing carbon flux into various end-products of phenylpropanoid metabolism, such as flavonoids and lignins (Wohl and Petersen, 2020). Studies have shown that inhibiting the activity of COMT and 4CL could lead to a decrease in lignin content (Awasthi et al., 2019; Wohl and Petersen, 2020). Therefore, we speculate that HT stress could also affect the heat tolerance of alfalfa by affecting the metabolic pathway of lignin.

Terpenoids are the most abundant and diverse compounds in plant secondary metabolites (Caputi and Aprea, 2011). In this experiment, HT stress affected the metabolic of terpenoids in MS37. Among the DEPs related to the biosynthesis of terpenoids in MS37, lycopene beta-cyclase (TRINITY_DN16506_c0_g1_Gene_6592) has been down-regulated at 35°C and up-regulated at 43°C. Lycopene beta-cyclase (LCYB) participates in the metabolic pathway of carotenoids (Yamaguchi, 2012). Lots of studies have shown that high expression of LCYB gene can significantly increase carotenoid biosynthesis and enhance the tolerance of plants to abiotic stress (Jia et al., 2011; Chen et al., 2018; Li Y. et al., 2018). In this experiment, HT stress affected the expression of LCYB, indicating that HT stress could affect the photosynthesis and heat tolerance of alfalfa through the metabolic pathway of carotenoids. The other DEPs related to the metabolic of terpenoids is 1-deoxy-D-xylulose 5-phosphate reductoisomerase (TRINITY_DN13041_c3_g1_Gene_16656) and 1-deoxy-D-xylulose 5-phosphate reductoisomerase (TRINITY_DN13041_c3_g1_Gene_16657). 1-deoxy-D-xylulose 5-phosphate reductoisomerase (DXR) catalyzes the second step of the methylerythritol phosphate (MEP) pathway that functions in several organisms and plants for the synthesis of isoprenoids (Takahashi et al., 1998; Kesharwani and Sundriyal, 2020). Studies have shown that inhibiting or increasing the DXR expression will affect the production of terpenes, thereby affecting photosynthesis (Hasunuma et al., 2008; Wang et al., 2018). Therefore, combined with MS37 photosynthesis results, we speculate that a certain degree of HT stress will promote

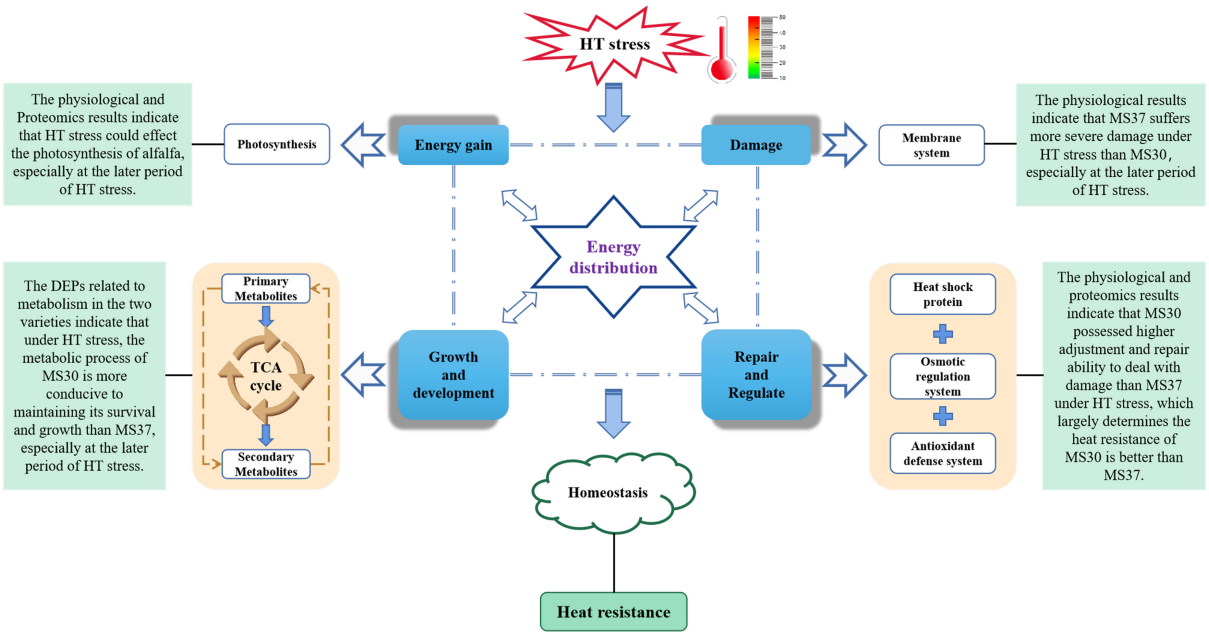

FIGURE 8 | Model shows the differential responses of two alfalfa varieties with contrasting heat tolerance to HT stress based on physiological and proteomic changes.

the synthesis of terpenoids in MS37, so as to maintain the photosynthesis of MS37. But excessive temperature will also inhibit the synthesis of terpenoids, which may be one of the factors leading to the decrease of the Fv/Fm ratio and the chlorophyll content in MS37 under 43°C HT stress.

The Change of Heat Shock Proteins Under Heat Stress

Heat shock proteins are molecular chaperones fulfiling stress-related and housekeeping functions, including protein folding, assembly, degradation and translocation, thus playing a central role in protein homeostasis (Fragkostefanakis et al., 2015). Here, we observed thirty-six and thirteen HSPs in MS30 and MS37 were differentially accumulated in response to heat stress, respectively. These DEHSPs were almost up-regulated during the entire high temperature stress, which indicated HSPs in both alfalfa varieties were playing an active role to protect alfalfa from high temperature stress. But it is noteworthy that compared with MS37, MS30 has more HSP quantity and classes. These results indicate that the difference in DEHSPs could be one of the reasons why MS30 has better heat tolerance than MS37.

When plants are subjected to abiotic stress, a large number of misfolded or unfolded proteins will accumulate in the endoplasmic reticulum, which can trigger endoplasmic reticulum stress (ERS). Studies have shown that ERS can induce an increase in the expression of various molecular chaperones and their auxiliary partners, such as HSPs, because they play important functions in Endoplasmic reticulum quality control (ERQC), unfolded protein response (UPR), and ER-associated degradation (ERAD) (Zhao et al., 2007; Fu et al., 2016). In this experiment, we found thirteen and five DEHSPs related to Protein processing in endoplasmic reticulum (KEEG: mtr04141) in MS30 and MS37, respectively. Among these, four DEHSPs (TRINITY_DN11338_c0_g1_Gene_18098, TRINITY_DN21025_c0_g2_Gene_8907, TRINITY_DN10929_c0_g1_Gene_4083, TRINITY_DN17416_c0_g2_Gene_3822) co-exist in two alfalfa varieties and have always been up-regulated under the HT stress, which indicates that these four DEHSPs can protect alfalfa from high temperature stress by regulating the endoplasmic reticulum stress. In addition, compared with MS37, MS30 has more DEHSPs involved in Protein processing in endoplasmic reticulum under HT stress, which suggests that MS30 can more actively respond to ERS to maintain the homeostasis and function of the endoplasmic reticulum. We also found five HSP60s were up-regulated in MS30 under the HT stress, which is absent in MS37. It has been reported that overexpression of HSP60 could improve plant stress resistance, while inhibiting the expression of HSP60 could affect the normal growth and development of plants (Hill and Hemmingsen, 2001; Cabiscol et al., 2002). These results clarify the reasons for the strong heat resistance of MS30. HSP100/ClpB (casein lytic proteinase B) could function in a non-degradative pathway of protein renaturation to liberate native functional proteins from aggregates, which is important to reactivate heat aggregated proteins under demanding, stressful conditions (Mishra and Grover, 2016). In this experiment, our data found that HT stress altered respectively the abundance of seven and six ClpB proteins in MS30 and MS37. Of these, we found that three ClpB3 proteins shared by two alfalfa varieties were up-regulated under HT stress. ClpB3 specifically targets unstructured polypeptides and mediates the reactivation of heat-denatured model substrates in an Hsp70-independent

manner (Parcerisa et al., 2020). Therefore, we speculate that ClpB3 proteins play an important role in the response of alfalfa to HT stress, and ClpB3 proteins were up-regulated under HT stress could contribute to enhance heat tolerance of alfalfa.

CONCLUSION

In summary, a model of HT-mediated stress response in *Medicago sativa* L. was proposed by conducting a comprehensive comparative analysis of two alfalfa varieties contrasting in heat tolerance based on their physiological and proteomic changes (**Figure 8**). HT induces the ROS accumulation and osmotic pressure in alfalfa, which significantly weakens the photosynthetic efficiency, destroys the cell membrane structure and causes endoplasmic reticulum stress. Our results demonstrated that MS30 was more tolerant to HT stress than MS37, which was evidenced by the differences at the physiological and proteomic levels. MS30 possessed higher abilities of adjustment and repair to deal with damage than those of MS37 under HT stress conditions. Meanwhile, the proteomic analysis revealed the metabolic process of MS30 is more conducive to maintaining its survival and growth than MS37, especially at the later period of HT stress. All these processes involve energy distribution and the maintenance of homeostasis in alfalfa, which ultimately determines the heat tolerance of alfalfa. These results provide basic information for exploring the physiological and molecular mechanisms of alfalfa adaptation or tolerance to HT stress. Nevertheless, a challenge for future work will be to elucidate the complex regulation networks of HT response and to identify key regulators and their function in the context of high temperature, which could contribute to accelerate the breeding progress of high-quality alfalfa varieties with heat resistance.

DATA AVAILABILITY STATEMENT

The datasets presented in this study can be found in online repositories. The names of the repository/repositories and accession number(s) can be found in the article/ **Supplementary Material**.

AUTHOR CONTRIBUTIONS

YL, XLi, and JY performed the experiments. YL, XLi, and JinZ analyzed the data and prepared the figures and tables. JY, XLi, and JinZ edited and revised the manuscript. XLi, JinZ, DL, LY, MY, JiaZ, DC, XJ, XLe, JA, ML, and SB conceived, designed research, and wrote this manuscript. YL, XLi, JinZ, DL, LY, MY, JiaZ, DC, XJ, XLe, JA, ML, SB, and JY approved the final version of this manuscript. All authors contributed to the article and approved the submitted version.

FUNDING

This work was financially supported by the Breeding Project of Sichuan Provincial Department of Science and Technology-Study on the selection and breeding of new varieties of multi-purpose forage in alpine pasturing area and its supporting technology (2021YFYZ0013), the basic scientific research business expense project of Sichuan non-profit scientific research institutes "Evaluation of production performance and resistance of multi-leaf alfalfa" project, National Modern Agricultural Industry Technology System Sichuan Forage Innovation Team for "Highland perennial forage species selection and breeding", Wild Plants Sharing and Service Platform of Sichuan Province (2019JDPT0028).

ACKNOWLEDGMENTS

We thank test support of laboratory staff in Sichuan Academy of Grassland Science and Sichuan Agricultural University College of Grassland Science and Technology.

SUPPLEMENTARY MATERIAL

The Supplementary Material for this article can be found online at: https://www.frontiersin.org/articles/10.3389/fpls.2021.753011/full#supplementary-material

REFERENCES

Anley, M. W. (2020). *Physiological and Transcriptomic Responses of (Medicago sativa* L.) to Heat Stress and Salicylic Acid-Induced Thermotolerance. Ph.D. thesis. Wuhan (HB): Wuhan Botanical Garden, Chinese Academy of Sciences

Awasthi, P., Mahajan, V., Jamwal, V. L., Chouhan, R., Kapoor, N., Bedi, Y. S., et al. (2019). Characterization of the gene encoding 4-coumarate: CoA ligase in Coleus forskohlii. *J. Plant Biochem. Biotechnol.* 28, 203–210. doi: 10.1007/s13562-018-0468-4

Ban, Z., Guan, J., Li, L., Feng, J., and Xu, X. (2012). Overview of research on the production of reactive oxygen species and the mechanisms of antioxidant in plants under abiotic stress. *Chin. Fruit Veg.* 05, 40–47. doi: 10.3969/j.issn.1008-1038.2012.05.023

Bates, L. S., Waldren, R. P., and Teare, I. (1973). Rapid determination of free proline for water-stress studies. *Plant Soil* 39, 205–207. doi: 10.1007/BF00018060

Blum, A., and Ebercon, A. (1981). Cell membrane stability as a measure of drought and heat tolerance in wheat 1. *Crop Sci.* 21, 43–47. doi: 10.2135/cropsci1981.0011183X002100010013x

Bradford, M. M. (1976). A rapid and sensitive method for the quantitation of microgram quantities of protein utilizing the principle of protein-dye binding. *Anal. Biochem.* 72, 248–254. doi: 10.1016/0003-2697(76)90527-3

Buysse, J., and Merckx, R. (1993). An improved colorimetric method to quantify sugar content of plant tissue. *J. Exp. Bot.* 44, 1627–1629. doi: 10.1093/jxb/44.10.1627

Cabiscol, E., Belli, G., Tamarit, J., Echave, P., Herrero, E., and Ros, J. (2002). Mitochondrial Hsp60, resistance to oxidative stress, and the labile iron pool are closely connected in Saccharomyces cerevisiae. *J. Biol. Chem.* 277, 44531–44538. doi: 10.1074/jbc.M206525200

Caputi, L., and Aprea, E. (2011). Use of terpenoids as natural flavouring compounds in food industry. *Recent Pat. Food Nutr. Agric.* 3, 9–16. doi: 10.2174/2212798411103010009

Carmo-Silva, E., Scales, J. C., Madgwick, P. J., and Parry, M. A. (2015). Optimizing Rubisco and its regulation for greater resource use efficiency. *Plant Cell Environ.* 38, 1817–1832. doi: 10.1111/pce.12425

Chao, Y. Y., Chen, C. Y., Huang, W. D., and Kao, C. H. (2010). Salicylic acid-mediated hydrogen peroxide accumulation and protection against Cd toxicity in rice leaves. *Plant Soil* 329, 327–337. doi: 10.1007/s11104-009-0161-4

Chen, H., Zeng, Y., Yang, Y., Huang, L., Tang, B., Zhang, H., et al. (2020). Allele-aware chromosome-level genome assembly and efficient transgene-free genome editing for the autotetraploid cultivated alfalfa. *Nat. Commun.* 11:2494. doi: 10.1038/s41467-020-16338-x

Chen, J., Burke, J. J., Velten, J., and Xin, Z. (2006). FtsH11 protease plays a critical role in Arabidopsis thermotolerance. *Plant J.* 48, 73–84. doi: 10.1111/j.1365-313x.2006.02855.x

Chen, K., Hong, Z., Xue, L., Zhao, N., He, S., and Liu, Q. (2018). A lycopene β-cyclase gene, IbLCYB2, enhances carotenoid contents and abiotic stress tolerance in transgenic sweetpotato. *Plant Sci.* 272, 243–254. doi: 10.1016/j.plantsci.2018.05.005

Chen, W., Zhu, X., Han, W., Wu, Z., and Lai, Q. (2016). Morphological, physiological and biochemical responses of gerbera cultivars to heat stress. *Hortic. Sci. Technol.* 34, 1–14. doi: 10.12972/kjhst.20160018

Chetty, K. A. (2017). *The Effects Of High Temperature Stress On The Enzymatic Antioxidant System In Zea Mays*. Ph.D. thesis. Tygerberg (Cape Town): University of the Western Cape.

Chołuj, D., Wiśniewska, A., Szafrański, K. M., Cebula, J., Gozdowski, D., and Podlaski, S. (2014). Assessment of the physiological responses to drought in different sugar beet genotypes in connection with their genetic distance. *J. Plant Physiol.* 171, 1221–1230. doi: 10.1016/j.jplph.2014.04.016

Das-Chatterjee, A., Goswami, L., Maitra, S., Dastidar, K. G., Ray, S., and Majumder, A. L. (2006). Introgression of a novel salt-tolerant L-myo-inositol 1-phosphate synthase from Porteresia coarctata (Roxb.) Tateoka (PcINO1) confers salt tolerance to evolutionary diverse organisms. *FEBS Lett.* 580, 3980–3988. doi: 10.1016/j.febslet.2006.06.033

Djanaguiraman, M., Boyle, D. L., Welti, R., Jagadish, S. V. K., and Prasad, P. V. V. (2018). Decreased photosynthetic rate under high temperature in wheat is due to lipid desaturation, oxidation, acylation, and damage of organelles. *BMC Plant Biol.* 18:55. doi: 10.1186/s12870-018-1263-z

Du, J. (2015). *Functional Sites Analysis of Vitamin K Epoxide Reductase on the Photosynthetic Growth and Activity of Photosystem II in Arabidopsis*. Ph.D. thesis. Qingdao (SD): Shandong Agricultural University.

Faiz, H., Ayyub, C. M., Khan, R. W., and Ahmad, R. (2020). Morphological, physiological and biochemical responses of eggplant (*Solanum melongena* L.) seedling to heat stress. *Pak. J. Agric. Sci.* 57, 371–380. doi: 10.21162/PAKJAS/20.9433

Foyer, C. H., Ruban, A. V., and Nixon, P. J. (2017). Photosynthesis solutions to enhance productivity. *Philos. Trans. R. Soc. Lond. B Biol. Sci.* 372:20160374. doi: 10.1098/rstb.2016.0374

Fragkostefanakis, S., Röth, S., Schleiff, E., and Scharf, K. D. (2015). Prospects of engineering thermotolerance in crops through modulation of heat stress transcription factor and heat shock protein networks. *Plant Cell Environ.* 38, 1881–1895. doi: 10.1111/pce.12396

Fu, C., Liu, X., Yang, W., Zhao, C., and Liu, J. (2016). Enhanced salt tolerance in tomato plants constitutively expressing heat-shock protein in the endoplasmic reticulum. *Genet. Mol. Res.* 15:15028301. doi: 10.4238/gmr.15028301

Gao, L., Ren, H. L., Zheng, J. W., and Chen, Q. L. (2019). Diagnosis features of extreme temperature variations in China based on the NCEP-GEFS reforecasts. *Trans. Atmos. Sci.* 42, 60–69. doi: 10.13878/j.cnki.dqkxxb.20180911001

Giannopolitis, C. N., and Ries, S. K. (1977). Superoxide dismutases: I. Occurrence in higher plants. *Plant Physiol.* 59, 309–314. doi: 10.1104/pp.59.2.309

Goswami, R., Bondoc, J. M. G., Wheeler, P. R., Jafari, A., Gonzalez, T., Mehboob, S., et al. (2018). Inositol Monophosphatase: a Bifunctional Enzyme in Mycobacterium smegmatis. *ACS Omega* 3, 13876–13881. doi: 10.1021/acsomega.8b01753

Guilioni, L., Wéry, J., and Lecoeur, J. (2003). High temperature and water deficit may reduce seed number in field pea purely by decreasing plant growth rate. *Funct. Plant Biol.* 30, 1151–1164. doi: 10.1071/fp03105

Guo, H. (2010). Research progress on adjustment material under water stress. *J. Anhui Agric. Sci.* 38, 7750–7753. doi: 10.3969/j.issn.0517-6611.2010.15.013

Guo, Y., Hou, L., Zhu, D., and Liu, X. (2017). Cloning and Functional Analysis of *VvMIPS* Relevant to Temperature Stress in Grape (*Vitis vinifera*). *J. Agric. Biotechnol.* 04, 558–566. doi: 10.3969/j.issn.1674-7968.2017.04.005

Han, X. (2014). *). Structural studies of L-sorbose dehydrogenase and nucleotide-rhamnose synthetase*. Ph.D. thesis. Tianjin: Nankai University.

Hashiguchi, A., Ahsan, N., and Komatsu, S. (2010). Proteomics application of crops in the context of climatic changes. *Food Res. Int.* 43, 1803–1813. doi: 10.1016/j.foodres.2009.07.033

Hasunuma, T., Takeno, S., Hayashi, S., Sendai, M., Bamba, T., Yoshimura, S., et al. (2008). Overexpression of 1-deoxy-D-xylulose-5-phosphate reductoisomerase gene in chloroplast contributes to increment of isoprenoid production. *J. Biosci. Bioeng.* 105, 518–526. doi: 10.1263/jbb.105.518

He, S., Liu, G., and Yang, H. (2012). Water use efficiency by alfalfa: mechanisms involving anti-oxidation and osmotic adjustment under drought. *Russ. J. Plant Physiol.* 59, 348–355. doi: 10.1134/S1021443712020033

Heide, H., Kalisz, H. M., and Follmann, H. (2004). The oxygen evolving enhancer protein 1 (OEE) of photosystem II in green algae exhibits thioredoxin activity. *J. Plant Physiol.* 161, 139–149. doi: 10.1078/0176-1617-01033

Hill, J. E., and Hemmingsen, S. M. (2001). *Arabidopsis thaliana* type I and II chaperonins. *Cell Stress Chaperones* 6, 190–200. doi: 10.1379/1466-12682001006<0190:attiai<2.0.co;2

Hinojosa, L., Matanguihan, J. B., and Murphy, K. M. (2019). Effect of high temperature on pollen morphology, plant growth and seed yield in quinoa (*Chenopodium quinoa* Willd.). *J. Agron. Crop Sci.* 205, 33–45. doi: 10.1111/jac.12302

Ibrahim, A. M. H., and Quick, J. S. (2001). Genetic Control of High Temperature Tolerance in Wheat as Measured by Membrane Thermal Stability. *Crop Sci.* 41, 1405–1407. doi: 10.2135/cropsci2001.4151405x

Ifuku, K., Ido, K., and Sato, F. (2011). Molecular functions of PsbP and PsbQ proteins in the photosystem II supercomplex. *J. Photochem. Photobiol. B Biol.* 104, 158–164. doi: 10.1016/j.jphotobiol.2011.02.006

Jia, F., Xu, W., Liu, W., and Wang, Y. (2011). Effects of Temperature and Light Intensity on Expression of Lycopene Cyclase Gene in Tobacco (*Nicotiana tabacum* L.). *Plant Physiol. J.* 47, 189–192. doi: 10.13592/j.cnki.ppj.2011.02.009

Jia, J., Li, S., Cao, X., Li, H., Shi, W., Polle, A., et al. (2016). Physiological and transcriptional regulation in poplar roots and leaves during acclimation to high temperature and drought. *Physiol. Plant.* 157, 38–53. doi: 10.1111/ppl.12400

Jiang, N., Dillon, F. M., Silva, A., Gomez-Cano, L., and Grotewold, E. (2020). Rhamnose in plants-from biosynthesis to diverse functions. *Plant Sci.* 302:110687. doi: 10.1016/j.plantsci.2020.110687

Johnen, P. (2021). *Cellular Functions of myo-Inositol-Derived Signaling Molecules in Yeast and Plants during Abiotic and Biotic Stresses*. Ph.D. thesis. Tübingen (Baden-Württemberg): Universität Tübingen.

Junmatong, C., Faiyue, B., Rotarayanont, S., Uthaibutra, J., Boonyakiat, D., and Saengnil, K. (2015). Cold storage in salicylic acid increases enzymatic and non-enzymatic antioxidants of Nam Dok Mai No. 4 mango fruit. *Sci. Asia* 41, 12–21. doi: 10.2306/scienceasia1513-1874.2015.41.012

Kato, Y., and Sakamoto, W. (2018). FtsH protease in the thylakoid membrane: physiological functions and the regulation of protease activity. *Front. Plant Sci.* 9:855. doi: 10.3389/fpls.2018.00855

Kawashima, Y., Watanabe, E., Umeyama, T., Nakajima, D., Hattori, M., Honda, K., et al. (2019). Optimization of data-independent acquisition mass spectrometry for deep and highly sensitive proteomic analysis. *Int. J. Mol. Sci.* 20:5932. doi: 10.3390/ijms20235932

Kesharwani, S., and Sundriyal, S. (2020). Non-hydroxamate inhibitors of 1-deoxy-D-xylulose-5-phosphate reductoisomerase (DXR): a critical review and future perspective. *Eur. J. Med. Chem.* 213:113055. doi: 10.1016/j.ejmech.2020.113055

Kim, H. J., Lin, D., Lee, H. J., Li, M., and Liebler, D. C. (2016). Quantitative profiling of protein tyrosine kinases in human cancer cell lines by multiplexed parallel reaction monitoring assays. *Mol. Cell. Proteom.* 15, 682–691. doi: 10.1074/mcp.O115.056713

Kolupaev, Y. E., Karpets, Y., Yastreb, T. O., Shemet, S. A., and Bhardwaj, R. (2020). "Antioxidant system and plant cross-adaptation against metal excess and other environmental stressors," in *Metal Toxicity in Higher Plants*, eds M. Landi, S. A. Shemet, and V. S. Fedenko (New York: FL: Nova Science Publishers), 21–67.

Krauss, A., and Marschner, H. (1984). Growth rate and carbohydrate metabolism of potato tubers exposed to high temperatures. *Potato Res.* 27, 297–303. doi: 10.1007/BF02357638

Kumar, S. (2020). Abiotic stresses and their effects on plant growth, yield and nutritional quality of agricultural produce. *Int. J. Food Sci. Agric*. 4, 367–378. doi: 10.26855/ijfsa.2020.12.002

Kundu, P., Gill, R., Nehra, A., Sharma, K. K., Hasanuzzaman, M., Prasad, R., et al. (2020). "Reactive oxygen species (ROS) management in engineered plants for abiotic stress tolerance," in *Advancement in Crop Improvement Techniques*, eds N. Tuteja, R. Tuteja, N. Passricha, S. K. Saifi (Amsterdam: Elsevier), 241–262. doi: 10.1016/b978-0-12-818581-0.00015-2

Li, B., Gao, K., Ren, H., and Tang, W. (2018). Molecular mechanisms governing plant responses to high temperatures. *J. Integr. Plant Biol.* 60, 757–779. doi: 10.1111/jipb.12701

Li, D. F. (2015). *Cause of Summer Yield Reduction of Alfalfa and Comparison of Different Traits as Indicators of Heat Tolerance in Alfalfa*. Ph.D. thesis. Zhengzhou (HN): Henan Agricultural University.

Li, X., Luo, J., Tian, S., and Zhang, S. (2015). Analysis of the overall situation of alfalfa production in China. *Chin. Dairy Cattle* 16, 58–64. doi: 10.3969/j.issn.1004-4264.2015.16.022

Li, X., Yuan, J., Liu, X., and Wang, J. (2006). Lignan: an important natural estrogen from plants. *Chin. J. Chin. Mater. Med.* 31, 2021–2025. doi: 10.3321/j.issn:1001-5302.2006.24.001

Li, Y., Chen, M., Zhu, H., Wen, Q., and Liu, J. (2018). Cloning and Expression Analysis of a Lycopene Beta-cyclase Gene in *Hibiscus esculentus* L. *J. Plant Genet. Resour.* 19, 167–176.

Li, Y. F., Wang, Y., Tang, Y., Kakani, V. G., and Mahalingam, R. (2013). Transcriptome analysis of heat stress response in switchgrass (*Panicum virgatum* L.). *BMC Plant Biol.* 13:153. doi: 10.1186/1471-2229-13-153

Lin, X., Bai, S., Zhang, X., and Zhang, Y. (2007). Research Progress of Alfalfa Introduction Adaptability in Southern China. *J. Anhui Agric. Sci.* 35, 7159–7161. doi: 10.13989/j.cnki.0517-6611.2007.23.048

Liu, D. L., Zhang, H., Cao, X. C., Hu, K. Q., Liu, Z. M., Wang, K., et al. (2014). Impacts of Heat Stress on the Photosynthetic Physiology of Alfalfa. *Acta Agrestia Sin*. 22, 657–660. doi: 10.11733/j.issn.1007-0435.2014.03.033

Liu, L., Wang, L., Deng, F., Huang, Y., Liu, D., Ren, W., et al. (2013). Response of different rice genotypes to osmotic regulation substance content and protective enzyme activities in leaves under shading. *Rice Sci.* 20, 276–283. doi: 10.1016/S1672-6308(13)60137-7

Liu, L., Zhou, L., Zhang, C., Wang, H., Liu, C., and Yang, Q. (2019). Cloning and characterization of UDP-L-rhamnose synthase 1/2 from *Fallopia multiflora*. *Acta Pharm. Sin*. 054, 1515–1523.

Liu, M., Zhao, W., Zhang, H., Wang, Y., and Sui, X. (2020). Contribution of Mitochondrial Structure and Respiratory Metabolism to The Cold-Resistance of Alfalfa Seedling Root. *Preprint* doi: 10.21203/rs.3.rs-59648/v1

Liu, S. J., Xu, H. H., Wang, W. Q., Li, N., Wang, W. P., Møller, I. M., et al. (2015). A proteomic analysis of rice seed germination as affected by high temperature and ABA treatment. *Physiol. Plant.* 154, 142–161. doi: 10.1111/ppl.12292

Machly, A. C., and Chance, P. (1955). Assay of catalase and peroxidases. *Methods Enzymol.* 2, 764–775. doi: 10.1016/s0076-6879(55)02300-8

Majee, M., Maitra, S., Dastidar, K. G., Pattnaik, S., Chatterjee, A., Hait, N. C., et al. (2004). A novel salt-tolerant L-myo-inositol-1-phosphate synthase from Porteresia coarctata (Roxb.) Tateoka, a halophytic wild rice: molecular cloning, bacterial overexpression, characterization, and functional introgression into tobacco-conferring salt tolerance phenotype. *J. Biol. Chem.* 279, 28539–28552. doi: 10.1074/jbc.M310138200

Markulin, L., Corbin, C., Renouard, S., Drouet, S., Gutierrez, L., Mateljak, I., et al. (2019). Pinoresinol–lariciresinol reductases, key to the lignan synthesis in plants. *Planta* 249, 1695–1714. doi: 10.1007/s00425-019-03137-y

Miguel, C., Dalmay, T., and Chaves, I. (2020). *Plant microRNAs: shaping Development and Environmental Responses*. Basingstoke: Springer Nature.

Mishra, R. C., and Grover, A. (2016). ClpB/Hsp100 proteins and heat stress tolerance in plants. *Crit. Rev. Biotechnol.* 36, 862–874. doi: 10.3109/07388551.2015.1051942

Miteva, E., Hristova, D., Nenova, V., and Maneva, S. (2005). Arsenic as a factor affecting virus infection in tomato plants: changes in plant growth, peroxidase activity and chloroplast pigments. *Sci. Hortic.* 105, 343–358. doi: 10.1016/j.scienta.2005.01.026

Mohammadi, P. P., Salavati, A., and Ismaili, A. (2014). A Comparative Proteomic Analysis of Responses to High Temperature Stress in Hypocotyl of Canola (*Brassica napus* L.). *Protein Pept. Lett.* 22, 285–299. doi: 10.2174/0929866521666141124102755

Musgrove, J. E., and Ellis, R. J. (1986). The Rubisco large subunit binding protein. *Philos. Trans. R. Soc. Lond. B Biol. Sci*. 313, 419–428. doi: 10.1098/rstb.1986.0048

Nakano, Y., and Asada, K. (1981). Hydrogen peroxide is scavenged by ascorbate-specific peroxidase in spinach chloroplasts. *Plant Cell Physiol.* 22, 867–880. doi: 10.1093/oxfordjournals.pcp.a076232

Navrot, N., Rouhier, N., Gelhaye, E., and Jacquot, J. P. (2007). Reactive oxygen species generation and antioxidant systems in plant mitochondria. *Physiol. Plant.* 129, 185–195. doi: 10.1111/j.1399-3054.2006.00777.x

Nishimura, T., Sato, F., and Ifuku, K. (2017). *In vivo* system for analyzing the function of the PsbP protein using *chlamydomonas reinhardtii*. *Photosynth. Res.* 133, 117–127. doi: 10.1007/s11120-017-0370-2

Niu, Y., and Xiang, Y. (2018). An overview of biomembrane functions in plant responses to high-temperature stress. *Front. Plant Sci.* 9:915. doi: 10.3389/fpls.2018.00915

Nogueira, F. C. S., Palmisano, G., Schwämmle, V., Campos, F. A. P., Larsen, M. R., Domont, G. B., et al. (2012). Performance of isobaric and isotopic labeling in quantitative plant proteomics. *J. Proteome Res.* 11, 3046–3052. doi: 10.1021/pr300192f

Nourbakhsh, A., Collakova, E., and Gillaspy, G. E. (2015). Characterization of the inositol monophosphatase gene family in Arabidopsis. *Front. Plant Sci.* 5:725. doi: 10.3389/fpls.2014.00725

Pagel, O., Loroch, S., Sickmann, A., and Zahedi, R. P. (2015). Current strategies and findings in clinically relevant post-translational modification-specific proteomics. *Expert Rev. Proteom.* 12, 235–253. doi: 10.1586/14789450.2015.1042867

Parcerisa, I. L., Rosano, G. L., and Ceccarelli, E. A. (2020). Biochemical characterization of ClpB3, a chloroplastic disaggregase from *Arabidopsis thaliana*. *Plant Mol. Biol.* 104, 451–465. doi: 10.1007/s11103-020-01050-7

Pu, M., Li, Y., Zhang, J., Bai, S., and Yan, J. (2019). Research Progress in the Heat-resistance of *Medicago sativa* L. *J. Grassland Forage Sci.* 06, 1–7.

Rivero, R. M., Mestre, T. C., Mittler, R., Rubio, F., Garcia-Sanchez, F., and Martinez, V. (2014). The combined effect of salinity and heat reveals a specific physiological, biochemical and molecular response in tomato plants. *Plant Cell Environ.* 37, 1059–1073. doi: 10.1111/pce.12199

Rykaczewska, K. (2015). The Effect of High Temperature Occurring in Subsequent Stages of Plant Development on Potato Yield and Tuber Physiological Defects. *Am. J. Potato Res.* 92, 339–349. doi: 10.1007/s12230-015-9436-x

Schrader, S. M., Wise, R. R., Wacholtz, W. F., Ort, D. R., and Sharkey, T. D. (2004). Thylakoid membrane responses to moderately high leaf temperature in Pima cotton. *Plant Cell Environ.* 27, 725–735. doi: 10.1111/j.1365-3040.2004.01172.x

Sergeant, K., and Renaut, J. (2010). Plant Biotic Stress and Proteomics. *Curr. Proteom.* 7, 275–297. doi: 10.2174/157016410793611765

Sévellec, F., and Drijfhout, S. S. (2018). A novel probabilistic forecast system predicting anomalously warm 2018-2022 reinforcing the long-term global warming trend. *Nat. Commun.* 9:3024. doi: 10.1038/s41467-018-05442-8

Sharma, D. K., Andersen, S. B., Ottosen, C.-O., and Rosenqvist, E. (2012). Phenotyping of wheat cultivars for heat tolerance using chlorophyll a fluorescence. *Funct. Plant Biol.* 39, 936–947. doi: 10.1071/FP12100

Sharma, D. K., Andersen, S. B., Ottosen, C.-O., and Rosenqvist, E. (2015). Wheat cultivars selected for high Fv/Fm under heat stress maintain high photosynthesis, total chlorophyll, stomatal conductance, transpiration and dry matter. *Physiol. Plant.* 153, 284–298. doi: 10.1111/ppl.12245

Sharma, P. (2020). "Responses and Tolerance of Brassicas to High Temperature," in *The Plant Family Brassicaceae: biology and Physiological Responses to Environmental Stresses*, ed. M. Hasanuzzaman (Singapore: Springer Singapore), 277–310.

Shen, H., Zhao, B., Xu, J., Zheng, X., and Huang, W. (2016). Effects of Salicylic Acid and Calcium Chloride on Heat Tolerance in Rhododendron 'Fen Zhen Zhu'. *J. Am. Soc. Hortic. Sci.* 141, 363–372. doi: 10.21273/JASHS.141.4.363

Soltabayeva, A., Ongaltay, A., Omondi, J. O., and Srivastava, S. (2021). Morphological, Physiological and Molecular Markers for Salt-Stressed Plants. *Plants* 10:243. doi: 10.3390/plants10020243

Sun, Z., Wei, D., Yang, M., and Lan, X. (2018). Biosynthesis and function of thiamine in plants. *Plant Physiol. J.* 54, 1791–1796. doi: 10.13592/j.cnki.ppj.2018.0329

Takahashi, S., Kuzuyama, T., Watanabe, H., and Seto, H. (1998). A 1-deoxy-D-xylulose 5-phosphate reductoisomerase catalyzing the formation of 2-C-methyl-D-erythritol 4-phosphate in an alternative nonmevalonate pathway for terpenoid biosynthesis. *Proc. Natl. Acad. Sci. U. S. A.* 95, 9879–9884. doi: 10.1073/pnas.95.17.9879

Ulsen, P. V., Kuhn, K., Prinz, T., Legner, H., Schmid, P., Baumann, C., et al. (2009). Identification of proteins of *Neisseria meningitidis* induced under iron-limiting conditions using the isobaric tandem mass tag (TMT) labeling approach. *Proteomics* 9, 1771–1781. doi: 10.1002/pmic.200800642

Wahid, A., Gelani, S., Ashraf, M., and Foolad, M. R. (2007). Heat tolerance in plants: an overview. *Environ. Exp. Bot.* 61, 199–223. doi: 10.1016/j.envexpbot.2007.05.011

Wang, C. H., Lei, X. Y., Xia, J., and Wang, J. W. (2018). Effect of down-regulating 1-deoxy-D-xylulose-5-phosphate reductoisomerase by RNAi on growth and artemisinin biosynthesis in *Artemisia annua* L. *Plant Growth Regul.* 84, 549–559. doi: 10.1007/s10725-017-0360-6

Wang, W. (2020). Improving China's alfalfa industry development: an economic analysis. *Chin. Agric. Econ. Rev.* 13, 211–228. doi: 10.1108/CAER-07-2019-0128

Wang, Y., Chen, X., Li, Y., Jiang, X., Liu, Q., and Li, S. (2001). The osmotic solute in plant resistance to adverse conditions and progress in relative genic engineering. *J. Beijing For. Univ.* 23, 66–70. doi: 10.3321/j.issn:1000-1522.2001.04.014

Wheeler, C. R., Salzman, J. A., Elsayed, N. M., Omaye, S. T., and Korte, D. W. Jr. (1990). Automated assays for superoxide dismutase, catalase, glutathione peroxidase, and glutathione reductase activity. *Anal. Biochem.* 184, 193–199. doi: 10.1016/0003-2697(90)90668-Y

Wilkins, O., Hafemeister, C., Plessis, A., Holloway-Phillips, M. M., Pham, G. M., Nicotra, A. B., et al. (2016). EGRINs (Environmental Gene Regulatory Influence Networks) in Rice That Function in the Response to Water Deficit, High Temperature, and Agricultural Environments. *Plant Cell* 28, 2365–2384. doi: 10.1105/tpc.16.00158

Wohl, J., and Petersen, M. (2020). Phenolic metabolism in the hornwort Anthoceros agrestis: 4-coumarate CoA ligase and 4-hydroxybenzoate CoA ligase. *Plant Cell Rep.* 39, 1129–1141. doi: 10.1007/s00299-020-02552-w

Xiao, Y., Shao, K., Zhou, J., Wang, L., Wu, D., Chen, J., et al. (2021). Structure based engineering for substrate specificity of pinoresinol-lariciresinol reductases. *Nat. Commun.* 12:2828. doi: 10.21203/rs.3.rs-41063/v1

Xu, L., Xu, D., Pang, H., Xin, X., Jing, D., Tang, X., et al. (2017). Chinese alfalfa habitat suitability regionalization. *Pratac. Sci.* 034, 2347–2358. doi: 10.11829/j.issn.1001-0629.2016-0551

Xu, X., Liu, T., Yang, J., Chen, L., Liu, B., Wang, L., et al. (2018). The first whole-cell proteome-and lysine-acetylome-based comparison between Trichophyton rubrum conidial and mycelial stages. *J. Proteome Res.* 17, 1436–1451. doi: 10.1021/acs.jproteome.7b00793

Yamaguchi, M. (2012). Role of carotenoid β-cryptoxanthin in bone homeostasis. *J. Biomed. Sci.* 19:36. doi: 10.1186/1423-0127-19-36

Yamamoto, Y. (2001). Quality control of photosystem II. *Plant Cell Physiol.* 42, 121–128. doi: 10.1093/pcp/pce022

Yan, X., Wang, Y., and Li, Y. (2007). Plant secondary metabolism and its response to environment. *Acta Ecol. Sin.* 06, 2554–2562. doi: 10.3321/j.issn:1000-0933.2007.06.050

Yang, N., Zhang, J., Wang, L., and Su, H. (2017). Research Progress in Myo-inositol and Its Metabolic Key Enzyme Genes with Plant Stress Response Mechanism. *J. Ludong Univ.* 33, 321–325. doi: 10.3969/j.issn.1673-8020.2017.04.007

Yuan, L. (2018). *Study on Effect from UV-C Treatment on Anthocyanin Biosynthesis and the Cloning of Anthocyanin Acyltransferase of Red Cabbage*. Ph.D. thesis. Beijing: Chinese Academy of Agricultural Sciences.

Zhang, C., Shi, S., Wang, B., and Zhao, J. (2018). Physiological and biochemical changes in different drought-tolerant alfalfa (*Medicago sativa* L.) varieties under PEG-induced drought stress. *Acta Physiol. Plant.* 40, 1–15. doi: 10.1007/s11738-017-2597-0

Zhang, H., Li, X., Nan, X., Sun, G., Sun, M., Cai, D., et al. (2017). Alkalinity and salinity tolerance during seed germination and early seedling stages of three alfalfa (*Medicago sativa* L.) cultivars. *Legume Res. Int. J.* 40, 853–858. doi: 10.18805/lr.v0i0.8401

Zhang, M., Xie, Y., Yang, H., and Yao, L. (2013). Myo-inositol Metamolism as the Precursor of Xylan and Pectin in Plants. *Chem. Ind. For. Prod.* 33, 106–114. doi: 10.3969/j.issn.0253-2417.2013.05.021

Zhang, X. X., Gao, Y. G., Yan, X. B., Wang, C. Z., Wang, Y. H., Peng, B. A., et al. (2010). Research progress on heat resistance identification and evaluation in alfalfa. *Pratac. Sci.* 27, 113–118. doi: 10.3969/j.issn.1001-0629.2010.02.021

Zhao, C., Shono, M., Sun, A., Yi, S., Li, M., and Liu, J. (2007). Constitutive expression of an endoplasmic reticulum small heat shock protein alleviates endoplasmic reticulum stress in transgenic tomato. *J. Plant Physiol.* 164, 835–841. doi: 10.1016/j.jplph.2006.06.004

Zheng, G., Tian, B., Zhang, F., Tao, F., and Li, W. (2011). Plant adaptation to frequent alterations between high and low temperatures: remodelling of membrane lipids and maintenance of unsaturation levels. *Plant Cell Environ.* 34, 1431–1442. doi: 10.1111/j.1365-3040.2011.02341.x

Zhou, J., Sun, A., Zeng, L., and Li, Z. (2012). Thiamin Promotes Plant Rapid Response to External Stress through Improving Mitochondrial Oxidation Status. *Acta Laser Biol. Sin.* 21, 340–345.

Conflict of Interest: The authors declare that the research was conducted in the absence of any commercial or financial relationships that could be construed as a potential conflict of interest.

Publisher's Note: All claims expressed in this article are solely those of the authors and do not necessarily represent those of their affiliated organizations, or those of the publisher, the editors and the reviewers. Any product that may be evaluated in this article, or claim that may be made by its manufacturer, is not guaranteed or endorsed by the publisher.

Copyright © 2021 Li, Li, Zhang, Li, Yan, You, Zhang, Lei, Chang, Ji, An, Li, Bai and Yan. This is an open-access article distributed under the terms of the Creative Commons Attribution License (CC BY). The use, distribution or reproduction in other forums is permitted, provided the original author(s) and the copyright owner(s) are credited and that the original publication in this journal is cited, in accordance with accepted academic practice. No use, distribution or reproduction is permitted which does not comply with these terms.

frontiers in Plant Science

ORIGINAL RESEARCH
published: 05 January 2022
doi: 10.3389/fpls.2021.804315

Identification of Heat Tolerant Cotton Lines Showing Genetic Variation in Cell Membrane Thermostability, Stomata, and Trichome Size and Its Effect on Yield and Fiber Quality Traits

Saifullah Abro[1], Muhammad Rizwan[1], Zaheer Ahmed Deho[1], Shafiq Ahmed Abro[2] and Mahboob Ali Sial[1]*

[1] Plant Breeding and Genetics Division, Nuclear Institute of Agriculture (NIA), Tando Jam, Pakistan, [2] Technical Services Division, Nuclear Institute of Agriculture (NIA), Tando Jam, Pakistan

OPEN ACCESS

Edited by:
Raul Antonio Sperotto, Universidade do Vale do Taquari, Brazil

Reviewed by:
Zhengwen Sun, Hebei Agricultural University, China
Pangirayi Tongoona, University of KwaZulu-Natal, South Africa

***Correspondence:**
Muhammad Rizwan
rzi_rizwan@yahoo.com

Specialty section:
This article was submitted to Plant Abiotic Stress, a section of the journal Frontiers in Plant Science

Received: *29 October 2021*
Accepted: *06 December 2021*
Published: *05 January 2022*

Citation:
Abro S, Rizwan M, Deho ZA, Abro SA and Sial MA (2022) Identification of Heat Tolerant Cotton Lines Showing Genetic Variation in Cell Membrane Thermostability, Stomata, and Trichome Size and Its Effect on Yield and Fiber Quality Traits. Front. Plant Sci. 12:804315. doi: 10.3389/fpls.2021.804315

Heat stress in cotton reduces its productivity. The development of heat-tolerant cotton varieties having resilience against changing climate is feasible. The purpose of this study was to probe the genetic variability in upland cotton for heat tolerance, the association of cell membrane thermostability (CMT), stomata, and trichome size with cotton adaptation to high temperature and effective breeding strategy to advance the valued traits. Relative cell injury percentage (RCI%) in studied genotypes ranged from 39 to 86%. Seventeen genotypes were found heat tolerant on the basis of low RCI%, heat susceptibility index (HSI <1), higher number of boll/plant, and seed cotton yield (SCY). Scanning electron microscopy (SEM) of heat-tolerant genotypes revealed the presence of different size of stomata (21.57 to 105.04 μm^2) and trichomes (177 to 782.6 μm) on leaves of selected genotypes. The regression analysis showed a strong and negative association of RCI% and stomata size with SCY. However, no association was observed between the trichome size, yield, and fiber traits. On the overall location basis, a significant genotype $\times$ environment interaction was observed. All selected genotypes produced a higher SCY as compared with check varieties. But the stability analysis showed that the high yielding genotypes NIA-M-30, NIA-80, NIA-83, and CRIS-342 were also wide adaptive with unit regression (bi$\sim$1) and non-significant deviation from the regression line ($S^2d\sim0$). The ability for the combination of some heat-tolerant genotypes was estimated by using the line $\times$ tester method among nine hybrids along with their 3 testers (i.e., male) and 3 lines (i.e., females). Genotypes, CRIS-342 and NIA-Perkh, were observed as best general combiners for SCY with a negative general combining ability effects for RCI%. Five hybrids showed a positive specific combining ability and heterotic effects for studied traits and also found lowest for HSI. RCI% and SCY/plant displayed higher estimates of heritability and genetic advance, indicating the heritability due to additive

gene effects and chances of effective selection. The identified heat-tolerant and wide adaptive germplasm can be further advanced and utilized in cotton breeding programs for developing heat-tolerant cultivars. Selection criteria involving CMT and stomata size concluded to be an effective strategy for the screening of heat-tolerant cotton.

Keywords: breeding, cotton, high temperature, germplasm, physiology, stress tolerance

INTRODUCTION

Cotton (*Gossypium hirsutum* L.) is an international agricultural product of which quality and quantity are subject to various whims of nature. It occupies an important position in global status of commercial crops with annual impact of >US$50 billion in the economy of the world (Organisation for Economic Co-operation Development/Food and Agriculture Organization [OECD/FAO], 2019). The lint quality in general, while the quantity of produce, i.e., the seed cotton yield (SCY) particularly is highly sensitive to climatic conditions. It can be seen in case of Pakistan where it was grown across 2.3 million hectares during 2018–2019 with an average per hectare yield of approximately 707 kg/ha (Anonymous, 2018–2019)) compared with 2,320 and 1,765 kg/ha for Australia and China, respectively (International Cotton Advisory Committee [ICAC], 2018). The quality of lint produced is also inferior, having a short fiber length, coarse fiber fineness, and lower uniformity, resulting in a higher import of longer fiber and lower price of locally produced cotton lint (Pakistan Central Cotton Committee [PCCC], 2014). The cotton belt of Pakistan is mainly located in the high-temperature zone where mean maximum temperature often exceed 48°C during the cotton-growing season. The optimum temperature for a successful cotton production is about 35°C, which may vary among cultivars. However, temperatures above this threshold level badly affect the peak time of cotton flowers and boll setting, resulting in excessive evapo-transpiration and abscission/no boll set at lower half of the plant (Bibi et al., 2003). Singh et al. (2007) reported a strong negative correlation between high temperature and the lint yield, resulting in a yield decrease of about 110 kg/ha for each unit increase in maximum temperature.

Identification of genotypes that have a greater ability to withstand the peaks of heat stress coupled with their limited water use is important to enhance the cotton productivity (Cottee et al., 2010). However, suitable selection standards are required for measuring resilience of cotton germplasm against heat stress. Plant phenological traits especially flowering and boll retention capacity in high temperature environments are effective in repeatable heat stress screening environments (Ismail and Hall, 1999). But genotypes with significant G × Y (genotype × year) and G × E (genotype × environment) interaction in the field often compromise genetic advance. Therefore, genetic gain in the cotton yield can be exploited by targeting those traits that are closely associated with plant adaptation to high-temperature environment (Singh et al., 2007). Cell membrane thermostability (CMT) has been reported as most relevant and suitable selection criteria for measuring heat tolerance (Abro et al., 2015). The ratio of trichomes to stomata is also found associated with the efficiency of water use (Galdon-Armero et al., 2018; Lei et al., 2018). Slow progress in development of heat tolerance in cotton cultivars due to its polygenic inheritance has been reported in earlier findings (Jones et al., 2014). A low heritability and time reliance of adaptive traits in high-temperature environments have also been reported as major obstacles (Singh et al., 2007; Jones et al., 2014). However, combining morphological and plant physiological traits for the elucidation of thermo tolerance in cotton is important and expected to result in improved heat tolerance in cotton (Rana et al., 2011). Better understanding of genetic, morphological, and physiological traits conferring heat tolerance in cotton is necessary, if climate change resilience, high yielding, and fine fiber quality of cotton cultivars are to be developed. An ability for the combination of genotypes in general (general combining ability [GCA]) and specific combining ability (SCA), heterotic effects and heritability of the traits coupled with genetic advance are also important in devising an effective breeding strategy for improving heat stress tolerance of cotton genotypes (Azhar et al., 2005).

The present study investigates the genetic variability in upland cotton for heat tolerance and identifies the association of CMT, stomata, and trichome size with cotton adaptation to high temperature and effects on yield and fiber quality parameters. The line × tester analysis was also performed for deciding the effective breeding strategy to advance the valued traits.

MATERIALS AND METHODS

Study Site and Experimental Material

The research work was conducted at Plant Breeding and Genetics Division, Nuclear Institute of Agriculture (NIA), Tando Jam, Pakistan, between the years 2015 and 2019. The experimental material consisted of fifty-eight diverse cotton genotypes including advance lines developed at NIA using hybridization and radiation-induced mutagenesis. History of breeding material used in the present study is given in **Supplementary Table 1**.

Evaluation of Cotton Genotypes for Heat Stress Tolerance

Heat tolerance of the experimental material in terms of high CMT, boll retention, SCY, ginning out turn percentage (GOT%), and staple length was tested in two sowing dates (i.e., early and normal) in a randomized complete block design (RCBD) with three replications. The RCBD was used to evaluate the large set of 58 genotypes because of the non-significant within-block variability and also because we were using the same piece of land every season for cotton breeding trials only. Further, the plot

size used was smaller than the normal plot size being used for advance line yield trials. One set of experimental material was sown early (15 March, 2015) to expose the genotypes to high temperature (up to 45°C in the months June and July) at the peak flowering and boll setting stage. Another set of same genotypes was planted in normal sowing (15 May, 2015) to experience mild temperature at the flowering and boll setting stage during late August. Cultivars CRIS-134 and CIM-469 were included as heat tolerant and susceptible check, respectively. Each genotype was planted in a plot size of 6.1 × 3.0 m in four rows with 30 cm plant-to-plant and 75 cm row-to-row distance. Standard agronomic and plant protection measures were performed throughout the growing season. From each genotype, five random plants were selected for data recording on number of bolls/plant. At maturity, seed cotton was picked, and the data were recorded on SCY. Further, seed cotton from each repeat of each genotype was ginned using the ginning machine. The staple length (in mm) was measured using the fibrograph by taking forty grams of lint from each sample. GOT% was calculated by following formula.

$$\text{GOT\%} = \frac{\text{Lint weight}}{\text{Weight of seed cotton}} \times 100$$

Analysis of Cell Membrane Thermostability

Relative cell injury percentage (RCI%), a measurement for CMT under a high temperature stress, was determined according to Sullivan (1972). RCI% was measured from fully developed green leaves of 20–22 days during the peak flowering season. A steel punch with a 10 mm inner diameter was used for collection of two sets of leaf disc from both sides of the midrib of selected leaves. One set was used for heat treatment, and other was kept as control. Leaf discs were collected at about 1 pm to 3 pm, and samples were immediately kept in glass vials having 2 ml of deionized water. Leaf discs were thoroughly washed two times with deionized water to rinse any electrolyte adhering on the outside. After the final rinse, 2 ml of deionized water was added in sterilized glass vials and covered with a lid to avoid evaporation during heat treatment. One set of glass vials was kept at room temperature and other at 50°C in a water bath for 1 h. After heat treatment, 10 ml of deionized water was added in vials and kept at 10°C for 24 h to allow diffusion of electrolytes. On the next day, vials were kept at room temperature and shaken three times for mixing of electrolytes. Initial electrical conductivity (EC) was measured using the EC meter (Model HI-933300, Hanna Instrument, United States). After the measurement of EC, the samples were autoclaved for 10 min at 0.10 MPa pressure for releasing all electrolytes. The same procedure for measurement of EC was repeated. RCI% was calculated by using the following formula:

RCI% = 1-[{1-(T1/T2)}/{1-(C1/C2)}] × 100

Where as

T1 and T2 = EC of sap at 50°C before and after autoclaving, respectively.

C1 and C2 = EC of sap at 25°C before and after autoclaving, respectively.

Measurement of Heat Susceptibility Index

Heat susceptibility index (HSI), a measurement of a relative decrease in yield influenced by non-favorable vs. favorable environments, was determined according to Fischer and Maurer (1978).

Heat susceptibility index = [(1-yh/yp)/H]

Where:

Yh = Average yield of genotypes under heat stress

Yp = Average yield of genotypes under non-stress condition or potential yield

H = Heat stress intensity = 1-(average yh of all genotypes/average yp of all genotypes).

Scanning Electron Microscopy of Leaves for Stomata and Trichome Size

For scanning electron microscopy (SEM) study of selected heat-tolerant genotypes along with the susceptible check, prepared leaf specimens were mounted on the stubs of a double-sided cellophane tape. The sputter was covered with Jeol, JFC-1500 ion Sputter device with C-30–50 mm gold. The sample specimens were observed, and pictures were taken by SEM, Jeol, JSM T-200, and Jeol-T6380 at voltage of 5–15 KV with a distinct magnification (Hayat, 1989). The stomata and trichome measurements with 4–5 repetitions were carried from an individual leaf using an SEM measuring bar. The SEM study was conducted at Central Research Laboratory, University of Karachi, Pakistan.

Multienvironment Field Trial of Selected Heat-Tolerant Genotypes for the Stability Analysis

Seventeen selected heat-tolerant genotypes along with one susceptible check (CIM-469) were evaluated for their stability analysis across five different locations of Sindh (i.e., Tando Jam, Matiari, Shaheed Benazirabad, Dadu, and Khairpur) during 2016–2017. The multienvironment trials were conducted in the RCBD with four replications. The plot size was 18 m^2 (6 × 3 m) with a row-to-row and plant-to-plant distance of 75 and 30 cm, respectively. Standard agronomic and plant protection measures were adopted throughout the growing season. At maturity, seed cotton was picked, and data were recorded on SCY (kg/plot).

Population Development for Genetic Studies of Heat Tolerance

To determine the pattern of inheritance and genetic variability, three heat-tolerant cotton genotypes (i.e., CRIS-342, NIA-Perkh, and CRIS-134) and three heat-susceptible genotypes (i.e., HariDost, Sohni, and NIA-148) were selected as parents for population development. The genetic population was developed by following the line × tester (3 × 3) method. Heat-tolerant genotypes were used as testers (i.e., male), whereas heat-susceptible genotypes were kept as lines (i.e., female). For crossing, unopened flowers commonly known as candles or buds were hand emasculated in the evening and covered with a butter

paper bag. Male parent flowers were also covered with butter paper bags to avoid insect-intervened pollen contamination. Pollination of flowers was carried out in the morning (10:00 AM), and pollinated flowers were again covered with butter paper bags. At maturity, seed cotton was picked from all cross combinations. Ginning was performed, and F_0 seeds were collected for evaluation in F_1 generation along with parents.

Evaluation of F_1 and F_2 Generations

Two sets of F_1 genetic material (i.e., 9 hybrids) along with six parents were planted in the field (i.e., normal) and glasshouse (i.e., elevated temperature) in the RCBD with 3 replications. The data were recorded on five random plants for RCI% and SCY (g/plant) in each cross and analyzed for combining ability and heterotic effects. Seeds harvested from F_1 generation were again evaluated in F_2 generation along with parents. Again two sets were planted, one in the field (i.e., normal) and other in the glasshouse (i.e., elevated temperature) conditions. In F_2, 10 and 20 plants were maintained in each cross under the glasshouse and field experiment, respectively. The data on five random plants in each cross along with parents were recorded for RCI% and SCY (g/plant). Genetic variance, heritability, and genetic advance were estimated from F_2 data.

Statistical Analysis

The data collected were analyzed separately for each parameter and subjected to analysis of variance (ANOVA) following Steel et al. (1997). The means comparison (honest significant difference [HSD] test at alpha 0.05) and correlation matrix were computed using the STATISTIX® VERSION 8.1 software. The values presented are mean of three replicates ± standard error (SE). The stability analysis of heat-tolerant genotypes was carried out for SCY data from replicated trials at multienvironments. The analysis comprised location-wise or environmental ANOVA and the combined ANOVA for any place/environment (Pooled ANOVA). Stability parameters were calculated following the model by Eberhart and Russell (1966). For the combining analysis, the mean squares of the line × tester design, the overall ability of the combination (i.e., GCA), and SCA variances and effects were calculated according to the method proposed by Kempthorne (1957). Mid-parent heterosis and better parent heterosis were worked out as percent mean deviation of the mean F1 performance over the mean performance of the mid-parent and better parent, respectively. Genetic variance was calculated by following Singh and Chaudhary (1999). Heritability was calculated by following Cochran and Cox (1957), and genetic advance was estimated according to Allard (1960).

RESULTS

Response of Different Genotypes of Cotton to Heat Stress

The analysis of variance showed highly significant differences among studied genotypes for RCI%, SCY, and number of bolls/plant. Differences were also observed among sowing dates for number of bolls/plant and SCY. Significant differences were present among sowing dates for RCI%, staple length, and GOT%. The sowing dates × genotypes interaction was also found highly significant for number of bolls/plant and SCY (**Supplementary Table 2**). The RCI% values of 58 genotypes are presented in **Table 1**. RCI% in studied genotypes ranged from 39 to 86%. The RCI level was noted >70% in 22 genotypes, while 60–70% in 20 genotypes and 50–60% in 08 genotypes. Eight genotypes showed < 50% level of cell damage, i.e., 40–50%. The tolerant genotypes, 50–60% levels of cell damage, were Sadori, NIA-Perkh, NIAB-111, CRIS-134, and CRIS-342. Whereas, some advance lines such as NIA-80, NIA-82, NIA-83, NIA-84, NIA-Bt1, NIA-Bt2, NIA-M-30, NIA-M31, NIA-HM-48, NIA-H-32, NIA-HM-327, and NIA-HM-2-1 had the lowest RCI level < 50% (i.e., higher CMT). The genotypes NIA-86, NIA-M2, NIA-M32, NIA-HM-1, NIA-H67, CRIS-121, and CIM-496 showed the highest RCI level (i.e., lower CMT). Out of 58, 17 genotypes were identified as more heat-tolerant because of having a higher CMT.

The SCY of 58 genotypes are presented in **Table 1**. SCY in studied genotypes ranged from 2,215 to 4,115 kg/ha under heat stress and non-heat stress conditions. The selected seventeen heat-tolerant genotypes performed well in both regimes. NIA-M-30 had the highest SCY (4,115 kg/ha) followed by NIA-HM-2 (3,936 kg/ha) and NIA-80 (3,912 kg/ha). NIA-HM-320 produced lowest SCY (2,215 kg/ha) under heat stress conditions. The HSI based on SCY varied in different genotypes (**Table 2**). In the present study, HSI values ranged between 0.32 and 10.85. Superior heat-tolerant genotypes gave the least values of HSI < 1 and high yield under heat stress conditions. Whereas, other genotypes, which were found as heat susceptible, had a higher HSI.

For the determination of heat tolerance, the data for bolls/plant in cotton genotypes were also considered. The mean values of number of bolls/plant showed that both heat stress and non-stress conditions had differently affected the boll retention capacity of fifty-eight genotypes. The heat-tolerant genotypes produced maximum bolls/plant in both heat stress and non-stress regimes. While other genotypes produced less number of bolls as a result of high temperature (**Table 1**). Superior heat-tolerant genotypes produced maximum bolls/plant under both sowing condition indicating that these genotypes could be less affected by heat stress (**Table 2**).

Table 1 represents the mean values of GOT% of studied genotypes, which ranged from 30 to 40.56% as a result of early and normal sowing dates. Less effects of high temperature stress were recorded in terms of GOT% in NIA-M-30, NIA-HM-48, NIA-H-32, NIA-Bt1, NIA-Perkh, CRIS-342, NIAB-111, CRIS-134, and Sadori. Non-significant differences in mean values were observed for the staple length (in mm). However, the staple length for all genotypes ranged from 27 to 30 mm. A decrease in fiber length can be attributed to high temperature. But in the present study, eighteen genotypes showed less reduction in the staple length and gave the lowest value of HSI < 1 (**Table 2**).

TABLE 1 | Mean performance of 58 cotton genotypes for relative cell injury percentage (RCI%), yield, and fiber traits.

Genotypes	RCI%		No. of bolls/plant		Seed cotton yield (Kg/ha)		Staple length (mm)		GOT%	
	SD 1	SD 2	SD 1	SD 2	SD 1	SD 2	SD 1	SD2	SD 1	SD 2
NIA-80	45 ± 1.7	42 ± 1.2	39 ± 0.1	41 ± 0.1	3871 ± 7	3912 ± 7	28.0 ± 0.3	28.5 ± 0.1	36.0 ± 0.6	37.5 ± 0.3
NIA-81	57 ± 0.6	55 ± 0.6	35 ± 0.1	37 ± 0.1	3669 ± 6	3732 ± 18	28.0 ± 0.3	28.5 ± 0.1	38.5 ± 0.3	39.4 ± 0.3
NIA-83	55 ± 0.6	53 ± 0.6	35 ± 0.1	38 ± 0.1	3584 ± 2	3610 ± 6	27.8 ± 0.1	28.1 ± 0.1	36.0 ± 0.3	37.0 ± 0.6
NIA-84	57 ± 0.6	55 ± 0.6	38 ± 0.1	39 ± 0.0	3678 ± 6	3710 ± 6	28.2 ± 0.1	28.5 ± 0.2	36.5 ± 0.3	38.4 ± 0.2
NIA-85	78 ± 0.6	73 ± 1.6	31 ± 0.1	36 ± 0.0	2415 ± 9	2934 ± 12	27.0 ± 0.0	28.0 ± 0.0	34.5 ± 0.3	37.5 ± 0.3
NIA-86	77 ± 1.6	78 ± 1.6	24 ± 0.2	33 ± 0.1	2625 ± 14	3298 ± 6	27.2 ± 0.1	27.5 ± 0.1	35.1 ± 0.1	40.1 ± 0.5
NIA-M-30	40 ± 1.6	39 ± 0.6	34 ± 0.1	36 ± 0.1	4065 ± 6	4115 ± 9	28.2 ± 0.1	28.6 ± 0.2	37.5 ± 0.1	38.0 ± 0.6
NIA-HM-327	46 ± 1.6	44 ± 1.2	36 ± 0.2	38 ± 0.1	3788 ± 5	3850 ± 3	28.0 ± 0.3	28.5 ± 0.1	37.8 ± 0.1	39.5 ± 0.3
NIA-HM-329	73 ± 1.7	71 ± 0.6	26 ± 0.1	34 ± 0.1	2423 ± 13	3023 ± 13	28.3 ± 0.2	29.5 ± 0.1	33.5 ± 0.3	38.4 ± 0.4
NIA-HM-335	83 ± 0.6	79 ± 1.7	20 ± 10	36 ± 5.8	2230 ± 17	3121 ± 6	27.9 ± 0.1	28.6 ± 0.1	34.4 ± 0.2	36.0 ± 0.6
NIA-H-1	81 ± 0.6	79 ± 0.0	23 ± 0.1	33 ± 0.1	2869 ± 12	3454 ± 12	27.6 ± 0.1	28.6 ± 0.2	33.5 ± 0.0	37.5 ± 0.8
NIA-H-24	82 ± 0.6	80 ± 1.2	23 ± 0.1	34 ± 0.0	2551 ± 29	3209 ± 5	27.5 ± 0.0	27.6 ± 0.1	36.4 ± 0.0	38.4 ± 0.2
NIA-M31	50 ± 1.6	49 ± 0.6	36 ± 0.1	38 ± 0.1	3561 ± 1	3606 ± 3	28.0 ± 0.0	28.5 ± 0.1	37.5 ± 0.3	39.2 ± 0.1
NIA-M32	85 ± 0.6	83 ± 0.6	27 ± 0.1	30 ± 0.0	2320 ± 12	2855 ± 6	28.5 ± 0.1	20.4 ± 9.2	35.5 ± 0.7	38.3 ± 0.4
NIA-M33	69 ± 0.6	65 ± 0.6	27 ± 0.2	34 ± 0.1	2431 ± 18	2931 ± 18	28.9 ± 0.1	29.2 ± 0.1	36.6 ± 0.1	39.6 ± 0.6
NIA-M34	74 ± 0.6	71 ± 0.6	30 ± 0.1	36 ± 0.1	3054 ± 5	3356 ± 6	27.8 ± 0.1	28.5 ± 0.1	35.8 ± 0.3	39.4 ± 0.2
NIA-Perkh	51 ± 0.6	48 ± 1.2	32 ± 0.1	37 ± 0.1	3681 ± 6	3740 ± 3	28.0 ± 0.3	28.7 ± 0.2	36.6 ± 0.1	39.6 ± 0.1
NIA-H-13	68 ± 0.0	66 ± 0.6	21 ± 0.0	32 ± 0.0	2653 ± 30	3155 ± 6	27.0 ± 0.0	27.5 ± 0.1	37.5 ± 0.6	38.6 ± 0.1
NIA-HM-2	54 ± 0.6	53 ± 0.6	37 ± 0.1	40 ± 0.1	3898 ± 12	3936 ± 12	27.5 ± 0.1	28.1 ± 0.1	37.9 ± 0.6	38.7 ± 0.1
NIA-HM-48	51 ± 0.6	59 ± 0.6	36 ± 0.1	39 ± 0.1	3589 ± 6	3621 ± 12	28.7 ± 0.1	29.3 ± 0.1	36.2 ± 0.1	37.3 ± 0.6
NIA-M-2	84 ± 0.6	82 ± 1.2	22 ± 1.2	30 ± 0.7	2512 ± 7	3040 ± 23	27.8 ± 0.1	28.5 ± 0.1	33.3 ± 0.2	39.3 ± 0.8
NIA-HM-1	86 ± 0.6	83 ± 0.0	31 ± 2.7	35 ± 1.6	2456 ± 32	3470 ± 17	27.3 ± 0.1	27.5 ± 0.1	35.2 ± 0.1	38.6 ± 0.6
NIA-H-36	75 ± 0.6	77 ± 0.9	32 ± 1.0	39 ± 0.6	3132 ± 18	3441 ± 12	27.9 ± 0.1	28.5 ± 0.1	34.4 ± 0.1	37.4 ± 0.1
NIA-H-12	65 ± 0.6	63 ± 0.6	32 ± 0.1	33 ± 0.1	2923 ± 13	3255 ± 6	28.1 ± 0.1	28.4 ± 0.2	32.5 ± 0.6	39.2 ± 0.5
NIA-Bt-1	55 ± 0.6	50 ± 0.7	37 ± 0.1	36 ± 0.0	3768 ± 6	3820 ± 6	27.5 ± 0.1	28.2 ± 0.1	36.9 ± 0.6	38.5 ± 0.4
NIA-Bt-2	58 ± 0.6	55 ± 0.6	38 ± 0.2	40 ± 0.1	3526 ± 6	3690 ± 6	28.0 ± 0.0	28.3 ± 0.2	39.5 ± 0.3	40.3 ± 0.4
NIA-Bt-3	76 ± 0.6	76 ± 1.2	36 ± 0.1	39 ± 0.1	2959 ± 6	3415 ± 9	28.0 ± 0.1	28.5 ± 0.1	32.2 ± 0.6	37.4 ± 0.8
NIA-Bt-4	78 ± 0.6	80 ± 1.2	34 ± 0.1	37 ± 0.1	3046 ± 27	3570 ± 6	27.0 ± 0.0	27.9 ± 0.1	35.8 ± 0.6	37.9 ± 0.6
NIA-Bt-5	65 ± 0.6	65 ± 0.0	31 ± 0.1	38 ± 0.1	2427 ± 16	3254 ± 105	27.6 ± 0.1	28.0 ± 0.0	35.4 ± 0.2	37.5 ± 0.6
NIA-HM-320	79 ± 0.6	77 ± 0.0	30 ± 1.2	35 ± 0.7	2215 ± 9	3515 ± 9	28.2 ± 0.1	29.5 ± 0.1	33.4 ± 0.3	37.3 ± 0.2
NIA-HM-322	64 ± 0.0	60 ± 1.2	32 ± 0.2	35 ± 0.1	3022 ± 13	3356 ± 6	28.6 ± 0.1	29.0 ± 0.0	30.3 ± 0.2	32.6 ± 0.6
NIA-HM-323	78 ± 0.6	78 ± 0.0	31 ± 0.1	38 ± 0.1	2910 ± 6	3469 ± 6	28.0 ± 0.0	28.5 ± 0.1	32.5 ± 0.9	35.0 ± 0.6
NIA-HM-337	69 ± 0.6	67 ± 1.2	25 ± 0.1	35 ± 0.1	3041 ± 24	3445 ± 26	28.6 ± 0.1	29.0 ± 0.0	31.8 ± 0.6	34.9 ± 0.6
NIA-HM-338	65 ± 0.6	63 ± 1.7	22 ± 0.2	30 ± 0.1	3123 ± 13	3398 ± 6	28.2 ± 0.1	28.5 ± 0.2	36.2 ± 0.6	38.9 ± 0.1
NIA-HM-321	64 ± 0.6	64 ± 1.2	34 ± 0.1	37 ± 0.1	2236 ± 21	3236 ± 21	28.6 ± 0.2	29.0 ± 0.1	31.8 ± 0.6	34.1 ± 0.1
NIA-H-31	71 ± 0.6	70 ± 0.0	23 ± 0.1	30 ± 0.1	3240 ± 23	3523 ± 13	29.5 ± 0.1	30.0 ± 0.1	30.2 ± 0.1	32.5 ± 0.3
NIA-H-32	51 ± 0.6	50 ± 0.6	34 ± 0.1	37 ± 0.1	3439 ± 6	3539 ± 6	27.9 ± 0.1	28.5 ± 0.2	36.1 ± 0.6	38.1 ± 0.5
NIA-H-01	71 ± 0.6	70 ± 0.6	30 ± 0.1	35 ± 0.1	3144 ± 25	3463 ± 6	28.6 ± 0.1	29.3 ± 0.2	34.3 ± 0.1	35.5 ± 0.6
NIA-Okra-24	86 ± 0.6	84 ± 1.2	29 ± 0.2	39 ± 0.1	2229 ± 6	3433 ± 6	27.4 ± 0.1	28.5 ± 0.3	34.6 ± 0.6	35.3 ± 0.4
NIA-H-29	69 ± 0.6	67 ± 0.6	23 ± 0.8	33 ± 0.4	3022 ± 13	3687 ± 6	27.9 ± 0.1	28.1 ± 0.1	33.6 ± 0.6	38.5 ± 0.6
NIA-H-30	65 ± 0.6	68 ± 1.2	34 ± 0.6	36 ± 0.3	2918 ± 10	3332 ± 12	27.6 ± 0.1	28.3 ± 0.1	35.1 ± 0.6	37.2 ± 0.4
NIA-HM-311	74 ± 0.6	70 ± 0.6	32 ± 0.6	35 ± 0.3	2913 ± 8	3535 ± 20	27.0 ± 0.0	27.1 ± 0.1	33.3 ± 0.2	37.2 ± 0.1
NIA-H-67	73 ± 0.6	74 ± 0.6	24 ± 0.1	32 ± 0.1	2996 ± 6	3296 ± 2	27.5 ± 0.1	27.8 ± 0.1	33.5 ± 0.3	35.3 ± 0.4
CRIS-121	83 ± 1.2	81 ± 0.6	34 ± 0.6	36 ± 0.3	2763 ± 6	3301 ± 2	28.0 ± 0.3	28.1 ± 0.1	33.3 ± 0.4	36.5 ± 0.6
CRIS-9	65 ± 0.6	68 ± 0.0	33 ± 0.4	38 ± 0.3	3002 ± 1	3532 ± 18	28.2 ± 0.1	28.5 ± 0.1	35.6 ± 0.3	39.6 ± 0.6
Sindh-1	67 ± 0.6	69 ± 0.6	30 ± 0.1	36 ± 0.0	2650 ± 29	3201 ± 3	27.2 ± 0.1	27.5 ± 0.1	34.8 ± 0.6	38.1 ± 0.5
Hari Dost	75 ± 0.0	73 ± 0.6	22 ± 0.6	32 ± 0.3	3108 ± 5	3532 ± 18	27.8 ± 0.1	28.0 ± 0.0	33.6 ± 0.6	38.2 ± 0.1
Sohni	68 ± 0.6	64 ± 0.6	32 ± 0.2	34 ± 0.1	3021 ± 12	3444 ± 2	27.9 ± 0.1	28.0 ± 0.0	36.4 ± 0.7	39.3 ± 0.4
NIA-Ufaq	63 ± 1.7	62 ± 1.2	34 ± 0.5	36 ± 0.3	3420 ± 12	3520 ± 12	28.0 ± 0.0	28.4 ± 0.1	35.2 ± 0.1	38.5 ± 0.6
CRIS-342	62 ± 1.2	62 ± 1.2	31 ± 0.7	32 ± 0.4	3331 ± 18	3356 ± 6	27.5 ± 0.3	28.1 ± 0.1	35.5 ± 0.6	38.3 ± 0.2
Chandi-95	65 ± 0.6	62 ± 1.2	33 ± 0.6	37 ± 0.3	3118 ± 10	3630 ± 17	29.6 ± 0.1	31.2 ± 0.1	33.4 ± 0.2	36.4 ± 0.2

(Continued)

TABLE 1 | (Continued)

Genotypes	RCI%		No. of bolls/plant		Seed cotton yield (Kg/ha)		Staple length (mm)		GOT%	
	SD 1	SD 2	SD 1	SD 2	SD 1	SD 2	SD 1	SD2	SD 1	SD 2
Sadori	51 ± 0.0	50 ± 1.2	36 ± 0.2	37 ± 0.1	3542 ± 24	3570 ± 17	28.3 ± 0.1	28.8 ± 0.1	37.6 ± 0.6	38.5 ± 0.6
Shahbaz	72 ± 0.6	71 ± 0.6	28 ± 0.1	32 ± 0.0	2354 ± 31	3099 ± 1	28.0 ± 0.0	28.2 ± 0.1	34.5 ± 0.3	38.2 ± 0.1
IR-3701	65 ± 0.6	64 ± 0.9	32 ± 0.1	36 ± 0.1	3332 ± 6	3390 ± 6	27.5 ± 0.2	28.0 ± 0.0	34.2 ± 0.5	37.1 ± 0.5
NIAB-78	70 ± 1.2	65 ± 0.6	27 ± 0.1	33 ± 0.1	3053 ± 6	3420 ± 12	27.2 ± 0.1	27.6 ± 0.1	30.7 ± 0.6	34.8 ± 0.1
NIAB-111	64 ± 1.2	62 ± 1.2	34 ± 0.2	36 ± 0.1	3489 ± 6	3526 ± 6	28.0 ± 0.0	28.3 ± 0.1	35.6 ± 0.6	36.4 ± 0.6
CIM-469	80 ± 0.6	77 ± 0.6	29 ± 0.6	29 ± 0.3	3122 ± 6	3290 ± 3	27.6 ± 0.1	28.0 ± 0.0	34.4 ± 0.6	35.2 ± 0.1
CRIS-134	50 ± 1.2	47 ± 0.6	32 ± 0.1	34 ± 0.1	3556 ± 6	3590 ± 6	27.8 ± 0.1	28.0 ± 0.1	36.7 ± 0.5	37.6 ± 0.3

RCI%, relative cell injury percentage, GOT%, ginning out turn percentage, SD 1, sowing date 1 (15 March), SD 2, sowing date 2 (15 May).

TABLE 2 | Heat susceptible index (HSI) of 58 cotton genotypes for yield and fiber traits.

Genotypes	NBP	SCY	SL	GOT%	Genotypes	NBP	SCY	SL	GOT%
NIA-80	0.59	0.31	0.56	1.19	NIA-HM-320	4.41	5.10	1.32	1.52
NIA-81	0.56	0.50	0.52	0.68	NIA-HM-322	3.05	2.97	1.54	2.06
NIA-83	0.32	0.20	0.32	0.84	NIA-HM-323	5.08	4.81	1.15	1.30
NIA-84	0.46	0.26	0.31	1.45	NIA-HM-337	8.48	3.50	1.03	1.80
NIA-85	2.72	2.39	1.07	1.56	NIA-HM-338	7.81	2.42	1.36	1.28
NIA-86	8.00	3.09	1.17	1.49	NIA-HM-321	2.41	4.53	1.44	1.56
NIA-M-30	0.34	0.36	0.42	0.38	NIA-H-31	6.78	2.40	1.19	2.09
NIA-HM-327	0.95	0.48	0.52	1.26	NIA-H-32	0.33	0.84	0.63	0.90
NIA-HM-329	7.33	3.29	1.21	1.44	NIA-H-01	4.31	2.75	1.32	1.07
NIA-HM-335	3.44	2.18	1.15	1.36	NIA-Okra-24	7.48	4.80	1.15	0.63
NIA-H-1	2.70	2.70	1.04	1.55	NIA-H-29	8.77	5.38	1.17	2.31
NIA-H-24	10.10	4.54	1.67	1.56	NIA-H-30	2.14	3.71	1.16	1.71
NIA-M31	0.86	0.37	0.52	1.29	NIA-HM-311	2.30	5.25	1.17	1.44
NIA-M32	3.48	4.71	1.03	2.14	NIA-H-67	7.97	2.72	1.35	1.58
NIA-M33	6.02	2.27	1.12	1.53	CRIS-121	2.23	4.87	1.06	1.74
NIA-M34	4.81	2.69	1.26	1.43	CRIS-9	4.05	4.48	1.05	1.48
NIA-Perkh	0.64	0.50	0.69	0.73	Sindh-1	4.61	5.14	1.27	1.02
NIA-H-13	10.85	4.75	1.57	0.85	Hari Dost	9.95	3.58	0.53	1.25
NIA-HM-2	0.60	0.29	0.64	0.59	Sohni	1.66	3.67	1.16	1.44
NIA-HM-48	0.54	0.26	0.61	0.86	NIA-Ufaq	1.80	0.85	0.42	1.76
NIA-M-2	7.66	4.35	0.73	4.56	CRIS-342	0.62	0.28	0.69	0.68
NIA-HM-1	3.46	5.17	1.26	2.59	Chandi-95	2.86	4.21	1.53	1.64
NIA-H-36	5.19	2.68	1.05	2.39	Sadori	0.64	0.23	0.52	0.70
NIA-H-12	1.44	3.04	1.14	5.08	Shahbaz	3.80	5.61	1.27	2.17
NIA-Bt-1	0.32	0.41	0.74	1.24	IR-3701	0.67	0.51	0.53	2.35
NIA-Bt-2	0.61	0.84	0.53	0.59	NIAB-78	6.02	3.20	1.15	1.88
NIA-Bt-3	2.00	3.99	1.26	1.75	NIAB-111	0.82	0.31	0.73	0.62
NIA-Bt-4	2.26	4.38	1.27	1.62	CIM-469	1.61	1.44	1.05	0.67
NIA-Bt-5	5.56	3.54	1.26	1.68	CRIS-134	0.64	0.32	0.43	0.75

NBP, no. of bolls/plant, SCY, seed cotton yield, SL, staple length (mm), GOT%, ginning out turn.

Scanning Electron Microscopy Study of Stomata and Trichome Size of Heat-Tolerant Cotton Genotypes

Highly significant and significant differences among genotypes were observed for the stomata and trichome size, respectively (**Supplementary Table 3**). The stomata and trichome size of different genotypes examined with SEM are presented in **Table 3**, and the difference in stomata and trichome size of heat-tolerant and heat-susceptible genotypes is shown in **Figures 1**, **2**. The minimum value of the stomata size on the surface of cotton leaf was recorded as 21.57 μm^2, and the maximum stomata size was recorded as 105 μm^2 with ± 23.3 standard deviation. The large size of stomata was observed in genotype CIM-469 (105.0 μm^2) followed by genotype NIAB-111 (87.0 μm^2). Whereas, two genotypes, namely, NIA-80 (21.6 μm^2) and

TABLE 3 | Mean stomata and trichome size of selected 18 cotton genotypes.

Genotypes	Open stomata			Trichome size (μm)		
	Length (μm)	Width (μm)	Size (μm^2)	Minimum value	Maximum value	Average
NIA-80	9.76	2.21	21.6 i	420	519	465.0 bc
NIA-81	15.2	4.77	72.5 e	725	823	782.7 a
NIA-83	14.8	4.96	73.4 c	234	790	419.3 bc
NIA-84	11.8	2.78	32.8 g	216	490	328.7 b-e
NIA-H32	11.9	3.64	44.3 f	89.6	510	348.2 b-e
NIA-M-30	7.81	2.89	22.6 i	147	372	257.0 c-e
NIA-HM-327	16.7	6.29	39.2 f	109	322	184.7 de
NIA-M31	14.3	2.88	41.2 f	311	685	446.0 bc
NIA-Perkh	9.95	2.68	26.7 h	160	634	438.0 bc
NIA-HM-2-1	11.1	3.18	35.3 g	73.5	584	256.8 c-e
NIA-HM-48	16.8	3.44	57.8 d	222	490	374.3 b-e
NIA-Bt-1	12.9	3.52	45.4 e	131	545	402.0 bc
NIA-Bt-2	11.8	5.01	59.1 d	176	471	317.7 b-e
NIAB-111	15.4	5.65	87.0 b	130	503	318.0 b-e
Sadori	12.7	3.65	46.4 e	317	557	468.0 b
CRIS-342	12.01	4.03	48.4 h	164	410	369.0 b
CIM-469	16.7	6.29	105.0 a	87	263	177.0 e
CRIS-134	13.2	4.47	56.0 d	143	565	388.0 b-d
Minimum value	7.81	2.21	21.57	73.5	263	177
Maximum value	16.8	6.29	105.04	725	823	782.7
Standard deviation	±2.63	±1.11	±23.23	±156.40	±144.12	±136.31

NIA-M30 (22.6 μm^2), gave small size stomata. The results of the electron micrograph obtained from the leaf epidermis tissues showed that all genotypes were non-glandular single-cell trichome. All the selected genotypes showed a high density of trichomes and large trichome size as compared with susceptible check. Among them, the highest average size and density of trichome were recorded (782.7 μm) in genotype NIA-81 followed by Sadori (468 μm) and NIA-80 (465 μm). Whereas, the average lowest density and trichome size (177 μm) were observed in the susceptible check (i.e., CIM-469). The standard deviation value for the minimum trichome length of all genotypes was ± 156.40, and maximum trichomes lengths were ± 144.12. The average standard deviation was observed to be ± 136.31.

Association of Relative Cell Injury Percentage, Stomata, and Trichome Size With Seed Cotton Yield and Ginning Out Turn Percentage

Coefficient of determination (R^2) depicted that the variation in SCY was due to the effects of RCI% and stomata size (**Figure 3**). This shows that a higher SCY among genotypes was significantly associated with a lower RCI% and stomata size. Therefore, the regression analysis illustrated that the RCI% and stomata size had a strong negative effect on SCY, with coefficients of determination (R^2) 0.61 and 0.51, respectively. The trichome size exhibited positive but non-significant relationships with SCY. Relationships between RCI%, stomata size, and trichome size with GOT% were observed to be weak or non-significant.

G × E Interaction Study of Selected Heat Tolerant Cotton Genotypes

Mean squares showed highly significant ($P < 0.01$) differences for mean SCY among genotypes, environments, and the G × E interaction (**Supplementary Table 4**). Highly significant differences among locations indicated the presence of the G × E interaction in this area. The stability analysis showed the presence of significant G × E interactions for SCY in this region. As per results, all selected genotypes showed higher yield and stability as compare to susceptible check. Among the genotypes, NIA-M30, NIA-80, and NIA-83 produced a high average yield (3.47, 3.47, and 3.31 tons/ha) and wide adaptability with unit regression (bi∼1) and non-significant deviation from the regression line (S^2d∼0). These genotypes are high yielding and stable (**Table 4**) and may be tested over all environments to attain an additional stable performance. Moreover, three genotypes, namely, NIA-M31, NIA-HM48, and NIA-Bt2, were considered suitable for the specific environment by way of expected performance as they possess a high seed yield (ton/ha) with increased regression average (bi > 1). Five other genotypes viz., NIA-Perkh, NIA-Bt2, Sadori, CRIS-134, and CIM-469 were found suitable to poor environments as they showed good performance in the seed yield with regression (bi < 1) and above average non-significant deviation from the regression (**Table 4**).

Genetic Improvement Through Hybridization for Heat Tolerance and Genetic Analysis of Relative Cell Injury and Seed Cotton Yield in F_1 and F_2 Generations

This research work was carried out to find out combining ability variance effects of parents and their F_1 hybrids of cotton and their efficient use in the improvement of breeding program. The ANOVA (**Supplementary Table 5**) reveals that the mean squares for the interaction of temperature regimes were highly significant ($P < 0.01$) for parents and their crosses. A significant variation was identified for RCI% in parents as well as their respective crosses under field regimes. Parents vs. crosses mean square, an indicator of average heterosis, was also significant under field regimes ($P < 0.01$), indicating that the mean RCI% among crosses deviated substantially from the mean of their parental cultivars. ANOVA of combining ability for RCI% and SCY (g/plant) was computed separately using two temperature regimes (March and May) indicated a significant variation for RCI% due to lines and testers ($P < 0.01$) under both regimes in the field.

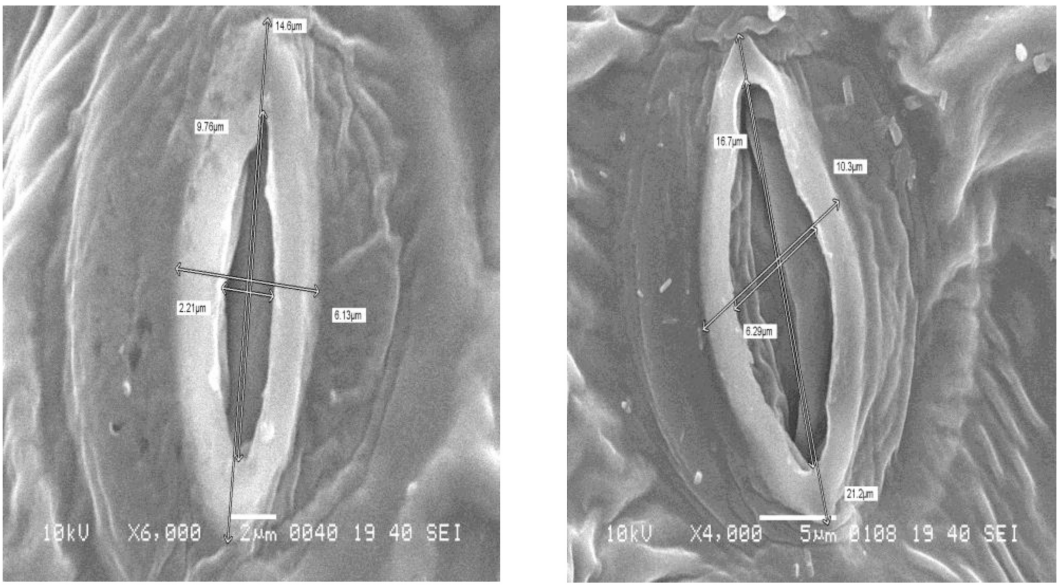

FIGURE 1 | Difference in stomata size of heat-tolerant (NIA-80) and heat-susceptible (CIM-469) cotton genotypes revealed through scanning electron microscopy (SEM).

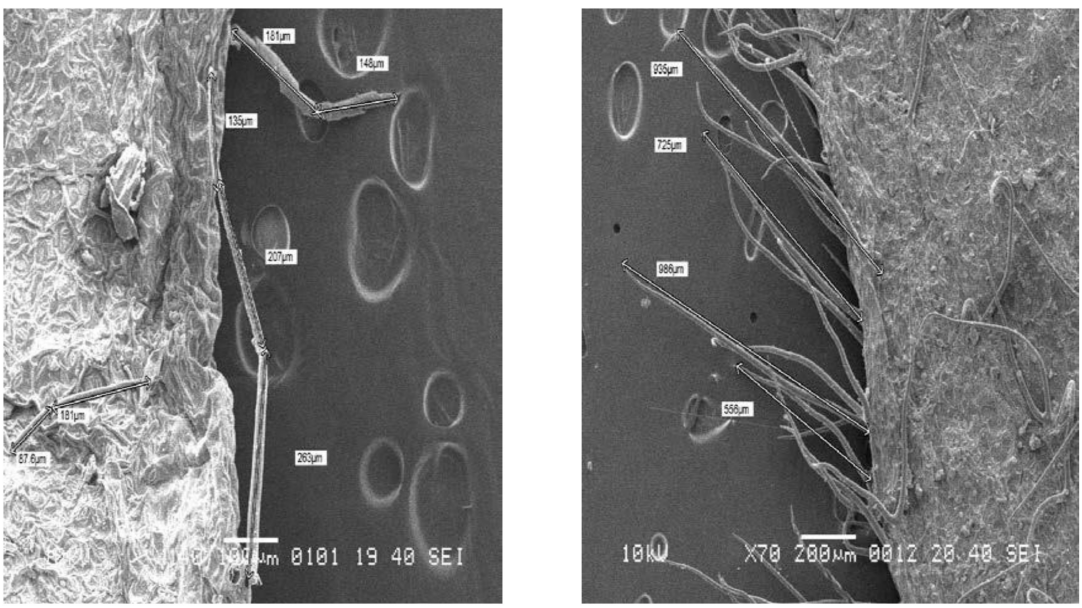

FIGURE 2 | Difference in trichome size of heat-susceptible (CIM-469) and heat-tolerant (NIA-81) cotton genotypes revealed through SEM.

Mean Performance of Parents and Their Hybrids for Relative Cell Injury and Seed Cotton Yield in F_1

In the presents study, lower RCI was interpreted as higher CMT due to heat sensitivity. The variation among parents as well as hybrids was significant ($P < 0.01$) for RCI under field and glasshouse regimes. The mean performance of parents and their hybrids for RCI% and SCY (g/plant) is presented in **Table 5**. Among parents, RCI ranged between 43 and 78% in the glasshouse and between 42 and 75% in the field, whereas tester NIA-Perkh, CRIS-342, and CRIS-134 showed minimum RCI in glasshouse (i.e., heat stress) and field (i.e., non-stress)

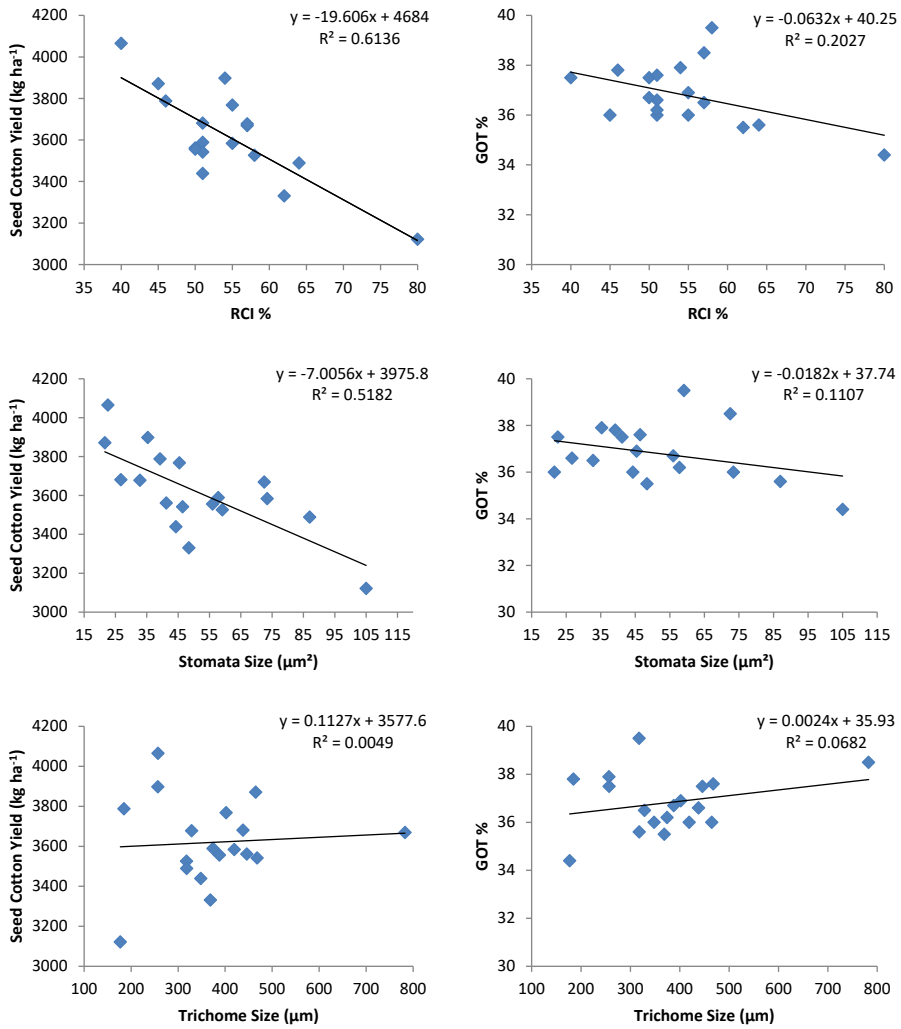

FIGURE 3 | Relationship of physiological traits with seed cotton yield (kg ha^{-1}) and ginning out turn percentage (GOT%) of selected heat-tolerant cotton genotypes.

regimes, respectively; however, line NIA-148 showed maximum RCI in both glasshouse and field temperature regimes. Among F_1 hybrids, RCI ranged between 42 and 70% in the glasshouse and 42 and 67% in the field regime. NIA-Perkh, CRIS-342, and CRIS-134 among parents had lowest, while NIA-148, Haridost, and Sohni had the highest relative cell injury percent. The crosses NIA-148 × NIA-Perkh, Sohni × CRIS-134, and NIA-148 × CRIS-342 had lowest RCI%, which showed stability in the cell membrane among hybrids was below average in both glasshouse and field regimes. Hybrid NIA-148 × CRIS-134 had maximum RCI%.

The results regarding stocktickerSCY (g/plant) are presented in **Table 5**, which showed that the testers stocktickerCRIS-324, NIA-Perkh, and stocktickerCRIS-134 produced the highest SCY, whereas, three lines gave the lowest yield under both temperature regimes. Among the crosses, HariDost × stocktickerCRIS-342, NIA-148 × NIA-Perkh, NIA-148 × stocktickerCRIS-342, Sohni × stocktickerCRIS-342, and Sohni × stocktickerCRIS-134 showed better performance under non-heat stress and heat stress regimes. The HSI for parents and F_1 hybrids was ranged from 0.32 to 2.0%. The parents and hybrids with a higher stocktickerSCY performance have also shown lowest values of HSI. The superior genotypes for heat tolerance gave the least values of HSI (HSI < 1) and high yield under heat stress conditions (**Figure 4**).

Combining Ability Variance and Effects

The effects of general combining ability associated with parental varieties were computed for RCI% under glasshouse and field conditions. The scatter diagram (**Figure 5**) revealed that CRIS-342 and NIA-Perkh could be categorized in high CMT and high GCA group under both temperature regimes, therefore, could be used as a suitable parent in breeding programs aimed to improve CMT in cotton. Cultivars CRIS-134, CRIS-342, NIA-Perkh, and Sohni were recognized in low CMT and low GCA group under both regimes. The variety CRIS-134, NIA-148, and Haridost showed positive GCA effects. The varieties NIA-148 and Haridost were recognized in low CMT and low GCA group under both temperature regimes, indicated that these cultivars

TABLE 4 | Seed cotton yield (tons/ha) and stability parameters for SCY of 18 selected genotypes tested over different locations during 2017–2018.

Genotypes	L1	L2	L3	L4	L5	Overall genotypic mean yield	b ± SE (b)	S^2d
NIA-80	3.668	3.570	3.240	3.054	3.055	3.317 b	1.186 ± 0.123	0.003
NIA-81	3.495	3.364	3.133	2.858	2.828	3.135 ef	1.240 ± 0.055	0.000
NIA-83	3.593	3.404	3.303	3.150	3.033	3.297 b	0.900 ± 0.091	0.002
NIA-84	3.343	3.186	2.779	2.447	2.481	2.847 h	1.684 ± 0.138	0.004
NIA-H32	2.943	3.559	2.915	2.547	2.788	2.950 g	0.964 ± 0.714	0.116
NIA-M-30	3.867	3.471	3.554	3.249	3.216	3.471 a	1.021 ± 0.242	0.013
NIA-HM-327	3.694	2.993	3.330	3.045	2.952	3.203 d	0.941 ± 0.523	0.062
NIA-M31	3.503	2.879	2.901	2.718	2.632	2.926 g	1.269 ± 0.379	0.033
NIA-Perkh	3.381	3.585	3.309	3.143	3.176	3.319 b	0.587 ± 0.263	0.016
NIA-HM-2-1	3.579	2.927	3.228	3.082	3.086	3.180 d-f	0.563 ± 0.501	0.057
NIA-HM-48	3.389	3.343	2.777	2.583	2.671	2.952 g	1.522 ± 0.300	0.020
NIA-Bt-1	3.570	3.466	3.131	2.957	2.814	3.187 de	1.335 ± 0.139	0.004
NIA-Bt-2	3.567	3.420	3.272	3.126	3.035	3.284 bc	0.897 ± 0.056	0.000
NIAB-111	3.145	3.153	2.954	2.855	2.762	2.974 g	0.697 ± 0.120	0.003
Sadori	3.476	3.360	3.267	3.069	2.977	3.230 cd	0.848 ± 0.083	0.002
CRIS-342	3.388	3.278	3.128	2.945	2.857	3.119 f	0.922 ± 0.063	0.000
CIM-469	2.927	2.774	2.660	2.501	2.439	2.660 i	0.831 ± 0.039	0.000
CRIS-134	2.962	2.971	2.856	2.684	2.664	2.827 h	0.592 ± 0.099	0.002
Overall site mean yield	3.416a	3.261b	3.096c	2.889d	2.859e			

L1, location 1 (Tando Jam), L2, location 2 (Matiari), L3, location 3 (Shaheed Benazirabad), L4, location 4 (Khairpur), L5, location 5 (Dadu), b, variance due to regression coefficient, SE, standard error, S^2d, deviation from regression coefficient.

TABLE 5 | Mean performance of parents and their hybrids for RCI% and SCY (g/plant) in F_1 and F_2 generations.

Parents and hybrids	F_1 generation				F_2 generation			
	RCI%		SCY (g/plant)		RCI%		SCY (g/plant)	
	Glasshouse	Field	Glasshouse	Field	Glasshouse	Field	Glasshouse	Field
CRIS-342	51	49.3	118.4	125.4	50	49.3	116.73	118
NIA-Perkh	43	42.3	113.4	118.9	40	38.9	121.46	115
CRIS-134	52	51.7	108.5	111.9	48	50	109.52	118
Haridost	71	71	72.6	95.7	75.3	74.3	72.81	121
Sohni	70	71.7	76.7	108.2	76	75.1	72.92	97
NIA-148	78	78.4	81.2	118.8	80	82.3	62.88	116
Haridost × CRIS-342	45.1	45.2	130.3	140.9	38.3	37.5	145	145
Haridost × NIA-Perkh	50	48.1	102.9	138.5	44.4	42.6	134.79	140
Haridost × CRIS-134	55	56.7	109.3	138	51	51	128.12	142
Sohni × CRIS-342	51	49.2	129.1	135.9	47.6	46.6	166.63	167
Sohni × NIA-Perkh	44.1	42.6	135.4	146.1	50.8	48.2	113.57	133
Sohni × CRIS-134	51	51.4	96.5	122.9	60	58.7	132	132
NIA-148 × CRIS-342	43	43.3	133.3	144.5	42.6	41.1	144.99	148
NIA-148 × NIA-Perkh	42.1	42.4	129.5	140.6	51.1	50.1	139.63	142
NIA-148 × CRIS-134	70	67.2	89.6	129.2	72.9	72.7	81.99	124

will not be suitable as donor parents for CMT studies. For SCY, the parents NIA-Perkh, CRIS-342, and Sohni displayed the positive GCA (**Figure 6**). Three tolerant (based on CMT) genotypes expressed differential patterns of GCA effects and also show differential response (i.e., SCA effects) in different cross combinations. The combinations NIA-148 × CRIS-342, Haridost × CRIS-342, Sohni × CRIS-134, and NIA-148 × NIA-Perkh had a negative RCI% value, which proved to be the best indicator showing tolerance to heat stress in hybrids (based on CMT) in both regimes. Three hybrids Sohni × CRIS-342, Sohni × NIA-Perkh, and NIA-148 × CRIS-134 showed a positive RCI%, indicating susceptibility to heat stress. Sohni × NIA-Perkh

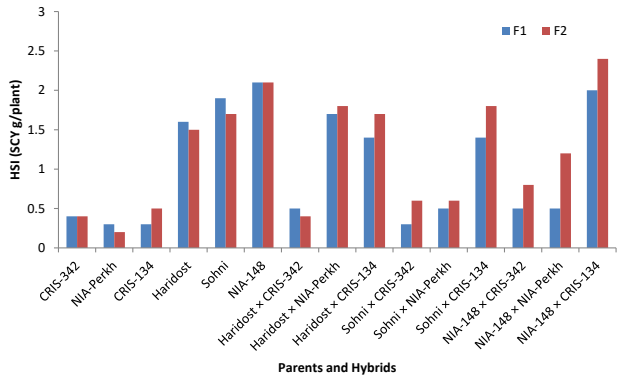

FIGURE 4 | Heat susceptibility index (HSI) for SCY (g/plant) among parents and their progenies in F_1 and F_2 generations.

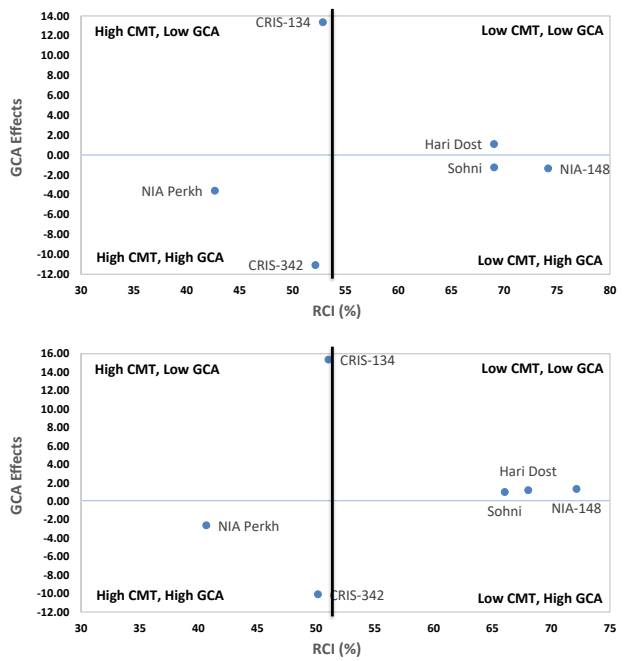

FIGURE 5 | Scatter diagram between RCI% and general combining ability (GCA) effects in upland cotton genotypes (parents) in the glasshouse (up) and field (down) data based on F_1 generation.

and NIA-148 × CRIS-342 crosses proved as the best combiners for SCY (**Figure 7**).

Heterotic Effects in F_1 Generation

The heterosis values for RCI% and SCY (g/plant) expressed as the percentage increase or decrease over mid-parent (i.e., relative heterosis or mid parent heterosis) and over better parent (i.e., hetrobeltiosis) are presented in **Table 6**. Results revealed that there was a general tendency of increase in the cell membrane stability of hybrids over mid- and better parents, respectively. Negative heterotic effects for RCI (%) indicated less damage to cellular membranes and vice versa. In the present study, maximum negative mid-parent and better parent heterosis were observed in HariDost × CRIS-342, Sohni × CRIS-342, NIA-148 × CRIS-342, and NIA-148 × NIA-Perkh, while the maximum positive heterotic effects were produced by hybrids NIA-148 × CRIS-134 and HariDost × NIA-Perkh under both temperature regimes. The results of heterosis for SCY (g/plant) have shown maximum significant positive heterosis and heterobeltiosis under both heat stress and non-heat stress regimes in the crosses HariDost × CRIS-342, Sohni × CRIS-342, Sohni × NIA-Perkh, NIA-148 × CRIS-342, and NIA-148 × NIA-Perkh. However, maximum negative heterotic effects were observed in cross NIA-148 × CRIS-134 in heat stress conditions (i.e., glasshouse).

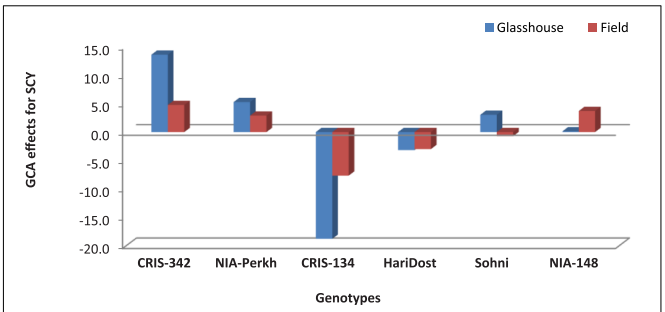

FIGURE 6 | Estimates of GCA effects for SCY (g/plant) in six parents data based on F_1 generation.

Performance of Parents and Their Hybrids for Relative Cell Injury and Seed Cotton Yield in F_2 Generation

The results for RCI and SCY in parents and F_2 progenies are presented in **Table 5**. Among parents, RCI ranged between 40 and 80% in glasshouse and between 38 and 82% in field conditions. Tester NIA-Perkh, CRIS-342, and CRIS-134 showed minimum RCI in both regimes, whereas line NIA-148 showed maximum RCI in both glasshouse and field conditions. Among F_2progenies, RCI ranged between 38 and 72% in the glasshouse and 37 to 72% in field conditions. NIA-Perkh, CRIS-342 and CRIS-134 among parents had lowest, while NIA-148, Haridost, and Sohni had the highest relative cell injury percent. The crosses NIA-148 × NIA-Perkh, HariDost × CRIS-342, Sohni × CRIS-342, and NIA-148 × CRIS-342 had a lowest relative cell injury level percentage, which showed the stability in cell membrane among hybrids was below average RCI in both heat stress (i.e., glasshouse) and non-stress (i.e., field) regimes. For SCY, the results showed that the testers CRIS-324, NIA-Perkh, and CRIS-134 produced the highest SCY, whereas, three lines gave the lowest SCY under both temperature regimes. Among the crosses, HariDost × CRIS-342, HariDost × NIA-Perkh, Sohni × CRIS-342, Sohni × NIA-Perkh, and NIA-148 × NIA-Perkh showed better performance under both temperature regimes.

Values of HSI in parents and F_2 progenies (**Figure 4**) were ranged between 0.2 and 2.3%. Genotypes NIA-Perkh, CRIS-342, and CRIS-134 gave the lowest value for HSI. Among the

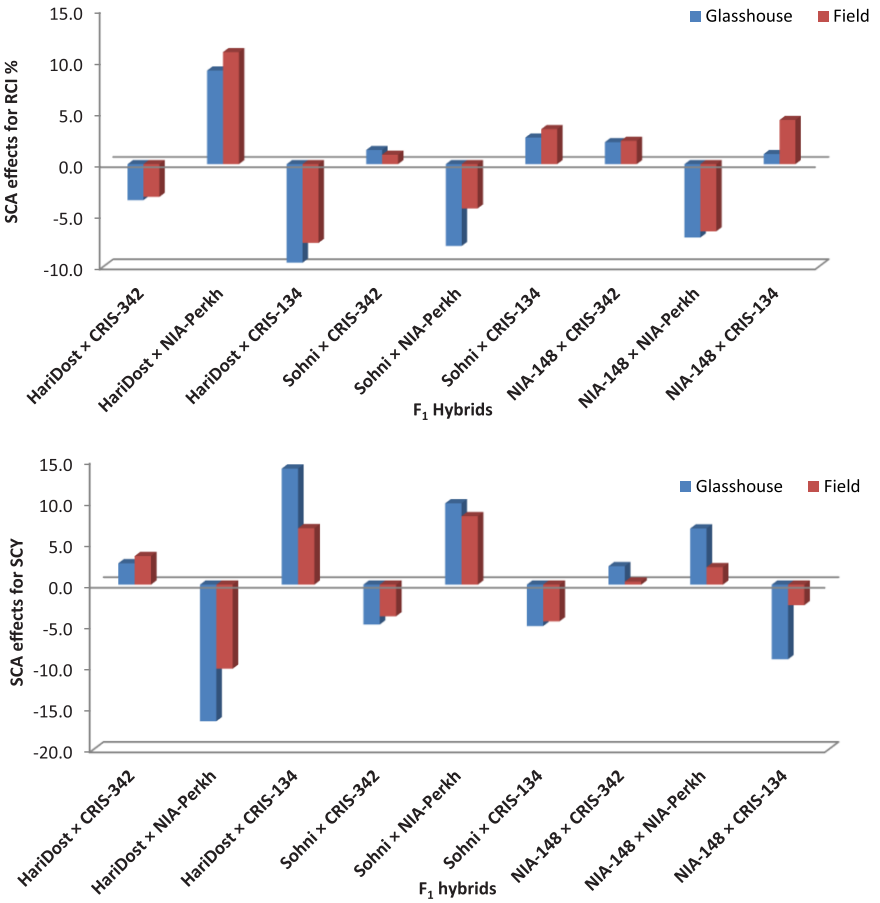

FIGURE 7 | Estimates of SCA effects for RCI% and SCY (g/plant) in F_1 generation of cotton genotypes in heat-stress (glasshouse) and non-heat-stress (field) conditions.

nine crosses, five crosses HariDost × CRIS-342, Sohni × NIA-CRIS-342, Sohni × NIA-Perkh, NIA-148 × NIA-Perkh, and NIA-148 × CRIS-342 gave the lowest value for HSI. The superior genotypes for heat tolerance gave the least values (HSI < 1) and high yield under heat stress conditions.

TABLE 6 | Heterotic effects for RCI% and SCY (g/plant) in F_1 generation.

Hybrids	RCI%				SCY (g/plant)			
	Glasshouse		Field		Glasshouse		Field	
	MPH	BPH	MPH	BPH	MPH	BPH	MPH	BPH
F_1 Generation								
Haridost × CRIS-342	−25	−7.8	−23	−8.4	36	10.1	27	12.3
Haridost × NIA-Perkh	−15	14.6	−13	13.7	10	−9.3	29	16.5
Haridost × CRIS-134	−8	9	−5	9.7	21	0.7	33	23.4
Sohni × CRIS-342	−18	0.5	−14	−0.2	32	9.1	16	8.4
Sohni × NIA-Perkh	−10	22.3	−4	21.3	42	19.4	29	22.8
Sohni × CRIS-134	−31	−18.1	−27	−17.5	4	−11.1	12	9.8
NIA-148 × CRIS-342	−32	−11.6	−27	−12.2	34	12.6	18	15.2
NIA-148 × NIA-Perkh	−29	0.9	−25	0.1	33	14.2	18	18.2
NIA-148 × CRIS-134	3	29.2	10	30.0	−6	−17.4	12	15.5

MPH, mid-parent heterosis; BPH, better parent heterosis.

Genetic Parameters of Relative Cell Injury and Seed Cotton Yield in F_2 Generation

As far as heritability and genetic advance for RCI% are concerned, crosses HariDost × CRIS-342, Sohni × CRI-342, Sohni × NIA-Perkh, and NIA-148 × NIA-Perkh displayed a high heritability and moderate genetic advance under both temperature regimes, while other crosses displayed a low heritability and low genetic advance. Lowest heritability and genetic advance were recorded in cross NIA-148 × CRIS-134 (**Table 7**).

For SCY, out of nine crosses, five crosses showed a high heritability along with high genetic advance. Sohni × CRIS-342, Sohni × NIA-Perkh, NIA-148 × CRIS-342, and HariDost × CRIS-342 displayed the highest heritability coupled with genetic advance under both temperature regimes, which is indicative of the additive type of gene action. However, NIA-148 × CRIS-134 and Sohni × CRIS-134 displayed the low heritability estimates coupled with low genetic advance (**Table 7**).

TABLE 7 | Genetic studies of RCI% and SCY (g/plant) in F_2 progenies.

Traits	F_2 Progenies	Genetic variance (σ^2g)		Heritability broad sense (h^2%)		Genetic advance (GA)	
		Glasshouse	Field	Glasshouse	Field	Glasshouse	Field
RCI%	Haridost × CRIS-342	5.10	22.0	82.95	87.2	20.23	21.0
	Haridost × NIA-Perkh	38.58	64.9	55.43	65.3	12.17	16.0
	Haridost × CRIS-134	61.42	51.2	51.28	65.8	15.42	11.3
	Sohni × CRIS-342	11.0	6.4	87.66	89.6	16.40	19.5
	Sohni × NIA-Perkh	53.42	17.8	92.10	88.1	14.45	17.1
	Sohni × CRIS-134	26.41	76.3	50.58	41.4	9.50	7.2
	NIA-148 × CRIS-342	3.76	26.6	60.05	45.4	3.09	7.2
	NIA-148 × NIA-Perkh	11.01	5.5	90.64	84.1	6.51	1.8
	NIA-148 × CRIS-134	145.04	86.4	43.94	53.3	11.34	10.4
SCY (g/plant)	Haridost × CRIS-342	783.45	237.8	88.67	84.4	54.29	41.2
	Haridost × NIA-Perkh	330.52	539.7	44.48	59.4	12.32	19.9
	Haridost × CRIS-134	1141.1	621.6	42.22	58.6	6.83	4.0
	Sohni × CRIS-342	1571.2	364.2	95.23	75.4	59.69	54.1
	Sohni × NIA-Perkh	1439.7	539.3	94.00	90.1	55.79	65.4
	Sohni × CRIS-134	521.90	840.6	47.46	42.6	4.01	4.3
	NIA-148 × CRIS-342	1116.6	1345.9	93.26	87.7	66.48	70.8
	NIA-148 × NIA-Perkh	519.96	564.0	85.37	81.3	43.40	44.1
	NIA-148 × CRIS-134	173.33	376.6	51.43	60.4	5.50	3.1

DISCUSSION

In the present study, the temperature at peak flowering in early sowing (March) was high (44.2/32.2°C) as compared with normal sowing (39.8/28.4°C) during the month of May. Both temperature regimes in the field were able to expose the studied genotypes to differential responses, resulting in significant sowing the date × genotypes interaction. Previously, Rahman et al. (2004) reported a highly significant genotype × temperature interaction in field. The present study reports seventeen heat-tolerant genotypes, identified on the basis of low RCI% (40–50) and HSI (<1), higher boll retention, and SCY. Differential responses of genotypes to heat in terms of RCI were consistent under heat stress and non-stress regimes. RCI is an indicator of cellular heat tolerance, i.e., high RCI (>70%) means low CMT and vice versa (Khan et al., 2008). Heat-tolerant genotypes produced a high SCY with high GOT% and staple length, while susceptible genotypes were low yielding with inferior fiber traits. Our results are in confirmation with the reports of Azhar et al. (2009) and Karademir et al. (2012). HSI was also used as an extent of relative decrease in yield influenced by non-favorable vs. favorable environments. Results indicated the values of HSI < 1 for heat-tolerant genotypes. Previously, Hafeez-ur-Rahman (2006) measures the heat tolerance in cotton at the whole-plant level using the heat-tolerant index. The SEM study of heat-tolerant genotypes along with susceptible check revealed a wide range of stomata and trichome size present on leaves of these genotypes. Galdon-Armero et al. (2018) reported that ratio of trichomes to stomata in cotton is associated with the efficiency of water use. Lei et al. (2018) observed the linkage of the efficiency of water use with variation between veins and stomata under drought stress. In the present study, a strong negative association of RCI% and stomata size with SCY suggested that low RCI% and small stomata are reliable indicators of genotypic heat tolerance response. This analysis indicated that simultaneous selection of high SCY and heat tolerance would be effective in the presence of heat stress. However, density and length of trichomes on the leaf surface, which protect against excessive radiation and reduce the effect of high temperature, were found non-significant, and these results are in contradiction with Celka et al. (2006) and Passos et al. (2009) who emphasized that trichomes play an important role in reducing biotic and abiotic effects. Another study was conducted for evaluating the heat tolerance and stability in multienvironments. The results showed that all selected genotypes were high yielding and stable as compared with the susceptible check and may be tested over all environments to attain an additional stable performance. These findings are in confirmation with some previous reports (Killi and Harem, 2006; Khan et al., 2007; Riaz et al., 2013), which observed the stability and G × E interaction in genotypes of cotton and the effect on SCY. The ability to the combination of some heat-tolerant genotypes was also estimated by a line × tester method among nine hybrids along with their 3 testers (i.e., male) and 3 lines (i.e., females). Genotypes CRIS-342 and NIA-Perkh were observed as best general combiners for SCY with negative GCA effects for RCI%. This finding is in confirmation with the reports of Jatoi et al. (2010) and Srinivas et al. (2014). Five hybrids showed positive SCA and negative heterotic effects for RCI% and also found lowest for HSI. This is in accordance with some previous studies of Abro et al. (2009) and Nidagundi et al. (2012). These findings suggested that the expression of RCI% under field regimes was predominantly controlled by combining ability because of additive genetic variability. Relative contribution of lines or testers individually as compared with lines × testers was

also high for RCI and SCY under both temperature regimes, depicting a comparatively significant role of additive genetic variability in the expression of RCI and SCY. In cotton heat tolerance breeding programs, these results are important for selection point of view from segregating populations (Baloch and Bhutto, 2003). In the present study, RCI% and SCY/plant also displayed higher estimates of heritability and genetic advance, indicating the heritability due to additive gene effects and chances of effective selection. Alike degree of heritability and genetic advance were also got by Khan (2002) and Ahsan et al. (2015). The combination of high heritability and genetic advance provides clear picture of the trait in the selection process. The results for additive gene action are in confirmation with the results of Kumaresan et al. (2000) and Larik et al. (2000).

CONCLUSION

Selection criteria involving CMT and stomata size concluded to be an effective strategy for the screening of heat-tolerant cotton. Low RCI% and small stomata are good indicators of heat tolerance in optimum as well as heat stress environment. These traits have a good association with SCY. The line × tester analysis revealed two best general combiners for SCY with negative GCA effects for RCI% and five hybrids with positive SCA and heterotic effects for studied traits. Vigilant and rigorous selection of the developed segregating material recognized the heat-tolerant progenies with improved reproductive traits. The identified heat tolerant and wide adaptive germplasm can be further advanced for the release of commercial heat-tolerant cotton varieties.

DATA AVAILABILITY STATEMENT

The original contributions presented in the study are included in the article/**Supplementary Material**, further inquiries can be directed to the corresponding author.

AUTHOR CONTRIBUTIONS

SaA conceived the idea, executed experiments, recorded the data in the field and laboratory, and prepared the draft manuscript. MR helped in the execution of field and lab experiments, data recording, and analysis and was a major contributor in writing and finalization of the manuscript. ZD helped in execution of field experiments including multilocation trials. ShA performed the data analysis. MS validated the idea, supervised the work, and provided technical inputs in the execution of field experiments. All authors have read and approved the manuscript.

SUPPLEMENTARY MATERIAL

The Supplementary Material for this article can be found online at: https://www.frontiersin.org/articles/10.3389/fpls.2021.804315/full#supplementary-material

REFERENCES

Abro, S., Kandhro, M. M., Laghari, S., Arain, M. A., and Deho, Z. A. (2009). Combining ability and heterosis for yield contributing traits in upland cotton (*Gossypium hirsutum* L.). *Pak. J. Bot.* 41, 1769–1774.

Abro, S., Rajput, M. T., Khan, M. A., Sial, M. A., and Tahir, S. S. (2015). Screening of cotton (*Gossypium hirsutum* L.) genotypes for heat tolerance. *Pak. J. Bot.* 47, 2085–2091.

Ahsan, M. Z., Majidano, M. S., Bhutto, H., Soomro, A. W., Panhwar, F. H., Channa, A. R., et al. (2015). Genetic variability, coefficient of variance, heritability and genetic advance of some Gossypium hirsutum L. accessions. *J. Agric. Sci.* 7, 147–153. doi: 10.5539/jas.v7n2p147

Allard, R. W. (1960). *Principles of Plant Breeding*. Hoboken, NJ: John Wiley and Sons Inc, 96.

Anonymous. (2018–2019). *Economic Survey of Pakistan*. Islamabad: Ministry of Finance, Govt. of Pakistan.

Azhar, F. M., Ali, Z., Akhtar, M. M., Khan, A. A., and Trethowan, R. (2009). Genetic variability of heat tolerance and its effect on yield and fibre quality traits in upland cotton (*Gossypium hirsutum* L.). *Plant Breed.* 128, 356–362. doi: 10.1111/j.1439-0523.2008.01574.x

Azhar, M. T., Khan, A. A., and Khan, I. A. (2005). Combining ability analysis of heat tolerance in *Gossypium hirsutum* L. *Czech J. Genet. Plant Breed.* 41, 23–28. doi: 10.17221/3678-CJGPB

Baloch, M. J., and Bhutto, H. U. (2003). Design–II analysis of estimating general and specific combining ability effects of cotton leaf curl virus resistant inbred parents. *Zagazig J. Agric. Res.* 30, 635–639.

Bibi, A. C., Oosterhuis, D. M., Brown, R. S., Gonias, E. D., and Bourland, F. M. (2003). "The physiological response of cotton to high temperatures for germplasm screening," in *Summaries of Arkansas Cotton Research*, Vol. 521, ed. D. M. Oosterhuis (Fayetteville, AR: Arkansas Agricultural Experiment Station), 87–93.

Celka, Z., Szkudlarz, P., and Bierężnoj, U. (2006). Morphological variation of hairs in *Malvaalcea L.* (Malvaceae). *Biodiv. Res.Conserv.* 3, 258–261.

Cochran, W. G., and Cox, G. M. (1957). *Experimental Designs*. New York, NY: John Wiley and Sons. Inc, 661.

Cottee, N. S., Tan, D. K. Y., Bange, M. P., Cothren, J. T., and Campbell, L. C. (2010). Multi-level determination of heat tolerance in cotton (*Gossypium hirsutum* L.) under field conditions. *Crop Sci.* 50, 2553–2564. doi: 10.2135/cropsci2010.03.0182

Eberhart, S. A., and Russell, W. A. (1966). Stability parameters for comparing varieties. *Crop Sci.* 6, 36–40. doi: 10.2135/cropsci1966.0011183X000600010011x

Fischer, R. A., and Maurer, R. (1978). Drought resistance in spring wheat cultivars. I. Grain yield responses. *Aust. J. Agric. Res.* 29, 897–912. doi: 10.1071/AR9780897

Galdon-Armero, J., Fullana-Pericas, M., Mulet, P. A., Conesa, M. A., Martin, C., and Galmes, J. (2018). The ratio of trichomes to stomata is associated with water use efficiency in *Solanum lycopersicum* (tomato). *Plant J.* 96, 607–619. doi: 10.1111/tpj.14055

Hafeez-ur-Rahman. (2006). Environmental interaction, additive and non-additive genetic variability is involved in the expression of tissue and whole-plant heat tolerance in upland cotton (*Gossypium hirsutum* L). *Genet. Mol. Biol.* 29, 525–532. doi: 10.1590/S1415-47572006000300022

Hayat, M. A. (1989). *Principles and Techniques of Electron Microscopy. Biological Applications*, 3rd Edn. Houndmills: Macmillan Press. doi: 10.1007/978-1-349-09857-6

International Cotton Advisory Committee [ICAC] (2018). 'Cotton: Review of the World Situation': The 2018/19 Season Featured Rollercoaster Prices, with Decreasing Production, Area and Yields. Available online at: https://icac.org/News/NewsDetails?NewsId=2314&YearId=2019 (accessed April 10, 2021).

Ismail, A. M., and Hall, A. E. (1999). Reproductive stage heat tolerance, leaf membrane thermostability and plant morphology in cowpea. *Crop Sci.* 39, 1762–1768. doi: 10.2135/cropsci1999.3961762x

Jatoi, W. A., Baloch, M. J., Khan, N. U., Veesar, N. F., and Batool, S. (2010). Identification of potential parents and hybrids in intraspecific crosses of upland cotton. *Sarhad J. Agric.* 26, 25–30.

Jones, D. C., Gore, M. A., Sanchez, P. A., Fang, D., Hunsaker, D., White, J., et al. (2014). "High- throughput phenotyping of drought-adaptive traits in cotton," in *Proceedings of the Abstracts Belt Wide Cotton Conference*. New Orleans, LA.

Karademir, E., Karademir, Ç, Ekinci, R., and Basbag, S. (2012). Screening cotton varieties (*Gossypium hirsutum* L.) for heat tolerance under field conditions. *Afr. J. Agric. Res.* 7, 6335–6342.

Kempthorne, O. (1957). *An Introduction to Genetic Statistics*. New York, NY: John Wiley & sons, 191–200.

Khan, A. I., Khan, I. A., and Sadaqat, H. A. (2008). Heat tolerance is variable in cotton (*Gossypium hirsutum* L.) and can be exploited for breeding of better yielding cultivars under high temperature regimes. *Pak. J. Bot.* 40, 2053–2058.

Khan, N. G., Naveed, M., Islam, N. U., and Iqbal, M. S. (2007). Assessment of new upland cotton genotypes (*Gossypium hirsutum* L.) for yield stability and adaptability. *Asian J. Plant Sci.* 6, 1012–1017. doi: /10.3923/ajps.2007.1012.1015

Khan, U. Q. (2002). Study of heterosis in fiber quality traits of upland cotton. *Asian J. Plant Sci.* 1, 593–595. doi: 10.3923/ajps.2002.593.595

Killi, F., and Harem, E. (2006). Genotype × environment interaction and stability analysis of cotton yield in Aegean region of Turkey. *J. Environ. Biol.* 37, 427–430.

Kumaresan, D., Ganesan, J., and Ashok, S. (2000). Genetic analysis of qualitative characters in cotton (*Gossypium hirsutum* L.). *Crop Res.* 19, 481–484.

Larik, A. S., Malik, S. I., Kakar, A. A., and Naz, M. A. (2000). Assessment of heritability and genetic advance for yield and yield components in *Gossypium hirsutum* L. *Sci. Khyb.* 13, 39–44.

Lei, Z. Y., Han, J. M., Yi, X. P., Zhang, W. F., and Zhang, Y. L. (2018). Coordinated variation between veins and stomata in cotton and its relationship with water-use efficiency under drought stress. *Photosynthetica* 56, 1326–1335. doi: 10.1007/s11099-018-0847-z

Nidagundi, J. M., Patil, S. S., Salimath, P. M., Kajjidoni, S. T., Patil, B. C., and Hegde, M. G. (2012). Heterobeltiosis in multiple environments for seed cotton yield and yield attributes in cotton (*Gossypium hirsutum* L.). *Karnataka J. Agric. Sci.* 25, 301–304.

Organisation for Economic Co-operation Development/Food and Agriculture Organization [OECD/FAO] (2019). *OECD-FAO Agricultural Outlook, OECD Agriculture statistics (database)*. Available online at: http://dx.doi.org/10.1787/agr-outl-data-en (accessed December 1, 2020).

Passos, J. L., Meira, R. M. S. A., and Barbosa, L. C. A. (2009). Foliar anatomy of the species *Lantana camara* and *L. radula* (Verbenaceae). *Planta Danin.* 27, 689–700. doi: 10.1590/S0100-83582009000400007

Pakistan Central Cotton Committee [PCCC] (2014). *Summary Progress Report of National Coordinated Varietal Trials, 2013-14*. Karachi: PCCC.

Rahman, H., Malik, S. A., and Saleem, M. (2004). Heat tolerance of upland cotton during the fruiting stage evaluated using cellular membrane thermostability. *Field Crop Res.* 85, 149–158. doi: 10.1016/S0378-4290(03)00159-X

Rana, R. M., Khan, S. H., Ali, Z., Khan, A. I., and Khan, I. A. (2011). Elucidation of thermo tolerance diversity in cotton (*Gossypium hirsutum* L.) using physio-molecular approaches. *Genet. Mol. Res.* 10, 1156–1167. doi: 10.4238/vol10-2gmr1180

Riaz, M., Naveed, M., Farooq, J., Farooq, A., Mahmood, A., Rafiq, C. M., et al. (2013). AMMI analysis for stability, adaptability and GE interaction studies in cotton (*Gossypium hirsutum* L.). *J. Anim. Plant Sci.* 23, 865–871.

Singh, R. K., and Chaudhary, B. D. (1999). *Biometrical Methods in Quantitative Genetic Analysis*. New Delhi: Kalyani Publisher, 1–303.

Singh, R. P., Prasad, P. V., Sunita, K., Giri, S. N., and Reddy, K. R. (2007). Influence of high temperature and breeding for heat tolerance in cotton: a review. *Adv. Agron.* 93, 313–385. doi: 10.1016/S0065-2113(06)93006-5

Srinivas, B., Bhadru, D., Rao, M. B., and Gopinath, M. (2014). Combining ability studies for yield and fibre quality traits in upland cotton (*Gossypium hirsutum* L.). *SABRAO J. Breed. Genet.* 46, 313–318.

Steel, R. G. D., Torrie, J. H., and Dickey, D. A. (1997). *Principles and Procedures of Statistics: A Biometrical Approach*. New York, NY: McGraw Hill Book Co. Inc, 400–428.

Sullivan, C. Y. (1972). "Mechanisms of heat and drought resistance in grain sorghum and methods of measurements," in *Sorghum in Seventies*, eds N. G. P. Rao and L. R. House (New Delhi: Oxford and IBH Publishing Co), 247–264.

Conflict of Interest: The authors declare that the research was conducted in the absence of any commercial or financial relationships that could be construed as a potential conflict of interest.

Publisher's Note: All claims expressed in this article are solely those of the authors and do not necessarily represent those of their affiliated organizations, or those of the publisher, the editors and the reviewers. Any product that may be evaluated in this article, or claim that may be made by its manufacturer, is not guaranteed or endorsed by the publisher.

Copyright © 2022 Abro, Rizwan, Deho, Abro and Sial. This is an open-access article distributed under the terms of the Creative Commons Attribution License (CC BY). The use, distribution or reproduction in other forums is permitted, provided the original author(s) and the copyright owner(s) are credited and that the original publication in this journal is cited, in accordance with accepted academic practice. No use, distribution or reproduction is permitted which does not comply with these terms.

frontiers in Plant Science

ORIGINAL RESEARCH
published: 05 January 2022
doi: 10.3389/fpls.2021.800081

Comparative Analysis of Physiological, Enzymatic, and Transcriptomic Responses Revealed Mechanisms of Salt Tolerance and Recovery in *Tritipyrum*

Ze Peng[1,2†], Yiqin Wang[1†], Guangdong Geng[1], Rui Yang[1], Zhifen Yang[1], Chunmiao Yang[1], Ruhong Xu[1,3], Qingqin Zhang[1], Kaleem U. Kakar[4], Zhenhua Li[1,3] and Suqin Zhang[1,3]**

[1]College of Agriculture, Guizhou University, Guiyang, China, [2]Research Institute of Pepper, Guizhou Academy of Agricultural Sciences, Guiyang, China, [3]Guizhou Subcenter of National Wheat Improvement Center, Guiyang, China, [4]Department of Microbiology, Faculty of Life Sciences and Informatics, Balochistan University of Information Technology, Engineering and Management Sciences, Quetta, Pakistan

OPEN ACCESS

Edited by:
Raul Antonio Sperotto, Universidade do Vale do Taquari - Univates, Brazil

Reviewed by:
Salah El-Sayed El-Hendawy, King Saud University, Saudi Arabia
Mahmoud Yaish, Sultan Qaboos University, Oman

***Correspondence:**
Zhenhua Li
zhli3@gzu.edu.cn
Suqin Zhang
zsqin2002@163.com

[†]These authors have contributed equally to this work

Specialty section:
This article was submitted to Plant Abiotic Stress, a section of the journal Frontiers in Plant Science

Received: 22 October 2021
Accepted: 30 November 2021
Published: 05 January 2022

Citation:
Peng Z, Wang Y, Geng G, Yang R, Yang Z, Yang C, Xu R, Zhang Q, Kakar KU, Li Z and Zhang S (2022) Comparative Analysis of Physiological, Enzymatic, and Transcriptomic Responses Revealed Mechanisms of Salt Tolerance and Recovery in Tritipyrum. Front. Plant Sci. 12:800081. doi: 10.3389/fpls.2021.800081

Salt stress results in the severe decline of yield and quality in wheat. In the present study, salt-tolerant *Tritipyrum* ("Y1805") and salt-sensitive wheat "Chinese Spring" ("CS") were selected from 121 wheat germplasms to test their physiological, antioxidant enzyme, and transcriptomic responses and mechanisms against salt stress and recovery. 56 chromosomes were identified in "Y1805" that comprised A, B, and D chromosomes from wheat parent and E chromosomes from *Thinopyrum elongatum*, adding to salt-tolerant trait. Salt stress had a greater inhibitory effect on roots than on shoots, and "Y1805" demonstrated stronger salt tolerance than "CS." Compared with "CS," the activities of superoxide dismutase and catalase in "Y1805" significantly increased under salt stress. "Y1805" could synthesize more proline and soluble sugars than "CS." Both the net photosynthetic rate and chlorophyll a/b were affected by salt stress, though the level of damage in "Y1805" was significantly less than in "CS." Transcriptome analysis showed that the differences in the transcriptional regulatory networks of "Y1805" were not only in response to salt stress but also in recovery. The functions of many salt-responsive differentially expressed genes were correlated closely with the pathways "peroxisome," "arginine and proline metabolism," "starch and sucrose metabolism," "chlorophyll and porphyrin metabolism," and "photosynthesis."

Keywords: wheat, salinity tolerance, growth, antioxidases, osmoregulators, molecular response

INTRODUCTION

Wheat is a global food crop that is fundamental to human civilization. Over 759 million metric tons were consumed in the 2020/2021 marketing year (Ahmad et al., 2016). Soil salinity is one of the most serious types of abiotic stress, known for its detrimental effects on plant growth, development, and productivity, it leads to significant crop yield losses. Soil salinity is

one of the most damaging abiotic stresses and a major global problem in modern agriculture (Isayenkov and Maathuis, 2019). Among different factors, salt stress primarily induces higher osmotic pressure in soil solutions due to the accumulation of salt. This results in the impairment of crop growth, overall development, and production. Studies on plant abiotic stress management have shown that both seed germination and subsequent seedling emergence are inhibited by salt stress because of retarded water absorption (Sohrabikertabad et al., 2012; Shu et al., 2017; Li et al., 2020; Zeng et al., 2021). Additionally, a reduction in leaf areas, stomatal conductance, plant heights, and shoot and root weights were observed under salt stress (Mahmood and Quarrie, 1993; Qureshi and Daba, 2019). Globally, about 6% of the soil surface is affected by salt stress, especially in arid and semi-arid regions, where there is insufficient rainfall to filter salt from the upper layers of the soil (Rai et al., 2018). Research has shown that 50% of the world's arable land will be lost by the middle of the 21st century due to increasing salinization (Goyal et al., 2016). Therefore, the improvement and use of saline soil are considered important for the sustainable development of agriculture. This necessitates a search for plants that are tolerant to salt stress in addition to providing food.

Salt stress induces many physiological responses in plants, mainly through ion stress, osmotic stress, and oxidative stress (Yang and Guo, 2018; Sikder et al., 2020). For instance, some initial responses, such as membrane rupture, accumulation of compatible solutes, and reduction of carbon assimilation, are stimulated by osmotic stress. Similarly, Na^+ and Cl^- are absorbed by plants through transporters and ion channels, resulting in ion toxicity and nutrient imbalance (Han et al., 2015). In addition, the levels of reactive oxygen species (ROS) in plant cells increase, leading to oxidative stress, lipid peroxidation, membrane degradation, and damage to DNA and proteins (Arif et al., 2020). Under salt stress, plants respond through osmotic regulation, ion homeostasis, hormone regulation, photosynthesis, and antioxidant defense systems (Mushtaq et al., 2020; Zhu et al., 2021). At the cellular level, the "salt overly sensitive" (SOS), "mitogen-activated protein kinase," and "abscisic acid (ABA) signal transduction" pathways are considered to be related to plant salt tolerance (Mishra et al., 2006; Huang et al., 2012; Zhu, 2016). Transporters, such as SOS1, high-affinity K^+ transporters, and Na^+/H^+ and K^+/H^+ exchangers, have been found to participate in K^+ and/or Na^+ homeostasis and stress tolerance in *Arabidopsis* (Shi et al., 2000; Baxter et al., 2010; Zhu, 2016). The molecular mechanism of plant salt tolerance is very complex, and a large amount of data is required to explore its regulatory network. Recently, genomic, transcriptomic, proteomic, and metabolomic methods have been used to predict regulatory genes and signal pathways in *Arabidopsis* and other species (Abdel-Farid et al., 2020; Han et al., 2020; Yan et al., 2021).

The E genome species (e.g., halophile wheatgrass *Thinopyrum elongatum*) of the *Triticeae* possess salt-tolerant properties, making them invaluable sources for genetic variation and the improvement of wheat crops (Jauhar, 1990; Munns and Tester, 2008; Margiotta et al., 2020). *Tritipyrum* derived from the wide crosses of *Triticum* and *Thinopyrum* displays salt tolerance (Omielan et al., 1991; Yuan and Tomita, 2015). The amphiploid from a cross between common wheat "Chinese Spring" ("CS") and salt-tolerant *T. elongatum* (Host) Löve, greatly outperformed "CS" in grain yield, biomass, and other characters under salt stress. The presence of the E genome of wheat was associated with the exclusion of Na^+ and $C1^-$ and inclusion of K^+ as well as retranslocation of K^+. In the current work, the potential salt tolerance in salt-tolerant *Tritipyrum* ("Y1805") was studied with an objective of understanding the physiological, biochemical, and molecular mechanisms of salt tolerance in *Tritipyrum* hybrids. The results of this work will provide valuable information for the breeding and improvement of salt-tolerant wheat.

MATERIALS AND METHODS

Plant Materials

A total of 121 germplasms were screened, including cultivars from common wheat, the progeny of wide cross and rye. Two wheat varieties, "Y1805" (salt-tolerant *Tritipyrum*) and "CS" (salt-sensitive common wheat "Chinese Spring") were used in this investigation (Omielan et al., 1991; Guo et al., 2012; Yuan and Tomita, 2015). "Y1805" is a stable progeny from a wide cross between common wheat and *T. elongatum*.

Preliminary Screening of Materials

For the current work, complete and uniform wheat seeds were thoroughly selected, disinfected with 70% alcohol for 1 min, and then washed repeatedly with sterilized distilled water. The seeds were soaked in Petri dishes with two layers of wet filter paper. After germination, seedlings with the same growth vigor were selected and planted in a 24-hole tray with peat substrate. Five seedlings were planted in each hole (36 cm^2 per hole), and three holes were sown for each germplasm. On the 7th day after germination, seedlings were subjected to salt stress treatment for 14 days by watering NaCl solution (180 mM), and sterilized distilled water was used as control. Plant growth was maintained at 24/18°C for a 16/8 h light/dark photoperiod with an irradiance of 400 $\mu mol\, m^{-2}\, s^{-1}$. The experiment was repeated three times. The roots were cleaned to remove peat substrate and then extracted from the root–stem interface. Root fresh weight (RFW), shoot fresh weight (SFW), root dry weight (RDW), and shoot dry weight (SDW) were measured for all 121 germplasms. RDW and SDW measurements were taken after that the roots and shoots were oven-dried at 90°C for 48 h. We evaluated RFW, SFW, RDW, and SDW of 121 germplasms through membership function (Ding et al., 2018), obtained the membership function value of each germplasm, and conducted cluster analysis based on within-group linkage and squared Euclidean distance (Hunter and Mccoy, 2004).

Sequential GISH-FISH Analysis

Genomic *in situ* hybridization (GISH) and fluorescence *in situ* hybridization (FISH) were performed as described by Kato et al. (2004) and Han et al. (2006). The labeled genomic DNA of *T. elongatum* was used as a probe for GISH analysis. Oligo-pAs1-1,

Oligo-pAs1-3, Oligo-pAs1-4, Oligo-pAs1-6, Oligo-AFA-3, Oligo-AFA-4 (red), Oligo-pSc119.2-1, and $(GAA)_{10}$ (green) probes were used according to Du et al. (2017). Oligonucleotide probes were synthesized by Shanghai Invitrogen Biotechnology Co. Ltd. (Shanghai, China). The slides were mounted in Vectashield antifade solution containing 4′-6-diamino-2-phenylindole (DAPI; Vector Laboratories Inc., Burlingame, CA, United States). A fluorescence microscope (BX60, Olympus Corp., Tokyo, Japan) fitted with a Spot CCD camera was used to capture hybridization signals. The images were compiled with CellSens Vers.1.5 Imaging software (Olympus Corp.).

Growth Conditions and Stress Treatment

The seeds of "Y1805" and "CS" were germinated in a growth chamber at 24/18°C and relative humidity of 75%. The seedlings were transferred to 1/2 Hoagland solution and incubated under 16/8 h of light/dark with an irradiance of 400 μmol $m^{-2} s^{-1}$ and germinated at the same temperature and humidity as in the chamber. The culture solution was refreshed every 3 days. On the 14th day (two-leaf stage), uniformed-sized roots and tops were collected as the first samples (T1 stage, no salt stress). Then, 250 mM NaCl salt stress treatment (NaCl +1/2 Hoagland solution) was applied. The second and third samples were selected at 5 h (T2 stage) and 24 h (T3 stage) respectively after salt stress treatment. Afterward, salt stress was removed, and the materials were recovered. The fourth and fifth samplings were performed at 1 h (R1 stage) and 24 h (R2 stage) after recovery. These sampling stages were chosen according to typical phenotypic observations. Normal (1/2 Hoagland solution) cultured materials were used as parallel controls. All the samples were immediately frozen in liquid nitrogen after sampling and stored at −80°C for physiological and biochemical analysis, transcriptomic analysis, and confirmational qRT-PCR.

Analysis of Growth, Physio-Biochemical Parameters

Analysis of Growth

Root dry weight and shoot dry weight were determined after roots and seedlings were oven-dried at 90°C for 48 h. Seminal root length (RL) and shoot height (SH) of "Y1805" and "CS" samples were measured at each stage.

Analysis of Photosynthesis

The chlorophyll contents of leaves were measured according to an assay by Arnon (Jain and Gadre, 1997). Chlorophyll a (Chl-a) and chlorophyll b (Chl-b) were extracted by 80% acetone, and their contents were read at 645 and 663 nm, respectively. The net photosynthetic rate (Pn) of leaves was measured using an LI-6400 XT portable photosynthesis system (Li-Cor Inc., Lincoln, NE, United States).

Analysis of Enzyme Activities

Enzyme Extraction

The subsequent biochemical and physiological parameters were measured using the roots of the wheat plants. Enzymes were extracted using the method of Xu et al. (2021). Briefly, 0.50 g of roots were collected and ground in 6 mL of 50 mM phosphate buffer (pH 5.5) containing 5 mM mercaptoethanol, 1 mM EDTA, and 1% polyvinylpyrrolidone in an ice bath, and then centrifuged at 3,550 *g* and 4°C for 10 min. The supernatant was used as the extract.

Spectrophotometric Assay

SOD (EC1.15.1.1). Total SOD activity was assayed by monitoring the inhibition of nitro blue tetrazolium (NBT) photochemical reduction by using the method by Jiang and Zhang (2001). The 3 mL reaction mixture contained 50 mM potassium phosphate buffer (pH 7.8), 13 mM methionine, 75 μm NBT, 2 μm riboflavin, 0.1 mM EDTA, and 100 μL enzyme extract. The reaction mixtures were illuminated for 15 min at a light intensity of 400 μmol $m^{-2} s^{-1}$. One unit of SOD activity was defined as the amount of enzyme required to cause 50% inhibition to the NBT reduction as monitored at 560 nm.

CAT (EC 1.11.1.6). The CAT activity was measured by its ability to decompose H_2O_2 (Aebi, 1984). The 3 mL mixture consisted of 50 mM potassium phosphate buffer (pH 7.0), 10 mM H_2O_2, and 200 μL of enzyme extract. The absorbance was observed at 240 nm.

Analysis of Osmoregulators

The Proline Content. A modified method by Bates et al. was used to measure the proline content (Bates et al., 1973). Briefly, 0.5 g of roots were extracted with 10 mL of 3% sulfosalicylic acid. After centrifugation of homogenate at 10,000 *g* for 10 min, 0.5 mL of the supernatant was added into 0.5 mL of ninhydrin and 0.5 mL of glycol acetic acid. The reaction was carried out at 100°C for 30 min. After cooling in an ice bath, 1 mL toluene was added and the absorbance of the mixture was measured at 520 nm. The proline content was determined according to a standard curve.

Soluble Sugar Content. The soluble sugar content was determined by the anthrone sulfuric acid method (Leyva et al., 2008). About 0.1 g anthrone was dissolved in 100 mL of 98% sulfuric acid and stored away from light. Then, 150 μL anthrone reagent was added into 50 μL of sample extraction solution. The samples were incubated at 100°C for 20 min. After cooling to room temperature, the absorbance was measured at 620 nm.

Transcriptome Analysis

The data obtained from phenotypic, physiological, and biochemical analysis were used to choose the two key sampling stages (T2 and R1) of "Y1805" and "CS" for further transcriptome analysis. Total RNA from the roots was extracted using TRIzol reagent (Thermo Fisher Scientific, Waltham, MA, United States) following the manufacturer's instructions, and then treated with TaKaRa RNase-free DNase I for 30 min. NanoDrop 1000 spectrophotometer was used to test the quantity and quality of the extracted RNA. A total of 20 μg RNA was used for cDNA library construction and transcriptome sequencing (BGISEQ-500) at the Beijing Genome Institute. After data

filtering, clean reads were obtained and then compared with the reference genome (wheat "CS," AABBDD) by using HISAT2 (version 2.1.0) software. Finally, fragments per kilobase of exon model per million mapped fragment (FPKM) values were calculated by RSEM (version 1.2.8), and the level of gene expression was quantified (Bates et al., 1973).

DEG Identification and Bioinformatics Analysis

The FPKM method was used to detect differentially expressed genes (DEGs) among the treatment and control samples (Trapnell et al., 2010). To compute the significance of the differences in gene expression levels, a false discovery rate (FDR) method was used to determine the threshold of the value of p. Then, the genes potentially regulated by treatment were identified using an FDR threshold <0.01, value of $p < 0.001$, and absolute $\log_2$fold change value ($|\log_2 FC| > 1$ between all three salt-treated and three salt-free samples using DESeq software (Anders and Huber, 2010). The Phyper function in the R package was used for enrichment analyses of Gene Ontology (GO) and Kyoto Encyclopedia of Genes and Genomes (KEGG).

Quantitative Real-Time PCR Validation

The candidate DEGs were verified by qRT-PCR. Total RNA extracted from root tissue was reverse transcribed into cDNA using PrimeScript™ RT reagent Kit with gDNA Eraser (Perfect Real-Time, Takara Bio, Dalian, China). An ABI step-one fluorescent quantitative PCR system (Applied Biosystems, Foster, CA, United States) was used to analyze the DEGs. The relative expression levels were calculated with the $2^{-\Delta\Delta Ct}$ method in three biological replications and three technical replications (Depuydt and Hardtke, 2011), and actin-7 (Accession No. LOC123057740) was used as the internal control.

Data Analysis

A randomized complete block design with three replications was employed in the experiments. The results were expressed as the mean and standard deviation of three separate replicates. Statistical software (SPSS 20.0, IBM Corp., Armonk, NY, United States) and graphics software (Origin 2018, OriginLab, Northampton, MA, United States) were used for the data analysis and subsequent representation. ANOVA and Duncan's multiple range tests were used to compare means and determine the differences between means at a significance level of $p < 0.05$. Pearson's correlation analysis of binary variables was performed, and two variables were considered significantly correlated at the $p < 0.05$ level. The cluster analysis was carried out by using the square Euclidean distance on the average linkage between groups.

RESULTS

Preliminary Salt-Tolerant Screening of Materials

We determined RFW, SFW, RDW, and SDW of 121 germplasm resources as indicators for salt tolerance. As shown in **Figure 1**, these germplasms were divided into three categories based on their salt tolerance indices (value for the sodium chloride treated plant/value for the control). Of these, "Y1805" was classified as salt-tolerant germplasm. "Y1805" is a distant hybrid of wheat, widely used in wheat breeding, and has been proven to be salt-tolerant. Whereas "CS" was classified as salt-sensitive germplasm (**Figure 1**), "CS" is considered an important variety in wheat genetics, and a proven salt-sensitive cultivar.

Sequential GISH-FISH Analysis of *Tritipyrum* "Y1805"

Using the labeled genomic DNA of *T. elongatum* as a probe, GISH analysis detected a group of chromosomes with a green signal in "Y1805" (**Figure 2A**), which confirmed that the alien chromosomes belonged to *T. elongatum*. "Y1805" chromosomes could be effectively distinguished by FISH analysis. It was demonstrated that "Y1805" not only had A, B, and D chromosomes from wheat parent but also contained a set of alien chromosomes that originated from the E genome of *T. elongatum* (**Figure 2**). For the E genome chromosomes, the red fluorescence signals were greater than the green signals and had a different karyotype pattern compared with the A, B, and D chromosomes of common wheat. Thus, both GISH and FISH analysis demonstrated that "Y1805" not only had three sets of chromosomes from common wheat but also had an E genome of chromosomes from *T. elongatum*. "Y1805" and "CS" were selected for subsequent molecular biology experiments.

Growth Responses to Salt Stress and Recovery in Two Wheat Varieties

The growth of crops under salt stress depends on their salt tolerance and resilience after the recovery (Guo et al., 2015). Our analysis of the growth indices indicated an inhibitory effect of salt stress in "CS" at the R2 stage, which was significantly less in "Y1805," especially in roots (**Figure 3**). Salt stress had a greater inhibitory effect on the root than the leaves (**Figure 3**). RL of salt-tolerant "Y1805" at the T3, R1, and R2 stages was significantly greater than the "CS" under both salt stress and recovery conditions, and there was no significant difference between the treatments and controls at each stage (**Figure 3A**). Compared with the control, the RL of salt-sensitive "CS" was reduced at each stage. A reduction in RL of 10.84% was observed at the R2 stage after recovery (**Figure 3A**). At the R2 stage, the RDW of recovered "Y1805" tissues did not show a significant difference compared with the control (**Figure 3B**) whereas that of the "CS" decreased significantly by 22.35% (**Figure 3B**). Relative to controls, no significant differences were observed in SH of "Y1805" at each stage of the salt stress and recovery, except for a slight increase at the R2 stage (**Figure 3C**). On the other hand, the SH of "CS" was comparatively higher, yet exhibited no significant difference compared with the controls at each stage (**Figure 3C**). Similar results were noted for SDW. At the R2 stage, the SDW of "Y1805" and "CS" decreased by 11.30 and 13.83%, respectively (**Figure 3D**). At the R2 stage, the absolute values of RDW and SDW in

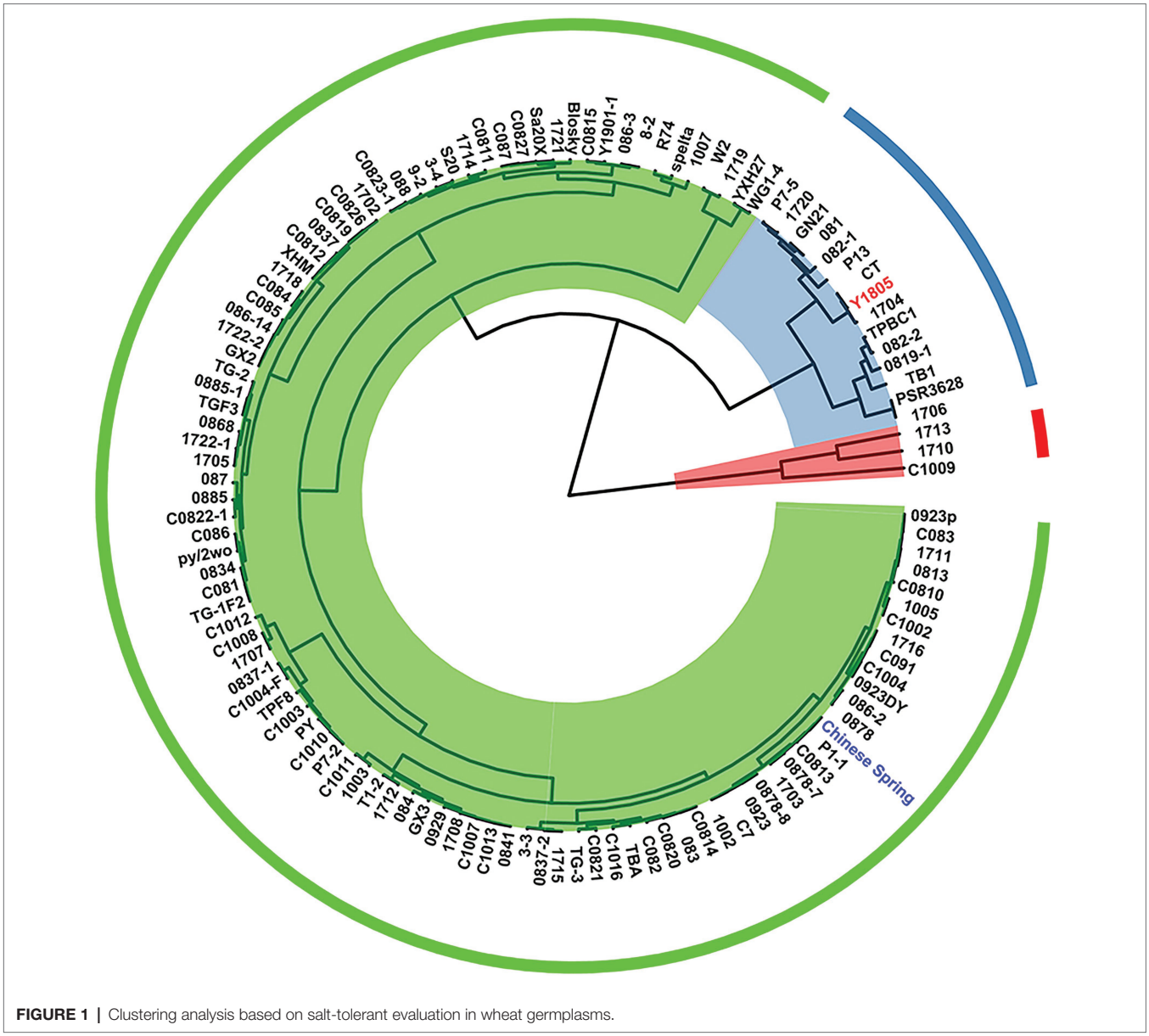

FIGURE 1 | Clustering analysis based on salt-tolerant evaluation in wheat germplasms.

"Y1805" were less than those of the "CS" under normal and treatment conditions because of their different genotypes. Overall, RL, RDW, and SDW of "CS" were significantly lower than those of the controls at the R2 stage, whereas there was no significant difference in RL and RDW shown by "Y1805," and an even slightly higher SH than that of the control, which may be attributed to differences in their mechanisms toward salt stress and recovery.

Physio-Biochemical Responses to Salt Stress and Recovery in Two Wheat Varieties

Analysis of Antioxidant Enzyme Activities

Antioxidant enzyme activity is an important index to measure the ability of plants to resist salt stress. Superoxide dismutase (SOD) and catalase (CAT) enzymes help plants in the defense against possible oxidative damage (Agami, 2014). Here, we assessed the activities of SOD and CAT in two wheat varieties subjected to salt stress and recovery. Compared with the controls, the activities of SOD and CAT sharply increased in "Y1805" during salt stress and recovery stages, whereas only CAT activity was dramatically increased in "CS" (**Figure 4**). The SOD activity of "Y1805" began to rise sharply at the T2 stage and peaked at the T3 stage under salt stress, which was ~2.16 and ~2.60-fold higher than the "CS" and control, respectively (**Figure 4A**). The SOD activity in "Y1805" was maintained at a higher level during the R1 and R2 recovery stages after a gradual decline. The SOD activity of "CS" increased slowly during salt stress, and the difference between the treatment and control was significant only at the T3 stage. The CAT activity of "Y1805"

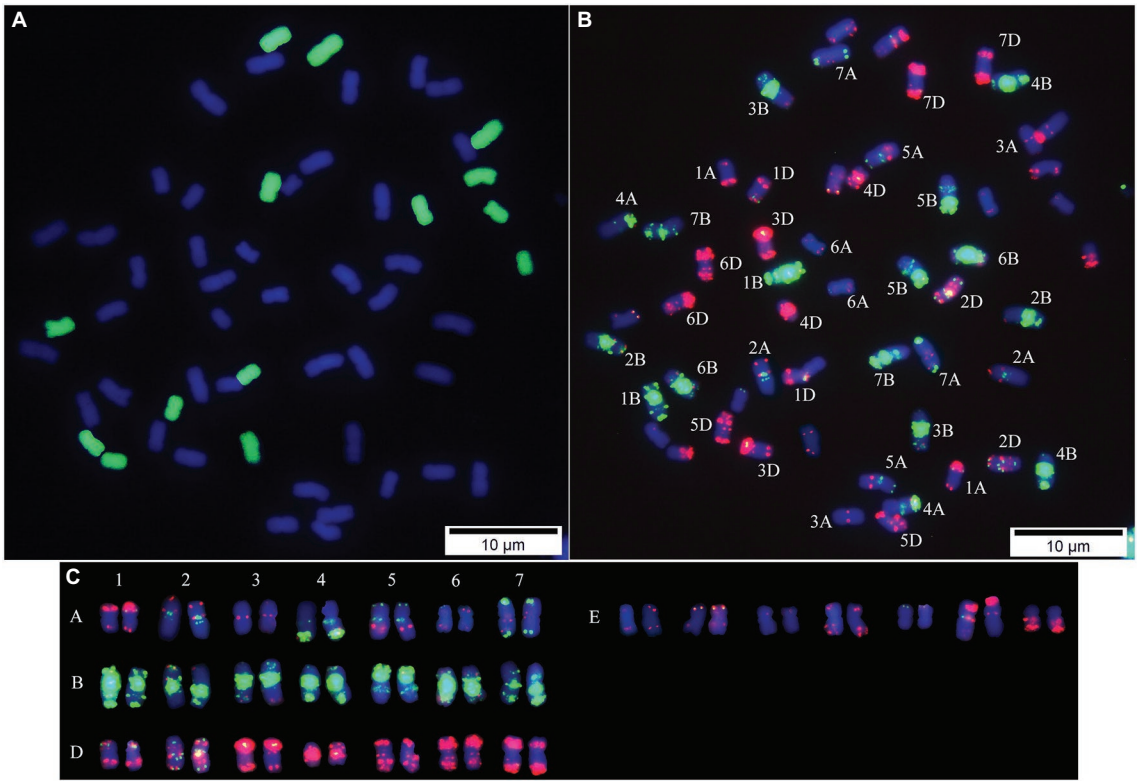

FIGURE 2 | Sequential GISH-FISH analysis of *Tritipyrum* ("Y1805"). **(A)** GISH patterns of chromosomes of "Y1805" using labeled genomic DNA of *Thinopyrum elongatum* as the probe (green). **(B)** FISH patterns of "Y1805" chromosomes using Oligo-pAs1-1, Oligo-pAs1-3, Oligo-pAs1-4, Oligo-pAs1-6, Oligo-AFA-3, Oligo-AFA-4 (red), Oligo-pSc119.2–1 and $(GAA)_{10}$ (green) probes, counterstained with DAPI (blue). **(C)** FISH karyotypes of "Y1805".

increased significantly from the T2 stage and reached a peak at the T3 stage, and then decreased rapidly after recovery (**Figure 4B**). This trend demonstrated that "Y1805" enhanced CAT activity rapidly under salt stress to protect the cells from damage caused by ROS, and reduced quickly after recovery. In "CS," the CAT activity increased slowly during salt stress, peaked at the R1 stage, and dropped afterward. The general trend of the two species was similar, the activities of antioxidant enzymes began to rise after salt stress, and began to decline during the recovery process, which indicated that wheat could cope with salt stress by adjusting the activities of antioxidant enzymes.

Analysis of Osmoregulation

Proline and soluble sugar are important regulators for the ability of plants to cope with osmotic stress caused by salt stress. Our results indicated that the salt stress and recovery responses of "Y1805" were stronger and faster than those of "CS." During development under normal conditions, and under stress and recovery, levels of osmoregulants were generally higher in "Y1805" than in "CS" (**Figure 5**). Under salt stress, the contents of both proline and soluble sugar in "Y1805" increased significantly from the T2 stage, peaked at the R1 stage, and then gradually declined. The proline content of "Y1805" began to rise at the T2 stage under salt stress and reached maximum at the R1 stage, which was ~2.00 and ~2.46-fold higher than "CS" and the control, respectively (**Figure 5A**). Similarly, the soluble sugar content in "Y1805" increased rapidly from the T2 stage, kept stable until the R1 stage, and returned to the control level at the R2 stage (**Figure 5B**). The soluble sugar content of the "Y1805" was ≥1.40-fold higher than the "CS" and control at the T2, T3, and R1 stages. In "CS," the proline content increased from the T1 to T2 stages, suddenly declined to a slightly lower level than the control at the T3 stage, and increased at the R1 stage. In addition, the soluble sugar level of "CS" was generally lower than the control during the T2 and T3 stages but gradually increased at the R1 stage.

Analysis of Chlorophyll Content and Photosynthesis

Salt stress is harmful to the photosynthesis of plants (Mbarki et al., 2018). In this experiment, we studied the impact of salt stress and recovery on the photosynthetic activities of two wheat varieties by measuring the levels of Chl-a, Chl-b, and Pn (**Figure 6**). The results showed that salt stress greatly affected the photosynthesis processes of "Y1805" and "CS," indicated by lower levels of Chl-a and Chl-b, and Pn than the control samples. However, the Chl-a content of "Y1805" was significantly higher than the "CS" after salt stress at

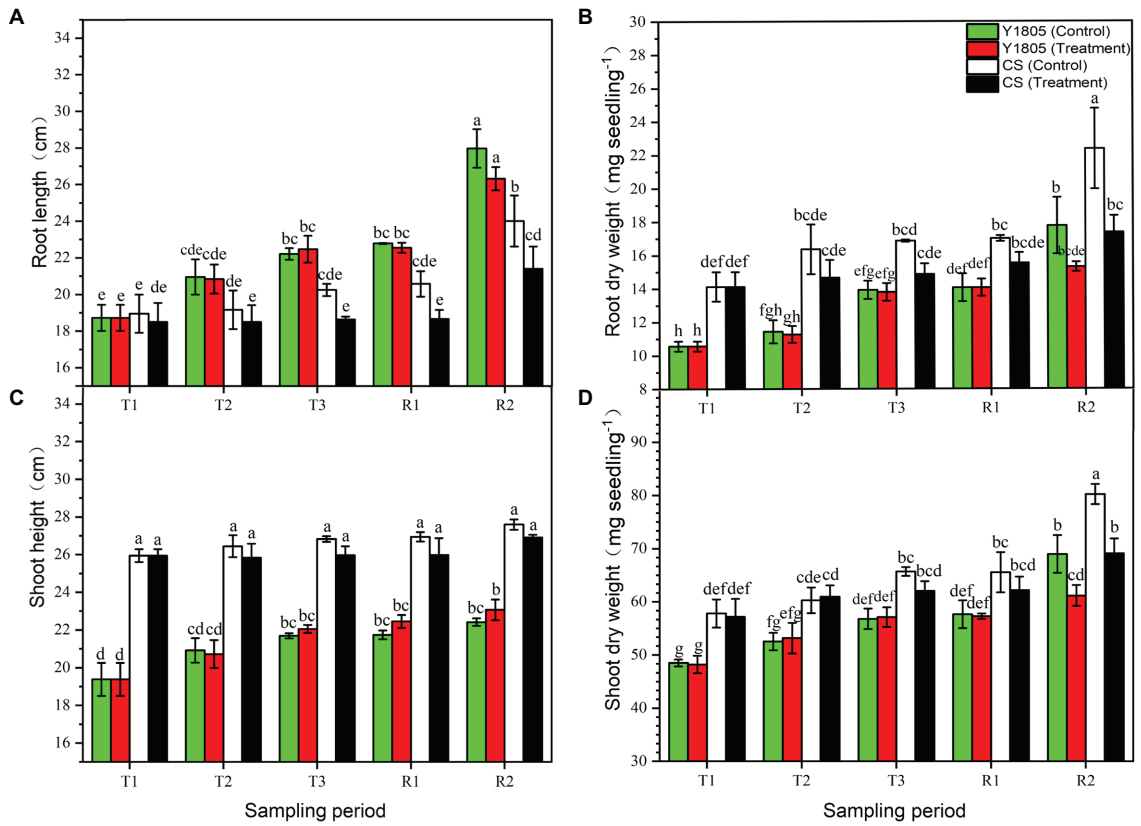

FIGURE 3 | Effect of salt stress and recovery on growth parameters of two wheat varieties. **(A)** Root length. **(B)** Root dry weight. **(C)** Shoot height. **(D)** Shoot dry weight. Bars indicate means with SDs ($n = 3$). Values with different letters are significantly different at $p < 0.05$.

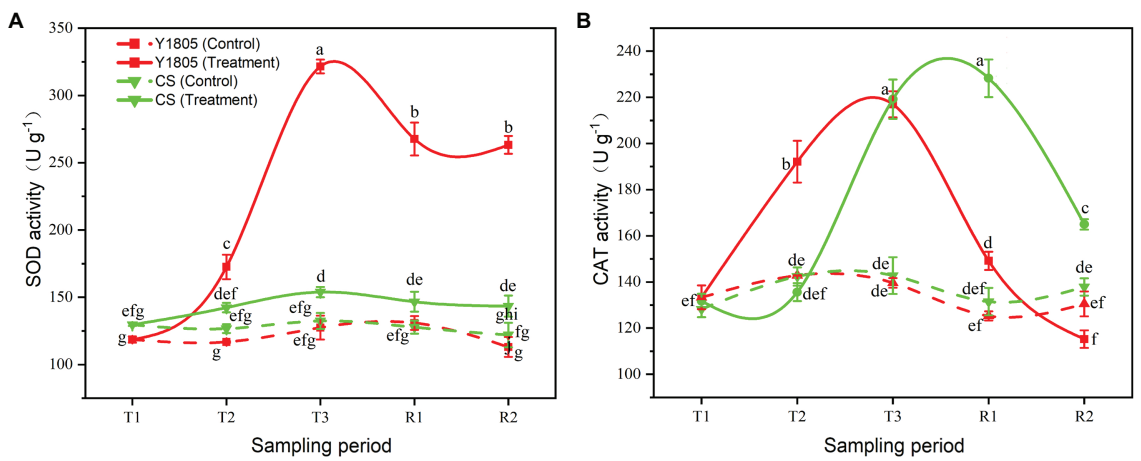

FIGURE 4 | Effect of salt stress on antioxidant enzyme activities in two wheat varieties. **(A)** SOD activity. **(B)** CAT activity. Bars indicate means with SDs ($n = 3$). Values with different letters are significantly different at $p < 0.05$.

the T2 stage and recovered well at the R2 stage. The Pn of both wheat varieties started to decline at the T2 stage, reached a minimum level at the T3 stage, and started to recover during the R1 and R2 stages (**Figure 6A**). At the T2 stage, the respective Pn of "Y1805" and "CS" decreased significantly by 56.13 and 75.07% under salt stress compared with the controls. The Pn of "Y1805" was significantly higher than that of "CS" at the R1 and R2 stages showing that "Y1805" could maintain a higher Pn under salt stress, and recover more rapidly than "CS." Similarly, the Chl-a content

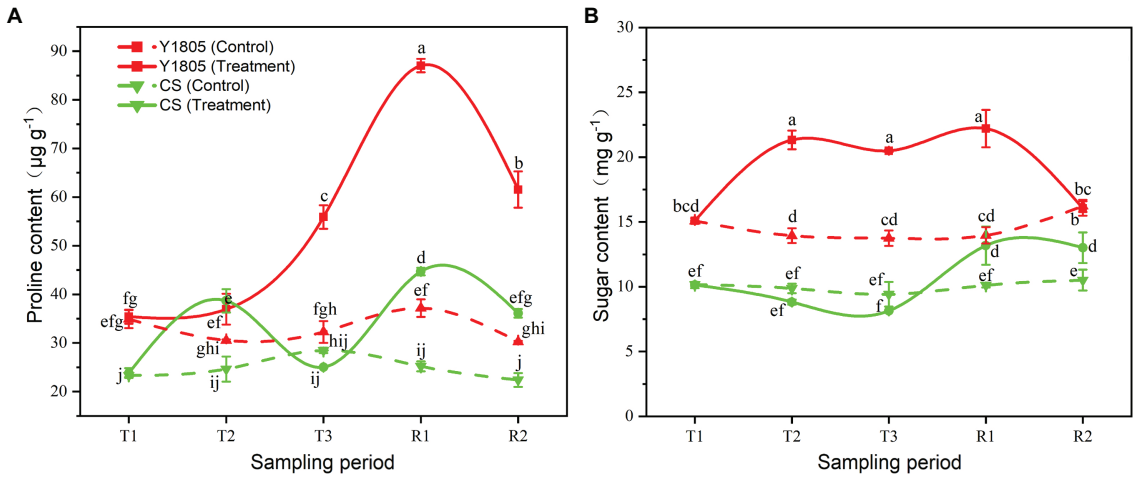

FIGURE 5 | Effect of salt stress and recovery on osmoregulator levels in two wheat varieties. **(A)** Proline content. **(B)** Sugar content. Bars indicate means with SDs ($n = 3$). Values with different letters are significantly different at $p < 0.05$.

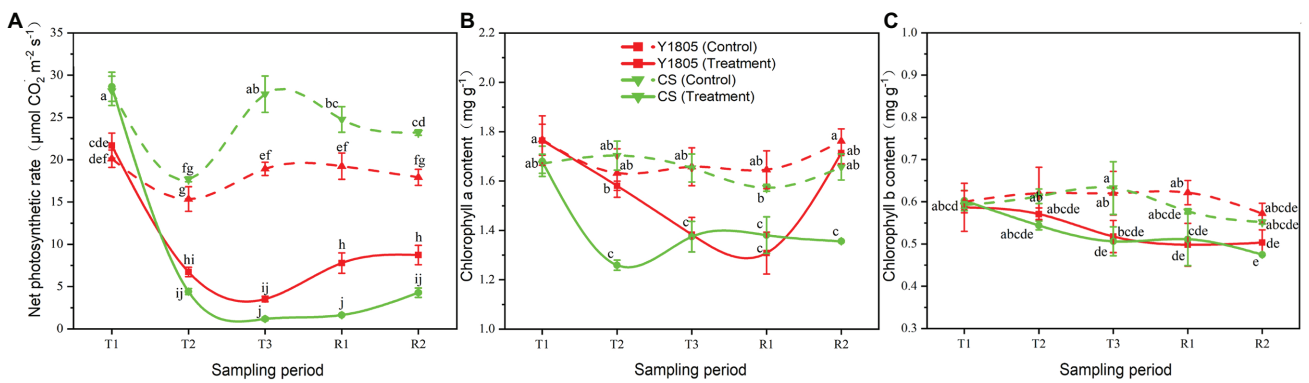

FIGURE 6 | Effect of salt stress and recovery on chlorophyll contents and photosynthetic rate in two wheat varieties. **(A)** Net photosynthetic rate. **(B)** Chlorophyll a content. **(C)** Chlorophyll b content. Bars indicate means with SDs ($n = 3$). Values with different letters are significantly different at $p < 0.05$.

of both "Y1805" and "CS" fell during salt stress (T2 and T3). The Chl-a content of "Y1805" at the T2 stage was higher than that of "CS" and recovered well at the R2 stage (**Figure 6B**). At the T2 stage, the Chl-a content of "CS" decreased significantly by 26.07% compared with "Y1805" under salt stress. After recovery, Chl-a content in "Y1805" rapidly returned to the control level at the R2 stage; however, little change occurred in "CS." These observations suggest that "Y1805" had a stronger Chl-a resilience ability after recovery, but "CS" suffered irreversible damage due to salt stress. Lastly, "Y1805" and "CS" showed a similar pattern of salt stress/recovery and Chl-b contents, that is, the Chl-b levels of both varieties dropped during salt stress and changed little after recovery (**Figure 6C**). The lower values of chlorophyll and Pn in "Y1805" and "CS" compare with those of the control under salt stress and the recovery period, indicating that salt stress inhibited the photosynthesis of the two wheat varieties, but "Y1805" was significantly less affected than "CS."

DEG Identification in Two Wheat Varieties Under Salt Stress and Recovery

To identify salt stress-responsive DEGs, we performed transcriptomic sequencing of root samples of salt-tolerant ("Y1805") and salt-sensitive ("CS") germplasms exposed to 250 mM NaCl solution (T2 stage) and after recovery (R1 stage). A total of 112,454 unigenes were obtained from RNA-seq data and 44,886 DEGs were found (**Figure 7**). Of these DEGs, 30,885 were identified in "Y1805" and 33,694 in "CS," respectively. Venn diagram analysis indicated that 23,183 and 23,505 unigenes were differentially expressed in response to salt stress in "Y1805" and "CS," respectively (**Figure 7**; DEGs at the T2 phase), and 17,804 and 21,513 unigenes were expressed in response to recovery (DEGs at the R1 stage). In "Y1805," there were 6,397 and 2,993 genes unique to the salt stress and recovery response, respectively, whereas 1,802 "Y1805"-specific DEGs were co-regulated by both salt stress and recovery. Likewise, there were 6,608 and 4,384 "CS"-specific DEGs, regulated under salt treatment and recovery only, while, 3,009 DEGs were co-expressed under both conditions.

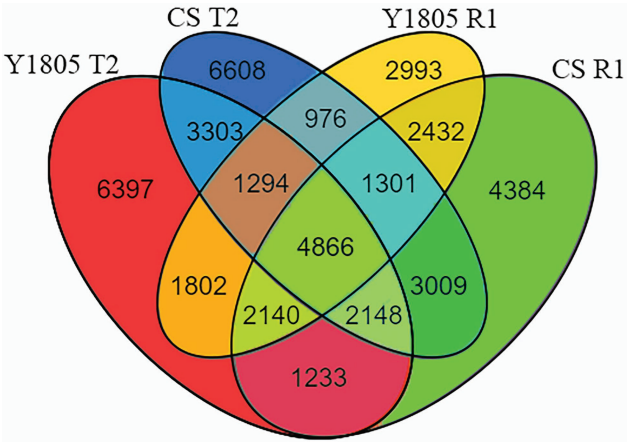

FIGURE 7 | Venn diagrams of DEGs under salt stress and recovery conditions. "Y1805" and "CS" are salt-tolerant and salt-sensitive wheat varieties, respectively. T2 and R1 indicate salt stress and recovery, respectively. False discovery rate (FDR) ≤ 0.01 and absolute $\log_2$fold change value ($|\log_2 FC| > 1$ are used as the thresholds to judge the significance of gene expression differences.

Annotation and GO Enrichment Analysis of Salt/Recovery Responsive DEGs in Two Wheat Varieties

We conducted GO enrichment analysis to characterize the biological functions of the DEGs in "Y1805" and "CS" under salt stress and recovery. The results indicated that the most significantly enriched GO term was markedly greater in "Y1805" (87) than "CS" (69). The top functional terms significantly ($p < 0.01$) enriched in both "Y1805" and "CS" under salt stress or recovery included oxidoreductase, catalytic activity, and amino acid metabolism (**Supplementary Tables S1 and S2**). The GO terms exclusively enriched in "Y1805" were related to cell cycle, proliferation and differentiation, ion homeostasis, carbohydrate metabolism, nucleoside phosphate binding, protein binding, photosynthesis, ion transport, and protein refolding. The GO terms enriched in "CS" were phenylpropanoid metabolism, organic acid metabolism, amine metabolism, and cellular hormone metabolism.

Under salt stress (T2 stage), 39 GO terms belonging to functional categories of ion homeostasis (9), catalytic activity (7), cellular process (6), photosynthesis (5), homeostatic process (4), signaling (3), transporter activity (2), protein refolding, ion transport, and lipid metabolic activity were exclusively enriched in "Y1805" at value of $Q < 0.01$ (**Supplementary Table S3**). Among the salt-responsive DEGs in "Y1805," 138 were associated with "transferase/phosphatase/dehydratase activity," 86 with "cell wall organization" or "biogenesis/chaperone-mediated protein folding/microtubule bundle formation," 85 with "ion transport," followed by "cellular chemical homeostasis" (76), "inorganic/metal ion homeostasis" (40), "photosynthesis-specific metabolic processes" (19), "transporter activity" (11), "protein refolding" (11), "tetraterpenoid metabolic process" (10), and "cell–cell signaling" (3). In "Y1805"-specific DEGs, GO terms for "acid phosphatase activity," "dihydroxy-acid dehydratase activity," "S-malonyltransferase activity," "plant-type secondary cell wall biogenesis," "chaperone-mediated protein folding," "microtubule bundle formation," "chlorophyll metabolic process," "carotenoid metabolic process," "inorganic phosphate transmembrane transporter activity," and "L-ascorbic acid transmembrane transporter activity" were enriched under salt stress. During the recovery process (R1 stage), the "organic substance metabolism" and RNA (LSU-rRNA/ncRNA/tRNA) processing related GO terms were significantly enriched in "Y1805," which indicated that "Y1805" had abundant gene expression pathways in response to salt stress compared to recovery response (**Supplementary Table S4**). The common DEGs of salt stress and recovery in "Y1805" were enriched in amino acid metabolism, oxidoreductase, catalytic activity, organic substance metabolism, and cellular process (**Supplementary Table S5**). There were fewer specific GO terms in "CS" than in "Y1805," especially in response to salt stress. Under salt stress, 21 GO terms mainly involved in diverse functions of secondary metabolism (61 DEGs), oxidoreductase (83), ion binding (83), amino acid metabolism (26), amine metabolic process (25), structural molecule activity (14), organic substance metabolism (11), transcription (8), and catalytic activity (6) were observed in "CS" (**Supplementary Table S6**). During the recovery process, GO terms mainly involved in binding (single-stranded RNA binding/organic cyclic compound binding/DNA binding), cellular process, catalytic activity, and organic substance metabolism, were significantly enriched in recovery-specific DEGs of "CS" (**Supplementary Table S7**). The GO terms associated with oxidoreductase, phospholipid metabolism, amino acid metabolism, organic acid metabolism, and response to stimulus were enriched in "CS" responsive to both salt stress and recovery (**Supplementary Table S8**).

Analysis of KEGG Pathways in Salt/Recovery Responsive DEGs in Two Wheat Varieties

Kyoto Encyclopedia of Genes and Genomes enrichment analysis revealed similar pathways in the DEGs of "Y1805" and "CS" under salt stress and recovery, but the number of genes in respective pathways differed (**Supplementary Tables S9 and S10**). Common pathways, namely, "transcription," "lipid metabolism," "folding, sorting, and degradation," "transport and catabolism," "signal transduction," "metabolism of terpenoids and polyketides," "glycan biosynthesis and metabolism," "nucleotide metabolism," "DNA replication and repair," "metabolism of cofactors and vitamins," "translation," "amino acid metabolism," and "biosynthesis of other secondary metabolites" appeared in both "Y1805" and "CS." The most significantly (value of $Q < 0.05$) enriched KEGG pathways in "Y1805"-specific DEGs were associated with "folding, sorting, and degradation," "transport and catabolism," "carbohydrate metabolism," and "glycan biosynthesis and metabolism." There were multiple pathways in "replication and repair," and their DEGs were more abundant in "Y1805" than "CS." Compared with "Y1805," the DEGs of

"CS" were more abundant in pathways related to "metabolism of terpenoids and polyketides," "energy metabolism," "amino acid metabolism," and "biosynthesis of other secondary metabolites" (**Supplementary Table S10**).

Furthermore, KEGG enrichment analysis of "Y1805"-DEGs identified under salt stress found that DEGs were significantly enriched in "metabolism" (carbohydrates, lipids, amino acids, nucleotides, terpenoids and polyketides, and cofactors and vitamins), "transcription," "translation," "replication and repair," "signal transduction," "environmental adaptation," "biosynthesis of other secondary metabolites," "folding, sorting, and degradation," and "membrane transport" pathways (**Supplementary Table S11**). We observed that pathways for "biosynthesis of secondary metabolites" and "synthesis and degradation of ketone bodies" were enriched exclusively in "Y1805" that were responsive to both salt stress and recovery (**Supplementary Table S12**). In addition to the activation of different "cellular processes" and "metabolism" pathways, the salt stress seemed to suppress autophagy-related genes in "CS" (**Supplementary Table S13**). During the recovery process, "lipoic acid metabolism" pathway was enriched solely in "CS" (**Supplementary Table S14**).

Participation of Key Genes in Salt Stress-Related Pathways

We looked for key genes involved in antioxidant enzymes, osmoregulation, and photosynthesis related metabolic pathways under salt stress in "Y1805." The "peroxisome" (ko04146), "arginine and proline metabolism" (ko00330), "starch and sucrose metabolism" (ko00500), "photosynthesis" (ko00195), and "chlorophyll and porphyrin metabolism" (ko00860) pathways were enriched under salt stress. There were three upregulated genes and four downregulated genes encoding CAT, four upregulated and five downregulated genes encoding SOD in the "peroxisome" pathway (**Supplementary Table S15**). In the "arginine and proline" pathway, three upregulated genes encoding 1-pyrroline-5-carboxylate synthetase (*BGI_novel_G009739*, *BGI_novel_G019140*, and *TraesCS3D02G357200*), three downregulated genes encoding proline dehydrogenase (*TraesCS1A02G209100*, *TraesCS1B02G223300*, and *TraesCS1D02G212400*), and four upregulated genes encoding prolyl 4-hydroxylase (including *TraesCS2B02G292200*, *TraesCS4B02G228600*, and *TraesCS4D02G229700*) were found. In the "starch and sucrose" pathway, there were four upregulated genes (including *TraesCS4D02G169800*, *TraesCS2D02G175600*, and *TraesCS4A02G140000*) encoding sucrase synthase, six upregulated genes encoding sucrose-phosphate synthase (including *TraesCS3A02G425500*, *TraesCS4A02G225100*, and *TraesCS4B02G091100*), five downregulated *MGAM* (maltase-glucoamylase) genes (including *TraesCS7D02G451800*, *TraesCS7A02G134500*, and *TraesCS7B02G364700*) encoding maltase-glucoamylase, 15 upregulated genes (including *TraesCS2A02G588300*, *TraesCS2B02G595000*, and *TraesCS2D02G570000*) encoding *SacA* of beta fructofuranosidase, 31 *amyA* genes (including *TraesCS2A02G309400*, *TraesCS2B02G183400*, and *TraesCS6B02G349500*) encoding alpha-amylase were downregulated. In the "photosynthesis" pathway, there was one upregulated *PsbC* gene (*BGI_novel_G013282*) encoding photosystem II CP43 chlorophyll apoprotein, two upregulated *PetA* genes (*TraesCS1D02G181700* and *TraesCS5D02G200200*) related to apocytochrome f, and one upregulated *psb27* gene (*TraesCS4D02G172800*) encoding the photosystem II psb27 protein. In the "chlorophyll and porphyrin" pathway, there were two downregulated *chlG*/*bchG* genes (*TraesCS1B02G237700* and *TraesCS1D02G226100*) encoding Chl-a synthase, two upregulated genes (*TraesCS3D02G103900* and *TraesCS5D02G364100*) encoding chlorophyllase, two upregulated *NOL*/*NYC*1 genes (*TraesCS3A02G151900* and *TraesCS3D02G159800*) encoding chlorophyll (ide) b reductase, three downregulated *CAO* genes (*TraesCS3A02G506200*, *TraesCS3B02G574300*, and *TraesCS3D02G514100*) encoding chlorophyllide a oxygenase, and nine upregulated *SGR/SGRL* (stay green rice/stay green rice like) genes (including *TraesCS6B02G143000*, *TraesCS3A02G447000*, and *TraesCS5B02G320200*) encoding magnesium dechelase.

Verification of DEGs by qRT-PCR

In total, 12 DEGs closely related to salt stress were selected for qRT-PCR analysis. All the gene amplification levels, as assessed by qRT-PCR, agreed well with the RNA-seq patterns, and the correlation between RNA-seq and qRT-PCR showed a positive correlation coefficient ($r = 0.902$, $p = 6.16E^{-5}$; **Figure 8**).

DISCUSSION

Crop models, such as *Tritipyrum*, are essential tools for assessing the threat of salt stress to local and global food production crops including wheat. In this work, we studied salt-tolerant mechanisms in *Tritipyrum* by assessing the growth, physiological, and antioxidant enzymatic responses of salt-tolerant *Tritipyrum* ("Y1805") and a salt-sensitive common wheat variety ("CS"). Sequential GISH-FISH technique were used to determine the genome structure and genetic diversity of salt-tolerant hybrid germplasm. Moreover, RNA-seq analysis, GO annotation, KEGG pathway enrichment, and qRT-PCR analyses were used to identify key candidate genes and investigate the molecular mechanisms of salt tolerance and recovery in "Y1805."

In recent years, RNA-seq analysis based DEGs and candidate gene identification has been used to study salt tolerance in numerous plants, including *Arabidopsis* (Sako et al., 2021), rice (Chandran et al., 2019), bread wheat (Amirbakhtiar et al., 2021), Chinese cabbage (Li et al., 2021), drought/salt-tolerant *Caragana korshinskii* (Li et al., 2016), a model halophytic *Chenopodium quinoa* (Ruiz et al., 2019), *Cenostigma pyramidale* (Frosi et al., 2021), and *Ricinus communis* (Lei et al., 2021). These studies have identified abundant DEGs, candidate upregulated genes, and the functional enrichment of GO terms and pathways related to salt stress responses in plants. Additionally, many physiological and biochemical genes have been verified experimentally to play key roles in the salt

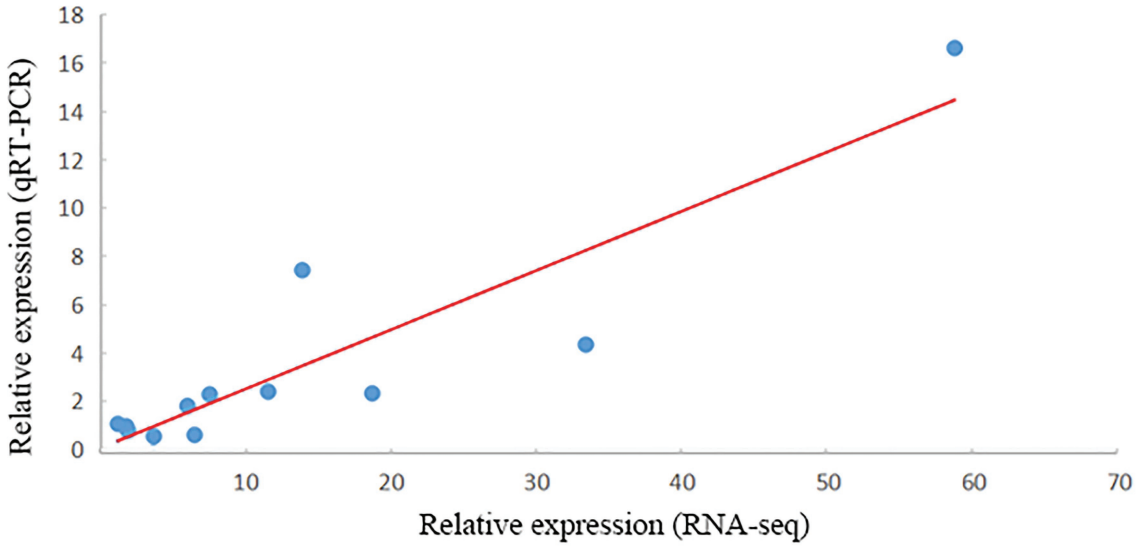

FIGURE 8 | Verification of RNA-seq results by qRT-PCR. The x- and y-axes show the relative expression levels analyzed independently by RNA-seq and qRT-PCR, respectively.

tolerance mechanism of plants. Singh et al. found that when the *SbpAPX* gene encoding peroxisome ascorbate peroxidase (APX) from *Salicornia brachiata* Roxb. was overexpressed in tobacco plants, the plants showed increased salt and drought tolerance compared to the wild type (Singh et al., 2014). Surender et al. (2015) found that the survival capability of transgenic *Sorghum bicolor* lines under salt stress was more enhanced when transformed with the mutated pyrroline-5-carboxylate synthetase gene, which encodes a key enzyme for glutamate proline synthesis and protects photosynthetic and antioxidant enzyme activities. Transformation of sugarcane plants with the *Vigna aconitifolia P5CS* gene not only conferred salt tolerance in transgenic lines but also the higher gene expression was accompanied by higher proline content, reduction of malondialdehyde, low accumulation of Na^+, and sustained photochemical efficiency of photosystem II compared with the control (Guerzoni et al., 2014). This suggests that proline protects the photosynthetic system and prevents oxidative damage under salt stress. Ahmad et al. showed that the expression of the SOD, CAT, and APX genes in chickpea (*Cicer arietinum* L.) plants was upregulated, and the exogenous nitric oxide was also significantly increased under salt stress (Ahmad et al., 2016). Studying transgenic wheat plants containing the *mtlD* gene, El-yazal et al. found that transgenic plants had improved salt tolerance over non-transgenics, showing better growth traits, physio-biochemical attributes, and activities of antioxidant enzymes (El-Yazal et al., 2016).

In the present study, salt-tolerant *Tritipyrum* hybrid and salt-sensitive common wheat ("CS") were evaluated for growth parameters, various biochemical attributes, and transcriptomic responses against salt stress and recovery. We found that salt stress inhibited the growth of the two cultivars as evidenced by examination of growth parameters. The RL and RDW of salt-tolerant "Y1805" showed no significant difference between the treatments and controls at each stage. Whereas those of salt-sensitive "CS" were significantly reduced by 10.84 and 22.35% of the controls at the R2 stage after recovery, salt stress had more inhibitory effects on the roots than the rest of the plant. "Y1805" represented stronger salt tolerance than "CS" according to its RL and plant dry weight. These results were in accordance with those of Basal et al. who observed a reduction in SDW and RDW with increasing salt levels in salt-tolerant and salt-sensitive cotton varieties (Basal et al., 2006). Moreover, the findings of Guo et al. corroborate our results and state that under salt stress, the dry matter accumulation rate of cotton varieties decreases, but it can be resumed in the salt-tolerant varieties after recovery (Guo et al., 2015).

Photosynthesis is the basis for the efficient conversion of light energy into the growth and development of plants. Leaf photosynthetic rate is an important indicator of photosynthesis, and the chlorophyll content of leaves is closely related to photosynthetic rate. Salt stress can lead to the decrease of chlorophyll content in plants, but the degree of Chl-a/b reduction will differ among different varieties (Ehsanzadeh et al., 2009; Sarwar and Shahbaz, 2019; Rehman et al., 2021). In this work, both the Pn and Chl-a/b levels of "Y1805" and "CS" were significantly affected by salt stress, though, the level of damage in the former was significantly less than in the latter, and these changes were subsequently reversed in "Y1805" during the recovery process. It was also shown that Chl-a was more sensitive to salt stress than Chl-b. At the T2 stage, the Chl-a content of "CS" decreased significantly by 26.07% compared with that of "Y1805." These results were in agreement with previous reports (Muhammad et al., 2012; Abdellaoui et al., 2017), where salt stress and subsequent Na^+ accumulation resulted in the degradation of photosynthetic pigment and Pn reduction in cactus and *Stipa lagascae* plants, respectively.

Salt stress induces the overproduction of ROS, which causes redox imbalance and oxidative damage in cells (Demiral and Türkan, 2005; Hossain and Dietz, 2016; Zhang et al., 2016; Ahmad et al., 2019). In response, antioxidant defense machinery is activated by various enzymatic and non-enzymatic antioxidants to alleviate this stress and scavenge ROS (Kakar et al., 2016, 2017; Vighi et al., 2017; Fan et al., 2020). SOD reacts with superoxide anion radical (O^{2-}) to produce H_2O_2, while CAT is an H_2O_2 scavenging enzyme, which can decompose H_2O_2 and avoid the accumulation of H_2O_2 in cells. The combination of SOD and CAT can effectively reduce the harm of ROS in plant cells. In this study, the SOD and CAT activities of the two wheat varieties were significantly upregulated under salt stress, which was consistent with the results of Esfandiari et al. (2007). Under salinity, salt-tolerant varieties are more likely to activate SOD and CAT than other varieties (Al Kharusi et al., 2019). Here, "Y1805" enhanced the SOD and CAT activities rapidly under salt stress, and they were reduced quickly after recovery, indicating that its ROS scavenging ability was higher than in "CS."

Cells accumulate free proline, soluble sugars, and other osmotic regulators under salt stress, which can regulate the osmotic potential of cells and maintain water balance. Proline accumulation is considered one of the important regulatory mechanisms for plants to adapt to saline and alkaline environment (Meena et al., 2019; Sharma et al., 2019), and its exogenous application has reportedly improved the salt tolerance of several crops (Sun and Hong, 2010; Nounjan et al., 2012; Sobahan et al., 2012; El Moukhtari et al., 2020). Moreover, proline is also a metal chelator, an antioxidative defense molecule, and a signaling molecule (Hayat et al., 2012). In this experiment, the ability of proline accumulation was different among the two varieties at different stages, where the proline in "Y1805" was accumulated at an increasing rate during each stage of salt stress, compared with "CS" that showed a zigzag trendline. Previously, Sivakumar et al., showed that the proline content of a few tomato varieties did not increase significantly after 24 h of short-term stress or under low salinity (Sivakumar et al., 2019). The proline content of "Y1805" began to rise at the T2 stage of salt stress and peaked at the R1 stage, and was 2.00-fold higher than that of "CS." These observations suggest that "Y1805" could synthesize more proline than "CS" to cope with salt stress damage. Soluble sugars, as osmotic regulators and signal molecules, participate in the response and adaptation of plants to environmental stress (Wang et al., 2018) and can be used to identify salt tolerance in plants (Bai et al., 2013). In a study conducted by Kerepesi and Galiba, the soluble sugar content of the salt-tolerant wheat variety "Sakha" was higher than that of "CS" under salt stress (Kerepesi and Galiba, 2000). Similar results were obtained in this study. The soluble sugar content in "Y1805" increased significantly from the T2 stage, and kept stable until the R1 stage, and returned to the control level at the R2 stage after recovery. In contrast, "CS" showed little change in soluble sugar content during salt stress and only showed an increase after recovery, indicating that "Y1805" had strong soluble sugar regulatory abilities.

In this study, we used a sequential GISH-FISH technique to determine the genomic composition of salt-tolerant *Tritipyrum* "Y1805" and identified 56 chromosomes. It was revealed that the "Y1805" genome comprised A, B, and D chromosomes from wheat parents, but also contained the E genome of chromosomes that originated from *T. elongatum*, adding to its genetic diversity and suitability as a hybrid with salt-tolerant traits.

Comparison of the DEGs between the two cultivars directly reflects the mechanism of plant salt tolerance. In this study, a total of 112,454 unigenes were obtained by RNA-seq analysis, including 44,886 DEGs. Transcriptome analysis showed that the differences in the transcriptional regulatory networks of salt-tolerant and salt-sensitive germplasm are not only in response to salt stress but also in recovery. The number of DEGs in each variety and treatment varied. Among these DEGs, some were expressed solely against salt stress or recovery, while others were co-expressed mutually between "Y1805" and "CS." The DEGs of "Y1805" at the T2 stage were enriched in several photosynthetic GO terms and KEGG pathways related to "fatty acid biosynthesis and metabolism." The results of Luo et al. showed that salt-tolerant wheat could enhance the photosynthetic system and improve the salt tolerance of wheat through pathways related to polyunsaturated fatty acid metabolism (Luo et al., 2019). In this experiment, it was found that there were more DEGs related to "fatty acid" and "photosynthesis" in "Y1805" under salt stress, but expression decreased rapidly after recovery. It may be that "Y1805" increased salt tolerance through fatty acid synthesis and metabolism and ensured that the photosynthetic machinery of the cells was actively regulated under salt stress, and remained almost intact during the recovery process. "Y1805" was enriched in the metabolic pathway of "start and conquer metabolism" at the T2 stage, and in "glutathione metabolism" and "arginine and proline metabolism" at the T2 and R1 stages, respectively. Starch and sucrose metabolism is considered to determine the soluble sugar content in plants and affect osmotic regulation (Balibrea et al., 2006). Differences in expression levels of related DEGs under salt stress will lead to differences in soluble sugar contents in the plant materials studied (Wei et al., 2020). The transcriptional level of enzymes related to glutathione biosynthesis and glutathione content can alleviate the effects of salt stress on photosynthesis (Nazar et al., 2015), maintain the dynamic balance of cell redox (Zhou et al., 2017), and reduce the toxicity of methylglyoxal induced by salt stress (Khunpon et al., 2018). Amirbakhtiar et al. (2019) also reported that DEGs in salt-tolerant bread wheat were enriched in "transporters," "phenylpropanoid biosynthesis," "transcription factors," "glycosyltransferases," "glutathione metabolism," and "plant hormone signal transduction" pathways during salt stress, which also support our results that these are significant pathways in the abiotic and biological stress response in plants.

"Arginine and proline metabolism" is the key pathway for proline accumulation in plants under salt stress, and as mentioned earlier, proline is an important osmotic regulator for salt tolerance (Sakr et al., 2012). Here, the high abundance of DEGs at the T2 and R1 stages indicated that the expression of DEGs in "Y1805" may be one of the important reasons

for its high salt tolerance. The KEGG pathway enrichment analysis of "Y1805" revealed that DEGs at the T2 stage were significantly enriched in "carbohydrates," "lipids," and "amino acids metabolism" along with "signal transduction," "environmental adaptation," "secondary metabolites biosynthesis," and "membrane transport." At the R1 stage, DEGs were enriched in "glycan biosynthesis and metabolism" and "carbohydrate metabolism." There were significant differences in the metabolic pathways regulated by DEGs in "Y1805" under salt stress and recovery conditions, which indicated that there were differences in the regulatory mechanisms of "Y1805" in response to salt stress and recovery.

Lastly, the expression patterns of salt stress and recovery responsive DEGs in "Y1805" were determined. The results indicated that the functions of many salt stress and recovery responsive DEGs in "Y1805" were closely correlated with the levels of SOD and CAT activities, as well as the levels of sugar, proline, chlorophyll, and Pn. These DEGs played key roles in the KEGG pathways of "peroxisome" (ko04146), "arginine and proline metabolism" (ko00330), "starch and sucrose metabolism" (ko00500), "chlorophyll and porphyrin metabolism" (ko00860), and "photosynthesis" (ko00195), respectively. Functional analysis revealed that these genes are involved in specific metabolic pathways and mechanisms, which might have a unique significance in wheat salt tolerance. After recovery, some genes were potentially upregulated at the R1 stage, thus contributing to the recovery of wheat growth and development. Through transcriptome analysis, it was found that "Y1805" had many specific DEGs under salt stress and recovery. These DEGs were enriched in multiple related pathways, and their enrichment differed under salt stress and recovery conditions, showing that plants can regulate specific DEGs under different conditions. Finally, the patterns of the up/downregulated genes combined with the detection of related growth indicators prompted us to conclude that the function of many stress-responsive DEGs is closely related to the activities of antioxidant enzymes and the levels of sugar, proline, chlorophyll, and Pn.

CONCLUSION

Salt-tolerant *Tritipyrum* ("Y1805") and salt-sensitive wheat ("CS") were chosen from 121 wheat germplasms using salt-tolerant experiments. Overall, 56 chromosomes were identified in "Y1805" using sequential GISH-FISH analysis, which comprised A, B, and D chromosomes from common wheat parent and E genome chromosomes that originated from *T. elongatum*, which added to its genetic diversity and salt-tolerant traits. Growth parameters revealed that salt stress had a greater inhibitory effect on the roots than on the shoots, and "Y1805" demonstrated stronger salt tolerance than "CS." "Y1805" could enhance the antioxidant activity more rapidly than "CS" under salt stress to protect the cells from damage caused by ROS. "Y1805" could synthesize more proline and soluble sugars than "CS' to cope with salt stress damage. Both Pn and Chlorophyll a/b contents were affected by salt stress, although the level of damage in "Y1805" was significantly lesser than in "CS." Using transcriptome analysis, the functions of many salt-responsive DEGs were closely correlated with "peroxisome," "arginine and proline metabolism," "starch and sucrose metabolism," "chlorophyll and porphyrin metabolism," "photosynthesis," and "fatty acid biosynthesis and metabolism" KEGG pathways. The strong salt tolerance of "Y1805" may be mainly attributed to ROS scavenging, osmoregulation, ion homeostasis, cell wall remodeling, and signal transduction. Some novel candidate genes related to antioxidase, osmoregulator, or photosynthesis pathways were also found under salt stress in "Y1805." The outcomes of growth and physio-biochemical analyses were consistent with the transcriptome data. The nature of the salt tolerance mechanisms –*per se*- is already known in other plant species and but seems to be more quantitatively effective in the tolerant wheat genotype. These findings provide useful information for the cultivation and breeding of salt-tolerant wheat.

DATA AVAILABILITY STATEMENT

The datasets presented in this study can be found in online repositories. The raw sequence reads were deposited into NCBI SRA database under accession no. PRJNA769794 (https://www.ncbi.nlm.nih.gov/sra/?term=PRJNA769794).

AUTHOR CONTRIBUTIONS

ZL, RX, and SZ designed the experiments. Material preparation, data collection, and analysis were performed by ZP, YW, RY, and ZY. ZP, YW, GG, QZ, KK, ZL, and SZ wrote the manuscript. All authors have read and approved the final manuscript.

FUNDING

This study was financially supported by the National Natural Science Foundation of China (31860380 and 32160442) and the Science Foundation of Guizhou Province [(2018)5781 and (2019)1110].

ACKNOWLEDGMENTS

Special thanks are due to Pr. Adam J. Lukaszewski (University of California Riverside, United States) for the technical assistance in the experiments. We thank International Science Editing (http://www.internationalscienceediting.com) for editing this manuscript.

SUPPLEMENTARY MATERIAL

The Supplementary Material for this article can be found online at: https://www.frontiersin.org/articles/10.3389/fpls.2021.800081/full#supplementary-material

REFERENCES

Abdel-Farid, I. B., Marghany, M. R., Rowezek, M. M., and Sheded, M. G. (2020). Effect of salinity stress on growth and metabolomic profiling of *Cucumis sativus* and *Solanum lycopersicum*. *Plan. Theory* 9:1626. doi: 10.3390/plants9111626

Abdellaoui, R., Boughalleb, F., Chebil, Z., Mahmoudi, M., and Belgacem, A. O. (2017). Physiological, anatomical and antioxidant responses to salinity in the Mediterranean pastoral grass plant *Stipa lagascae*. *Crop Pasture Sci.* 68, 872–884. doi: 10.1071/CP16365

Aebi, H. (1984). Catalase in vitro. *Methods Enzymol.* 105, 121–126. doi: 10.1016/s0076-6879(84)05016-3

Agami, R. A. (2014). Applications of ascorbic acid or proline increase resistance to salt stress in barley seedlings. *Biol. Plant.* 58, 341–347. doi: 10.1007/s10535-014-0392-y

Ahmad, P., Abdel Latef, A. A., Hashem, A., Abd Allah, E. F., Gucel, S., and Tran, L. S. (2016). Nitric oxide mitigates salt stress by regulating levels of osmolytes and antioxidant enzymes in chickpea. *Front. Plant Sci.* 7:347. doi: 10.3389/fpls.2016.00347

Ahmad, R., Hussain, S., Anjum, M. A., Khalid, M. F., Saqib, M., Zakir, I., et al. (2019). "Oxidative stress and antioxidant defense mechanisms in plants under salt stress," in *Plant Abiotic Stress Tolerance*. eds. M. Hasanuzzaman et al. (Cham: Springer), 191–205.

Al Kharusi, L., Al Yahyai, R., and Yaish, M. W. (2019). Antioxidant response to salinity in salt-tolerant and salt-susceptible cultivars of date palm. *Agriculture* 9:8. doi: 10.3390/agriculture9010008

Amirbakhtiar, N., Ismaili, A., Ghaffari, M. R., Firouzabadi, F. N., and Shobbar, Z. S. (2019). Transcriptome response of roots to salt stress in a salinity-tolerant bread wheat cultivar. *PLoS One* 14:e0213305. doi: 10.1371/journal.pone.0213305

Amirbakhtiar, N., Ismaili, A., Ghaffari, M. R., Mirdar Mansuri, R., Sanjari, S., and Shobbar, Z. S. (2021). Transcriptome analysis of bread wheat leaves in response to salt stress. *PLoS One* 16:e0254189. doi: 10.1371/journal.pone.0254189

Anders, S., and Huber, W. (2010). Differential expression analysis for sequence count data. *Genome Biol.* 11:R106. doi: 10.1186/gb-2010-11-10-r106

Arif, Y., Singh, P., Siddiqui, H., Bajguz, A., and Hayat, S. (2020). Salinity induced physiological and biochemical changes in plants: an omic approach towards salt stress tolerance. *Plant Physiol. Biochem.* 156, 64–77. doi: 10.1016/j.plaphy.2020.08.042

Bai, J., Liu, J., Zhang, N., Sa, R., and Jiang, L. (2013). Effect of salt stress on antioxidant enzymes, soluble sugar and yield of oat. *Adv. J. Food Sci. Technol.* 5, 303–309. doi: 10.19026/ajfst.5.3261

Balibrea, M. E., Martínez-Andújar, C., Cuartero, J., Bolarín, M. C., and Pérez-Alfocea, F. (2006). The high fruit soluble sugar content in wild *Lycopersicon* species and their hybrids with cultivars depends on sucrose import during ripening rather than on sucrose metabolism. *Funct. Plant Biol.* 33, 279–288. doi: 10.1071/FP05134

Basal, H., Hemphill, J. K., and Smith, C. W. (2006). Shoot and root characteristics of converted race stocks accessions of upland cotton (*Gossypium hirsutum* L.) grown under salt stress conditions. *Am. J. Plant Pathol.* 1, 99–106. doi: 10.3923/ajpp.2006.99.106

Bates, L. S., Waldren, R. P., and Teare, I. D. (1973). Rapid determination of free proline for water-stress studies. *Plant Soil* 39, 205–207. doi: 10.1007/BF00018060

Baxter, I., Brazelton, J. N., Yu, D., Huang, Y. S., Lahner, B., Yakubova, E., et al. (2010). A coastal cline in sodium accumulation in *Arabidopsis thaliana* is driven by natural variation of the sodium transporter AtHKT1, 1. *PLoS Genet.* 6:e1001193. doi: 10.1371/journal.pgen.1001193

Chandran, A. K. N., Kim, J. W., Yoo, Y. H., Park, H. L., Kim, Y. J., Cho, M. H., et al. (2019). Transcriptome analysis of rice-seedling roots under soil–salt stress using RNA-Seq method. *Plant Biotechnol. Rep.* 13, 567–578. doi: 10.1007/s11816-019-00550-3

Demiral, T., and Türkan, İ. (2005). Comparative lipid peroxidation, antioxidant defense systems and proline content in roots of two rice cultivars differing in salt tolerance. *Environ. Exp. Bot.* 53, 247–257. doi: 10.1016/j.envexpbot.2004.03.017

Depuydt, S., and Hardtke, C. S. (2011). Hormone signaling crosstalk in plant growth regulation. *Curr. Biol.* 21, R365–R373. doi: 10.1016/j.cub.2011.03.013

Ding, T., Yang, Z., Wei, X., Yuan, F., Yin, S., and Wang, B. (2018). Evaluation of salt-tolerant germplasm and screening of the salt-tolerance traits of sweet sorghum in the germination stage. *Funct. Plant Biol.* 45, 1073–1081. doi: 10.1071/FP18009

Du, P., Zhuang, L. F., Wang, Y. Z., Yuan, L., Wang, Q., and Wang, D. R. (2017). Development of oligonucleotides and multiplex probes for quick and accurate identification of wheat and *Thinopyrum bessarabicum* chromosomes. *Genome* 60, 93–103. doi: 10.1139/gen-2016-0095

Ehsanzadeh, P., Nekoonam, M. S., Azhar, J. N., Pourhadian, H., and Shaydaee, S. (2009). Growth, chlorophyll, and cation concentration of tetraploid wheat on a solution high in sodium chloride salt: hulled versus free-threshing genotypes. *J. Plant Nutr.* 32, 58–70. doi: 10.1080/01904160802531019

El Moukhtari, A., Cabassa-Hourton, C., Farissi, M., and Savouré, A. (2020). How does proline treatment promote salt stress tolerance during crop plant development? *Front. Plant Sci.* 11:1127. doi: 10.3389/fpls.2020.01127

El-Yazal, M. A. S., Eissa, H. F., Ahmed, S. M. A. E., Howladar, S. M., Zaki, S. S., and Rady, M. M. (2016). The *mtlD* gene-overexpressed transgenic wheat tolerates salt stress through accumulation of mannitol and sugars. *Plant* 4, 78–90. doi: 10.11648/j.plant.20160406.15

Esfandiari, E., Shekari, F., Shekari, F., and Esfandiari, M. (2007). The effect of salt stress on antioxidant enzymes' activity and lipid peroxidation on the wheat seedling. *Not. Bot. Horti Agrobot. Cluj Napoca* 35, 48–56. doi: 10.15835/nbha351251

Fan, D., Subramanian, S., and Smith, D. L. (2020). Plant endophytes promote growth and alleviate salt stress in *Arabidopsis thaliana*. *Sci. Rep.* 10:12740. doi: 10.1038/s41598-020-69713-5

Frosi, G., Ferreira-Neto, J. R. C., Bezerra-Neto, J. P., Pandolfi, V., Silva, M. D. D., Morais, D. A. D. L., et al. (2021). Transcriptome of *Cenostigma pyramidale* roots, a woody legume, under different salt stress times. *Physiol. Plant.* 173, 1463–1480. doi: 10.1111/ppl.13456

Goyal, E., Amit, S. K., Singh, R. S., Mahato, A. K., Chand, S., and Kanika, K. (2016). Transcriptome profiling of the salt-stress response in *Triticum aestivum* cv. Kharchia local. *Sci. Rep.* 6:27752. doi: 10.1038/srep27752

Guerzoni, J. T. S., Belintani, N. G., Moreira, R. M. P., Hoshino, A. A., Domingues, D. S., Filho, J. C. B., et al. (2014). Stress-induced Δ1-pyrroline-5-carboxylate synthetase (*P5CS*) gene confers tolerance to salt stress in transgenic sugarcane. *Acta Physiol. Plant.* 36, 2309–2319. doi: 10.1007/s11738-014-1579-8

Guo, G. F., Ge, P., Ma, C. Y., Li, X. H., Lv, D. W., Wang, S. L., et al. (2012). Comparative proteomic analysis of salt response proteins in seedling roots of two wheat varieties. *J. Proteome* 75, 1867–1885. doi: 10.1016/j.jprot.2011.12.032

Guo, W. Q., Zhang, P. T., Li, C. H., Yin, J. M., and Han, X. Y. (2015). Recovery of root growth and physiological characters in cotton after salt stress relief. *Chil. J. Agric. Res.* 75, 85–91. doi: 10.4067/S0718-58392015000100012

Han, F., Lamb, J. C., and Birchler, J. A. (2006). High frequency of centromere inactivation resulting in stable dicentric chromosomes of maize. *Proc. Natl. Acad. Sci.* 103, 3238–3243. doi: 10.1073/pnas.0509650103

Han, Z. J., Sun, Y., Zhang, M., and Zhai, J. T. (2020). Transcriptomic profile analysis of the halophyte *Suaeda rigida* response and tolerance under NaCl stress. *Sci. Rep.* 10:15148. doi: 10.1038/s41598-020-71529-2

Han, Y., Yin, S., and Huang, L. (2015). Towards plant salinity tolerance-implications from ion transporters and biochemical regulation. *Plant Growth Regul.* 76, 13–23. doi: 10.1007/s10725-014-9997-6

Hayat, S., Hayat, Q., Alyemeni, M. N., Wani, A. S., Pichtel, J., and Ahmad, A. (2012). Role of proline under changing environments: a review. *Plant Signal. Behav.* 7, 1456–1466. doi: 10.4161/psb.21949

Hossain, M. S., and Dietz, K. J. (2016). Tuning of redox regulatory mechanisms, reactive oxygen species and redox homeostasis under salinity stress. *Front. Plant Sci.* 7:548. doi: 10.3389/fpls.2016.00548

Huang, G. T., Ma, S. L., Bai, L. P., Zhang, L., Ma, H., Jia, P., et al. (2012). Signal transduction during cold, salt, and drought stresses in plants. *Mol. Biol. Rep.* 39, 969–987. doi: 10.1007/s11033-011-0823-1

Hunter, J. C., and Mccoy, R. A. (2004). Applying randomization tests to cluster analyses. *J. Veg. Sci.* 15, 135–138. doi: 10.1111/j.1654-1103.2004.tb02246.x

Isayenkov, S. V., and Maathuis, F. J. (2019). Plant salinity stress, many unanswered questions remain. *Front. Plant Sci.* 10:80. doi: 10.3389/fpls.2019.00080

Jain, M., and Gadre, R. (1997). Effect of as on chlorophyll and protein contents and enzymic activities in greening maize tissues. *Water Air Soil Pollut.* 93, 109–115. doi: 10.1007/BF02404750

Jauhar, P. P. (1990). Multidisciplinary approach to genome analysis in the diploid species, *Thinopyrum bessarabicum* and *Th. elongatum* (*Lophopyrum elongatum*), of the triticeae. *Theor. Appl. Genet.* 80, 523–536. doi: 10.1007/BF00226755

Jiang, M., and Zhang, J. (2001). Effect of abscisic acid on active oxygen species, antioxidative defence system and oxidative damage in leaves of maize seedlings. *Plant Cell Physiol.* 42, 1265–1273. doi: 10.1093/pcp/pce162

Kakar, K. U., Nawaz, Z., Cui, Z., Almoneafy, A. A., Ullah, R., and Shu, Q. Y. (2017). Rhizosphere-associated *Alcaligenes* and *Bacillus* strains that induce resistance against blast and sheath blight diseases, enhance plant growth and improve mineral content in rice. *J. Appl. Microbiol.* 124, 779–796. doi: 10.1111/jam.13678

Kakar, K. U., Ren, X. L., Nawaz, Z., Cui, Z. Q., Li, B., Xie, G. L., et al. (2016). A consortium of rhizobacterial strains and biochemical growth elicitors improve cold and drought stress tolerance in rice (*Oryza sativa* L.). *Plant Biol.* 18, 471–483. doi: 10.1111/plb.12427

Kato, A., Lamb, J. C., and Birchler, J. A. (2004). Chromosome painting using repetitive DNA sequences as probes for somatic chromosome identification in maize. *Proc. Natl. Acad. Sci.* 101, 13554–13559. doi: 10.1073/pnas.0403659101

Kerepesi, I., and Galiba, G. (2000). Osmotic and salt stress-induced alteration in soluble carbohydrate content in wheat seedlings. *Crop Sci.* 40, 482–487. doi: 10.2135/cropsci2000.402482x

Khunpon, B., Cha-um, S., Faiyue, B., Uthaibutra, J., and Saengnil, K. (2018). Paclobutrazol mitigates salt stress in indica rice seedlings by enhancing glutathione metabolism and glyoxalase system. *Biologia* 73, 1267–1276. doi: 10.2478/s11756-018-0132-4

Lei, P., Liu, Z., Hu, Y., Kim, H., Liu, S., Liu, J., et al. (2021). Transcriptome analysis of salt stress responsiveness in the seedlings of wild and cultivated *Ricinus communis* L. *J. Biotechnol.* 327, 106–116. doi: 10.1016/j.jbiotec.2020.12.020

Leyva, A., Quintana, A., Sánchez, M., Rodríguez, E. N., Cremata, J., and Sánchez, J. C. (2008). Rapid and sensitive anthrone–sulfuric acid assay in microplate format to quantify carbohydrate in biopharmaceutical products: method development and validation. *Biologicals* 36, 134–141. doi: 10.1016/j.biologicals.2007.09.001

Li, S., Fan, C., Li, Y., Zhang, J., Sun, J., Chen, Y., et al. (2016). Effects of drought and salt-stresses on gene expression in *Caragana korshinskii* seedlings revealed by RNA-seq. *BMC Genomics* 17:200. doi: 10.1186/s12864-016-2562-0

Li, N., Zhang, Z., Chen, Z., Cao, B., and Xu, K. (2021). Comparative transcriptome analysis of two contrasting Chinese cabbage (*Brassica rapa* L.) genotypes reveals that ion homeostasis is a crucial biological pathway involved in the rapid adaptive response to salt stress. Frontiers. *Plant Sci.* 12:683891. doi: 10.3389/fpls.2021.683891

Li, W., Zhang, H., Zeng, Y., Xiang, L., Lei, Z., Huang, Q., et al. (2020). A salt tolerance evaluation method for sunflower (*Helianthus annuus* L.) at the seed germination stage. *Sci. Rep.* 10:10626. doi: 10.1038/s41598-020-67210-3

Luo, Q., Teng, W., Fang, S., Li, H., Li, B., Chu, J., et al. (2019). Transcriptome analysis of salt-stress response in three seedling tissues of common wheat. *Crop J.* 7, 378–392. doi: 10.1016/j.cj.2018.11.009

Mahmood, A., and Quarrie, S. A. (1993). Effects of salinity on growth, ionic relations and physiological traits of wheat, disomic addition lines from *Thinopyrum bessarabicum*, and two amphiploids. *Plant Breed.* 110, 265–276. doi: 10.1111/j.1439-0523.1993.tb00589.x

Margiotta, B., Colaprico, G., Urbano, M., Veronico, G., Tommasi, F., and Tomaselli, V. (2020). Halophile wheatgrass *Thinopyrum elongatum* (host) D.R. Dewey (poaceae) in three Apulian coastal wetlands: vegetation survey and genetic diversity. *Plant Biosyst.* 6, 1–15. doi: 10.1080/11263504.2020.1829732

Mbarki, S., Sytar, O., Cerda, A., Zivcak, M., Rastogi, A., and He, X., et al. (2018). "Strategies to mitigate the salt stress effects on photosynthetic apparatus and productivity of crop plants," in *Salinity Responses and Tolerance in Plants. Vol. 1*. eds. V. Kumar, S. H. Wani and P. Suprasanna et al. (Cham: Springer), 85–136.

Meena, M., Divyanshu, K., Kumar, S., Swapnil, P., Zehra, A., Shukla, V., et al. (2019). Regulation of L-proline biosynthesis, signal transduction, transport, accumulation and its vital role in plants during variable environmental conditions. *Heliyon* 5:e02952. doi: 10.1016/j.heliyon.2019.e02952

Mishra, N. S., Tuteja, R., and Tuteja, N. (2006). Signaling through MAP kinase networks in plants. *Arch. Biochem. Biophys.* 452, 55–68. doi: 10.1016/j.abb.2006.05.001

Muhammad, J., Samina, B., Soma, A., Sara, B., Asia, B., and Farman, U. (2012). Effect of salinity on physiological and biochemical characteristics of different varieties of rice. *Pak. J. Bot.* 44, 7–13. doi: 10.1080/12538078.2012.673824

Munns, R., and Tester, M. (2008). Mechanisms of salinity tolerance. *Annu. Rev. Plant Biol.* 59, 651–681. doi: 10.1146/annurev.arplant.59.032607.092911

Mushtaq, Z., Faizan, S., and Gulzar, B. (2020). Salt stress, its impacts on plants and the strategies plants are employing against it: a review. *J. Appl. Biol. Biotechnol.* 8, 81–91. doi: 10.7324/JABB.2020.80315

Nazar, R., Umar, S., and Khan, N. A. (2015). Exogenous salicylic acid improves photosynthesis and growth through increase in ascorbate-glutathione metabolism and S assimilation in mustard under salt stress. *Plant Signal. Behav.* 10:e1003751. doi: 10.1080/15592324.2014.1003751

Nounjan, N., Nghia, P. T., and Theerakulpisut, P. (2012). Exogenous proline and trehalose promote recovery of rice seedlings from salt-stress and differentially modulate antioxidant enzymes and expression of related genes. *J. Plant Physiol.* 169, 596–604. doi: 10.1016/j.jplph.2012.01.004

Omielan, J. A., Epstein, E., and Dvořák, J. (1991). Salt tolerance and ionic relations of wheat as affected by individual chromosomes of salt-tolerant *Lophopyrurn elongaturn*. *Genome* 34, 961–974. doi: 10.1139/g91-149

Qureshi, A. S., and Daba, A. W. (2019). Differential analysis of five quinoa (*Chenopodium quinoa* W.) genotypes under different salt stresses in a controlled environment. *Am. Eurasian J. Sustain. Agric.* 14, 14–21. doi: 10.22587/aejsa.2020.14.1.2

Rai, A., Cherif, A., Cruz, C., and Nabti, E. (2018). Extracts from marine macroalgae and *Opuntia ficus-indica* cladodes enhance halotolerance and enzymatic potential of diazotrophic rhizobacteria and their impact on wheat germination under salt stress. *Pedosphere* 28, 241–254. doi: 10.1016/S1002-0160(17)60333-3

Rehman, F., Munir, H., Raza, M. A., and Saeed, A. (2021). Uncover the salt tolerance potential of accessions based on photosynthetic attributes and interaction plot in tomato (*Solanum lycopersicum*). *Plant Breed.* 140, 130–141. doi: 10.1111/pbr.12881

Ruiz, K. B., Maldonado, J., Biondi, S., and Silva, H. (2019). RNA-seq analysis of salt-stressed *versus* non salt-stressed transcriptomes of *Chenopodium quinoa landrace* R49. *Genes* 10:1042. doi: 10.3390/genes10121042

Sako, K., Ha, V. C., Matsui, A., Tanaka, M., Sato, A., and Seki, M. (2021). Transcriptome analysis of *Arabidopsis thaliana* plants treated with a new compound Natolen128, enhancing salt stress tolerance. *Plan. Theory* 10:978. doi: 10.3390/plants10050978

Sakr, M. T., El-Sarkassy, N. M., and Fuller, M. P. (2012). Osmoregulators proline and glycine betaine counteract salinity stress in canola. *Agron. Sustain. Dev.* 32, 747–754. doi: 10.1007/s13593-011-0076-3

Sarwar, Y., and Shahbaz, M. (2019). GR24 triggered variations in morpho-physiological attributes of sunflflower (*Helianthus annuus*) under salinity. *Int. J. Agric. Biol.* 21, 34–40. doi: 10.17957/IJAB/15.0000

Sharma, A., Shahzad, B., Kumar, V., Kohli, S. K., Sidhu, G. P. S., Bali, A. S., et al. (2019). Phytohormones regulate accumulation of osmolytes under abiotic stress. *Biomol. Ther.* 9:285. doi: 10.3390/biom9070285

Shi, H., Ishitani, M., Kim, C., and Zhu, J. K. (2000). The Arabidopsis thaliana salt tolerance gene *SOS1* encodes a putative Na^+/H^+ antiporter. *Proc. Natl. Acad. Sci.* 97, 6896–6901. doi: 10.1073/pnas.120170197

Shu, K., Qi, Y., Chen, F., Meng, Y., Luo, X., Shuai, H., et al. (2017). Salt stress represses soybean seed germination by negatively regulating GA biosynthesis while positively mediating ABA biosynthesis. *Front. Plant Sci.* 8:1372. doi: 10.3389/fpls.2017.01372

Sikder, R. K., Wang, X., Jin, D., Zhang, H., Gui, H., Dong, Q., et al. (2020). Screening and evaluation of reliable traits of upland cotton (*Gossypium hirsutum* L.) genotypes for salt tolerance at the seedling growth stage. *J. Cotton Res.* 3:11. doi: 10.1186/s42397-020-00049-1

Singh, N., Mishra, A., and Jha, B. (2014). Over-expression of the peroxisomal ascorbate peroxidase (*SbpAPX*) gene cloned from halophyte *Salicornia brachiata* confers salt and drought stress tolerance in transgenic tobacco. *Mar. Biotechnol.* 16, 321–332. doi: 10.1007/s10126-013-9548-6

Sivakumar, J., Prashanth, J. E. P., Rajesh, N., and Osman, B. P. (2019). Effect of time-course salt stress on chlorophyll, proline and catalase activity in *Solanum lycopersicum* L. *Res. J. Biotechnol.* 14, 108–116.

Sobahan, M. A., Akter, N., Ohno, M., Okuma, E., Hirai, Y., and Mori, I. C. (2012). Effects of exogenous proline and glycinebetaine on the salt tolerance of rice cultivars. *Biosci. Biotechnol. Biochem.* 76, 1568–1570. doi: 10.1271/bbb.120233

Sohrabikertabad, S., Ghanbari, A., Mohassel Mohamad, H. R., Mahalati, M. N., and Gherekhloo, J. (2012). Effect of desiccation and salinity stress on seed germination and initial plant growth of *Cucumis melo*. *Planta Daninha* 31, 833–841. doi: 10.1590/S0100-83582013000400009

Sun, Y. L., and Hong, S. K. (2010). Exogenous proline mitigates the detrimental effects of saline and alkaline stresses in *Leymus chinensis* (Trin.). *J. Plant Biotechnol.* 37, 529–538. doi: 10.5010/JPB.2010.37.4.529

Surender, R. P., Jogeswar, G., Rasineni, G. K., Maheswari, M., Reddy, A. R., Varshney, R. K., et al. (2015). Proline over-accumulation alleviates salt stress and protects photosynthetic and antioxidant enzyme activities in transgenic sorghum [*Sorghum bicolor* (L.) Moench]. *Plant Physiol. Biochem.* 94, 104–113. doi: 10.1016/j.plaphy.2015.05.014

Trapnell, C., Williams, B. A., Pertea, G., Mortazavi, A., Kwan, G., Baren, V. M., et al. (2010). Transcript assembly and quantification by RNA-Seq reveals unannotated transcripts and isoform switching during cell differentiation. *Nat. Biotechnol.* 28, 511–515. doi: 10.1038/nbt.1621

Vighi, I., Benitez, L. C., Amaral, M. N., Moraes, G. P., Auler, P. A., Rodrigues, G. S., et al. (2017). Functional characterization of the antioxidant enzymes in rice plants exposed to salinity stress. *Biol. Plant.* 61, 540–550. doi: 10.1007/s10535-017-0727-6

Wang, H., Gong, M., Xin, H., Tang, L., Dai, D., Gao, Y., et al. (2018). Effects of chilling stress on the accumulation of soluble sugars and their key enzymes in *Jatropha curcas* seedlings. *Physiol. Mol. Biol. Plants* 24, 857–865. doi: 10.1007/s12298-018-0568-6

Wei, T., Wang, Y., and Liu, J. H. (2020). Comparative transcriptome analysis reveals synergistic and disparate defense pathways in the leaves and roots of trifoliate orange (*Poncirus trifoliata*) autotetraploids with enhanced salt tolerance. *Hortic. Res.* 7:88. doi: 10.1038/s41438-020-0311-7

Xu, Y., Guo, H., Geng, G. D., Zhang, Q. Q., and Zhang, S. Q. (2021). Changes in defense-related enzymes and phenolics in resistant and susceptible common wheat cultivars under aphid stress. *Acta Physiol. Plant.* 43:36. doi: 10.1007/s11738-021-03207-3

Yan, M., Zheng, L., Li, B., Shen, R., and Lan, P. (2021). Comparative proteomics reveals new insights into the endosperm responses to drought, salinity and submergence in germinating wheat seeds. *Plant Mol. Biol.* 105, 287–302. doi: 10.1007/s11103-020-01087-8

Yang, Y., and Guo, Y. (2018). Elucidating the molecular mechanisms mediating plant salt-stress responses. *New Phytol.* 217, 523–539. doi: 10.1111/nph.14920

Yuan, W. Y., and Tomita, M. (2015). *Thinopyrum ponticum* chromatin-integrated wheat genome shows salt-tolerance at germination stage. *Int. J. Mol. Sci.* 16, 4512–4517. doi: 10.3390/ijms16034512

Zeng, P., Zhu, P., Qian, L., Qian, X., Mi, Y., Lin, Z., et al. (2021). Identification and fine mapping of qGR6. 2, a novel locus controlling rice seed germination under salt stress. *BMC Plant Biol.* 21:36. doi: 10.1186/s12870-020-02820-7

Zhang, M., Smith, J. A. C., Harberd, N. P., and Jiang, C. (2016). The regulatory roles of ethylene and reactive oxygen species (ROS) in plant salt stress responses. *Plant Mol. Biol.* 91, 651–659. doi: 10.1007/s11103-016-0488-1

Zhou, Y., Wen, Z., Zhang, J., Chen, X., Cui, J., and Xu, W. (2017). Exogenous glutathione alleviates salt-induced oxidative stress in tomato seedlings by regulating glutathione metabolism, redox status, and the antioxidant system. *Sci. Hortic.* 220, 90–101. doi: 10.1016/j.scienta.2017.02.021

Zhu, J. K. (2016). Abiotic stress signaling and responses in plants. *Cell* 167, 313–324. doi: 10.1016/j.cell.2016.08.029

Zhu, D., Luo, F., Zou, R., Liu, J., and Yan, Y. (2021). Integrated physiological and chloroplast proteome analysis of wheat seedling leaves under salt and osmotic stresses. *J. Proteome* 234:104097. doi: 10.1016/j.jprot.2020.104097

Conflict of Interest: The authors declare that the research was conducted in the absence of any commercial or financial relationships that could be construed as a potential conflict of interest.

Publisher's Note: All claims expressed in this article are solely those of the authors and do not necessarily represent those of their affiliated organizations, or those of the publisher, the editors and the reviewers. Any product that may be evaluated in this article, or claim that may be made by its manufacturer, is not guaranteed or endorsed by the publisher.

Copyright © 2022 Peng, Wang, Geng, Yang, Yang, Yang, Xu, Zhang, Kakar, Li and Zhang. This is an open-access article distributed under the terms of the Creative Commons Attribution License (CC BY). The use, distribution or reproduction in other forums is permitted, provided the original author(s) and the copyright owner(s) are credited and that the original publication in this journal is cited, in accordance with accepted academic practice. No use, distribution or reproduction is permitted which does not comply with these terms.

frontiers in Plant Science

ORIGINAL RESEARCH
published: 13 January 2022
doi: 10.3389/fpls.2021.785267

Select and Sequence of a Segregating Sugar Beet Population Provides Genomic Perspective of Host Resistance to Seedling *Rhizoctonia solani* Infection

Paul Galewski[1,2]*, *Andrew Funk*[2,3] and *J. Mitchell McGrath*[4]

[1] United States Department of Agriculture – Agricultural Research Service (USDA-ARS) Northwest Irrigation and Soils Research Laboratory, Kimberly, ID, United States, [2] Department of Plant, Soil, and Microbial Science, Plant Breeding, Genetics, and Biotechnology Program, Michigan State University, East Lansing, MI, United States, [3] United States Department of Agriculture – National Institute of Food and Agriculture (USDA-NIFA) Institute of Food Production and Sustainability, Kansas City, MO, United States, [4] United States Department of Agriculture – Agricultural Research Service (USDA-ARS) Sugar Beet and Bean Research Unit USDA-ARS, East Lansing, MI, United States

OPEN ACCESS

Edited by:
Magdalena Arasimowicz-Jelonek,
Adam Mickiewicz University, Poland

Reviewed by:
Piergiorgio Stevanato,
University of Padua, Italy
Khaled Michel Hazzouri,
United Arab Emirates University,
United Arab Emirates

***Correspondence:**
Paul Galewski
paul.galewski@usda.gov

Specialty section:
This article was submitted to Plant Pathogen Interactions, a section of the journal Frontiers in Plant Science

Received: 28 September 2021
Accepted: 12 November 2021
Published: 13 January 2022

Citation:
Galewski P, Funk A and McGrath JM (2022) Select and Sequence of a Segregating Sugar Beet Population Provides Genomic Perspective of Host Resistance to Seedling Rhizoctonia solani Infection. Front. Plant Sci. 12:785267. doi: 10.3389/fpls.2021.785267

Understanding the genetic basis of polygenic traits is a major challenge in agricultural species, especially in non-model systems. Select and sequence (SnS) experiments carried out within existing breeding programs provide a means to simultaneously identify the genomic background of a trait while improving the mean phenotype for a population. Using pooled whole genome sequencing (WGS) of selected and unselected bulks derived from a synthetic outcrossing sugar beet population EL57 (PI 663212), which segregates for seedling rhizoctonia resistance, we identified a putative genomic background involved in conditioning a resistance phenotype. Population genomic parameters were estimated to measure fixation (*He*), genome divergence (F_{ST}), and allele frequency changes between bulks (DeltaAF). We report on the genome wide patterns of variation resulting from selection and highlight specific genomic features associated with resistance. Expected heterozygosity (*He*) showed an increased level of fixation in the resistant bulk, indicating a greater selection pressure was applied. In total, 1,311 biallelic loci were detected as significant F_{ST} outliers ($p < 0.01$) in comparisons between the resistant and susceptible bulks. These loci were detected in 206 regions along the chromosomes and contained 275 genes. We estimated changes in allele frequency between bulks resulting from selection for resistance by leveraging the allele frequencies of an unselected bulk. DeltaAF was a more stringent test of selection and recovered 186 significant loci, representing 32 genes, all of which were also detected using F_{ST}. Estimates of population genetic parameters and statistical significance were visualized with respect to the EL10.2 physical map and produced a candidate gene list that was enriched for function in cell wall metabolism and plant disease resistance, including pathogen perception, signal transduction, and pathogen

response. Specific variation associated with these genes was also reported and represents genetic markers for validation and prediction of resistance to Rhizoctonia. Select and sequence experiments offer a means to characterize the genetic base of sugar beet, inform selection within breeding programs, and prioritize candidate variation for functional studies.

Keywords: *Beta vulgaris*, sugar beet, Rhizoctonia resistance, synthetic populations, gene discovery

INTRODUCTION

The characterization of resistance sources for the genetic improvement of beet (*Beta vulgaris*) is a long-standing challenge. The USDA sugar beet germplasm is enriched for important traits such as resistance to disease and adaptation to local production regions. The pedigrees of this material suggest many of these traits can be traced back to wide hybridizations between sugar beet and wild beet *(Beta maritima*) (Doney, 1995; Panella et al., 2015). Beet is an outcrossing species, wind pollinated and generally self-incompatible. As a result, beet populations are highly heterozygous. Historically, crop improvement has been carried out via recurrent phenotypic selection and sib mating (Doney and Theurer, 1978). Commercial sugar beets are hybrid, and the production of hybrid seed relies on a narrow but well characterized genetic base where the frequencies of cytoplasmic male sterility (CMS) and CMS restorers are well understood. The need to maintain the genetic backgrounds required for hybrid seed production while breeding for multiple disease resistance traits, local adaptation, and yield makes the utilization of novel genetic variation a slow and resource-intensive process. Beet reference genomes and sequencing technologies have increased our ability to characterize genome variation within diverse beet lineages and breeding lines (Funk et al., 2018; Galewski and McGrath, 2020). The use of whole genome sequencing (WGS) to inform traditional beet breeding programs provides a system for "select and sequence" (SnS) experiments. These methods are a powerful tool for detecting the genetic basis of phenotypic selection in experimental populations (Schlötterer et al., 2015; Burghardt et al., 2018) and is an efficient way to prioritize candidate variation for functional studies and marker validation in the future (Burny et al., 2020).

Advances in genomic resources, population genomic methods and experimental design have improved the process of gene discovery in agricultural species. Reference genomes provide an anchor to link genetic variation with coding sequences underlying phenotypic variation (Hufford et al., 2012). Accurate gene models determined from ab-initio gene prediction, transcript evidence, and gene ontology can help to infer gene function and provide hypotheses for biological mechanisms (Salzberg, 2019). The genome EL10.2 is a contiguous chromosome level assembly (McGrath et al., 2020) with high homology to other beet reference genomes such as RefBeet (Dohm et al., 2014). Reference genomes have increased our ability to rapidly catalog and compare variation within and between populations using genome scans (Nielsen et al., 2005), bulk segreant analysis (BSA) (Michelmore et al., 1991) and mapping by sequencing approaches (Schneeberger et al., 2009). WGS has also been used to provide a complete picture of genetic variation within a population including structural variants (SV) and presence-absence variation (PAV) (Pinosio et al., 2016; Wang et al., 2018). Recent research has demonstrated the impact of SV and PAV on important phenotypic variation observed between cultivars and adaptative trait variation including disease resistance (Zhou et al., 2019; Hämälä et al., 2021). SnS experiments show potential to detect genetic variation linked to selection and adaptation in experimentally generated populations (Schlötterer et al., 2015). Additionally, numerous methods to detect positive selection within populations have been established (reviewed in Weigand and Leese, 2018) which facilitates the adoption of SnS experiments within breeding programs for agricultural crops such as beet.

Phenotypic variation in beets is often measured at the level of the population due to difficulties inbreeding and fixing variation in single plants, fostering comparisons between populations rather than comparisons between individuals. Pooled sequencing of populations is an effective way to capture and compare causal genetic variation in beet, either by partitioning variation according to phenotypes within a segregating population, or by comparing different populations. The utility of pooled data has been demonstrated (Schlötterer et al., 2014) and can provide accurate estimates of allele frequency (Lynch et al., 2014) and population genetic parameters (Ferretti et al., 2013). Pooled sequencing increases the effective number of assayed recombination events, improving our ability to resolve causal variation vs. traditional mapping approaches. In beets, pooled sequencing has been utilized to understand how diversity is distributed in crop type lineages (Galewski and McGrath, 2020) and within selected breeding populations (Ries et al., 2016). The later research used pooled data and a mapping by sequencing approach to discover causal variation associated with hypocotyl color, a monogenic trait. Our hypothesis is that pooled sequencing could also be effective for resolving polygenic traits with continuous phenotypes, which are more difficult to detect with traditional marker-based approaches. For example, disease resistance traits have been a major target of sugar beet breeding for more than a century and the application of pooled sequence data to inform polygenic traits such as Rhizoctonia resistance is warranted.

Rhizoctonia solani Kühn is a soil borne pathogen which can cause seedling dampening off and crown and root rot, both of which can severely impact sugar yield for growers (Gaskill et al., 1970). Various management practices are used to mitigate *R. solani* infection in the field and maintain crop profitability. This includes crop rotation, seed treatments and fungicide applications (Bolton et al., 2010). Genetic resistances

have been identified but appear to be derived from relatively few sources (Panella, 2005) which highlights the need for identifying new sources. Unfortunately, genetic resistance to rhizoctonia is poorly characterized, and while no single germplasm source can be attributed to Rhizoctonia resistance in beet, the long history of selection for resistance to crown and root rot from the USDA-ARS Ft. Collins, CO, United States germplasm enhancement program likely represents the major resistance source in commercial materials. Seedling resistance was identified from these materials and from the USDA-ARS East Lansing, MI, United States germplasm enhancement program (Panella et al., 2015). Early reports describe resistance as polygenic with many small-effect alleles (Hecker and Ruppel, 1975). Some major resistance quantitative trait loci (QTL) have been described in greenhouse studies (Lein et al., 2008) but the added complexity of field conditions and year effects (Strausbaugh et al., 2013a), host growth stage (Nagendran et al., 2009; Liu et al., 2019), cultivar and pathogen interactions (Strausbaugh et al., 2013b), and confounding infections from bacterial pathogens (Strausbaugh et al., 2013a) suggest many genes contribute to rhizoctonia resistance in sugar beet. Other research suggests the involvement of additional compounds and proteins in rhizoctonia resistance, such as reactive oxygen species (Taheri and Tarighi, 2010), polygalacturonase-inhibiting proteins (Li and Smigocki, 2018), and major latex protein-like proteins (Holmquist et al., 202). Newly sequenced rhizoctonia genomes have further detailed the complexity of host-pathogen interactions resulting from different anastomosis groups, putative genes, enzymes, and effectors molecules (Wibberg et al., 2016).

This research is focused on understanding plant host resistance to seedling Rhizoctonia by sequencing bulks of phenotypically distinct individuals derived from a synthetic outcrossing population, EL57 (PI 663212). Using WGS, existing reference genomes, and selection for resistance we highlight a genomic background associated with seedling Rhizoctonia resistance. In identifying the genetic determinants underlying resistance we show how these methods can be used to characterize polygenic traits in beet (*B. vulgaris)*, inform future experiments, and provide genetic solutions to long standing challenges faced by sugar beet producers.

MATERIALS AND METHODS

Populations and Sequencing

The population EL57 is a unique synthetic population combining mostly Eastern US germplasm traits in a self-fertile genetic background, and is diploid, multigerm, and biennial. EL57 is a very broad genetic base diploid combining genetics of 660 mother roots with the unique feature that 98% of the 133 parental used lines are self-fertile due to a dominant gene (Sf) introgressed from C869 (PI 628754) or C869 CMS (PI 628755). 21% of the parents were derived from C869 CMS and thus have the S-cytoplasm. Male sterility, both nuclear male sterility from C869 and CMS, was used to capture pollen from open-pollinated increases of a wide variety of pollinators from 1997 through 2007. Traits expected to be segregating in the population include Aphanomyces seedling disease and Cercospora leaf spot resistances contributed by sugar beet germplasms SP7622 (aka SP6822, 20% of original pollinators), USH20 (8% of original pollinators), and SP85303 (PI 590770, 6% of original pollinators), Rhizoctonia resistance derived from EL51 (PI 598074, 13% of original pollinators), curly top and rhizomania resistance selections from C931 (PI 636340) and EL0204 (PI 655951) (5% of original pollinators), a series of Aphanomyces resistant or salt-tolerant germination breeding lines and selections (derived from PI 165485, PI 271439, PI 518160, PI 546409, PI 562591, PI 562599, and PI 562601) (20% of original pollinators in total), a series of 17 nematode resistant breeding lines from the Salinas, CA USDA-ARS breeding program (13% of original pollinators), and a mixture of released and unreleased breeding lines derived from high sucrose, smooth-root selections (23% of original pollinators).

EL57 was planted in the SVREC seedling Rhizoctonia nursery on May 15, 2017, as a large selection block of 161 plots and inoculated with Rhizoctonia isolate RG2-2 on June 6. Seven plots of EL57 were not inoculated as a control. Approximately 8 weeks later leaves were harvested from non-inoculated and inoculated plots, representing three bulks. Resistant and susceptible bulks were chosen from the inoculated plots, and an unselected bulk was taken from non-inoculated plots. Leaf material from 25 plants was harvested and pooled for each of the three bulks. Pooled leaf material was homogenized, and DNA was extracted using the Macherey-Nagel NucleoSpin Plant II Genomic DNA extraction kit (Bethlehem, PA). One microgram of DNA for each population was submitted to Admera Health, LLC, where NGS libraries were constructed using TruSeq bar-code adapters. The sequencing reactions were carried out on the Illumina Hi-Seq 2500 in a 2 × 150 bp paired-end format with a target coverage of 80x relative to the predicted 758 Mb genome size of beet (Arumuganathan and Earle, 1991). Post-sequencing read quality was assessed using FastQC (Andrews, 2010). Library bar-code adapters were removed and reads were trimmed according to a quality threshold using TRIMMOMATIC (Bolger et al., 2014) invoking the following options (ILLUMINACLIP:adapters.fa:2:30:10 LEADING:3 TRAILING:3 SLIDINGWINDOW:4:15 MINLEN:36). These filtered reads were used for downstream analysis.

Alignment and Variant Detection

Reads from each population were aligned to the *B. vulgaris* reference genome assembly EL10.2 (McGrath et al., 2020) using BWA mem (Li, 2013). The resulting alignment files were sorted and merged using SAMtools (Li et al., 2009). Variants for each population were called simultaneously on all three populations using the program Freebayes (Garrison and Marth, 2012). Variants were filtered for mapping quality, number of variants detected and depth across sites. After the initial variant detection step, the vcf file was filtered for genotype quality, GQ $\geq$ 20, and read depth, $N < 300$. Variants were then partitioned into those that were detected as biallelic and those that were multi-allelic. The biallelic sites were used for the estimation of population genetic parameters and the multiallelic sites were retained for consequence on phenotype after significant regions

were determined. In addition, structural variants were cataloged in each sample using the program Manta (Chen et al., 2016).

Genome Divergence—Allele Frequency, F_{ST} and DeltaAF

A python program was used to count alleles for all biallelic variants within the three populations. Allele frequency was estimated for the resistant, susceptible, and unselected EL57 populations. Population genetic parameters were estimated using the allele frequency within each population such that ($p + q = 1$). The variable p was designated as the reference allele of the EL10.2 reference genome and q as the alternate state. The degree of fixation was estimated at all biallelic sites using the expected heterozygosity (*He)* or *2pq*. Global levels of fixation with respect to selection were calculated as the average of *He* across all sites. F_{ST} was used to calculate differentiation between the resistant and susceptible populations at each locus (Eq. 1). The parameter $F_{ST}24$ was estimated by calculating F_{ST} within a sliding window of 25 biallelic variant sites, or 12 variant sites flanking a single biallelic locus across the genome. Significant regions along chromosomes were determined by loci that showed a significant F_{ST} value at a given locus. Significance thresholds were defined by P-values < 0.01, calculated using the empirical distribution of all F_{ST} values.

$$F_{ST} = \frac{\sigma_s^2}{\sigma_T^2} = \frac{\sigma_s^2}{\bar{p}\left(1-\bar{p}\right)} \quad (1)$$

Equation 1: shows F_{ST} is defined as the ratio of variance in allele frequency of the subpopulation (s) relative to the total population (t), where p is the allele frequency of allele (p).

Delta allele frequency was calculated by using a series of Boolean operators to determine the loci which pass allele frequency thresholds in selected populations relative to the unselected population. This provided a null distribution from which to derive the genomic locations of large changes in allele frequency with respect to selection for resistance.

$$\begin{aligned} &DeltaAF(RS) = max(AFR,AFS)—min(AFR,AFS)\\ &DeltaAF(RW) = max(AFR,AFS)—min(AFR,AFS)\\ &DeltaAF(SW) = max(AFR,AFS)—min(AFR,AFS)\\ &Delta\ AF\ =\ (DeltaAF(RS) > 0.8; DeltaAF(SW) < 0.15) \end{aligned} \quad (2)$$

Equation 2: determines sites where the relative change in allele frequency between resistant and susceptible bulks is > 0.8 and the allele frequency change between susceptible and unselected bulks is low, >0.15.

Genome Visualization

Visualization of significant genomic regions was carried out by plotting $F_{ST}24$ along chromosomes with a density plot of all significant F_{ST} values. Python was used for the manipulation of data sets and estimation of population genetic parameters, while R libraries were used for plotting the final data matrixes. DeltaAF was also plotted across the genome, highlighting only those regions where divergence in allele frequency between the resistant and susceptible bulk was high and the susceptible and unselected population was low. Regions along the chromosome of high significance were determined by investigating a significant locus and searching within a 50 kb window upstream to determine the size and significance of a region with respect to selection. All regions with significant F_{ST} or DeltaAF were visualized using R. The density and distribution of variation was also considered by plotting data relative to the physical map provided by the EL10.2 genome assembly along with EL10 gene models and annotations. SNPeff (Cingolani et al., 2012) was used to annotate variants based on physical position and determine functional consequences in terms of protein coding changes.

Determination of Resistance Genes Involved in Resistance to *Rhizoctonia solani*

A combination of statistical analysis and genome resources were leveraged to identify targets within or adjacent to significant regions across the genome (e.g., F_{ST}, $F_{ST}24$, and DeltaAF). Determination of putative gene loci involved in resistance were based on all previous analysis as well as significant homology to functional validated candidates in other species. Markers were derived for use in predicting seedling rhizoctonia resistance by extracting significant variation from .vcf files.

RESULTS

Nearly 3,500 plants from the synthetic, outcrossing sugar beet population EL57 (PI 663212) were sown, inoculated with *Rhizoctonia solani* isolate RG2-2, and allowed to grow for 8 weeks before being evaluated for seedling dampening off. Rhizoctonia symptoms became progressively worse throughout the growing season: average stand counts prior to inoculation were 21.3 plants/plot (*SD* = 3.33) and post-inoculation at the end of the season (October 17) were 4.9 plants/plot (*SD* = 1.74), or approximately 77% plant death. This suggested that the disease nursery provided a strong selection pressure for resistance to *Rhizoctonia solani* infection and an opportunity to identify a genetic basis for this important trait. Three bulks were sampled for WGS each representing 25 plants (0.7% of the total population). Susceptible individuals (S bulk) were selected with respect to leaf symptoms and confirmed as showing root symptoms as well. Resistant individuals (R bulk) showed no visual leaf or root symptoms (**Figure 1**). An unselected bulk was also sampled which helped to identify allele frequency changes resulting from selection vs. historical population dynamics and/or genetic drift.

An average of 259,888,506 reads were generated for each of the three bulks, representing an average coverage of 80.3X per sample. The raw reads were trimmed and mapped to the EL10.2 reference genome: 98.1% of bases were retained after filtering and 95% of reads successfully aligned. The aligned reads were used to identify sequence variation across the three populations. A total of 3,235,162 variants were detected, consisting of biallelic, multi-allelic, and structural variants (SV). Biallelic variation accounted for 2,812,301 loci (86.93%) of the total variation and multi-allelic variation accounted for 249,045 (7.70%). Biallelic and multi allelic variation was further categorized by type,

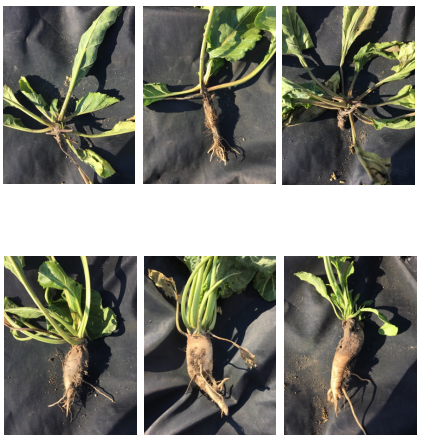

FIGURE 1 | Phenotypic selection of EL57 bulks segregating for resistance to seedling Rhizoctonia.

TABLE 1 | Summary of variant detection.

	Number	Percent (%)
Total variants	3,235,162	100.00%
Biallelic	2,812,301	86.93%
Multiallelic	249,045	7.70%
Structural variant (SV)	173,816	5.37%
SV insertion	*26,837*	
SV deletion	*68,922*	
SV translocations	*78,057*	
Biallelic	2,812,301	100.00%
Single nucleotide polymorphism (SNP)	1,939,590	68.97%
Insertion	454,829	16.17%
Deletion	186,790	6.64%
Complex substitution	168,053	5.98%
Multi nucleotide polymorphism (MNP)	63,039	2.24%
Population	**Expected heterozygocity (2pq)**	
EL57 unselected bulk	0.304	
EL57 resistant bulk	0.298	
EL57 susceptible bulk	0.305	

including insertions, deletions, single nucleotide polymorphisms (SNP), multi nucleotide polymorphisms (mnp) and complex substitutions (**Table 1**). The biallelic variation was used for statistical analysis due to its ease in estimating allele frequency and population genomic parameters. Expected heterozygosity (*He*) showed the degree of fixation resulting from selection for a resistance phenotype. A reduction in *He* was observed between the unselected (0.304) and the resistant bulk (0.298). *He* for the susceptible bulk (0.305) was closer to the unselected bulk (**Table 1**). This is consistent with selection pressure applied and the frequency that resistance was observed in the base EL57 population. We also found 173,817 SVs (5.37%), which were subcategorized as insertions (26,837), deletions (68,922), and putative translocations (78,057) relative to the EL10.2 genome (**Table 1**).

Selection was investigated across the genome using the parameters F_{ST} and DeltaAF. F_{ST} estimated the apportionment of variation in allele frequency between bulks. The empirical distribution of F_{ST} allowed us to assign significance values (p-values) to all biallelic loci. At significance levels of $p < 0.05$, $p < 0.01$, and $p < 0.001$. F_{ST} values were equal to 0.22, 0.84, and 0.91 respectively. In total, 1,311 loci were detected with significant F_{ST} ($p < 0.01$). Since F_{ST} shows divergence at a single site, it can be hard to interpret if the divergence is the result of genetic drift or selection. To address this issue, F_{ST} was also calculated in a sliding window ($F_{ST}24$) which considered 24 adjacent variant sites as a single entity. This could reduce noise from genetic drift under the assumption that if selection was acting on a site, linkage disequilibrium would cause adjacent sites to diverge along with the causal variant. As expected, the $F_{ST}24$ analysis reduced the number of significant regions associated with divergence between the resistant and susceptible bulks (**Figure 2** and **Table 2**). Divergence between resistant and susceptible bulks, measured by F_{ST}, occurred on all chromosomes but some chromosomes contained more divergent loci than others. It was also noted that divergent sites appeared to be within gene rich regions, and not associated with centromeric or telomeric sequences.

Delta AF was used to test changes in allele frequency between populations selected for resistance and susceptibility to rhizoctonia vs. an unselected population. Our expectation for DeltaAF was that large differences in allele frequency detected between susceptible and resistant bulk would not be found between susceptible and unselected bulks, given the frequency of resistant individuals in the unselected bulk was estimated at 23%. In terms of significant sites, DeltaAF was a more stringent statistic. In total, 186 sites were detected as significant, representing 42 genes. The complete table of all DeltaAF loci are presented in **Supplementary Table 2**. Comparisons between significant loci produced by F_{ST}, F_{ST} 24, and DeltaAF across the chromosomes are present in **Table 2**.

Significant genomic regions were defined by taking all 1311 F_{ST} values which passed the significance threshold of 0.84 ($p < 0.01$) and looking for physical clusters of significant F_{ST} values within 50 kb of a given locus. This produced a list of regions along the chromosome which were the most diverged between the resistant and susceptible bulks (**Table 3**). In total 206 regions were identified and the size and magnitude of significance for each region were evaluated. In total 83 of the regions were represented by only one locus with significant F_{ST}. These appeared less likely to reflect a selective sweep but represent potential functional variants between pools and may contribute to the phenotype. The remaining 43 regions were represented by more than a single locus (3–17 loci) within 50 kb of another significant variant site. The average size of a significant region was 27,624 bp, with a range from 3 to 130,093 bp in length. The complete table with F_{ST} values is presented in **Supplementary Table 1**. Significant DeltaAF loci were associated with 136 regions across the chromosome and were determined the same way as F_{ST}.

Genes that were associated with significant F_{ST} and DeltaAF values were extracted by using a significance threshold and determining their physical position relative to gene boundaries (5′ URT and 3′ UTR) or the upstream promoter sequences,

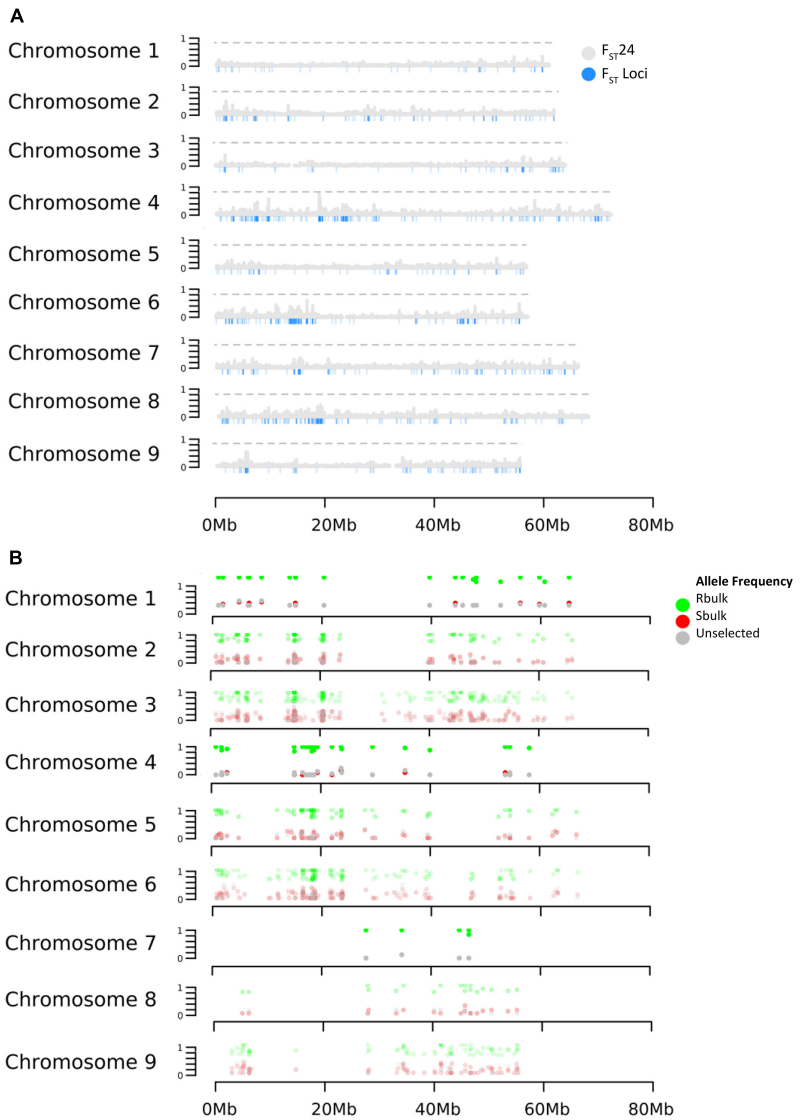

FIGURE 2 | Effects of selection on allele frequency across *B. vulgaris* chromosomes. **(A)** Distribution of F_{ST} 24 and F_{ST} **(B)** Distribution of DeltaAF.

defined as 3 kb flanking the gene. In total, 1,316 loci with high F_{ST} were associated with 206 regions, containing 311 genes. These could be further subdivided into variants associated with the gene sequences (275) (**Supplementary Table 3**) and those associated promoter sequences of genes (36) (**Supplementary Table 4**). In total, DeltaAF recovered 42 genes, and 32 were identified as having high DeltaAF signals within the gene boundaries (**Supplementary Table 5**) and 10 were identified in putative promoter sequence (3 kb flanking the genes) (**Supplementary Table 6**). All of the genes associated with Delta AF genes were found within the larger F_{ST} gene set. The total biallelic variant set was analyzed using SNPeff and produced 56,451 annotations predicted to have high consequences on gene function. Only 11 of these coincide with loci determined to have significant F_{ST} or DeltaAF.

We combined data from statistical tests for enrichment (e.g., F_{ST} and DeltaAF) with custom visualization tools to inspect regions of significance with respect to the EL10.2 physical map (**Figure 3**). A preliminary set of 41 candidate

TABLE 2 | Accumulation of significant loci among chromosomes.

	FST ($p < 0.01$)	FST24 ($p < 0.01$)	DeltaAF
Chromosome 1	314	153	37
Chromosome 2	204	18	32
Chromosome 3	145	0	25
Chromosome 4	79	4	13
Chromosome 5	117	26	14
Chromosome 6	50	0	7
Chromosome 7	235	112	48
Chromosome 8	69	0	5
Chromosome 9	103	52	5

TABLE 3 | Comparison of regions derived from F_{ST} and Delta AF.

	Number of regions	Genes associated with regions	Promoters associated with regions	Average number of loci in regions	Average size of region (bp)
FST	206	275	36	6.39	14,998
DeltaAF	136	32	10	1.37	3,559

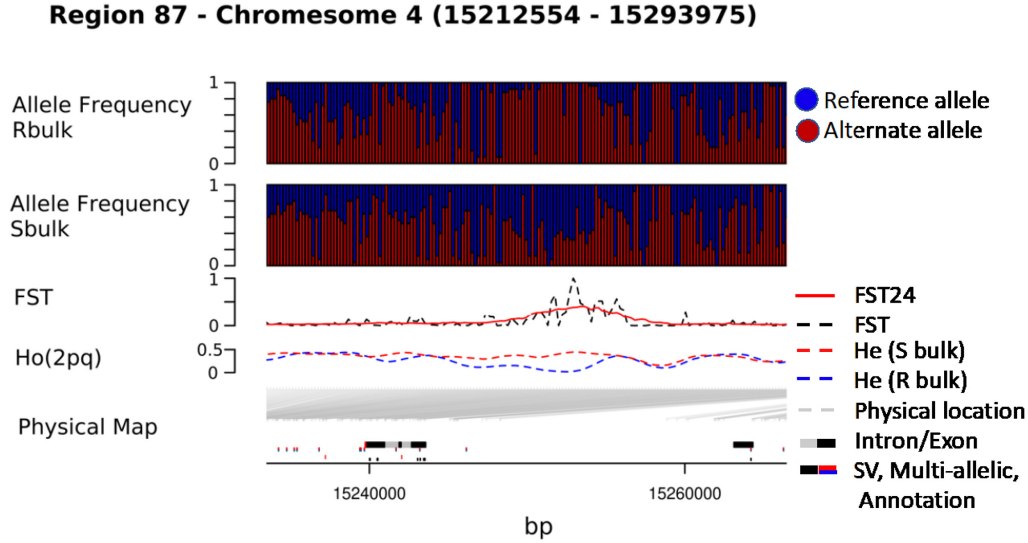

FIGURE 3 | Visualization of chromosome regions on the basis significant F_{ST} (p-value<0.01).

regions was generated based on their proximity and effect of genetic variation relative to gene models. We queried publicly available databases and the scientific literature to determine the functional identity of the candidate genes to prioritize targets of future research. This analysis revealed 18 genes with known or putative function in pathogen resistance and six genes likely involved in cell wall metabolism (**Table 4**). The pathogen defense related genes included multiple representatives from three classes: four chitinases (EL10Ac3g05998, EL10Ac3g06002, EL10Ac3g06003, EL10Ac3g05996), three putative pathogen-responsive Ser/Thr receptor kinases (EL10Ac4g07999, EL10Ac3g06055, EL10Ac3g06056), and two genes involved in defense-associated volatile ester catabolism (EL10Ac6g14646 and EL10Ac3g05812). The cell wall-related genes included five metabolic genes (EL10Ac6g13717, EL10Ac6g13257, EL10Ac5g13023, EL10Ac3g05157, and EL10Ac3g05159) as well as one Myb-related transcription factor EL10Ac1g00142. It is noteworthy that the Peroxidase 5 genes EL10Ac3g05157 and EL10Ac3g05159 are likely a single gene with a transposon inserted into the coding region in the EL10.2 reference genome (the transposon is recorded as EL10Ac3g05158 "Retrovirus-related Pol polyprotein from transposon TNT1–94" in the EL10.2 annotation). Unfortunately, the variant detection strategy employed in this report cannot determine if this peroxidase gene is intact in either the resistant or susceptible bulks. However, the combination of F_{ST}, DeltaAF, and visualization of variant positions was able to generate a plausible candidate gene list for further investigation. Potential markers and their significance were reported which could be used for the prediction of resistance (**Table 5**). Subsequent rounds of the "Select and Sequence" strategy would help to validate the markers generated and inform how genomic prediction might be applied to beet populations segregating for phenotypes of interest.

DISCUSSION

Identifying the genetic basis of quantitative traits is a longstanding challenge in crop improvement. In this report, we used a select and sequence (SnS) approach to identify contrasting genetic variants between resistant and susceptible bulks drawn from a synthetic breeding population segregating for resistance to seedling rhizoctonia infection. Using pooled sequencing, we estimated population genetic parameters to investigate fixation (He), genome divergence (F_{ST}) and changes in allele frequency (DeltaAF) resulting from selection and identified candidate genomic variation underlying Rhizoctonia resistance. We generated a list of putative candidate genes by visualizing the population genetic data with respect to the EL10.2 physical map. The candidate gene list was enriched for genes associated with pathogen defense and cell—wall biosynthesis, both of which are plausible components of rhizoctonia resistance. Additional rounds of selection within the EL57 base population or the advancement of generations in the presence of divergent selection could further resolve causal genetic variation and validate the genetic basis of Rhizoctonia resistance in beet.

TABLE 4 | Candidate genes derived from F_{ST}, DeltaAF and proximity to chromosomal regions of high significance.

Data	Chr	Gene	Scaffold	Start	Stop	Strand	Identity
FSTG	1	EL10Ac1g00142	lcl| Scaffold_4	62288988	62293643	–	Myb-related protein Zm1
Region	3	EL10Ac3g05118	lcl| Scaffold_7	2505514	2508049	+	Mitochondrial metalloendopeptidase OMA1
DAF/FSTG	3	EL10Ac3g05157	lcl| Scaffold_7	2964465	2988432	+	Peroxidase 5 {ECO:0000250| UniProtKB:P22195}
Region	3	EL10Ac3g05158	lcl| Scaffold_7	2975394	2980297	–	Retrovirus-related Pol polyprotein from transposon TNT1-94
Region	3	EL10Ac3g05159	lcl| Scaffold_7	2986817	2992340	–	Peroxidase 5 {ECO:0000250| UniProtKB:P22195}
FSTG	3	EL10Ac3g05812	lcl| Scaffold_7	11447524	11463930	–	Probable carboxylesterase 1
FSTG	3	EL10Ac3g05814	lcl| Scaffold_7	11478272	11491769	+	Putative disease resistance protein RGA1
FSTG	3	EL10Ac3g05956	lcl| Scaffold_7	13796358	13808136	–	Cytosolic sulfotransferase 15
Region	3	EL10Ac3g05996	lcl| Scaffold_7	14499893	14502240	+	Endochitinase CH25
Region	3	EL10Ac3g05998	lcl| Scaffold_7	14524198	14525516	+	Endochitinase
Region	3	EL10Ac3g06002	lcl| Scaffold_7	14553565	14555809	+	Endochitinase A
FSTG	3	EL10Ac3g06003	lcl| Scaffold_7	14553822	14558536	–	Chitinase 9
FSTG	3	EL10Ac3g06012	lcl| Scaffold_7	14703412	14714093	–	3beta-hydroxysteroid-dehydrogenase/decarboxylase isoform 3
FSTG	3	EL10Ac3g06014	lcl| Scaffold_7	14744397	14756713	–	Calreticulin-3
Region	3	EL10Ac3g06055	lcl| Scaffold_7	15643877	15645017	+	Wall-associated receptor kinase 1
FSTP	3	EL10Ac3g06056	lcl| Scaffold_7	15666223	15687673	+	Wall-associated receptor kinase 2
Region	4	EL10Ac4g07999	lcl| Scaffold_3	6786108	6793448	–	Probable leucine-rich repeat receptor-like serine/threonine-protein kinase At5g15730
Region	5	EL10Ac5g12121	lcl| Scaffold_2	16531411	16538896	+	zinc-binding in reverse transcriptase
FSTG	5	EL10Ac5g13023	lcl| Scaffold_2	787508	799504	–	Oxysterol-binding protein-related protein 2A
FSTG	6	EL10Ac6g13257	lcl| Scaffold_1	69644352	69648601	–	Endo-1,4-beta-xylanase F1
FSTP	6	EL10Ac6g13717	lcl| Scaffold_1	62821741	62829006	+	Anthocyanidin 3-O-glucoside 2"-O-glucosyltransferase
NA	6	EL10Ac6g14646	lcl| Scaffold_1	22176769	22179875	–	Valencene synthase
FSTG	6	EL10Ac6g15325	lcl| Scaffold_1	7486762	7502133	+	transmembrane protein 184A
FSTG	6	EL10Ac6g15331	lcl| Scaffold_1	7409666	7416329	–	Probable E3 ubiquitin-protein ligase HERC2
Region	6	EL10Ac6g15568	lcl| Scaffold_1	3124396	3127216	+	hypothetical protein
FSTG	8	EL10Ac8g19585	lcl| Scaffold_5	30096389	30106598	+	Cationic amino acid transporter 1
FSTG	3	EL10Ac9g21282	lcl| Scaffold_9	41429473	41431399	–	Vacuolar amino acid transporter 1
Region	5	EL10As14g24073	lcl| Scaffold_2	14271095	14272339	+	Protein SLE2 {ECO:0000303| Ref.3}
FSTP	5	EL10As14g24074	lcl| Scaffold_2	14288341	14294899	+	Dynamin-related protein 1E

FSTG, significant FST loci within gene; FSTP, significant FST loci within promoter sequence; DAF, significant DeltaAF loci; Region, gene found within significant region; NA, gene found within significant region.

SnS experiments using segregating populations provide a system to study the underlying genetics of polygenic traits as part of ongoing selection activities within a breeding program. Here we show how pooled sequencing could be used for discovery of key genetic variation when applied to polygenic traits within a population with an extremely broad genetic base. In this case, Rhizoctonia resistance stored within the synthetic EL57 population was derived from EL51, which can be traced to FC701 as the likely source (Panella et al., 2015). Significant signals of divergence as the result of selection were distributed across the genome indicative of a polygenic trait. This is consistent with previous reports of trait heritability (Hecker and Ruppel, 1975). Expected heterozygosity (*He*) estimated using all biallelic sites showed a greater level of fixation in the resistant bulk, suggesting that the genetic background that conditions resistance to Rhizoctonia could be selected and identified within a highly heterozygous population. The fact that only a few resistance sources have been identified even with considerable effort suggests genome informed approaches may be key to characterizing the source under study here as well as identifying new sources for Rhizoctonia resistance in other diverse populations.

F_{ST} and DeltaAF are complementary statistics that were both able to identify the effects of selection across the genome. DeltaAF was a more stringent statistic in terms of the number of significant loci and putative genes detected, as evidenced by all significant DeltaAF loci appearing as a subset of significant F_{ST} loci. It has been shown that generating a null distribution of allele frequency in an unselected population is important for separating signal from noise when detecting selection (Galtier and Duret, 2007). Therefore, DeltaAF could have an advantage in identifying causal variation due to its ability to leverage unselected allele frequencies to further distinguish significant loci resulting from selection, as opposed to differences resulting from historical population dynamics or genetic drift.

The final candidate gene list was strongly enriched for disease resistance genes and cell wall biosynthesis genes, suggesting complementary mechanisms involved in host resistance. To better define the genomic background associated with the putative EL51/FC701 resistance source, we specifically focused on genes which can explain resistance and are documented in the literature with known disease resistance functions, such as pathogen perception, signal transduction and cellular response to pathogens. The wide array of obvious defense genes such

TABLE 5 | Marker variation — high consequence (SNPeff), F_{ST}, and DeltaAF.

Data	EL10.2 Scaffold	Position	Ref	Alt	Allele Frequency			FST	EL10.1 Gene ID	Gene Annotation
					Unseleted	Resistant	Suceptible			
SNPeff	lcl| Scaffold_1	10,879,102	TGG	TGGG	0.00	0.00	1.00	1.00	EL10Ac6g15089	RNA recognition motif. (a.k.a. RRM, RBD, or RNP domain)
SNPeff	lcl| Scaffold_1	26,110,683	CAA	CAAA	1.00	0.00	0.92	0.85	EL10Ac6g14526	Zinc finger CCHC domain-containing protein 8
SNPeff	lcl| Scaffold_2	56,034,911	GG	GCA	0.88	1.00	0.16	0.72	EL10Ac5g11051	NEP1-interacting protein-like 2;TMhmm_ExpAA:32.25
SNPeff	lcl| Scaffold_4	62,342,250	CTC	CTTG	1.00	0.00	1.00	1.00	EL10Ac1g00136	Carboxymethylenebutenolidase homolog
SNPeff	lcl| Scaffold_7	52,713,203	TA	TGG	0.92	0.00	1.00	1.00	EL10Ac3g07219	Nucleolar protein 10
SNPeff	lcl| Scaffold_8	452,635	TT	TAGGA	0.88	0.00	0.84	0.72	EL10Ac2g02429	Histidine kinase 5
SNPeff	lcl| Scaffold_9	48,328,478	AGA	AGGG	0.92	0.00	1.00	1.00	EL10Ac9g21727	Probable receptor-like serine/threonine-protein kinase At4g34500;TMhmm_ExpAA:23.97
SNPeff	lcl| Scaffold_9	52,891,057	TA	TGGC	0.80	0.00	1.00	1.00	EL10Ac9g22099	GATA transcription factor 12
SNPeff	lcl| Scaffold_9	53,136,509	GAG	GAAC	0.68	1.00	0.16	0.72	EL10Ac9g22117	MADS-box transcription factor 27
DAF/FST	lcl| Scaffold_4	63,029,953	C	T	0.08	1.00	0.00	1.00	EL10Ac6g15080	Protein FAR-RED ELONGATED HYPOCOTYL 3
DAF/FST	lcl| Scaffold_4	63,029,962	A	G	0.08	1.00	0.00	1.00	EL10Ac6g14731	Probable inactive receptor kinase At5g10020;TMhmm_ExpAA:41.51
DAF/FST	lcl| Scaffold_4	53,504,844	T	C	0.00	1.00	0.00	1.00	EL10Ac6g14670	Replication factor C subunit 1
DAF/FST	lcl| Scaffold_4	40,900,804	TGGGGGGGG GGGGGGGA	TGGGGGGGGGG GGGGGGA	0.04	0.96	0.00	0.92	EL10Ac6g14562	Importin-9;TMhmm_ExpAA:27.48
DAF/FST	lcl| Scaffold_4	1,904,674	CA	AG	0.00	0.84	0.00	0.72	EL10Ac6g13913	Sugar transport protein 14
DAF/FST	lcl| Scaffold_4	1,904,696	T	A	0.00	0.88	0.00	0.79	EL10Ac5g12073	Putative disease resistance protein RGA3
DAF/FST	lcl| Scaffold_8	2,814,345	A	G	0.00	1.00	0.00	1.00	EL10Ac5g12061	Transcription factor MYB39
DAF/FST	lcl| Scaffold_8	3,930,082	G	A	0.00	0.88	0.00	0.79	EL10Ac5g11572	Metallothionein
DAF/FST	lcl| Scaffold_7	1,850,367	A	T	0.16	1.00	0.12	0.79	EL10Ac4g08331	Putative ribonuclease H protein At1g65750
DAF/FST	lcl| Scaffold_7	2,965,251	AT	ATACAGT	0.00	1.00	0.00	1.00	EL10Ac4g09188	Guanine deaminase
DAF/FST	lcl| Scaffold_7	2,965,294	C	T	0.00	1.00	0.00	1.00	EL10Ac4g09998	Protein kri1
DAF/FST	lcl| Scaffold_7	14,304,193	GAA	GA	0.00	1.00	0.00	1.00	EL10Ac1g02366	Heptahelical transmembrane protein 4;TMhmm_ExpAA:151.43
DAF/FST	lcl| Scaffold_7	15,181,123	GTAAACTAGTAAC	GGCCAG	0.00	1.00	0.00	1.00	EL10Ac1g02366	Heptahelical transmembrane protein 4;TMhmm_ExpAA:151.43
DAF/FST	lcl| Scaffold_7	15,643,326	A	G	0.08	1.00	0.00	1.00	EL10Ac1g02366	Heptahelical transmembrane protein 4;TMhmm_ExpAA:151.43
DAF/FST	lcl| Scaffold_7	15,665,864	G	A	0.00	1.00	0.00	1.00	EL10Ac1g01440	Small RNA degrading nuclease 5
DAF/FST	lcl| Scaffold_7	15,665,870	GTAAGAAAGTGACAT	GTAAGAAAGTGACATA AGAAAGTGACAT	0.00	1.00	0.00	1.00	EL10Ac1g00071	ABC transporter E family member 2
DAF/FST	lcl| Scaffold_7	16,724,330	GGATC	AGATT	0.00	1.00	0.00	1.00	EL10Ac1g00071	ABC transporter E family member 2
DAF/FST	lcl| Scaffold_7	16,724,391	TATC	AATT	0.00	1.00	0.00	1.00	EL10Ac8g18254	BNR repeat-like domain

(Continued)

TABLE 5 | (Continued)

Data	EL10.2 Scaffold	Position	Ref	Alt	Allele Frequency			FST	EL10.1 Gene ID	Gene Annotation
					Unseleted	Resistant	Suceptible			
DAF/FST	lcl| Scaffold_7	16,724,418	A	C	0.00	1.00	0.00	1.00	EL10Ac8g18254	BNR repeat-like domain
DAF/FST	lcl| Scaffold_7	25,250,059	AGTGGTTGTGGTTGTG GTTGTGGTTGTGGTTG TGGTTGTGGTTGTGGT TGTGGTTGTGGTTGTGG TTGTGGTTG	AGTGGTTGTGGTTGTGG TTGTGGTTGTGGTTGTG GTTGTGGTTGTGGTTGT GGTTGTGGTTG	0.08	0.92	0.04	0.78	EL10Ac8g20189	U4/U6.U5 tri-snRNP-associated protein 2
DAF/FST	lcl| Scaffold_7	52,512,965	TG	GG	0.00	1.00	0.00	1.00	EL10Ac7g17584	Major allergen Pru ar 1
DAF/FST	lcl| Scaffold_3	19,694,86	G	A	0.00	1.00	0.04	0.92	EL10Ac3g05987	Lysine–tRNA ligase;TMhmm_ExpAA:77.60
DAF/FST	lcl| Scaffold_3	15,282,274	GGG	AAA	0.00	1.00	0.00	1.00	EL10Ac3g06032	Hypothetical protein;TMhmm_ExpAA:36.46
DAF/FST	lcl| Scaffold_3	48,281,437	A	C	0.00	1.00	0.00	1.00	EL10Ac3g06055	Wall-associated receptor kinase 1
DAF/FST	lcl| Scaffold_3	56,318,571	TTATATATATATATATATATA TATATATATATATATATATATA TATATATATATATAT	TTATATATATATATATA TATATATATAT	0.04	1.00	0.08	0.85	EL10Ac3g06056	Wall-associated receptor kinase 2;TMhmm_ExpAA:46.88
DAF/FST	lcl| Scaffold_3	60,769,635	G	C	0.00	0.84	0.00	0.72	EL10Ac3g06056	Wall-associated receptor kinase 2;TMhmm_ExpAA:46.88
DAF/FST	lcl| Scaffold_2	35,363,747	GTTTTTTTTTTTTTG	GTTTTTTTTTTTTTTTTTTG	0.16	0.96	0.08	0.78	EL10Ac3g06056	Wall-associated receptor kinase 2;TMhmm_ExpAA:46.88
DAF/FST	lcl| Scaffold_2	18,141,331	A	T	0.00	1.00	0.00	1.00	EL10Ac3g06056	Wall-associated receptor kinase 2;TMhmm_ExpAA:46.88
DAF/FST	lcl| Scaffold_2	17,790,729	T	A	0.00	1.00	0.00	1.00	EL10Ac3g06102	Protein FAM136A
DAF/FST	lcl| Scaffold_2	15,093,093	C	T	0.00	1.00	0.00	1.00	EL10Ac3g06102	Protein FAM136A
DAF/FST	lcl| Scaffold_1	54,208,817	AAGGGTTAGGGTTT	AAGGGTTAGGGTTAGGGTTT	0.08	1.00	0.08	0.85	EL10Ac3g06102	Protein FAM136A
DAF/FST	lcl| Scaffold_1	24,987,470	CGGGGGGGGGGGGT	CGGGGGGGGGGGGGGT	0.16	1.00	0.12	0.79	EL10Ac3g06102	Protein FAM136A
DAF/FST	lcl| Scaffold_1	21,263,551	TAAAAAG	TAAAAAAG	0.00	0.88	0.00	0.79	EL10Ac3g06102	Protein FAM136A
DAF/FST	lcl| Scaffold_1	19,398,911	C	A	0.00	1.00	0.00	1.00	EL10Ac3g06102	Protein FAM136A
DAF/FST	lcl| Scaffold_1	19,217,784	G	A	0.00	1.00	0.00	1.00	EL10Ac3g06102	Protein FAM136A
DAF/FST	lcl| Scaffold_1	11,698,071	C	A	0.12	1.00	0.12	0.79	EL10Ac3g06102	Protein FAM136A
DAF/FST	lcl| Scaffold_1	11,468,948	A	T	0.00	1.00	0.00	1.00	EL10Ac3g06102	Protein FAM136A
DAF/FST	lcl| Scaffold_1	2,848,411	GAA	GAAA	0.00	1.00	0.00	1.00	EL10Ac3g05053	Hypothetical protein
DAF/FST	lcl| Scaffold_6	33,124,391	AATATATATATATATAT ATATATATATATA	AATATATATATATATATA TATATATATATA	0.00	0.92	0.08	0.71	EL10Ac3g06365	Light-mediated development protein DET1
DAF/FST	lcl| Scaffold_5	61,709,065	GT	AC	0.00	1.00	0.00	1.00	EL10Ac3g05157	Peroxidase 5 {ECO:0000250| UniProtKB:P22195}
DAF/FST	lcl| Scaffold_5	61,709,075	G	A	0.08	1.00	0.00	1.00	EL10Ac3g05157	Peroxidase 5 {ECO:0000250| UniProtKB:P22195}
DAF/FST	lcl| Scaffold_5	48,904,484	C	T	0.00	1.00	0.08	0.85	EL10Ac3g07201	Two-component response regulator ARR9
DAF/FST	lcl| Scaffold_5	42,132,982	C	A	0.04	1.00	0.00	1.00	EL10Ac2g02580	Cytochrome b-c1 complex subunit 7
DAF/FST	lcl| Scaffold_5	7,244,134	GCC	GC	0.08	0.88	0.00	0.79	EL10Ac2g02645	Hypothetical protein
DAF/FST	lcl| Scaffold_9	34,647,812	GCTGGACTGGAC	GCTGGACTGGACTGGAC	0.12	1.00	0.12	0.79	EL10Ac9g21035	Exosome component 10
DAF/FST	lcl| Scaffold_9	45,146,825	G	T	0.00	1.00	0.00	1.00	EL10Ac9g21479	Calmodulin-binding transcription activator 1

as Ser/Thr kinases, resistance gene analogs, chitinases, and peroxidases is in line with our expectations of how plants could defend themselves against a generalist pathogen such as Rhizoctonia. Other members of the candidate gene list do not have established roles in plant defense. These are genes with plausible but speculative roles, such as transcription factors and putative cell membrane-associated proteins. The combination of known defense genes along with additional genes of unknown function provides direction for developing testable hypotheses regarding the mechanisms of defense. In addition to genes involved in host-pathogen interactions, variation in cell wall biosynthesis could make some plants more resistant to infection. Previous studies have identified seedling resistance in comparisons between susceptible (USH20) and resistant (EL51) varieties (Nagendran et al., 2009). Resistant plants showed a durable resistance including the ability to limit the spread of infection beyond the epidermis, including maintenance of cell wall integrity in the presence of pathogen-derived enzymes that varied with respect to plant age. For this reason, identifying numerous cell wall-related genes among our significant loci adds evidence to the importance of cell wall biosynthesis in limiting Rhizoctonia infection, especially at the seedling stage.

In conclusion, this research provides a genomic perspective to seedling Rhizoctonia resistance in beets, a complex polygenic trait with agricultural importance. We think it is a useful exercise to develop methods and generate lists of candidate genes involved with important traits in order to validate results and prioritize candidate variation for functional studies. A better understanding of the limitations of these experiments and our ability to detect significant variation is warranted. The detection of PAV in pooled data is perhaps the most visible limitation of this experiment. If PAV is causal and not represented in the genomic data then we rely on linkage, which is not a strength of pooled sequencing designs. Future experiments should address the ability of pooled assemblies to represent the genomes of populations under investigation with respect to PAV, and whether PAV frequency can be measured. Starting with the best possible catalog of variants for population genetic parameters represents the highest degree of resolution for the identification of causal variation. Select and sequence experiments have the potential to explore the genetic base of beet through the identification of alleles in wild material as well as characterize existing germplasm for agriculturally important traits. Using this approach, beet breeding programs can simultaneously generate markers and improve the genetic base of populations using phenotypic selection.

DATA AVAILABILITY STATEMENT

The original contributions presented in the study are publicly available. This data can be found here: EL57 Illumina reads for the resistance, susceptible and unselected populations were deposited to NCBI under BioProject (PRJNA563463). The EL10.2 genome assembly (https://genomevolution.org/coge/GenomeInfo.pl?gid=57232). All variant files (.vcf) and files used for visualization are available at (Data Dryad - https://doi.org/10.5061/dryad.3j9kd51kg). All code is available at (https://github.com/BetaGenomeNinja/EL57). This includes bash scripts, Jupyter-note books for python code development, python scripts for data manipulation and pop gen estimators and R code for plotting and visualization of data.

AUTHOR CONTRIBUTIONS

JM developed the synthetic EL57 population. PG, JM, and AF conceived and designed the experiments and edited reviewed and approved the final manuscript. JM and PG performed the experiments. PG and AF analyzed the data. PG wrote the draft manuscript. All authors contributed to the article and approved the submitted version.

FUNDING

This research was supported by the U.S. Department of Agriculture (USDA), Agricultural Research Service (ARS) under CRIS projects: 3635-21000-011-00D and 2054-21220-005-000D.

ACKNOWLEDGMENTS

We would like to thank Ashley Wieczorek for help with the sampling plants and Linda Hanson, Tom Goodwill and the Michigan State SVREC staff for their expertise managing the Seedling Rhizoctonia nursery.

SUPPLEMENTARY MATERIAL

The Supplementary Material for this article can be found online at: https://www.frontiersin.org/articles/10.3389/fpls.2021.785267/full#supplementary-material

REFERENCES

Andrews, S. (2010). *FastQC – A Quality Control Tool for High Throughput Sequence Data*. Available online at: http://www.bioinformatics.babraham.ac.uk/projects/fastqc/ (accessed October 20, 2020).

Arumuganathan, K., and Earle, E. D. (1991). Nuclear DNA content of some important plant species. *Plant Mol. Biol. Rep.* 9, 208–221.

Bolger, A. M., Lohse, M., and Usadel, B. (2014). Trimmomatic: a flexible trimmer for Illumina sequence data. *Bioinformatics* 30, 2114–2120. doi: 10.1093/bioinformatics/btu170

Bolton, M. D., Panella, L., Campbell, L., and Khan, M. F. R. (2010). Temperature, moisture, and fungicide effects in managing *Rhizoctonia* root and crown rot of sugar beet. *Phytopathology* 100, 689–697. doi: 10.1094/PHYTO-100-7-0689

Burghardt, L. T., Epstein, B., Guhlin, J., Nelson, M. S., Taylor, M. R., Young, N. D., et al. (2018). Select and resequence reveals relative fitness of bacteria in symbiotic and free-living environments. *Proc. Natl. Acad. Sci. U.S.A.* 115, 2425–2430. doi: 10.1073/pnas.1714246115

Burny, C., Nolte, V., Nouhaud, P., Dolezal, M., Schlötterer, C., and Baer, C. (2020). Secondary evolve and resequencing: an experimental confirmation of putative selection targets without phenotyping. *Genome Biol. Evol.* 12, 151–159. doi: 10.1093/gbe/evaa036

Chen, X., Schulz-Trieglaff, O., Shaw, R., Barnes, B., Schlesinger, F., Källberg, M., et al. (2016). Manta: rapid detection of structural variants and indels for

germline and cancer sequencing applications. *Bioinformatics* 32, 1220–1222. doi: 10.1093/bioinformatics/btv710

Cingolani, P., Platts, A., Wang, L. L., Coon, M., Nguyen, T., Wang, L., et al. (2012). A program for annotating and predicting the effects of single nucleotide polymorphisms, SnpEff: SNPs in the genome of *Drosophila melanogaster* strain w1118; iso-2; iso-3. *Fly* 6, 80–92. doi: 10.4161/fly.19695

Dohm, J. C., Minoche, A. E., Holtgräwe, D., Capella-Gutiérrez, S., Zakrzewski, F., Tafer, H., et al. (2014). The genome of the recently domesticated crop plant sugar beet (*Beta vulgaris*). *Nature* 505, 546–549. doi: 10.1038/nature12817

Doney, D. L. (1995). USDA-ARS sugarbeet releases. *J. Sugar Beet Res.* 32, 229–257.

Doney, D. L., and Theurer, J. C. (1978). Reciprocal recurrent selection in sugarbeet. *Field Crops Res.* 1, 173–181. doi: 10.1016/0378-4290(78)90020-5

Ferretti, L., Ramos-Onsins, S. E., and Pérez-Enciso, M. (2013). Population genomics from pool sequencing. *Mol. Ecol.* 22, 5561–5576. doi: 10.1111/mec.12522

Funk, A., Galewski, P., and McGrath, J. M. (2018). Nucleotide-binding resistance gene signatures in sugar beet, insights from a new reference genome. *Plant J.* 95, 659–671. doi: 10.1111/tpj.13977

Galewski, P., and McGrath, J. M. (2020). Genetic diversity among cultivated beets (*Beta vulgaris*) assessed via population-based whole genome sequences. *BMC Genomics* 21:189. doi: 10.1186/s12864-020-6451-1

Galtier, N., and Duret, L. (2007). Adaptation or biased gene conversion? Extending the null hypothesis of molecular evolution. *Trends Genet.* 23, 273–277. doi: 10.1016/j.tig.2007.03.011

Garrison, E., and Marth, G. (2012). Haplotype-based variant detection from short-read sequencing. *arXiv* [Preprint] arXiv: 1207.3907,

Gaskill, J. O., Mumford, D. L., and Ruppel, E. G. (1970). Preliminary report on breeding sugarbeet for combined resistance to leaf spot, curly top, and *Rhizoctonia*. *J. Am. Soc. Sugar Beet Technol.* 16, 207–213.

Hämälä, T., Wafula, E. K., Guiltinan, M. J., Ralph, P. E., dePamphilis, C. W., and Tiffin, P. (2021). Genomic structural variants constrain and facilitate adaptation in natural populations of *Theobroma cacao*, the chocolate tree. *Proc. Natl. Acad. Sci. U.S.A.* 118:e2102914118. doi: 10.1073/pnas.2102914118

Hecker, R. J., and Ruppel, E. G. (1975). Inheritance of resistance to *Rhizoctonia* root rot in sugarbeet. *Crop Sci.* 15, 487–490.

Hufford, M. B., Xu, X., van Heerwaarden, J., Pyhäjärvi, T., Chia, J. M., Cartwright, R. A., et al. (2012). Comparative population genomics of maize domestication and improvement. *Nat. Genet.* 44, 808–811. doi: 10.1038/ng.2309

Lein, J. C., Sagstetter, C. M., Schulte, D., Thurau, T., Varrelmann, M., Saal, B., et al. (2008). Mapping of *Rhizoctonia* root rot resistance genes in sugar beet using pathogen response-related sequences as molecular markers. *Plant Breed.* 127, 602–611. doi: 10.1111/j.1439-0523.2008.01525.x

Li, H. (2013). Aligning sequence reads, clone sequences and assembly contigs with BWA-MEM. *arXiv* [Preprint] arXiv: 1303.3997,

Li, H., and Smigocki, A. C. (2018). Sugar beet polygalacturonase-inhibiting proteins with 11 LRRs confer *Rhizoctonia*, *Fusarium* and *Botrytis* resistance in *Nicotiana* plants. *Physiol. Mol. Plant Pathol.* 102, 200–208. doi: 10.1016/j.pmpp.2018.03.001

Li, H., Handsaker, B., Wysoker, A., Fennell, T., Ruan, J., Homer, N., et al. (2009). The sequence alignment/map format and SAMtools. *Bioinformatics* 25, 2078–2079. doi: 10.1093/bioinformatics/btp352

Liu, Y., Qi, A., and Khan, M. F. R. (2019). Age-dependent resistance to *Rhizoctonia solani* in sugar beet. *Plant Dis.* 103, 2322–2329. doi: 10.1094/PDIS-11-18-2001-RE

Lynch, M., Bost, D., Wilson, S., Maruki, T., and Harrison, S. (2014). Population-genetic inference from pooled-sequencing data. *Genome Biol. Evol.* 6, 1210–1218. doi: 10.1093/gbe/evu085

McGrath, J. M., Funk, A., Galewski, P., Ou, S., Townsend, B., Davenport, K., et al. (2020). A contiguous de novo genome assembly of sugar beet EL10 *Beta vulgaris* L. *bioRxiv* [Preprint] doi: 10.1101/2020.09.15.298315

Michelmore, R. W., Paran, I., and Kesseli, R. (1991). Identification of markers linked to disease-resistance genes by bulked segregant analysis: a rapid method to detect markers in specific genomic regions by using segregating populations. *Proc. Natl. Acad. Sci. U.S.A.* 88, 9828–9832. doi: 10.1073/pnas.88.21.9828

Nagendran, S., Hammerschmidt, R., and Mcgrath, J. M. (2009). Identification of sugar beet germplasm EL51 as a source of resistance to post-emergence *Rhizoctonia* damping-off. *Eur. J. Plant Pathol.* 123, 461–471. doi: 10.1007/s10658-008-9384-0

Nielsen, R., Williamson, S., Kim, Y., Hubisz, M. J., Clark, A. G., and Bustamante, C. (2005). Genomic scans for selective sweeps using SNP data. *Genome Res.* 15, 1566–1575.

Panella, L. (2005). "Root rots," in *Genetics and Breeding of Sugar Beet*, eds E. Biancardi, L. G. Campbell, G. N. Skaracis, and M. de Biaggi (Enfield, NH: Science Publishers), 95–98.

Panella, L., Campbell, L. G., Eujayl, I. A., Lewellen, R. T., and McGrath, J. M. (2015). USDA-ARS sugarbeet releases and breeding over the past 20 years. *J. Sugar Beet Res.* 52, 22–67. doi: 10.5274/jsbr.52.3.40

Pinosio, S., Giacomello, S., Faivre-Rampant, P., Taylor, G., Jorge, V., le Paslier, M. C., et al. (2016). Characterization of the poplar pan-genome by genome-wide identification of structural variation. *Mol. Biol. Evol.* 33, 2706–2719. doi: 10.1093/molbev/msw161

Ries, D., Holtgräwe, D., Viehöver, P., and Weisshaar, B. (2016). Rapid gene identification in sugar beet using deep sequencing of DNA from phenotypic pools selected from breeding panels. *BMC Genomics* 17:236. doi: 10.1186/s12864-016-2566-9

Salzberg, S. L. (2019). Next-generation genome annotation: we still struggle to get it right. *Genome Biol.* 20:92. doi: 10.1186/s13059-019-1715-2

Schlötterer, C., Kofler, R., Versace, E., Tobler, R., and Franssen, S. U. (2015). Combining experimental evolution with next-generation sequencing: a powerful tool to study adaptation from standing genetic variation. *Heredity* 114, 431–440. doi: 10.1038/hdy.2014.86

Schlötterer, C., Tobler, R., Kofler, R., and Nolte, V. (2014). Sequencing pools of individuals-mining genome-wide polymorphism data without big funding. *Nat. Rev. Genet.* 15, 749–763. doi: 10.1038/nrg3803

Schneeberger, K., Ossowski, S., Lanz, C., Juul, T., Petersen, A. H., Nielsen, K. L., et al. (2009). SHOREmap: simultaneous mapping and mutation identification by deep sequencing. *Nat. Methods* 6, 550–551. doi: 10.1038/nmeth0809-550

Strausbaugh, C. A., Eujayl, I. A., and Foote, P. (2013a). Selection for resistance to the *Rhizoctonia*-bacterial root rot complex in sugar beet. *Plant Dis.* 97, 93–100. doi: 10.1094/PDIS-05-12-0511-RE

Strausbaugh, C. A., Eujayl, I. A., and Panella, L. W. (2013b). Interaction of sugar beet host resistance and *Rhizoctonia solani* AG-2-2 IIIB strains. *Plant Dis.* 97:11751180. doi: 10.1094/PDIS-11-12-1078-RE

Taheri, P., and Tarighi, S. (2010). Riboflavin induces resistance in rice against *Rhizoctonia solani* via jasmonate-mediated priming of phenylpropanoid pathway. *J. Plant Physiol.* 167, 201–208. doi: 10.1016/j.jplph.2009.08.003

Wang, W., Mauleon, R., Hu, Z., Chebotarov, D., Tai, S., Wu, Z., et al. (2018). Genomic variation in 3,010 diverse accessions of Asian cultivated rice. *Nature* 557, 43–49. doi: 10.1038/s41586-018-0063-9

Weigand, H., and Leese, F. (2018). Detecting signatures of positive selection in non-model species using genomic data. *Zool. J. Linn. Soc.* 184, 528–583. doi: 10.7717/peerj.4077

Wibberg, D., Andersson, L., Tzelepis, G., Rupp, O., Blom, J., Jelonek, L., et al. (2016). Genome analysis of the sugar beet pathogen *Rhizoctonia solani* AG2-2IIIB revealed high numbers in secreted proteins and cell wall degrading enzymes. *BMC Genomics* 17:245. doi: 10.1186/s12864-016-2561-1

Zhou, Y., Minio, A., Massonnet, M., Solares, E., Lv, Y., Beridze, T., et al. (2019). The population genetics of structural variants in grapevine domestication. *Nat. Plants* 5, 965–979. doi: 10.1038/s41477-019-0507-8

Conflict of Interest: The authors declare that the research was conducted in the absence of any commercial or financial relationships that could be construed as a potential conflict of interest.

Publisher's Note: All claims expressed in this article are solely those of the authors and do not necessarily represent those of their affiliated organizations, or those of the publisher, the editors and the reviewers. Any product that may be evaluated in this article, or claim that may be made by its manufacturer, is not guaranteed or endorsed by the publisher.

Copyright © 2022 Galewski, Funk and McGrath. This is an open-access article distributed under the terms of the Creative Commons Attribution License (CC BY). The use, distribution or reproduction in other forums is permitted, provided the original author(s) and the copyright owner(s) are credited and that the original publication in this journal is cited, in accordance with accepted academic practice. No use, distribution or reproduction is permitted which does not comply with these terms.

frontiers in Plant Science

ORIGINAL RESEARCH
published: 21 February 2022
doi: 10.3389/fpls.2022.792079

Genome-Wide Expression Analysis of Root Tips in Contrasting Rice Genotypes Revealed Novel Candidate Genes for Water Stress Adaptation

*Somayeh Abdirad[1,2], Mohammad Reza Ghaffari[1], Ahmad Majd[2], Saeed Irian[3], Armin Soleymaniniya[4], Parisa Daryani[1], Parisa Koobaz[5], Zahra-Sadat Shobbar[1], Laleh Karimi Farsad[1], Parisa Yazdanpanah[1,2], Amirhossein Sadri[1], Mehdi Mirzaei[6], Zahra Ghorbanzadeh[1], Mehrbano Kazemi[1], Naghmeh Hadidi[7], Paul A. Haynes[8] and Ghasem Hosseini Salekdeh[1,8]**

[1] Department of Systems and Synthetic Biology, Agricultural Biotechnology Research Institute of Iran, Agricultural Research, Education and Extension Organization, Karaj, Iran, [2] Department of Plant Biology, Faculty of Biological Sciences, Kharazmi University, Tehran, Iran, [3] Department of Cell and Molecular Biology, Faculty of Biological Sciences, Kharazmi University, Tehran, Iran, [4] Department of Biotechnology, University of Tehran, Tehran, Iran, [5] Department of Molecular Physiology, Agricultural Biotechnology Research Institute of Iran, Agricultural Research, Education and Extension Organization, Karaj, Iran, [6] Faculty of Medicine, Health and Human Sciences, Macquarie University, Sydney, NSW, Australia, [7] Department of Clinical Research and Electronic Microscope, Pasteur Institute of Iran, Tehran, Iran, [8] Department of Molecular Sciences, Macquarie University, Sydney, NSW, Australia

OPEN ACCESS

Edited by:
Guihua Bai,
Independent Researcher, Manhattan, United States

Reviewed by:
Dong-Ha Oh,
Louisiana State University, United States
Shunwu Yu,
Shanghai Agrobiological Gene Center, China

***Correspondence:**
Ghasem Hosseini Salekdeh
hosseini.salekdeh@mq.edu.au;
h_salekdeh@abrii.ac.ir

Specialty section:
This article was submitted to Plant Abiotic Stress, a section of the journal Frontiers in Plant Science

Received: 09 October 2021
Accepted: 05 January 2022
Published: 21 February 2022

Citation:
Abdirad S, Ghaffari MR, Majd A, Irian S, Soleymaniniya A, Daryani P, Koobaz P, Shobbar Z-S, Farsad LK, Yazdanpanah P, Sadri A, Mirzaei M, Ghorbanzadeh Z, Kazemi M, Hadidi N, Haynes PA and Salekdeh GH (2022) Genome-Wide Expression Analysis of Root Tips in Contrasting Rice Genotypes Revealed Novel Candidate Genes for Water Stress Adaptation. Front. Plant Sci. 13:792079. doi: 10.3389/fpls.2022.792079

Root system architecture (RSA) is an important agronomic trait with vital roles in plant productivity under water stress conditions. A deep and branched root system may help plants to avoid water stress by enabling them to acquire more water and nutrient resources. Nevertheless, our knowledge of the genetics and molecular control mechanisms of RSA is still relatively limited. In this study, we analyzed the transcriptome response of root tips to water stress in two well-known genotypes of rice: IR64, a high-yielding lowland genotype, which represents a drought-susceptible and shallow-rooting genotype; and Azucena, a traditional, upland, drought-tolerant and deep-rooting genotype. We collected samples from three zones (Z) of root tip: two consecutive 5 mm sections (Z1 and Z2) and the following next 10 mm section (Z3), which mainly includes meristematic and maturation regions. Our results showed that Z1 of Azucena was enriched for genes involved in cell cycle and division and root growth and development whereas in IR64 root, responses to oxidative stress were strongly enriched. While the expansion of the lateral root system was used as a strategy by both genotypes when facing water shortage, it was more pronounced in Azucena. Our results also suggested that by enhancing meristematic cell wall thickening for insulation purposes as a means of confronting stress, the sensitive IR64 genotype may have reduced its capacity for root elongation to extract water from deeper layers of the soil. Furthermore, several members of gene families such as *NAC*, *AP2/ERF*, *AUX/IAA*, *EXPANSIN*, *WRKY,* and *MYB* emerged as main players in RSA and drought adaptation. We also found that *HSP*

and *HSF* gene families participated in oxidative stress inhibition in IR64 root tip. Meta-quantitative trait loci (QTL) analysis revealed that 288 differentially expressed genes were colocalized with RSA QTLs previously reported under drought and normal conditions. This finding warrants further research into their possible roles in drought adaptation. Overall, our analyses presented several major molecular differences between Azucena and IR64, which may partly explain their differential root growth responses to water stress. It appears that Azucena avoided water stress through enhancing growth and root exploration to access water, whereas IR64 might mainly rely on cell insulation to maintain water and antioxidant system to withstand stress. We identified a large number of novel RSA and drought associated candidate genes, which should encourage further exploration of their potential to enhance drought adaptation in rice.

Keywords: rice, root tip, water stress, root system architecture, RNAseq, transcriptome

INTRODUCTION

Rice (*Oryza sativa* L.) is a staple food for nearly half of the world's population (Bhuiyan, 1992). Drought, estimated to affect a large portion of the world's rice production (Lesk et al., 2016), is defined as a decrease in water input into an ecosystem over time and being sufficient to result in soil water deficit (Gilbert and Medina, 2016; Abdirad et al., 2020). Water-deficit stress limits crop growth and development, eventually leading to a sharp decline in productivity (Michaletti et al., 2018). Therefore, developing plants capable of tolerating conditions of water deficit while maintaining a high yield is of great interest (Salekdeh et al., 2009).

Root system architecture (RSA) is an important agronomic trait with vital roles in plant adaptation and productivity in water-limited environments. A deep, thick, and branched root system may help plants to avoid water stress by enabling them to acquire more water and nutrient resources (Ye et al., 2018). Deep rooting is a complex trait affected by growth angle and root length (Araki et al., 2002; Uga et al., 2013). Other deep-rooting determinants include root thickness and penetrability, with thicker roots penetrating deeper through soil-layers (Yu et al., 1995; Zheng et al., 2000). Also, branched and proliferate rooting, mainly determined by the number and length of adventitious and lateral roots (LRs), is considered as an important contributor to water uptake efficiency under water-deficit conditions (Ye et al., 2018).

From a developmental biological perspective, a developmental gradient is apparent at the growing root tips from meristematic to mature zones, with each responding differentially to water stress and performing specific functions during RSA formation. The major longitudinal regions of a typical root include: The meristematic region wherein cell division and cell production originate; the elongation zone wherein the growing cells elongate and lose the power of division; the zone of maturation with completely differentiated cells wherein the root hairs and LRs initiate and emerge, and specialized tissues are differentiated.

Lowland rice, accounting for 80% of the total rice produced worldwide, is generally grown under flooded conditions, and is susceptible to drought due to its shallow root distribution and limited capacity to extract water from deep soil layers (Kondo et al., 2003). Upland rice, however, is mainly planted in unbounded fields without irrigation facilities, and thus by being exposed to drought has accumulated a relatively greater morphological and genetic variations contributing to its drought resistant traits, including the development of deeper roots for enhanced water uptake (Bernier et al., 2008).

A strategy envisaged to enhance drought resistance in lowland rice cultivars would be to introduce the deep rooting traits of the upland rice into the commercial lowland rice cultivars. Such cultivars would also be better suited to the Alternate Wetting and Drying irrigation systems, wherein the field is not continuously flooded. This involves periodic introduction of unsaturated soil conditions during the growing season, and has been shown to decrease water demand for irrigation up to 30%, and reduce greenhouse gas emissions without reducing crop yields (Carrijo et al., 2017).

Progress has been made in detecting large effect quantitative trait loci (QTL) conferring the ratio of deep roots in rice (Uga et al., 2011; Lou et al., 2015). The root transcriptomes of the extreme shallow or deep-rooting genotypes, surveyed under abiotic stresses have led to the identification of numerous stress-responsive genes and pathways (Mehra et al., 2016; Singh et al., 2016; Sinha et al., 2018; Subudhi et al., 2020; Tiwari et al., 2020). However, our knowledge of the genetics and molecular control mechanisms of deep rooting in rice is still relatively limited as only a few genes involved in RSA traits have been identified. In addition, these studies by applying hydroponic media have ignored the impact of soil texture on RSA development (Mehra et al., 2016; Singh et al., 2016; Subudhi et al., 2020; Tiwari et al., 2020). Furthermore, by using whole roots, the important signaling events localized to particular areas, such as the root tips, go undetected. Root tips, by encompassing the root cap, apical meristem and elongation zones, are considered to be of great functional significance as these regions determine the fate of root traits (Uga et al., 2013; Wu et al., 2016).

The integration of RSA Meta-QTLs analysis with transcriptome profiling may assist in generating a more reliable list of potential candidate genes involved in RSA. Meta-analysis of QTLs is a powerful statistical technique for reducing the confidence interval of QTL position through refining and

confirming QTL positions on a consensus map via mathematical models. In Meta-QTL analysis, a number of independent QTL studies performed across different genetic backgrounds and environments are combined to determine the number of true QTLs enabling researchers to reduce the intervals and the number of candidate genes (Coudert et al., 2010; Comas et al., 2013; Daryani et al., 2021).

Here we aimed at monitoring the transcriptome response to water stress of three different root regions in two well-known genotypes of rice, namely IR64, a high-yielding, lowland, drought-susceptible, and shallow-rooting genotype, and Azucena, a traditional, upland, drought-tolerant and deep-rooting genotype. The transcriptome data were collected from two consecutive 5 mm sections and the following next 10 mm section starting from the distal tip, namely Z1–Z3, aimed to be enriched for undifferentiated, differentiating and differentiated cells, respectively. Z1, containing meristematic and elongating cells, is the region of cell division, and elongation, and is enriched for root traits such as length, thickness and angle. In zones 2 and 3, root tissues are gradually differentiating and enriched for LR production (Takehisa et al., 2012). We then integrated the transcriptome data into Meta-QTLs, resulting in identification of a large number of novel RSA/drought associated candidate genes.

MATERIALS AND METHODS

Sample Preparation

Seeds of two genotypes of rice (*Oryza sativa* L.), Azucena (a japonica-type, traditional, upland, and deep-rooting genotype) and IR64 (an *indica*-type, cultivated, lowland, and shallow-rooting genotype) (Yadav et al., 1997; Shashidhar et al., 1999) were provided by the IRRI International Rice Genebank Collection in the Philippines. Sterilized seeds were germinated on water-soaked filter paper, and uniformly sized 7-day-old seedlings were cultured hydroponically in Yoshida solution (Yoshida, 1976) at 22–25°C, relative humidity of 85% and a photoperiod of 16 h for 2 weeks. Then, 20-day-old seedlings were transferred to 400 root boxes (two plants in each box) filled with a mix ratio of 1:1:2 of clay, pit, and sand, respectively (**Figure 1A**). The root boxes were made of plexiglass sheets with a thickness of 5 mm (the root box dimensions: 25 cm × 3 cm × 40 cm L × W × H) and placed in a greenhouse of ABRII (Agricultural Biotechnology Research Institute of Iran) (**Figures 1A,C**). In a randomized design (100 root boxes and 200 plants per each treatment), water stress was imposed on 35-day-old plants by withholding water for 14 days till the level of field capacity was reduced to 25–35%. The control plants were watered regularly. Field capacity was measured twice a day during the treatment period for at least 40 root boxes, randomly (Puértolas et al., 2017). The Soil moisture of the 40 root boxes were also monitored using a Soil Moisture Sensor SM150 (Delta-T Devices, Cambridge, United Kingdom). Relative water content (RWC) of fresh leaves (the last expanded leaf) was measured 14 days after water withholding using the following formula (Martinez et al., 2004): RWC = (FW – DW) 100/(SW – DW) × 100, where FW corresponds to the leaf fresh weight, DW to the leaf dry weight (determined after 48 h in an oven at 80°C), and SW to the leaf water-saturated weight measured after 24 h of saturation on deionized water in the dark.

To assay the dry weight, shoots and roots were separated and dried in an oven at 110°C for 2 days (Morant-Manceau et al., 2004). Also, the length of the longest root was measured. The collected data (six biological replicates) were subjected to analysis of variance (ANOVA), and the mean differences were compared using Duncan's range test at P values ≤ 0.05. All calculations were performed using SPSS software, version 19.

Fourteen days after stress initiation, crown root tips were dissected from both well-watered and stressed 50-day-old plants and were immediately snap-frozen in liquid nitrogen, and then stored at −80°C. Root tip samples were collected from three zones: two consecutive 5 mm sections (Z1 and Z2) and the following next 10 mm section (Z3) (**Figure 1B**). Only the root tips located in one third of the bottom of root boxes, were considered for sampling. Three biological replicates were considered for each genotype/zone/condition. Biological replicates were collected on different dates (12 days) and pooled, separately, to allow for day-to-day variation within each genotype/zone/condition and other environmental variables. Approximately root tip sections of 70 plants were pooled as a biological replicate.

Microscopic Analysis

Root samples were cut into small pieces of 2.5 mm (serial sections), fixed in 4% glutaraldehyde (in PBS buffer), dried under vacuum for 3 h, shaken for 2 h, washed in PBS buffer (pH 7.2, 100 mM) six times and then kept in PBS buffer at 4°C overnight. The fixed samples were post fixed in 1% osmium tetroxide (OsO4) (in PBS buffer) for 2 h, and washed in PBS buffer and distilled water, three times each, respectively. Then, they were dehydrated stepwise in 5, 10, 30, 50, 70, 80, 90, 95, and 100% acetone for 15 min in each step and then twice in 100% acetone again for 20 min. Finally, the samples were embedded stepwise in different mixtures of Spurs resin/100% acetone, 25%/75%, 50%/50%, 75%/25% for 4, 1, and 4 h, respectively, followed by pure Spurs resin, three times and for 4, 12, and 24 h and oven-cured at 65°C for 48 h. For light microscopy, serial semi thin transverse and longitudinal sections (1–2 μm) were obtained from resin blocks cutting. Then the sections were mounted on glass slides, stained with 0.05% methylene blue (w/v), and observed and recorded with a light microscope (Olympus BX53, Tokyo, Japan). For transmission electron microscopy (TEM), the blocks were cut into ultrathin sections of 40–50 nm thick with an RMC MT-7000 Ultramicrotome (Tucson, AZ, United States) by a glass knife, and then stained with 2% uranyl acetate and 2% lead citrate, respectively (Bozzola and Russell, 1999). Ultimately, the ultrastructural analysis and photography were performed using a Zeiss EM900 Transmission Electron Microscope (Carl Zeiss, Oberkochen, Germany).

RNA Extraction, RNA-Seq Library Construction and Sequencing

A total of 24 root samples were collected for RNAseq profiling from three different zones of the two contrasting genotypes of

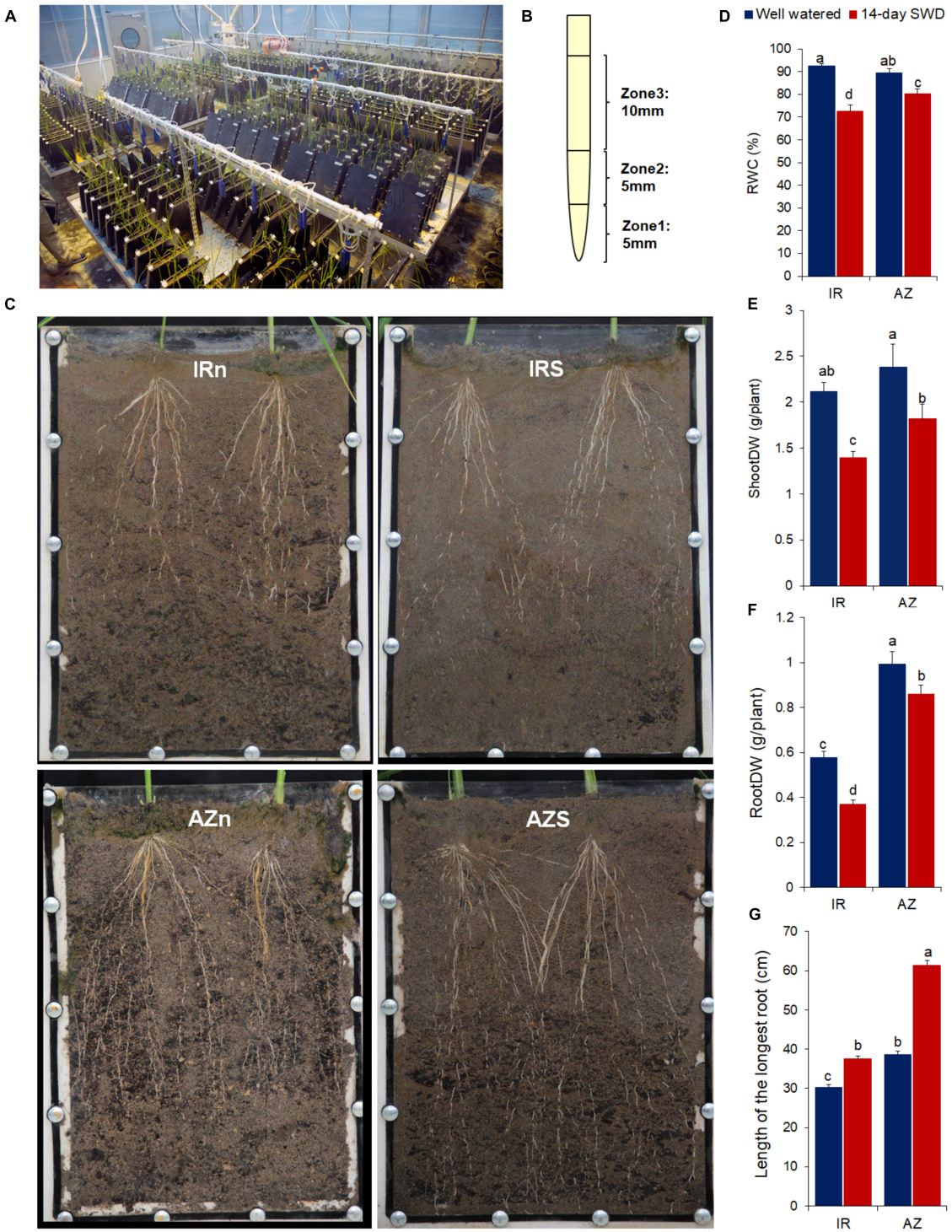

FIGURE 1 | Root sampling and phenotypic responses of two contrasting rice genotypes, Azucena and IR64, to water stress. **(A)** Soil-filled root boxes containing rice plants in the greenhouse; **(B)** root tip sampling; **(C)** the root length of IR64 (top panel, IRn and IRs) and Azucena (bottom panel, AZn and AZs) under well-watered (Left panel, IRn and AZn) and 14-day water withholding (right panel, IRs and AZs) conditions, shown in the transparent root boxes; 14-day-treated root boxes were watered prior to taking photos for a better resolution; **(D)** relative water content (RWC); **(E)** shoot dry weight; **(F)** root dry weight; and **(G)** length of the longest root of two contrasting genotypes of rice, IR64 (IR), the shallow rooting and sensitive genotype and Azucena (AZ), the deep rooting and tolerant genotype, grown in soil-filled root boxes in response to a 14-day water-deficit stress compared to well-watered samples. Values represent mean ± SE from six independent samples. The different letters indicate significant difference ($p \leq 0.05$) by Duncan's test. **(E)** DW, dry weight; IRn, IR64 genotype under normal condition; IRs, IR64 genotype under water-deficit stress condition; AZn, Azucena genotype under normal condition; AZs, Azucena genotype under water-deficit stress condition.

rice under two different growth conditions with two independent biological replicates for each treatment. Total RNA was isolated from 100 mg root tissue using the Invitrogen TRIzol Reagent (Thermo Fisher Scientific, Waltham, MA, United States) as previously described (Mardi et al., 2015).

The RNA was analyzed for quality and concentration determination using a Nanodrop 2000 spectrophotometer (NP80 NanoPhotometer, IMPLEN, Munich, Germany) and an Agilent Technologies 2100 Bio Analyzer. All the RNA samples had A260/A280 nm ratios between 2 and 2.1 and RNA integrity number (RIN) between 9 and 10.

RNA-Seq Data Processing

RNA-seq (Illumina Hiseq 2500 system with 150-bp paired end reads, Beijing Genomics Institute, BGI) were performed on 24 samples, and approximately 15–22 million read pairs were collected for each sample (a total of 70 Gb data). The sequencing data has been submitted to SRA of NCBI with accession no. PRJNA716593.

Quality assessment of the raw sequencing reads using FASTQC tool showed that all data were clean and did not require trimming. The clean reads were aligned to the *O. sativa* cv. Nipponbare (ssp. *japonica*) reference genome sequences IRGSP 1.0[1] using Hisat2 (Kim et al., 2015; Pertea et al., 2016). Then, for assembly, Cufflinks utility (Trapnell et al., 2012) was used on the Hisat2-generated alignment and the transcriptome assembly was performed by cuffmerge meta-assembler. The Cuffcompare utility was used to identify novel transcripts.

Raw read counts were normalized by library size and accounted for the effect of extremely differentially expressed genes using the trimmed Mean of the *M*-values (TMM) normalization approach (Robinson and Oshlack, 2010) to give counts per million reads mapped (CPM) values for each gene in each sample. CPM values were then normalized by gene coding sequence (CDS) lengths to give fragments per kilo base of exon per million reads (FPKM) values.

The silent genes were selected where there were no doublet sets of biological replicates with FPKM values of more than one in all 24 samples. The expressed genes were detected where at least both replicates of one doublet set had FPKM values of more than one. The constitutive, intermediate frequency and low frequency genes were identified from expressed genes as having FPKM $>$ 1 in more than 80%, between 20 and 80%, and less than 20% of samples, respectively. Genes actively expressed in all replicates of the three zones of one genotype, but not expressed in the other, were referred to as genotype-specific genes. Similar approaches were used to determine-zone specific and condition-specific genes.

Identification of Differentially Expressed Genes

Genes with differential expression between control and stress (stress vs. control) were identified for each zone in each genotype using Cuffdiff (FDR adjusted p-value < 0.05) (Trapnell et al., 2012), and the fold changes (FC) were calculated for each gene in response to stress. Differentially expressed genes (DEGs) were further classified into different fold-change categories (i.e., $2 >$ FC, $4 >$ FC > 2, $8 >$ FC > 4, $16 >$ FC > 8, FC > 16) considering their directions for upregulation and downregulation. An upset plot (showing the intersections of DEGs sets), generated by Upset package in R, was performed on total DEGs to identify general, zone-specific and genotype-specific DEGs.

Gene Ontology Enrichment Analysis

Gene Ontology (GO) enrichment analysis was performed using Cytoscape software (version 3.8.2) with the ClueGO V2.5.7 plug-in (Bindea et al., 2009). The *P*-value was calculated by two-sided hypergeometric tests, and Benjamini–Hochberg adjustment was used for multiple test correction. GO terms with a *P*-value < 0.05 were considered significant.

Finding Gene Family Members and Genes Known to Be Involved in Root Development

The members of 24 important gene families, *NAC domain transcription factor* (TF), *APETALA2/Ethylene-Responsive Factor* (*AP2/ERF*), *Auxin/Indole-3-Acetic Acid* (*Aux/IAA*), *auxin response factor* (*ARF*), *WRKY TF* (*WRKY*), *MYB TF*, *MYB-Related TF*, *EXPANSIN*, *GRAS TF*, *late embryogenesis abundant* (*LEA*) *protein*, *heat-shock protein* (*HSP*), *heat shock factor* (*HSF*) *TF*, *ARID*, *basic helix-loop-helix* (*bHLH*) *TF*, *basic leucine zipper* (*bZIP*), *lateral organ boundaries domain* (*LOB*), *WUSCHEL-related homeobox* (*WOX*) *TF*, *ethylene insensitive3-like* (*EIL*) *TF*, *growth-regulating factor* (*GRF*) *TF*, *golden 2-like* (*G2-like*) *TF*, *TIP*, and *PIP aquaporins*, *SWEET*, *response regulator* (*RR*), and *MADS-box* were collected by searching through the following databases: fun rice genes[2], oryza base[3], Rapdb[4], Rice phylogenomics[5], and uniprot[6].

An expanded list of previously reported genes involved in root elongation, lateral root formation, root growth and development, and root cell wall biogenesis and modification was also prepared from the literature and by searching through the same databases using relevant keywords.

To identify gene family members with significant interactions between genotypes and conditions, the expression level of members was extracted from the transcriptome profiling data followed by the statistical analysis of their expression pattern using a two-way analysis of variance (ANOVA) for each zone, separately (p-value cutoff of <0.05).

Quantitative Trait Loci Meta-Analysis

Collection and Projection of Related Quantitative Trait Loci

Quantitative trait loci controlling rice RSA traits (based on RFLP, AFLP, SSR, and SNP genetic markers and including the RIL,

[1]https://plants.ensembl.org/info/data/ftp/index.html

[2]https://funricegenes.github.io/

[3]https://shigen.nig.ac.jp/rice/oryzabase/

[4]https://rapdb.dna.affrc.go.jp/

[5]http://planttfdb.gao-lab.org/index.php

[6]https://www.uniprot.org

F_2, DH, and NIL populations) were collected from reviewing of 20 independent experiments that studied two sets of bi-parental populations: IR64 × Azucena population (8 articles) and Azucena (the tolerant and deep-rooting genotype) × other rice genotypes population (12 articles) under drought and normal conditions. The root traits considered were included maximum root length (MRL), deep rooting weight (DRW), root number (RN), root length (RL), root thickness (RTHK), root volume (RV), root dry weight (RDW), deep rooting ratio (DRR), root to shoot ratio (RSR), drought stress (DS), root surface area (RSAr) and root growth angle (RGA). Afterward, the chromosome number, trait type, proportion of phenotypic variance explained by the QTL (R^2), logarithm of odds ratio (LOD score), QTL confidence interval (CI), QTL chromosomal position and population size were also extracted.

A high-density marker integrated genetic map (Daryani et al., 2021) was used as a reference map for Meta-QTL analysis. The primary QTLs were projected on the consensus map based on a simple scaling method using flanking markers. Using a Gaussian distribution, new confidence intervals of the primary QTLs were approximated based on their original genetic map before the QTLs projection on the consensus map. Based on the population type, the 95% CI for each QTL position was calculated according to Daryani et al. (2021).

Meta-Analysis and Identification of Candidate Genes Within the Meta-Quantitative Trait Loci Regions

Applying BioMercator V4.2 (Arcade et al., 2004) contained algorithms from the MetaQTL software (Sosnowski et al., 2012), meta-analysis was performed according to the QTL clusters on each chromosome following QTL projection on the consensus map for both sets of IR64 × Azucena and Azucena × other rice genotypes populations, separately).

To identify candidate genes, the flanking markers of the positional CIs belonged to the extracted Meta-QTLs were applied. As the reference genome, the genome assembly of cultivated rice (*Oryza sativa* L.) was considered (Temnykh et al., 2001)[7] and the flanking markers were mapped. Then, the physical positions were also calculated. Lastly, the identification of candidate genes was performed using BioMart data mining tools from the Ensembl Website Gramene[8]. A total of 5787 and 3511 genes were obtained for IR64 × Azucena and Azucena × other rice genotypes populations, respectively which 1047 genes were common between them. To narrow down the candidate genes, only the 1047 common genes were considered for integration with RNAseq data.

Integrating Transcriptome Profiling and Meta-Quantitative Trait Loci Analysis

The expression level of the 1047 selected candidate genes (see the pervious section) were extracted from the transcriptome profiling data for all samples (the genes with FPKM values less than one in more than 80% of samples were removed) and their significance was analyzed by a two-way ANOVA for each zone, separately (with a p-value cutoff of < 0.05) to identify genes with significant interactions between genotypes and conditions.

Quantitative Real-Time PCR Analysis

Total RNA was extracted as described above. Quantitative real-time PCR (qRT-PCR) was performed as previously described (Taheri et al., 2011). Briefly, cDNA was synthesized from 2 μL of each RNA sample (iScript cDNA Synthesis kit, Bio-Rad). The sequence information from our RNA-seq data was utilized for primer design using the Oligo 7.0 software (National Bioscience Inc., Plymouth, MA, United States), and the primer sequences were double-checked by IDT-oligo analyzer tool[9]. The qRT-PCR with three independent biological replicates was performed using a LightCycler 96 Real-Time PCR System (Roche Life Science, Germany) and TB SYBR Premix Ex Taq II based on the manufacturers' protocol.

The expression level of each target mRNA and the housekeeping gene (UBQ) were determined in parallel for each sample. Results were expressed as the normalized ratio of the mRNA level of each gene of interest over that of UBQ using the difference between the threshold cycle values, or ΔΔCt method. Ct values for individual target genes were calculated and the ΔCt average for the housekeeping gene (UBQ) was treated as an arbitrary constant and used to calculate ΔΔCt values for all samples. Three independent biological replicates were used for qRT-PCR.

RESULTS

Phenotypic Responses of Two Contrasting Rice Genotypes to Water Stress

Following exposure to a 14-day water stress treatment, RWC of the susceptible and shallow-rooting genotype, IR64, dropped to 72%, while Azucena, the tolerant and deep-rooting genotype, maintained 80% of its RWC (**Figure 1D** and **Supplementary Tables S1, S2**). A significant reduction in shoot dry weight was evident in Azucena (24%), and to a greater extent in IR64 (34%) (**Figure 1E** and **Supplementary Tables S1, S2**). Changes in the root dry weight also showed a similar trend, with 36 and 13% reduction in IR64 and Azucena, respectively (**Figure 1F** and **Supplementary Tables S1, S2**).

In addition, Azucena had significantly longer roots compared to IR64 under both control and stress conditions (**Figures 1C,E** and **Supplementary Tables S1, S2**), and the rates of root elongation induced by water stress were significantly higher in Azucena (58%) compared to IR64 (23%) (**Supplementary Table S2**).

Lateral roots expansion, evident in both genotypes in response to stress, was more significant in Azucena (**Figure 2A**). The number of macroscopic lateral roots was counted along a 30-cm section (from tip) of the longest crown roots of both genotypes

[7] http://archive.gramene.org/markers/microsat/

[8] https://plants.ensembl.org/biomart/martview/

[9] https://www.idtdna.com/pages/tools/oligoanalyzer

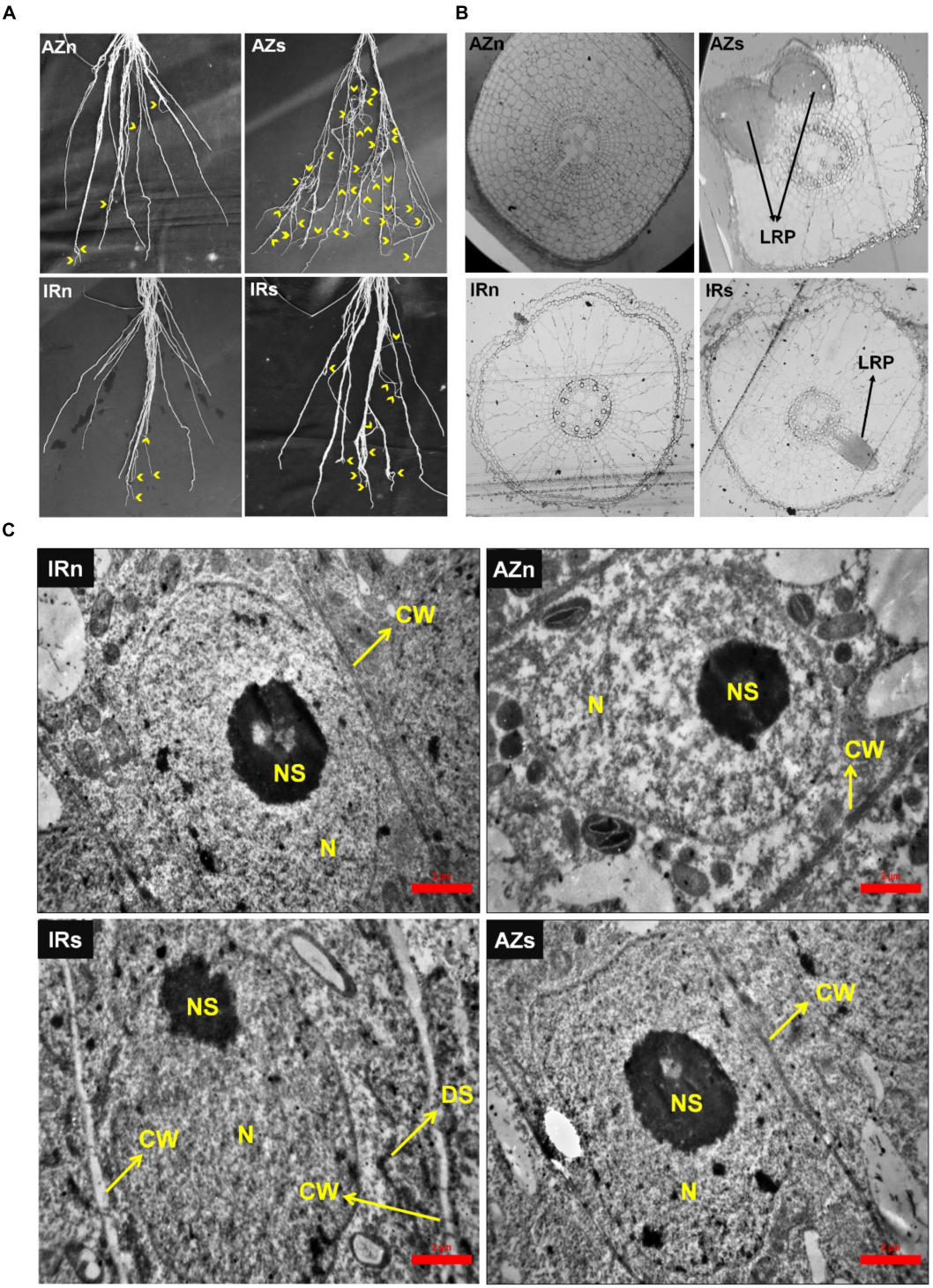

FIGURE 2 | Lateral root expansion and structural and ultrastructural studies of Azucena and IR64 root tips in response to water stress. **(A)** Lateral root expansion in Azucena and IR64 under normal and stress conditions; Yellow arrows indicate lateral roots. **(B)** Tissue structural studies of root (zone3) in both genotypes under normal and stress conditions shows the number of lateral root primordia. **(C)** Ultrastructural studies of root meristematic cells in both genotypes under normal and stress conditions shows cell wall thickening in IR64 in response to stress. IRn, IR64 genotype under normal condition; IRs, IR64 genotype under water-stress condition; AZn, Azucena genotype under normal condition; AZs, Azucena genotype under water-stress condition; Z1, Root Z1; Z2, Root Z2; Z3, Root Z3; CW, cell wall; N, nucleus; NS, nucleolus; DS, dictyosome; LRP, lateral root primordium.

under both conditions (**Supplementary Figure S1**). The number of lateral roots were increased 4.5 fold in Azucena under water stress while in IR64 it was only 2.5 fold. Structural studies revealed different numbers of LR primordia in a 2 mm section of Z3. Our transverse serial sections showed no LR primordia in the two genotypes grown under well-watered conditions (**Figure 2B**). However, under water stress, LR primordia were observed in both genotypes with Azucena having a greater number. These observations may be reflective of the role of LR growth and development in assisting the tolerant genotypes to cope with water shortage.

Furthermore, cellular ultrastructural studies of meristematic root zone (Z1) revealed cell wall thickening of meristematic cells in IR64 roots, in response to water stress, with no change in those of Azucena (**Figure 2C**). Plant cells are surrounded by plasma membrane and cell wall, with the former appearing dark, after fixation in osmium tetroxide and staining with uranyl acetate and lead citrate, due to their lipid structure, and the latter appearing white due to its polysaccharide content (Alberts, 2018). The very thin cell wall surrounding a typical meristematic cell makes it barely detectable, as shown in Azucena under both conditions and IR64 under the normal condition. However, in IR64 samples exposed to stress, it presented in the form of a white boundary, possibly indicating an increase in the thickness of the cell wall (**Figure 2C**).

Transcriptome Profiling of Root Zones Under Control and Water Stress Conditions

RNAseq profiling was performed on three consecutive root tip zones in the two contrasting genotypes of rice under two different conditions and approximately 15–22 million read pairs were obtained for each sample (A total of 452,452,035 read pairs; **Supplementary Table S3** and **Supplementary Figure S2**). Reads were aligned to the *O. sativa* cv. Nipponbare (ssp. *japonica*) reference genome sequences IRGSP1.0[10] using Hisat2 (Kim et al., 2015). The percentage of mapping rates and unique mapping rates for all samples were between 94–96% (with an average of 95.17%) and 84–90% (with an average of 88.57%), respectively (**Supplementary Table S3** and **Supplementary Figure S2**). Expression levels for the transcripts were calculated by quantifying the reads according to the FPKM method (Trapnell et al., 2010).

A total of 37846 annotated genes were identified, 65% of which (24742 genes) were actively expressed (FPKM $>$ 1 in at least two biological replicates of one sample), whereas, about 35% (13104 genes) were not expressed (FPKM = 0) or expressed at very low levels (1 $>$ FPKM $>$ 0) and thus considered as silent genes. Among all expressed genes (24742), there was evidence of expression for 18364 genes (48% of all annotated genes) in at least 80% of all samples (referred to constitutive expression), 5580 genes (15% of all annotated genes) in 20–80% of all samples (intermediate frequency), and 798 genes (2% of all annotated genes) in less than 20% of all samples (low frequency) (**Figure 3A**). The enriched biological processes (BPs) terms for the identified gene sets are shown in **Supplementary Table S4**.

There were 1053 and 1675 genes specifically expressed in IR64 and Azucena, respectively (referred to genotype specific), and 1723 and 916 genes expressed specifically in control and stress conditions, respectively (referred to condition specific). In the zone-specific category, 661, 250, and 503 genes were only expressed in Z1, Z2, and Z3, respectively (**Figure 3B**). These results suggest substantial differences in expression patterns in all genotypes, conditions, and the zones examined here. The enriched BPs terms for these identified gene sets are shown in **Supplementary Table S5**.

Principal component analysis (PCA) on the 24742 expressed genes illustrated the clustering of samples by zones, genotypes and conditions. Pearson correlation coefficients based on gene expression levels (FPKMs) between each pair of samples are shown as a heatmap, indicating the consistency between biological replicates of each sample (**Supplementary Figure S3**). The first two PC dimensions, accounting for 91% of the variation, was sufficient for clear separation of the genotypes and conditions (**Figure 3C** and **Supplementary Figure S3**). The PCA analysis clearly presented the distinct expression patterns between stress and normal conditions. Furthermore, Z1 grouped separately from Z2 and Z3 (**Figure 3C** and **Supplementary Figure S3**).

Differential Expression Analysis

Differentially Expressed Genes Between Control and Stress Conditions

Differentially expressed genes for each genotype and zone were identified and the fold change was calculated by dividing the expression level under stress conditions by control conditions. An Upset plot was used for visualization of the number of up- (red boxes) and down- (blue boxes) regulated DEGs across different genotypes and zones (**Figure 3D**). The data on DEGs in Z1, Z2, and Z3 of IR64 and Azucena identified a fraction of nearly 35–45% with modest levels of change (less than twofold change), while the remainder showed greater levels of change (more than twofold change) in transcript abundance. Interestingly, about 5–10% of DEGs showed 8- to 16-fold change (**Figure 3D**).

The intersections of DEGs across these six groups, labeled C1-C40, indicated their dynamic patterns in different zones and genotypes, as shown in the vertical bar graph (**Figure 3E**). The significantly enriched BPs of eleven important intersections representing zone-, genotype-, and zone and genotype-specific responses are shown in bar plots (based on –log10 adjusted *p*-values) at the bottom panel (**Figure 3F**) while the remains are exhibited in the **Supplementary Table S6**. The results from zone and genotype-specific DEGs revealed the enrichment of different BPs by IR64 and Azucena: In Z1 of Azucena roots (C07), six BPs were specifically enriched, such as those involved in cell cycle and division and ATPase activity (**Figure 3F**). In IR64 (C04), on the other hand, of the six enriched BPs, four were related to signaling, and transporting (**Figure 3F**). The BPs specifically enriched in Z2 of Azucena (C09) included peptidyl-proline modification and regulation of mRNA metabolic processes, while, in Z2 of IR64 (C12) different BPs were enriched

[10]https://plants.ensembl.org/info/website/ftp/index.html

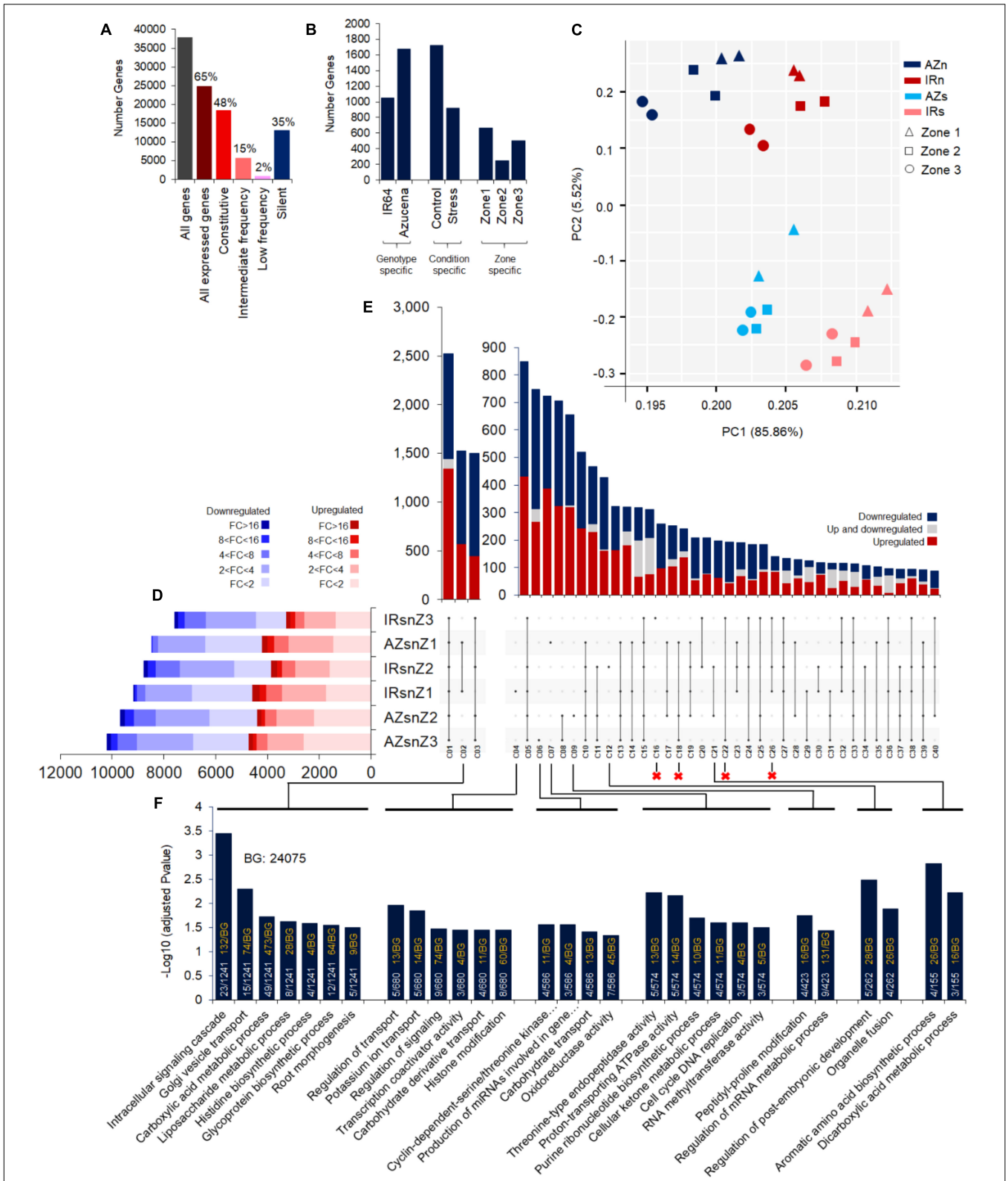

FIGURE 3 | Transcriptome profiling of Azucena and IR64 root zones under control and water stress conditions and the intersections of DEGs across 6 interaction of genotypes, zones and conditions. **(A)** The number of genes not expressed in any sample (the silent group) (FPKM < 1 in none of the doublet sets of replicates), expressed in less than 20% of samples (Low frequency), expressed in 20–80% of samples (Intermediate frequency), and expressed in more than 80% of samples

(Continued)

FIGURE 3 | (Constitutive). **(B)** The number of genes expressed in only one genotype (All replicates of three zones; Genotype specific), one condition (All replicates of the condition; Condition specific), and one zone (All replicates of the zone; Zone specific). **(C)** Principal component analysis (PCA) visualization of all 24 samples in a 2D space. PCA were used on Log2 transformed FPKM values of a set of 24742 genes (about 65% of all identified annotated genes) expressed in at least one set of doublet replicates (FPKM > 1) in this analysis. The color indicates genotype and condition (IRn, IR64 under normal condition; AZn, Azucena under normal condition; IRs, IR64 under stress condition; AZs, Azucena under stress condition) and the shapes indicates root zones. **(D)** Horizontal bar graph represents the number of up- (Red boxes) and down- (Blue boxes) regulated DEGs (FDR adjusted *p*-value cut-off of ≤ 0.05) based on their fold changes. **(E)** The intersections of DEGs across the six gene lists in the vertical bar graph (40 out of 62 intersections presented and the information on the others can be found in **Supplementary Table S6**). Sections colored in red/blue depict genes up/down regulated synchronously, while the gray sections are the ones upregulated in one and downregulated in the other and vice versa. The circles below each bar with black color indicate which sets are in the intersection. **(F)** The significantly enriched BPs are shown as barplots in the bottom panel based on their –log10 adjusted *p*-values. The proportion of gene numbers included in each BP in annotated gene numbers of the cluster (white text) along with the proportion of total gene numbers included in each BP in annotated gene numbers of the background (yellow text) were mentioned in the bars. IRsnZ1, expression changes in zone1 of IR64 (Stress vs. Control); IRsnZ2, expression changes in zone2 of IR64 (Stress vs. Control); IRsnZ3, expression changes in zone3 of IR64 (Stress vs. Control); AZsnZ1, expression changes in zone1 of Azucena (Stress vs. Control); AZsnZ2, expression changes in zone2 of Azucena (Stress vs. Control); AZsnZ3, expression changes in zone3 of Azucena (Stress vs. Control).

including the regulation of post-embryonic development and organelle fusion (**Figure 3F**). Genes specifically expressed in Z3 of Azucena (C06) corresponded to BPs including cyclin-dependent protein serine/threonine kinase activity, production of miRNAs involved in gene silencing, carbohydrate transport and oxidoreductase activity. In contrast, no significantly enriched BPs were detected in Z3 of IR64 (C16) (**Figure 3F**).

To present an overview of data and identify major co-expressed clusters across both genotypes and all root zones in response to water stress, a hierarchical clustering was performed on DEGs based on the fold-change values by complete method and Euclidean distance measurement (**Figure 4**). The matrix was included the FC values of those genes that were DEG in at least one zone (the non-differentially expressed FC values were set to zero.). The 11 main clusters (C1–C11) were considered for GO enrichment analysis. **Supplementary Table S7** shows the significantly enriched GO terms belonged to the clusters 1–5 and 9–11 (C1–C5 and C9–C11) however, no enriched GO terms were obtained for the clusters 6, 7, and 8. Interestingly, the genes belonged to C5 strongly upregulated in zone one of Azucena, were enriched for generation of precursor metabolites and energy, electron transport chain, and cell cycle BPs while the C11 containing genes with upregulation patterns in zone 1 and 2 of IR64 root were enriched for response to water stress and polysaccharide catabolic process (**Supplementary Table S7** and **Figure 4**).

Differentially Expressed Genes With a High Fold Change Between Control and Stress Conditions

To analyze highly up- and down-regulated DEGs, transcripts with more than fourfold change between control and stress conditions were filtered. The filter was applied to all DEG groups belonging to all three root zones of the two genotypes, and the values of each list in the other zones and other genotype were determined. To find the genotype-specific responsive genes, only those genes with more than fourfold change differences between genotypes were kept. The collective list (1440 genes) was clustered based on fold changes in different zones and genotypes by average linkage method and Euclidean distance measurement (**Figure 5A**). We observed six distinct clusters corresponding to up- or down-regulated genes in response to stress. Cluster 3 consisted of genes highly upregulated in Z1 of Azucena, and included a total of 375 genes, 194 of which had functional annotation according to rice databases. Interestingly, a total of 40 genes, listed in **Figure 5B**, are involved in root development (18 genes) and drought tolerance (22 genes). These were included genes with important roles in rice RSA, such as *OsbHLH120* (root thickness), *OsNAC10* (root thickness and drought tolerance), *OsPHR3* (LR development), PIP1;3/RWC3 (root length and water stress avoidance), *OsMADS18* (root elongation), and *OsNLA1* (root length and growth), as well as those with key roles in enhancing drought tolerance such as *DIP3*, *CIPK10*, *CIPK17*, *CIPK29*, *OsERF101*, *OsWRKY11,* and *ONAC58*/*OsNAP*.

Gene ontology enrichment analysis was performed on all six clusters in **Figure 5A**, and the significant BPs (p-value < 0.05) are presented in **Figure 5C** based on their –log10 (p-value). Interestingly, cluster 3 (C3) containing highly up-regulated genes in zone 1 of Azucena, was specifically enriched for transcripts involved in regulation of transcription, and terpenoid, lipid and monocarboxylic acid metabolic processes, while cluster 1 (C1) containing highly up-regulated genes in zone 1 of IR64, was specifically enriched for response to oxidative stress and isoprenoid metabolic process. Response to oxidative stress was also enriched for cluster 6 (C6), which containing a gene set with upregulation patterns in all three zones of IR64 but only in zone 1 of Azucena (**Figure 5C**).

Differentially Expressed Genes Involved in Root Elongation, Lateral Roots Expansion and Meristematic Cell Wall Thickening

The main goal of this study was identification of genes involved in rice RSA traits. To find more associated candidate genes, an expand literature review was performed to prepare a list of related genes reported previously in the research articles and the rice databases. According to the results of our phenotypic observations indicating induced root elongation, LR expansion and meristematic cell wall thickening in response to stress, three lists of 230, 154, and 581 genes affecting root length, LR development and cell wall formation and modification, respectively, were considered for surveying of their expression

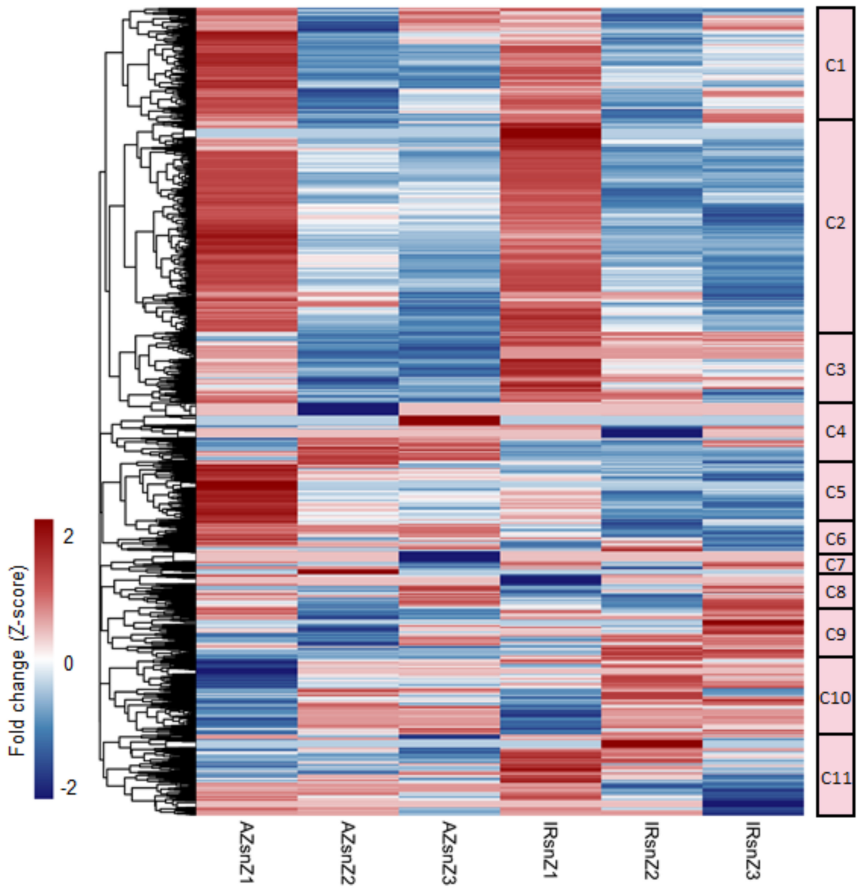

FIGURE 4 | An overview of DEGs and co-expressed clusters across rice genotypes and root zones in response to water stress. Heatmap representing the hierarchical clustering of DEGs based on the fold-change values (clustering method: complete; clustering distance: euclidean). The color bar depicts the gradient of fold changes in response to water stress. The matrix was included the FC values of those genes that were DEG in at least one zone (the non-differentially expressed FC values were set to zero.). The 11 main clusters (C1–C11) were marked. Please see the enriched GO terms belonged to each cluster in **Supplementary Table S7**.

patterns using our dataset (**Supplementary Table S8**). Of these, a total of 186, 113, and 403 genes with FPKM values of more than one in at least 20% of the samples, respectively, were selected for further analysis. The two-way ANOVA led to the identification of interesting DEGs with significant interactions for genotypes and conditions.

Our phenotypic analysis revealed Azucena roots were longer than those of IR64 under both well-watered and water-deficit conditions (**Figures 1C,G**). In addition, stress-induced increase in root elongation rate was about 2.5 fold higher in Azucena than in IR64 (**Supplementary Table S2**). Out of 186, 34 DEGs with significant interactions for genotypes and conditions were detected in Z1, the region including meristematic and elongation regions responsible for cell division and cell expansion, the two major determinants in root growth and elongation (Krizek, 2009) (**Supplementary Figure S4A**). Among them, 17 DEGs were upregulated in Azucena (**Figure 6A**), including *OsRBG1*, *OsRMC*, and *OsERF2*/*OsWR4*.

Since Azucena had longer roots than IR64 under both conditions, to identify DEGs between the two genotypes, irrespective of the treatment, a t-test analysis was performed on the genes with insignificant differences according to the ANOVA analysis. Eleven genes (**Supplementary Figure S4B**) showed significant differences (p-value < 0.05) between genotypes under both normal and stress conditions, of which seven were over-expressed in the Azucena genotype, including *OsDEL1*/*OsPLL12* and *OsDOF7*/*11* (**Figure 6B**).

Also, we detected LR expansion in both genotypes in response to water stress, though to a greater level in Azucena (**Figures 2A,B**). The analysis revealed 48 (out of 113) DEGs (**Supplementary Figure S4C**) significantly induced (significant at least in one zone) of which 18 were upregulated in the Azucena roots (**Figure 6C**), included *OsACS*, *OsARF16*, *OsPTR9*, *OsMADS27*, *OsHO1*/*OsSE5*, *OsRAA1*, and *OsAUX*/*LAX1* (**Figure 6C**). It is interesting to note that all 18 DEGs were significantly induced in response to stress in both zones 2 and 3, enriched for lateral root growth and development (**Figure 6C**).

Meristematic cell wall thickening was observed in IR64 in response to stress (**Figure 2C**). Out of a total of 58 DEGs with significant interaction between genotype and condition in Z1 (**Supplementary Figure S4D**), 32 genes were upregulated in IR64 (**Figure 6D**) including three

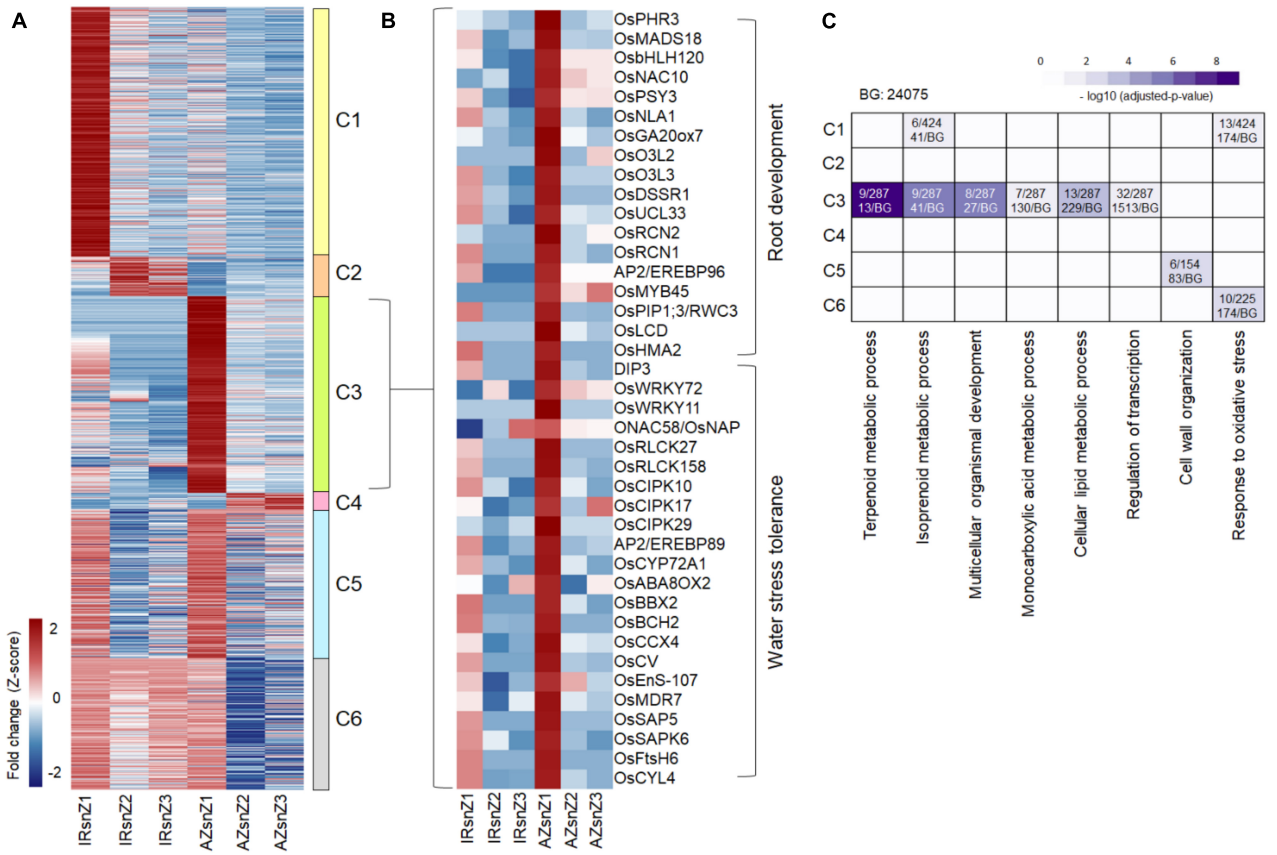

FIGURE 5 | Differentially expressed genes with a high fold change between control and stress conditions in two contrasting genotypes of rice. **(A)** Heatmap representing the DEGs with high fold changes (more than fourfold) between control and stress in the six clusters with distinct expression patterns across the three root zones of two contrasting genotypes of rice. The color bar depicts the gradient of fold changes in response to water stress. **(B)** Heatmap representing a subset of 40 genes extracted from cluster 3 with roles in root development and water stress tolerance. **(C)** BPs enriched in clusters 1–6 (C1–C6). The color bar depicts the gradient of –log10 (adjusted *P*-value) where *P*-value is the significance of individual GO-BPs enriched with each cluster. The proportion of gene numbers included in each BP in annotated gene numbers of the cluster (on top) along with the proportion of total gene numbers included in each BP in annotated gene numbers of the background (at bottom) were mentioned in the boxes. IRsnZ1, expression changes in zone1 of IR64 (Stress vs. Control); IRsnZ2, expression changes in zone2 of IR64 (Stress vs. Control); IRsnZ3, expression changes in zone3 of IR64 (Stress vs. Control); AZsnZ1, expression changes in zone1 of Azucena (Stress vs. Control); AZsnZ2, expression changes in zone2 of Azucena (Stress vs. Control); AZsnZ3, expression changes in zone3 of Azucena (Stress vs. Control).

members of the *CAD* gene family (*OsCAD3*, *OsCAD8D*, and *OsCAD9*) along with *OsMYB52/54*, *OsSUS3*, *OsPRX1*, and *BSH1/OsCYP96B4*.

Gene Family Studies Across Contrasting Genotypes

To maximize the benefit of transcriptome analysis, the expression pattern of 24 important gene families with roles in RSA growth and development and drought stress response were further analyzed including *NAC*, *AP2/ERF*, *AUX/IAA*, *EXPANSIN*, *WRKY*, *MYB*, *MYB-related*, *ARF*, *EXPANSIN*, *GRAS*, *LEA*, *HSP*, *HSF*, *ARID*, *bHLH*, *bZIP*, *LOB*, *WOX*, *EIL*, *GRF*, *G2-like*, *TIP* and *PIP*, *SWEET*, *RR*, and *MADS* (Hu et al., 2009; Dal Santo et al., 2013; Janiak et al., 2016; Yoon et al., 2020). A complete list of the members, collected by searching through four databases, along with their IDs, names, and descriptions is presented in the **Supplementary Table S9**. By performing a two-way ANOVA for each zone, separately, we searched for genes with significant interactions for genotypes and conditions (at least in one zone). The expression patterns of DEG members (p-value < 05) in two genotypes in response to water stress are shown in **Supplementary Figures S5–S7**. It should be emphasized that the majority of the 24 families showed dynamic expression patterns, however, we have focused on six important families, namely *NAC*, *AP2/ERF*, *AUX/IAA*, *EXPANSIN*, *WRKY*, and *MYB*, while the information on the remaining families is shown in **Supplementary Figures S6, S7**. These six families are involved in a wide range of BPs such as plant life cycle, root growth and development and water deficit tolerance.

Out of the 121, 164, 31, 103, 120, and 56, members detected of *NAC*, *AP2/ERF*, *AUX/IAA*, *WRKY*, *MYB TF*, and *EXPANSIN* gene families, respectively, 69, 103, 27, 70, 81, and 39 had FPKM values of more than one at least in 20% of the samples considered for two-way ANOVA.

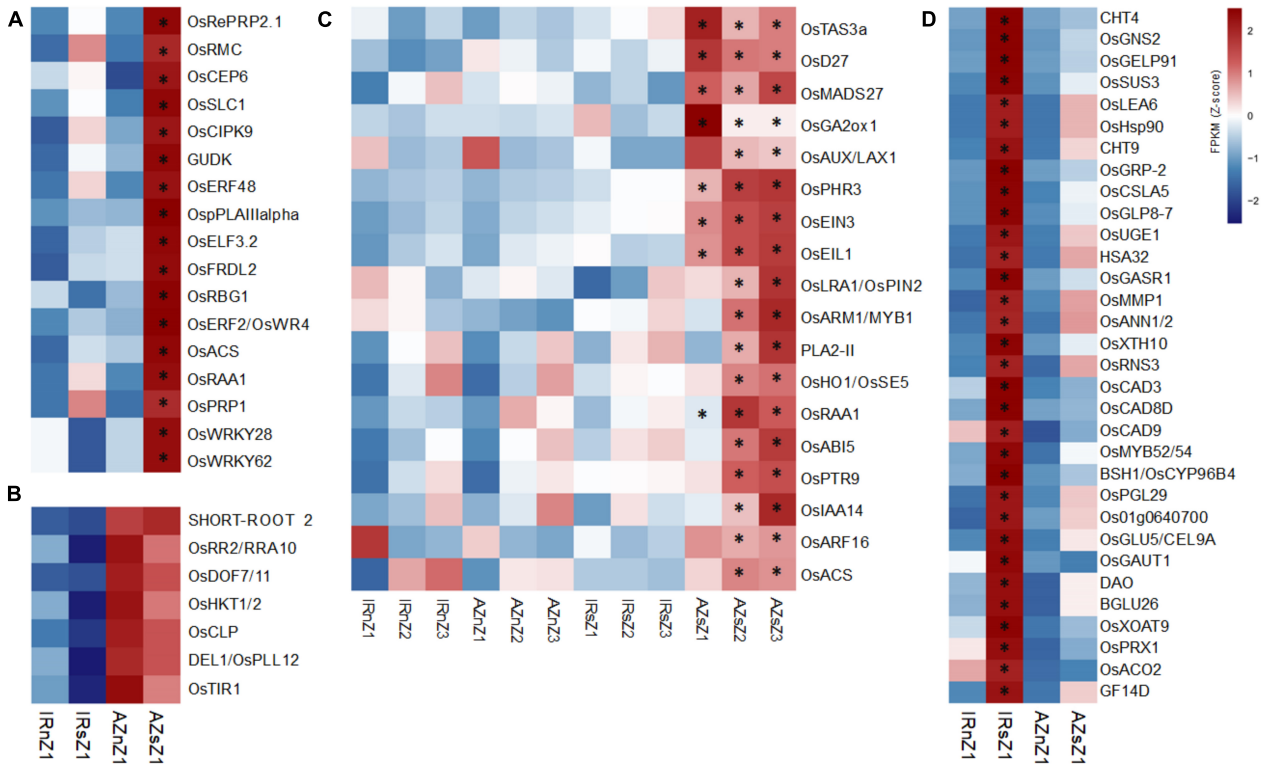

FIGURE 6 | The expression pattern of DEGs involved in root elongation, LR expansion and meristematic cell wall thickening across two contrasting genotypes under water stress. **(A)** Heatmap showing the expression patterns of genes affecting root length and significantly upregulated in Z1 of Azucena roots under stress conditions. The asterisks indicate significant interactions between genotypes and conditions (p-value cut-off ≤ 0.05) analyzed by a two-way ANOVA test. **(B)** Genes affecting root length were expressed at much higher levels (p-value cut-off of ≤ 0.05, analyzed by t-tests between genotypes in both conditions) in Z1 of Azucena roots under both conditions compared to IR64. **(C)** Heatmap showing the expression pattern of genes involved in lateral root formation, growth and development, induced and upregulated in response to stress only in Azucena root zones. The asterisks indicate significant interactions between genotypes and conditions (p-value cut-off ≤ 0.05) analyzed by two-way ANOVA test. **(D)** Heatmap showing the expression pattern of genes involved in cell wall biogenesis and modification induced and upregulated in Z1 of IR64 roots under stress. The asterisks indicate significant interactions between genotypes and conditions (p-value cut-off ≤ 0.05) analyzed by two-way ANOVA test. IRnZ1, root Z1 of IR64 under normal condition; IRnZ2, root Z2 of IR64 under normal condition; IRnZ3, root Z3 of IR64 under normal condition; IRsZ1, root Z1 of IR64 under stress condition; IRsZ2, root Z2 of IR64 under stress condition; IRsZ3, root Z3 of IR64 under stress condition; AZnZ1, root Z1 of Azucena under normal condition; AZnZ2, root Z2 of Azucena under normal condition; AZnZ3, root Z3 of Azucena under normal condition; AZsZ1, root Z1 of Azucena under stress condition; AZsZ2, root Z2 of Azucena under stress condition; AZsZ3, root Z3 of Azucena under stress condition.

Of the 33 DEGs identified of the *NAC* family (**Supplementary Figure S5B**), 19 showed significant upregulation in Azucena root in response to water stress while they did not change significantly in IR64 (**Figure 7A**) and included those involved in RSA development [*OsNAC10*, *OsNAC5*, *ONAC54* (*RIM1*), *ONAC58* (*OsNAP*), and *ONAC3* (SNAC3)]. Of the 45 DEGs detected of the *AP2/ERF* gene family (**Supplementary Figure S5A**), 16 were upregulated in Azucena in response to water stress, with no significant changes in IR64 (**Figure 7B**). The roles of six of them in water-stress tolerance and rice root development have previously been reported; *OsERF50* (*OsDREB6*), *OsERF48*, *OsERF101*, *OsERF95* (*OsSta2*), *OsERF93/ERF1*, and *OsERF2/OsWR*. Fourteen members of *AUX/IAA* gene family showed differential expression under water stress at least in one zone (**Supplementary Figure S5E**). Of these, a total of 6 indicated significant upregulation under stress only in the Azucena genotype including *OsIAA26*, *OsIAA2*, *OsIAA18*, *OsIAA20*, *OsIAA14*, and *OsIAA24* (**Figure 7D**). Also, 22 DEGs were detected of *WRKY* gene family (**Supplementary Figure S5C**) in which seven DEGs were upregulated in Azucena under water stress with no significant changes in IR64. These include *OsWRKY51*, *OsWRKY72*, *OsWRKY3*, *OsWRKY9*, *OsWRKY11*, *OsWRKY28*, and *OsWRKY62* (**Figure 7C**). The analysis led to the identification of 33 DEGs of the *MYB TF* family (**Supplementary Figure S5F**). Six genes (*OsMYB12*, *OsMYB20*, *OsDLN31*, *OsMYB10*, *OsMYB1/ARM1*, and *Os01g0685400*) showed significant upregulation in Azucena roots in response to water stress while they did not change significantly in IR64 (**Figure 7F**). Thirteen DEGs were detected of the *EXPANSIN* gene family (**Supplementary Figure S5D**). Despite the ten DEGs downregulated in both genotypes the expression level of 3 members (*EXPA2*, *EXPB11*, and *EXPA5*) only increased only in Azucena roots, especially in Z1 in response to water stress with no significant changes in IR64 (**Figure 7E**).

In addition, our results revealed that the members of two *HSP* (heat shock protein) and *HSF* (heat shock

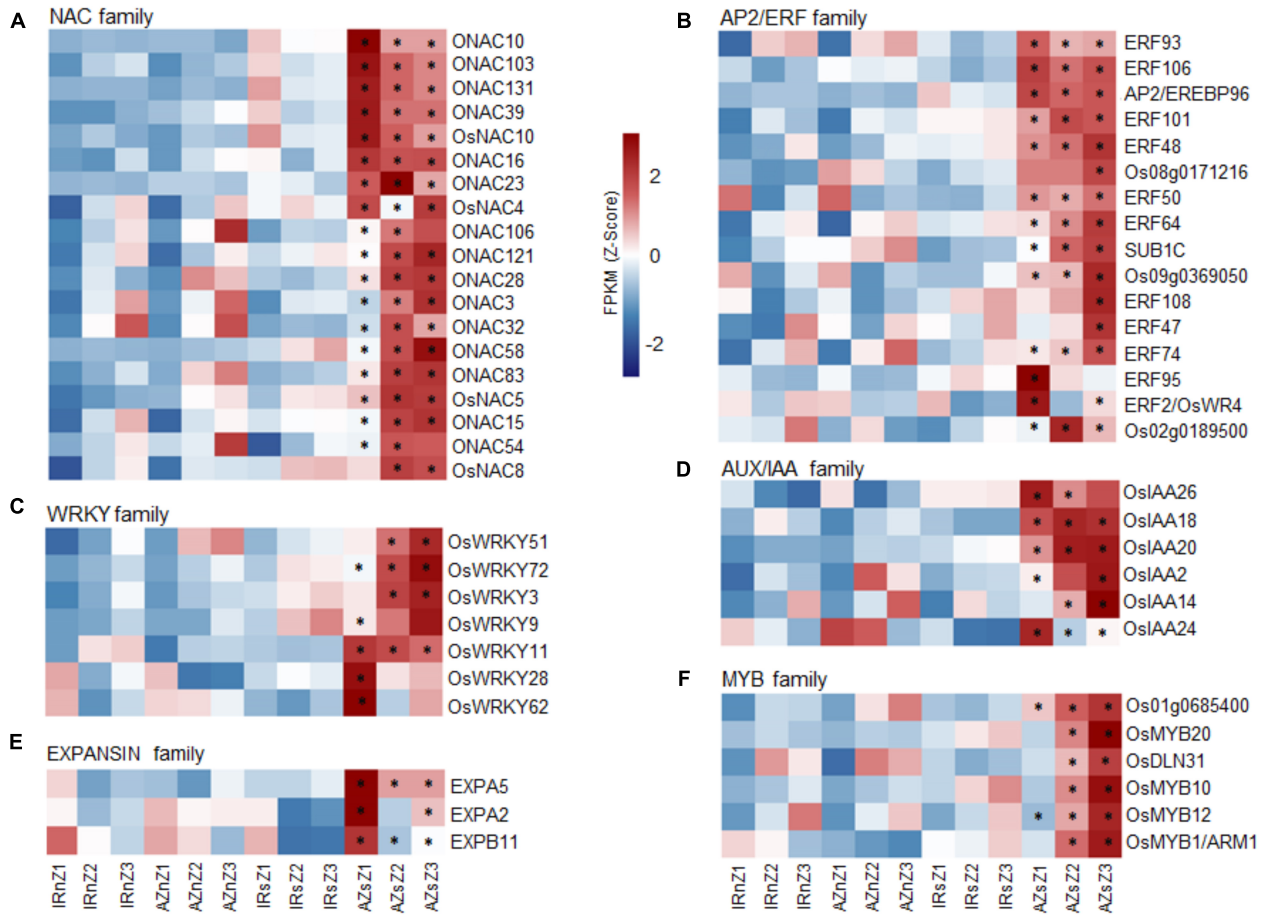

FIGURE 7 | Gene family studies across contrasting genotypes in response to water stress. Heatmaps showing the expression pattern of members of **(A)** *NAC*, **(B)** *AP2/ERF*, **(C)** *WRKY*, **(D)** *AUX/IAA*, **(E)** *EXPANSIN*, **(F)** *MYB* gene families, upregulated in Azucena roots in response to water stress compared to IR64 genotype. The color bar depicts the gradient of FPKM mean (*Z*-score) for each sample. The asterisks indicate genes with significant interactions between genotypes and conditions ($p \leq 0.05$) by two-way ANOVA test. IRnZ1, root zone 1 of IR64 under normal condition; IRnZ2, root zone 2 of IR64 under normal condition; IRnZ3, root zone 3 of IR64 under normal condition; IRsZ1, root zone 1 of IR64 under stress condition; IRsZ2, root zone 2 of IR64 under stress condition; IRsZ3, root zone 3 of IR64 under stress condition; AZnZ1, root zone 1 of Azucena under normal condition; AZnZ2, root zone 2 of Azucena under normal condition; AZnZ3, root zone 3 of Azucena under normal condition; AZsZ1, root zone 1 of Azucena under stress condition; AZsZ2, root zone 2 of Azucena under stress condition; AZsZ3, root zone 3 of Azucena under stress condition.

factor) gene families were strongly upregulated in IR64 root in response to water stress, compared to Azucena. Out of 25 and 39 members detected for *HSF* and *HSP* gene families, respectively, 19 and 24 members showed significant interactions for genotypes and conditions at least in one zone. Of these 14 *HSF* genes (including *OsHSFA2a*, *OsHSF-16*, *OsHSFB2b*, *OsHSFC1b*, *OsHSFA2c*, *OsHSFA3*, *OsHSFB2a*, *OsHSFB4a*, *OsHSFB2c*, *OsHSFA7*, *OsHSFA2d*, *OsHSFA9*, *OsHSF15*, and *OsHSFA2b*) and 19 *HSP* genes (including *OsHSP70-4*, *OsHSP18.6*, *OsHSP70CP1*, *OsHSP101*, *OsHSP18.0-CIII*, *OsHSP90.1*, *OsHSP17.9B*, *OsHSP26*, *OsHSP74.8*, *OsctHSP70-1*, *OsHSP17.3*, *OsHSP17.7*, *OsHSP70CP2*, *OsHSP90-1*, *OsHSP16.9C*, *OsHSP17.9A*, *OsHSP24.1*, *OsHSP16.9A*, and *OsHSBP2*) were significantly upregulated in IR64, the sensitive and lowland genotype, while they did not change significantly in Azucena (**Supplementary Figures S7A,B**). These results may suggest the important roles of *HSP* and *HSF* families in IR64 to cope with water-deficit stress.

Collectively, several RSA associated genes were identified as drought responsive genes in both gene family and root elongation, LR expansion and meristematic cell wall thickening studies (from sections "Differentially Expressed Genes Involved in Root Elongation, Lateral Roots Expansion and Meristematic Cell Wall Thickening" and "Gene Family Studies Across Contrasting Genotypes") which their roles in response to drought have not been reported yet. For example, we found two subsets of 17 (*OsPHR3*, *OsMADS18*, *OsACS*, *OsARF16*, *OsHO1*, *OsPTR9*, *OsRAA1*, *OsRMC*, *OsDOF11*, *OsERF2*, *OsDEL1*, *ONAC52*/*RIM1*, *OsEXPA2*, *OsIAA20*, *OsIAA26*, and *OsWRKY72*) and 7 (*OsCAD3*, *OsCAD8D*, *OsCAD9*, *OsMYB52*/*54*, *OsSUS3*, *OsPRX1*, and *BSH1*/*OsCYP96B4*) genes with positive and negative roles in RSA formation and modification, respectively. Considering their induction in response to water deficit stress,

their potential roles in adaptation of rice to water stress needs to be further investigated.

Integrating Transcriptome Profiling and Meta-Quantitative Trait Loci Analysis

Many QTLs related to rice RSA traits were identified by linkage analysis from different populations across different water conditions, so far, which are valuable resources for integrating with transcriptome profiling and finding novel candidate genes. In this study, 20 independent experiments (**Supplementary Table S10** and **Figure 8A**) based on bi-parental populations were reviewed included two sets of IR64 × Azucena and Azucena × other rice genotypes populations (with emphasis on Azucena, the tolerant and deep-rooting genotype). A total of 132 QTLs controlling RSA traits under drought and normal conditions (including 82 and 50 from the two mentioned population sets, respectively) were collected (**Figure 8A** and **Supplementary Table S11**). The RSA traits included were MRL, DRW, RN, RL, RTHK, RV, RDW, DRR, RSR, DS, RSAr, and RGA. Meta-QTL analysis were performed on both sets of collected QTLs separately. It led to identification of 31 and 23 significant Meta-QTLs with confidence interval (CI) of 0.11–17.67 cM and 0.055–5.2 cM which were 2.52 and 3.07 times narrower than the mean CI of the original QTLs for IR64 × Azucena and Azucena × other rice genotypes populations, respectively. They were located on all 12 rice chromosomes (**Figure 8A** and **Supplementary Table S12**) and were included a total of 5787 and 3511 genes (**Figure 8B** and **Supplementary Table S13**). Among them, 1047 common genes were detected located on chromosomes 1, 2, 3, 4, 7, and 9. To narrow down the candidate genes, only the 1047 common genes (**Figure 8B**), were considered for integrating with RNAseq data. The locations of these genes along with the information about the associated Meta-QTLs are shown in **Supplementary Figure S8**. A two-way ANOVA analysis of the expression levels in 1047 common genes across the two genotypes and two conditions showed that the expression level of 121, 159, and 130 genes changed significantly ($p < 0.05$) in zones 1, 2, and 3, respectively (**Figure 8C** and **Supplementary Table S14**). Of these, some were common between all three zones while others were zone-specific. Subsets of 22, 48, 64, and 33 genes overlapped between all zones, zones 1 and 2, zones 2 and 3, and zones 1 and 3, respectively (**Figure 8C**). The expression patterns of the DEGs in Z1 (the region enriched for root traits such as length, thickness and angle) are shown in **Figure 8D**, while those in Z2 and Z3 are shown in **Supplementary Figure S9**. In zone one 14, 7, 18, 18, 46, and 18 genes were differentially expressed in chromosomes 1, 2, 3, 4, 7, and 9, respectively (**Figure 8D** and **Supplementary Figure S8**). These genes, in particular those induced in the tolerant and deep-rooting genotype Azucena, may represent novel candidate genes potentially involved in RSA modification and response to water stress conditions. Some of them had functional descriptions, while others lacked. For example, in obtained Meta-QTLs on chromosome 9 (which control DRR trait), three annotated genes, *CYP76L1* (Cytochrome P450 76L1), *OsFbox490* and *ACO1,* along with a set of six unannotated genes adjacent to each other (surrounded by orange lines) were detected which were co-upregulated significantly in Azucena (**Figure 8D**).

As shown in **Figure 8D**, two another co-expressed regions (surrounded by orange lines) on chromosomes 4 and 7 were observed upregulated significantly in Z1 of Azucena. They may be considered as important regions including key candidate genes involved in RSA traits and tolerance to water stress. Due to the importance of these regions, their expression patterns were also examined in zones 2 and 3. The majority of which were found to be insignificant (**Figure 9**). Only 2, 3, and 2 genes on chromosomes 4, 7, and 9, respectively, showed significant differential expression in zones 2 and 3, while the remainder were zone 1-specific, the zone enriched for deep-rooting traits (**Figure 9**). Collectively, these results may be indicative of the potential roles of these genes in determining RSA traits.

The co-expressed region on chromosome 4 included a total of nine genes: *Os04g0108300*, *Os04g0110100* [GO-Molecular function (MF): carbohydrate binding], *Os04g0111500* (GO-BP: exocytosis and protein transport), *PIC22* (resistance gene analog *PIC22*/*Os04g0111900*; GO-BP: defense response; GO-MF: ADP binding; NB-ARC domain), *Os04g0112100* (GO-MF: ADP binding; NB-ARC domain), *OsFbox179* (*F-box protein 179*/*Os04g0113000*), *Os04g0115200*, *OsAMI1/2* (*Amidase2*/*Os04g0117900*; GO-BP: response to abscisic acid, IAA biosynthesis; GO-MF: amidase activity), and *Os04g0128300*. These genes were extracted by overlaying Meta-QTL 4.1 (IR64 × Azucena population) and Meta-QTL 4.1 (Azucena × other rice genotypes population) which control the RDW and RN traits (**Figure 9** and **Supplementary Figure S8**).

The region on chromosome 7 contains the following 8 genes: *Os07g0642100* (GO-BP: DNA repair; GO-MF: DNA binding), *Os07g0642600*, *Os07g0643100* (putative esterase; GO-MF: hydrolase activity), *Os07g0645200*, *Os07g0648300*, *Os07g0649300*, *Os07g0650100* (transmembrane helix, integral component of membrane), and *Os07g0653900*. They were identified by the overlap between two Meta-QTLs (Meta-QTL 7.4 and 7.4) controlling the RSR and DRW traits (**Figure 9** and **Supplementary Figure S8**).

Moreover, six genes were included in the region on chromosome 9, namely *Os09g0436000*, *Os09g0436300*, *Os09g0436400*, *Os09g0436500* (GO-BP: branched-chain amino acid biosynthesis, isoleucine and valine biosynthesis; GO-MF: oxidoreductase activity, ketol-acid reductoisomerase activity), *Os09g0437500*, and *Os09g0442400*. This region was obtained by overlaying of two Meta-QTLs which control DRR traits (Meta-QTL 9.3 and 9) (**Figure 9** and **Supplementary Figure S8**).

Considering the lack of functional annotation for the majority of these transcripts, they are reported here as novel candidate genes potentially involved in RSA modification and response to water stress conditions.

Validation by qRT-PCR

Technical and biological variations in the data were checked by performing qRT-PCR of 3 independent biological replicates

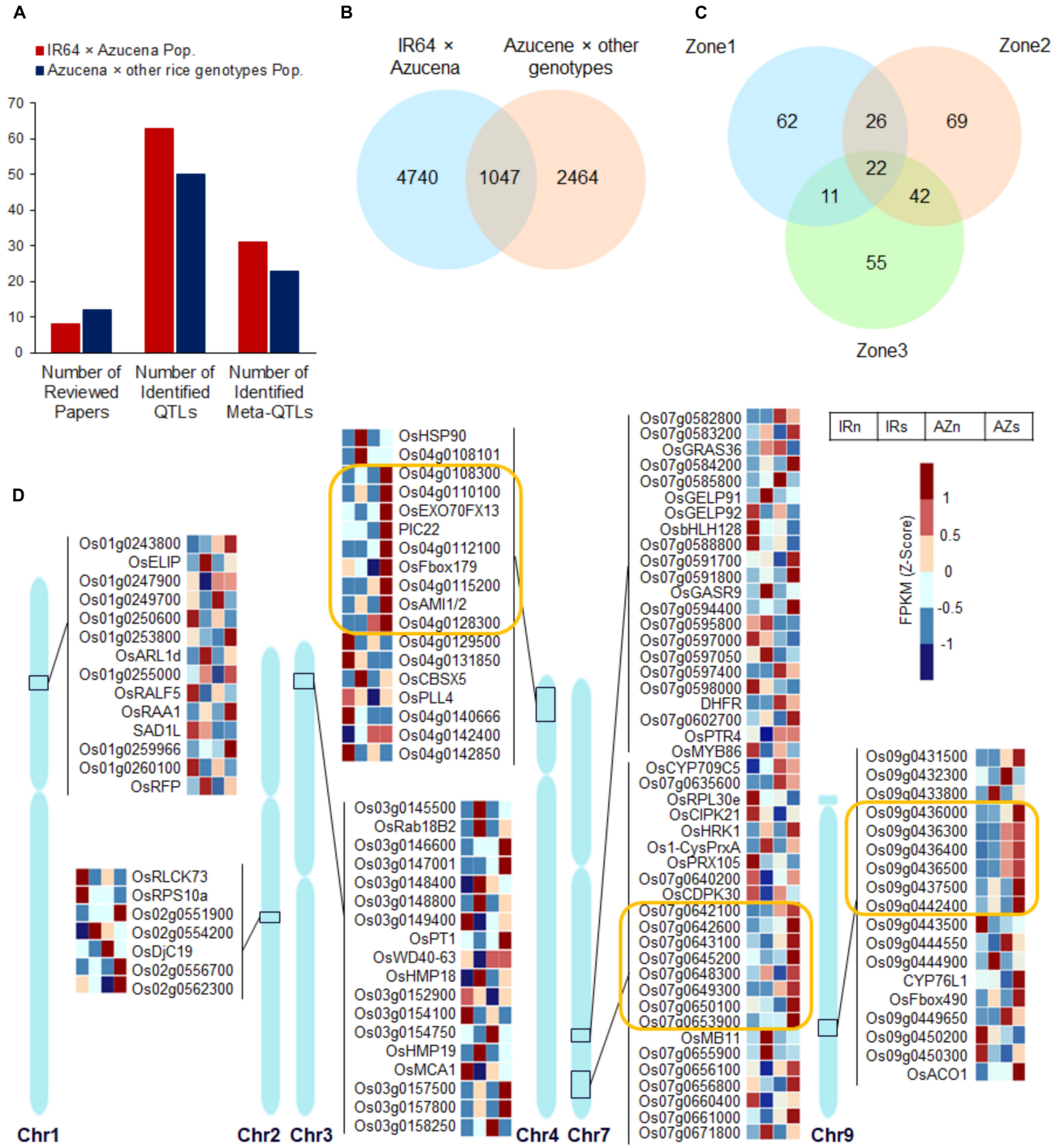

FIGURE 8 | The expression patterns of the genes extracted from integrating transcriptome profiling and Meta-QTL analysis which had significant interactions between genotypes and conditions. **(A)** Barplot showing the number of reviewed articles, collected QTLs, and the identified Meta-QTLs across the populations. **(B)** Venn diagram for extracted genes belonged to Meta-QTLs identified across the populations and their overlaps. **(C)** Venn diagram showing the number of genes with significant interactions (with a *p*-value cutoff of <0.05) between genotypes and conditions (a two-way ANOVA was performed on 1047 genes detected from the overlapping of the populations) in three zones and their overlaps. **(D)** The expression pattern of the DEGs belonged to Z1, on their chromosomal regions; three subsets of genes on chromosomes 4, 7, and 9 showing co-upregulation in response to water stress in Azucena were surrounded by orange lines. IRnZ1, root Z1 of IR64 under normal condition; IRsZ1, root Z1 of IR64 under stress condition; AZnZ1, root Z1 of Azucena under normal condition; AZsZ1, root Z1 of Azucena under stress condition.

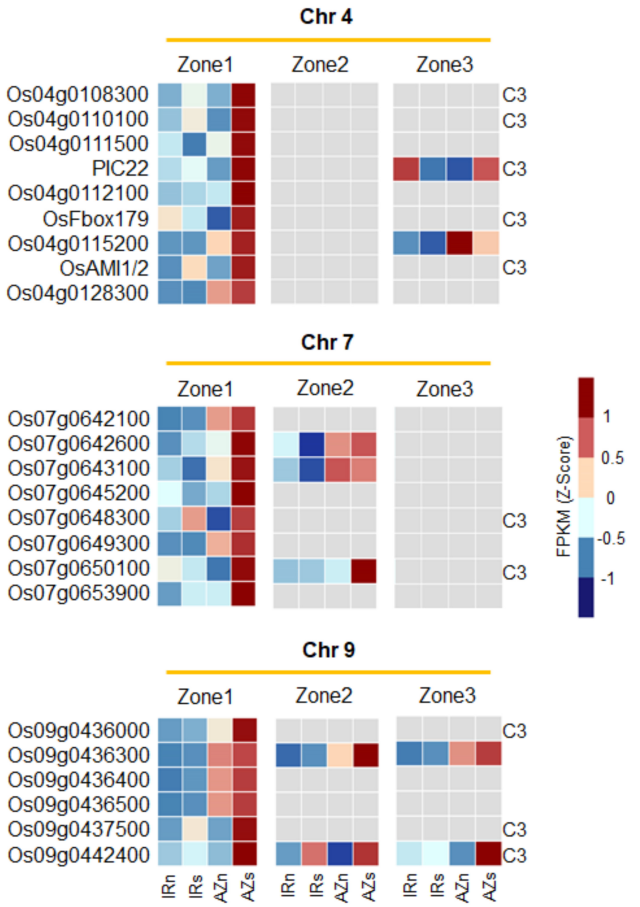

FIGURE 9 | The expression pattern of the co-expressed regions on chromosome 4, 7, and 9 across all three root zones revealing they are zone 1-specific. Three subsets of genes on chromosomes 4, 7 and 9 co-upregulated in zone 1 of Azucena in response to water stress, and their expression pattern in Zones 2 and 3. Gray color depicts no significant change under stress. The genes co-localized with cluster 3 in the **Figure 4A** (highly upregulated DEGs in Z1 of Azucena) were labeled as C3. IRn, IR64 under normal condition; IRs, IR64 under stress condition; AZn, Azucena under normal condition; AZs, Azucena under stress condition.

on 17 DEGs. These include six genes from integrating Meta-QTLs and RNAseq data (*Os04g0110100*, *Os07g0650100*, *Os07g0637300/OsHRK1/PDK*, *Os09g0437500*, *Os07g0591800*, and *Os09g0436000*), three genes from *NAC* gene family (*Os11g0126900/OsNAC10*, *Os07g0566500/ONAC010*, and *Os01g0104200/OsNAC16*), five genes with a high-fold change in expression levels (*Os07g0605200/OsMAD18*, *Os02g0139000 /OsPHR3*, *Os09g0455300/OsbHLH120*, *Os05g0247100/DIP3*, and *Os11g0126900/OsNAC10*), and four randomly selected DEGs (*Os01g0757200/OsGA2ox3*, *Os03g0198600/OsHOX12*, *Os08g0499300/OsWRKY30*, *Os06g0141200/OsZFP1*). The qRT-PCR results were highly consistent with those of RNA sequencing in all three root zones in both genotypes in response to water-deficit stress (**Figure 10A**). The small variations in Log2FC values are probably due to a combinatorial effect of biological variation and the different mathematical models used to calculate expression levels from either qRT-PCR or RNA-Seq data (Kyndt et al., 2012). Scatter plots showed simple linear regression, and the *R*-squared (r^2) between relative expression, based on log2FC obtained by FPKM values of RNAseq data (X), and the analyzed values from qRT-PCR (Y) (**Figure 10B**). The coefficient of variation was 0.79 for all samples.

DISCUSSION

In this study we investigated the transcriptomic response to water stress of three parts of root tips in two contrasting rice genotypes; Azucena, with a deep-rooting system, and IR64, with a shallow-rooting system. The aim of this was to develop a better understanding of RSA, an important developmental and agronomic trait with vital roles in plant adaptation and productivity under water-limited environments.

As expected, Azucena maintained a higher level of leaf RWC, less reduction in root and shoot dry weight, and a higher growth rate of roots in response to water stress, when compared to IR64. The transcriptomics analysis of the three consecutive root tip zones identified thousands of genes differentially expressed in the two genotypes under normal and stress conditions. A major challenge of big data is how to analyze and translate it into new biological knowledge, and generate a short list of the most important differentially expressed genes. Here we discuss several approaches we utilized to maximize the benefit of transcriptome analysis of root tips in our contrasting rice genotypes.

Differentially Expressed Genes Between Control and Stress Conditions: Differentially Expressed Genes in Z1 of Azucena Root Are Specifically Enriched for Root Growth Maintenance Biological Processes

The results revealed different BPs which were enriched in zones 1, 2, and 3 of Azucena and IR64. Of great interest was Z1 of Azucena, as it was the only group enriched for genes involved in cell cycle and division and ATPase activities and energy generation. This may suggest intrinsic differences between Azucena and IR64, used to maintain root growth under water stress condition. Cell cycle regulation which plays key roles in maintaining plant growth at times of stress must be balanced with adoption to dynamic environmental conditions (Qi and Zhang, 2020). The ATPases extrude protons from cells to generate an electrochemical proton gradient which has a major role in providing the energy for physiological functions such as cell growth (Falhof et al., 2016). Activation of the ATPases is important in auxin-mediated cell elongation during wheat embryo development (Rober-Kleber et al., 2003). In Arabidopsis, auxin induces hypocotyl elongation through phosphorylation and activation of the ATPases (Takahashi et al., 2012). Also, ATPase activities are responsible for water maintenance, osmotic

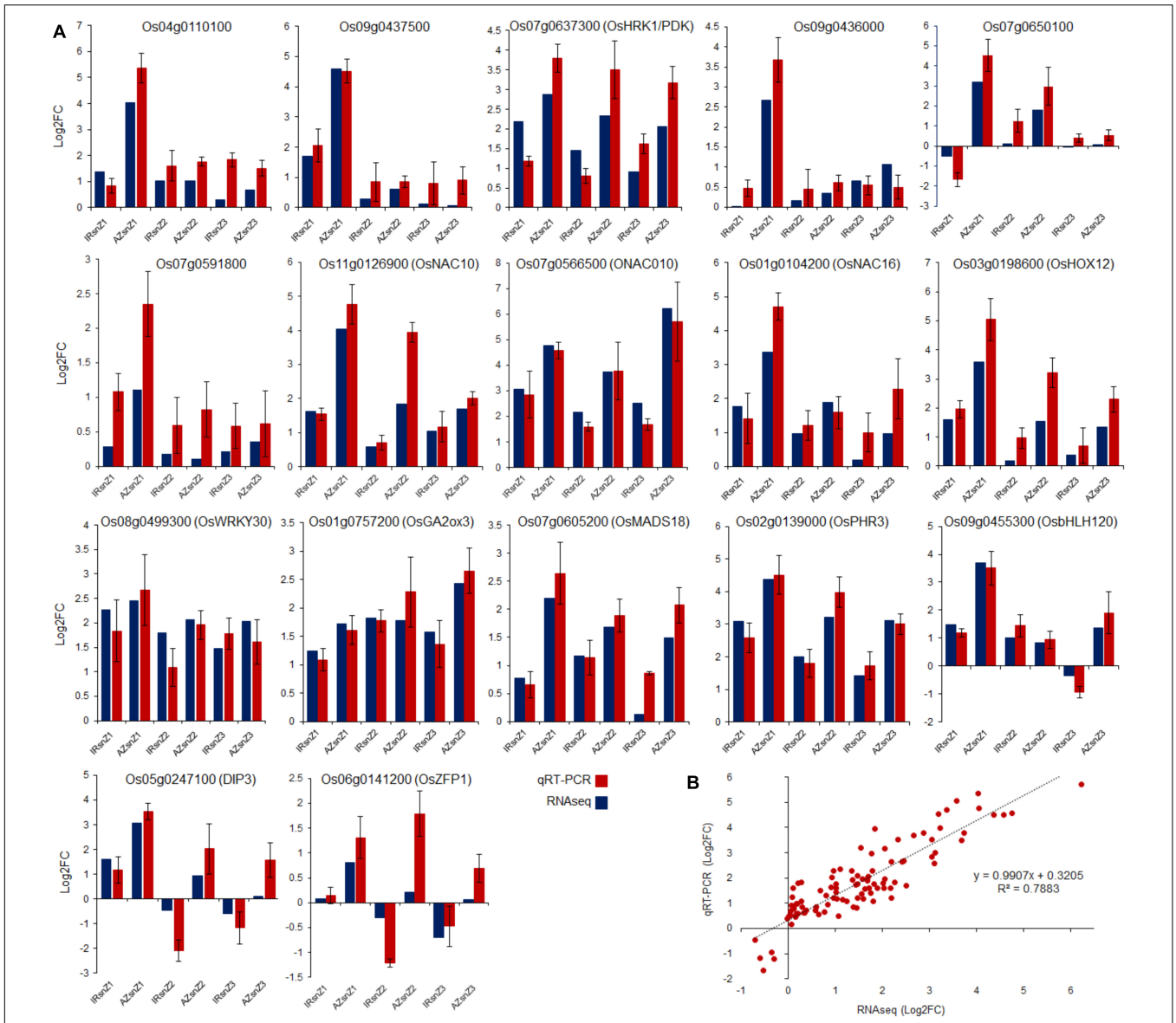

FIGURE 10 | Validation by qRT-PCR. **(A)** Validations of selected genes using qRT-PCR in all three root zones of both genotypes, Azucena and IR64, in response to water stress. Data points are represented as log2fold change values. **(B)** Linear regression analysis between qRT-PCR and RNA-seq results (R^2 = 0.7883) for 17 genes. *X*-axis numbers represent the log2fold-change values of mRNA-seq results. *Y*-axis numbers represent the log2fold-change values of qRT-PCR results.

regulation and other adaptive mechanisms under drought stress (Ober and Sharp, 2003; Liu et al., 2005).

Highly Upregulated Differentially Expressed Genes in Z1 of Azucena Are Enriched for Genes Involved in Root System Architecture Development While in IR64, Response to Oxidative Stress Is Enriched

Interestingly, about 2000 DEGs showed more than a fourfold change in response to stress across different genotypes and zones, and these clustered in 6 expression groups, labeled C1 to C6. Among them, C3 included 375 genes highly upregulated, specifically in Z1 of Azucena. Our GO enrichment analysis revealed that the C3 group was specifically enriched for transcripts involved in the regulation of transcription processes, as well as terpenoid, lipid and monocarboxylic acid metabolic processes. Terpenoids and their derivatives play essential roles in plant growth and development, and represent specialized metabolites mediating environmental adaptation (Tholl, 2015). Their functions in water stress response have also been reported (Vaughan et al., 2015; Savoi et al., 2016). Lipids are important components of cell membranes, and a change in their composition may help maintain membrane integrity and preserve cell compartmentation under water

stress conditions (Gigon et al., 2004). Drought-tolerant plants have reaction mechanisms to maintain cellular homeostasis by lipid metabolism, and can regulate metabolic homeostasis (De Paula et al., 1990).

The C3 cluster was also enriched for genes involved in RSA development and water stress tolerance. These included the five key genes *OsNAC10*, *OsbHLH120*, *OsPHR3*, *PIP1;3*/*RWC3*, *OsMADS18*, and *OsNLA1*. Rice root-specific overexpression of *OsNAC10* increases root thickness and improves drought tolerance and grain yield under field drought conditions (Jeong et al., 2010). *OsbHLH120*, is known to control root thickness and length in upland rice genotypes, and is strongly induced by drought and salt stress (Li et al., 2015). *OsPHR3* is involved in root hair formation. Loss-of-function mutations in *OsPHR3* impair root hair growth and elongation (Guo et al., 2015). Overexpression of *PIP1;3*/*RWC3* in lowland rice exhibited higher levels of drought avoidance (Lian et al., 2004) and in Arabidopsis showed longer roots under stress conditions (Mosa et al., 2016). *OsMADS18*, strongly expressed in root meristems, causes a reduction in the number and elongation rate of adventitious root primordia when mutated (Fornara et al., 2004).

The C3 was also included several key genes involved in drought adaptation such as *DIP3*, *CIPK10*, *CIPK17*, *CIPK29*, *OsERF101*, *OsWRKY11,* and *ONAC58*/*OsNAP*. *DIP3*, annotated as a stress-induced protein, codes for a chitinase III, and is involved in the regulation of drought stress response in upland rice (Guo et al., 2013). *OsCIPK17* seems to participate in cross-talk among drought, salt stress and ABA treatment signaling pathways (Xiang et al., 2007). Rice plants overexpressing *OsERF101*, an important positive regulator in the adaptive response to water stress, are relatively more tolerant toward water stress (Jin et al., 2018). Overexpression of *OsWRKY11* confers heat and drought tolerance in rice seedlings (Wu et al., 2009), and its ectopic expression induces constitutive expression of drought-responsive genes in rice (Lee et al., 2018). Finally, the upregulation of *ONAC58*/*OsNAP* in rice in response to ABA and abiotic stresses, including high salinity, drought and low temperature, have been reported, and plants overexpressing *ONAC58*/*OsNAP* show enhanced tolerance and improved yield under drought stress (Chen et al., 2014).

In addition, our result showed that the cluster 1 (C1), containing genes highly upregulated in zone 1 of IR64, was enriched for genes involved in oxidative stress response. Response to oxidative stress was also enriched for cluster 6 (C6) which containing a gene set with upregulation patterns in all three zones of IR64. An important consequence of water stress is the closure of stomata which leads limits CO2 fixation and causes excessive production of reactive oxygen species (Das and Roychoudhury, 2014). When plants are exposed to water limitation and dehydration, oxidative or secondary stress occurs, thereby plants have to adjust their signaling pathways and metabolisms to ensure their growth and development (Scarpeci et al., 2008). It appears that IR64 is incapable of avoiding long-lasting water stress (Uga et al., 2013), shows an oxidative-stressed status while the upland Azucena genotype is in a water deficit avoidance stage. The enriched pathways of growth maintenance along with the increase in root length, observed in Azucena, is in accordance with the strategy of plants coping with water stress through root exploration to access water in deeper soil layers (Gilbert and Medina, 2016). IR64 probably resists water stress by limiting the growth rate and starting antioxidant system to deal with excess reactive oxygen species. It has been reported that, under severe stress, the oxidative stress markers and enzymes revealed a significant and strong upregulation by drought in IR64 (Melandri et al., 2021). However, there are studies that claimed that the inefficient antioxidant defense system in IR64 made it susceptible to water stress (Nahar et al., 2018; Sevanthi et al., 2021).

To cope with environmental stresses, plants have developed different adaptive strategies in a genotype-dependent manner (Rosa et al., 2009). Differential adaptation strategies to water stress in upland and lowland genotypes of rice have been previously reported (Xia et al., 2019; Abdirad et al., 2020; Luo et al., 2020).

Molecular Mechanisms Associated With Enhanced Root Elongation in Azucena Under Stress Conditions

Root length, a contributing trait to RSA, strongly fluctuated between the two genotypes under the two conditions. Azucena not only had significantly longer roots than did IR64 under the two conditions, but also an increased rate of root growth and elongation induced by stress. With the onset of drought and drying of soil surface, plants capable of accessing water from deeper layers of soil by expanding their root systems can adapt more readily to water deficit stress, and maintain osmotic pressure. Root elongation is an important strategy used by tolerant genotypes to reach the moist layers of the soil (Comas et al., 2013). The root apical meristem, along with the elongation region, are responsible for root elongation, and are located in zone 1 of the plants in the present study.

Our expression analysis led to the identification of 17 genes upregulated in Z1 of Azucena including *OsRBG1*, *OsRMC*, and *OsERF2*/*OsWR4*. Ectopic expression of *OsRBG1*, preferentially expressed in meristematic tissues, increases auxin accumulation and facilitates crown root development. *OsRBG1* overexpression increases root length, primarily due to elevated cell numbers rather than cell enlargement. Also, *OsRBG1* co-localizes with microtubules known to be involved in cell division, which may account for the increase in organ size (Lo et al., 2020). Rice lines with *OsRMC* silenced had shorter primary roots and showed reduced total length of adventitious root (Jiang et al., 2007). *OsRMC*-overexpressing rice seedlings under Fe-deficient showed higher total root length than those of the wild types (Yang et al., 2013). Finally, *OsERF2*/*OsWR4* is required for the control of root architecture by regulating the expression of pivotal genes involved in rice root development. Its mutant lines showed shorter roots (Xiao et al., 2016).

Moreover, seven over-expressed genes (under both conditions) were found in the Azucena, including *OsDEL1*/*OsPLL12* and *OsDOF7*/*11*. Elongation of roots does not occur in transgenic rice seedlings with mutations in *OsDOF7*/*11* due to a reduced sucrose uptake (Wu et al., 2018).

OsDEL1/*OsPLL12* is expressed predominantly in elongating tissues and is also involved in the maintenance of normal cell division. Mutation in *OsDEL1*/*OsPLL12* exhibited a clear 50% reduction in root length relative to the wild type (Leng et al., 2017).

Water Stress Enhances Lateral Roots Formation in Both Genotypes, but More So in Azucena

It appears that expansion of the LR system is used as a strategy by both genotypes in facing water shortage, but it is employed to a greater extent by Azucena. LRs constitute a large proportion of the root system in total length and number, and are responsible for the greatest amount of water and nutrient uptake from the soil (Gowda et al., 2011). LR formation is influenced by the soil environment, and exhibits a high level of plasticity (Wangenheim et al., 2020). Proliferative roots have a relatively high-water uptake efficiency in water deficient soils (Ye et al., 2018). Although there are few studies on root branching patterns under abiotic stresses, increased lateral root density in response to drought has previously been reported in an article examining 11 Egyptian rice genotypes (Hazman and Brown, 2018).

Our transcriptomic approach revealed 18 genes significantly upregulated in Azucena roots that are related to LR growth and development, included *OsACS*, *OsARF16*, *OsPTR9*, *OsMADS27*, *OsHO1*/*OsSE5*, *OsRAA1,* and *OsAUX*/*LAX1*. Interestingly, all 18 DEGs were significantly induced in both zones 2 and 3, which are enriched for LR growth and development. Rice *OsACS* mutants fail to promote LR growth and elongation especially in response to inorganic phosphate deficiency, however, the most common morphological changes in response to inorganic phosphate deficiency was the increase in LR growth (Lee et al., 2019). Rice *ARF16,* along with several other genes involved in auxin biosynthesis and transport, control the phosphate-dependent LR formation (Shen et al., 2013). *OsPTR9*, when overexpressed in transgenic rice, results in promotion of LR growth and development and enhanced ammonium uptake, while its mutant lines have a lower number of LRs (Fang et al., 2013). *OsMADS27* strongly induces proliferation and the length of LRs when overexpressed (Liu et al., 2020) while under constitutive expression it significantly enhances the formation of lateral roots in a nitrate-dependent manner (Chen et al., 2018b). Overexpression of *OsHO1*/*OsSE5* enhances LR formation in rice (Chen et al., 2012). *OsRAA1* is expressed in LR primordia and the pericycles of the branch zones. Its overexpression led to longer LRs (Han et al., 2008). *OsAUX*/*LAX1* was upregulated in Azucena roots in response to stress. In Arabidopsis, auxin influx via *AUX1,* and its close homologs *LAX1*, *LAX2* and *LAX3*, three transmembrane proteins with a highly conserved permease activity, participate in LR formation and emergence (Ugartechea-Chirino et al., 2009).

Cell Wall Thickening in IR64 Under Stress May Reduce Root Growth

Cell wall thickening occurred in meristematic cells of IR64 roots in response to water stress. Cell wall dynamics and modifications under abiotic stress are variable depending on the genotype, the organ, the tissue, and the intensity of the stress (Le Gall et al., 2015). Cell wall thickening, by granting further rigidity to the wall, limits water loss. It also promotes water transport and maintains cell turgor pressure, in addition to restricting cell movement, elongation and enlargement by reducing cell wall flexibility (Yamaguchi et al., 2010; Liu et al., 2018). Thus, by enhancing cell wall thickening for insulation purposes as a mean of mitigating stress, the sensitive IR64 genotype may have reduced its capacity for root elongation to extract water from deeper layers of the soil. To strengthen this hypothesis, a list of genes known to take part in cell wall growth and development was prepared and their expression patterns were surveyed in our transcriptomic data. This led to the identification of 32 genes upregulated in Z1 of IR64 including three members of the *CAD* gene family (*OsCAD3*, *OsCAD8D*, and *OsCAD9*) along with *OsMYB52*/*54*, *OsSUS3*, *OsPRX1*, and *BSH1*/*OsCYP96B4*. CADs are an important group of enzymes which catalyzed lignin biosynthesis. In particular, the involvement of *OsCAD3* in lignin biosynthesis was recently reported in loss-of-function mutants with reduced levels of lignin (Tobias and Chow, 2005; Park et al., 2018). *OsMYB52*/*54*, is a secondary wall-associated gene. Its product acts downstream from *CEF1*/*OsMYB103L*, a master switch that regulates the regulatory cascade of secondary wall biosynthesis in rice. Loss-of-function mutation in *CEF1*/*OsMYB103L* reduces cellulose content and decrease thickness of the cell walls (Ye et al., 2015). *OsSUS3* participates in carbon-partitioning regulation for the direct biosynthesis of cellulose and callose. Overexpression of *OsSUS3* reduces cellulose crystallinity and increases cell wall polysaccharide deposition and thickness in transgenic rice (Fan et al., 2020). *OsPRX1*, a class III peroxidase, catalyzes a variety of reactions in cell wall formation and modification, including the cross-linking of structural polysaccharides, oxidative lignin polymerization, and ROS production, all of which are involved in modulation of the mechanical properties of cell walls (Passardi et al., 2004). *BSH1*/*OsCYP96B4* encodes a cytochrome P450 monooxygenase that functions mainly in secondary cell wall formation and thickening. *bsh1* mutants have been shown to have reduced levels of cell wall components such as cellulose and xylose (Wang et al., 2016; Jiang et al., 2020).

Members of the *NAC, AP2/ERF, AUX/IAA, EXPANSIN, WRKY,* and *MYB* Gene Families May Play Important Roles in Root System Architecture and Drought Adaptation

Differential expression of members of a gene family across three root zones of both genotypes under both normal and stress conditions suggested their potential roles in RSA and drought adaptation. For example, 19 members of the *NAC* gene family were upregulated in Azucena roots in response to stress, five of which are known to be involved in rice RSA and drought stress response and tolerance. Overexpression of *OsNAC5* (Jeong et al., 2013) and *OsNAC10* (Jeong et al., 2010) in rice roots enlarge root diameter and enhance drought tolerance and grain yield

under field conditions. Overexpression of *ONAC3* (*SNAC3*) in rice enhances tolerance to drought and oxidative stress while its suppression increases sensitivity to stress (Fang et al., 2015). *ONAC106* plays roles in osmotic stress-responsive signaling and plant architecture (Sakuraba et al., 2015). Mutation in *ONAC54* (*OsRIM1*) leads to shorter roots in rice (Yoshii et al., 2010). *ONAC58* (*OsNAP*)-overexpressing rice enhances tolerance to drought (Chen et al., 2014) and shows longer roots (Zhou et al., 2013). Downregulation of *ONAC58* lead to reduction in root growth and total root length, and fewer root tips (Lu et al., 2017).

Sixteen members of the *AP2/ERF* were significantly upregulated in Azucena in response to stress, among which six members are known to play roles in water stress tolerance and rice root development. Overexpression of *OsERF50* (*OsDREB6*, *AP2/EREBP113*) increases tolerance to osmotic stress in transgenic rice, whereas, *OsERF50* RNAi knockdown lines are more sensitive to stress than the wild type (Ke et al., 2014). Overexpression of *OsERF48* produces a longer and denser root phenotype. Under drought condition the transgenics exhibit a more vigorous root growth and a higher grain yield (Jung et al., 2017). The role of *OsERF101* in improving rice yield under drought, and its predominant expression in reproductive tissues have been reported (Jin et al., 2018) while in the present study *OsERF101* expression was detected in all 3 root zones in both genotypes and was induced by stress in Azucena. *OsERF95* (*OsSta2*)-overexpressing lines show more tolerance to osmotic stress (Kumar et al., 2017). *OsERF93* (*ERF1*) is involved in the induction of RSOsPR10 [root specific *Oryza sativa* pathogenesis-related (PR) protein 10] which plays a role in protecting the inner vascular system in the root during drought stress (Takeuchi et al., 2011). *OsERF2*/*OsWR4* controls root architecture and affects primary root growth in rice, and mutant lines of the same gene have shorter roots (Xiao et al., 2016).

The expression level of three genes *EXPA2*, *EXPB11*, and *EXPA5* increased significantly in response to water stress in Azucena roots. *OsEXPA2* has been shown to be linked to a QTL for seminal root length under water deficit conditions (Yang et al., 2004). The specific expression of *OsEXPA2* in the pericycle in the root-hair zone and the lateral and adventitious root primordia has also been reported (Cho and Kende, 1998).

We observed a significant upregulation of 6 members of this family under stress in Azucena. Of these, *OsIAA18* participates in tolerance against drought stress in rice (Song et al., 2009). A recent study in rice seedlings revealed *OsIAA26* and *OsIAA20* functioning in the reduction of inhibitory effects of ethylene on root growth and elongation (Chen et al., 2018a). *OsIAA20* and *OsIAA23* participate in the maintenance of the root quiescent center during the primary, lateral and crown root development (Jun et al., 2011).

Six and seven members of *MYB* and *WRKY* gene families were upregulated in the Azucena roots. In rice roots, the expression of *OsWRKY11* is highly upregulated under mild drought stress, implying a role in drought avoidance (Kakar et al., 2016). *OsWRKY11* may also play a role in stimulating root growth, enhancing the plants ability to extract water from soil in water stress condition (Nuruzzaman et al., 2014). A reduction in the expression level of OsWRKY72 in del1 rice mutants leads to a reduction in root length and number (Leng et al., 2017). The constitutive expression of OsWRKY72 in transgenic Arabidopsis also affects root growth and stress tolerance (Song et al., 2010). OsWRKY3 has previously been identified as a drought responsive gene in rice (Berri et al., 2009; Yu et al., 2017).

Our results showed that *HSPs* and *HSF*s were specifically abundant in IR64 root in response to a 14-day water withholding compared to Azucena. It reveals the important roles of *HSP* and *HSF* families in IR64 adaptive strategies when confronting water-deficit stress. Plant *HSP*s as chaperones and *HSF*s as *HSP*s' transcriptional regulators have been identified for playing a vital role in protecting proteins that might lose their potential functional conformation during biotic and/or abiotic stress (Khan et al., 2019). Also, *HSP*s and *HSF*s detoxify the reactive oxygen species by positively regulating the antioxidant enzymatic system and thus enhance membrane stability when plants face oxidative stress (Khan et al., 2019). Consequently, *HSP*s and *HSF*s might be considered as the main components of IR64 adaptation strategy against oxidative stress. A study on chickpea reported that *HSP*s were down-regulated in drought-tolerant genotypes while they were abundant in drought-sensitive genotypes (Sato and Yokoya, 2008). Theses finding might suggest that *HSP*s respond to drought in a genotype specific manner.

Integrating Transcriptome Profiling and Meta-Quantitative Trait Loci Analysis: Identification of Novel Root System Architecture-Associated Candidate Genes

Many QTLs related to rice RSA traits were identified so far, including a number of genes which their expressions were not studied yet under different genotypes and conditions. They may be valuable resources for integrating with transcriptome profiling of RSA-contrasted genotypes and finding novel associated candidate genes. Meta-analysis of QTLs is a powerful statistical technique for reducing the confidence interval of QTL position through refining and confirming QTL positions on a consensus map via mathematical models. In Meta-QTL analysis, a number of independent QTL studies performed across different genetic backgrounds and environments, are combined to determine the number of true QTLs enabling researchers to position consensus QTLs with a greater precision, and to further reduce the intervals and the number of candidate genes (Coudert et al., 2010; Comas et al., 2013; Daryani et al., 2021). QTL meta-analysis method was initially developed by Goffinet and Gerber (2000) using maximum likelihood estimation and was then improved by Veyrieras et al. (2007). The integration of RSA Meta-QTLs analysis with transcriptome profiling may assist in generating a more reliable list of potential candidate genes involved in RSA. In this study, a total of 132 QTLs controlling RSA traits under drought and normal conditions, including 82 and 50 from IR64 × Azucena and Azucena × other rice genotypes populations, respectively, were collected and 31 and 23 significant Meta-QTLs were identified according to Daryani et al. (2021) method. The confidence interval (CI) of the

identified M-QTLs was obtained as 0.11–17.67 cM and 0.055–5.2 which were 2.52 and 3.07 times narrower than the mean CI of the original QTLs belonged to IR64 × Azucena populations and Azucena × other rice genotypes populations, respectively. Also, the physical intervals of most of the obtained M-QTLs (14 M-QTLs and 10 M-QTLs belonged to IR64 × Azucena populations and Azucena × other rice genotypes populations, respectively) were below 1 Mb.

To narrow down the candidate genes, only the 1047 common genes between two sets of populations (see section "Materials and Methods") were considered for searching in our transcriptome data, with 291 of these corresponding to DEGs in our study. These included 125, 159, and 130 DEGs in zones 1, 2, and 3, respectively. Some were common between all three zones while others were zone-specific, some had functional descriptions, while others lacked functional annotations and thus represent novel candidates with potential roles in RSA related pathways.

OsACO1, a highly upregulated gene in Z1 of Azucena roots in response to water stress, was located on meta-QTLs on chromosome 9 which controls the deep-rooting ratio trait. This gene is known to be involved in ethylene biosynthesis and salt stress response. Despite a lack of information on the role of *ACO1* in root traits, its positive role in internode elongation in rice has been reported (Iwamoto et al., 2010). *OsFbox490* (*Os09g0449600*), an F-box domain protein, was also found on chromosome 9, upregulated in Z1 of Azucena. A number of QTLs, related to maximum root length, are associated with a small region on chromosome 9 in rice. Containing three genes encoding F-box domain proteins, one Meta-QTL with a confidence interval of 20 kb were detected on rice chromosome 9 from resolving 14 QTLs for maximum root length (Courtois et al., 2009).

Interestingly, genes (adjacent to each other) located on three regions on chromosomes 4, 7, and 9 showed significant specific co-upregulation in Z1 of Azucena root. The regions belonged to the overlapped Meta-QTLs which control several root traits under drought (chromosome 4: RDW and RN; chromosome 7: RSR and DRW; chromosome 9: DRR). It was also noteworthy that only 2, 3 and 2 genes on chromosomes 4, 7, and 9, respectively, showed differential expression in zones 2 and 3, with the rest being specific to Z1. Specific expression of these genes in Z1, encompassing meristematic and elongating cells, reinforces the hypothesis on their roles in RSA trait determination. For example, *OsAMI1/2*, found on chromosome 4, encodes an enzyme involved in the biosynthesis of indole-3-acetamide to indole acetic acid. Auxins, as plant root forming hormones, promote root initiation, growth, development and branching (Overvoorde et al., 2010). Auxins are also involved in the control of cell division and elongation in root tips (Takatsuka and Umeda, 2014). Moreover, the role of *OsAMI1/2* in rice root hair development has also been reported (Wang et al., 2017). *Os09g0436500*, which is also located on chromosome 9, which controls the deep rooting ratio, is involved in the biosynthesis of isoleucine and valine. Reduction in the rate of isoleucine biosynthesis has been reported to lead to defects in both cell division and expansion processes during root development in Arabidopsis. Reduction in the number of root meristematic cells and the length of roots and root hairs has also been associated with mutations in isoleucine biosynthesis genes (Yu et al., 2013). The lack of functional annotation for the majority of these genes would represent them as potential novel candidates involved in RSA modification and response to water stress condition.

It was interesting to note that 17 of the highly upregulated DEGs in Z1 of Azucena (cluster 3, **Figure 5A**) were also co-localized with Meta-QTLs including *Os01g0253800*, *Os01g0257300* (*OsRAA1*), *Os01g0259966*, *Os04g0110100*, *Os04g0117900* (*OsAMI1/2*), *Os04g0108300*, *Os04g0111900* (*PIC22*), *Os04g0113000*, *Os07g0591700*, *Os07g0637300* (*OsHRK1/PDK*), Os07g0648300, *Os07g0650100*, *Os07g0594400*, *Os09g0436000*, *Os09g0442400*, *Os09g0447300* (*CYP76L1/Cytochrome P450 76L1*), and *Os09g0437500*. The expression pattern of five of these (*Os04g0110100*, *Os07g0650100*, *Os07g0637300*, *Os09g0437500*, and *Os09g0436000*) was also confirmed by qRT-PCR. These 17 candidate genes are located on meta-QTLs of chromosomes 1, 4, 7, and 9, controlling several root traits under drought stress (chromosome 1: RN, chromosome 4: RDW and RN; chromosome 7: RSR and DRW; chromosome 9: DRR).

CONCLUSION

Detailed analyses of the transcriptome responses of three consecutive root tip zones to water stress in two contrasting genotypes of rice, IR64 (a susceptible and shallow-rooting genotype) and Azucena (a tolerant and deep-rooting genotype) lead to the identification of a number of DEGs and differential pathways involved in RSA and water stress adaptation. Our results revealed that Z1 of Azucena was specifically enriched for genes involved in cell cycle and division while in IR64 root, responses to oxidative stress were strongly enriched. It may suggest main intrinsic differences between Azucena and IR64 to maintain root growth under water stress condition. Also, a number of highly upregulated DEGs were identified in Z1 of Azucena involved in RSA development and water-stress adaptation. Our phenotypic analysis revealed that Azucena not only had significantly longer roots than IR64 under the two conditions, but also an increased rate of root growth and elongation induced by stress. It appears that expansion of the LR system is used as a strategy by both genotypes in facing water shortage, and to a greater extent by the upland tolerant genotype Azucena. By enhancing meristematic cell wall thickening for insulation purposes as a means of confronting stress, the sensitive IR64 genotype may have reduced its capacity for root elongation to extract water from deeper layers of the soil. In this study 28, 18, and 32 DEGs which may be involved in root elongation, lateral root development and cell wall formation and modification, respectively, were introduced. Furthermore, several members of gene families such as *NAC*, *AP2/ERF*, *AUX/IAA*, *EXPANSIN*, *WRKY,* and *MYB* emerged as main players in RSA and drought adaptation, while in IR64 root tip, members of *HSP* and *HSF* gene families were enriched. Integrating Meta-QTL analysis and transcriptome profiling revealed that 288 DEGs were co-localized with RSA QTLs previously reported

under drought and normal conditions from two bi-parental populations. Considering the lack of functional annotation for the majority of these transcripts, they are reported here as novel candidate genes potentially involved in RSA modification and response to water stress conditions. We also found three co-expressed regions on Meta-QTLs on chromosomes 4, 7, and 9 (controlling the RDW and RN, the RSR and DRW, and DRR traits, respectively) specifically upregulated in Z1 of Azucena including 9, 7, and 9 genes, respectively. Lastly, it was interesting to note that 13 of the highly upregulated DEGs in Z1 of Azucena were also co-localized with Meta-QTLs. This finding warrants further research into their possible roles in drought adaptation and RSA. Overall, our analyses presented several major molecular differences between Azucena and IR64, which may partly explain their differential root growth responses to water stress. It appears that Azucena avoided water stress through enhancing growth and root exploration to access water, whereas IR64 with a shallow root system might mainly rely on cell insulation and antioxidant system to resist stress.

DATA AVAILABILITY STATEMENT

The original contributions presented in the study are publicly available. This data can be found here: National Center for Biotechnology Information (NCBI) BioProject database under accession number PRJNA716593.

AUTHOR CONTRIBUTIONS

GHS and SA designed the experiment. GHS supervised the experiment and revised the manuscript. SA prepared the samples and wrote the manuscript. MG, ArS, SA, and AmS analyzed the data. PD and Z-SS performed the Meta-QTL analysis. SA, PK, NH, PY, and AM performed the microscopic analysis. LF, SA, ZG, and MK performed the qRT-PCR section. PH, SI, and MM cooperated in data interpretation and manuscript revision. All authors contributed to the article and approved the submitted version.

ACKNOWLEDGMENTS

The authors thank the Agricultural Biotechnology Research Institute of Iran (ABRII) and the Australian Research Council (ARC) for providing funding for this work.

SUPPLEMENTARY MATERIAL

The Supplementary Material for this article can be found online at: https://www.frontiersin.org/articles/10.3389/fpls.2022.792079/full#supplementary-material

REFERENCES

Abdirad, S., Majd, A., Irian, S., Hadidi, N., and Salekdeh, G. H. (2020). Differential adaptation strategies to different levels of soil water deficit in two upland and lowland genotypes of rice: a physiological and metabolic approach. *J. Sci. Food Agricult.* 100, 1458–1469. doi: 10.1002/jsfa.10153

Alberts, B. (2018). *Molecular biology of the cell*. New York, NY: Garland Science.

Araki, H., Morita, S., Tatsumi, J., and Iijima, M. (2002). Physiol-morphological analysis on axile root growth in upland rice. *Plant Prod. Sci.* 5, 286–293.

Arcade, A., Labourdette, A., Falque, M., Mangin, B., Chardon, F., Charcosset, A., et al. (2004). BioMercator: integrating genetic maps and QTL towards discovery of candidate genes. *Bioinformatics* 20, 2324–2326. doi: 10.1093/bioinformatics/bth230

Bernier, J., Atlin, G. N., Serraj, R., Kumar, A., and Spaner, D. (2008). Breeding upland rice for drought resistance. *J. Sci. Food Agricult.* 88, 927–939.

Berri, S., Abbruscato, P., Faivre-Rampant, O., Brasileiro, A. C., Fumasoni, I., Satoh, K., et al. (2009). Characterization of WRKYco-regulatory networks in rice and Arabidopsis. *BMC Plant Biol.* 9:120.

Bhuiyan, S. I. (1992). Water management in relation to crop production: case study on rice. *Outlook Agricult.* 21, 293–299.

Bindea, G., Mlecnik, B., Hackl, H., Charoentong, P., Tosolini, M., Kirilovsky, A., et al. (2009). ClueGO: a Cytoscape plug-in to decipher functionally grouped gene ontology and pathway annotation networks. *Bioinformatics* 25, 1091–1093. doi: 10.1093/bioinformatics/btp101

Bozzola, J. J., and Russell, L. D. (1999). *Electron microscopy: principles and techniques for biologists*. Burlington: Jones and Bartlett Learning.

Carrijo, D. R., Lundy, M. E., and Linquist, B. A. (2017). Rice yields and water use under alternate wetting and drying irrigation: a meta-analysis. *Field Crops Res.* 203, 173–180. doi: 10.1016/j.fcr.2016.12.002

Chen, H., Xu, N., Wu, Q., Yu, B., Chu, Y., Li, X., et al. (2018b). OsMADS27 regulates the root development in a NO_3^-—Dependent manner and modulates the salt tolerance in rice (*Oryza sativa* L.). *Plant Sci.* 277, 20–32. doi: 10.1016/j.plantsci.2018.09.004

Chen, H., Ma, B., Zhou, Y., He, S. J., Tang, S. Y., Lu, X., et al. (2018a). E3 ubiquitin ligase SOR1 regulates ethylene response in rice root by modulating stability of Aux/IAA protein. *Proc. Natl. Acad. Sci.* 115, 4513–4518. doi: 10.1073/pnas.1719387115

Chen, X., Wang, Y., Lv, B., Li, J., Luo, L., Lu, S., et al. (2014). The NAC family transcription factor OsNAP confers abiotic stress response through the ABA pathway. *Plant Cell Physiol.* 55, 604–619. doi: 10.1093/pcp/pct204

Chen, Y. H., Chao, Y. Y., Hsu, Y. Y., Hong, C. Y., and Kao, C. H. (2012). Heme oxygenase is involved in nitric oxide-and auxin-induced lateral root formation in rice. *Plant Cell Rep.* 31, 1085–1091. doi: 10.1007/s00299-012-1228-x

Cho, H. T., and Kende, H. (1998). Tissue localization of expansins in deepwater rice. *Plant J.* 15, 805–812. doi: 10.1046/j.1365-313x.1998.00258.x

Comas, L., Becker, S., Cruz, V. M. V., Byrne, P. F., and Dierig, D. A. (2013). Root traits contributing to plant productivity under drought. *Front. Plant Sci.* 4:442. doi: 10.3389/fpls.2013.00442

Coudert, Y., Perin, C., Courtois, B., Khong, N. G., and Gantet, P. (2010). Genetic control of root development in rice, the model cereal. *Trends Plant Sci.* 15, 219–226. doi: 10.1016/j.tplants.2010.01.008

Courtois, B., Ahmadi, N., Khowaja, F., Price, A. H., Rami, J.-F., Frouin, J., et al. (2009). Rice root genetic architecture: meta-analysis from a drought QTL database. *Rice* 2, 115–128.

Dal Santo, S., Vannozzi, A., Tornielli, G. B., Fasoli, M., Venturini, L., Pezzotti, M., et al. (2013). Genome-wide analysis of the expansin gene superfamily reveals grapevine-specific structural and functional characteristics. *PLoS One* 8:e62206. doi: 10.1371/journal.pone.0062206

Daryani, P., Ramandi, H. D., Dezhsetan, S., Mansuri, R. M., Salekdeh, G. H., and Shobbar, Z. S. (2021). Pinpointing Genomic Regions Associated with Root System Architecture in Rice Through an Integrative Meta-Analysis Approach. *Theor. Appl. Genet.* 2021:342601. doi: 10.21203/rs.3.rs-342601/v1

Das, K., and Roychoudhury, A. (2014). Reactive oxygen species (ROS) and response of antioxidants as ROS-scavengers during environmental stress in plants. *Front. Env. Sci.* 2:53.

De Paula, F. M., Thi, A. P., De Silva, J. V., Justin, A., Demandre, C., and Mazliak, P. (1990). Effects of water stress on the molecular species composition of polar

lipids from Vigna unguiculata L. leaves. *Plant Sci.* 66, 185–193. doi: 10.1016/0168-9452(90)90203-z

Falhof, J., Pedersen, J. T., Fuglsang, A. T., and Palmgren, M. (2016). Plasma membrane H(+)-ATPase regulation in the center of plant physiology. *Mole. Plant* 9, 323–337. doi: 10.1016/j.molp.2015.11.002

Fan, C., Wang, G., Wu, L., Liu, P., Huang, J., Jin, X., et al. (2020). Distinct cellulose and callose accumulation for enhanced bioethanol production and biotic stress resistance in OsSUS3 transgenic rice. *Carbohydr. Poly.* 232:115448. doi: 10.1016/j.carbpol.2019.115448

Fang, Y., Liao, K., Du, H., Xu, Y., Song, H., Li, X., et al. (2015). A stress-responsive NAC transcription factor SNAC3 confers heat and drought tolerance through modulation of reactive oxygen species in rice. *J. Exp. Bot.* 66, 6803–6817. doi: 10.1093/jxb/erv386

Fang, Z., Xia, K., Yang, X., Grotemeyer, M. S., Meier, S., Rentsch, D., et al. (2013). Altered expression of the PTR/NRT 1 homologue Os PTR 9 affects nitrogen utilization efficiency, growth and grain yield in rice. *Plant Biotechnol. J.* 11, 446–458. doi: 10.1111/pbi.12031

Fornara, F., Pařenicová, L., Falasca, G., Pelucchi, N., Masiero, S., Ciannamea, S., et al. (2004). Functional characterization of OsMADS18, a member of the AP1/SQUA subfamily of MADS box genes. *Plant Physiol.* 135, 2207–2219. doi: 10.1104/pp.104.045039

Gigon, A., Matos, A. R., Laffray, D., Zuily-Fodil, Y., and Pham-Thi, A. T. (2004). Effect of drought stress on lipid metabolism in the leaves of Arabidopsis thaliana (ecotype Columbia). *Ann. Bot.* 94, 345–351. doi: 10.1093/aob/mch150

Gilbert, M. E., and Medina, V. (2016). Drought adaptation mechanisms should guide experimental design. *Trends Plant Sci.* 21, 639–647. doi: 10.1016/j.tplants.2016.03.003

Goffinet, B., and Gerber, S. (2000). Quantitative trait loci: a meta-analysis. *Genetics* 155, 463–473. doi: 10.1093/genetics/155.1.463

Gowda, V. R., Henry, A., Yamauchi, A., Shashidhar, H. E., and Serraj, R. (2011). Root biology and genetic improvement for drought avoidance in rice. *Field Crops Res.* 122, 1–13. doi: 10.1016/j.fcr.2011.03.001

Guo, M., Ruan, W., Li, C., Huang, F., Zeng, M., Liu, Y., et al. (2015). Integrative comparison of the role of the PHOSPHATE RESPONSE1 subfamily in phosphate signaling and homeostasis in rice. *Plant Physiol.* 168, 1762–1776. doi: 10.1104/pp.15.00736

Guo, X. L., Bai, L. R., Su, C. Q., Shi, L. R., and Wang, D. W. (2013). Molecular cloning and expression of drought-induced protein 3 (DIP3) encoding a class III chitinase in upland rice. *Genet. Mole. Res.* 12, 6860–6870.

Han, Y., Cao, H., Jiang, J., Xu, Y., Du, J., Wang, X., et al. (2008). Rice ROOT ARCHITECTURE ASSOCIATED1 binds the proteasome subunit RPT4 and is degraded in a D-box and proteasome-dependent manner. *Plant Physiol.* 148, 843–855. doi: 10.1104/pp.108.125294

Hazman, M., and Brown, K. M. (2018). Progressive drought alters architectural and anatomical traits of rice roots. *Rice* 11, 1–16. doi: 10.1186/s12284-018-0252-z

Hu, W., Hu, G., and Han, B. (2009). Genome-wide survey and expression profiling of heat shock proteins and heat shock factors revealed overlapped and stress specific response under abiotic stresses in rice. *Plant Sci.* 176, 583–590. doi: 10.1016/j.plantsci.2009.01.016

Iwamoto, M., Baba−Kasai, A., Kiyota, S., Hara, N., and Takano, M. (2010). ACO1, a gene for aminocyclopropane−1−carboxylate oxidase: effects on internode elongation at the heading stage in rice. *Plant Cell Env.* 33, 805–815. doi: 10.1111/j.1365-3040.2009.02106.x

Janiak, A., Kwaśniewski, M., and Szarejko, I. (2016). Gene expression regulation in roots under drought. *J. Exp. Bot.* 67, 1003–1014. doi: 10.1093/jxb/erv512

Jeong, J. S., Kim, Y. S., Baek, K. H., Jung, H., Ha, S. H., Do Choi, Y., et al. (2010). Root-specific expression of OsNAC10 improves drought tolerance and grain yield in rice under field drought conditions. *Plant Physiol.* 153, 185–197. doi: 10.1104/pp.110.154773

Jeong, J. S., Kim, Y. S., Redillas, M. C., Jang, G., Jung, H., Bang, S. W., et al. (2013). OsNAC5 overexpression enlarges root diameter in rice plants leading to enhanced drought tolerance and increased grain yield in the field. *Plant Biotechnol. J.* 11, 101–114. doi: 10.1111/pbi.12011

Jiang, J., Li, J., Xu, Y., Han, Y., Bai, Y., Zhou, G., et al. (2007). RNAi knockdown of *Oryza sativa* root meander curling gene led to altered root development and coiling which were mediated by jasmonic acid signalling in rice. *Plant Cell Env.* 30, 690–699. doi: 10.1111/j.1365-3040.2007.01663.x

Jiang, L., Ramamoorthy, R., Ramachandran, S., and Kumar, P. P. (2020). Systems Metabolic Alteration in a Semi-Dwarf Rice Mutant Induced by OsCYP96B4 Gene Mutation. *Internat. J. Mole. Sci.* 21:1924. doi: 10.3390/ijms21061924

Jin, Y., Pan, W., Zheng, X., Cheng, X., Liu, M., Ma, H., et al. (2018). OsERF101, an ERF family transcription factor, regulates drought stress response in reproductive tissues. *Plant Mole. Biol.* 98, 51–65. doi: 10.1007/s11103-018-0762-5

Jun, N., Gaohang, W., Zhenxing, Z., Huanhuan, Z., Yunrong, W., and Ping, W. (2011). OsIAA23−mediated auxin signaling defines postembryonic maintenance of QC in rice. *Plant J.* 68, 433–442. doi: 10.1111/j.1365-313X.2011.04698.x

Jung, H., Chung, P. J., Park, S. H., Redillas, M. C. F. R., Kim, Y. S., Suh, J. W., et al. (2017). Overexpression of Os ERF 48 causes regulation of Os CML 16, a calmodulin−like protein gene that enhances root growth and drought tolerance. *Plant Biotechnol. J.* 15, 1295–1308. doi: 10.1111/pbi.12716

Kakar, K. U., Ren, X. L., Nawaz, Z., Cui, Z. Q., Li, B., Xie, G. L., et al. (2016). A consortium of rhizobacterial strains and biochemical growth elicitors improve cold and drought stress tolerance in rice (*Oryza sativa* L.). *Plant Biol.* 18, 471–483. doi: 10.1111/plb.12427

Ke, Y. G., Yang, Z. J., Yu, S. W., Li, T. F., Wu, J. H., Gao, H., et al. (2014). Characterization of OsDREB6 responsive to osmotic and cold stresses in rice. *J. Plant Biol.* 57, 150–161. doi: 10.1007/s12374-013-0480-0

Khan, A., Ali, M., Khattak, A. M., Gai, W. X., Zhang, H. X., Wei, A. M., et al. (2019). Heat shock proteins: dynamic biomolecules to counter plant biotic and abiotic stresses. *Internat. J. Mole. Sci.* 20:5321. doi: 10.3390/ijms20215321

Kim, D., Langmead, B., and Salzberg, S. L. (2015). HISAT: a fast spliced aligner with low memory requirements. *Nat. Methods* 12, 357–360. doi: 10.1038/nmeth.3317

Kondo, M., Pablico, P. P., Aragones, D. V., Agbisit, R., Abe, J., Morita, S., et al. (2003). Genotypic and environmental variations in root morphology in rice genotypes under upland field conditions. *Plant Soil* 255, 189–200. doi: 10.1023/a:1026142904714

Krizek, B. A. (2009). Making bigger plants: key regulators of final organ size. *Curr. Opinion Plant Biol.* 12, 17–22. doi: 10.1016/j.pbi.2008.09.006

Kumar, M., Choi, J., An, G., and Kim, S. R. (2017). Ectopic expression of OsSta2 enhances salt stress tolerance in rice. *Front. Plant Sci.* 8:316. doi: 10.3389/fpls.2017.00316

Kyndt, T., Denil, S., Haegeman, A., Trooskens, G., De Meyer, T., Van Criekinge, W., et al. (2012). Transcriptome analysis of rice mature root tissue and root tips in early development by massive parallel sequencing. *J. Exp. Bot.* 63, 2141–2157. doi: 10.1093/jxb/err435

Le Gall, H., Philippe, F., Domon, J. M., Gillet, F., Pelloux, J., and Rayon, C. (2015). Cell wall metabolism in response to abiotic stress. *Plants* 4, 112–166. doi: 10.3390/plants4010112

Lee, H., Cha, J., Choi, C., Choi, N., Ji, H. S., Park, S. R., et al. (2018). Rice WRKY11 plays a role in pathogen defense and drought tolerance. *Rice* 11, 1–12. doi: 10.1186/s12284-018-0199-0

Lee, H. Y., Chen, Z., Zhang, C., and Yoon, G. M. (2019). Editing of the OsACS locus alters phosphate deficiency-induced adaptive responses in rice seedlings. *J. Exp. Bot.* 70, 1927–1940. doi: 10.1093/jxb/erz074

Leng, Y., Yang, Y., Ren, D., Huang, L., Dai, L., Wang, Y., et al. (2017). A rice PECTATE LYASE-LIKE gene is required for plant growth and leaf senescence. *Plant Physiol.* 174, 1151–1166. doi: 10.1104/pp.16.01625

Lesk, C., Rowhani, P., and Ramankutty, N. (2016). Influence of extreme weather disasters on global crop production. *Nature* 529, 84–87. doi: 10.1038/nature16467

Li, J., Han, Y., Liu, L., Chen, Y., Du, Y., Zhang, J., et al. (2015). qRT9, a quantitative trait locus controlling root thickness and root length in upland rice. *J. Exp. Bot.* 66, 2723–2732. doi: 10.1093/jxb/erv076

Lian, H. L., Yu, X., Ye, Q., Ding, X. S., Kitagawa, Y., Kwak, S. S., et al. (2004). The role of aquaporin RWC3 in drought avoidance in rice. *Plant Cell Physiol.* 45, 481–489. doi: 10.1093/pcp/pch058

Liu, B., Wu, J., Yang, S., Schiefelbein, J., and Gan, Y. (2020). Nitrate regulation of lateral root and root hair development in plants. *J. Exp. Bot.* 71, 4405–4414. doi: 10.1093/jxb/erz536

Liu, H. P., Yu, B. J., Zhang, W. H., and Liu, Y. L. (2005). Effect of osmotic stress on the activity of H+-ATPase and the levels of covalently and noncovalently conjugated polyamines in plasma membrane preparation from wheat seedling roots. *Plant Sci.* 168, 1599–1607. doi: 10.1016/j.plantsci.2005.01.024

Liu, Q., Luo, L., and Zheng, L. (2018). Lignins: Biosynthesis and biological functions in plants. *Internat. J. Mole. Sci.* 19:335. doi: 10.3390/ijms19020335

Lo, S. F., Cheng, M. L., Hsing, Y. I. C., Chen, Y. S., Lee, K. W., Hong, Y. F., et al. (2020). Rice Big Grain 1 promotes cell division to enhance organ development, stress tolerance and grain yield. *Plant Biotechnol. J.* 18, 1969–1983. doi: 10.1111/pbi.13357

Lou, Q., Chen, L., Mei, H., Wei, H., Feng, F., Wang, P., et al. (2015). Quantitative trait locus mapping of deep rooting by linkage and association analysis in rice. *J. Exp. Bot.* 66, 4749–4757. doi: 10.1093/jxb/erv246

Lu, G., Casaretto, J. A., Ying, S., Mahmood, K., Liu, F., Bi, Y. M., et al. (2017). Overexpression of OsGATA12 regulates chlorophyll content, delays plant senescence and improves rice yield under high density planting. *Plant Mole. Biol.* 94, 215–227. doi: 10.1007/s11103-017-0604-x

Luo, Z., Xiong, J., Xia, H., Ma, X., Gao, M., Wang, L., et al. (2020). Transcriptomic divergence between upland and lowland ecotypes contributes to rice adaptation to a drought−prone agroecosystem. *Evol. Appl.* 13, 2484–2496. doi: 10.1111/eva.13054

Mardi, M., Farsad, L. K., Gharechahi, J., and Salekdeh, G. H. (2015). In-depth transcriptome sequencing of Mexican lime trees infected with Candidatus Phytoplasma aurantifolia. *PLoS One* 10:e0130425. doi: 10.1371/journal.pone.0130425

Martinez, J. P., Lutts, S., Schanck, A., Bajji, M., and Kinet, J. M. (2004). Is osmotic adjustment required for water stress resistance in the Mediterranean shrub Atriplex halimus L? *J. Plant Physiol.* 161, 1041–1051. doi: 10.1016/j.jplph.2003.12.009

Mehra, P., Pandey, B. K., and Giri, J. (2016). Comparative morphophysiological analyses and molecular profiling reveal Pi-efficient strategies of a traditional rice genotype. *Front. Plant Sci.* 6:1184. doi: 10.3389/fpls.2015.01184

Melandri, G., AbdElgawad, H., Floková, K., Jamar, D. C., Asard, H., Beemster, G. T., et al. (2021). Drought tolerance in selected aerobic and upland rice varieties is driven by different metabolic and antioxidative responses. *Planta* 254, 1–16. doi: 10.1007/s00425-021-03659-4

Michaletti, A., Naghavi, M. R., Toorchi, M., Zolla, L., and Rinalducci, S. (2018). Metabolomics and proteomics reveal drought-stress responses of leaf tissues from spring-wheat. *Sci. Rep.* 8, 1–18. doi: 10.1038/s41598-018-24012-y

Morant-Manceau, A., Pradier, E., and Tremblin, G. (2004). Osmotic adjustment, gas exchanges and chlorophyll fluorescence of a hexaploid triticale and its parental species under salt stress. *J. Plant Physiol.* 161, 25–33. doi: 10.1078/0176-1617-00963

Mosa, K. A., Kumar, K., Chhikara, S., Musante, C., White, J. C., and Dhankher, O. P. (2016). Enhanced boron tolerance in plants mediated by bidirectional transport through plasma membrane intrinsic proteins. *Sci. Rep.* 6:21640. doi: 10.1038/srep21640

Nahar, S., Vemireddy, L. R., Sahoo, L., and Tanti, B. (2018). Antioxidant protection mechanisms reveal significant response in drought-induced oxidative stress in some traditional rice of Assam, India. *Rice Sci.* 25, 185–196. doi: 10.1016/j.rsci.2018.06.002

Nuruzzaman, M., Sharoni, A. M., Satoh, K., Kumar, A., Leung, H., and Kikuchi, S. (2014). Comparative transcriptome profiles of the WRKY gene family under control, hormone-treated, and drought conditions in near-isogenic rice lines reveal differential, tissue specific gene activation. *J. Plant Physiol.* 171, 2–13. doi: 10.1016/j.jplph.2013.09.010

Ober, E. S., and Sharp, R. E. (2003). Electrophysiological responses of maize roots to low water potentials: relationship to growth and ABA accumulation. *J. Exp. Bot.* 54, 813–824. doi: 10.1093/jxb/erg060

Overvoorde, P., Fukaki, H., and Beeckman, T. (2010). Auxin control of root development. *Cold Spring Harb. Perspect. Biol.* 2:a001537.

Park, H. L., Kim, T. L., Bhoo, S. H., Lee, T. H., Lee, S. W., and Cho, M. H. (2018). Biochemical characterization of the rice cinnamyl alcohol dehydrogenase gene family. *Molecules* 23:2659. doi: 10.3390/molecules23102659

Passardi, F., Longet, D., Penel, C., and Dunand, C. (2004). The class III peroxidase multigenic family in rice and its evolution in land plants. *Phytochemistry* 65, 1879–1893. doi: 10.1016/j.phytochem.2004.06.023

Pertea, M., Kim, D., Pertea, G. M., Leek, J. T., and Salzberg, S. L. (2016). Transcript-level expression analysis of RNA-seq experiments with HISAT, StringTie and Ballgown. *Nat. Protocols* 11:1650. doi: 10.1038/nprot.2016.095

Puértolas, J., Larsen, E. K., Davies, W. J., and Dodd, I. C. (2017). Applying drought to potted plants by maintaining suboptimal soil moisture improves plant water relations. *J. Exp. Bot.* 68, 2413–2424. doi: 10.1093/jxb/erx116

Qi, F., and Zhang, F. (2020). Cell Cycle Regulation in the Plant Response to Stress. *Front. Plant Sci.* 10:1765. doi: 10.3389/fpls.2019.01765

Rober-Kleber, N., Albrechtova, J. T., Fleig, S., Huck, N., Michalke, W., Wagner, E., et al. (2003). Plasma membrane H+-ATPase is involved in auxin-mediated cell elongation during wheat embryo development. *Plant Physiol.* 131, 1302–1312. doi: 10.1104/pp.013466

Robinson, M. D., and Oshlack, A. (2010). A scaling normalization method for differential expression analysis of RNA-seq data. *Genome Biol.* 11:R25. doi: 10.1186/gb-2010-11-3-r25

Rosa, M., Prado, C., Podazza, G., Interdonato, R., González, J. A., Hilal, M., et al. (2009). Soluble sugars: Metabolism, sensing and abiotic stress: a complex network in the life of plants. *Plant Signal. Behav.* 4, 388–393. doi: 10.4161/psb.4.5.8294

Sakuraba, Y., Piao, W., Lim, J. H., Han, S. H., Kim, Y. S., An, G., et al. (2015). Rice ONAC106 inhibits leaf senescence and increases salt tolerance and tiller angle. *Plant Cell Physiol.* 56, 2325–2339. doi: 10.1093/pcp/pcv144

Salekdeh, G. H., Reynolds, M., Bennett, J., and Boyer, J. (2009). Conceptual framework for drought phenotyping during molecular breeding. *Trends Plant Sci.* 14, 488–496. doi: 10.1016/j.tplants.2009.07.007

Sato, Y., and Yokoya, S. (2008). Enhanced tolerance to drought stress in transgenic rice plants overexpressing a small heat-shock protein, sHSP17.7. *Plant Cell Rep.* 27, 329–334. doi: 10.1007/s00299-007-0470-0

Savoi, S., Wong, D. C., Arapitsas, P., Miculan, M., Bucchetti, B., Peterlunger, E., et al. (2016). Transcriptome and metabolite profiling reveals that prolonged drought modulates the phenylpropanoid and terpenoid pathway in white grapes (Vitis vinifera L.). *BMC Plant Biol.* 16, 1–17. doi: 10.1186/s12870-016-0760-1

Scarpeci, T. E., Zanor, M. I., and Valle, E. M. (2008). Investigating the role of plant heat shock proteins during oxidative stress. *Plant Signal. Behav.* 3, 856–857. doi: 10.4161/psb.3.10.6021

Sevanthi, A. M., Sinha, S. K., Sureshkumar, V., Rani, M., Saini, M. R., Kumari, S., et al. (2021). Integration of dual stress transcriptomes and major QTLs from a pair of genotypes contrasting for drought and chronic nitrogen starvation identifies key stress responsive genes in rice. *Rice* 14, 1–28. doi: 10.1186/s12284-021-00487-8

Shashidhar, H. E., Hemamalini, G. S., Hittalmani, S., Ito, O., O'Toole, J., and Hardy, B. (1999). *Molecular marker-assisted tagging of morphological and physiological traits at the peak vegetative stage: two contrasting moisture regimes. Genetic improvement of rice for water-limited environments*. Philippines: International Rice Research Institute, Manila, 239–256.

Shen, C., Wang, S., Zhang, S., Xu, Y., Qian, Q., Qi, Y., et al. (2013). OsARF16, a transcription factor, is required for auxin and phosphate starvation response in rice *(Oryza sativa* L.). *Plant Cell Env.* 36, 607–620. doi: 10.1111/pce.12001

Singh, A., Kumar, P., Gautam, V., Rengasamy, B., Adhikari, B., Udayakumar, M., et al. (2016). Root transcriptome of two contrasting indica rice cultivars uncovers regulators of root development and physiological responses. *Sci. Rep.* 6:39266. doi: 10.1038/srep39266

Sinha, S. K., Sevanthi, V. A. M., Chaudhary, S., Tyagi, P., Venkadesan, S., Rani, M., et al. (2018). Transcriptome analysis of two rice varieties contrasting for nitrogen use efficiency under chronic N starvation reveals differences in chloroplast and starch metabolism-related genes. *Genes* 9:206. doi: 10.3390/genes9040206

Song, Y., Chen, L., Zhang, L., and Yu, D. (2010). Overexpression of OsWRKY72 gene interferes in the abscisic acid signal and auxin transport pathway of Arabidopsis. *J. Biosci.* 35, 459–471. doi: 10.1007/s12038-010-0051-1

Song, Y., Wang, L., and Xiong, L. (2009). Comprehensive expression profiling analysis of OsIAA gene family in developmental processes and in response to phytohormone and stress treatments. *Planta* 229, 577–591. doi: 10.1007/s00425-008-0853-7

Sosnowski, O., Charcosset, A., and Joets, J. (2012). BioMercator V3: an upgrade of genetic map compilation and quantitative trait loci meta-analysis algorithms. *Bioinformatics* 28, 2082–2083. doi: 10.1093/bioinformatics/bts313

Subudhi, P. K., Garcia, R. S., Coronejo, S., and Tapia, R. (2020). Comparative Transcriptomics of Rice Genotypes with Contrasting Responses to Nitrogen Stress Reveals Genes Influencing Nitrogen Uptake through the Regulation of Root Architecture. *Internat. J. Mole. Sci.* 21:5759. doi: 10.3390/ijms21165759

Taheri, F., Nematzadeh, G., Zamharir, M. G., Nekouei, M. K., Naghavi, M., Mardi, M., et al. (2011). Proteomic analysis of the Mexican lime tree response to Candidatus Phytoplasma aurantifolia infection. *Mole. Biosyst.* 7, 3028–3035. doi: 10.1039/c1mb05268c

Takahashi, K., Hayashi, K., and Kinoshita, T. (2012). Auxin activates the plasma membrane H+-ATPase by phosphorylation during hypocotyl elongation in Arabidopsis. *Plant Physiol.* 159, 632–641. doi: 10.1104/pp.112.196428

Takatsuka, H., and Umeda, M. (2014). Hormonal control of cell division and elongation along differentiation trajectories in roots. *J. Exp. Bot.* 65, 2633–2643. doi: 10.1093/jxb/ert485

Takehisa, H., Sato, Y., Igarashi, M., Abiko, T., Antonio, B. A., Kamatsuki, K., et al. (2012). Genome−wide transcriptome dissection of the rice root system: implications for developmental and physiological functions. *Plant J.* 69, 126–140. doi: 10.1111/j.1365-313X.2011.04777.x

Takeuchi, K., Gyohda, A., Tominaga, M., Kawakatsu, M., Hatakeyama, A., Ishii, N., et al. (2011). RSOsPR10 expression in response to environmental stresses is regulated antagonistically by jasmonate/ethylene and salicylic acid signaling pathways in rice roots. *Plant Cell Physiol.* 52, 1686–1696. doi: 10.1093/pcp/pcr105

Temnykh, S., DeClerck, G., Lukashova, A., Lipovich, L., Cartinhour, S., and McCouch, S. (2001). Computational and experimental analysis of microsatellites in rice (*Oryza sativa* L.): frequency, length variation, transposon associations, and genetic marker potential. *Genome Res.* 11, 1441–1452. doi: 10.1101/gr.184001

Tholl, D. (2015). Biosynthesis and biological functions of terpenoids in plants. *Adv. Biochem. Eng. Biotechnol.* 148, 63–106. doi: 10.1007/10_2014_295

Tiwari, P., Srivastava, D., Chauhan, A. S., Indoliya, Y., Singh, P. K., Tiwari, S., et al. (2020). Root system architecture, physiological analysis and dynamic transcriptomics unravel the drought-responsive traits in rice genotypes. *Ecotoxicol. Env. Safety* 207:111252. doi: 10.1016/j.ecoenv.2020.111252

Tobias, C. M., and Chow, E. K. (2005). Structure of the cinnamyl-alcohol dehydrogenase gene family in rice and promoter activity of a member associated with lignification. *Planta* 220, 678–688. doi: 10.1007/s00425-004-1385-4

Trapnell, C., Roberts, A., Goff, L., Pertea, G., Kim, D., Kelley, D. R., et al. (2012). Differential gene and transcript expression analysis of RNA-seq experiments with TopHat and Cufflinks. *Nat. Prot.* 7, 562–578. doi: 10.1038/nprot.2012.016

Trapnell, C., Williams, B. A., Pertea, G., Mortazavi, A., Kwan, G., Van Baren, M. J., et al. (2010). Transcript assembly and quantification by RNA-Seq reveals unannotated transcripts and isoform switching during cell differentiation. *Nat. Biotechnol.* 28, 511–515. doi: 10.1038/nbt.1621

Uga, Y., Okuno, K., and Yano, M. (2011). Dro1, a major QTL involved in deep rooting of rice under upland field conditions. *J. Exp. Bot.* 62, 2485–2494. doi: 10.1093/jxb/erq429

Uga, Y., Sugimoto, K., Ogawa, S., Rane, J., Ishitani, M., Hara, N., et al. (2013). Control of root system architecture by DEEPER ROOTING 1 increases rice yield under drought conditions. *Nat. Genet.* 45, 1097–1102. doi: 10.1038/ng.2725

Ugartechea-Chirino, Y., Swarup, R., Swarup, K., Péret, B., Whitworth, M., Bennett, M., et al. (2009). The AUX1 LAX family of auxin influx carriers is required for the establishment of embryonic root cell organization in Arabidopsis thaliana. *Ann. Bot.* 105, 277–289. doi: 10.1093/aob/mcp287

Vaughan, M. M., Christensen, S., Schmelz, E. A., Huffaker, A., Mcauslane, H. J., Alborn, H. T., et al. (2015). Accumulation of terpenoid phytoalexins in maize roots is associated with drought tolerance. *Plant, Cell Env.* 38, 2195–2207. doi: 10.1111/pce.12482

Veyrieras, J. B., Goffinet, B., and Charcosset, A. (2007). MetaQTL: a package of new computational methods for the meta-analysis of QTL mapping experiments. *BMC Bioinform.* 8, 1–16. doi: 10.1186/1471-2105-8-49

Wang, T., Li, C., Wu, Z., Jia, Y., Wang, H., Sun, S., et al. (2017). Abscisic acid regulates auxin homeostasis in rice root tips to promote root hair elongation. *Front. Plant Sci.* 8:1121. doi: 10.3389/fpls.2017.01121

Wang, X., Cheng, Z., Zhao, Z., Gan, L., Qin, R., Zhou, K., et al. (2016). BRITTLE SHEATH1 encoding OsCYP96B4 is involved in secondary cell wall formation in rice. *Plant Cell Rep.* 35, 745–755. doi: 10.1007/s00299-015-1916-4

Wangenheim, D., Banda, J., Schmitz, A., Boland, J., Bishopp, A., Maizel, A., et al. (2020). Early developmental plasticity of lateral roots in response to asymmetric water availability. *Nat. Plants* 6, 73–77. doi: 10.1038/s41477-019-0580-z

Wu, Q., Pagès, L., and Wu, J. (2016). Relationships between root diameter, root length and root branching along lateral roots in adult, field-grown maize. *Ann. Bot.* 117, 379–390. doi: 10.1093/aob/mcv185

Wu, X., Shiroto, Y., Kishitani, S., Ito, Y., and Toriyama, K. (2009). Enhanced heat and drought tolerance in transgenic rice seedlings overexpressing OsWRKY11 under the control of HSP101 promoter. *Plant Cell Rep.* 28, 21–30. doi: 10.1007/s00299-008-0614-x

Wu, Y., Lee, S. K., Yoo, Y., Wei, J., Kwon, S. Y., Lee, S. W., et al. (2018). Rice transcription factor OsDOF11 modulates sugar transport by promoting expression of sucrose transporter and SWEET genes. *Mole. Plant* 11, 833–845. doi: 10.1016/j.molp.2018.04.002

Xia, H., Luo, Z., Xiong, J., Ma, X., Lou, Q., Wei, H., et al. (2019). Bi-directional selection in upland rice leads to its adaptive differentiation from lowland rice in drought resistance and productivity. *Mole. Plant* 12, 170–184. doi: 10.1016/j.molp.2018.12.011

Xiang, Y., Huang, Y., and Xiong, L. (2007). Characterization of stress-responsive CIPK genes in rice for stress tolerance improvement. *Plant Physiol.* 144, 1416–1428. doi: 10.1104/pp.107.101295

Xiao, G., Qin, H., Zhou, J., Quan, R., Lu, X., Huang, R., et al. (2016). OsERF2 controls rice root growth and hormone responses through tuning expression of key genes involved in hormone signaling and sucrose metabolism. *Plant Mole. Biol.* 90, 293–302. doi: 10.1007/s11103-015-0416-9

Yadav, R., Courtois, B., Huang, N., and McLaren, G. (1997). Mapping genes controlling root morphology and root distribution in a doubled-haploid population of rice. *Theoret. Appl. Genet.* 94, 619–632. doi: 10.1007/s001220050459

Yamaguchi, M., Valliyodan, B., Zhang, J., Lenoble, M. E., Yu, O., Rogers, E. E., et al. (2010). Regulation of growth response to water stress in the soybean primary root. I. Proteomic analysis reveals region−specific regulation of phenylpropanoid metabolism and control of free iron in the elongation zone. *Plant Cell Env.* 33, 223–243. doi: 10.1111/j.1365-3040.2009.02073.x

Yang, A., Li, Y., Xu, Y., and Zhang, W. H. (2013). A receptor-like protein RMC is involved in regulation of iron acquisition in rice. *J. Exp. Bot.* 64, 5009–5020. doi: 10.1093/jxb/ert290

Yang, L., Zheng, B., Mao, C., Qi, X., Liu, F., and Wu, P. (2004). Analysis of transcripts that are differentially expressed in three sectors of the rice root system under water deficit. *Mole. Genet. Genom.* 272, 433–442. doi: 10.1007/s00438-004-1066-9

Ye, H., Roorkiwal, M., Valliyodan, B., Zhou, L., Chen, P., Varshney, R. K., et al. (2018). Genetic diversity of root system architecture in response to drought stress in grain legumes. *J. Exp. Bot.* 69, 3267–3277. doi: 10.1093/jxb/ery082

Ye, Y., Liu, B., Zhao, M., Wu, K., Cheng, W., Chen, X., et al. (2015). CEF1/OsMYB103L is involved in GA-mediated regulation of secondary wall biosynthesis in rice. *Plant Mole. Biol.* 89, 385–401. doi: 10.1007/s11103-015-0376-0

Yoon, Y., Seo, D. H., Shin, H., Kim, H. J., Kim, C. M., and Jang, G. (2020). The role of stress-responsive transcription factors in modulating abiotic stress tolerance in plants. *Agronomy* 10:788. doi: 10.3390/agronomy10060788

Yoshida, S. (1976). Routine procedure for growing rice plants in culture solution. *Lab. Man. Physiol. Stud. Rice* 1976, 61–66.

Yoshii, M., Yamazaki, M., Rakwal, R., Kishi−Kaboshi, M., Miyao, A., and Hirochika, H. (2010). The NAC transcription factor RIM1 of rice is a new regulator of jasmonate signaling. *Plant J.* 61, 804–815. doi: 10.1111/j.1365-313X.2009.04107.x

Yu, H., Zhang, F., Wang, G., Liu, Y., and Liu, D. (2013). Partial deficiency of isoleucine impairs root development and alters transcript levels of the genes involved in branched-chain amino acid and glucosinolate metabolism in Arabidopsis. *J. Exp. Bot.* 64, 599–612. doi: 10.1093/jxb/ers352

Yu, J., Zao, W., He, Q., Kim, T. S., and Park, Y. J. (2017). Genome-wide association study and gene set analysis for understanding candidate genes involved in salt tolerance at the rice seedling stage. *Mole. Genet. Genom.* 292, 1391–1403. doi: 10.1007/s00438-017-1354-9

Yu, L. X., Ray, J. D., OToole, J. C., and Nguyen, H. T. (1995). Use of wax−petrolatum layers for screening rice root penetration. *Crop Sci.* 35, 684–687.

Zheng, H. G., Babu, Md, R. C., Pathan, M. S., Ali, L., Huang, N., et al. (2000). Quantitative trait loci for root-penetration ability and root thickness in rice: comparison of genetic backgrounds. *Genome* 43, 53–61. doi: 10.1139/g99-065

Zhou, Y., Huang, W., Liu, L., Chen, T., Zhou, F., and Lin, Y. (2013). Identification and functional characterization of a rice NAC gene involved in the regulation of leaf senescence. *BMC Plant Biol.* 13, 1–13. doi: 10.1186/1471-2229-13-132

Conflict of Interest: The authors declare that the research was conducted in the absence of any commercial or financial relationships that could be construed as a potential conflict of interest.

Publisher's Note: All claims expressed in this article are solely those of the authors and do not necessarily represent those of their affiliated organizations, or those of the publisher, the editors and the reviewers. Any product that may be evaluated in this article, or claim that may be made by its manufacturer, is not guaranteed or endorsed by the publisher.

Copyright © 2022 Abdirad, Ghaffari, Majd, Irian, Soleymaniniya, Daryani, Koobaz, Shobbar, Farsad, Yazdanpanah, Sadri, Mirzaei, Ghorbanzadeh, Kazemi, Hadidi, Haynes and Salekdeh. This is an open-access article distributed under the terms of the Creative Commons Attribution License (CC BY). The use, distribution or reproduction in other forums is permitted, provided the original author(s) and the copyright owner(s) are credited and that the original publication in this journal is cited, in accordance with accepted academic practice. No use, distribution or reproduction is permitted which does not comply with these terms.

frontiers in Plant Science

ORIGINAL RESEARCH
published: 04 March 2022
doi: 10.3389/fpls.2022.821647

Genome-Wide Analysis of *DREB* Genes Identifies a Novel Salt Tolerance Gene in Wild Soybean (*Glycine soja*)

Zhihong Hou[1,2†], Yongli Li[2†], Yuhan Cheng[3†], Weiwei Li[4†], Tai Li[2], Hao Du[2], Fanjiang Kong[2], Lidong Dong[2], Dianfeng Zheng[1,5,6], Naijie Feng[1,5,6*], Baohui Liu[2*] and Qun Cheng[2*]*

[1] College of Agriculture, Heilongjiang Bayi Agricultural University, Daqing, China, [2] Innovative Center of Molecular Genetics and Evolution, School of Life Sciences, Guangzhou University, Guangzhou, China, [3] Beijing Zhongnong Futong Horticulture Co., Ltd., Beijing, China, [4] Keshan Branch of Heilongjiang Academy of Agricultural Sciences, Keshan, China, [5] College of Coastal Agricultural Sciences, Guangdong Ocean University, Zhanjiang, China, [6] Shenzhen Research Institute of Guangdong Ocean University, Shenzhen, China

Salt stress is a major factor limiting the growth and yield of soybean (*Glycine max*). Wild soybeans (*Glycine soja*) contain high allelic diversity and beneficial alleles that can be re-introduced into domesticated soybeans to improve adaption to the environment. However, very few beneficial alleles have been identified from wild soybean. Here, we demonstrate that wild soybean is more salt tolerant than cultivated soybean and examine dehydration responsive element-binding (DREB) family transcription factor genes to look for advantageous alleles that might improve drought tolerance in cultivated soybean. Our genome-wide analysis identified 103 *DREB* genes from the *Glycine max* genome. By combined RNA-sequencing and population genetics of wild, landrace, and cultivated soybean accessions, we show that the natural variation in *DREB3a* and *DREB3b* is related to differences in salt tolerance in soybean accessions. Interestingly, *DREB3b*, but not *DREB3a*, appears to have undergone artificial selection. Soybean plants carrying the wild soybean *DREB3b* allele ($DREB3b^{39Del}$) are more salt tolerant than those containing the reference genome allele ($DREB3b^{Ref}$). Together, our results suggest that the loss of the $DREB3b^{39Del}$ allele through domestication of cultivated soybean may be associated with a reduction in salt tolerance. Our findings provide crucial information for improving salt tolerance in soybean through molecular breeding.

Keywords: artificial selection, DREB, natural variation, salt tolerance, cultivated soybean, wild soybean

OPEN ACCESS

Edited by:
Guihua Bai, Independent Researcher, New York, NY, United States

Reviewed by:
Milad Eskandari, University of Guelph, Canada
Kareem A. Mosa, University of Sharjah, United Arab Emirates

***Correspondence:**
Dianfeng Zheng
zdffnj@263.net
Naijie Feng
fengnj@gdou.edu.cn
Baohui Liu
liubh@gzhu.edu.cnr
Qun Cheng
chengqun0118@gzhu.edu.cn

† These authors have contributed equally to this work

Specialty section:
This article was submitted to Crop and Product Physiology, a section of the journal Frontiers in Plant Science

Received: *24 November 2021*
Accepted: *17 January 2022*
Published: *04 March 2022*

Citation:
Hou Z, Li Y, Cheng Y, Li W, Li T, Du H, Kong F, Dong L, Zheng D, Feng N, Liu B and Cheng Q (2022) Genome-Wide Analysis of DREB Genes Identifies a Novel Salt Tolerance Gene in Wild Soybean (Glycine soja). Front. Plant Sci. 13:821647. doi: 10.3389/fpls.2022.821647

INTRODUCTION

High salt levels in soil cause stress that affects plant growth and salinization of farmland restricts global agricultural production (Flowers, 2004; Munns and Tester, 2008; Ondrasek et al., 2011). Soil salinization is exacerbated by natural and human activities, including irrigation (Munns et al., 2020). Under salt stress, plants experience dehydration, metabolic toxicity, nutrient deficiencies, and membrane dysfunction, leading to tissue damage and early senescence (Essah et al., 2003). To

adapt to various environmental stresses, plants have evolved many complexes signaling networks, and the molecular basis of these pathways is currently being studied (Zhu, 2001).

Soybean [*Glycine max* (L.) Merr.] is an economically important crop for oil and protein (Graham and Vance, 2003). It is classified as a moderately salt-sensitive crop; under salt stress, soybean yields may be reduced by up to 40% (Papiernik et al., 2005; Munns and Tester, 2008). Moreover, soybean cultivars show variation in their salt sensitivity: under saline conditions, salt-sensitive cultivars have a 37% decrease in yield compared with salt-tolerant cultivars (Parker et al., 1983). This natural variation in salt tolerance provides opportunities to increase soybean production under saline conditions (Guan et al., 2014; Qi et al., 2014). However, few salt-tolerant variants have been identified (Guan et al., 2014; Qi et al., 2014). This lack of knowledge has greatly inhibited attempts to improve salt tolerance in crops.

Cultivated soybean was domesticated from its wild counterpart *Glycine soja* Sieb. & Zucc. 6,000–9,000 years ago (Hymowitz, 1970; Carter et al., 2004). Due to artificial selection and population/genetic bottlenecks, cultivated soybeans have much lower genetic diversity than their wild relative (Hyten et al., 2006; Lam et al., 2010). This reduced variation may have led to the loss of some genes or alleles that are important for adapting to different environments. Therefore, wild soybean, with its high allelic diversity, may be a good source for beneficial alleles that can be re-introduced into domesticated soybean cultivars through breeding.

The dehydration responsive element-binding (DREB) family is a subgroup of the APETALA2/ethylene-responsive factor (AP2/ERF) transcription factor (TF) superfamily; in multiple plants, *DREB* genes respond to a wide variety of abiotic stresses, such as drought, high salt, cold, and heat (Xu et al., 2011; Kudo et al., 2017; Ali and Hadi, 2018; Eckardt, 2019). Some DREBs are involved in the salt stress response in soybean (Gao et al., 2005; Li et al., 2005; Chen et al., 2007). However, the variation in the *DREB* family in wild soybean remains to be explored. To fill this gap, we combined genome-wide analysis, association studies, population genetics, and RNA-sequencing to identify candidate causal *DREB* genes for salt tolerance. Our results show that *DREB3b* contributes to salt tolerance and may have undergone natural and artificial selection. In addition, the $DREB3b^{39Del}$ allele from wild soybean improves salt tolerance compared to the $DREB3b^{Ref}$ allele from cultivated soybean. The identification of these *DREB3b* alleles provides important information for improving the yield of soybean and other crops.

MATERIALS AND METHODS

Plant Materials, Salt Treatment, and Primers

The soybean cultivar Williams 82 (W82) and 424 soybean varieties (Lu et al., 2020) were used in this study. 424 soybean accessions were grown in a greenhouse using vermiculite as the growth medium, and maintained at 25°C and 70% relative humidity with a 16 h light/8 h dark. Fifteen days after planting, seedlings at the first-node stage (V1; Fehr et al., 1971) were subjected to 200 mM NaCl treatment. After being treated for 2 weeks, salt tolerance index was determined with two independent experiments. Briefly, five to eight plants of each accession in each replication were scored for salt tolerance. A salt-tolerance rating for each of the accession was assigned by the respective level of leaf chlorosis (Liu et al., 2020). The salt-tolerance ratings ranged on a scale from 1 (normal green leaves) to 5 (complete death). All primers used for vector construction, PCR, and quantitative reverse transcription (qRT)-PCR assays for all target genes are listed in **Supplementary Table 3**.

Identification and Bioinformatic Analysis of *DREB* Genes in Soybean Genome

The soybean genome in Phytozome[1] was used to identify all members of *DREB* family genes. A database search was carried out against all the genome-coded soybean proteins with the BLASTP program (*E*-value < 1e–20 and coverage >75%) in TBtools (Chen et al., 2020) using 56 full-length amino acid sequences of DREB homologs from *A. thaliana* (Sakuma et al., 2002). Multiple alignment of the protein sequences of 159 *DREB* genes (56 from *A. thaliana* and 103 from soybean) were aligned by ClustalW. A neighbor-joining phylogenetic tree was generated using MEGA_X with bootstrap repeated 1,000 times. The expression data of 103 *DREB* genes in different tissues (leaf, stem, root, flower, seed, pod, and cotyledon) of soybean were obtained from RNA-seq database (Machado et al., 2020).[2] Location of *DREB* genes was visualized using the soybean genome generic feature format (.gff) using TBtools.

RNA Extraction, Transcriptome Sequencing, and Quantitative Reverse Transcription–PCR

For RNA-sequencing, the W82 seedlings were grown in a growth chamber maintained at 25°C and 70% relative humidity with a 16-h light/8-h dark. Fifteen days after planting, seedlings at the first-node stage (V1; Fehr et al., 1971) were subjected to 200 mM NaCl treatment. The control plants were treated with water. After being treated for 2 weeks, total RNA was isolated using TRIzol reagent kit (Invitrogen, Carlsbad, CA, United States). cDNA synthesis was conducted using an M-MLV reverse transcriptase kit (Takara, Dalian, China) according to the manufacturer's protocol. The cDNA fragments were purified using a QiaQuick PCR extraction kit, and ligated to Illumina sequencing adapters. The ligation products were size-selected by agarose gel electrophoresis, PCR amplified, and sequenced using an Illumina HiSeq 2500 system by Gene *Denovo* Biotechnology Co. (Guangzhou, China).

Haplotype Network Construction

The full-length coding sequence of *DREB3a* and *DREB3b* in 1295 soybean accessions were retrieved from the 1295 resequencing data (Lu et al., 2020). The resequencing data of 1295 accessions

[1] https://phytozome.jgi.doe.gov/pz/portal.html

[2] http://venanciogroup.uenf.br/cgi-bin/gmax_atlas/index.cgi

were deposited into the NCBI database under accession number PRJNA394629, and the GSA database in BIG Data Center under accession numbers PRJCA000205 and PRJCA001691. Only haplotypes found in ≥3 soybean accessions were recorded. A haplotype network was constructed based on polymorphic sites of the whole coding sequences of *DREB3a* and *DREB3b* using the Median-Joining method in the NETWORK version 4.6.1.2 software (Fluxus Technology Ltd., Sudbury, Suffolk, United Kingdom) with data preparation using DNASP version 5 (Librado and Rozas, 2009).

Nucleotide Diversity of *DREB3a* and *DREB3b*

A 20-kb sequence set (Chr01:48411780.48452989 and Chr15:1392382. . .1433465) centered on the candidate genes (*DREB3a* and *DREB3b*) were obtained from the 1295 soybean accessions whole-genome dataset. Nucleotide diversity (π) of each accession was estimated using the script vcftools with parameters–window-pi 20000–window-pi-step 10000.

Plasmid Construction and Soybean Hairy Root Transformation

The coding sequence of *DREB3b* was obtained from W82 and GDW013 (wild soybean variety) by KOD-Plus-Neo (TOYOBO) with the primer in **Supplementary Table 3**. The coding sequence of *DREB3b* was cloned into plant expression vector pCAMBIA3301 with gene-specific primers. Transgenic soybean hairy roots were generated by *Agrobacterium rhizogenes*-mediated transformation as described by Graham et al. (2007) and Kereszt et al. (2007) with some modifications. The cotyledons were cut into rough triangles and immediately placed in Petri dishes containing 0.6% agar medium to keep them moist. The cut surface was treated with 20 μl *A. rhizogenes* suspension. The dishes were sealed with Parafilm and placed in an incubator at 25°C. Transformed hairy roots were abundant along a callus ridge on the inoculated cotyledons after approximately 3 weeks. Overexpression of the target gene in transgenic hairy roots was tested via quantitative PCR (qPCR) and GUS staining.

Molecular Marker Development

The sequences of the $DREB3b^{39Del}$ allele and $DREB3b^{Ref}$ allele were obtained by sequencing. Primers were designed using Primer Premier 5.0, with a product size < 200 bp. The InDel marker was developed on the basis of the variation in *DREB3b*. **Supplementary Table 3** lists the InDel markers that were used in this study.

Statistical Analyses

In this study, for 424 accessions phenotypic evaluation, at least 6 individual plants were analyzed. all values were presented as mean ± s.e.m. and numbers (n) of samples or replicates are indicated in figure legends. Data were analyzed with GraphPad Prism 8 (ver. 8.0.1). Significance levels of differences were calculated by one-tailed, two-sample Student's t-tests or one-way ANOVA with GraphPad Prism 8 (ver. 8.0.1).

RESULTS

Genetic Diversity and Salt Tolerance Index in Soybean Accessions

Owing to "domestication syndrome" through artificial selection for traits to increase yield, cultivated soybean has lost substantial genetic diversity (Qiu et al., 2013; Li et al., 2014). Here, we examined a panel of 424 previously described accessions (Lu et al., 2020), which comprised 85 wild soybeans, 153 landraces, and 186 cultivars. To assess the genetic diversity in this panel, we compared the shapes of the wild, landrace, and cultivated soybean seeds (**Figure 1A**) and estimated the number of single-nucleotide polymorphisms (SNPs) and the nucleotide diversity across chromosome 1 in the 424 accessions. The number of SNPs and the nucleotide diversity are lowest in cultivated soybean and highest in wild soybean (**Figures 1B,C**). These results are consistent with a previous preliminary report (Lam et al., 2010).

We also measured the salt tolerance indexes of the 424-accession panel. Phenotype was evaluated in a growth chamber at 25°C, revealing significantly reduced salt tolerance in landrace and cultivated soybean compared to wild accessions in two biological replicates (**Figures 1D,E**). These results suggest that artificial selection may have had a strong effect on the genetic diversity in the cultivated soybeans.

Genome-Wide Identification and Annotation of the *DREB* Gene Family

The DREB family plays an important role in plant responses to abiotic stresses (Gao et al., 2005; Chen et al., 2007; Ali and Hadi, 2018; Eckardt, 2019), so it would be meaningful to identify the genes encoding DREB TFs in soybean. In this study, 56 *Arabidopsis thaliana DREB* sequences (Sakuma et al., 2002) were used as a query to search the soybean database. This identified 103 *DREB* genes from the *Glycine max* genome (**Supplementary Table 1**), 73 of which have been reported previously (Zhou et al., 2020b). The *DREB* genes were distributed on all chromosomes of soybean, with 8, 3, 4, 5, 6, 8, 4, 3, 4, 5, 7, 7, 8, 9, 3, 2, 8, 2, 5, and 2 *DREB* genes on chromosome 1, 2, 3, 4, 5, 6, 7, 8, 9, 10, 11, 12, 13, 14, 15, 16, 17, 18, 19, and 20, respectively (**Supplementary Figure 1**). Phylogenetic analyses based on previously reported Arabidopsis *DREB* sequences (Sakuma et al., 2002) classified these genes into six subgroups: 14 genes in A-1 group, 35 genes in A-2 group, 19 genes in A-3 group, 2 genes in A-4 group, 21 genes in A-5 group, and 12 genes in A-6 group (**Figure 2A** and **Supplementary Table 1**).

Expression Analysis of *DREB* Genes in Different Tissues

The transcript levels of 103 *DREB* genes in different soybean tissues were analyzed using the Phytozome database.[3] The A-1 subgroup was highly expressed in stem and flower; the A-2 subgroup was highly expressed in root, flower, pod, and leaves; the A-3 subgroup was highly expressed in stem, root, and flower; the A-4 subgroup and the A-6 subgroup were highly expressed

[3]https://phytozome-next.jgi.doe.gov/

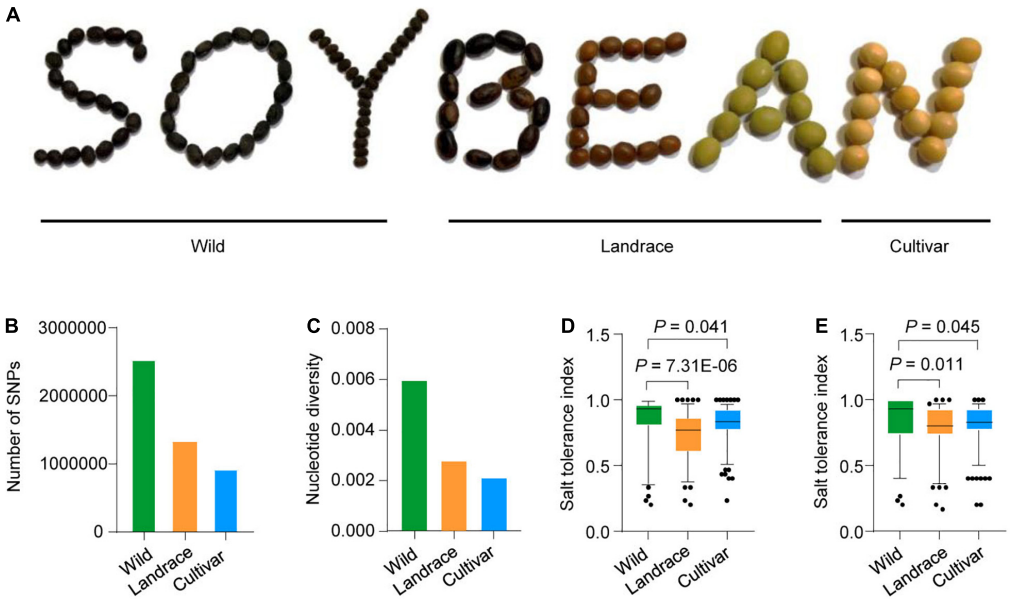

FIGURE 1 | The morphologic characteristics and salt tolerance of wild, landrace and cultivated soybean. **(A)** The morphologic characteristics of wild, landrace, and cultivated soybean. **(B)** Number of SNPs of 424 accessions in chromosome 1 genomic region. **(C)** Nucleotide diversity of 424 accessions in chromosome 1 genomic region. **(D,E)** Comparison of the salt tolerance index of 424 accessions (85 wild soybeans, 153 landraces and 186 improved cultivars); two biological replicates in greenhouse.

in seed and cotyledon; the A-5 subgroup was highly expressed in stem (**Figure 2B**). These data suggest that *DREB* genes of the same subgroup may have similar functions, whereas *DREB* genes of different subgroups may have functional differentiation.

Expression Analysis of *DREB* Genes Under Salinity Stress

As a few *DREB* genes have been shown to be induced by salinity stress (Chen et al., 2007, 2009; Zhou et al., 2020a), we asked whether other *DREB* family members also control salt tolerance and whether these homologs could be used in agricultural applications. We thus performed RNA-sequencing experiments with three biological replicates, comparing the cultivated soybean Williams 82 (W82) grown under control conditions (W82-Water) with W82 treated with 200 mM NaCl for 15 days (W82-NaCl). The differentially expressed genes (DEGs) were identified by a pairwise comparison of the transcriptome datasets (W82-Water vs. W82-NaCl). As expected, the gene expression patterns were similar between three biological replicates but differed significantly between the control and salt treatments (**Figure 3A**).

We identified 24 differentially expressed *DREB* genes in the W82-water vs. W82-NaCl comparison. There were nine up-regulated genes in the A-2 subgroup, one up-regulated gene each in the A-3 and A-5 subgroups, three up-regulated genes in the A-6 subgroup, four down-regulated genes in the A-2 and A-3 subgroups, and two down-regulated genes in the A-5 subgroup (**Figures 3B,C** and **Supplementary Table 2**).

The gene structures of the 24 differentially expressed *DREB* genes were diagrammed, including the untranslated regions (UTRs) and the locations of exons and introns (**Supplementary Figure 2**). Among the up-regulated *DREB* genes, nine genes had no introns and five genes contained one intron (**Supplementary Figure 2A**). Among the down-regulated *DREB* genes, nine genes had no introns and only one gene contained one intron (**Supplementary Figure 2B**). This observation is consistent with the structural characteristics described by Zhou et al. (2020b).

The Natural Variation of *DREB3a* and *DREB3b* Affects Salt Tolerance

Some *DREB* genes positively regulate tolerance to abiotic stress in soybean (Chen et al., 2007, 2009; Zhou et al., 2020a); therefore, we focused on the 14 up-regulated *DREB* genes. To systematically study natural variation of *DREB* genes, we investigated the variation of all 14 up-regulated *DREB* genes in the 424-accession panel and found that only nine *DREB* genes arose through natural variation: *Glyma.01G147600*, *Glyma.15G018400*, *Glyma.04G084000*, *Glyma.08G035000*, *Glyma.16G023800*, *Glyma.09G233800*, *Glyma.08G137600*, *Glyma.12G103100*, *Glyma.06G301300* (**Figures 4A,B** and **Supplementary Figures 3–6**).

We then measured the salt tolerance indexes of the population to determine if salt tolerance is associated with any of the nine genes. After correcting for population structure (at least ten individual plants were analyzed per accession), two out of the nine *DREB* genes were significantly correlated with the salt tolerance index ($p < 0.05$): *Glyma.01G147600* and *Glyma.15G018400* (**Figures 4A,B**).

Phylogenetic investigation indicated that *Glyma.01G147600* and *Glyma.15G018400* are orthologs of *DREB3* in other plants. The two orthologs were thus named *DREB3a* and *DREB3b*,

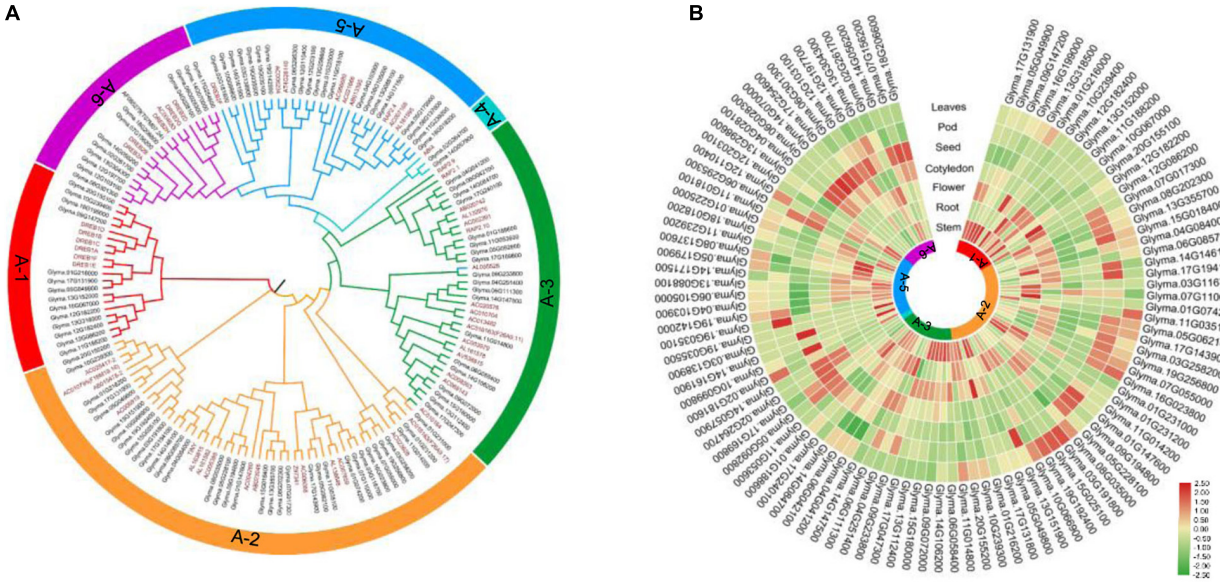

FIGURE 2 | Phylogenetic tree of the *DREB* genes of *Arabidopsis thaliana* and soybean, and gene expression profile of soybean *DREB* genes in different tissues. **(A)** The NJ tree was constructed using MEGA_X based on alignment of a total of 159 DREB proteins, including 56 *Arabidopsis* DREBs and 103 *Glycine max* DREBs. DREB subfamilies are divided into six groups (A-1 to A-6). **(B)** The normalized microarray expression data of 103 *Glycine max* DREBs was downloaded from PLEXdb (http://www.plexdb.org/). The heatmap was produced using TBtools.

respectively (**Figure 4C**). To determine whether *DREB3a* and *DREB3b* respond to salt stress, we performed qRT-PCR to examine their expression profiles under salt stress. The results showed that *DREB3a* and *DREB3b* were up-regulated under salt stress (**Figures 4D,E**), consistent with RNA-sequencing data (**Figure 3C**).

Interestingly, Hap. 2-4 of *DREB3a* harbored a 15-bp InDel predicted to insert 5 amino acids, and Hap. 2–3 of *DREB3b* lacked a 6-bp InDel predicted to lack 2 amino acids (hereafter referred to as $DREB3a^{167Ins}$ and $DREB3b^{39Del}$, respectively). We then compared the phenotypic differences of the accessions carrying either the reference genome *DREB3a* allele ($DREB3a^{Ref}$) or $DREB3a^{167Ins}$ allele, and the two accessions carrying either the reference genome *DREB3b* allele ($DREB3b^{Ref}$) or $DREB3b^{39Del}$ allele. The salt tolerance indexes of $DREB3a^{167Ins}$ and $DREB3b^{39Del}$ allele accessions were significantly higher than $DREB3a^{Ref}$ and $DREB3b^{Ref}$ accessions in two biological replicates (**Figures 4F–I**). These results strongly suggest that *DREB3a* and *DREB3b* are excellent candidate genes that respond to salt stress.

DREB3b, but Not *DREB3a*, Has Undergone Artificial Selection in the Domestication Process

To gain further insight into the evolutionary history of *DREB3a* and *DREB3b*, we examined the variation in the *DREB3a* and *DREB3b* coding sequences in our previously described collection of 1295 resequenced accessions (**Supplementary Figure 7A**), of which four (Hap. 1, 2, 3, and 4) are described above (**Figure 4A**), and identified five haplotypes in *DREB3b* (**Supplementary Figure 7B**), of which three (Hap. 1, 2, 3) are described above (**Figure 4B**). The residues of Hap. 2 for both *DREB3a* and *DREB3b* are identical to all other homologs in legume (**Supplementary Figures 8A,B**), suggesting that Hap. 2 is the original haplotype in the soybean species. Median-joining network analysis of *DREB3a* showed that Hap. 5 is derived from Hap. 2, Hap. 1, and Hap. 3 are derived from Hap. 5, and Hap. 4 is derived from Hap. 3 (**Supplementary Figure 9A**). Median-joining network analysis of *DREB3b* showed that Hap. 1, 3, and 5 are derived from Hap. 2, and Hap. 4 is derived from Hap. 3 (**Supplementary Figure 9B**).

We then analyzed the percentage of $DREB3a^{167Ins}$ and $DREB3b^{39Del}$ alleles in 1295 resequenced soybean accessions. Surprisingly, the most common allele $DREB3b^{Ref}$ was present in the vast majority of improved cultivars (507/515) and in most landraces (418/485) (**Figure 5A**), indicating that the $DREB3b^{Ref}$ allele is nearly fixed in the landrace population. This dramatic increase of the $DREB3b^{Ref}$ allele in the soybean population indicates that the $DREB3b^{Ref}$ allele might have been under strong artificial selection during domestication.

To examine whether selection has acted on $DREB3b^{Ref}$, we analyzed the nucleotide diversity of the 20-kb region flanking $DREB3b^{Ref}$ in domesticated and wild soybean lines. Landraces carrying the $DREB3b^{39Del}$ allele retained 84.16% of the nucleotide diversity of their wild counterparts, and improved cultivars retained 47.38% of the nucleotide diversity of landraces (**Figure 5C**). Whereas, landraces carrying the $DREB3b^{Ref}$ allele retained only 33.77% of the nucleotide diversity of wild lines, and improved cultivars retained only 2.18% of the nucleotide diversity of landraces (**Figure 5C**). We identified strong evidence of selection in a region of 380 kb around the *DREB3b* gene (**Figure 5D**). These results suggest that the $DREB3b^{Ref}$ allele

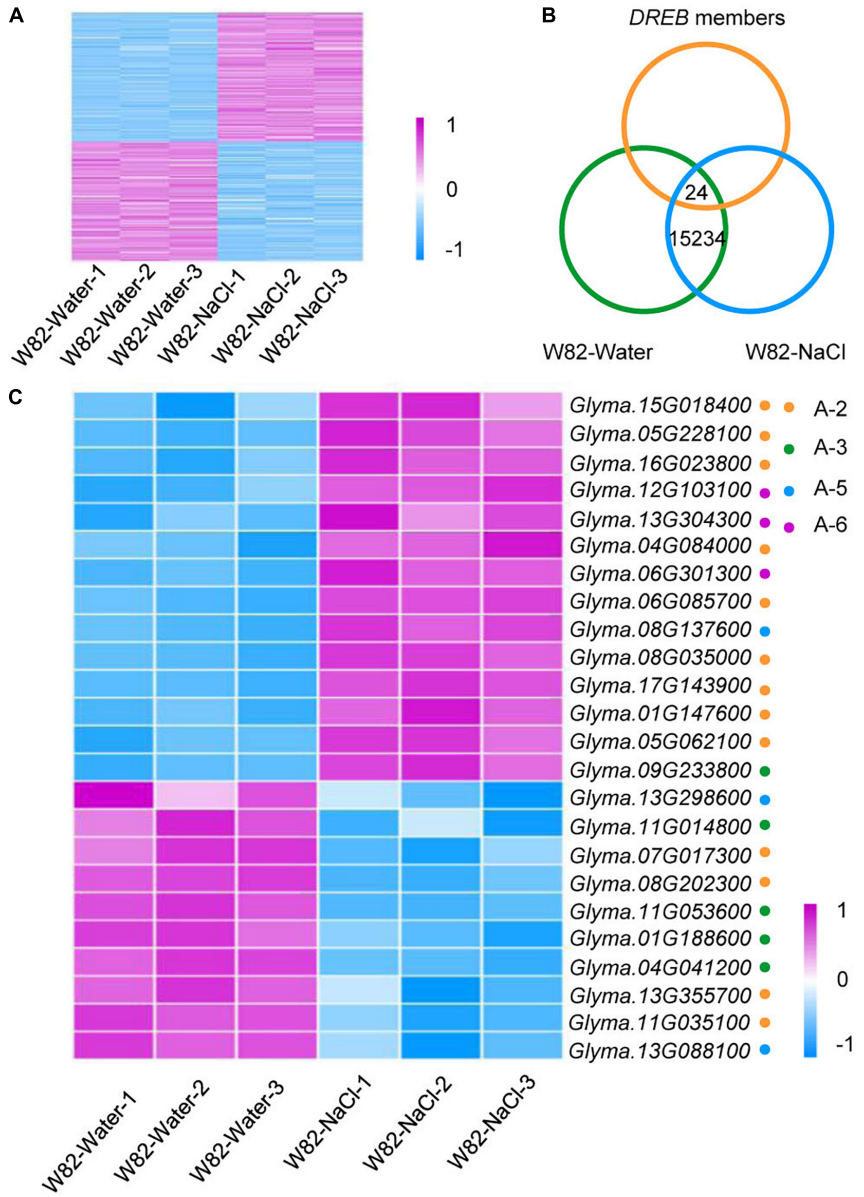

FIGURE 3 | Identification of differentially expressed *DREB* genes in NaCl-treated W82 vs. mock treated. **(A)** Heat map of differentially expressed genes in W82-Water and W82-NaCl; $n = 3$ for each group. Relative transcript level is indicated on a color scale from purple (high) to blue (low). **(B)** Overlap between W82-Water, W82-NaCl and *DREB* genes. **(C)** Heat map of differentially expressed 24 *DREB* genes under NaCl treatment.

was targeted by selection, thereby causing its rapid accumulation in domesticated soybeans. This is also supported by similar negative values of Tajima's *D* statistic for *DREB3b* in domesticated soybeans (**Supplementary Table 5**), indicating that *DREB3b* (and in particular the $DREB3b^{Ref}$ allele) experienced selection during the transition from wild soybean to landrace.

Given that salt tolerance is not considered a soybean domestication trait, it is not clear why $DREB3b^{Ref}$ was selected during early domestication. We propose that the *DREB3b* region is a hotspot for many domestication and agronomic traits. Consistent with expectation, the $DREB3b^{Ref}$ allele improves flowering, increases seed size, and decreases plant height relative to the $DREB3b^{39Del}$ allele (**Supplementary Figures 10A–C**). Therefore, $DREB3b^{Ref}$ may have been selected for an effect on flowering time, seed size and plant height, and the change in salt tolerance was a correlated response. Considering the enrichment of the $DREB3b^{39Del}$ allele in wild soybeans, and the higher salt tolerance index of the $DREB3b^{39Del}$ allele compared to that of the $DREB3b^{Ref}$ allele, the $DREB3b^{39Del}$ allele may be undergoing strong natural selection to facilitate the response of wild soybeans to salt stress.

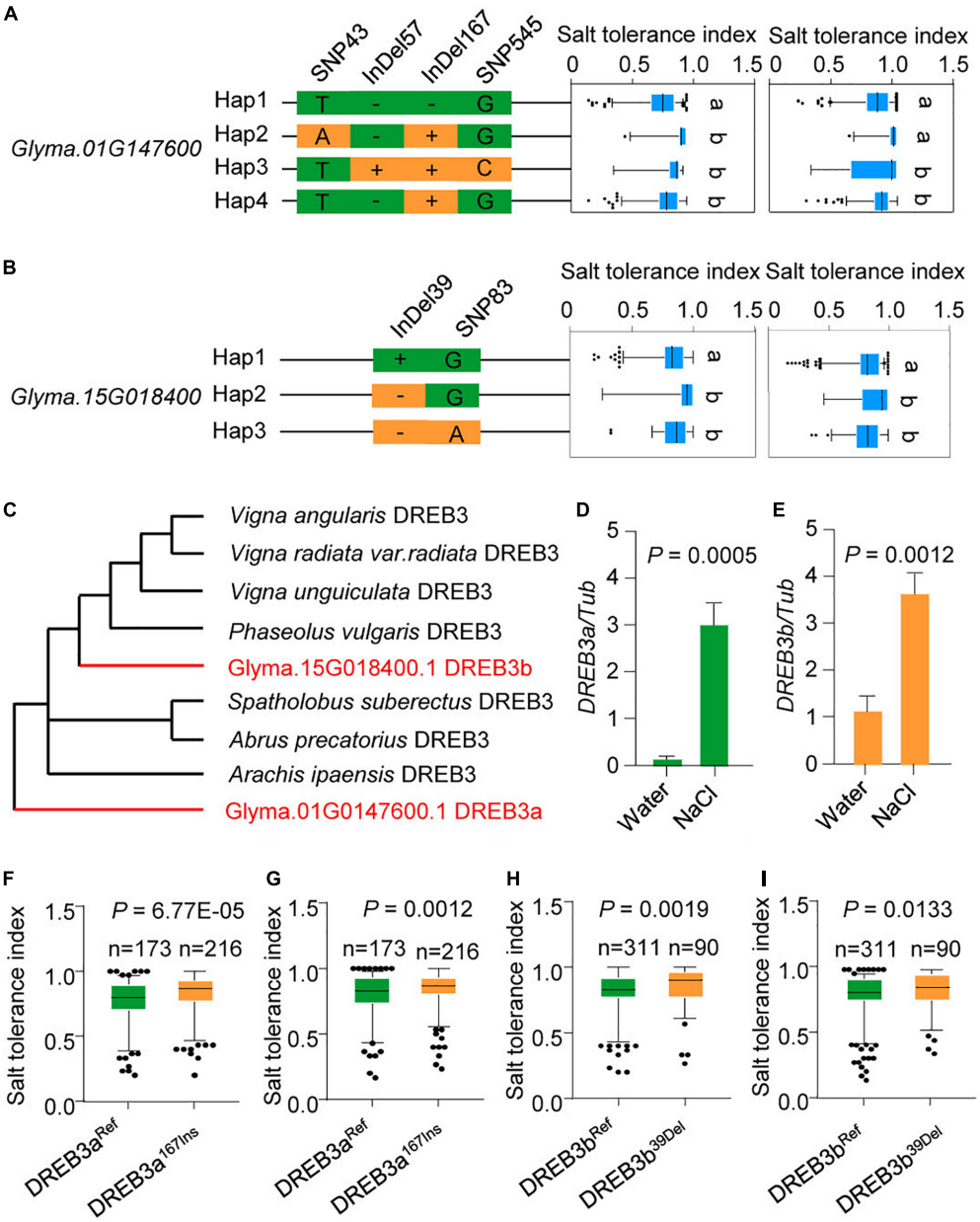

FIGURE 4 | Natural variation of *DREB3a* and *DREB3b* are significantly associated with the salt tolerance. **(A)** Boxplots for salt tolerance index based on the haplotypes of *Glyma.01G147600* among 424 soybean accessions. The *Glyma.01G147600* haplotypes (Hap1–Hap4) were categorized by the four significant variants. **(B)** Boxplots for salt tolerance index based on the haplotypes of *Glyma.15G018400* among 424 soybean accessions. The *Glyma.15G018400* haplotypes (Hap1–Hap3) were categorized by the two significant variants. The experiment was performed using two biological replicates in **(A,B)**. The same lowercase letters above the histogram bars in **(A,B)** denote non-significant differences across the two panels ($P > 0.05$). One-way ANOVA was used to generate the *P*-values. **(C)** Phylogenetic tree of DREB proteins in plants. Red indicates DREB3a and DREB3b protein. **(D)** The transcription levels of *DREB3a* under salt stress (200 mM NaCl). **(E)** The transcript levels of *DREB3b* under salt stress (200 mM NaCl). All data were given as mean ± s.e.m. ($n = 3$ biological replicates). **(F,G)** $GmDREB3a^{Ref}$ and $DREB3a^{167Ins}$ alleles associated with salt tolerance index. **(H,I)** $DREB3b^{Ref}$ and $DREB3b^{39Del}$ alleles associated with salt tolerance index. One-tailed Student's *t*-test was used to generate the *P*-values in **(D–I)**.

For *DREB3a*, the $DREB3a^{Ref}$ allele was the most abundant in landraces (274/360) and in improved cultivars (230/401) (**Figure 5A**). However, landraces carrying the $DREB3a^{167Ins}$ allele retained 30.08% of the nucleotide diversity of their wild counterparts, and improved cultivars retained 18.90% of the nucleotide diversity of landraces (**Figure 5B**). Whereas, landraces carrying $DREB3a^{Ref}$ allele retained 29.22% of the nucleotide diversity of wild, and cultivated retained 33.05% of the nucleotide diversity of landraces (**Figure 5B**). We identified no strong evidence of selection in a region of the *DREB3a* gene (**Figure 5D**,

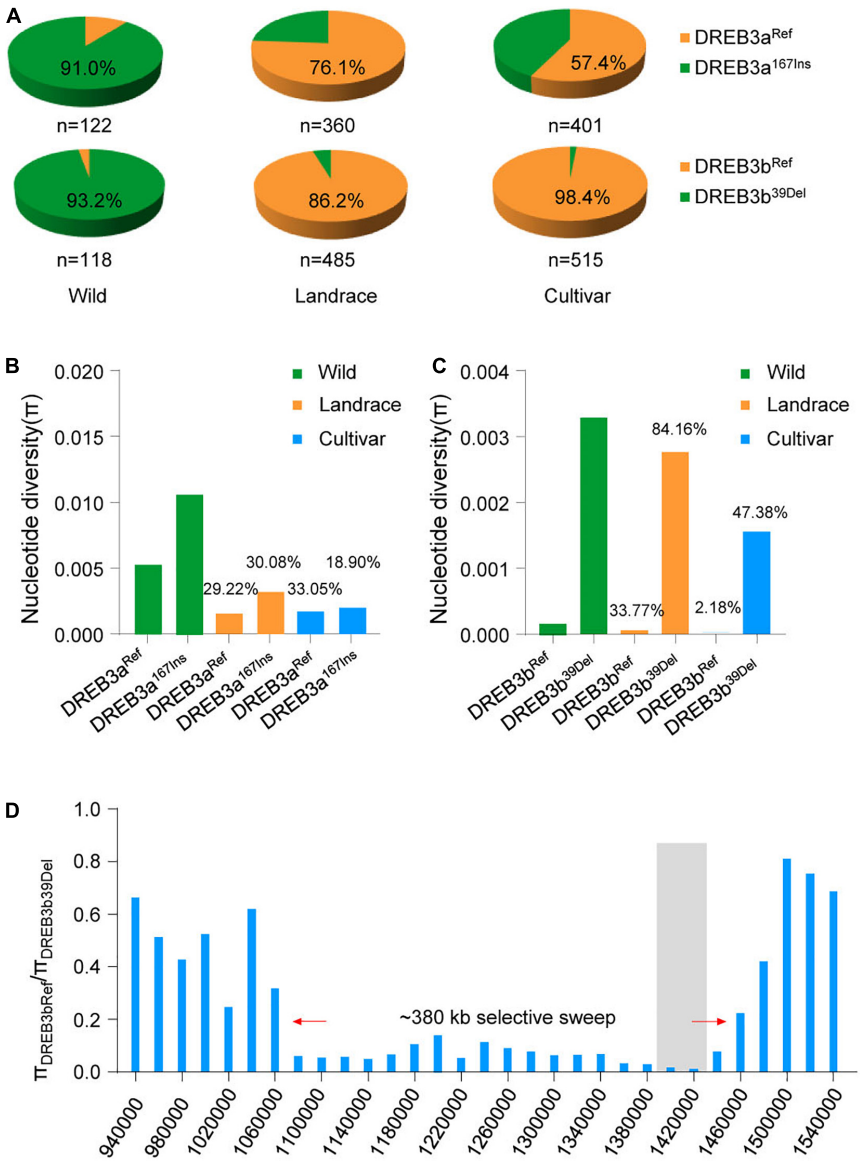

FIGURE 5 | *DREB3b* underwent artificial selection but *DREB3a* did not. **(A)** Proportions of *DREB3a* and *DREB3b* alleles and their co-occurrence with each of the three germplasm groups (wild, landrace, and cultivar). **(B)** Nucleotide diversity analysis of the region surrounding *DREB3a* in wild, landrace, and cultivated soybean. **(C)** Nucleotide diversity analysis of the region surrounding *DREB3b* in wild, landrace, and cultivated soybean. **(D)** Selective sweep in the 380-kb *DREB3b* genomic region.

Supplementary Figure 11, and **Supplementary Table 5**). This implies that *DREB3b*, but not *DREB3a*, has undergone artificial selection during in the domestication process.

DREB3b^{39Del} Enhances Salt Tolerance in Soybean

We next focused on the function of *DREB3b*. To further characterize the potential contribution of *DREB3b* to salt tolerance in different soybean varieties, we generated *DREB3b*^{Ref}-overexpressing and *DREB3b*^{39Del}-overexpressing transgenic soybean hairy roots by high-efficiency *A. rhizogenes*-mediated transformation (Graham et al., 2007; Kereszt et al., 2007). We examined the *DREB3b*^{Ref}-overexpressing and *DREB3b*^{39Del}-overexpressing transgenic hairy roots by GUS staining and qRT-PCR (**Figures 6A,B**). Under normal conditions (0 mM NaCl), all soybean hairy roots grew well, with no noticeable difference (**Figure 6C**). Under 100 mM NaCl stress, the average root length of *DREB3b*^{39Del}-overexpressing soybean hairy roots was much longer than that of *DREB3b*^{Ref}-overexpressing transgenic hairy roots and much longer than that of non-transgenic hairy roots (**Figures 6C,D**).

Many positive and negative regulators of salt tolerance in soybean have been identified (Zhou et al., 2008; Wang et al., 2015; Shi et al., 2018; Li et al., 2019). To test whether DREB3b can

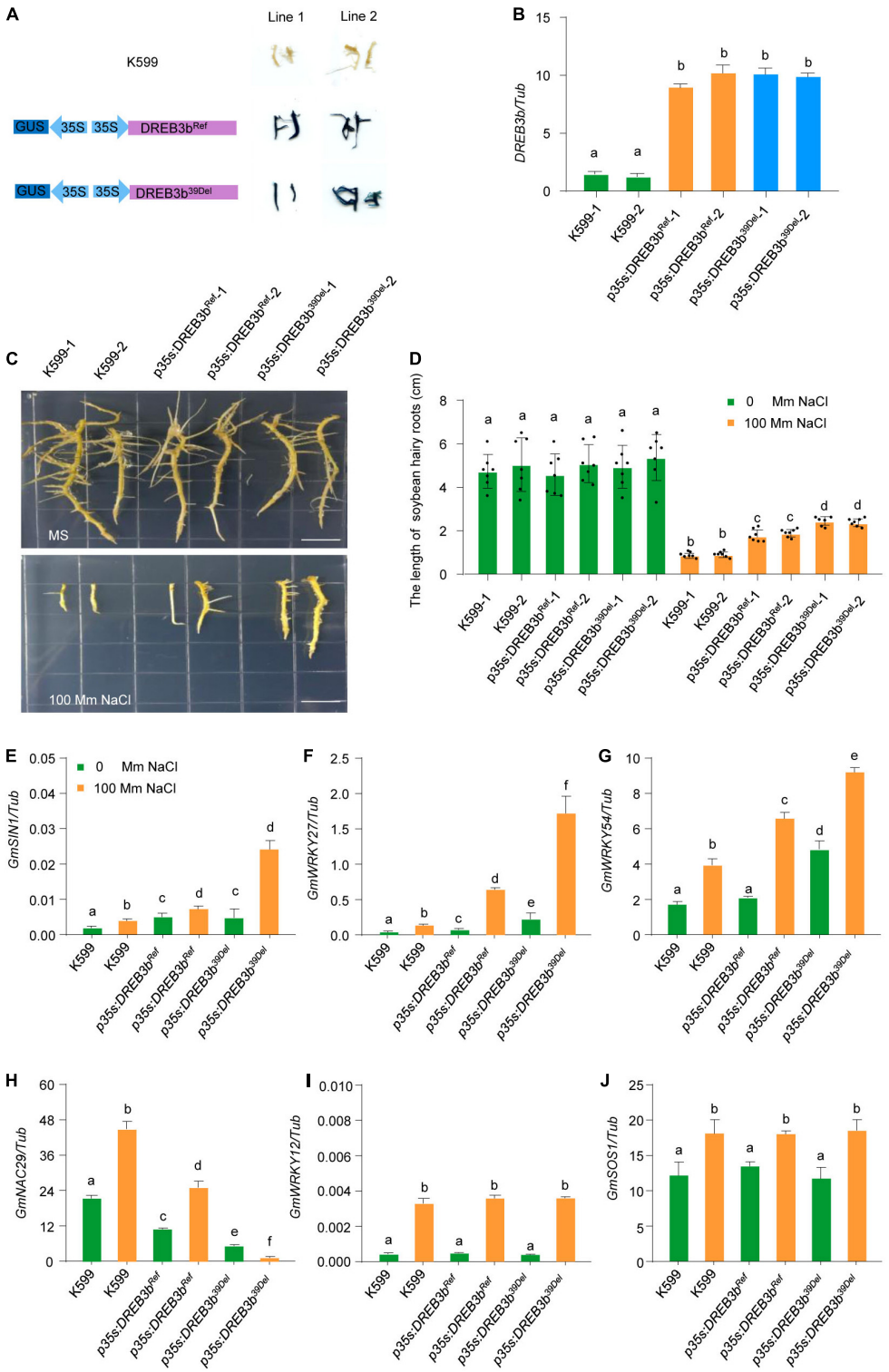

FIGURE 6 | *DREB3b*^{39Del} improves salt tolerance more than *DREB3b*^{Ref} in transgenic soybean hairy roots. **(A)** Schematic diagram of overexpression vector and GUS staining of overexpressing *DREB3b*^{39Ref} and *DREB3b*^{39Del} in soybean hairy roots. **(B)** The transcript levels of *DREB3b* in W82 and two independent *DREB3b*^{39Ref} and *DREB3b*^{39Del} transgenic lines grown under normal growth conditions. **(C,D)** Phenotype of the transgenic lines overexpressing *DREB3b*^{39Ref} and *DREB3b*^{39Del} with or without 100 mM NaCl treatment. The lengths of soybean hairy roots were obtained from at least seven roots. **(E–J)** DREB3b regulates the expression of salt stress-tolerant gene in soybean with or without 100 mM NaCl treatment. Experiment was performed using three biological replicates. The same lowercase letters above the histogram bars denote non-significant differences across the two panels ($P > 0.05$). One-way ANOVA was used to generate the *P*-values.

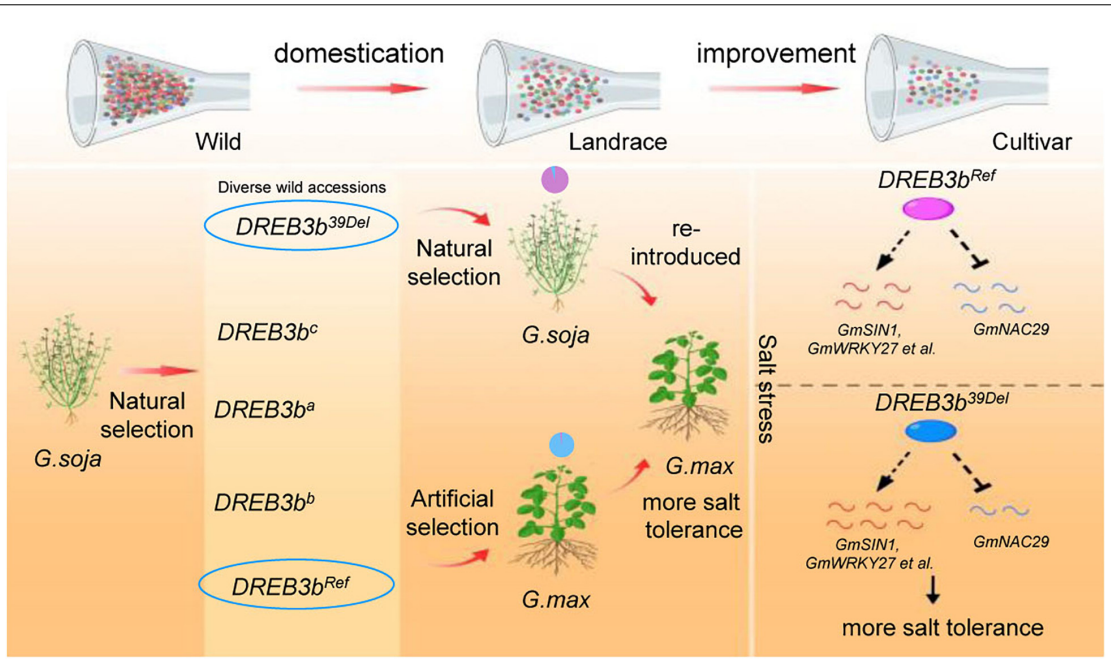

FIGURE 7 | Model of artificial selection in *DREB3b* in soybean and the underlying mechanism. A large number of potentially advantageous alleles were lost during domestication and cultivar improvement, resulting in lower salt tolerance of cultivated soybean than wild soybean. The *DREB3b*^{Ref} allele underwent artificial selection in cultivated soybean. The *DREB3b*^{Ref} allele reduced the salt tolerance of cultivated soybean. DREB3b up-regulates positive regulators of salt tolerance and down-regulates negative regulators of salt tolerance.

regulate the expression of these genes, we performed qRT-PCR analysis in *DREB3b*^{Ref}-overexpressing and *DREB3b*^{39Del}-overexpressing soybean hairy roots under mock and NaCl treatment (100 mM). *DREB3b*^{Ref} and *DREB3b*^{39Del} up-regulated the expression of the positive regulators of salt tolerance *SIN1*, *WRKY27*, and *WRKY54*, and down-regulated the expression of negative regulator of salt tolerance *NAC29*, but could regulate the expression of *WRKY12* and *SOS1* under mock and NaCl treatment (**Figures 6E–J**). Interestingly, the transcript levels of *SIN1*, *WRKY27* and *WRKY54* were higher in *DREB3b*^{39Del} soybean hairy roots than in *DREB3b*^{Ref} soybean hairy roots, and the transcript level of *NAC29* was lower in *DREB3b*^{39Del} soybean hairy roots than in *DREB3b*^{Ref} soybean hairy roots under NaCl treatment (**Figures 6E–J**). These results show that the *DREB3b*^{39Del} allele enhances salt tolerance more than the *DREB3b*^{Ref} allele in soybean.

Genetic markers are an important and effective tool for identifying mutant alleles in molecular-assisted studies, and could accelerate the genotyping procedure in future generations. We thus developed an InDel marker to identify the *DREB3b*^{39Del} allele. After PCR amplification using *DREB3b*-specific primers (**Supplementary Table 3**), the *DREB3b*^{Ref} allele produced 106-bp amplicons, whereas the *DREB3b*^{39Del} allele produced 100-bp amplicons, and the differences could be detected by electrophoresis (**Supplementary Figure 12**). We used this InDel marker to detect the genotypes of soybean accessions at random, and the results were consistent with the sequencing results (**Supplementary Figure 12** and **Supplementary Table 4**). Therefore, this InDel marker can be used to improve the breeding efficiency of salt tolerant soybean varieties in molecular breeding.

DISCUSSION

Soybean is a leguminous plant that is capable of closed flower fertilization (closed flower pollination). This feature may be helpful for maintaining genomic homogeneity and reducing genomic variation, which may have been further intensified by the domestication process (Lam et al., 2010). Due to bottlenecks and artificial selection, some genes that play important roles for adaptation to different environments have been lost during the soybean domestication process. Wild soybean (*Glycine soja*) may have high allelic diversity at certain loci, including advantageous alleles that can be re-introduced into domesticated soybeans via breeding to improve their adaption to the environment (Zhang et al., 2017). Consistent with a previous report (Lam et al., 2010), we show that the SNPs number of both landrace and improved cultivars were significantly lower than that of wild soybeans (**Figure 1B**), and wild soybeans have retained higher genetic diversity, but have been lost in cultivated soybeans (**Figure 1C**). We also show that the salt tolerance index of wild soybeans was much higher than that of improved cultivars (**Figures 1D,E**). These data indicate that a large number of useful alleles and genes from wild soybeans may be great significance for improving the salt tolerance of soybean. Importantly, to explore the variation in excellent alleles in wild soybeans, we combined genome-wide analysis

and RNA-sequencing and identified an excellent allele from wild soybean, which could be useful in breeding for improved salt tolerance in soybean.

Farmlands worldwide are increasingly affected by soil salinization, and most crops are sensitive to salt stress (Ren et al., 2005; Munns et al., 2012; An et al., 2017). Therefore, salt tolerance is an ecologically significant trait for crop breeding. Previous studies have confirmed that genetic variation in salt tolerance exists widely within and among major crops, providing an opportunity to use salt tolerance variation to improve crop salt tolerance (Wu et al., 2012; Qi et al., 2014; Zhang et al., 2018). For example, natural variation in *SALT3*/*CHX1*, a cation H^+ exchanger gene, could modulate salt tolerance in soybean (Guan et al., 2014; Qi et al., 2014). Moreover, the DREB family is one of the most important TF families in vascular plants, and DREB TFs are involved in salt stress responses (Li et al., 2005; Xu et al., 2011; Kudo et al., 2017; Ali and Hadi, 2018; Eckardt, 2019). For example, *DREBa*, *DREBb,* and *DREBc* are up-regulated under salt stress conditions (Li et al., 2005); GmDREB2, a soybean DRE-binding transcription factor, confers drought- and salt-tolerance in transgenic Arabidopsis and tobacco (*Nicotiana tabacum*) plants (Chen et al., 2007). However, the natural variation of *DREB* genes has not been examined in soybean. Here, we have identified one *DREB* gene in soybean, *DREB3b*, which conferred salt tolerance in soybean (**Figure 4B**). The molecular footprint showed strong selection at *DREB3b* during domestication (**Figure 5D**). The $DREB3b^{39Del}$ allele was highly abundant in wild soybeans (about 95%), and the $DREB3b^{Ref}$ allele was highly abundant in improve cultivar (about 98%, **Figure 5A**). Together, the data suggest that the DREB3bRef allele may have undergone artificial selection during domestication. We also demonstrate that, compared to $DREB3b^{Ref}$ overexpression, $DREB3b^{39Del}$ overexpression led to (i) better salt tolerance in soybean hairy root, and (ii) stronger up-regulation of positive regulators of salt tolerance and stronger down-regulation of a negative regulator of salt tolerance. Therefore, the loss of the $DREB3b^{39Del}$ allele in the domestication of improved cultivar may be a reason for its reduced salt tolerance.

Based on our data, we propose a model (**Figure 7**) describing how the artificial selection of the $DREB3b^{Ref}$ allele occurred in cultivated soybean, thereby reducing salt tolerance. According to this model, wild soybeans contain a large number of alleles in *DREB3b* but the $DREB3b^{Ref}$ allele underwent artificial selection in the domestication of cultivated soybean, resulting in the reduction of salt tolerance. Overexpression of *DREB3b* could improve salt tolerance by up-regulating positive regulators of salt tolerance and down-regulating negative regulators of salt tolerance.

DATA AVAILABILITY STATEMENT

The datasets presented in this study can be found in online repositories. The names of the repository/repositories and accession number(s) can be found at: NCBI BioProject, PRJNA797227.

AUTHOR CONTRIBUTIONS

QC and BL designed and interpreted the results. QC, BL, DZ, and NF coordinated the projects. QC, LD, FK, HD, TL, YC, YL, and ZH performed the experiments. LD, QC, YL, and ZH performed the data analysis. QC and ZH wrote the manuscript. WL revised the manuscript. All authors contributed to the article and approved the submitted version.

FUNDING

This work was supported by the National Natural Science Foundation of China (Grant Nos. 32090065 and 32001508 to LD, 32090064 and 31725021 to FK, 31930083 to BL, and 31901568 to QC) and the Major Program of Guangdong Basic and Applied Research (Grant No. 2019B030302006 to FK and BL).

SUPPLEMENTARY MATERIAL

The Supplementary Material for this article can be found online at: https://www.frontiersin.org/articles/10.3389/fpls.2022.821647/full#supplementary-material

Supplementary Figure 1 | Distribution of 103 *DREB* genes on 20 chromosomes in soybean.

Supplementary Figure 2 | Gene structures of 24 *DREB* genes. **(A)** Gene structures of up-regulated *DREB* genes. **(B)** Gene structures of down-regulated *DREB* genes. The exon-intron organization and UTRs of *DREB* genes were analyzed by aligning the DNA sequences using the GSDS 2.0 server (http://gsds.gao-lab.org/index.php). Introns and exons are shown as black lines and orange boxes, respectively. Green boxes at 5' and 3' ends represent untranslated regions (UTRs).

Supplementary Figure 3 | Boxplots for salt tolerance index based on the haplotypes of salt-induced *DREB* genes from the A-2 subgroup. The experiment was performed using two biological replicates. The same lowercase letters above the histogram bars denote non-significant differences across the two panels ($P > 0.05$). One-way ANOVA was used to generate the *P*-values.

Supplementary Figure 4 | Boxplots for salt tolerance index based on the haplotypes of salt-induced *DREB* gene from the A-3 subgroup. The experiment was performed using two biological replicates. The same lowercase letters above the histogram bars denote non-significant differences across the two panels ($P > 0.05$). One-way ANOVA was used to generate the *P*-values.

Supplementary Figure 5 | Boxplots for salt tolerance index based on the haplotypes of salt-induced *DREB* gene from the A-5 subgroup. The experiment was performed using two biological replicates. The same lowercase letters above the histogram bars denote non-significant differences across the two panels ($P > 0.05$). One-way ANOVA was used to generate the *P*-values.

Supplementary Figure 6 | Boxplots for salt tolerance index based on the haplotypes of salt-induced *DREB* genes from the A-6 subgroup. The experiment was performed using two biological replicates. The same lowercase letters above the histogram bars denote non-significant differences across the two panels ($P > 0.05$). One-way ANOVA was used to generate the *P*-values.

Supplementary Figure 7 | Haplotypes of *DREB3a* and *DREB3b*. **(A)** Haplotypes of *DREB3a.* **(B)** Haplotypes of *DREB3b.* Haplotype was extracted from the 1,295 panel of 146 wild soybeans, 575 landraces and 574 improved cultivars.

Supplementary Figure 8 | Comparison of the amino acid sequences of DREB3a, DREB3b and its homologs in plants. **(A)** Protein sequence comparisons of DREB3a alleles and its homologs in plants. **(B)** Protein sequence comparisons of DREB3b alleles and its homologs in plants.

Supplementary Figure 9 | Haplotype origins of *DREB3a* and *DREB3b*.

Supplementary Figure 10 | Boxplots for yield-related traits based on the haplotypes of *DREB3b* gene. **(A)** Flowering time. **(B)** Plant height. **(C)** 100-grain weight. One-tailed Student's *t*-test was used to generate the *P*-values.

Supplementary Figure 11 | Selective sweep in the *DREB3a* genomic region.

Supplementary Figure 12 | Development of functional genetic markers for $DREB3b^{Ref}$ and $DREB3b^{39Del}$ alleles. Lines 1–7, soybean plants harbor DREB3bRef allele. Lines 8–13, soybean plants harbor DREB3bRef allele.

REFERENCES

Ali, N., and Hadi, F. (2018). CBF/DREB transcription factor genes play role in cadmium tolerance and phytoaccumulation in *Ricinus communis* under molybdenum treatments. *Chemosphere* 208, 425–432. doi: 10.1016/j.chemosphere.2018.05.165

An, D., Chen, J. G., Gao, Y. Q., Li, X., Chao, Z. F., Chen, Z. R., et al. (2017). *AtHKT1* drives adaptation of *Arabidopsis thaliana* to salinity by reducing floral sodium content. *PLoS Genet*. 13:e1007086. doi: 10.1371/journal.pgen.1007086

Carter, T. E., Nelson, R., Sneller, C. H., and Cui, Z. (2004). *Soybeans: Improvement, Production and Uses*, 3rd Edn. Madison, WI: American Society of Agronomy. doi: 10.1016/j.agsy.2004.06.006

Chen, C., Chen, H., Zhang, Y., Thomas, H. R., Frank, M. H., He, Y., et al. (2020). TBtools: an integrative toolkit developed for interactive analyses of big biological data. *Mol. Plant* 13, 1194–1202. doi: 10.1016/j.molp.2020.06.009

Chen, M., Wang, Q. Y., Cheng, X. G., Xu, Z. S., Li, L. C., Ye, X. G., et al. (2007). *GmDREB2*, a soybean DRE-binding transcription factor, conferred drought and high-salt tolerance in transgenic plants. *Biochem. Biophys. Res. Commun*. 353, 299–305. doi: 10.1016/j.bbrc.2006.12.027

Chen, M., Xu, Z., Xia, L., Li, L., Cheng, X., Dong, J., et al. (2009). Cold-induced modulation and functional analyses of the DRE-binding transcription factor gene, *GmDREB3*, in soybean (*Glycine max* L.). *J. Exp. Bot*. 60, 121–135. doi: 10.1093/jxb/ern269

Eckardt, N. A. (2019). DREB duo defines distinct drought and cold response pathways. *Plant Cell* 31, 1196–1197. doi: 10.1105/tpc.19.00331

Essah, P. A., Davenport, R., and Tester, M. (2003). Sodium influx and accumulation in Arabidopsis. *Plant Physiol*. 133, 307–318. doi: 10.1104/pp.103.022178

Fehr, W. R., Caviness, C. E., Burmood, D. T., and Pennington, J. S. (1971). Stage of development descriptions for soybeans. *Crop Sci.* 11, 929–931. doi: 10.2135/cropsci1971.0011183x001100060051x

Flowers, T. J. (2004). Improving crop salt tolerance. *J. Exp. Bot*. 55, 307–319. doi: 10.1093/jxb/erh003

Gao, S. Q., Xu, H. J., Cheng, X. G., Chen, M., Xu, Z. S., Li, L. C., et al. (2005). Improvement of wheat drought and salt tolerance by expression of a stress-inducible transcription factor *GmDREB* of soybean (*Glycine max*). *Chin. Sci. Bull.* 50, 2714–2723. doi: 10.1360/982005-1234

Graham, P. H., and Vance, C. P. (2003). Legumes: importance and constraints to greater use. *Plant Physiol*. 131, 872–877. doi: 10.1104/pp.017004

Graham, T. L., Graham, M. Y., Subramanian, S., and Yu, O. (2007). RNAi silencing of genes for elicitation or biosynthesis of 5-deoxyisoflavonoids suppresses race-specific resistance and hypersensitive cell death in *Phytophthora sojae* infected tissues. *Plant Physiol*. 144, 728–740. doi: 10.1104/pp.107.097865

Guan, R., Qu, Y., Guo, Y., Yu, L., Liu, Y., Jiang, J., et al. (2014). Salinity tolerance in soybean is modulated by natural variation in *GmSALT3*. *Plant J*. 80, 937–950. doi: 10.1111/tpj.12695

Hymowitz, T. (1970). On the domestication of the soybean. *Econ. Bot*. 24, 408–421. doi: 10.1007/BF02860745

Hyten, D. L., Song, Q., Zhu, Y., Choi, I. Y., Nelson, R. L., Costa, J. M., et al. (2006). Impacts of genetic bottlenecks on soybean genome diversity. *Proc. Natl. Acad. Sci. U.S.A*. 103, 16666–16671. doi: 10.1073/pnas.0604379103

Kereszt, A., Li, D., Indrasumunar, A., Nguyen, C. D., Nontachaiyapoom, S., Kinkema, M., et al. (2007). *Agrobacterium rhizogenes*-mediated transformation of soybean to study root biology. *Nat. Protoc*. 2, 948–952. doi: 10.1038/nprot.2007.141

Kudo, M., Kidokoro, S., Yoshida, T., Mizoi, J., Todaka, D., Fernie, A. R., et al. (2017). Double overexpression of DREB and PIF transcription factors improves drought stress tolerance and cell elongation in transgenic plants. *Plant Biotechnol. J*. 15, 458–471. doi: 10.1111/pbi.12644

Lam, H. M., Xu, X., Liu, X., Chen, W., Yang, G., Wong, F. L., et al. (2010). Resequencing of 31 wild and cultivated soybean genomes identifies patterns of genetic diversity and selection. *Nat. Genet*. 42, 1053–1059. doi: 10.1038/ng.715

Li, S., Wang, N., Ji, D., Zhang, W., Wang, Y., Yu, Y., et al. (2019). A GmSIN1/GmNCED3s/GmRbohBs feed-forward loop acts as a signal amplifier that regulates root growth in soybean exposed to salt stress. *Plant Cell* 31, 2107–2130. doi: 10.1105/tpc.18.00662

Li, X. P., Tian, A. G., Luo, G. Z., Gong, Z. Z., Zhang, J. S., and Chen, S. Y. (2005). Soybean DRE-binding transcription factors that are responsive to abiotic stresses. *Theor. Appl. Genet*. 110, 1355–1362. doi: 10.1007/s00122-004-1867-6

Li, Y. H., Zhou, G., Ma, J., Jiang, W., Jin, L. G., Zhang, Z., et al. (2014). De novo assembly of soybean wild relatives for pan-genome analysis of diversity and agronomic traits. *Nat. Biotechnol*. 32, 1045–1052. doi: 10.1038/nbt.2979

Librado, P., and Rozas, J. (2009). DnaSP v5: a software for comprehensive analysis of DNA polymorphism data. *Bioinformatics* 25, 1451–1452. doi: 10.1093/bioinformatics/btp187

Liu, X. X., Chang, R. Z., Guan, R. X., and Qiu, L. J. (2020). Establishment of screening method for salt tolerant soybean at emergence stage and screening of tolerant germplasm. *Acta Agron. Sin*. 46, 1–8. doi: 10.3724/SP.J.1006.2020.94062

Lu, S., Dong, L., Fang, C., Liu, S., Kong, L., Cheng, Q., et al. (2020). Stepwise selection on homeologous *PRR* genes controlling flowering and maturity during soybean domestication. *Nat. Genet*. 52, 428–436. doi: 10.1038/s41588-020-0604-7

Machado, F. B., Moharana, K. C., Almeida-Silva, F., Gazara, R. K., Pedrosa-Silva, F., Coelho, F. S., et al. (2020). Systematic analysis of 1298 RNA-Seq samples and construction of a comprehensive soybean (*Glycine max*) expression atlas. *Plant J*. 103, 1894–1909. doi: 10.1111/tpj.14850

Munns, R., Day, D. A., Fricke, W., Watt, M., Arsova, B., Barkla, B. J., et al. (2020). Energy costs of salt tolerance in crop plants. *New Phytol*. 225, 1072–1090. doi: 10.1111/nph.15864

Munns, R., James, R. A., Xu, B., Athman, A., Conn, S. J., and Jordans, C. (2012). Wheat grain yield on saline soils is improved by an ancestral Na^+ transporter gene. *Nat. Biotechnol*. 30, 360–364. doi: 10.1038/nbt.2120

Munns, R., and Tester, M. (2008). Mechanisms of salinity tolerance. *Annu. Rev. Plant Biol*. 59, 651–681. doi: 10.1146/annurev.arplant.59.032607.092911

Papiernik, S. K., Grieve, C. M., Lesch, S. M., and Yates, S. R. (2005). Effects of salinity, imazethapyr, and chlorimuron application on soybean growth and yield. *Commun. Soil Sci. Plant Anal*. 36, 951–967. doi: 10.1081/CSS-200050280

Parker, M. B., Gascho, G. J., and Gaines, T. P. (1983). Chloride toxicity of soybeans grown on Atlantic coast flatwoods soils. *Agron. J*. 75, 439–443. doi: 10.2134/agronj1983.00021962007500030

Qi, X., Li, M. W., Xie, M., Liu, X., Ni, M., Shao, G., et al. (2014). Identification of a novel salt tolerance gene in wild soybean by whole-genome sequencing. *Nat. Commun*. 5:4340. doi: 10.1038/ncomms5340

Qiu, L. J., Xing, L. L., Guo, Y., Wang, J., Jackson, S. A., and Chang, R. Z. (2013). A platform for soybean molecular breeding: the utilization of core collections for food security. *Plant Mol. Biol*. 83, 41–50. doi: 10.1007/s11103-013-0076-6

Ren, Z. H., Gao, J. P., Li, L. G., Cai, X. L., Huang, W., and Chao, D. Y. (2005). A rice quantitative trait locus for salt tolerance encodes a sodium transporter. *Nat. Genet*. 37, 1141–1146. doi: 10.1038/ng1643

Sakuma, Y., Liu, Q., Dubouzet, J. G., Abe, H., Shinozaki, K., and Yamaguchi-Shinozaki, K. (2002). DNA-binding specificity of the ERF/AP2 domain of *Arabidopsis* DREBs, transcription factors involved in dehydration- and cold-inducible gene expression. *Biochem. Biophys. Res. Commun*. 290, 998–1009. doi: 10.1006/bbrc.2001.6299

Ondrasek, G., Rengel, Z., Veres, S. (2011). "Soil salinisation and salt stress in crop production," in *Abiotic Stress in Plants: Mechanisms and Adaptations*, eds A. K. Shanker and B. Venkateswarlu (Rijeka: INTECH Press), 171–190. doi: 10.5772/22248

Shi, W. Y., Du, Y. T., Ma, J., Min, D. H., Jin, L. G., Chen, J., et al. (2018). The WRKY transcription factor GmWRKY12 confers drought and salt tolerance in soybean. *Int. J. Mol. Sci*. 19:4087. doi: 10.3390/ijms19124087

Wang, F., Chen, H. W., Li, Q. T., Wei, W., Li, W., Zhang, W. K., et al. (2015). GmWRKY27 interacts with GmMYB174 to reduce expression of *GmNAC29* for stress tolerance in soybean plants. *Plant J.* 83, 224–236. doi: 10.1111/tpj.12879

Wu, H. J., Zhang, Z., Wang, J. Y., Oh, D. H., Dassanayake, M., Liu, B., et al. (2012). Insights into salt tolerance from the genome of *Thellungiella salsuginea*. *Proc. Natl. Acad. Sci. U.S.A.* 109, 12219–12224. doi: 10.1073/pnas.1209954109

Xu, Z. S., Chen, M., Li, L. C., and Ma, Y. Z. (2011). Functions and application of the AP2/ERF transcription factor family in crop improvement. *J. Integr. Plant Biol.* 53, 570–585. doi: 10.1111/j.1744-7909.2011.01062.x

Zhang, H., Li, Y., and Zhu, J. K. (2018). Developing naturally stress-resistant crops for a sustainable agriculture. *Nat. Plants* 4, 989–996. doi: 10.1038/s41477-018-0309-4

Zhang, H., Song, Q., Griffin, J. D., and Song, B. H. (2017). Genetic architecture of wild soybean (*Glycine soja*) response to soybean cyst nematode (*Heterodera glycines*). *Mol. Genet. Genomics* 292, 1257–1265. doi: 10.1007/s00438-017-1345-x

Zhou, Q. Y., Tian, A. G., Zou, H. F., Xie, Z. M., Lei, G., Huang, J., et al. (2008). Soybean WRKY-type transcription factor genes, *GmWRKY13*, *GmWRKY21*, and *GmWRKY54*, confer differential tolerance to abiotic stresses in transgenic *Arabidopsis* plants. *Plant Biotechnol. J.* 6, 486–503. doi: 10.1111/j.1467-7652.2008.00336.x

Zhou, Y., Chen, M., Guo, J., Wang, Y., Min, D., Jiang, Q., et al. (2020a). Overexpression of soybean *DREB1* enhances drought stress tolerance of transgenic wheat in the field. *J. Exp. Bot.* 71, 1842–1857. doi: 10.1093/jxb/erz569

Zhou, Y. X., Zhou, W., Liu, H., Liu, P., and Li, Z. G. (2020b). Genome-wide analysis of the soybean *DREB* gene family: identification, genomic organization and expression profiles in response to drought stress. *Plant Breed.* 139, 1158–1167. doi: 10.1111/pbr.12867

Zhu, J. K. (2001). Cell signaling under salt, water and cold stresses. *Curr. Opin. Plant Biol.* 4, 401–406. doi: 10.1016/s1369-5266(00)00192-8

Conflict of Interest: YC is employed by Beijing Zhongnong Futong Horticulture Co., Ltd.

The remaining authors declare that the research was conducted in the absence of any commercial or financial relationships that could be construed as a potential conflict of interest.

Publisher's Note: All claims expressed in this article are solely those of the authors and do not necessarily represent those of their affiliated organizations, or those of the publisher, the editors and the reviewers. Any product that may be evaluated in this article, or claim that may be made by its manufacturer, is not guaranteed or endorsed by the publisher.

Copyright © 2022 Hou, Li, Cheng, Li, Li, Du, Kong, Dong, Zheng, Feng, Liu and Cheng. This is an open-access article distributed under the terms of the Creative Commons Attribution License (CC BY). The use, distribution or reproduction in other forums is permitted, provided the original author(s) and the copyright owner(s) are credited and that the original publication in this journal is cited, in accordance with accepted academic practice. No use, distribution or reproduction is permitted which does not comply with these terms.

frontiers in Plant Science

ORIGINAL RESEARCH
published: 16 March 2022
doi: 10.3389/fpls.2022.848893

Shade-Tolerant Soybean Reduces Yield Loss by Regulating Its Canopy Structure and Stem Characteristics in the Maize–Soybean Strip Intercropping System

Bin Cheng[1,2,3†], Li Wang[1,2,4†], Ranjin Liu[3,5†], Weibing Wang[6], Renwei Yu[6], Tao Zhou[7], Irshan Ahmad[1,2,4], Ali Raza[8], Shengjun Jiang[9], Mei Xu[1,2,4], Chunyan Liu[1,2,4], Liang Yu[1,2,4], Wenyan Wang[1,2,4], Shuzhong Jing[3,5], Weiguo Liu[1,2,4]* and Wenyu Yang[1,2,4]*

[1] College of Agronomy, Sichuan Agricultural University, Chengdu, China, [2] Sichuan Engineering Research Center for Crop Strip Intercropping System, Chengdu, China, [3] Chengdu Da Mei Seeds Co., Ltd., Chengdu, China, [4] Key Laboratory of Crop Ecophysiology and Farming System in Southwest, Ministry of Agriculture, Chengdu, China, [5] Crop Research Institute, Sichuan Academy of Agricultural Sciences, Chengdu, China, [6] Quxian Agricultural and Rural Bureau, Dazhou, China, [7] State Key Laboratory of Southwestern Chinese Medicine Resources, Chengdu University of Traditional Chinese Medicine, Chengdu, China, [8] CAS Key Laboratory of Mountain Ecological Restoration and Bioresource Utilization, Ecological Restoration Biodiversity Conservation Key Laboratory of Sichuan Province, Chengdu Institute of Biology, Chinese Academy of Sciences, Chengdu, China, [9] Chuanshanqu Agricultural and Rural Bureau, Suining, China

The shading of maize is an important factor, which leads to lodging and yield loss of soybean in the maize–soybean strip intercropping system, especially in areas with low solar radiation. This study was designed to explore how shade-tolerant soybean reduces yield loss by regulating its canopy structure and stem characteristics in the maize–soybean strip intercropping system. The soybean cultivars Tianlong No.1 (TL-1, representative of shade-tolerant plants) and Chuandou-16 (CD-16, representative of shade-intolerant plants) were grown in monocropping and intercropping systems from 2020 to 2021 in Chongzhou, Sichuan, China. Regardless of shade-intolerant or shade-tolerant soybean, the canopy and stem of soybean in strip intercropping were weaker than those of the corresponding monoculture. But compared with shade-intolerant soybean, the shade-tolerant soybean slightly changed its spatial structure of canopy and stem morphology and physiology in maize–soybean strip intercropping system, especially in the later growth stages. On the one hand, the canopy of shade-tolerant soybean showed relatively high transmission coefficient (TC) and relatively low leaf area index (LAI) and mean leaf angle (MLA). On the other hand, the stem of shade-tolerant soybean was obviously stronger than that of shade-intolerant soybean in terms of external morphology, internal structure, and physiological characteristics. Additionally, compared with shade-intolerant soybean, shade-tolerant soybean showed higher APnWP (the average net photosynthetic rate of the whole plant) and seed yield in the strip intercropping. The results showed that shade-tolerant soybean increased light energy capture and photosynthesis in the different canopy levels to promote the morphological and physiological development of the stem and ultimately reduce the

OPEN ACCESS

Edited by:
Raul Antonio Sperotto,
Universidade do Vale do Taquari (UNIVATES), Brazil

Reviewed by:
Fábio Luiz Partelli,
Federal University of Espirito Santo, Brazil
Paul F. Devlin,
Royal Holloway, University of London, United Kingdom
Budiastuti Kurniasih,
Gadjah Mada University, Indonesia
Oqba Basal,
University of Debrecen, Hungary

***Correspondence:**
Shuzhong Jing
155650836@qq.com
Weiguo Liu
lwgsy@126.com

[†] These authors have contributed equally to this work

Specialty section:
This article was submitted to Crop and Product Physiology, a section of the journal Frontiers in Plant Science

Received: 05 January 2022
Accepted: 17 February 2022
Published: 16 March 2022

Citation:
Cheng B, Wang L, Liu R, Wang W, Yu R, Zhou T, Ahmad I, Raza A, Jiang S, Xu M, Liu C, Yu L, Wang W, Jing S, Liu W and Yang W (2022) Shade-Tolerant Soybean Reduces Yield Loss by Regulating Its Canopy Structure and Stem Characteristics in the Maize–Soybean Strip Intercropping System. Front. Plant Sci. 13:848893. doi: 10.3389/fpls.2022.848893

yield loss of the strip intercropping system. However, the molecular mechanism of low radiation regulating soybean canopy structure (LAI, TC, and MLA) needs further in-depth research to provide theoretical guidance for cultivating plants with ideal canopy shape that can adapt to changing light environment in intercropping system.

Keywords: canopy structure, intercropping, lodging, soybean, photosynthesis

INTRODUCTION

Intercropping of maize (*Zea mays* L.) and soybean (*Glycine max* L.) has been practiced on a large scale in the world, especially in China (Du et al., 2018; Iqbal et al., 2019). This planting pattern can harvest an extra-season of soybean seeds without reducing the yield or slightly reducing the yield of maize (Hussain et al., 2020a). However, soybean plants suffer severe shading stress from maize during the intergrowth in maize–soybean intercropping systems (Zhou et al., 2019a,b; Hussain et al., 2020b), which reduces the red-to-far-red ratio of light inside the soybean canopy (Yang et al., 2014, 2020; Fan et al., 2018). These plants in this shaded environment show strong shade avoidance responses, which include reduced stem thickness, longer stem length, and petiole length and also lower photosynthetic capacity and biomass (Yang et al., 2014; Liu et al., 2016; Fan et al., 2018). In the maize–soybean strip intercropping system, similar shade avoidance responses occur in the middle and later stages of growth, which results in lodging and yield loss of soybean (Chen et al., 2020). Fortunately, the phenotypes and physiology of soybean cultivars with a different shade tolerance have corresponding shade-avoiding strategies and plasticity under shade stress.

Light is one of the essential abiotic factors for crop growth, and its intensity and quality (spectral composition) can regulate the spatial structure of canopy and photosynthesis of leaves (Huber et al., 2021; Paradiso and Proietti, 2021). In the low radiation or shading environment, the net photosynthetic rate (Pn) of soybean decreases due to the reduction in light energy captured by the soybean canopy (Yang et al., 2020), which results in the decrease of photosynthate in the whole plant (Liu et al., 2006; Fan et al., 2018). However, because of the different overlapping degrees of leaves at different canopy levels, the photosynthetic capacity of leaves at the corresponding canopy levels is also different (Jiang et al., 1993). Compared with the leaves inside the canopy, those leaves exposed to the outside can receive more light radiation (Klich, 2000), which results in an increase in Pn of leaves (Zhou et al., 2019a,b). In addition, the Pn of soybean leaves decreases with the increase in self-shading degrees, among which the Pn of the lower leaves decreases faster, which results in the accelerated aging and shedding of the lower leaves and consequently yield loss (Miyaji and Tagawa, 1979). However, the soybean cultivars differ significantly in Pn in different environments (Dornhoff and Shibles, 1970), especially in a shady environment (Hussain et al., 2020b).

The canopy spatial structure of crops can be quantitatively visualized by leaf area index (LAI), transmission coefficient (TC) and mean leaf angle (MLA). The LAI, as an important indicator of crop development, can be used to show different canopy structures (Kross et al., 2015) and plant foliage density (Walthall et al., 2004). The TC is closely related to the content and composition of pigments in the crop canopy, which can be used to comprehend spatial and temporal dynamics of photosynthetically active radiation (PAR), photosynthesis, and vegetation productivity (Gitelson et al., 2019). Increasing the MLA in the upper canopy can increase the interception of PAR (IPAR), which improves lodging resistance of stalk while increasing grain yield of maize (Xue et al., 2021). In addition, soybean cultivars with a different shade tolerance show different shade avoidance responses in intercropping systems, especially in canopy spatial structure (Gong et al., 2015). Based on the above understanding, how to improve the canopy structure of intercropping soybean to intercept more light energy has become the focus of many scholars (Keating and Carberry, 1993; Feng et al., 2018, 2019; Ren et al., 2021). Consequently, in the maize–soybean strip intercropping system, what are relationships between the spatial structure of soybean canopy and the establishment of plant morphological structure and the formation of seed yield?

Regardless of the aggravation of shade degree or long-term exposure to shade, plant is prone to lodging under the external forces such as wind (Liu et al., 2019; Hussain et al., 2020a). The phenotype and physiology of stems change when plants are subjected to shade stress, such as slender stems and lower content of structural carbohydrates (Liu et al., 2019; Hussain et al., 2021). Some studies showed that the stem strength of soybean was negatively correlated with lodging, but positively correlated with lignin content (LC) and the activity of phenylalanine ammonia lyase (PAL) and 4-coumaric acid: CoA-ligase (4CL) (Cheng et al., 2020). Cotton (Chen et al., 2014) and soybean (Liu et al., 2019) had lower LC in stems, which results in a decrease in lodging resistance index (LRI) of plants, which in turn increased lodging risk. In addition, the characteristics of stem anatomical structure are closely related to the LRI of plant stems (Hussain et al., 2021). Moreover, intercropping with low-light environment makes soybean stem slender, and the areas of xylem, phloem, and pith decrease, which further leads to the decrease of stem strength (Liu et al., 2019). However, the characteristics of stem anatomical structure are different in different soybean cultivars (Yao et al., 2018). In short, high-strength stem can reduce the lodging risk and yield loss of soybean in low-light environment.

Soybean morphology changes significantly in shading environment, which is used to describe by shading-tolerance coefficient (STC) (Li et al., 2014). The plant height (PH), stem diameter (SD), seed yield, branch, and canopy structure can be regarded as the target trait of soybean (Chen et al., 2003). Moreover, the comprehensive shading-tolerance coefficient (CSTC) is used to carefully and objectively evaluate the shade tolerance of soybean in intercropping systems (Li et al., 2014).

In this study, Tianlong No. 1 (TL-1) with high yield and Chuandou-16 (CD-16) with low yield represent shade-tolerant and shade-intolerant soybean cultivars, respectively, which had been proved by the previous research (Zhao et al., 2014; Cheng et al., 2020). The suitable density (20 plants/m^2) with higher yield was selected for this study, according to the previous research (Cheng et al., 2020, 2021). Additionally, the strip intercropped soybean in this study was shaded by maize, which results in lodging after 49 days of sowing (V5 stage), which was proved by early study (Cheng et al., 2020, 2021). The objectives of this study are to explore how shade-tolerant soybean reduces yield loss by regulating its spatial structure of canopy and stem characteristics in the maize–soybean strip intercropping system. The results can provide theoretical reference for phenotypic modeling and soybean breeding research in maize–soybean intercropping systems.

MATERIALS AND METHODS

Site Description

The experiment was conducted from 2020 to 2021 at Chongzhou experimental site of Sichuan Agricultural University, Sichuan, China (30°33′N, 103°39′E). The daily average maximum and minimum temperature from sowing to harvest were 27.0 and 19.0°C in 2020, respectively (**Figure 1A**). The daily average maximum and minimum temperature from sowing to harvest were 26.8 and 17.8°C in 2021, respectively (**Figure 1B**). The annual sunshine and precipitation were 1,161.5 h and 1,012.4 mm, respectively. The field soil was a light loam with pH 7.1, 24.3 g/kg organic matter, 1.6 g/kg total N, 1.3 g/kg total P, 15.2 g/kg total K, 299.5 mg/kg available-P, and 169.4 mg/kg available-K.

Experimental Design

The field experiment was conducted using the two-factor randomized block design, with planting patterns (maize–soybean strip intercropping and monocropping) as the main factor whereas soybean cultivars as the secondary factor. The variety of maize was zhenghong-505 (ZH-505, semicompact plant) and soybean cultivars included Chuandou-16 (CD-16, shade-intolerant plant) and Tianlong No. 1 (TL-1, shade-tolerant plant). The classical wide and narrow row planting was adopted in maize–soybean strip intercropping system (Yang et al., 2014; Cheng et al., 2020), with 2 m of each strip width and 6 m of each strip length (**Figures 2A,C**). Regardless of strip intercropping or monoculture, the planting density of TL-1 and CD-16 was 20 plants/m^2, and the planting density of ZH-505 was 10 plants/m^2. In the monocropping system, the same planting way as strip intercropping soybean without maize strip was conducted as the control (**Figures 2B,D**). The maize and soybean with few differences in growth period were directly broadcast in the field in the form of seeds. The area of each individual treatment plot was 12 m^2 for both strip intercropping and monocropping, with a row × plant spacing of 40 cm × 20 cm for maize and a row × plant spacing of 40 cm × 10 cm for soybean. Each treatment that includes six biological repetitions was randomly planted in the whole experimental field. As base fertilizer for maize, 80 g/m^2 of compound fertilizer (N: P: K = 15: 15: 15) was applied before sowing. The urea ($N \geq 46\%$) of 7.8 g/m^2 and 13.2 g/m^2 was applied at jointing stage and heading stage, respectively (Cheng et al., 2020), whereas soybean did not apply fertilizer in the whole growth period because of fertile experimental site.

Sampling Time and Measurements

After 35 days of sowing, the samples of nine soybean plants with uniform and continuous growth for each treatment were collected every 14 days until harvest, with a total of five times. These samples were used for physiological and biochemical analyses. The collecting data information included the lodging rate (LR), LRI, PH, SD, LC, and activity of 4CL and PAL, canopy structure parameters that include LAI, MLA, and TC. Additionally, the Pn of the inverted trifoliate (PnIT, net photosynthetic rate), the average Pn of the whole plant (APnWP), and also stem anatomical structure that includes vascular, phloem, xylem, and pith were measured at R1 stage (early blooming stage). Grain yield and yield composition that include seed yield, full-pods, non-full-pods, and branches were measured at mature stage.

Lodging Rate and Lodging Resistance Index

Lodging rate (Eq. 1) was calculated by randomly investigating a soybean strip without damage for each treatment according to the previous method (Cheng et al., 2020). LRI (Eq. 2) from the third to fifth internodes at the base of soybean stem, as an important and comprehensive stem strength index, was measured as reported earlier (Hussain et al., 2020a,b).

$$LR\,(\%) = \frac{TNLSP}{TNSP} * 100 \quad (1)$$

where the LR represents the lodging rate of soybean in a plot, the TNLPP represents the total number of lodging soybeans in a plot, and the TNPP represents the total number of soybeans in a plot.

$$LRI = \frac{SBR}{MSL * AGW} \quad (2)$$

where the LRI represents the lodging resistance index of soybean stem, SBR represents soybean stem bending resistance, the MSL represents the main stem length of soybean, and the AGW represents the above-ground biomass fresh weight of soybean.

Leaf Area Index, Mean Leaf Angle, and Transmission Coefficient

The LAI, MLA, and TC of soybean canopy of each treatment were measured by Digital Plant Canopy Imager (CI-110, Zealquest Scientific Technology Co., Ltd., China), which measured four uniform measuring points in every treatment between two rows of soybean and took three more diagonal cells for repetition.

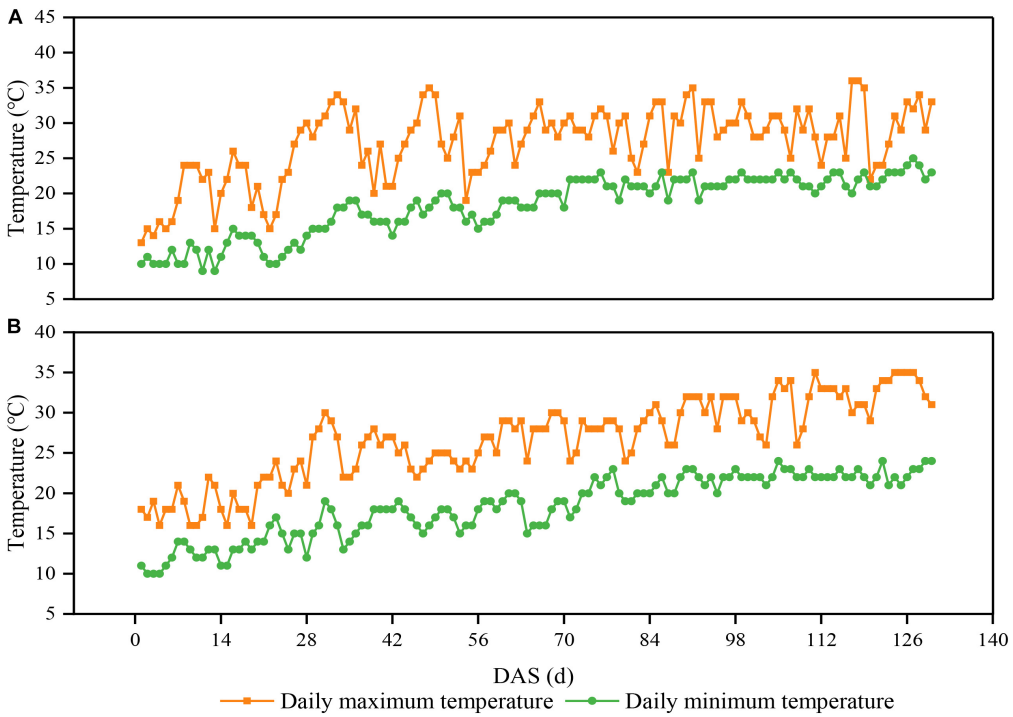

FIGURE 1 | Daily maximum and minimum temperatures above the soybean canopy from sowing to harvest in 2020 **(A)** and 2021 **(B)** in Chongzhou, Sichuan, China. Orange lines and boxes represent the daily maximum temperature, whereas green lines and circles represent the daily minimum temperature. DAS represents the number of days after sowing.

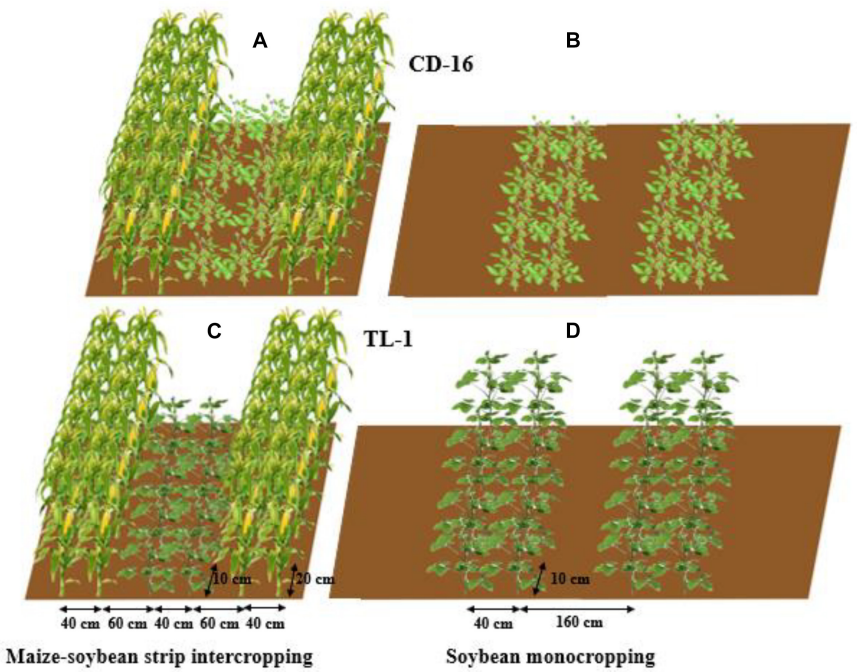

FIGURE 2 | The patterns of maize–soybean strip intercropping system **(A,C)** and monoculture **(B,D)** in 2020 and 2021. Regardless of Chuandou-16 (CD-16) **(A,B)** or Tianlong NO. 1 (TL-1) **(C,D)**, the soybean plant spacing is 10 cm and the row spacing is 40 cm. The maize plant spacing is 20 cm and the row spacing is 40 cm. In monoculture, the row spacing between each soybean strip is 160 cm.

Pn of the Inverted Trifoliate and Average Net Photosynthetic Rate of the Whole Plant

Between 9:00 a.m. to 11:00 a.m. on a sunny day, the PnIT and APnWP were measured with the portable photosynthetic analyzer LI-COR 6400 (Li-Cor Inc., Lincoln, NE, United States) at R1 stage of soybean. Totally, five plants with uniform growth were selected from each treatment and three repetitions, according to the earlier reported research (Cheng et al., 2020).

Vascular, Phloem, Xylem, and Pith of Soybean

The stem anatomical structure that includes vascular, phloem, xylem, and pith were measured according to the previous method (Rajput et al., 2018) with slight modification. The third internode of soybean stem was kept in FAA fixing solution for one month to soften. According to the following **Table 1**, the stem samples were dehydrated and transparent. Next, the stem samples were processed according to the following steps. ① Soaking wax: the paraffin wax (melting point: 57–63°C) was put into a beaker and melted it in a water bath pan (DXY-5H, Shenzhen Dingxinyi Experimental equipment Co., Ltd., China), in which the samples were soaked for about 8 h. ② Slicing: the wax block with stem samples was fixed on the slicer (RM 2245, Leica Microsystems Ltd., Wetzlar, Germany), and the slice thickness was set to 10 μm and sliced automatically (the blade was changed frequently). ③ Exhibition: the cut samples were unfolded in a water bath pan (40°C), then placed on the slide glass (marked), and put the slide glass on the baking machine (HI 1210, Leica Microsystems Ltd., Germany) at 40°C for drying. ④ Dewaxing: in a ventilated place, the slide glasses containing the samples were dissolved in a container containing xylene for 30 min and dried. ⑤ Dyeing: the safranin was dropped on the stem samples for 10 min, slowly removed by distilling water, and dried naturally. Then, the fixed o-fast green dye was dropped on the treated samples for 10 s, slowly removed by distilling water, and dried naturally. ⑥ Decolorization and observation: the slide glasses containing the samples were put in 75% alcohol to remove the residual dye and observed with a microscope (M205 FA, Leica Microsystems Ltd., Wetzlar Germany) after dried naturally. The final result is shown in **Figure 3**.

Seed Yield and Yield Composition

A total of 15 soybean plants with uniform and continuous growth were selected for each treatment. The number of full-pods, non-full-pods, and branches per plant, and also grain yield per unit area of soybean, were measured after natural drying. Likewise, 15 maize plants with uniform and continuous growth after natural drying were selected to measure grain yield per unit area.

TABLE 1 | Proportion of mixed chemical reagents and treatment time.

Mixed chemical reagent	Time
50% ethanol + 50% distilled water	6 h
50% ethanol + 30% *n*-butanol + 20 distilled water	5 h
40% ethanol + 50% *n*-butanol + 10% distilled water	4 h
30% ethanol + 80% *n*-butanol	3 h
10% ethanol + 90% *n*-butanol	2 h
100% *n*-butanol	1 h

Plant Height, Stem Diameter, Lignin Content, and Activity of 4CL and Phenylalanine Ammonia Lyase

The stem length of soybean plant was regarded as PH, which was measured with flexible rule. The SD in the middle of the third internode of the stem was measured with the Vernier caliper. The LC, 4CL, and PAL from the third to fifth internode of the stem were determined by the test kits (Lignin, 4CL and PAL Test Kits, Suzhou Grace Biotechnology Co., Ltd., China) according to the previous methods (Cheng et al., 2020).

The Shading-Tolerance Coefficient and Comprehensive Shading-Tolerance Coefficient

Shading-tolerance coefficient (Eq. 3) was used to describe the changes in target traits value of soybean between intercropping and monocropping, respectively. The CSTC (Eq. 4) was used to objectively evaluate the shade tolerance of soybean in intercropping systems (Li et al., 2014).

$$STC_j = 1 - \frac{|TTV_i - TTV_m|}{TTV_m} \quad (3)$$

where the STC represents shading-tolerance coefficient. The j represents different target traits of soybean. The TTV_i and TTV_m represent target traits value of soybean in monocropping and intercropping, respectively. When the value of STC is large, which means the target trait of soybean is less affected by shading; otherwise, it is more affected by shading.

$$CSTC = \frac{1}{n}\sum_{j=1}^{n} STC_j \quad (4)$$

where the CSTC represents CSTC. The n represents the number of target character of soybean. The j represents different target traits of soybean. When the value of CSTC is large, which means in the low-light environment, soybean shows a strong shade tolerance; otherwise, it possesses a weak shade tolerance (Liang and Li, 2004; Li et al., 2014).

Statistical Analysis of Data and Graphing

All data were collected and stored by Microsoft Excel 2019 software. The Adobe Photoshop 2020 software was used to draw the maize and soybean plants and image typesetting. The Image Pro Plus software was used to process and calculate the areas of stem cross-section, vascular, phloem, xylem, and pith, etc. The LRI, LC, Pn, and the areas of stem cross-section, vascular, phloem, xylem, and pith and also seed yield, full-pods, non-full-pods, and branches were subjected to two-way ANOVA using the Origin Pro 2021 software. Significant differences among means of

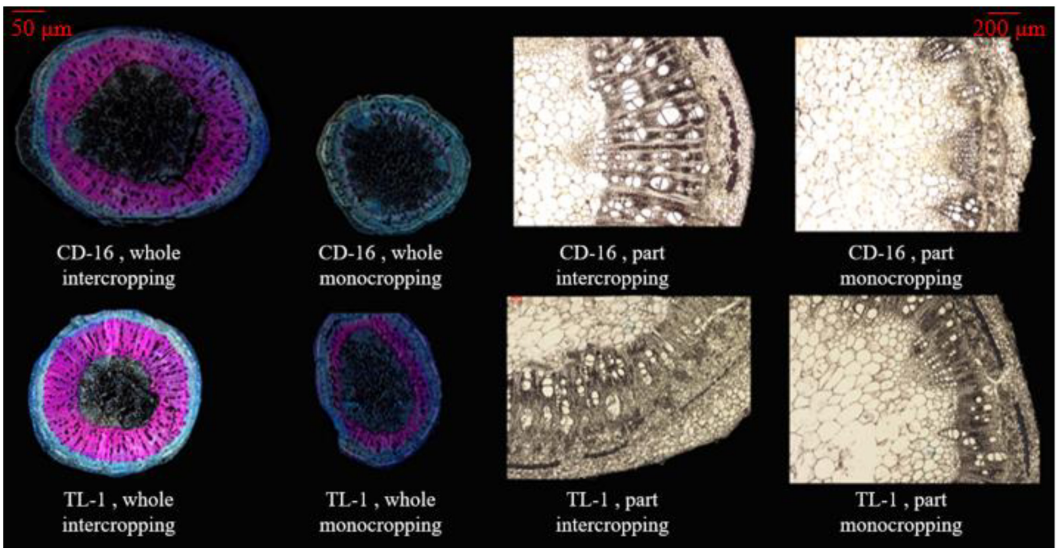

FIGURE 3 | The anatomical structure of soybean stem, whole section **(left)**, and local section **(right)**. The xylem in the stem is dyed pink by turning safranin, using to characterize the LC. The phloem in the stem is dyed light blue by fixed o-fast green dye, using to characterize the cellulose content. In the local section, the white bundle structure is the vascular bundle.

every treatment were separated according to Fisher's LSD at the level of $p \leq 0.05$. The *t*-test at $p \leq 0.05$ was applied for correlation analysis. The LR, PH, SD LAI, MLA, and TC were subjected to one-way ANOVA to assess the effects of shading of maize and variety difference in this study.

RESULTS

Seed Yield and Yield Composition

In the strip intercropping condition, the seed yield, the number of full-pods, and branches of CD-16 and TL-1 were significantly lower than those of monoculture, whereas the number of non-full-pods was the opposite (**Table 2**). The seed yield of TL-1 was 13.5% higher than that of CD-16 in the monocropping, whereas 21.8% higher than that of CD-16 in the strip intercropping (average of 2 years) (**Table 2**). A number of full-pods, non-full-pods, and branches of TL-1 were 16.6, 17.0, and 9.0% higher than those of CD-16, respectively, in the monocropping (**Table 2**). Similarly, in the strip intercropping, a number of full-pods, non-full-pods, and branches of TL-1 were 26.6, 22.4, and 29.6% higher than those of CD-16, respectively (**Table 2**). However, there was no significant difference between monoculture and intercropping in maize yield. The result showed that, compared with CD-16, the low decrease in grain yield of TL-1 in strip intercropping was due to its relatively high the number of full-pods and branches.

Lodging Rate and Lodging Resistance Index

Different soybean cultivars and planting patterns had significant impacts on LR (**Figure 4A**) and LRI (**Figure 4B**) of soybean. We noticed that whether CD-16 or TL-1, the lodging only occurred in the strip intercropping system, and with the development of soybean and maize growth, the LR increased continuously (**Figure 4B**). However, the LR of TL-1 was significantly lower than that of CD-16 (38.2% lower on average), and the lodging time of TL-1 in the field was approximately 14 days later than that of CD-16 (**Figure 4B**). To explain these phenomena, we further measured the LRI of soybean and found that the LRI of soybean in the strip intercropping was significantly lower than that of monocropping regardless of CD-16 or TL-1 (**Figure 4A**). Furthermore, the LRI of TL-1 was 30.0% lower than that of CD-16 in monocropping; however, but it was 15.1% higher than that of CD-16 in the strip intercropping (**Figure 4A**). This phenomenon could be explained according to the Eq. 2. Consequently, in the maize–soybean strip intercropping system, TL-1, a shade-tolerant plant, had relatively strong stem strength compared with CD-16, which was beneficial to maintain the upright growth of the plant.

Canopy Structure of Soybean

There was no significant difference in the LAI between TL-1 and CD-16 before soybean shaded by maize (0–49 days after sowing) in the strip intercropping (**Figures 5A,B**). Thereafter, the LAI of TL-1 was significantly lower than that of CD-16 during the whole later growth period of soybean, irrespective of the cropping system (**Figures 5A,B**). Notably, the LAI of TL-1 in the monocropping was 20.01% lower than that of CD-16, whereas that of TL-1 in the strip intercropping was only 16.0% lower than that of CD-16 (average of the last four sampling times). Additionally, the peak time of LAI of TL-1 and CD-16 in strip intercropping (63 days after sowing) was approximately 14 days earlier than that in monoculture (77 days after sowing), due to the shading stress of maize on soybean (**Figures 5A,B**).

Irrespective of the cropping system, the TC of TL-1 was significantly higher than that of CD-16 during the whole growth

TABLE 2 | The seed yield and composition of soybean and maize yield response to soybean cultivars and patterns in 2020 and 2021.

Years	Treatments		Soybean				Maize
			Seed yield	Full-pods	Non-full-pods	Branches	Seed yield
			g/m^2	Numbers/plant	Numbers/plant	Numbers/plant	g/m^2
2020	Inter.	CD-16	119.72^d	23.00^d	12.67^b	1.33^d	1248^a
		TL-1	163.86^c	31.33^c	16.33^a	1.89^c	1260^a
		P_{SV}	**	**	**	**	n.s.
	Mono.	CD-16	288.21^b	61.33^b	7.67^d	4.33^b	1105^a
		TL-1	323.86^a	73.51^a	9.24^c	4.76^a	
		P_{SV}	*	**	**	**	–
	P_{PP}		*	**	**	**	–
	P_{SV*PP}		**	**	*	*	–
2021	Inter.	CD-16	98.45^d	15.4^d	–	–	1470^a
		TL-1	115.32^c	23.87^c	–	–	1432^a
		P_{SV}	**	**	–	–	n.s.
	Mono.	CD-16	308.2^b	75.26^b	–	–	–
		TL-1	365.54^a	88.83^a	–	–	
		P_{SV}	**	**	–	–	–
	P_{PP}		**	**	–	–	–
	P_{SV*PP}		**	**	–	–	–

*Plants are grown in the strip intercropping (Inter.) and monocropping (Mono.). SV represented soybean variety. PP represents planting pattern. Data are average of three replicates. Different lowercase letters in the same column indicate significant differences among different cultivars ($p < 0.05$). p-Value is the result from two-way ANOVA. The * and ** indicate significant differences among different cultivars and planting patterns at the levels of $p < 0.05$ and $p < 0.01$, respectively. The n.s. means not significant at the level of $p \geq 0.05$. The – indicates no data here.*

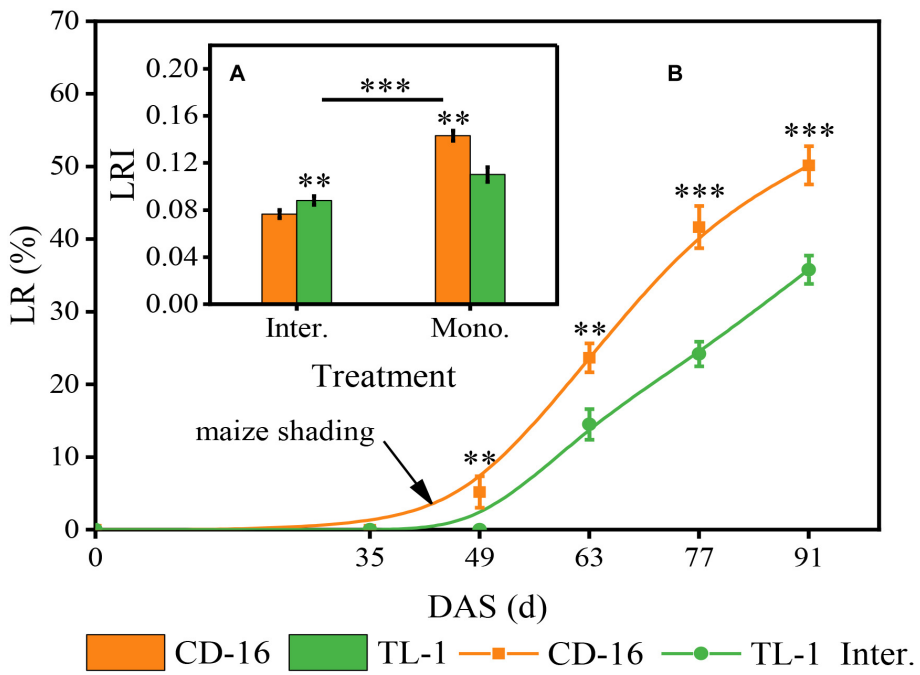

FIGURE 4 | Effects of different cultivars and planting patterns on LR **(A)** and LRI **(B)**. The ** and *** indicate significant differences between CD-16 and TL-1 at the levels of $p < 0.01$ and $p < 0.001$, respectively. The *** on the black short line indicates extremely significant differences between intercropping and monocropping at the levels of $p < 0.001$. Data are average of three replicates. Error bars represent standard errors. Mono. and Inter. are the abbreviation of monoculture and strip intercropping, respectively. DAS represents the number of days after sowing.

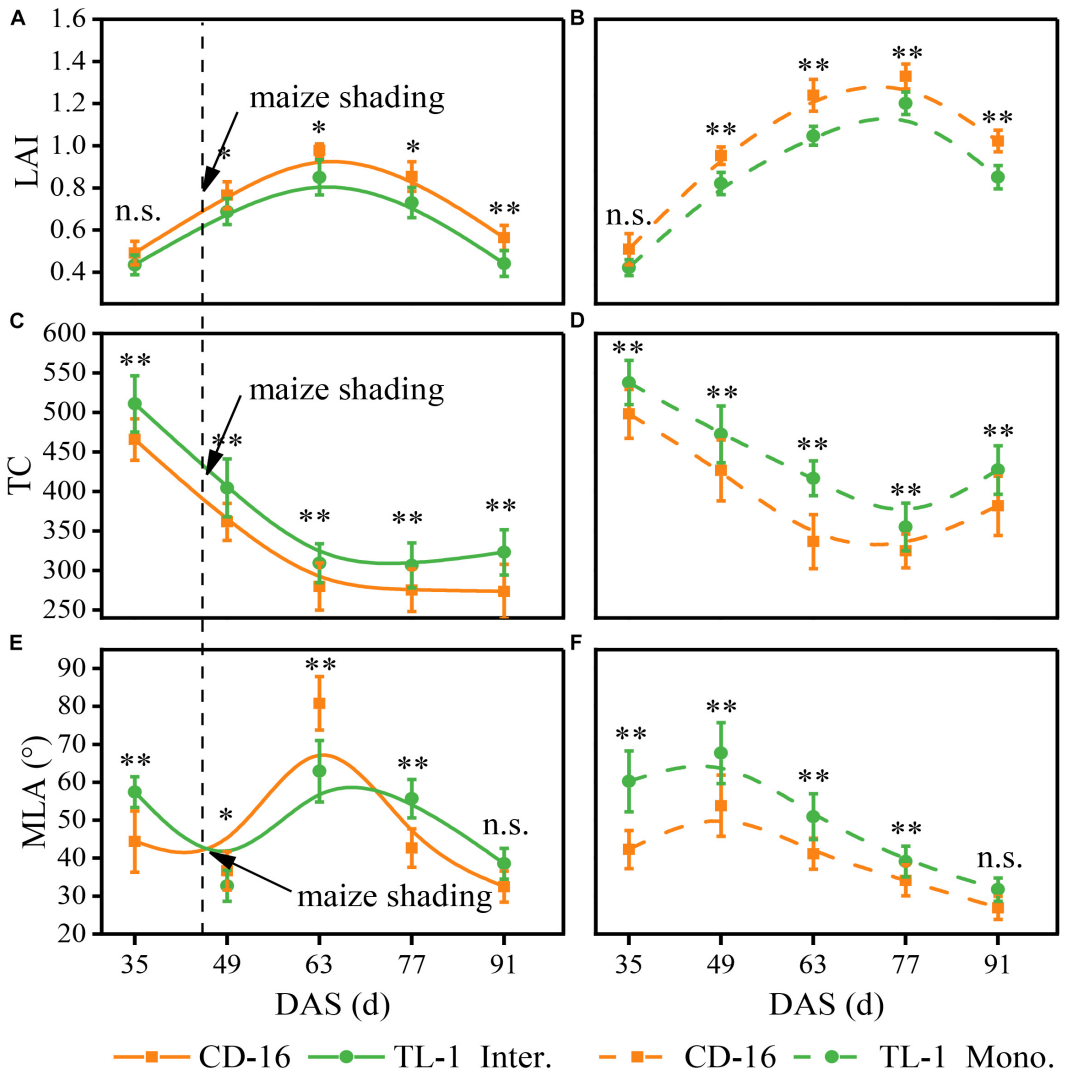

FIGURE 5 | Effects of different cultivars and planting patterns on LAI **(A,B)**, TC **(C,D)** and MLA **(E,F)**. The * and ** indicate significant differences between CD-16 and TL-1 at the levels of $P < 0.05$ and $P < 0.01$, respectively. The n.s. means not significant at the level of $p \geq 0.05$. The vertical black dotted line indicates that the maize begins to shade the intercropping soybean at this time. Data are average of three replicates. Error bars represent standard errors. The solid line indicates strip intercropping, and the dashed line indicates monoculture. The Mono. and Inter. are the abbreviation of monoculture and strip intercropping, respectively. DAS represents the number of days after sowing.

period of soybean (**Figures 5C,D**). After shaded soybean by maize, the TC of TL-1 and CD-16 in the strip intercropping was lower than that of in monocropping (**Figures 5C,D**). It was noteworthy that the TC of TL-1 in the monocropping was 10.91% higher than that of CD-16, but the TC of TL-1 was 11.42% higher than that of CD-16 (average of the last four sampling times) in the late maize shading.

Whether it was in strip intercropping or monoculture, the MLA of TL-1 was significantly higher than that of CD-16 from 0 to 49 days after sowing, whereas that of TL-1 in the strip intercropping was lower than that of CD-16 from 49 to 63 days after sowing (**Figures 5E,F**). Immediately, the MLA of T-1L and CD-16 decreased rapidly in the strip intercropping after the 63rd day of sowing, but the decreasing rate of TL-1 was faster as compared to CD-16 (**Figures 5E,F**). What should be of concern was that the MLA of TL-1 in the monocropping was 20.55% lower than that of CD-16, whereas the MLA of TL-1 was only 4.15% lower than that of CD-16 (average of the last four sampling times) in the late maize shading.

In a word, the shading of maize decreased the LAI and TC, but increased the MLA of intercropping soybean canopy, regardless of CD-16 or TL-1; however, the variation range of these canopy parameters of TL-1 were lower as compared to CD-16. The result showed that in the strip intercropping system, the canopy spatial structure of shade-tolerant plants (TL-1) was slightly changed by the shading stress, which was conducive to increasing light energy capture and the photosynthesis of leaves at different canopy levels in a low-light environment.

Photosynthetic Efficiency

Regardless of CD-16 or TL-1, the PnIT and APnWP of strip intercropping soybean were significantly lower than those of monoculture soybean at R1 stage (**Figures 6A,B**). Furthermore, the PnIT of TL-1 was obviously lower than that of CD-16 (14.0% lower on average), irrespective of planting patterns (**Figure 6A**). However, compared with CD-16, most of the leaves of TL-1 in both strip intercropping and monocropping maintained a relatively high level of Pn, which led to a higher APnWP of TL-1 (12.3% higher on average) (**Figure 6B**). The result showed that in the strip intercropping system, the shade-tolerant plant (TL-1) which was not easy to change in spatial structure could maintain the relatively high Pn of leaves at different canopy levels.

Morphology and Anatomical Structure of Stem

Compared with monoculture, maize shading reduced the SD but increased the PH of strip intercropped soybean regardless of CD-16 or TL-1, but the change range of SD and PH of TL-1 was smaller than that of CD-16 (**Figures 7A–D**). However, the SD of TL-1 in the strip intercropping was even higher than that of CD-16 as compared to monocropping (**Figure 7A**).

Anatomical structure of stems showed that planting patterns, soybean cultivars, and their interactions have significant effects on the number of vascular bundles and the area ratio of vascular/stem, phloem/stem, xylem/stem, and pith/stem at R1 stage (**Table 3** and **Figure 3**). The number of vascular bundles and the area ratio of phloem/stem and xylem/stem of TL-1 in the monocropping were significantly lower than those of CD-16 (**Table 3** and **Figure 3**). In addition, for TL-1, the percentage of decline in the number of vascular bundles between monoculture and intercropping was 4.08%, whereas for CD-16, the percentage of decline was 19.50% (**Table 3**). In contrast, those anatomical structure parameters of TL-1 in the strip intercropping were significantly higher than CD-16 (**Table 3** and **Figure 3**).

Consequently, in the maize–soybean strip intercropping system, there were relatively high number of vascular bundles and the area of vascular, phloem, xylem, and pith in shade-tolerant plant (TL-1) compared with CD-16, which was beneficial to maintain a relatively thick stem.

Lignin Content and Related Enzyme Activity

As compared to monoculture, regardless of CD-16 or TL-1, maize shading decreased the activity of PAL (**Figure 8A**) and 4CL (**Figure 8B**) of strip intercropped soybean, which led to the LC of intercropping soybean decreasing (**Figure 8C**). Furthermore, compared with CD-16, the TL-1 had lower PAL and 4CL activities and lower LC in monoculture (lower than 22.1, 21.4, and 21.0%, respectively), but it was opposite in the strip intercropping (higher than 116.4, 30.6, and 12.0%, respectively) (**Figures 8A–D**). Consequently, in the maize–soybean strip intercropping system, there was a relatively high activity of PAL and 4CL in shade-tolerant plant (TL-1) compared with CD-16, which was beneficial to maintain a relatively high LC of stem.

Correlation Analysis

To demonstrate the effect of plant canopy structure on stem morphology and yield components of soybean, we further analyzed the correlation between the canopy structure of plants and the key morphological and physiological parameters of stem and also yield, etc. (**Figure 9**). The result showed that the LAI was significantly and positively correlated with seed yield, full-pods, and branches, but significantly and negatively correlated with PH and non-full-pods (**Figure 9**). Additionally, the TC significantly and positively correlated with LRI, PnIT, APnWP, LC, PAL, 4CL, seed yield, full-pods, and branches, whereas significant negative correlation existed between the TC and MLA (**Figure 9**). Additionally, there was significant and negative correlation between the MLA and SD, LC, PAL, seed yield, full-pods, and branches (**Figure 9**). Consequently, these parameters, such as LAI, TC, and MLA, could be potentially used to evaluate canopy structure of plants and reflect the growth status of plants and final yield formation.

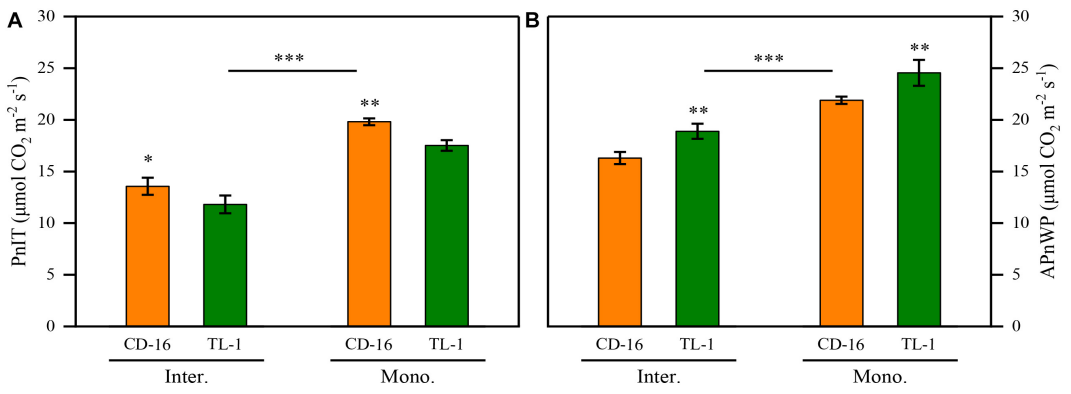

FIGURE 6 | Effects of different cultivars and planting patterns on the PnIT **(A)** and the APnWP **(B)** at R1 stage. The * and ** indicate significant differences between CD-16 and TL-1 at the levels of $p < 0.05$ and $p < 0.01$, respectively. The *** on the black short line indicates extremely significant differences between intercropping and monocropping at the levels of $p < 0.001$. Data are average of three replicates. Error bars represent standard errors. Mono. and Inter. are the abbreviation of monoculture and strip intercropping, respectively.

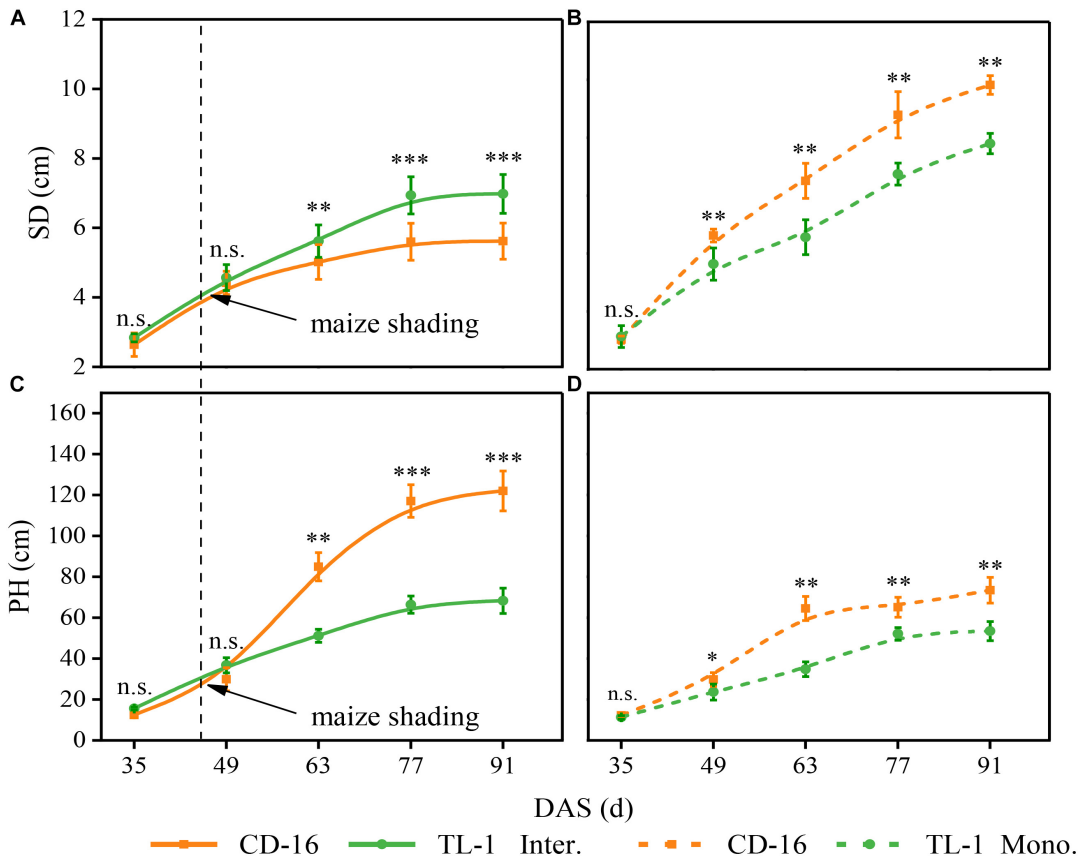

FIGURE 7 | Effects of different cultivars and planting patterns on SD **(A,B)** and PH **(C,D)**. The *, **, and *** indicate significant differences between CD-16 and TL-1 at the levels of $p < 0.05$, $p < 0.01$, and $p < 0.001$, respectively. The n.s. means not significant at the level of $p \geq 0.05$. The vertical black dotted line indicates that the maize begins to shade the intercropping soybean at this time. Data are average of three replicates. Error bars represent standard errors. The solid line indicates strip intercropping, and the dashed line indicates monoculture. Mono. and Inter. are the abbreviation of monoculture and strip intercropping, respectively. DAS represents the number of days after sowing.

TABLE 3 | The number of vascular bundles and the area ratio of vascular/stem, phloem/stem, xylem/stem, and pith/stem response to planting patterns and soybean cultivars at R1 stage.

Treatment		Vascular	Vascular/stem	Phloem/stem	Xylem/stem	Pith/stem
		Unit/mm^2	%	%	%	%
Mono.	CD-16	57.00^{a}	0.96^{c}	17.17^{b}	41.49^{a}	40.35^{c}
	TL-1	49.00^{b}	1.28^{b}	15.40^{c}	22.64^{d}	43.72^{a}
	P_{SV}	*	*	*	**	*
Inter.	CD-16	25.00^{d}	0.90^{c}	18.73^{b}	30.23^{c}	41.96^{b}
	TL-1	47.00^{c}	1.59^{a}	42.71^{a}	36.80^{b}	42.71^{ab}
P_{SV}		**	*	*	**	**
P_{PP}		**	**	**	**	**
P_{SV*PP}		**	*	**	**	**

*Plants are grown in the strip intercropping (Inter.) and monocropping (Mono.). SV represented soybean variety. PP represents planting pattern. Data are average of three replicates. Different lowercase letters in the same column indicate significant differences among different cultivars ($p < 0.05$). p-Value is the result from two-way ANOVA. The * and ** indicate significant differences among different cultivars and planting patterns at the levels of $p < 0.05$ and $p < 0.01$, respectively. The – indicates no data here.*

Evaluation of Shading-Tolerance Target Traits in Soybean

The STC of shading-tolerance target traits in TL-1 (e.g., LAI, MLA, SD, PH, APnWP, seed yield, and branches) significantly larger than those of CD-16 (**Figures 10A–E,G–I**). The STC of PnIT was not significant in TL-1 and CD-16 (**Figure 10F**). The possible reason is that the decrease of PnIT caused by shading stress is roughly the same, regardless of CD-16 or

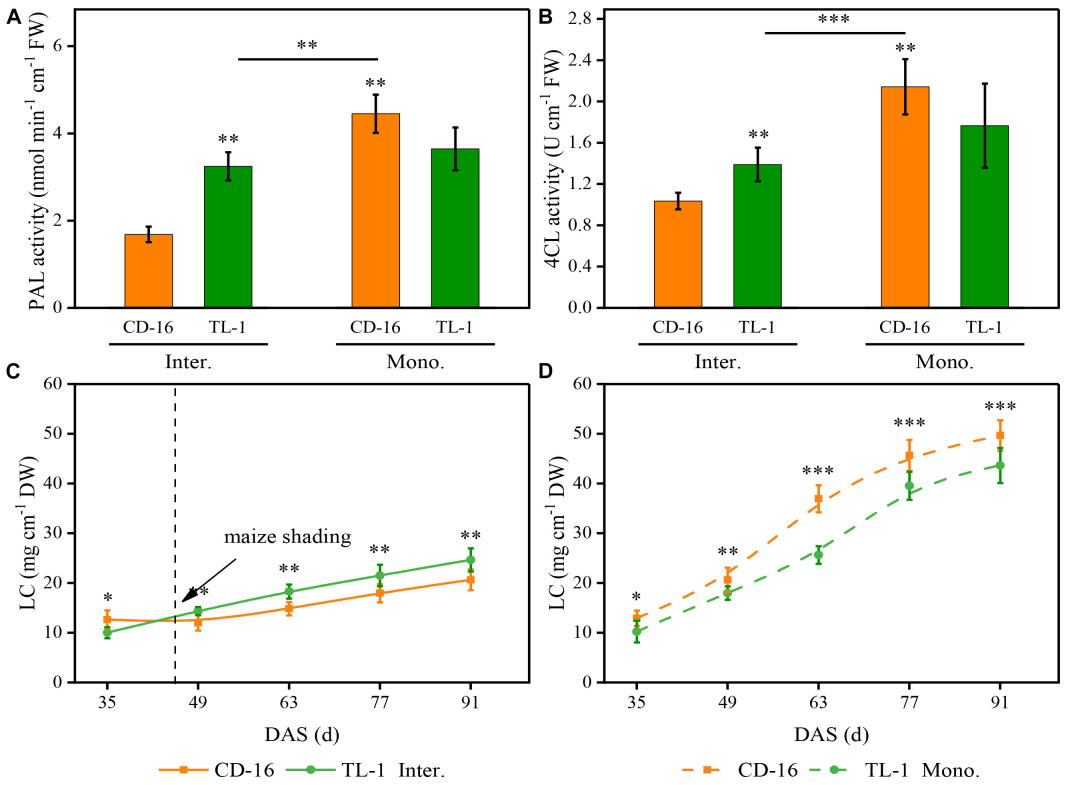

FIGURE 8 | Effects of different cultivars and planting patterns on PAL **(A)**, 4CL **(B)**, and LC **(C,D)**. The *, **, and *** Proportion of mixed chemical reagents indicate significant differences between CD-16 and TL-1 at the levels of $p < 0.05$, $p < 0.01$, and $p < 0.001$, respectively. The ** and *** on the black short line indicate significant differences between intercropping and monocropping at the levels of $p < 0.005$ and $p < 0.001$, respectively. The vertical black dotted line indicates that the maize begins to shade the intercropping soybean at this time. Data are average of three replicates. Error bars represent standard errors. The solid line and dashed line indicate strip intercropping and monoculture, respectively. Mono. and Inter. are the abbreviation of monoculture and strip intercropping, respectively. DAS represents the number of days after sowing.

TL-1. Moreover, compared with CD-16 (CSTC = 0.608), TL-1 (CSTC = 0.716) had a higher CSTC, which indicated that it had a stronger shade tolerance in strip intercropping system.

DISCUSSION

Photosynthesis and Yield in Strip Intercropping Enhanced by Regulating the Canopy Structure

In the maize–soybean strip intercropping system, soybean was vulnerable to shading stress from maize during the intergrowth, which thus affected its canopy structure and photosynthesis (Hideki et al., 2005; Feng et al., 2019). A large number of studies have shown that crop canopy structure was closely related to interception and utilization of photosynthetic active radiation (Yang et al., 2014; Feng et al., 2016; Charbonnier et al., 2017). In this study, the LAI, MLA, and TC of strip intercropped soybean were significantly lower than those of monoculture (**Figure 5**). Consequently, a serious impact was that the PnIT and APnWP of strip intercropped soybean were significantly lower than those of monoculture soybean at R1 stage (**Figures 6A,B**). In addition, the photosynthetic rate of intercropped soybean had been proved to be weaker than that of monoculture soybean (Su et al., 2014; Yao et al., 2017; Fan et al., 2018; Raza et al., 2019), which provided additional evidence to support that the intercropped soybean with lower the PnIT and APnWP experienced a shaded environment. Another important evidence showed that the low-light intensity aggravated senescence of leaves, which results in a decrease in leaf numbers (Lim et al., 2007; Zhou et al., 2019a,b), which in turn weakened canopy structure and photosynthesis of strip intercropped soybean (**Figures 5**, **6**).

Variations in leaf area distributions of different soybean cultivars in the field grown were largely determined by differences in the light intensities at the lower canopy levels, but independent of the angle of leaf inclination (Blad and Baker, 1972). In this study, the shade-tolerant soybean TL-1 had high STC of canopy structure (STC_{LAI} = 0.799, STC_{TC} = 0.839, and STC_{MLA} = 0.949) (**Figures 10A–C**), which was conducive to maintaining the relative stability of spatial structure of the canopy in low-light environment. Importantly, compared with the shade-intolerant soybean CD-16, the shade-tolerant soybean TL-1 had a more perfect canopy structure such as higher TC and lower LAI and MLA (**Figure 5**), which would allow greater penetration of light to the lower canopy

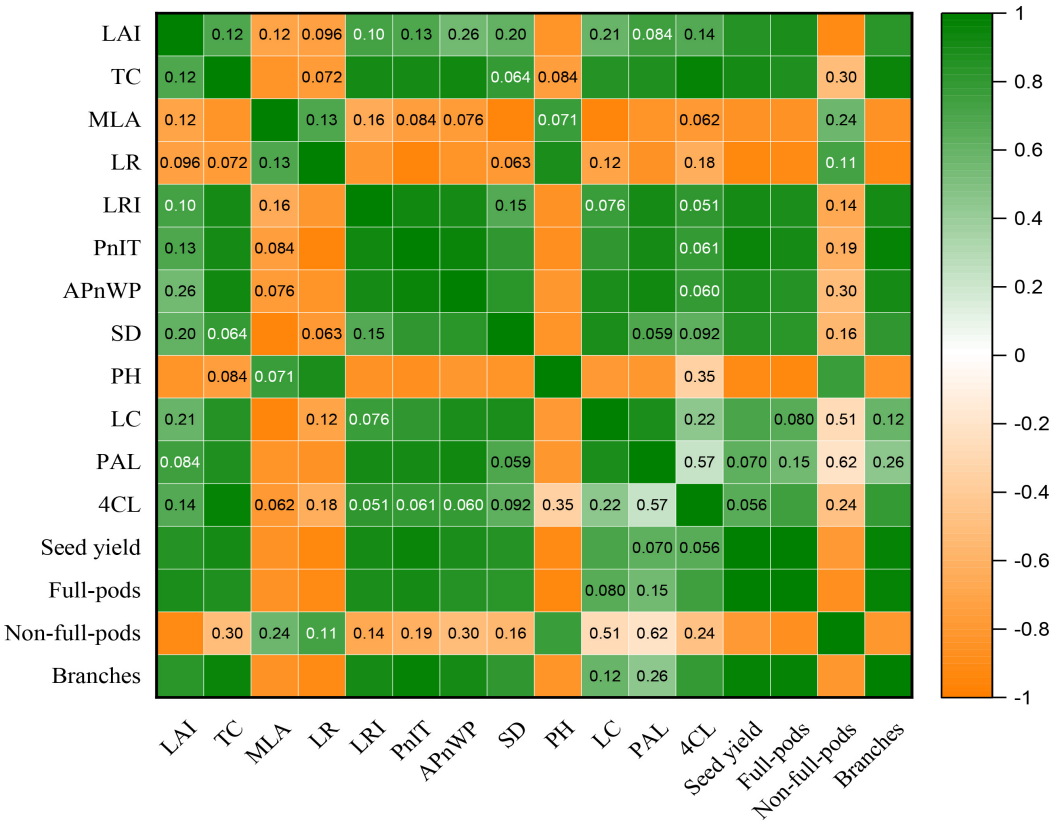

FIGURE 9 | Correlation analysis of LAI, TC, MLA, LR, LRI, the PnIT, the APnWP, SD, PH, LC, PAL, 4CL, seed yield, full-pods, non-full-pods, and branches by using the *t*-test at $p \leq 0.05$ for both TL-1 and CD-16 in the strip intercropping. Orange means positive correlation, and green means negative correlation. The darkness of the color represents strength of correlation. The numbers in the boxes indicate *p*-value, and a box without numbers indicates a strong correlation.

levels (Blad and Baker, 1972; Sakowska et al., 2018). Therefore, compared with shade-intolerant soybean CD-16, the shade-tolerant soybean TL-1 had a higher APnWP (**Figure 6B**), even though its PnIT was lower (**Figure 6A**). As a result, a good canopy structure of soybean is the prerequisite for maintaining high APnWP in low-radiation areas. However, in the intercropping system, the molecular mechanism of low-light environment regulating soybean canopy structure (LAI, TC, and MLA) was still unclear, which needs further research.

Most crops in the intercropping system showed yield advantages as compared to the corresponding monoculture (Li et al., 2001, 2020a; Ghosh, 2004; Chen et al., 2019; Feng et al., 2019). In this study, the soybeans in the strip intercropping system showed no yield advantages as compared to monoculture, irrespective of cultivars, across the two years in field experiments (**Table 2**). One possible explanation was that the canopy morphological formation of strip intercropped soybean was severely inhibited during the intergrowth with maize, which results in plant lodging (**Figure 4B**) and yield reduction (**Table 2**). Correlation analysis showed that the canopy structure of strip intercropped soybean was significantly correlated with LR and yield (**Figure 9**). A compact-type canopy structure was beneficial to intercept more light energy to promote stem morphogenesis and yield formation (Wang et al., 2017; Li et al., 2020b). In addition, the low dry matter allocation index limiting the yield of strip intercropped soybean might be another reason, because in the reproductive stage, the dense canopy structure with relatively low PAR reduced the number of full-pods and branches (**Table 2**), which increases the allocation of dry matter to leaves and stems and thus decreases the allocation of photosynthetic products to seeds (Board, 2000; Liu et al., 2010; Cheng et al., 2020). In contrast, the shade-tolerant soybean TL-1 with high STC ($STC_{Seedyield}$ = 0.526 and $STC_{Branches}$ = 0.397) (**Figures 10H,I**) had relatively high seed yield, full-pods, and branches in the strip intercropping system (**Table 2**). This was one of the important strategies to increase the yield of shade-tolerant soybean in areas with low-light radiation.

Stem Morphological and Physiological Responses to Canopy Structure

Crops with the perfect canopy structure were propitious to intercept more light energy to promote stem morphogenesis and yield formation (Board, 2000; Wang et al., 2017; Cheng et al., 2020; Li et al., 2020b), especially in the condition of intercropping. Some studies have shown that crops in intercropping showed strong shade avoidance responses, which include thinner stem thickness, longer stem, and petiole and also lower PAR inside

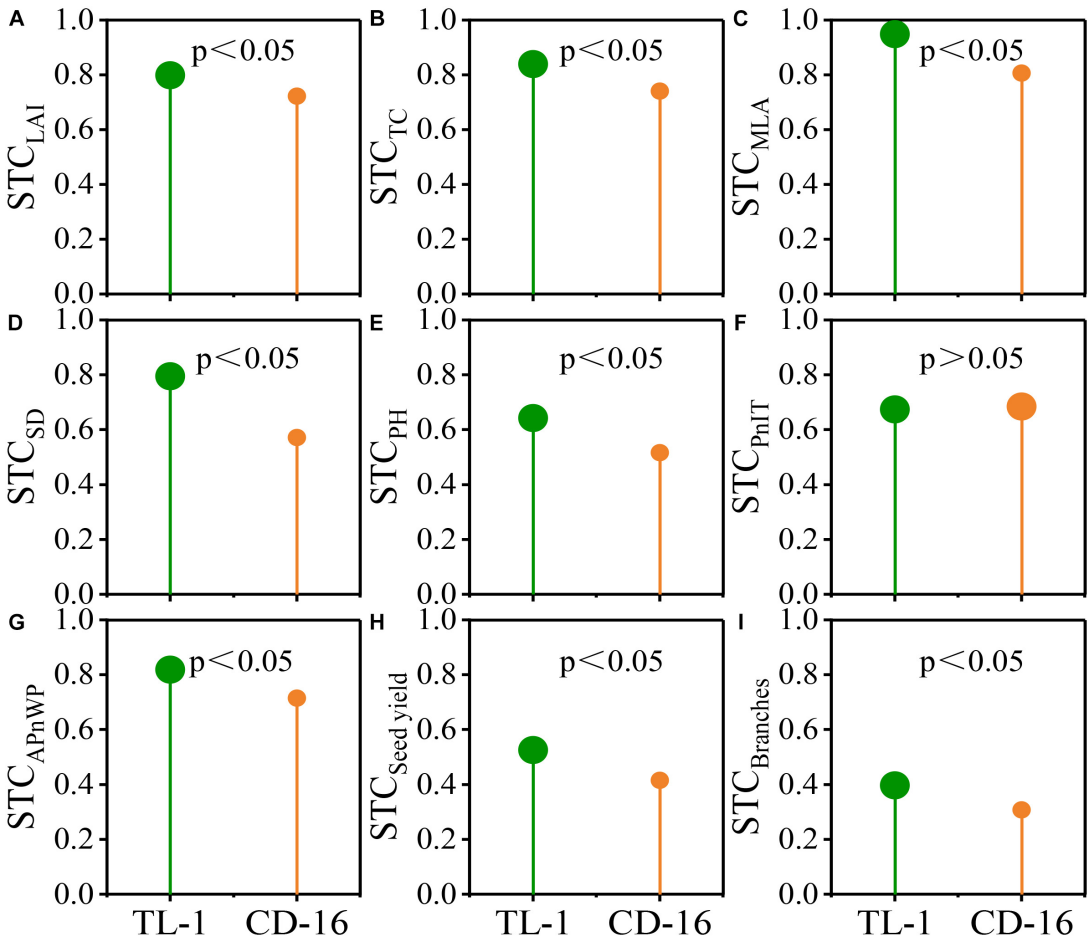

FIGURE 10 | Evaluation of shade-tolerance target traits such as LAI **(A)**, TC **(B)**, MLA **(C)**, SD **(D)**, PH **(E)**, the PnIT **(F)**, the APnWP, **(G)**, seed yield **(H)**, and branches **(I)** in soybean at the levels of $p \leq 0.05$.

the canopy and photosynthetic capacity (Yang et al., 2014; Liu et al., 2016; Fan et al., 2018). In this study, regardless of shade-intolerant soybean CD-16 or shade-tolerant soybean TL-1, The stem of strip intercropped soybean was obviously weaker than that of monoculture in terms of external morphology (lower SD and higher PH) (**Figure 7**) or internal structure (less vascular bundles and smaller area ratio of vascular/stem, phloem/stem, xylem/stem, and pith/stem) (**Table 3** and **Figure 6**), which provided additional evidence to support that there was less PAR inside the canopy of intercropped soybean. In addition, regardless of soybean cultivars, some studies (Cheng et al., 2020; Hussain et al., 2021) were consistent with the observations that the strip intercropped soybean with an unfilled canopy showed a lower activity of PAL and 4CL (**Figures 8A,B**), and also LC (**Figures 8C,D**) compared with monocropping. Regardless of planting system or cultivars, the stem with low LC was one of the key factors for plant lodging and yield reduction (Lourenco et al., 2016; Hussain et al., 2020a; **Figures 4**, **8C,D**). Additionally, the cellulose content in soybean stem was also closely related to plant lodging in intercropping (Liu et al., 2016). In this study, the canopy structure, LC, stem morphology, leaf photosynthesis, and yield components were also closely correlated (**Figure 9**). Thus, it could be seen that improving the canopy structure and the LC in the stem during intercropping was beneficial to decrease the lodging risk of soybean.

Fortunately, soybean cultivars of different genotypes had different responses to various shade environments. The shade-tolerant soybean (CSTC = 0.713) slightly changed its spatial structure of canopy and stem morphology and physiology in maize–soybean strip intercropping system (**Figures 3**, **5**, **7**). Some studies showed the morphology of shade-tolerant plants had lower plasticity (Gong et al., 2015; Chmura et al., 2017), so as to maintain the canopy structure stability of the plant in low-light conditions. Therefore, compared to the shade-intolerant CD-16, the shade-tolerant TL-1 with a relatively perfect canopy had the stronger external morphology (**Figure 7**) and internal structure (**Table 3** and **Figure 3**) in the strip intercropping, in favor of increasing LRI and reducing the LR of soybean in the field (**Figure 4**). Interestingly, for TL-1, the percentage of decline in the number of vascular bundles between monoculture and intercropping was 4.08%, whereas for CD-16, the percentage of decline was 19.50% (**Table 3**), which shows that the TL-1

could slightly reduce the number of vascular bundles in the stem and maintain the stem strength in strip intercropping (Hussain et al., 2021). Besides, high-light intensity was one of the important abiotic factors to improve photosynthesis of plants (Yang et al., 2014; Xue et al., 2016; Feng et al., 2019; Zhou et al., 2019a,b). As compared to shade-intolerant CD-16, most of the leaves of shade-tolerant TL-1 in both strip intercropping and monocropping maintained a relatively high level of APnWP (**Figure 6B**), which led to a higher accumulation of photosynthetic outcome in stem (**Figures 3**, **7**, **8** and **Table 3**) and grains (**Table 2**). Finally, intercropping could improve the microclimate conditions of coffee plants, such as lowering temperature and irradiance level and increasing air relative humidity (Partelli et al., 2014). Thus, what is the relationship between soybean field microclimate and plant lodging resistance and yield formation in the maize–soybean strip intercropping systems? Which needs to be further explored.

CONCLUSION

Our results demonstrated that compared with shade-intolerant soybean, the shade-tolerant soybean (CSTC = 0.713) slightly changed its spatial structure of canopy and stem morphology and physiology in maize–soybean strip intercropping system, especially in the middle and later growth stages. On the one hand, the canopy structure of shade-tolerant soybean showed relatively high TC and relatively low LAI and MLA. Importantly, the shade-tolerant soybean had high STC of canopy structure (STC_{LAI} = 0.799, STC_{TC} = 0.839, and STC_{MLA} = 0.949), which was conducive to maintaining the relative stability of spatial structure of the canopy in low-light environment. On the other hand, the stem of shade-tolerant soybean was obviously stronger than that of shade-intolerant plant in terms of external morphology (shorter PH and thicker stem), internal structure (more vascular bundles and higher area ratio of vascular/stem, phloem/stem, xylem/stem, and pith/stem), and physiological characteristics (higher LC and enzyme activity of PAL and 4CL). In brief, shade-tolerant soybean increased light energy capture and the photosynthesis of the different canopy levels to promote the morphological and physiological development of the stem and ultimately reduce the yield loss of the strip intercropping system. This study provided new insights into the mechanism of soybean lodging resistance in the strip intercropping system, which was of great significance for understanding the potential mechanism of how shade-tolerant plants reduce soybean yield loss in the strip intercropping system by regulating its spatial structure and the morphology and physiology of stems, especially in areas with low solar radiation. Moreover, the spatial structure of canopy with high TC and low LAI and MLA could be used as one of the important bases for screening soybean cultivars with shade resistance and lodging resistance in the future, especially in low radiation areas. However, the molecular mechanism of low-light regulating soybean canopy structure (LAI, TC, and MLA) needs further study, to provide theoretical guidance for cultivating plants with ideal canopy shape that can adapt to changing light environment in intercropping system.

DATA AVAILABILITY STATEMENT

The original contributions presented in the study are included in the article/supplementary material, further inquiries can be directed to the corresponding author/s.

AUTHOR CONTRIBUTIONS

BC and LW carried out the writing–riginal draft, data analysis and plotting. SZJ, RL, WBW, RY, TZ, and SJJ provided the manuscript overall guidance and some references. BC, LW, IA, and AR carried out the soybean sowing, investigation and analysis of physiological and biochemical. MX, CL, WY, and LY carried out the data curation. WL and WY provided financial support. All authors contributed to the article and approved the submitted version.

FUNDING

This work was supported by the Physiological Mechanism of Light-regulated Branching Development of Intercropping Soybean (31871570), the Demonstration Base Construction/ Demonstration Base Project for Poverty Alleviation and the Development of Oil Industry in Plateau Tibetan area (2021ZHFP0010), and the Sichuan Innovation team Project of National Modern Agricultural Industrial Technology system (SC-CXTD-2020-20).

REFERENCES

Blad, B. L., and Baker, D. G. (1972). Orientation and distribution of leaves within soybean canopies. *Agron. J.* 64, 26–29. doi: 10.2134/agronj1972.00021962006400010009x

Board, J. (2000). Light interception efficiency and light quality affect yield compensation of soybean at low plant populations. *Crop Sci.* 40, 1285–1294. doi: 10.2135/cropsci2000.4051285x

Charbonnier, F., Roupsard, O., Le Maire, G., Guillemot, J., Casanoves, F., Lacointe, A., et al. (2017). Increased light-use efficiency sustains net primary productivity of shaded coffee plants in agroforestry system. *Plant Cell Environ.* 40, 1592–1608. doi: 10.1111/pce.12964

Chen, H., Sun, Z., and Yang, S. (2003). Effect of shading on major charaters of soybean and preliminary study on the identification method of soybean shade endurance. *Chin. J. Oil Crop Sci.* 25, 78–82. doi: 10.3321/j.issn:1007-9084.2003.04.018

Chen, J., Lv, F., Liu, J., Ma, Y., Wang, Y., Chen, B., et al. (2014). Effect of late planting and shading on cellulose synthesis during cotton fiber secondary wall development. *PLoS One* 9:e105088. doi: 10.1371/journal.pone.0105088

Chen, P., Song, C., Liu, X., Zhou, L., Yang, H., Zhang, X., et al. (2019). Yield advantage and nitrogen fate in an additive maize-soybean relay intercropping system. *Sci. Total Environ.* 657, 987–999. doi: 10.1016/fj.scitotenv.2018.11.376

Chen, X., Sun, N., Gu, Y., Liu, Y., Li, J., Wu, C., et al. (2020). Maize-soybean strip intercropping improved lodging resistance and productivity of maize. *Int. J. Agric. Biol.* 24, 1383–1392. doi: 10.17957/ijab/15.1574

Cheng, B., Liu, W., Wang, L., Xu, M., Qin, S., Lu, J., et al. (2021). Effects of planting density on photosynthetic characteristics, yield and stem lodging resistance of soybean in maize-soybean strip intercropping system. *Sci. Agric. Sin.* 54, 4084–4096. doi: 10.3864/j.issn.0578-1752.2021.19.005

Cheng, B., Raza, A., Wang, L., Xu, M., Lu, J., Gao, Y., et al. (2020). Effects of multiple planting densities on lignin metabolism and lodging resistance of the strip intercropped soybean stem. *Agronomy* 10:1177. doi: 10.3390/agronomy10081177

Chmura, D. J., Modrzyński, J., Chmielarz, P., and Tjoelker, M. G. (2017). Plasticity in seedling morphology, biomass allocation and physiology among ten temperate tree species in response to shade is related to shade tolerance and not leaf habit. *Plant Biol.* 19, 172–182. doi: 10.1111/plb.12531

Dornhoff, G. M., and Shibles, R. (1970). Varietal differences in net photosynthesis of soybean leaves. *Crop Sci.* 10, 42–45. doi: 10.2135/cropsci1970.0011183X001000010016x

Du, J., Han, T., Gai, J., Yong, T., Xin, S., Wang, X., et al. (2018). Maize-soybean strip intercropping: achieved a balance between high productivity and sustainability. *J. Integr. Agr.* 17, 747–754. doi: 10.1016/S2095-3119(17)61789-1

Fan, Y., Chen, J., Cheng, Y., Raza, M. A., Wu, X., Wang, Z., et al. (2018). Effect of shading and light recovery on the growth, leaf structure, and photosynthetic performance of soybean in a maize-soybean relay-strip intercropping system. *PLoS One* 13:e0198159. doi: 10.1371/journal.pone.0198159

Feng, G., Luo, H., Zhang, Y., Gou, L., Yao, Y., Lin, Y., et al. (2016). Relationship between plant canopy characteristics and photosynthetic productivity in diverse cultivars of cotton (Gossypium hirsutum L.). *Crop J.* 4, 499–508. doi: 10.1016/j.cj.2016.05.012

Feng, L., Raza, M. A., Chen, Y., Khalid, M. H. B., Meraj, T. A., Ahsan, F., et al. (2019). Narrow-wide row planting pattern improves the light environment and seed yields of intercrop species in relay intercropping system. *PLoS One* 14:e0212885. doi: 10.1371/journal.pone.0212885

Feng, L., Raza, M. A., Li, Z., Chen, Y., Khalid, M. H. B., Du, J., et al. (2018). The influence of light intensity and leaf movement on photosynthesis characteristics and carbon balance of soybean. *Front. Plant Sci.* 9:1952. doi: 10.3389/fpls.2018.01952

Ghosh, P. (2004). Growth, yield, competition and economics of groundnut/cereal fodder intercropping systems in the semi-arid tropics of India. *Field Crop Res.* 88, 227–237. doi: 10.1016/j.fcr.2004.01.015

Gitelson, A., Viña, A., Solovchenko, A., Arkebauer, T., and Inoue, Y. (2019). Derivation of canopy light absorption coefficient from reflectance spectra. *Remote Sens. Environ.* 231:111276. doi: 10.1016/j.rse.2019.111276

Gong, W., Jiang, C., Wu, Y., Chen, H., Liu, W., and Yang, W. (2015). Tolerance vs. avoidance: two strategies of soybean (Glycine max) seedlings in response to shade in intercropping. *Photosynthetica* 53, 259–268. doi: 10.1007/s11099-015-0103-8

Hideki, S., Yonny, K., and Yukiyo, N. M. (2005). Canopy photosynthesis of maize-soybean intercropping system. *J. Agric. Meteorol.* 60, 937–940. doi: 10.2480/agrmet.937

Huber, M., Nieuwendijk, N. M., Pantazopoulou, C. K., and Pierik, R. (2021). Light signalling shapes plant–plant interactions in dense canopies. *Plant Cell Environ.* 44, 1014–1029. doi: 10.1111/pce.13912

Hussain, S., Pang, T., Iqbal, N., Shafiq, I., Skalicky, M., Brestic, M., et al. (2020a). Acclimation strategy and plasticity of different soybean genotypes in intercropping. *Funct. Plant Biol.* 47, 592–610. doi: 10.1071/fp19161

Hussain, S., Liu, T., Iqbal, N., Brestic, M., Pang, T., Mumtaz, M., et al. (2020b). Effects of lignin, cellulose, hemicellulose, sucrose and monosaccharide carbohydrates on soybean physical stem strength and yield in intercropping. *Photochem. Photobiol. Sci.* 19, 462–472. doi: 10.1039/cspp00369j

Hussain, S., Shuxian, L., Mumtaz, M., Shafiq, I., Iqbal, N., Brestic, M., et al. (2021). Foliar application of silicon improves stem strength under low light stress by regulating lignin biosynthesis genes in soybean (Glycine max (L.) Merr.). *J. Hazard. Mater.* 401:123256. doi: 10.1016/j.jhazmat.2020.123256

Iqbal, N., Hussain, S., Ahmed, Z., Yang, F., Wang, X., Liu, W., et al. (2019). Comparative analysis of maize–soybean strip intercropping systems: a review. *Plant Prod. Sci.* 22, 131–142. doi: 10.1080/1343943x.2018.1541137

Jiang, C., Rodermel, S. R., and Shibles, R. M. (1993). Photosynthesis, Rubisco activity and amount, and their regulation by transcription in senescing soybean leaves. *Plant Physiol.* 101, 105–112. doi: 10.1104/pp.101.1.105

Keating, B., and Carberry, P. (1993). Resource capture and use in intercropping: solar radiation. *Field Crop Res.* 34, 273–301. doi: 10.1016/0378-4290(93)90118-7

Klich, M. G. (2000). Leaf variations in Elaeagnus angustifolia related to environmental heterogeneity. *Environ. Exp. Bot.* 44, 171–183. doi: 10.1016/s0098-8472(00)00056-3

Kross, A., Mcnairn, H., Lapen, D., Sunohara, M., and Champagne, C. (2015). Assessment of RapidEye vegetation indices for estimation of leaf area index and biomass in corn and soybean crops. *Int. J. Appl. Earth Obs.* 34, 235–248. doi: 10.1016/j.jag.2014.08.002

Li, C., Hoffland, E., Kuyper, T. W., Yu, Y., Zhang, C., Li, H., et al. (2020a). Syndromes of production in intercropping impact yield gains. *Nat. Plants* 6, 653–660. doi: 10.1038/s41477-020-0680-9

Li, C., Hoffland, E., Kuyper, T. W., Yu, Y., Li, H., Zhang, C., et al. (2020b). Yield gain, complementarity and competitive dominance in intercropping in China: a meta-analysis of drivers of yield gain using additive partitioning. *Eur. J. Agron.* 113:125987. doi: 10.1016/fj.eja.2019.125987

Li, C., Yao, X., Ju, B., Zhu, M., Wang, H., Zhang, H., et al. (2014). Analysis of shade-tolerance and determination of shade-tolerance evaluation indicators in different soybean genotypes. *Sci. Agric. Sin.* 47, 2927–2939. doi: 10.3864/j.issn.0578-1752.2014.15.003

Li, L., Sun, J., Zhang, F., Li, X., Yang, S., and Rengel, Z. (2001). Wheat/maize or wheat/soybean strip intercropping: I. Yield advantage and interspecific interactions on nutrients. *Field Crop Res.* 71, 123–137. doi: 10.1016/S0378-4290(01)00156-3

Liang, Y., and Li, J. (2004). The varietal difference of tolerance to low light intensity in rape (Brassica napus L.) plants. *Acta Agronomica Sin.* 30, 360–364. doi: 10.1300/j064v24n01-09

Lim, P. O., Kim, H. J., and Gil Nam, H. (2007). Leaf senescence. *Annu. Rev. Plant Biol.* 58, 115–136. doi: 10.1146/annurev.arplant.57.032905.105316

Liu, B., Liu, X. B., Wang, C., Jin, J., Herbert, S. J., and Hashemi, M. (2010). Response of soybean yield and yield components to light enrichment and planting density. *Int. J. Plant Prod.* 4, 1–10. doi: 10.1016/j.indcrop.2009.09.012

Liu, W., Deng, Y., Hussain, S., Zou, J., Yuan, J., Luo, L., et al. (2016). Relationship between cellulose accumulation and lodging resistance in the stem of relay intercropped soybean [Glycine max (L.) Merr.]. *Field Crop Res.* 196, 261–267. doi: 10.1016/j.fcr.2016.07.008

Liu, W., Hussain, S., Ting, L., Zou, J., Meng, R., Tao, Z., et al. (2019). Shade stress decreases stem strength of soybean through restraining lignin biosynthesis. *J. Integr. Agr.* 18, 43–53. doi: 10.1016/S2095-3119(18)61905-7

Liu, X., Herbert, S., Baath, K., and Hashemi, A. (2006). Soybean (Glycine max) seed growth characteristics in response to light enrichment and shading. *Plant Soil Environ.* 52:176. doi: 10.17221/3363-pse

Lourenco, A., Rencoret, J., Chemetova, C., Gominho, J., Gutierrez, A., Del Rio, J. C., et al. (2016). Lignin composition and structure differs between xylem, phloem and phellem in quercus suber L. *Front. Plant Sci.* 7:1612. doi: 10.3389/fpls.2016.01612

Miyaji, K., and Tagawa, H. (1979). Longevity and productivity of leaves of a cultivated annual, Glycine max Merrill. I. Longevity of leaves in relation to density and sowing time. *New Phytol.* 82, 233–244. doi: 10.2307/2485094

Paradiso, R., and Proietti, S. (2021). Light-quality manipulation to control plant growth and photomorphogenesis in greenhouse horticulture: the state of the art and the opportunities of modern LED systems. *J. Plant Growth Regul.* 15, 1–39. doi: 10.1007/s00344-021-10337-y

Partelli, F. L., Araújo, A. V., Vieira, H. D., Dias, J. R. M., and Ramalho, J. C. (2014). Microclimate and development of 'Conilon' coffee intercropped with rubber trees. *Pesqui. Agropecu. Bras.* 49, 872–881. doi: 10.1590/S0100-204X2014001100006

Rajput, K. S., Gondaliya, A. D., Lekhak, M. M., and Yadav, S. R. (2018). Structure and ontogeny of intraxylary secondary xylem and phloem development by the internal vascular cambium in *Campsis radicans* (L.) seem (Bignoniaceae). *J. Plant Growth Regul.* 37, 755–767. doi: 10.1007/s00344-017-9771-x

Raza, M. A., Feng, L. Y., Van Der Werf, W., Iqbal, N., Khan, I., Hassan, M. J., et al. (2019). Optimum leaf defoliation: a new agronomic approach for increasing nutrient uptake and land equivalent ratio of maize soybean relay intercropping system. *Field Crop Res.* 244:107647. doi: 10.1016/j.fcr.2019.107647

Ren, Y., Zhang, L., Yan, M., Zhang, Y., Chen, Y., Palta, J. A., et al. (2021). Effect of sowing proportion on above-and below-ground competition in maize–soybean intercrops. *Sci. Rep.* 11:15760. doi: 10.1038/s41598-021-95242-w

Sakowska, K., Alberti, G., Genesio, L., Peressotti, A., Delle Vedove, G., Gianelle, D., et al. (2018). Leaf and canopy photosynthesis of a chlorophyll deficient soybean mutant. *Plant Cell Environ.* 41, 1427–1437. doi: 10.1111/pce.13180

Su, B., Song, Y., Song, C., Cui, L., Yong, T., and Yang, W. (2014). Growth and photosynthetic responses of soybean seedlings to maize shading in relay intercropping system in Southwest China. *Photosynthetica* 52, 332–340. doi: 10.1007/s11099-014-0036-7

Walthall, C., Dulaney, W., Anderson, M., Norman, J., Fang, H., and Liang, S. (2004). A comparison of empirical and neural network approaches for estimating corn and soybean leaf area index from Landsat ETM+ imagery. *Remote Sens. Environ.* 92, 465–474. doi: 10.1016/j.rse.2004.06.003

Wang, Z., Zhao, X., Wu, P., Gao, Y., Yang, Q., and Shen, Y. (2017). Border row effects on light interception in wheat/maize strip intercropping systems. *Field Crop Res.* 214, 1–13. doi: 10.1016/j.fcr.2017.08.017

Xue, J., Gou, L., Zhao, Y., Yao, M., Yao, H., Tian, J., et al. (2016). Effects of light intensity within the canopy on maize lodging. *Field Crop Res.* 188, 133–141. doi: 10.1016/j.fcr.2016.01.003

Xue, J., Qi, B., Ma, B., Li, B., and Gou, L. (2021). Effect of altered leaf angle on maize stalk lodging resistance. *Crop Sci.* 61, 689–703. doi: 10.1002/cSC2.20284

Yang, F., Huang, S., Gao, R., Liu, W., Yong, T., Wang, X., et al. (2014). Growth of soybean seedlings in relay strip intercropping systems in relation to light quantity and red:far-red ratio. *Field Crop Res.* 155, 245–253. doi: 10.1016/j.fcr.2013.08.011

Yang, F., Liu, Q., Cheng, Y., Feng, L., Wu, X., Fan, Y., et al. (2020). Low red/far-red ratio as a signal promotes carbon assimilation of soybean seedlings by increasing the photosynthetic capacity. *BMC Plant Biol.* 20:148. doi: 10.1186/s12870-020-02352-0

Yao, X., Zhou, H., Zhu, Q., Li, C., Zhang, H., Wu, J., et al. (2017). Photosynthetic response of soybean leaf to wide light-fluctuation in maize-soybean intercropping system. *Front. Plant Sci.* 8:1695. doi: 10.3389/fpls.2017.01695

Yao, Y., You, Q., Zhan, W., Guo, W., Shen, X., Xiang, L., et al. (2018). Comparison and analysis of stem anatomical structure between wild soybean YD63 (Glycine soja) and cultivated soybean ZD19 (G. max). *Chin. J. Oil Crop Sci.* 40:199. doi: 10.7505/j.issn.1007-9084.2018.02.005

Zhao, Z. S., Wang, R. Z., Zhao, X. W., Xiong, W. H., Tao, G. H., Wu, S. G., et al. (2014). Introduction, popularization and application of a new spring soybean variety "Tianlong No.1" with high yield and good quality. *Soybean Sci. Technol.* 2, 49–52. doi: 10.3969/j.issn.1674-3547.2014.02.016

Zhou, T., Wang, L., Yang, H., Gao, Y., Liu, W., and Yang, W. (2019a). Ameliorated light conditions increase the P uptake capability of soybean in a relay-strip intercropping system by altering root morphology and physiology in the areas with low solar radiation. *Sci. Total Environ.* 688, 1069–1080. doi: 10.1016/j.scitotenv.2019.06.344

Zhou, T., Wang, L., Li, S., Gao, Y., Du, Y., Zhao, L., et al. (2019b). Interactions Between Light intensity and phosphorus nutrition affect the P uptake capacity of maize and soybean seedling in a low light intensity area. *Front. Plant Sci.* 10:183. doi: 10.3389/fpls.2019.00183

Conflict of Interest: BC, RL, and SJJ was employed by the company Chengdu Da Mei Seeds Co., Ltd.

The remaining authors declare that the research was conducted in the absence of any commercial or financial relationships that could be construed as a potential conflict of interest.

Publisher's Note: All claims expressed in this article are solely those of the authors and do not necessarily represent those of their affiliated organizations, or those of the publisher, the editors and the reviewers. Any product that may be evaluated in this article, or claim that may be made by its manufacturer, is not guaranteed or endorsed by the publisher.

Copyright © 2022 Cheng, Wang, Liu, Wang, Yu, Zhou, Ahmad, Raza, Jiang, Xu, Liu, Yu, Wang, Jing, Liu and Yang. This is an open-access article distributed under the terms of the Creative Commons Attribution License (CC BY). The use, distribution or reproduction in other forums is permitted, provided the original author(s) and the copyright owner(s) are credited and that the original publication in this journal is cited, in accordance with accepted academic practice. No use, distribution or reproduction is permitted which does not comply with these terms.

frontiers | Frontiers in Plant Science

ORIGINAL RESEARCH
published: 14 April 2022
doi: 10.3389/fpls.2022.843227

Bulked Segregant RNA Sequencing Revealed Difference Between Virulent and Avirulent Brown Planthoppers

*Wei Guan, Junhan Shan, Mingyang Gao, Jianping Guo, Di Wu, Qian Zhang, Jing Wang, Rongzhi Chen, Bo Du, Lili Zhu and Guangcun He**

State Key Laboratory of Hybrid Rice, College of Life Sciences, Wuhan University, Wuhan, China

The brown planthopper (*Nilaparvata lugens* Stål, BPH) is one of the most devastating insect pests of rice (*Oryza sativa* L.), but BPH populations have varying degrees of virulence to rice varieties carrying different resistance genes. To help efforts to characterize these variations we applied bulked segregant RNA sequencing (BSR-seq) to identify differentially expressed genes (DEGs) and genetic loci associated with BPH virulence to YHY15 rice plants carrying the resistance gene *Bph15.* BPHs that are highly virulent or avirulent to these plants were selected from an F2 population to form two contrasting bulks, and BSR-seq identified 751 DEGs between the bulks. Genes associated with carbohydrate, amino acid and nucleotide metabolism, the endocrine system, and signal transduction were upregulated in the avirulent insects when they fed on these plants. The results also indicated that shifts in lipid metabolism and digestive system pathways were crucial for the virulent BPHs' adaptation to the resistant rice. We identified 24 single-nucleotide polymorphisms (SNPs) in 21 genes linked with BPH virulence. Possible roles of genes apparently linked to BPH virulence are discussed. Our results provide potentially valuable information for further studies of BPH virulence mechanisms and development of robust control strategies.

Keywords: brown planthopper, rice, insect virulence, biotype, bulked segregant RNA sequencing (BSR-seq)

OPEN ACCESS

Edited by:
Raul Antonio Sperotto, Universidade do Vale do Taquari – Univates, Brazil

Reviewed by:
Weihua Ma, Huazhong Agricultural University, China
Wenwu Zhou, Zhejiang University, China
Jing Huang Hu, Chinese Academy of Agricultural Sciences (CAAS), China

****Correspondence:***
Guangcun He
gche@whu.edu.cn

Specialty section:
This article was submitted to Plant Pathogen Interactions, a section of the journal Frontiers in Plant Science

Received: *25 December 2021*
Accepted: *08 March 2022*
Published: *14 April 2022*

Citation:
Guan W, Shan J, Gao M, Guo J, Wu D, Zhang Q, Wang J, Chen R, Du B, Zhu L and He G (2022) Bulked Segregant RNA Sequencing Revealed Difference Between Virulent and Avirulent Brown Planthoppers. Front. Plant Sci. 13:843227. doi: 10.3389/fpls.2022.843227

INTRODUCTION

The brown planthopper (*Nilaparvata lugens* Stål, BPH) is a monophagous piercing-sucking herbivore that has become the most destructive insect pest of rice (*Oryza sativa* L.) (Sogawa, 1982; Hibino, 1996; Guo et al., 2018). BPHs occur widely throughout Asia and can migrate several 100 km across national borders (Jing et al., 2017). When feeding on rice plants, BPH nymphs and adults ingest phloem sap by inserting a stylet into their vascular tissues, thereby directly damaging the plants (Sogawa, 1982). They can also directly damage the plants by transmitting pathogenic viruses (Jena and Kim, 2010; Guo et al., 2018). Rice varieties that are resistant to BPH can inhibit the pest's feeding, growth, and fecundity (Zheng et al., 2021). In recent decades, many BPH resistance genes and QTLs have been detected in cultivated rice and wild species (Guo et al., 2018; Shi et al., 2021; Zhou et al., 2021). However, new BPH biotypes may evolve that are virulent to resistant rice varieties (Claridge and Den Hollander, 1980; Saxena et al., 1991). A virulent biotype is defined as a BPH population that can damage a rice variety that was previously resistant (Claridge and Den Hollander, 1980; Jena and Kim, 2010). The first BPH-resistant variety (IR26 carrying the

Bph1 resistance gene) was developed by the International Rice Research Institute (IRRI) in 1973. However, within several years BPH biotype 2 had adapted and become virulent to IR26 in the field (Jena and Kim, 2010). Rice varieties resistant to biotype 2, carrying *Bph2*, were subsequently widely deployed in the field, but BPH biotype 3, which can overcome *Bph2*-mediated resistance, was detected in 1981 (Pathak and Heinrichs, 1982; Jena and Kim, 2010). Several additional BPH biotypes have been developed by rearing biotype 1 insects on specific resistant rice varieties in the laboratory (Claridge and Den Hollander, 1982). Analyses of various biotypes have clearly shown that BPH's virulence to resistant rice varieties is a genetic trait (Kobayashi, 2016), but the mechanisms underlying BPH virulence are poorly understood.

Previous studies have shown that BPHs exhibit distinct responses to feeding on resistant plants carrying different resistance genes (Kobayashi, 2016; Yue et al., 2019). For instance, their responses to the resistant rice variety Mudgo, which carries the *Bph1* resistance gene, include activation of various metabolic, digestive, and absorption pathways (Ji et al., 2013). Wang et al. (2015) also found that feeding on the resistant rice variety B5 induced significant changes in expression of genes involved in metabolism of lipids, amino acids, carbohydrates, nucleotides, and TCA cycle intermediates in the salivary glands of BPH insects. Zhang et al. (2019) showed that expression levels of genes related to detoxification and starvation responses were significantly upregulated in BPHs that fed on resistant *Bph6*-transgenic rice. In addition, Zheng et al. (2020) observed stronger expression of genes involved in lipid metabolism in BPHs fed on NIL-*Bph6* and NIL-*Bph9* resistant rice plants than in insects fed on susceptible wild type rice. These studies have provided valuable insights. However, most data on BPH responses have been obtained by temporarily feeding avirulent insects on different rice varieties, and there have been few comparisons of virulent and avirulent BPHs fed on resistant varieties.

Various techniques have been used to study plant-insect interactions (Zogli et al., 2020). For instance, genome sequencing of the pea aphid showed that most chemosensory genes had undergone rapid expansion in the genome under positive selection (Smadja et al., 2009). Genome sequencing has detected the expansions of detoxification gene families in *Tetranychus urticae* (Grbić et al., 2011). The genome-wide analysis found the expansion of Cytochrome P450 (CYP) genes in the rice striped stem borer in response to rice defense secondary metabolites (Wang et al., 2014). MS/MS *de novo* peptide sequencing has found several enzymes responsible for digesting carbohydrates, proteins, and lipids in the midgut lumen of the cotton bollworm (Pauchet et al., 2008). In addition, insects have evolved effectors to adapt to host plants (Chen et al., 2019). The functional genomics approach has found effectors required for thrips to reproduce on tomatoes (Abd-El-Haliem et al., 2018). Additionally, some insect avirulence genes have been identified in Hessian fly associated with virulence to wheat R genes *H6* and *H13* by bulked segregant analysis (BSA)-seq analysis (Navarro-Escalante et al., 2020). A useful approach for studying disease resistance in plants is BSA, initially developed by Michelmore et al. (1991). BSA is based on the theory that different genotypes are likely to have differing phenotypic extremes, which can be used to rapidly identify genetic markers linked to genomic regions related to targeted traits (Michelmore et al., 1991; Wang et al., 2013). However, due to complications caused by repetitive genomic sequences and high genome sequencing depth requirements, BSA is not suitable for analyses of populations with numerous mutants and large genomes (Liu et al., 2012). Another approach, RNA sequencing (RNA-seq), is widely applied in next-generation sequencing (NGS) efforts to quantify relative quantities of specific transcripts from read counts (Górczak et al., 2020). RNA-seq reads can also be used to identify DNA sequence polymorphisms, such as single nucleotide polymorphisms (Chepelev et al., 2009). Bulked segregant RNA-seq (BSR-seq) couples BSA with RNA-seq (Liu et al., 2012) and can be used not only to identify differentially expressed genes (DEGs) but also single-nucleotide polymorphisms (SNPs) that are tightly linked to targeted traits (Du et al., 2017). BSR-seq has been successfully applied in analyses of many species. For instance, BSR-seq has identified 1,255 DEGs between catfish that are resistant and susceptible to enteric septicemia, and 56,419 SNPs of 4,304 unique genes of the fish (Wang et al., 2013). In addition, it has identified 18 high-probability SNPs and six genes that may be involved in responses to waterlogging stress in maize (Du et al., 2017), as well as the maize *glossy13* gene, which encodes a putative ABC transporter and is crucial for accumulation of epicuticular waxes (Li et al., 2013). As it combines advantages of BSA and RNA-seq it is highly efficient for analyses of complex traits involving multiple genes (Du et al., 2017; Li et al., 2020).

The BPH resistance gene *Bph15* was introduced into *O. sativa* from the wild rice species *Oryza officinalis* (Yang et al., 2004; Lv et al., 2014). Rice variety YHY15 is a recombinant inbred line (RIL) selected from the RI93 × TN1 F2 population and carries a single resistance gene *Bph15* (Yang et al., 2004). BPH population, designed biotype Y, was developed by rearing biotype 1 BPHs on YHY15 from January 2007 (Jing et al., 2012). Biotype Y can overcome the resistance conferred by *Bph15*, grow and reproduce normally on YHY15 plants. Thus, this combination of insects and plants provides a suitable model system for examining virulence mechanisms, and in this study we applied BSR-seq to identify DEGs and SNPs associated with BPH virulence to rice. Comparison of virulent and avirulent BPH extreme bulks after feeding on resistant YHY15 rice plants for 48 h identified 751 DEGs, with illuminating differences in transcriptomic profiles. Moreover, we identified 24 polymorphic SNPs related to BPH virulence located on six chromosomes, and 21 genes that may play key roles in virulence mechanisms. The results may facilitate further study of the mechanisms that enable BPH to overcome host resistance.

MATERIALS AND METHODS

Insect and Plant Materials

The brown planthopper biotype 1 insects were reared on the susceptible rice variety Taichung Native 1 (TN1), which does not contain any BPH resistance gene. BPH biotype Y was developed by forcing biotype 1 BPHs to feed and reproduce on

the resistant rice variety YHY15 for multiple generations (Jing et al., 2012). YHY15 is a RIL carrying the *Bph15* resistance gene (Yang et al., 2004). The BPHs used in the experiments reported here were reared on 1-month-old rice seedlings growing in 24 × 19 cm plastic buckets in controlled environmental conditions (26 ± 1°C, 16 h light/8 h dark cycles) at Wuhan University Institute of Genetics.

Brown Planthopper Weight Gain and Honeydew Excretion Assay

The brown planthopper weight gain and honeydew excretion were measured as previously described (Shi et al., 2021). Newly emerged female adults were weighed using an AUW120D electronic balance (AUW120D, Shimadzu, Japan) then introduced into separate pre-weighed parafilm sachet (2 × 2.5 cm) fixed to leaf sheaths of a 4-week-old rice plant. After 48 h the insects were carefully removed from the sachets, and then the insect and the honeydew in each sachet were weighed. Each insect's weight gain was determined from its weight before and after ingestion, and its weight gain ratio was calculated by dividing its weight gain by its initial weight. Both BPH weight gain and honeydew excretion assays were repeated three times with 25 BPHs for each replicate.

Brown Planthopper Survival Rate

The brown planthopper survival rates were determined as previously described (Shi et al., 2021). Briefly, rice plants were grown in plastic pots (12 cm tall, 9 cm diameter, one plant per pot). When they were 1-month-old the pots were covered with plastic cages and 10 third-instar nymphs were released into each cage to infest the plants. The number of surviving BPH nymphs in each cage was recorded every day until 10 days after their introduction, and survival rates were calculated by dividing the number of surviving nymphs in each cage by the number initially released. The experiment was repeated three times, with 20 BPHs per replicate.

Formation of Brown Planthopper Extreme Bulks

An extremely virulent BPH female biotype Y adult, which gained 2.06 mg weight in the weight gain assay described above, was mated with an avirulent male adult of biotype 1. The F1 offspring were allowed to intermate and female F2 adults resulting from their mating, with similar body sizes, were subjected to the assay. Forty that gained 1.89–2.8 mg weight were classified as virulent to YHY15, and 40 that lost 0.4–1.04 mg were classified as avirulent. These sets were used to form a *Bph15*-virulent bulk (vB15) and a *Bph15*-avirulent bulk (aB15), respectively, which were used to prepare bulked RNA samples for the BSR-seq analysis.

Illumina cDNA Library Construction and RNA Sequencing

Each BPH individual in the extreme bulks was dissected into two parts under an Olympus stereoscopic microscope, the heads with intestines and the remaining carcasses. The two resulting bulks from the sets of 40 virulent and avirulent F2 individuals were each randomly divided into four replicates, with parts of 10 insects in each replicate. The tissue samples in each replicate were mixed, and total RNA was extracted from them using a mirVana miRNA Isolation Kit (Ambion-1561, Austin, TX, United States). After testing its integrity using a 2100 Bioanalyzer (Agilent Technologies, Santa Clara, CA, United States), sequencing libraries were constructed using a TruSeq Stranded mRNA LTSample Prep Kit (Illumina, San Diego, CA, United States) following the manufacturer's instructions. The cDNA library preparations were then sequenced using an Illumina HiSeq 4000 sequencing platform. Raw reads were processed using Trimmomatic (Pérez-Rubio et al., 2019). To obtain clean data, reads containing poly-n and low-quality reads were removed. Then the clean reads were used for the BSR-seq analysis.

SNP Calling and Bulked Segregant RNA-Seq Analysis

The reads were mapped to the latest chromosome-level BPH reference genome (BioProject accession no. PRJNA591478) (Ma et al., 2021) using Burrows–Wheeler Aligner (BWA, v. 0.7.5a) (Rajan-Babu et al., 2021). The bwa index command and BWA–MEM were used to create reference genome index and map the reference genome, respectively. Then, the mapped reads were sorted and indexed by SAMtools (v. 1.3.1) (Danecek et al., 2021), following recommended procedures.[1] SNPs were called using SAMtools and BCFtools (v. 1.3.1) (Lam et al., 2020). The Variant Call Format (VCF) files are shown in **Supplementary Materials**. Then SnpEff v. 4.1g (Cingolani et al., 2012) was used to annotate and predict the effects of genetic variants on genes. And SNP index was calculated at each SNP position to indicate the proportion of reads harboring SNPs that differed from the reference sequences (Abe et al., 2012). SNP positions with SNP index less than 0.3 were eliminated, and those with depth less than four were excluded, as these SNPs may be due to sequencing or alignment errors (Hisano et al., 2017; Feng et al., 2020; Li et al., 2020). After filtration, ΔSNP-index value (Takagi et al., 2013; Li et al., 2020) was calculated for each position by subtracting the SNP index of the aB15-bulk from that of the vB15-bulk. The average ΔSNP-index was calculated using a sliding window analysis with a window size of 3-Mb and a slide size of 1-Mb. We computed confidence intervals of ΔSNP-index values for all SNP positions under the null hypothesis that no QTLs were present.

Differential Expression Gene Analysis

The clean reads were mapped to the BPH reference genome (Ma et al., 2021) using Hisat2 (v. 2.2.1.0) software[2] (Kim et al., 2015). To quantify gene expression levels, fragments per kilobase of transcript per million mapped reads (FPKM) values (Roberts et al., 2011) were calculated using Cufflinks (Trapnell et al., 2010), and read counts of each gene were determined by htseq-count (Srinivasan et al., 2020). DEGs were clustered using the DESeq package (Anders and Huber, 2012) with thresholds of $\log_2 FC \geq 1$ and $P < 0.05$ for significantly differential expression. The DEGs' expression patterns were explored by hierarchical cluster analysis

[1] http://samtools.sourceforge.net/mpileup.shtml

[2] https://daehwankimlab.github.io/hisat2/

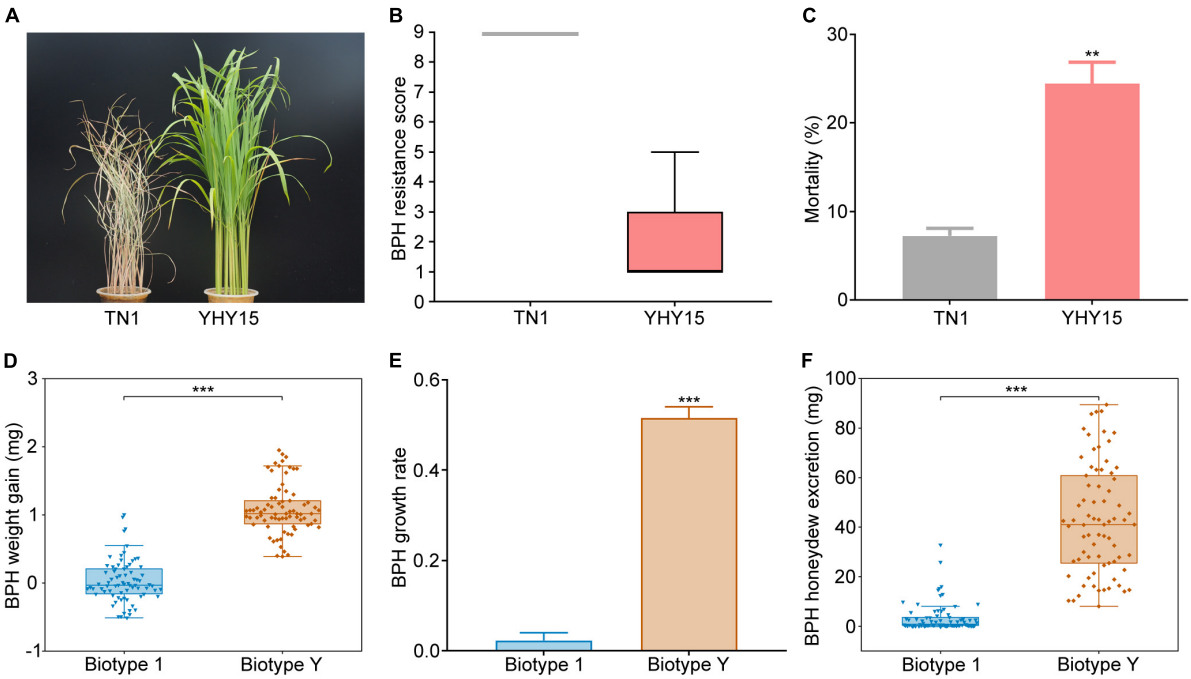

FIGURE 1 | Bph15-mediated resistance verification and virulence assessment of BPH biotype Y. **(A)** Photo showing the difference in TN1 and YHY15 rice plants' BPH resistance. **(B)** BPH-resistance scores of TN1 and YHY15 plants (negatively related to BPH resistance) obtained from observations 7 days after BPH infestation ($n = 3$ independent experiments, each with 15 rice plants). **(C)** Mortality of BPH insects fed on TN1 and YHY15 plants after 48 h. Weight gain **(D)** and growth rate **(E)** of BPH biotypes 1 and biotype Y feeding on YHY15 rice plants for 48 h. Three independent experiments were repeated with 25 BPHs per replicate. **(F)** Amounts of honeydew excreted by newly emerged female adults of biotype 1 and biotype Y on YHY15 plants after 48 h. Three independent experiments were performed with 25 BPHs per replicate. All data presented are means ± SE of three replicates. In the box charts, the bottom and top edges of the box charts represent the 25th and 75th percentiles, respectively, and center values are medians. The whiskers mark ranges of the data, excluding outliers. **, *** on the bars indicate significance at $P < 0.01$, and $P < 0.001$ (according to Student's *t*-test), respectively.

and they were functionally annotated by comparing with entries in the Nr, eukaryotic orthologous groups (KOG), Swiss-Prot, Gene ontology (GO), Pfam, and Kyoto Encyclopedia of Genes and Genomics (KEGG) databases (with $P \leq 0.05$ as the threshold in GO term and KEGG pathway enrichment analyses).

Real-Time Quantitative PCR Analysis

For expression analyses of candidate genes in *Bph15*-virulent (Vr-B15) and *Bph15*-avirulent (Avr-B15) BPHs. The weight gain of newly emerged female adults from biotype Y was measured after feeding on YHY15 for 48 h. The virulent insects (average weight gain in 2.0 mg) and the avirulent (weight gain –0.4 mg) were used for qRT-PCR, respectively. Total RNA was isolated from the insects using a RNAiso Plus kit (Takara, Kyoto, Japan) following the manufacturer's instructions. RNA samples were reverse-transcribed into cDNA using a PrimeScript RT Reagent Kit with gDNA Eraser (Takara, Kyoto, Japan). The resulting sequences were then used in qRT-PCR analysis with a CFX96 Touch^{TM} Real-Time System and iTaq Universal SYBR Green Supermix Kit (Bio-Rad, Hercules, CA, United States) according to the manufacturer's protocols. Relative expression levels were calculated using the $2^{-\Delta\Delta Ct}$ method with the BPH housekeeping gene *actin* serving as an internal control. Three independent biological replicates were employed in each experiment.

Statistical Analysis

The significance of differences in recorded variables was assessed using Student's *t*-test or Tukey's honestly Significant Difference test implemented in IBM SPSS Statistics v. 23.0. Differences were considered significant, very significant and highly significant (indicated by *, **, *** in the figures) if $P < 0.05$, $P < 0.01$, and $P < 0.001$, respectively.

RESULTS

The Performance of Brown Planthopper Insects on YHY15 Rice Plants

To verify the BPH resistance conferred by *Bph15*, YHY15 plants carrying *Bph15* were used for seedling stage insect resistance analysis, with susceptible TN1 plants as controls. After infestation by biotype 1 BPHs for 7 days, the TN1 plants were dead, but the YHY15 plants survived well, proving YHY15's resistance to biotype 1 BPHs (**Figures 1A,B** and **Supplementary Figure 1**). Moreover, the mortality rate of biotype 1 insects was also significantly higher on YHY15 (24.44%) than on TN1 (7.22%) plants (**Figure 1C**). These results clearly indicate that the YHY15 plants were resistant to BPH.

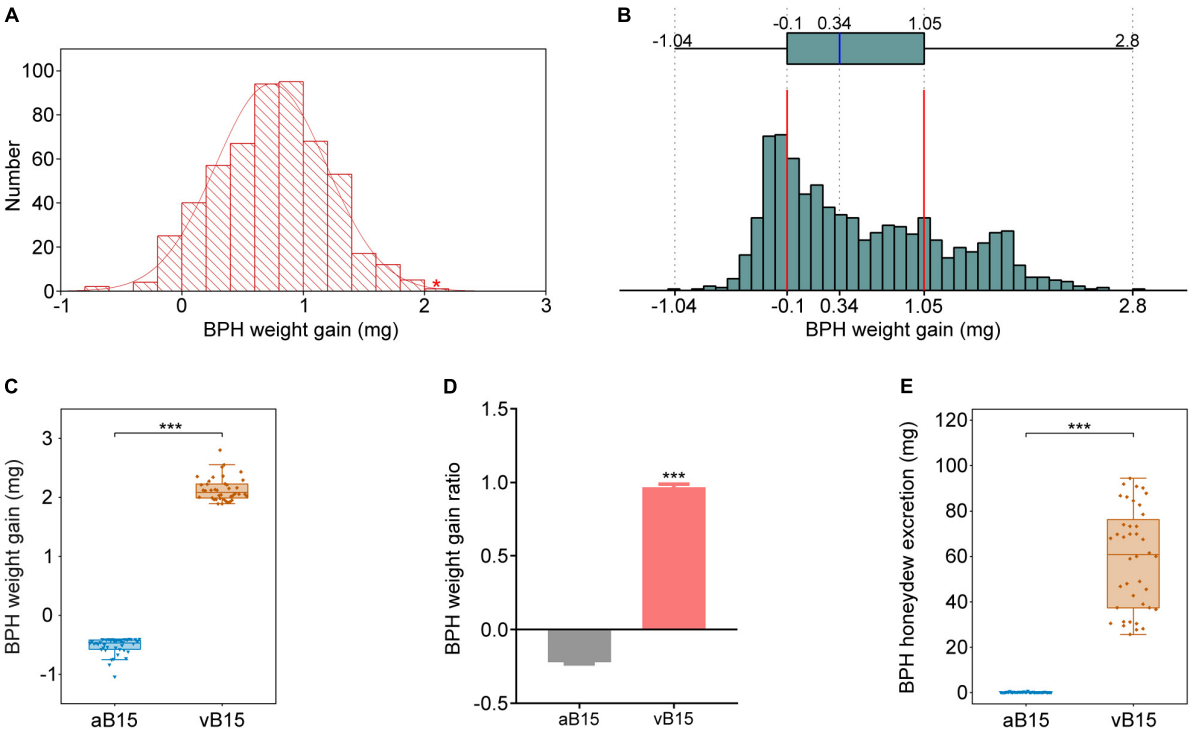

FIGURE 2 | Construction of the two extreme BPH bulks. **(A)** Frequency distribution of weight gain of 504 biotype Y BPHs after feeding on YHY15 plants for 48 h. A single extremely virulent BPH female, with 2.06 mg weight gain (indicated by the red asterisk), was selected. **(B)** Frequency distribution of weight gain of F2 BPHs (n = 1202) fed on YHY15 plants for 48 h. The histogram shows the BPHs' weight gain. The chart above it shows the range of BPH weight gain, with 25th and 75th percentiles (excluding outliers) indicated by right and left edges of the box, respectively, and the median within the box. Panels **(C–E)** show the weight gain, weight gain ratio, and honeydew excretion, of the two bulks after feeding on YHY15 for 48 h (three independent experiments were performed). vB15-bulk and aB15-bulk refer to BPHs extremely virulent and extremely avirulent to YHY15, respectively. ***P < 0.001 (Student's t-test).

To further investigate the virulence of BPH biotype Y to YHY15 rice, we observed the performance of adult female biotype 1 and Y insects (with similar initial body weight, ranging from 1.8 to 2.7 mg) on YHY15 plants. After feeding on YHY15 plants for 48 h, the biotype Y and 1 insects had average weight gain of 1.08 and 0.03 mg, respectively (**Figure 1D**), with average growth rate of 51.58 and 2.24%, respectively (**Figure 1E**). In addition, the biotype Y and 1 BPHs had average honeydew excretion of 42.78 and 3.55 mg, respectively (**Figure 1F**). These results indicate that the biotype Y has adapted to the resistant YHY15 rice plants.

Construction of Extremely Virulent and Avirulent Brown Planthopper Bulks

To construct the virulent and avirulent BPH bulks, 504 BPH female adults of biotype Y were randomly selected and we recorded the weight gain of each insect after feeding on YNY15 plants for 48 h. Their weight gain of BPH insects was continuously distributed in range of –0.79–2.06 mg (**Figure 2A**), indicating significant heterogeneity in virulence in the biotype Y population. Therefore, a virulent female with 2.06 mg weight gain from biotype Y (indicated by the red asterisk in **Figure 2A**) was selected and crossed with an avirulent male of the biotype 1 population. The emerging male and female offspring were then intercrossed to breed a F2 generation for bulk construction.

In total, the virulence of 1202 newly emerged F2 female adults was assessed by allowing them to feed on resistant YHY15 plants for 48 h and recording their weight gain, which ranged from –1.04 to 2.8 mg (**Figure 2B**), clearly showing that their virulence widely varied. We selected 40 extremely virulent and 40 avirulent BPHs with weight gains ranging from 1.89 to 2.8 mg and weight losses ranging from 0.4 to 1.04 mg, respectively (**Figure 2C**), and average weight gain ratios of 96.49 and –22.27%, respectively (**Figure 2D**). In addition, BPH honeydew excretion is a reliable indicator of BPH feeding activity. It has been applied to determine the virulence of the biotypes (Claridge and Den Hollander, 1980). The virulent BPHs produced 25.62–94.45 mg honeydew, and the avirulent 0–0.77 mg honeydew, respectively (**Figure 2E**). Hence, the 40 extremely virulent F2 insects and 40 extremely avirulent counterparts were designated the *Bph15*-virulent (vB15) bulk and *Bph15*-avirulent (aB15) bulk, respectively (**Supplementary Figure 2**).

Transcriptome Annotation of the Assembled Unigenes

We subjected the two extreme BPH bulks to deep RNA-sequencing. For this, the 40 F2 individuals in each extreme

TABLE 1 | Summary of the RNA sequencing data.

Sample	Raw bases	Clean bases	Q30 (%)	GC (%)	Total mapped reads	Mapping ratio (%)
aB15_1	7.14G	6.61G	91.94	42.33	38742958	85.87
aB15_2	7.38G	6.83G	91.89	42.42	40139950	86.03
aB15_3	7.41G	6.84G	91.58	42.67	40055545	85.69
aB15_4	7.76G	7.20G	92.13	42.16	40356826	82.09
vB15_1	7.35G	6.81G	92.08	41.37	38729806	83.34
vB15_2	7.46G	7.04G	93.51	42.16	39970460	83.47
vB15_3	7.38G	7.01G	93.91	40.40	39937855	83.91
vB15_4	7.72G	7.33G	94.05	40.97	41755631	83.82
Total	59.6G	55.67G	–	–	–	–

bulk were randomly divided into four replicates with 10 insects in each replicate, and each insect was divided into two parts (heads + intestines and remaining carcasses). RNA transcripts were extracted from the pooled pairs of tissue samples of each set of 10 BPHs then sequenced using an Illumina HiSeq 4000 sequencing platform, generating eight transcriptome libraries with 59.6 G raw data in total. After filtering out low-quality sequences, incorrect adapters, and redundant sequences, 55.67 G clean data were obtained. In addition, 82.09–86.03% of clean reads were mapped to the latest chromosomal-level BPH reference genome (Ma et al., 2021), and the Q30 percentage exceeded 91.58% (**Table 1**).

Results of the correlation analysis showed that the gene expression profiles of the four biological replicates of each bulked RNA sample correlated well (**Supplementary Figure 3** and **Supplementary Table 1**). Principle component analysis (PCA) showed that the first two principal components (PC1 and 2) explained 61 and 12.7% of the variance, respectively. Samples within each group clustered together (**Supplementary Figure 4**). In particular, 18,559 unigenes were identified based on the clean reads obtained from the two BPH extreme bulks. Based on the sequence homology, 10,450 unigenes were assigned to KOG functional classifications. These included 25 KOG categories, most commonly general function prediction only (21.48%), followed by: signal transduction mechanisms (14.08%); post-translational modification, protein turnover, chaperones (8.871%); transcription (6.134%); intracellular trafficking, secretion, and vesicular transport (5.33%); lipid transport and metabolism (4.813%); amino acid transport and metabolism (4.584%); and translation, ribosomal structure and biogenesis (3.962%) (**Figure 3**). Transcripts of numerous genes involved in basic processes such as translation and transcription, as well as functions including lipid transport, signal transduction, and post-translational modification mechanisms were detected.

Transcriptomic Profiles of Avirulent and Virulent Brown Planthoppers

Transcriptomic profiles of the vB15- and aB15-bulks were compared to identify DEGs with fold-change (FC) ≥ 2 and $P < 0.05$ (**Supplementary Figure 5**). In total, 751 DEGs were detected (**Supplementary Table 2**), of which 418 were more strongly expressed in the aB15-bulk and 333 in the vB15-bulk (**Figure 4A**). These findings indicate that feeding on the YHY15 plants induced stronger transcriptomic changes in the avirulent BPHs than in the virulent BPHs. We subsequently subjected to the DEGs to gene ontology (GO) analysis to identify the key processes that were enriched in each extreme bulk. The GO analysis (level 2) illustrated that GO terms that were mainly enriched in both aB15 and vB15-bulks were involved in single-organism, cellular, metabolic, binding, and catalytic activity processes (**Supplementary Figure 6** and **Supplementary Table 3**). Additionally, KEGG analysis (level 2) revealed that the 418 DEGs more strongly expressed in the aB15-bulk were mainly involved in: carbohydrate, amino acid and nucleotide metabolism; signal transduction; the endocrine system; and protein folding, sorting and degradation (**Figure 4B**). These changes indicate that *Bph15*-mediated resistance mechanisms induced substantial changes in diverse physiological processes of avirulent BPHs. The 333 DEGs more strongly expressed in the vB15-bulk were mainly assigned to lipid metabolism and digestive system categories (**Figure 4B**), suggesting that these pathways are crucial for BPH adaption to *Bph15*-mediated resistance.

We also subjected the DEGs to KEGG enrichment analysis (with a $P < 0.05$ threshold) to further pinpoint key pathways in each bulk. The 418 more strongly expressed in the aB15-bulk were mainly involved in: purine, carbohydrate, and amino acid metabolism; longevity regulation; and MAPK signaling pathways. Genes associated with six amino acids (Gly, Ser, Thr, Val, Leu, and Ile) were more strongly expressed in the aB15-bulk after feeding on resistant YHY15 rice plants. Genes of the glycolysis/gluconeogenesis, citrate cycle (TCA cycle), and pentose phosphate pathways of carbohydrate metabolism categories were significantly enriched in the avirulent BPHs (**Figure 4C** and **Supplementary Table 4**). In contrast, assignations of the 333 DEGs more strongly expressed in the vB15-bulk indicated significant enrichment of lipid metabolism (including steroid hormone and unsaturated fatty acid biosynthesis, fatty acid elongation, arachidonic acid metabolism, and glycerophospholipid metabolism pathways) in the virulent insects. Pancreatic secretion, vitamin digestion and absorption, and protein digestion and absorption pathways of the digestive system category were also significantly enriched

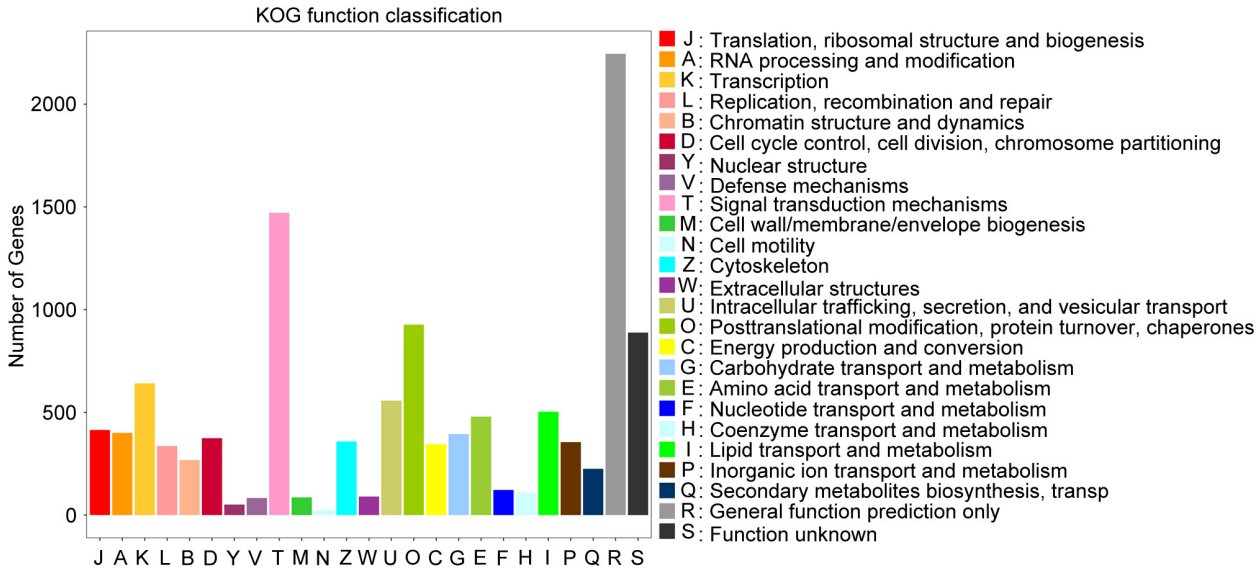

FIGURE 3 | Histogram of numbers of genes in orthologous group classes. In total 10,450 unigenes were annotated into 25 KOG categories and the number of unigenes in each specific functional clump is indicated on the *y*-axis.

in the vB15-bulk (**Figure 4D** and **Supplementary Table 4**). These results indicate that the virulent BPHs' adaption to YHY15 is related to lipid metabolism, protein digestion, and absorption pathways.

Verification of Differentially Expressed Genes in Key Pathways

To verify the reliability of the RNA sequencing data, we validated 30 randomly selected DEGs by quantitative reverse transcription-PCR (qRT-PCR) analysis with gene-specific primers (**Supplementary Table 5**). Expression levels of these 30 randomly selected DEGs (13 and 17 that were more strongly expressed in the vB15-bulk and aB15-bulk, respectively) were determined in both bulks, normalized with respect to *actin* expression, and then compared with the corresponding transcript read counts. Their expression levels according to the RNA-seq and qRT-PCR analyses correlated extremely well, with an R^2 value of 0.9574 (**Figure 5A**), clearly confirming the credibility of our RNA-seq data.

We also analyzed nine DEGs in the lipid metabolism pathway that were significantly enriched using qRT-PCR (**Supplementary Table 5**). These nine DEGs' annotations indicate that they are UDP-glucuronosyltransferases (**Supplementary Table 2**), which play diverse roles, including detoxification (Bock, 2016), by catalyzing the transfer of sugar molecules to lipid and protein acceptors (Zielinski et al., 2016). Expression levels of these genes were examined, by qRT-PCR, in representatives of the *Bph15*-virulent (Vr-B15) and *Bph15*-avirulent (Avr-B15) insects of biotype Y, with 2.0 mg weight gain and 0.4 mg weight loss after feeding on YHY15 plants for 48 h, respectively. The results showed that all these genes were expressed significantly more strongly in the Vr-B15 insect than the Avr-B15 insect (**Figure 5B**). These results are consistent with the pathway enrichment results, indicating that lipid metabolism pathways were regulated differentially in the virulent and avirulent insects in response to rice plants carrying the *Bph15* resistance gene.

Identification of Single-Nucleotide Polymorphisms Linked to Virulence

In total, 63127 SNPs with high confidence were obtained from the transcriptomic data of the two bulks. Application of the ΔSNP-index method identified 24 SNPs localized in 21 genes on six chromosomes at a significance level of 99% (**Supplementary Table 6**; Feng et al., 2020; Li et al., 2020; He et al., 2022). Moreover, two chromosome regions harboring SNPs were identified on chromosome 3 (73413752-83702207 and 88874910-94058321), as shown in **Figure 6** and **Supplementary Figure 7**. In addition, 33 of the 751 DEGs were located near identified SNPs linked to virulence (**Supplementary Table 7**). These results clearly suggest that multiple loci control BPH virulence to plants with *Bph15*-mediated resistance.

Putative functions of the 21 genes hosting the 24 identified SNPs were annotated (**Supplementary Table 8**). One of these genes, *LOC111057305*, encodes a fatty acyl-CoA reductase (FAR), which plays a crucial role in insect pheromone biosynthesis (Teerawanichpan et al., 2010). Another, *LOC111052455*, encodes a member of the aldo–keto reductase 6 (AKR6) family involved in channel trafficking and membrane localization (Barski et al., 2009). One of these genes, *LOC111054236*, encodes a dipeptidyl peptidase 4 (DPP 4) protein, a vital digestive peptidase in *Tenebrio molitor* larvae (Tereshchenkova et al., 2016). Another, *LOC111046750*, encodes a peroxidasin homolog protein involved in basement membrane biogenesis, tissue development, and innate immune defense (Nelson et al., 1994). And *LOC120354300* encodes a zinc finger

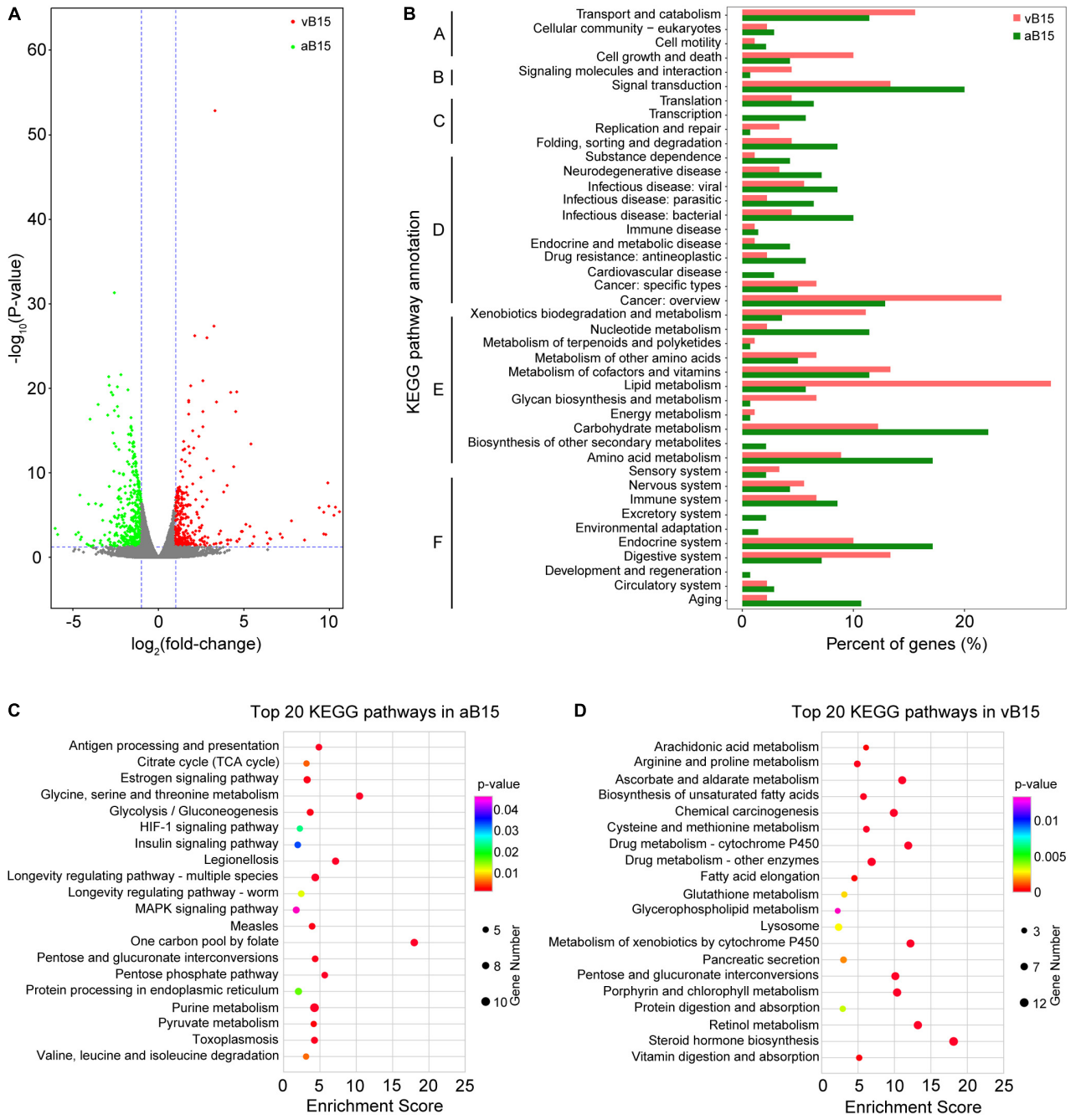

FIGURE 4 | Functional analyses of the differentially expressed genes (DEGs). **(A)** Volcano plots of DEGs ($P < 0.05$ and log2FC = 1.) between the vB15- and aB15-bulks, based on log2FC and FDR values. Green and red scatterpoints indicate DEGs more strongly expressed in the aB15-bulk and vB15-bulk, respectively. The results are based on comparison of expression of genes in vB15-bulk and aB15-bulk. **(B)** Kyoto Encyclopedia of Genes and Genomes (KEGG) classification of the DEGs more strongly expressed in the aB15- and vB15-bulks, respectively. The DEGs were assigned to KEGG pathways associated with: (A) Cellular processes; (B) Environmental information processing; (C) Genetic information processing; (D) Human diseases; (E) Metabolism; (F) Organismal systems. The DEGs more strongly expressed in the aB15-bulk were assigned to 42 KEGG categories, and those more strongly expressed in the vB15-bulk were assigned to 36 categories. **(C,D)** The 20 most highly enriched KEGG pathways in the aB15 and vB15 bulks, respectively.

protein, which has diverse functions, including lipid binding, transcriptional activation, regulation of apoptosis, and protein folding and assembly (Laity et al., 2001). Others include *LOC111055290*, an integrator complex subunit implicated in adipose differentiation (Otani et al., 2013), and *LOC111048257*, encoding a basement membrane specific heparan sulfate proteoglycan core protein. These candidate genes encode enzymes, zinc finger proteins, and other functional proteins

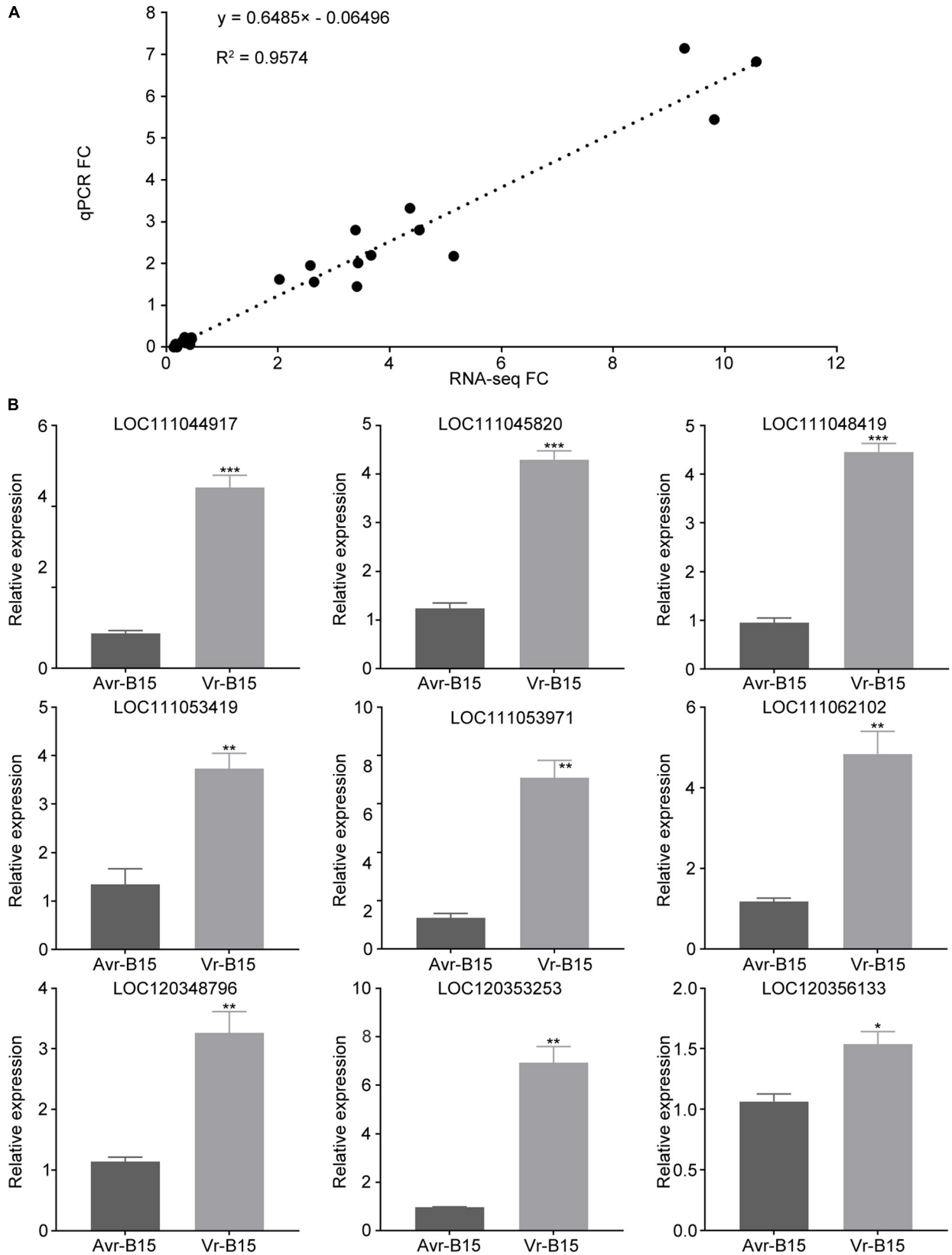

FIGURE 5 | (Continued)

FIGURE 5 | Validation of the transcriptome sequencing quality. **(A)** Correlation of the RNA-seq and RT-qPCR results. Expression levels of 30 randomly selected DEGs, including 13 and 17 more strongly expressed in the vB15-bulk and aB15-bulks, according to analyses of the RNA samples (normalized with respect to the BPH β-*actin* gene; three biological replicates). Fold-change values of these genes obtained from the RNA-seq and RT-qPCR analyses are strongly positively correlated. **(B)** Expression levels of nine DEGs related to lipid metabolism in Avr-B15 and Vr-B15 (avirulent and virulent BPHs with 0.4 mg weight loss and 2.0 mg weight gain after feeding on a YHY15 plant for 48 h, respectively). Presented data are means ± SE of three replicates. Error bars indicate SEM, $n = 3$ independent experiments. Asterisks above the bars indicate significant differences, according to Student's *t*-test (*$P < 0.05$; **$P < 0.01$; ***$P < 0.001$).

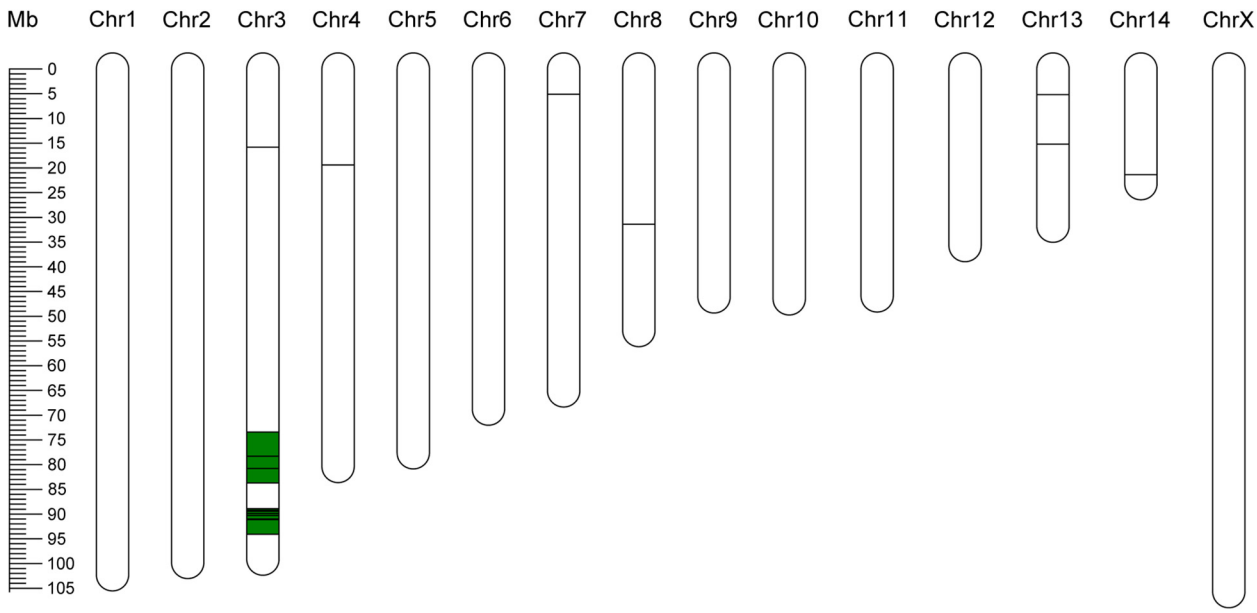

FIGURE 6 | Distribution of polymorphic SNPs on chromosomes. The horizontal lines indicate positions of SNPs with a significance level of 99%. The green blocks indicate chromosome regions linked to BPH virulence.

that may participate in BPH virulence to plants with *Bph15*-mediated resistance.

DISCUSSION

Previous studies have revealed significant genetic variations in virulence within BPH populations (Den Hollander and Pathak, 1981; Tanaka, 1999). Accordingly, this study found substantial variation in the virulence of randomly selected individuals of BPH biotype Y (**Figure 2A**). Thus, direct comparison of wild BPH populations may not readily identify genetic factors of BPH virulence (Via, 1990; Kobayashi, 2016). The heterogeneity of the parental BPH population also reportedly complicates inheritance of BPH virulence (Sogawa, 1981). Therefore, we mated a virulent female and an avirulent male to produce a F1 generation, and F1s were intermated to produce the F2 generation. Two BPH extreme bulks were constructed from the F2 population by the BSR approach. Virulence assessment validated these two extreme bulks (**Figure 2**), then 751 DEGs and 24 SNPs in 21 candidate genes were identified by BSR-seq analysis, confirming its suitability for studying BPH biotype Y's virulence to rice plants with *Bph15*-mediated resistance. To our knowledge, this is the first reported use of the BSR-seq method to identify candidate genes involved in BPH virulence to rice resistance.

Functional analyses of the identified DEGs showed that feeding on plants with *Bph15*-mediated resistance induced more extensive transcriptomic changes in the avirulent BPHs than in the virulent insects. Carbohydrates are the main chemical components in the phloem sap of rice and essential nutrients for phloem-sucking insects (Foyer et al., 2007). In this study, we detected 42 DEGs associated with carbohydrate metabolism in the two BPH bulks. More of these were expressed more strongly in avirulent BPHs than in virulent BPHs (**Figure 4B**). The expression patterns also showed that the glycolysis/gluconeogenesis, citrate cycle (TCA cycle), and pentose phosphate pathways were significantly enriched in the avirulent BPHs after feeding on resistant YHY15 rice plants (**Figure 4B**). These findings indicate that feeding on YHY15 plants induces upregulation of carbohydrate metabolism in avirulent BPH. We also found that it induced significant increases in expression of genes involved in synthesis of six amino acids (Gly, Ser, Thr, Val, Leu, and Ile) in the avirulent BPHs (**Figure 4C**). This has clear physiological implications as amino acids are the raw materials for protein synthesis and participate in myriads of fundamental processes in insects, including energy provision (Hargrove, 1976), sclerotization of newly formed cuticle (Andersen, 2007), and detoxification of harmful exogenous substances (Novoselov et al., 2015). Similarly, Peng et al. (2017) found that levels of six amino acids (Val, Leu,

Ser, Thr, Pro, and Gln) were higher in BPHs fed on resistant YHY15 rice plants than in counterparts fed on susceptible TN1 rice. Moreover, Liu et al. (2017) found that levels of 19 amino acids were lower in BPH nymphs after feeding on YHY15 rice than after feeding on TN1 plants for 12 h. These results suggest that the higher amino acid levels may contribute to the feeding and survival of avirulent BPHs on resistant YHY15 rice. MAPK signaling, purine metabolism, and longevity regulating pathways were also enriched in the avirulent BPHs after feeding on the resistant rice (**Figure 4C**). Collectively, these findings suggest that feeding on rice with *Bph15*-mediated resistance may perturb diverse physiological processes in avirulent BPHs.

In contrast, feeding on the YHY15 plants more specifically altered lipid metabolism in virulent biotype Y BPHs, in accordance with previous findings that lipid mobilization in their bodies is crucial for BPHs feeding on resistant rice plants (Yue et al., 2019). In this study, we found that it induced stronger expression of lipid metabolism-related pathways in virulent BPHs than in avirulent BPHs. Biosynthesis of steroid hormones and unsaturated fatty acids, fatty acid elongation, arachidonic acid metabolism, and glycerophospholipid metabolism pathways were significantly enriched in the virulent-BPH bulk (**Figure 4D**). These results indicate that lipid metabolism pathways are important for BPH virulence to *Bph15* resistance, and are consistent with previous reports that lipid metabolism in BPH fat bodies is activated when the insects feed on rice plants carrying *Bph6* or *Bph9* resistance genes (Zheng et al., 2020). In addition, efficient digestion and nutrient uptake are vital for insects to acquire essential nutrients from their diet (Holtof et al., 2019). Comparative analysis of salivary gland transcriptomes of two BPH populations derived from TN1 and Mudgo has revealed that genes related to "digestion and absorption" might be associated with BPH virulence (Ji et al., 2013). Results presented here indicate that feeding on the resistant plants induced stronger expression of pathways involved in the digestive system, including pancreatic secretion, as well as the digestion and absorption of vitamins and proteins in virulent BPHs (**Figures 4B,D**). These findings corroborate the importance of the digestive system's importance in BPH virulence. In sum, the findings indicate that lipid metabolism and digestive system pathways are strongly involved in BPHs' adaptation to resistant YHY15 plants.

Previous studies showed that the polygenic system controls BPH virulence (Claridge and Den Hollander, 1980; Tanaka, 1999; Jing et al., 2017). For example, BPH virulence to rice plants with *Bph1*-mediated resistance is influenced by a recessive gene located on linkage group 10 (Kobayashi et al., 2014), a gene on chromosome 7 influences the preference for *Bph1* plants, and two major QTLs on chromosomes 5 and 14 influence the insect's growth rates on resistant rice plants (Jing et al., 2014). The BSR-seq approach in this study extended these findings by identifying 24 SNPs linked with BPH virulence on six chromosomes. Most of these SNPs are located on chromosomes 3, followed by chromosomes 13, 4, 7, 8, and 14 (**Supplementary Table 6**). Furthermore, two chromosome regions (Chr3, 73413752-83702207 and 88874910-94058321) were identified (**Figure 6**). All the results suggest that the mechanism underlying BPH virulence is complex and involves multiple genes. In this analysis, we crossed a virulent female from biotype Y and an avirulent male from biotype 1 to produce an F2 population and performed a BSR-sequencing between the two extreme bulks. In the future, more BPH crosses and repeated BSR-sequencing analysis should be carried out to confirm and fine map the identified loci. Loci harboring the SNPs and candidate genes are expected to greatly facilitate determination of mechanisms involved in BPH virulence.

CONCLUSION

We identified 751 DEGs between the virulent and avirulent BPHs and mapped 24 SNPs linked to BPH virulence to rice plants with *Bph15*-mediated resistance by BSR-seq analysis. Functional analysis of 418 DEGs highly expressed in the avirulent insects showed that BPH upregulates carbohydrate, amino acid, and nucleotide metabolism, endocrine system, and signal transduction pathways in response to feeding on these plants. Lipid metabolism and digestive system pathways may play roles for BPH adaption to resistant rice. We expect the identification of relevant genetic loci and genes presented here to facilitate further research on BPH virulence mechanisms and responses to resistant plants.

DATA AVAILABILITY STATEMENT

The datasets presented in this study can be found in online repositories. The names of the repository/repositories and accession number(s) can be found below: https://www.ncbi.nlm.nih.gov/, PRJNA792102.

AUTHOR CONTRIBUTIONS

WG and GH designed the research, analyzed data, and wrote the manuscript. WG performed most of the experiments. JS, MG, JG, DW, QZ, JW, RC, BD, LZ, and GH performed some of the experiments. All authors read and approved the manuscript.

FUNDING

This work was supported by a grant (no. 31630063) from the National Natural Science Foundation of China.

SUPPLEMENTARY MATERIAL

The Supplementary Material for this article can be found online at: https://www.frontiersin.org/articles/10.3389/fpls.2022.843227/full#supplementary-material

REFERENCES

Abd-El-Haliem, A. M., Hoogstrate, S. W., and Schuurink, R. C. (2018). A robust functional genomics approach to identify effector genes required for thrips (*Frankliniella occidentalis*) reproductive performance on tomato leaf discs. *Front. Plant Sci.* 9:1852. doi: 10.3389/fpls.2018.01852

Abe, A., Kosugi, S., Yoshida, K., Natsume, S., Takagi, H., Kanzaki, H., et al. (2012). Genome sequencing reveals agronomically important loci in rice using MutMap. *Nat. Biotechnol.* 30, 174–178. doi: 10.1038/nbt.2095

Anders, S., and Huber, W. (2012). *Differential Expression of RNA-Seq Data at the Gene Level – The DESeq Package*. Heidelberg: European Molecular Biology Laboratory.

Andersen, S. O. (2007). Involvement of tyrosine residues, N-terminal amino acids, and beta-alanine in insect cuticular sclerotization. *Insect Biochem. Mol. Biol.* 37, 969–974. doi: 10.1016/j.ibmb.2007.05.002

Barski, O. A., Tipparaju, S. M., and Bhatnagar, A. (2009). Kinetics of nucleotide binding to the beta-subunit (AKR6A2) of the voltage-gated potassium (Kv) channel. *Chem. Biol. Interact.* 178, 165–170. doi: 10.1016/j.cbi.2008.10.016

Bock, K. W. (2016). The UDP-glycosyltransferase (UGT) superfamily expressed in humans, insects and plants: animal-plant arms-race and co-evolution. *Biochem. Pharmacol.* 99, 11–17. doi: 10.1016/j.bcp.2015.10.001

Chen, C. Y., Liu, Y. Q., Song, W. M., Chen, D. Y., Chen, F. Y., Chen, X. Y., et al. (2019). An effector from cotton bollworm oral secretion impairs host plant defense signaling. *Proc. Natl. Acad. Sci. U.S.A.* 116, 14331–14338. doi: 10.1073/pnas.1905471116

Chepelev, I., Wei, G., Tang, Q., and Zhao, K. (2009). Detection of single nucleotide variations in expressed exons of the human genome using RNA-Seq. *Nucleic Acids Res.* 37:e106. doi: 10.1093/nar/gkp507

Cingolani, P., Platts, A., Wang le, L., Coon, M., Nguyen, T., Wang, L., et al. (2012). A program for annotating and predicting the effects of single nucleotide polymorphisms, SnpEff: SNPs in the genome of *Drosophila melanogaster* strain w1118; iso-2; iso-3. *Fly* 6, 80–92. doi: 10.4161/fly.19695

Claridge, M. F., and Den Hollander, J. (1980). The "biotypes" of the rice brown planthopper, *Nilaparvata lugens*. *Entomol. Exp. Appl.* 27, 23–30. doi: 10.1111/j.1570-7458.1980.tb02942.x

Claridge, M. F., and Den Hollander, J. (1982). Virulence to rice cultivars and selection for virulence in populations of the brown planthopper *Nilaparvata lugens*. *Entomol. Exp. Appl.* 32, 213–221. doi: 10.1111/j.1570-7458.1982.tb03208.x

Danecek, P., Bonfield, J. K., Liddle, J., Marshall, J., Ohan, V., Pollard, M. O., et al. (2021). Twelve years of SAMtools and BCFtools. *Gigascience* 10:giab008. doi: 10.1093/gigascience/giab008

Den Hollander, J., and Pathak, P. K. (1981). The genetics of the "biotypes" of the rice brown planthopper, *Nilaparvata lugens*. *Entomol. Exp. Appl.* 29, 76–86. doi: 10.1111/j.1570-7458.1981.tb03044.x

Du, H., Zhu, J., Su, H., Huang, M., Wang, H., Ding, S., et al. (2017). Bulked Segregant RNA-seq reveals differential expression and SNPs of candidate genes associated with waterlogging tolerance in maize. *Front. Plant Sci.* 8:1022. doi: 10.3389/fpls.2017.01022

Feng, X., Li, X., Yang, X., and Zhu, P. (2020). Fine mapping and identification of the leaf shape gene *BoFL* in ornamental kale. *TAG* 133, 1303–1312. doi: 10.1007/s00122-020-03551-x

Foyer, C. H., Noctor, G., and van Emden, H. F. (2007). An evaluation of the costs of making specific secondary metabolites: does the yield penalty incurred by host plant resistance to insects result from competition for resources? *Int. J. Pest Manage.* 53, 175–182. doi: 10.1080/09670870701469146

Górczak, K., Claesen, J., and Burzykowski, T. (2020). A conceptual framework for abundance estimation of genomic targets in the presence of ambiguous short sequencing reads. *J. Comput. Biol.* 27, 1232–1247. doi: 10.1089/cmb.2019.0272

Grbić, M., Van Leeuwen, T., Clark, R. M., Rombauts, S., Rouzé, P., Grbić, V., et al. (2011). The genome of *Tetranychus urticae* reveals herbivorous pest adaptations. *Nature* 479, 487–492. doi: 10.1038/nature10640

Guo, J., Xu, C., Wu, D., Zhao, Y., Qiu, Y., Wang, X., et al. (2018). *Bph6* encodes an exocyst-localized protein and confers broad resistance to planthoppers in rice. *Nat. Genet.* 50, 297–306. doi: 10.1038/s41588-018-0039-6

Hargrove, J. W. (1976). Amino acid metabolism during flight in tsetse flies. *J. Insect Physiol.* 22, 309–313. doi: 10.1016/0022-1910(76)90040-8

He, P., Wei, P., Ma, Y., Hu, S., Yao, J., Jiang, X., et al. (2022). Candidate sex-associated gene identification in *Trachinotus ovatus* (Carangidae) using an integrated SLAF-seq and bulked segregant analysis approach. *Gene* 809:146026. doi: 10.1016/j.gene.2021.146026

Hibino, H. (1996). Biology and epidemiology of rice viruses. *Annu. Rev. Phytopathol.* 34, 249–274. doi: 10.1146/annurev.phyto.34.1.249

Hisano, H., Sakamoto, K., Takagi, H., Terauchi, R., and Sato, K. (2017). Exome QTL-seq maps monogenic locus and QTLs in barley. *BMC Genomics* 18:125. doi: 10.1186/s12864-017-3511-2

Holtof, M., Lenaerts, C., Cullen, D., and Vanden Broeck, J. (2019). Extracellular nutrient digestion and absorption in the insect gut. *Cell Tissue Res.* 377, 397–414. doi: 10.1007/s00441-019-03031-9

Jena, K. K., and Kim, S. M. (2010). Current status of brown planthopper (BPH) resistance and genetics. *Rice* 3, 161–171. doi: 10.1007/s12284-010-9050-y

Ji, R., Yu, H., Fu, Q., Chen, H., Ye, W., Li, S., et al. (2013). Comparative transcriptome analysis of salivary glands of two populations of rice brown planthopper, *Nilaparvata lugens*, that differ in virulence. *PLoS One* 8:e79612. doi: 10.1371/journal.pone.0079612

Jing, S., Liu, B., Peng, L., Peng, X., Zhu, L., Fu, Q., et al. (2012). Development and use of EST-SSR markers for assessing genetic diversity in the brown planthopper (*Nilaparvata lugens* Stål). *Bull. Entomol. Res.* 102, 113–122. doi: 10.1017/S0007485311000435

Jing, S., Zhang, L., Ma, Y., Liu, B., Zhao, Y., Yu, H., et al. (2014). Genome-wide mapping of virulence in brown planthopper identifies loci that break down host plant resistance. *PLoS One* 9:e98911. doi: 10.1371/journal.pone.0098911

Jing, S., Zhao, Y., Du, B., Chen, R., Zhu, L., and He, G. (2017). Genomics of interaction between the brown planthopper and rice. *Curr. Opin. Insect Sci.* 19, 82–87. doi: 10.1016/j.cois.2017.03.005

Kim, D., Langmead, B., and Salzberg, S. L. (2015). HISAT: a fast spliced aligner with low memory requirements. *Nat. Methods* 12, 357–360. doi: 10.1038/nmeth.3317

Kobayashi, T. (2016). Evolving ideas about genetics underlying insect virulence to plant resistance in rice-brown planthopper interactions. *J. Insect Physiol.* 84, 32–39. doi: 10.1016/j.jinsphys.2015.12.001

Kobayashi, T., Yamamoto, K., Suetsugu, Y., Kuwazaki, S., Hattori, M., Jairin, J., et al. (2014). Genetic mapping of the rice resistance-breaking gene of the brown planthopper *Nilaparvata lugens*. *Proc. Biol. Sci.* 281:20140726. doi: 10.1098/rspb.2014.0726

Laity, J. H., Lee, B. M., and Wright, P. E. (2001). Zinc finger proteins: new insights into structural and functional diversity. *Curr. Opin. Struct. Biol.* 11, 39–46. doi: 10.1016/s0959-440x(00)00167-6

Lam, S., Zeidan, J., Miglior, F., Suárez-Vega, A., Gómez-Redondo, I., Fonseca, P., et al. (2020). Development and comparison of RNA-sequencing pipelines for more accurate SNP identification: practical example of functional SNP detection associated with feed efficiency in Nellore beef cattle. *BMC Genomics* 21:703. doi: 10.1186/s12864-020-07107-7

Li, L., Li, D. L., Liu, S. Z., Ma, X. L., Dietrich, C. R., Hu, H. C., et al. (2013). The maize *glossy13* gene, cloned via BSR-seq and seq-walking, encodes a putative ABC transporter required for the normal accumulation of epicuticular waxes. *PLoS One* 9:e99563. doi: 10.1371/journal.pone.0082333

Li, Q., Pan, Z., Gao, Y., Li, T., Liang, J., Zhang, Z., et al. (2020). Quantitative Trait Locus (QTLs) mapping for quality traits of wheat based on high density genetic map combined with Bulked Segregant Analysis RNA-seq (BSR-Seq) indicates that the *basic 7s globulin* gene is related to falling number. *Front. Plant Sci.* 11:600788. doi: 10.3389/fpls.2020.600788

Liu, C., Du, B., Hao, F., Lei, H., Wan, Q., He, G., et al. (2017). Dynamic metabolic responses of brown planthoppers towards susceptible and resistant rice plants. *Plant Biotechnol. J.* 15, 1346–1357. doi: 10.1111/pbi.12721

Liu, S. Z., Yeh, C. T., Tang, H. M., Nettleton, D., and Schnable, P. S. (2012). Gene mapping via bulked segregant RNA-seq (BSR-seq). *PLoS One* 7:e36406. doi: 10.1371/journal.pone.0036406

Lv, W., Du, B., Shangguan, X., Zhao, Y., Pan, Y., Zhu, L., et al. (2014). BAC and RNA sequencing reveal the brown planthopper resistance gene *BPH15* in a recombination cold spot that mediates a unique defense mechanism. *BMC Genomics* 15:674. doi: 10.1186/1471-2164-15-674

Ma, W., Xu, L., Hua, H., Chen, M., Guo, M., He, K., et al. (2021). Chromosomal-level genomes of three rice planthoppers provide new insights into sex chromosome evolution. *Mol. Ecol. Resour.* 21, 226–237. doi: 10.1111/1755-0998.13242

Michelmore, R. W., Paran, I., and Kesseli, R. V. (1991). Identification of markers linked to disease-resistance genes by bulked segregant analysis: a rapid method to detect markers in specific genomic regions by using segregating populations. *Proc. Natl. Acad. Sci. U.S.A.* 88, 9828–9832. doi: 10.1073/pnas.88.21.9828

Navarro-Escalante, L., Zhao, C., Shukle, R., and Stuart, J. (2020). BSA-Seq discovery and functional analysis of candidate hessian fly (*Mayetiola destructor*) avirulence genes. *Front. Plant Sci.* 11:956. doi: 10.3389/fpls.2020.00956

Nelson, R. E., Fessler, L. I., Takagi, Y., Blumberg, B., Keene, D. R., Olson, P. F., et al. (1994). Peroxidasin: a novel enzyme-matrix protein of drosophila development. *EMBO J.* 13, 3438–3447. doi: 10.1002/j.1460-2075.1994.tb06649.x

Novoselov, A., Becker, T., Pauls, G., von Reuß, S. H., and Boland, W. (2015). *Spodoptera littoralis* detoxifies neurotoxic 3-nitropropanoic acid by conjugation with amino acids. *Insect Biochem. Mol. Biol.* 63, 97–103. doi: 10.1016/j.ibmb.2015.05.013

Otani, Y., Nakatsu, Y., Sakoda, H., Fukushima, T., Fujishiro, M., Kushiyama, A., et al. (2013). Integrator complex plays an essential role in adipose differentiation. *Biochem. Biophys. Res. Commun.* 434, 197–202. doi: 10.1016/j.bbrc.2013.03.029

Pathak, P. K., and Heinrichs, E. A. (1982). Selection of biotype populations 2 and 3 of *Nilaparvata lugens* by exposure to resistant rice varieties. *Environ. Entomol.* 11, 85–90. doi: 10.1093/ee/11.1.85

Pauchet, Y., Muck, A., Svatos, A., Heckel, D. G., and Preiss, S. (2008). Mapping the larval midgut lumen proteome of *Helicoverpa armigera*, a generalist herbivorous insect. *J. Proteome Res.* 7, 1629–1639. doi: 10.1021/pr7006208

Peng, L., Zhao, Y., Wang, H., Song, C., Shangguan, X., Ma, Y., et al. (2017). Functional study of cytochrome p450 enzymes from the brown planthopper (*Nilaparvata lugens* Stål) to analyze its adaptation to BPH-resistant rice. *Front. Physiol.* 8:972. doi: 10.3389/fphys.2017.00972

Pérez-Rubio, P., Lottaz, C., and Engelmann, J. C. (2019). FastqPuri: high-performance preprocessing of RNA-seq data. *BMC Bioinformatics* 20:226. doi: 10.1186/s12859-019-2799-0

Rajan-Babu, I. S., Peng, J. J., Chiu, R., Imagine Study, Causes Study, Li, C., et al. (2021). Genome-wide sequencing as a first-tier screening test for short tandem repeat expansions. *Genome Med.* 13:126. doi: 10.1186/s13073-021-00932-9

Roberts, A., Trapnell, C., Donaghey, J., Rinn, J. L., and Pachter, L. (2011). Improving RNA-Seq expression estimates by correcting for fragment bias. *Genome Biol.* 12:R22. doi: 10.1186/gb-2011-12-3-r22

Saxena, R. C., Demayo, C. G., and Barrion, A. A. (1991). Allozyme variation among biotypes of the brown planthopper *Nilaparvata lugens* in the Philippines. *Biochem. Genet.* 29, 115–123. doi: 10.1007/BF00554205

Shi, S., Wang, H., Nie, L., Tan, D., Zhou, C., Zhang, Q., et al. (2021). Bph30 confers resistance to brown planthopper by fortifying sclerenchyma in rice leaf sheaths. *Mol. Plant.* 14, 1714–1732. doi: 10.1016/j.molp.2021.07.004

Smadja, C., Shi, P., Butlin, R. K., and Robertson, H. M. (2009). Large gene family expansions and adaptive evolution for odorant and gustatory receptors in the pea aphid, *Acyrthosiphon pisum*. *Mol. Biol. Evol.* 26, 2073–2086. doi: 10.1093/molbev/msp116

Sogawa, K. (1981). Hybridization experiments on 3 biotypes of the brown planthopper, *Nilaparvata lugens* (Homoptera: Delphacidae) at the IRRI, the Philippines. *Appl. Entomol. Zool.* 16, 193–199. doi: 10.1303/aez.16.193

Sogawa, K. (1982). The rice brown planthopper: feeding physiology and host plant interactions. *Ann. Rev. Entomol.* 27, 49–73. doi: 10.1146/annurev.en.27.010182.000405

Srinivasan, K. A., Virdee, S. K., and McArthur, A. G. (2020). Strandedness during cDNA synthesis, the stranded parameter in htseq-count and analysis of RNA-Seq data. *Brief. Funct. Genomics* 19, 339–342. doi: 10.1093/bfgp/elaa010

Takagi, H., Abe, A., Yoshida, K., Kosugi, S., Natsume, S., Mitsuoka, C., et al. (2013). QTL-seq: rapid mapping of quantitative trait loci in rice by whole genome resequencing of DNA from two bulked populations. *Plant J.* 74, 174–183. doi: 10.1111/tpj.12105

Tanaka, K. (1999). Quantitative genetic analysis of biotypes of the brown planthopper *Nilaparvata lugens*: heritability of virulence to resistant rice varieties. *Entomol. Exp. Appl.* 90, 279–287. doi: 10.1046/j.1570-7458.1999.00448.x

Teerawanichpan, P., Robertson, A. J., and Qiu, X. (2010). A fatty acyl-CoA reductase highly expressed in the head of honey bee (*Apis mellifera*) involves biosynthesis of a wide range of aliphatic fatty alcohols. *Insect Biochem. Mol. Biol.* 40, 641–649. doi: 10.1016/j.ibmb.2010.06.004

Tereshchenkova, V. F., Goptar, I. A., Kulemzina, I. A., Zhuzhikov, D. P., Serebryakova, M. V., Belozersky, M. A., et al. (2016). Dipeptidyl peptidase 4 – An important digestive peptidase in *Tenebrio molitor* larvae. *Insect Biochem. Mol. Biol.* 76, 38–48. doi: 10.1016/j.ibmb.2016.07.003

Trapnell, C., Williams, B. A., Pertea, G., Mortazavi, A., Kwan, G., van Baren, M. J., et al. (2010). Transcript assembly and quantification by RNA-Seq reveals unannotated transcripts and isoform switching during cell differentiation. *Nat. Biotechnol.* 28, 511–515. doi: 10.1038/nbt.1621

Via, S. (1990). Ecological genetics and host adaptation in herbivorous insects: the experimental study of evolution in natural and agricultural systems. *Annu. Rev. Entomol.* 35, 421–446. doi: 10.1146/annurev.en.35.010190.002225

Wang, B., Shahzad, M. F., Zhang, Z., Sun, H., Han, P., Li, F., et al. (2014). Genome-wide analysis reveals the expansion of Cytochrome P450 genes associated with xenobiotic metabolism in rice striped stem borer, *Chilo suppressalis*. *Biochem. Biophys. Res. Commun.* 443, 756–760. doi: 10.1016/j.bbrc.2013.12.045

Wang, R. J., Sun, L. Y., Bao, L. S., Zhang, J. R., Jiang, Y. L., Yao, J., et al. (2013). Bulk segregant RNA-seq reveals expression and positional candidate genes and allele-specific expression for disease resistance against enteric septicemia of catfish. *BMC Genomics* 14:929. doi: 10.1186/1471-2164-14-929

Wang, X., Zhang, M., Feng, F., and He, R. (2015). Differentially regulated genes in the salivary glands of brown planthopper after feeding in resistant versus susceptible rice varieties. *Arch. Insect Biochem. Physiol.* 89, 69–86. doi: 10.1002/arch.21226

Yang, H., You, A., Yang, Z., Zhang, F., He, R., Zhu, L., et al. (2004). High-resolution genetic mapping at the Bph15 locus for brown planthopper resistance in rice (*Oryza sativa* L.). *Theor. Appl. Genet.* 110, 182–191. doi: 10.1007/s00122-004-1844-0

Yue, L., Kang, K., and Zhang, W. (2019). Metabolic responses of brown planthoppers to IR56 resistant rice cultivar containing multiple resistance genes. *J. Insect Physiol.* 113, 67–76. doi: 10.1016/j.jinsphys.2018.10.001

Zhang, J., Guan, W., Huang, C., Hu, Y., Chen, Y., Guo, J., et al. (2019). Combining next-generation sequencing and single-molecule sequencing to explore brown plant hopper responses to contrasting genotypes of japonica rice. *BMC Genomics* 20:682. doi: 10.1186/s12864-019-6049-7

Zheng, X., Xin, Y., Peng, Y., Shan, J., Zhang, N., Wu, D., et al. (2020). Lipidomic analyses reveal enhanced lipolysis in planthoppers feeding on resistant host plants. *Sci. China Life Sci.* 64, 1502–1521. doi: 10.1007/s11427-020-1834-9

Zheng, X., Zhu, L., and He, G. (2021). Genetic and molecular understanding of host rice resistance and *Nilaparvata lugens* adaptation. *Curr. Opin. Insect Sci.* 45, 14–20. doi: 10.1016/j.cois.2020.11.005

Zhou, C., Zhang, Q., Chen, Y., Huang, J., Guo, Q., Li, Y., et al. (2021). Balancing selection and wild gene pool contribute to resistance in global rice germplasm against planthopper. *J. Integr. Plant Biol.* 63, 1695–1711. doi: 10.1111/jipb.13157

Zielinski, T., Reichman, M., Donover, P. S., and Lowery, R. G. (2016). Development and validation of a universal high-throughput UDP-glycosyltransferase assay with a time-resolved FRET signal. *Assay Drug Dev. Technol.* 14, 240–251. doi: 10.1089/adt.2016.711

Zogli, P., Pingault, L., Grover, S., and Louis, J. (2020). Ento(o)mics: the intersection of 'omic' approaches to decipher plant defense against sap-sucking insect pests. *Curr. Opin. Plant Biol.* 56, 153–161. doi: 10.1016/j.pbi.2020.06.002

Conflict of Interest: The authors declare that the research was conducted in the absence of any commercial or financial relationships that could be construed as a potential conflict of interest.

Publisher's Note: All claims expressed in this article are solely those of the authors and do not necessarily represent those of their affiliated organizations, or those of the publisher, the editors and the reviewers. Any product that may be evaluated in this article, or claim that may be made by its manufacturer, is not guaranteed or endorsed by the publisher.

Copyright © 2022 Guan, Shan, Gao, Guo, Wu, Zhang, Wang, Chen, Du, Zhu and He. This is an open-access article distributed under the terms of the Creative Commons Attribution License (CC BY). The use, distribution or reproduction in other forums is permitted, provided the original author(s) and the copyright owner(s) are credited and that the original publication in this journal is cited, in accordance with accepted academic practice. No use, distribution or reproduction is permitted which does not comply with these terms.

frontiers | Frontiers in Plant Science

ORIGINAL RESEARCH
published: 25 May 2022
doi: 10.3389/fpls.2022.880519

Response of Physiological, Reproductive Function and Yield Traits in Cultivated Chickpea (*Cicer arietinum* L.) Under Heat Stress

Poonam Devi[1], Uday Chand Jha[2], Vijay Prakash[3], Sanjeev Kumar[4], Swarup Kumar Parida[5]*, Pronob J. Paul[6], P. V. Vara Prasad[7], Kamal Dev Sharma[8], Kadambot H. M. Siddique[9]* and Harsh Nayyar[1]**

[1] Department of Botany, Panjab University, Chandigarh, India, [2] ICAR–Indian Institute of Pulses Research, Kanpur, India, [3] Agricultural Research Station (S.K.R.A.U, Bikaner), Sri Ganganagar, India, [4] Department of Plant Sciences, Central University of Punjab, Bhatinda, India, [5] National Institute of Plant Genome Research, New Delhi, India, [6] International Rice Research Institute South-Asia Hub, Hyderabad, India, [7] Sustainable Intensification Innovation Lab, Kansas State University, Manhattan, KS, United States, [8] Department of Agricultural Biotechnology, CSK Himachal Pradesh Agricultural University, Palampur, India, [9] The UWA Institute of Agriculture, The University of Western Australia, Perth, WA, Australia

OPEN ACCESS

Edited by:
Raul Antonio Sperotto,
Universidade do Vale do Taquari - Univates, Brazil

Reviewed by:
Daniel Kean Yuen Tan,
The University of Sydney, Australia
Teklehaimanot Haileselassie,
Addis Ababa University, Ethiopia
Cengiz Toker,
Akdeniz University, Turkey

***Correspondence:**
Uday Chand Jha
u9811981@gmail.com
Swarup Kumar Parida
swarup@nipgr.ac.in
Kadambot H. M. Siddique
kadambot.siddique@uwa.edu.au
Harsh Nayyar
harshnayyar@hotmail.com

Specialty section:
This article was submitted to Plant Abiotic Stress, a section of the journal Frontiers in Plant Science

Received: 21 February 2022
Accepted: 28 March 2022
Published: 25 May 2022

Citation:
Devi P, Jha UC, Prakash V, Kumar S, Parida SK, Paul PJ, Prasad PVV, Sharma KD, Siddique KHM and Nayyar H (2022) Response of Physiological, Reproductive Function and Yield Traits in Cultivated Chickpea (Cicer arietinum L.) Under Heat Stress. Front. Plant Sci. 13:880519. doi: 10.3389/fpls.2022.880519

Under global climate change, high-temperature stress is becoming a major threat to crop yields, adversely affecting plant growth, and ultimately resulting in significant yield losses in various crops, including chickpea. Thus, identifying crop genotypes with increased heat stress (HS) tolerance is becoming a priority for chickpea research. Here, we assessed the response of seven physiological traits and four yield and yield-related traits in 39 chickpea genotypes grown in normal-sown and late-sown environments [to expose plants to HS (>32/20°C) at the reproductive stage] for two consecutive years (2017–2018 and 2018–2019). Significant genetic variability for the tested traits occurred under normal and HS conditions in both years. Based on the tested physiological parameters and yield-related traits, GNG2171, GNG1969, GNG1488, PantG186, CSJ515, RSG888, RSG945, RVG202, and GNG469 were identified as promising genotypes under HS. Further, ten heat-tolerant and ten heat-sensitive lines from the set of 39 genotypes were validated for their heat tolerance (32/20°C from flowering to maturity) in a controlled environment of a growth chamber. Of the ten heat-tolerant genotypes, GNG1969, GNG1488, PantG186, RSG888, CSJ315, and GNG1499 exhibited high heat tolerance evidenced by small reductions in pollen viability, pollen germination, and pod set %, high seed yield plant^{-1} and less damage to membranes, photosynthetic ability, leaf water status, and oxidative processes. In growth chamber, chlorophyll, photosynthetic efficiency, pollen germination, and pollen viability correlated strongly with yield traits. Thus, GNG1969, GNG1488, PantG186, RSG888, CSJ315, and GNG1499 genotypes could be used as candidate donors for transferring heat tolerance traits to high-yielding heat-sensitive varieties to develop heat-resilient chickpea cultivars.

Keywords: chickpea, heat stress, climate resilience, genotype, physiological trait

INTRODUCTION

Plants have an optimum temperature range where they perform best based on their genetic makeup; exposure to temperatures beyond the threshold is considered heat stress (HS; Hatfield and Prueger, 2015). Extreme temperature adversely affects crop growth by damaging morphological, physiological, biochemical, and molecular characteristics and ultimately reducing yield (Hemantaranjan et al., 2014; Sehgal et al., 2018; Jameel et al., 2021). At the sub-cellular level, HS impairs vital processes such as photosynthesis, respiration, membrane functioning, and water relations, affecting the functioning of enzymes, proteins, hormones, and primary and secondary metabolites (Bita and Gerats, 2013; Chaudhary et al., 2020). Additionally, HS can induce the accumulation of reactive oxygen species, cause organelles to malfunction, alter phytohormone production and signaling, and induce transcriptomic re-programming and metabolomic changes (Hasanuzzaman et al., 2013). Heat stress is frequently associated with reduced water availability; thus, crops grown in tropical and sub-tropical environments should be evaluated for their HS response (Barnabás et al., 2008; Krishnamurthy et al., 2011).

Temperatures are rising globally due to climate change and anthropogenic reasons (Mukherjee et al., 2018), posing a serious threat to various agricultural crops, including cool-season legumes such as chickpea. Heat stress at critical stages during plant development, especially the reproductive stage, severely constrains chickpea production. Chickpea performs well when the reproductive stage coincides with average temperatures of 20–28°C (Devasirvatham et al., 2013). However, temperatures (>32°C) during flowering and pod filling lead to various anomalies in reproductive organs resulting in flower drop, pollen sterility, pod abortion, and substantial losses in seed yield (Singh et al., 2016; Gaur et al., 2019; Pareek et al., 2019; Jha et al., 2021). Therefore, it is vital to develop heat tolerance in chickpea under the prevailing HS conditions.

Substantial reductions in chickpea yield have been observed for even a 1°C rise in temperature beyond the threshold (Kalra et al., 2008). Canci and Toker (2009) reported large-scale genetic variation in a field evaluation of 377 chickpea germplasm lines and 68 accessions of wild *Cicer* species, identifying several heat-tolerant genotypes and suggesting that harvest index, seed yield, and pods plant^{-1} be considered as selection traits. Similarly, Gaur et al. (2010) studied 180 chickpea genotypes at two locations in India and found large genetic variation for pod number. Information about genotypic diversity in terms of specific morpho-physiological and reproductive traits in chickpea is rarely available, hence the existing chickpea germplasm need to be assessed to identify heat tolerant genotypes and the underlying mechanisms. This study developed an effective, simple, and reliable screening method with well-defined traits for selecting heat-tolerant chickpea genotypes under field conditions. The screening method could be used to identify germplasm with increased heat tolerance for introgression into commercial chickpea breeding programs.

MATERIALS AND METHODS

Field and Growth Chamber Experiments

The seeds of 39 chickpea (*Cicer arietinum* L.) genotypes (**Supplementary Table 1**) were procured from various sources (Punjab Agricultural University, Ludhiana, India; Indian Institute of Pulse Research, Kanpur, India; Agricultural Research Station Sriganganagar, Rajasthan, India). Genotype ICC92944 (Source: ICRISAT) was used as a heat-tolerant check. Chickpea seeds were sown in pots (8 L capacity) containing a mixture of air-dried soil, sand, and farmyard manure [2:1:1 (v/v)]. The loam soil (pH 7.1) contained 54, 43, and 158 kg ha^{-1} of available N, P, and K, respectively. The seeds were inoculated with *Mesorhizobium* sp. at the recommended rate of 1.95 g kg^{-1} seeds. Five seeds were planted in each pot and thinned to three per pot after emergence (10 pots genotype^{-1} in triplicate). The experiment had a randomized complete block design. Meteorological information (mainly daily temperature and relative humidity profiles) from sowing date to maturity was recorded throughout the cropping season. The plants were grown in a natural environment outdoors in a wire-covered dome to protect them from birds and small animals at Panjab University, Chandigarh, India.

The chickpea genotypes were sown in pots on two sowing dates: (1) first week of November for normal sowing and (2) first week of January for late sowing to impose HS at the reproductive stage following CRBD. The year-wise weather details (Temperature, relative humidity, and light intensity) are given in **Supplementary Figure 1** and **Supplementary Table 2**.

In a separate experiment, conducted in controlled environment in a growth chamber (CRBD), plants of some selected genotypes (10 heat-tolerant, 10 heat-sensitive) at the onset of the bud stage were initially exposed to 25/15°C for a day, followed by a gradual increase by 2°C d^{-1} to obtain the required temperature (32/22°C). The plants were fully irrigated with (water applied twice daily at 10.00 a.m. and 7.00 p.m.) to avoid any drought stress during the heat treatment. The chamber had a light intensity of about 500 μmol m^{-2} s^{-1} and RH of 65–70% during the experiment.

Fresh leaves located at 2nd and 3rd branches from the top in control and heat-stressed plants (15 day after exposure to stress) were assessed for seven physiological traits [Electrolyte leakage (EL); leaf chlorophyll (CHL) content, stomatal conductance (gS), Fv/Fm photosystem II efficiency (PSII), malondialdehyde concentration (MDA)]. At the same time, the flowers (2 days before anthesis) were collected to measure pollen germination % (PGP), pollen viability % (PVP). The plants were also analyzed for pod set % (PSP), and yield-related traits [number of total pods plant^{-1} (NPP), seed yield plant^{-1} (SYP), single seed weight plant^{-1} (SSWP), biological mass]. The screening experiment (outdoors; conducted for two consecutive years) comprised of 10 pots for each of 39 genotypes (three plants pot^{-1}) grown in triplicate in a randomized block design. The validation experiment CRBD comprised of five pots for each selected genotypes (10 heat-tolerant and 10

heat-sensitive; three plants pot^{-1}) grown in triplicate in a complete randomized block design.

Physiological Traits

Electrolyte Leakage %

The leaves were assessed for membrane damage (as EL) to measure the permeability of cell membranes. Fresh leaves (100 mg) from the topmost branches were collected and washed with deionized water to remove surface-adhered electrolytes. The leaf tissue was placed in closed glass vials containing 10 mL deionized water and incubated at 25°C on a rotary shaker for 24 h. Electrical conductivity of the solution (L_1) was measured with a conductivity meter (ELICO CM 180, Hyderabad, India), expressed in mmhos g^{-1} dry weight (DW). The samples were then heated in a water bath at 120°C for 20 min before measuring final electrical conductivity (L_2) after equilibration at 25°C (Lutts et al., 1996). Electrolyte leakage was defined as EL (%) = $(L_1/L_2) \times 100$.

Stomatal Conductance

The stomatal conductance of fully expanded leaves (from the second or third branches from the top) was measured using a portable leaf porometer (model SC1, Decagon Devices, Pullman, WA, United States) at 11:00 h at the end of the stress period and expressed as mmol m^{-2} s^{-1} (Awasthi et al., 2014).

Chlorophyll Content (SPAD)

The chlorophyll (CHL; as SPAD value) of a tagged leaf was measured using a SPAD chlorophyll meter between 10.00 and 11.00 h using an Apogee-SPAD meter on alternative days for 2 weeks from 30 DAS (days after sowing).

Malondialdehyde

Lipid peroxidation of membranes was estimated in terms of MDA concentration, a lipid peroxidation product, following the method of Heath and Packer (1968). Fresh plant tissue (500 mg) was homogenized in 0.1% trichloroacetic acid (TCA), followed by centrifugation at 15,000 rpm for 5 min. A fraction of the supernatant (0.1 mL) was reacted with 0.5% thiobarbituric acid (4 mL) prepared in 20% TCA. The mixture was heated at 95°C for 30 min and then quickly cooled in an ice bath, followed by centrifugation at 10,000 rpm for 10 min at 4°C. The supernatant was used to measure absorbance at 532 nm. The MDA content was calculated using its extinction coefficient (155 mM^{-1} cm^{-1}) and expressed as nmol g^{-1} DW.

Leaf Photosynthetic Function

Photochemical efficiency was measured as chlorophyll fluorescence using the dark-adapted test of the modulated chlorophyll fluorometer OS1-FL (Opti-Sciences, Tyngsboro, MA, United States) at 11:00 h (Awasthi et al., 2014).

Reproductive Function

For assessing reproductive function, flowers were collected 15 days after exposure to stress.

Pollen Germination

In vitro pollen germination experiments were conducted using pollen grains collected from five flowers genotype^{-1} in three replications, as described by Brewbaker and Kwack (1963). The germination medium comprised 10% sucrose, 990 mM potassium nitrate (pH 6.5), 1.3 mM calcium nitrate, 1.64 mM boric acid, and 812 mM magnesium sulfate. Pollen grains are considered germinated when the diameter of the tube exceeds the diameter of the pollen grain. PGP was calculated from at least 100 pollen grains per replicate (Kaushal et al., 2013).

Pollen Viability

For PVP, pollen grains were collected from flowers that opened on the same day and pooled (Alexander, 1969), before adding 0.5% acetocarmine/Alexander stain. Viable pollen grains were selected based on shape and size (spherical or triangular) and the intensity of stain uptake (Kaushal et al., 2013). The observations were recorded for at least ten microscopic fields.

Yield Traits

Pod set %, NPP, SSWP, and SYP significantly varied ($P < 0.01$) among genotypes (**Table 1**). Under HS, these traits had high heritability, with 90.7, 89.4, and 89.7% in 2017–2018 and 90, 90.4, and 90.1% in 2018–2019, respectively, (**Table 2**).

Statistical Analyses

The plants were raised in outdoor and growth chamber environments using CRBD. Data were analyzed as a two-factorial (temperature and genotypes) experimental design using AGRISTAT statistical software (ICAR Research Complex, Goa, India). Standard errors and least significant differences ($P < 0.05$) for genotypes, treatments, and their interaction were computed. Phenotypic correlations were estimated to determine trait associations in GenStat 15. Using the R package cluster (Patterson and Thompson, 1971), the Euclidean dissimilarity matrix was constructed using all the traits and the accessions were clustered following Ward's method. Similarly, using the R package factoextra, the principal component analysis was performed. Heat map analysis was done as per Babicki et al. (2016).

RESULTS

Significant genetic variability for the tested traits was observed under normal and HS environment in both years (2017–2018 and 2018–2019). In accordance with the various tested physiological parameters and yield-related traits in the screening experiments, genotypes GNG2171, GNG1969, GNG1488, PantG186, CSJ515, RSG888, RSG945, RVG202, and GNG469 were identified as promising under HS in both years. In contrast, genotypes ICC10685, ICC96030, DCP92-3, PDG3, PDG4, GL15026, and GL15017 were identified as highly heat-sensitive due to their low pod set, SYP and other physiological parameters in both years.

Accordingly, ten heat-tolerant and ten heat-sensitive lines were selected from the set of 39 genotypes and further validated in a growth chamber under normal and heat-stressed conditions.

TABLE 1 | ANOVA for various traits recorded in chickpea genotypes grown outdoors in 2017–2018 and 2018–2019, and in a growth chamber under heat stress.

	Outdoor environment 2017–2018			Outdoor environment 2018–2019			Growth chamber		
	T	*G*	*T* × *G*	*T*	*G*	*T* × *G*	*T*	*G*	*T* × *G*
Electrolyte leakage	<0.01	<0.01	<0.01	<0.01	<0.01	<0.01	<0.01	<0.01	<0.01
Chlorophyll	<0.01	<0.01	<0.01	<0.01	<0.01	<0.01	<0.01	<0.01	<0.01
Photosynthetic efficiency (Fv/Fm)	<0.01	<0.01	ns	<0.01	<0.01	<0.01	<0.01	<0.01	<0.01
Stomatal conductance	ns	<0.01	<0.01	<0.01	<0.01	<0.01	<0.01	<0.01	<0.01
Malondialdehyde	<0.01	<0.01	<0.01	<0.01	<0.01	<0.01	<0.01	<0.01	<0.01
Pollen viability (%)	<0.01	<0.01	<0.01	<0.01	<0.01	<0.01	<0.01	<0.01	<0.01
Pollen germination (%)	<0.01	<0.01	<0.01	<0.01	<0.01	<0.01	<0.01	<0.01	<0.01
Pod set (%)	<0.01	<0.01	<0.01	<0.01	<0.01	<0.01	<0.01	<0.01	<0.01
Number of pods/plants	<0.01	<0.01	<0.01	<0.01	<0.01	<0.01	<0.01	<0.01	<0.01
Single seed weight per plant	<0.01	<0.01	<0.01	<0.01	<0.01	<0.01	<0.01	<0.01	<0.01
Seedyield per plant	<0.01	<0.01	<0.01	<0.01	<0.01	<0.01	<0.01	<0.01	<0.01
Biological mass	<0.01	<0.01	<0.01	<0.01	<0.01	<0.05	<0.01	<0.01	<0.01

ns, non significant.

Among the ten heat-tolerant lines, GNG1969, GNG1488, PantG186, RSG888, CSJ315, and GNG1499 exhibited high heat tolerance evidenced by small reductions in PVP, PGP, PSP, and SYP. Among the ten heat-sensitive lines, CSG8962, DCP92-3, IPC13-8, IPC14-9, and RSG931 exhibited high heat sensitivity evidenced by large reductions in these traits.

Physiological Traits

Electrolyte Leakage %

Heat stress significantly ($P < 0.01$) affected EL, a measure of membrane damage (**Supplementary Figure 2** and **Table 1**). Under HS, GNG 1969 (15.3%), GNG 1499 (16.4%), and Pant G186 (15.6%) had the lowest EL values in 2017–2018, and GNG 469, GNG 217, and Pant G186 had the lowest EL values in 2018–2019, similar to the heat-tolerant check ICC92944 (**Supplementary Figure 2**). EL had medium–high heritability under normal conditions (65.5 and 56.5%) and high heritability under HS (91.5 and 89.3%; **Table 2**). The heritability (h^2; %) of other traits is listed in **Table 2**.

Stomatal Conductance

Stomatal conductance (**Supplementary Figure 3**) varied among genotypes ($P < 0.01$; **Table 1**). Under normal conditions, GL13042 had the maximum value (485.7 mmol m^{-2} s^{-1}) in 2017–2018, and Pant G186 had the maximum value (511.70 mmol m^{-2} s^{-1}) in 2018–2019. Under HS, GNG1969 had the highest stomatal conductance (565.6) in 2017–2018, and GNG1488 (513.17) and GNG469 (511.73) had the highest in 2018–2019.

Chlorophyll (SPAD)

SPAD chlorophyll (**Supplementary Figure 4**) content declined drastically under HS and varied among genotypes ($P < 0.01$; **Table 1**). Mean SPAD values were 23.28 and 23.77 under normal conditions and 14.47 and 14.9 under HS in 2017–2018 and 2018–2019, respectively. GNG2171 (18.13) and GNG2299 (19) had the highest chlorophyll contents under HS in 2017–2018 and 2018–2019, respectively.

Chlorophyll Fluorescence

Chlorophyll fluorescence (Fv/Fm; **Supplementary Figure 5**) declined significantly under HS and varied among genotypes ($P < 0.01$; **Table 1**). Mean Fv/Fm values were 0.74 and 0.73 under normal conditions and 0.45 and 0.46 under HS in 2017–2018 and 2018–2019, respectively. GNG469 (0.62) and GNG1488 (0.63) had the highest Fv/Fm values under HS in 2017–2018 and 2018–2019, respectively.

Malondialdehyde

Malondialdehyde content varied significantly ($P < 0.01$) among genotypes (**Supplementary Figure 6** and **Table 1**), with mean values of 14.06 and 14.25 nmol g^{-1} DW under normal conditions and 43.5 and 44.17 under HS in 2017–2018 and 2018–2019, respectively. Under HS, GNG1488, GNG 1581, GNG 2207, RSG 888, and RSG 931 had the lowest Malondialdehyde contents (22.80–25.43) in 2017–2018, while GNG2207, GNG1488, GNG1499, and GNG663 had the lowest (22.8–23.77) in 2018–2019.

Reproductive Traits

Pollen Viability (%)

A considerable amount of genetic variability ($P < 0.01$; **Table 1**) was recorded for PVP (**Supplementary Figure 7**) and PGP (**Supplementary Figure 8**). Mean PVP values were 75.3 and 73.7 under normal conditions and 37.77 and 36.74 under HS. Maximum PVP values under normal conditions were recorded in GNG1499 and ICCV10 in 2017–2018 and 2018–2019, respectively. Under HS, PVP in GNG 2171 (24.45%) and RSG 931 (26.03%) in 2017–2018 and GNG 2144 (23.7%), GNG 469 (24%), and PantG 186 (23.9%) in 2018–2019 declined less than the heat-tolerant check ICCV 92944 (37.2 and 59.7%, respectively), relative to normal conditions.

Pollen Germination (%)

Under HS, PGP in GNG2171 (12.30%), RSG888 (12.16%), and GNG469 (13.96%) in 2017–2018 and GNG1581 (12.34%), CSJ515 (13.44%), and GNG2171 (13.57%) in 2018–2019 declined less

TABLE 2 | General statistics of various traits in chickpea genotypes under heat stress environment.

Traits	Mean	SE	Range	Heritability h^2 (%)
Heat-stress environment, 2017–2018				
Electrolyte leakage (%)	22.4	1.3	15.33–27.33	91.5
SPAD chlorophyll	14.47	0.6	12.3–18.13	92.1
Photosynthetic efficiency (Fv/Fm)	0.45	0	0.31–0.62	90
Stomatal conductance	427.4	19.3	308.7–571.9	94.8
Malondialdehyde	43.5	3.2	22.8–57.4	94.3
Pollen viability (%)	37.77	3.5	24–58.7	92.4
Pollengermination (%)	44.6	3.3	24.5–66.17	94.8
Pod set (%)	30.2	3	20.77–45.63	90.7
Number of podsplant^{-1}	12.58	1.3	5.33–20.67	89.4
Single seed weight (g)	0.19	0	0.11–0.29	93.2
Seed yield plant^{-1} (g)	2.47	0.4	0.71–4.94	89.7
Biological mass (g)	4.51	0.4	2.15–7.4	87.7
Heat-stress environment, 2018–2019				
Electrolyte leakage (%)	22.77	1.7	14.33–27.53	89.3
Chlorophyll	14.9	0.7	12.77–19	91.5
Photosynthetic efficiency (Fv/Fm)	0.46	0	0.33–0.63	90.6
Stomatal conductance	410.5	15.3	307.8–518.03	95.5
Malondialdehyde	44.17	3.2	22.77–58.03	95.5
Pollen viability (%)	36.74	3.1	23.47–55.83	94.5
Pollengermination (%)	42.85	3.9	21.37–64	93.3
Pod set (%)	31.36	3	22.83–45.73	90
Number of pods plant^{-1}	12.38	1.1	6.67–18.67	90.4
Single seed weight (g)	0.18	0	0.11–0.24	95
Seedyield plant^{-1} (g)	2.36	0.3	0.66–4.73	90.1
Biological mass (g)	4.45	0.3	2.62–5.61	84.8
Heat-stress environment under growth chamber				
Electrolyte leakage (%)	40.3	2.4	23.8–55.43	96.6
Chlorophyll	10.8	0.8	6.13–14.83	94.8
Photosynthetic efficiency (Fv/Fm)	0.51	0	0.34–0.64	96.8
Stomatal conductance	340.4	22.1	273.6–430.8	88
Malondialdehyde	21.7	1.3	14.8–32.4	96.8
Pollen viability (%)	0.51	0	0.34–0.64	96.8
Pollengermination (%)	45.6	2.2	32.07–61.07	96.2
Pod set (%)	51.38	1.7	33.63–64.6	98.4
Number of pods plant^{-1}	7.8	0.7	4.67–11.33	91.4
Single seed weight (g)	0.27	0.1	0.1–0.93	95.7
Seed yield plant^{-1} (g)	1.86	0.2	0.68–3.81	94.6
Biological mass (g)	4.1	0.2	3.17–4.82	90.8

than the heat-tolerant check ICCV92944 (43.93 and 53.83%, respectively), relative to normal conditions (**Figure 8**).

Yield Traits

Pod set % (**Figure 1**), NPP (**Figure 2**), SSWP (**Figure 3**), and SYP (**Figure 4**) significantly varied ($P < 0.01$) among genotypes (**Table 1**). Under HS, these traits had high heritability, with 90.7, 89.4, and 89.7% in 2017–2018 and 90, 90.4, and 90.1% in 2018–2019, respectively, (see **Table 2** for heritability of other traits).

GNG2144 (45.63%), GNG (44.97%), GNG1958 (44.80%), KWR (44.4%), RSG888 (43.63%), and GNG1488 (42.6%) in 2017–2018 and GNG1499 (43.97%), GNG1488 (44.875), GNG469 (44.97%) genotypes, and PantG186 (45.17%) in 2018–2019 had the highest PSP under HS, relative to heat-tolerant check ICCV92944 (24.6%; **Figure 1**).

GNG1581 (20.67), GNG2299 (19), RSG888 (17.3), and GNG469 (16.67) in 2017–2018 and GNG1581 (18.67), GNG2171 (16.67), and GNG663 (18) in 2018–2019 had the highest NPP under HS (**Figure 2**).

GNG1581 (0.29), GNG2144 (0.27), and GNG1958 (0.27) in 2017–2018 and GNG1581 (0.24) and GNG2144 (0.25) in 2018–2019 had higher single seed weights plant^{-1} than the heat-tolerant check ICC92944 (0.15 and 0.17 *g*, respectively) under HS (**Figure 3**).

Pant G186 (19.7%) in 2017–2018 and KWR108 (22.60%) in 2018–2019 had somewhat similar reductions

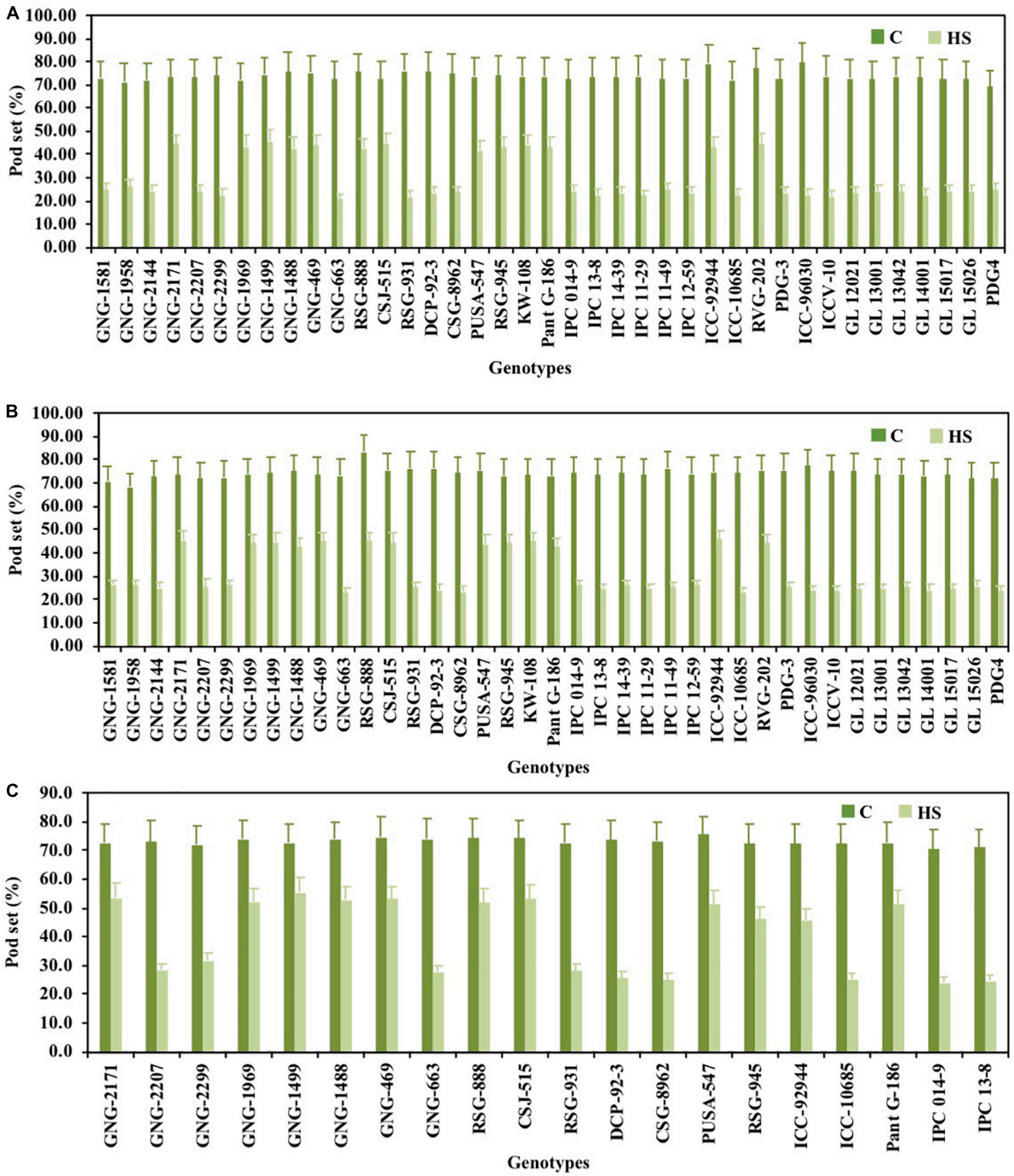

FIGURE 1 | Pod set (%) of chickpea genotypes under control (normal-sown; C) and heat stress (late-sown; HS) environment during 2017–2018 **(A)**, 2018–2019 **(B)** and in control environment of growth chamber (GC; C-control; HS-heat stress; **C)**. LSD values ($P < 0.05$); genotype × treatment: 9.3 (2017–2018), 11.3 (2018–2019), 11.7 (GC). Values are means + SE. ($n = 3$).

in SYP as the heat-tolerant check ICCV92944 (21.6 and 26.15%, respectively) under HS, relative to normal conditions (**Figure 4**).

Images 1, **2** illustrate the effects of HS on vegetative and reproductive components of chickpea plants.

Validation of Selected Genotypes Under Growth Chamber

The validation experiment in the growth chamber revealed significant differences ($P < 0.01$) between the ten heat-tolerant and ten heat-sensitive genotypes for the assessed traits

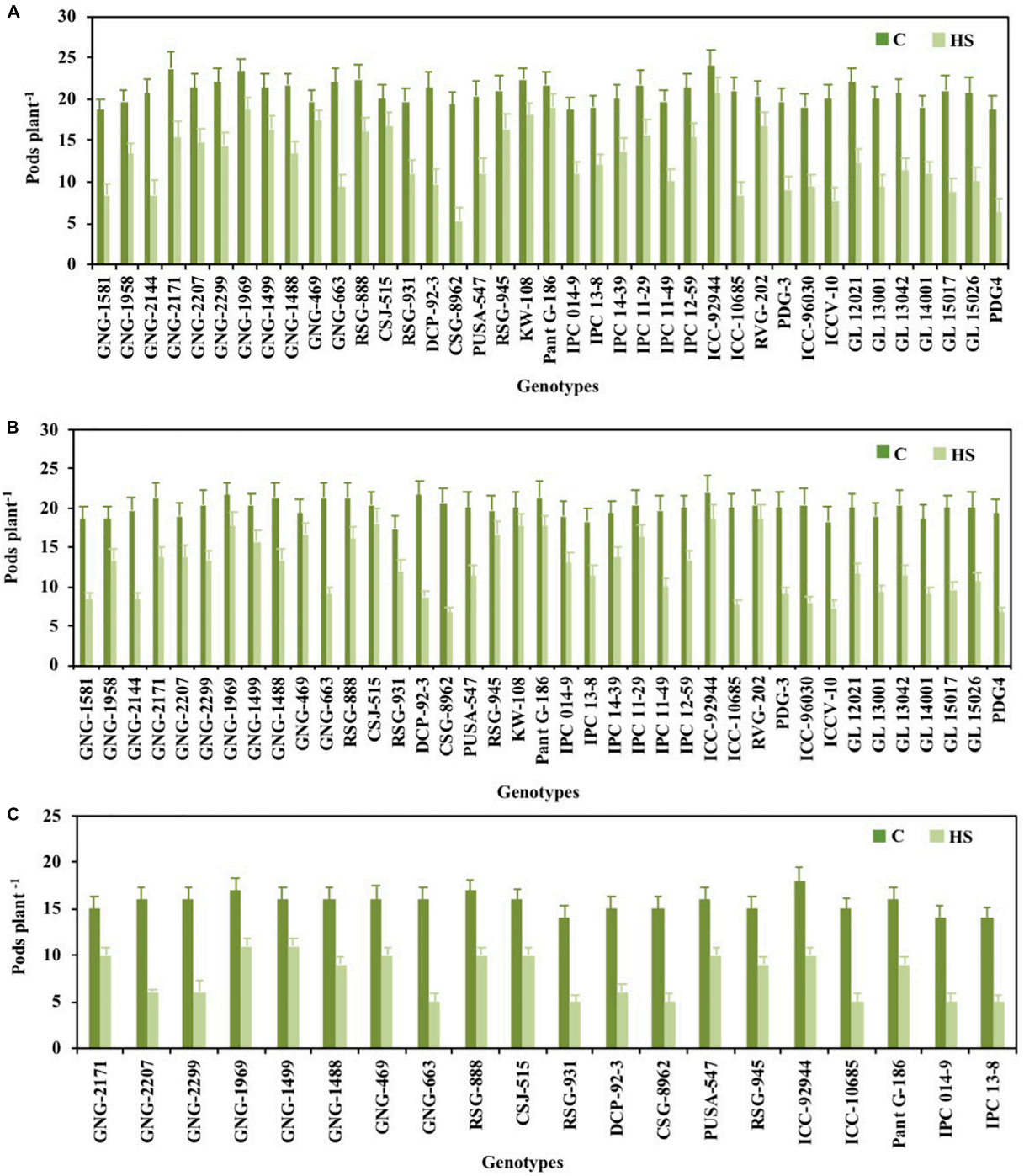

FIGURE 2 | Pod number plant^{-1} of chickpea genotypes under control (normal-sown; C) and heat stress (late-sown; HS) environment during 2017–2018 **(A)**, 2018–2019 **(B)** and in control environment of growth chamber (GC; C-control; HS-heat stress; **C)**. LSD values ($P < 0.05$); genotype × treatment: 2.9 (2017–2018), 3.6 (2018–2019), 3.1 (GC). Values are means + SE. ($n = 3$).

(**Table 1**). On the basis of chlorophyll content and stomatal conductance, genotypes GNG1488 (chlorophyll: 17.83 mg g^{-1} DW; **Supplementary Figure 4C**) and RSG888 (stomatal conductance; 388.2 mmol m^{-2} s^{-1}; **Supplementary Figure 3C** were identified as heat-tolerant. Likewise, GNG469 had high PVP (58.9%; **Supplementary Figure 7C**) and chlorophyll fluorescence values (**Supplementary Figure 5C**) and RSG888 had high PGP (64.6%; **Supplementary Figure 8C**) under HS. Genotype GNG1499 had the highest NPP (11.3; **Figure 2C**) under HS. The SYP of GNG1499 (16.9%), GNG 469 (22.6%), Pant

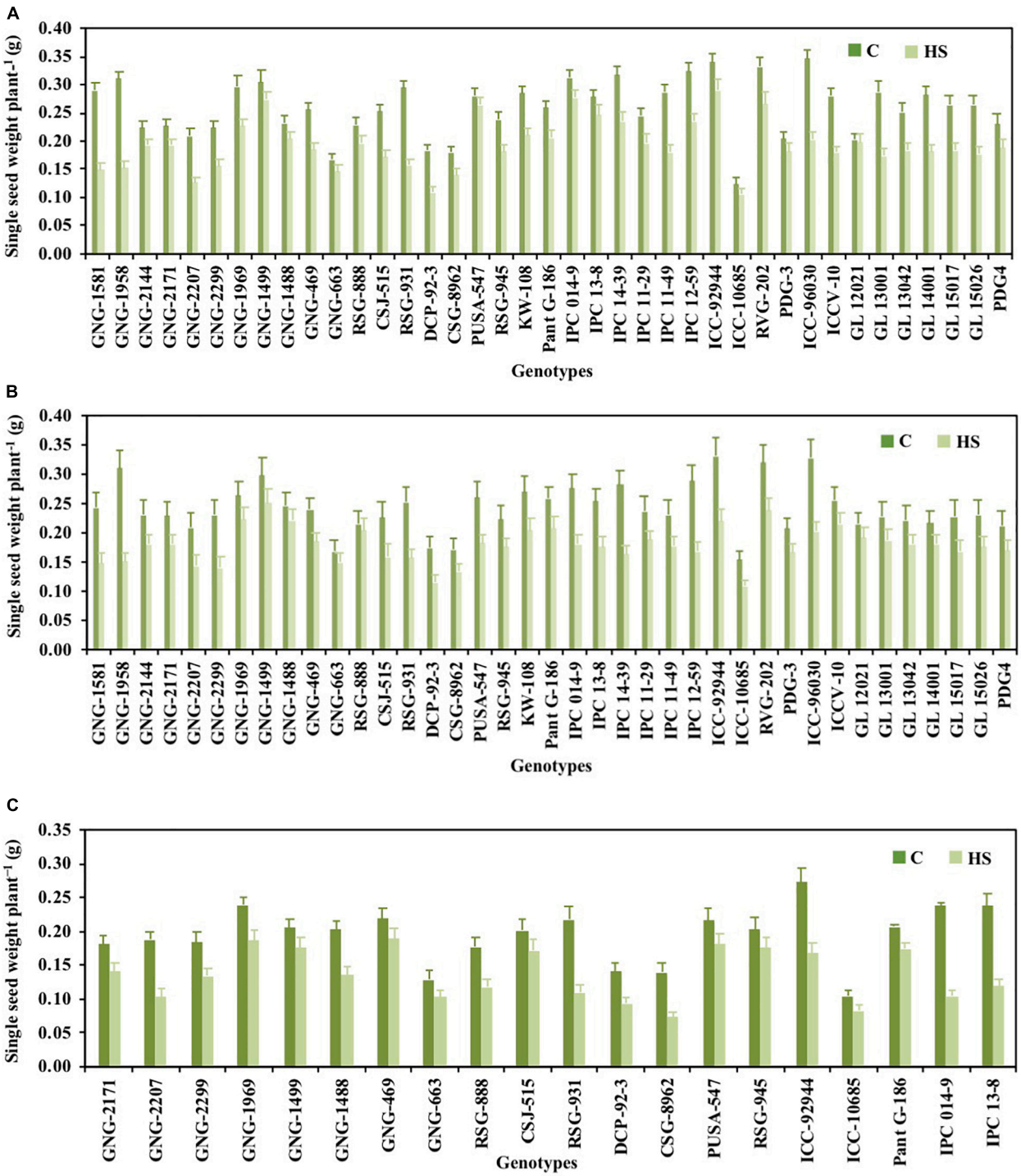

FIGURE 3 | Single seed weight of chickpea genotypes under control (normal-sown; C) and heat stress (late-sown; HS) environment during 2017–2018 **(A)**, 2018–2019 **(B)** and in control environment of growth chamber (GC; C-control; HS-heat stress; **C)**. LSD values ($P < 0.05$); genotype × treatment: 0.15 (2017–2018), 0.17 (2018–2019), 0.14 (GC). Values are means + SE. ($n = 3$).

G186 (6.8%), and RSG888 (27.5%) declined the least under HS (**Figure 4C**). Thus, the controlled environment study validated the heat tolerance of the selected genotypes based on various leaf-based reproductive and yield traits.

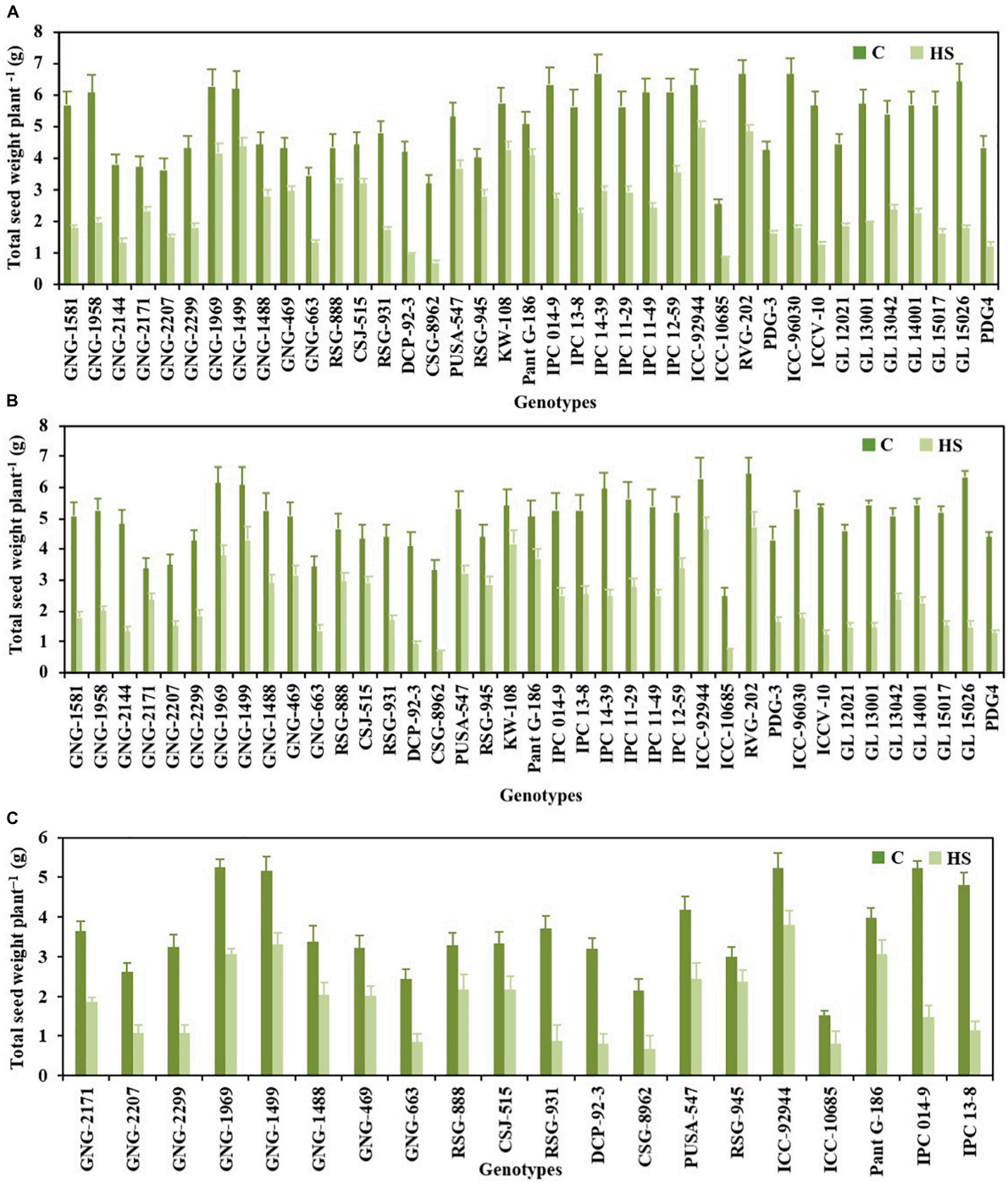

FIGURE 4 | Seed weight plant^{-1} of chickpea genotypes under control (normal-sown; C) and heat stress (late-sown; HS) environment during 2017–2018 **(A)**, 2018–2019 **(B)** and in control environment of growth chamber (GC; C-control; HS-heat stress; **C)**. Values are means + SE. (n = 3).

Correlation Analysis

Electrolyte leakage significantly correlated with NPP and SYP in all growth environments (**Table 3**). Similarly, significant negative correlations occurred between malondialdehyde and yield traits. Other leaf-based traits such as chlorophyll, photosynthetic efficiency, and stomatal conductance had strong positive correlations with NPP and SYP. Pollen-based traits such as PVP and PGP had significant positive correlations with yield traits. PSP strongly correlated with NPP and SYP (**Table 3**). In general, all of the measured traits, except

IMAGE 1 | Morphological symptoms of heat stress (HS) observed on in chickpea plants, showing plant height; under in the control condition **(a)**, reduced plant height; under the HS environment **(b)**, healthy leaves in the; under control condition **(c)**, leaf chlorosis under HS **(d)**, and leaf scorching ofleaves **(e)**, and leaf bleaching **(f)** ofleaflets due to photooxidation under HS **(e,f)**.

malondialdehyde and EL, had strong positive correlations with NPP and SYP.

Principal Component Analysis

In 2017–2018, four principal components, correlated to 12 traits, accounting for 96.6% of the total variability under HS. The individual contribution of each component was 74, 11.3, 7.7, and 3.4% (**Figure 5**). For PC1, major contributors are EL (0.3163) and malondialdehyde (0.31062) and chlorophyll (-0.31184) contributed the most negatively to PC1. For PC2, chlorophyll fluorescence (0.244) and PGP (0.225) had the greatest positive contributions, and SSWP (-0.584) and biomass (-0.409) had the greatest negative contributions. For PC4, SC (0.628) and SSWP (0.481) had the greatest positive contribution, and NPP (-0.488) had the greatest negative contribution.

In 2018–2019, four principal components, correlated to 12 traits, accounted for 96% of the total variability under HS. The individual contribution of each component was 74.5, 10.7, 7.2, and 3% (**Figure 6**). Analysis of the factor loadings of the characters in the retained PCs revealed that EL (0.314) and malondialdehyde (0.312) contributed most positively, and PSP (-0.316) contributed most negatively to PC1. For PC2, biomass

IMAGE 2 | Effects of heat stress (HS) in chickpea (reproductive phase) in comparison to control plants. Healthy flower bud under in the control condition **(a)**, aborted bud under HS **(b)**, healthy flower under in the control condition **(c)**, aborted flower under HS **(d)**, healthy pod under in the control condition **(e)**, aborted pod under HS **(f)**, mature filled pod under in the control condition **(g)**, unfilled mature pod under HS **(h)**, dissected flower showing the healthy anther under in the control condition **(i,j)**, distorted exposed anther under HS **(k,l)**, healthy style and stigma under in the control condition **(m,n)**, noticeable distorted shriveled stigma and style under HS **(o,p)**, healthy flower pollen load under in the control condition **(q,r)**, reduced pollen load under HS **(s,t)**, healthy viable pollen grains under in the control condition **(u,v)**, and distorted and shriveled pollen grains **(w,x)** as a sign of HS sensitivity to heat stress (HS).

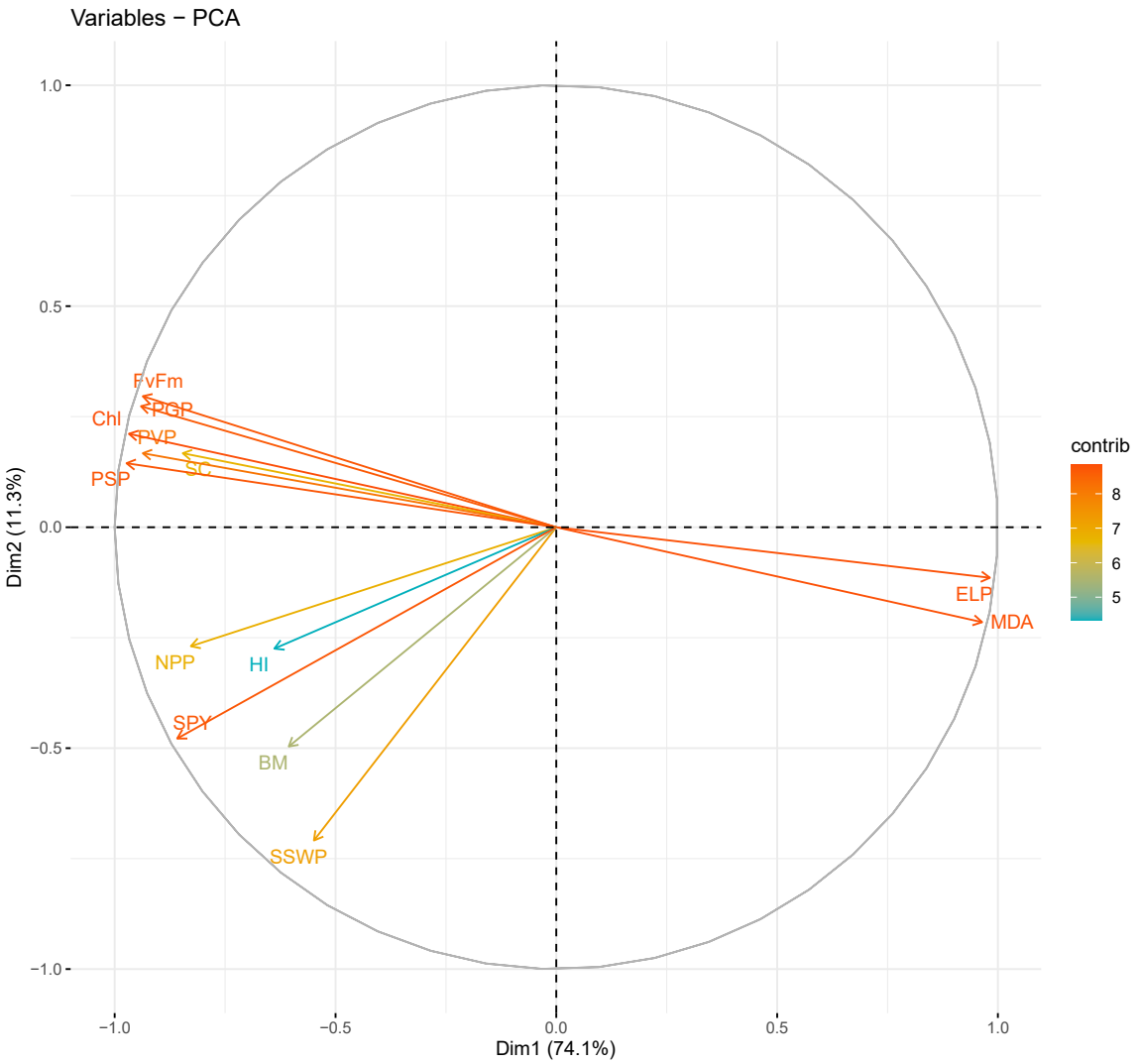

FIGURE 5 | Principal component analysis (PCA) of various traits in chickpea genotypes under heat stress in 2017–2018.

TABLE 3 | Correlation coefficients of various traits with yield traits in plants under heat stress environment.

	Outdoor environment 2017–2018		Outdoor environment 2018–2019		Growth chamber	
	Number of pods plant^{-1}	Seedyield plant^{-1}	Number of pods plant^{-1}	Seedyield plant^{-1}	Number of pods plant^{-1}	Seedyield plant^{-1}
Electrolyte leakage (%)	–0.77**	–0.79**	–0.77**	–0.77**	–0.79**	–0.77**
Chlorophyll	0.73**	0.73**	0.76**	0.77**	0.96**	0.86**
Photosynthetic efficiency (Fv/Fm)	0.68**	0.65**	0.74**	0.73*	0.97**	0.85**
Stomatal conductance	0.58**	0.61**	0.62**	0.67**	0.92**	0.83**
Malondialdehyde	–0.72**	–0.73**	–0.74**	0.75**	–0.85**	–0.73**
Pollen viability (%)	0.77**	0.72**	0.73**	0.67**	0.98**	0.84**
Pollen germination (%)	0.71**	0.68**	0.72**	0.67**	0.97**	0.84**
Pod set (%)	0.74**	0.77**	0.78**	0.80**	0.98**	0.81**
Number of pods plant^{-1}	1	0.84**	1	0.85**	1	0.87**
Single seed weight	0.46**	0.77**	0.50**	0.72**	–0.42**	–0.47**
Biological mass	0.80**	0.72**	0.70**	0.37*	0.80**	0.73**
Harvest index	0.56**	0.75**	0.82**	0.91**	0.81**	0.98**

*Significance at 5% and ** Significance at 1%.

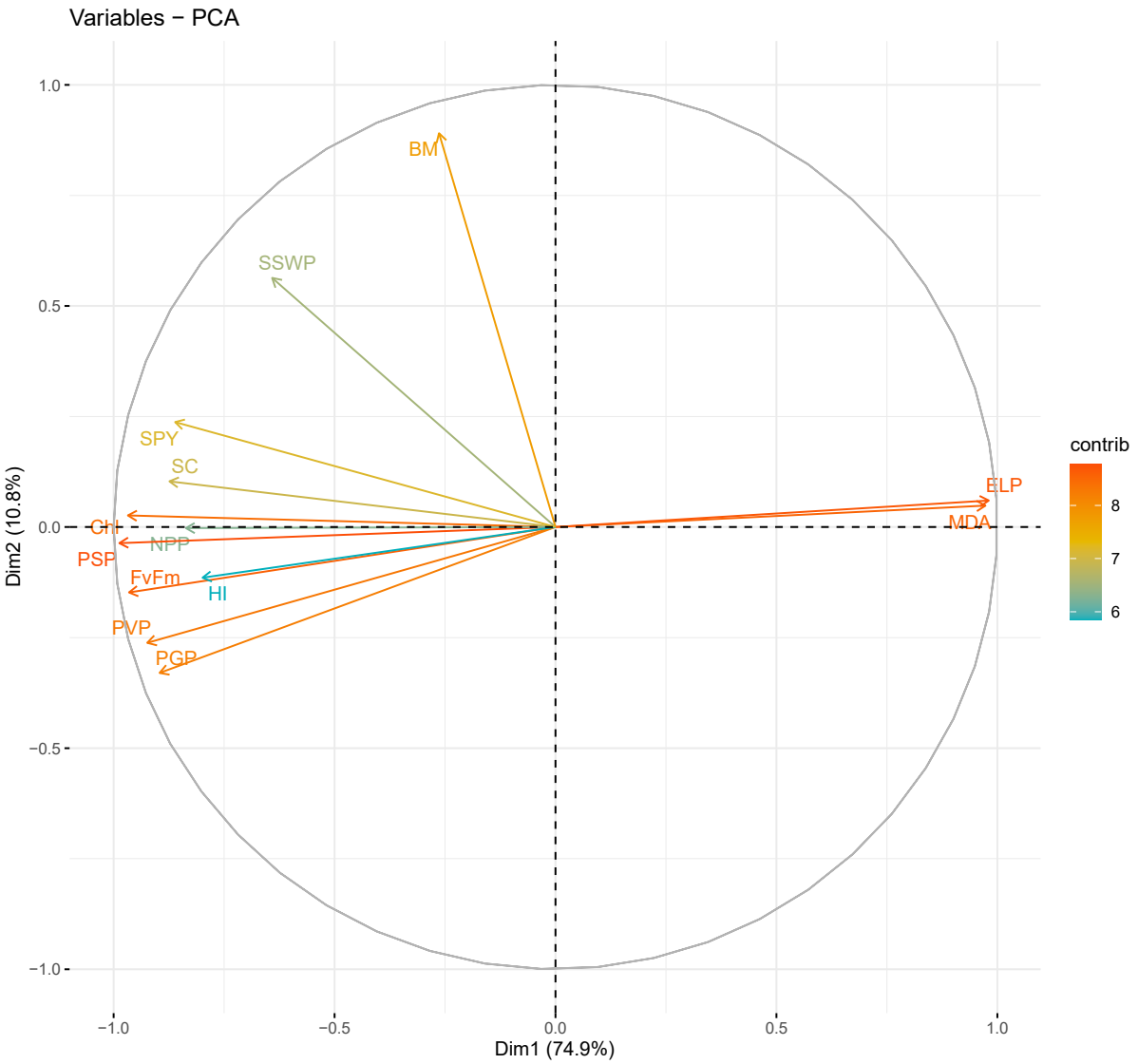

FIGURE 6 | Principal component analysis (PCA) of various traits in chickpea genotypes under heat stress in 2018–2019.

(0.75) and SSWP (0.476) had the greatest positive contributions and PGP (-0.27) had the greatest negative contribution. For PC3, NPP (0.347), SYP (0.416), and harvest index (0.58) had the greatest positive contributions, and stomatal conductance (-0.278) had the greatest negative contribution. For PC4, NPP (0.53) and biomass (0.38) had the greatest positive contribution and SSWP (-0.68) had the greatest negative contribution.

For the growth chamber environment, the extracted sums of squares loadings and component correlation matrix revealed three principal components correlated to all evaluated traits accounting for 94.7% of the total variability. The individual contribution of each component was 83.6, 6.9, and 4.2%. Analysis of the factor loadings of the characters in the retained PCs revealed that malondialdehyde (0.25) had the highest positive value and PGP (-0.2997) had the highest negative value for PC1 (**Figure 7**). For PC2, malondialdehyde (0.408) and biomass (0.102) had the highest positive values and SSWP (-0.886) had the highest negative value. For PC3, harvest index (0.68) and SYP (0.497) had the highest positive values, whereas biomass (-0.409) had the highest negative value.

Cluster Analysis for Identifying Heat-Tolerant Chickpea Genotypes Based on Physiological Yield Attributes in an Outdoor Environment

In 2017–2018, the heat map based on physiological attributes and yield responses of 39 chickpea genotypes to HS in an out-door environment revealed three clusters. Cluster I contained highly heat-sensitive genotypes based on high SYP reduction, PDG4 (71.53%), GL15026 (72.23%), GL15017 (71.28%), DCP92-3 (76.75%), CSG8962 (77.73%), and ICC10685 (66.77%; **Figure 8**).

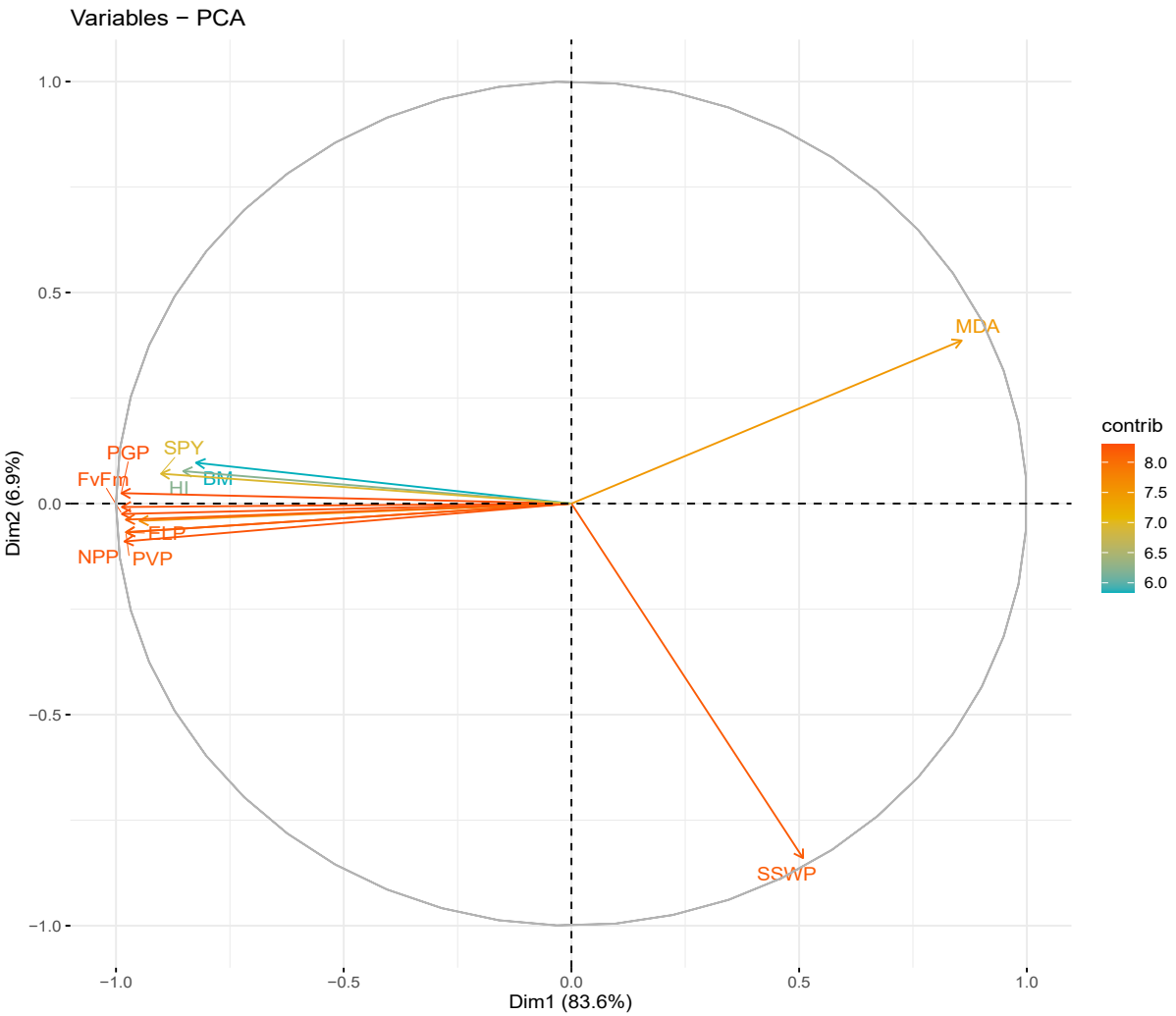

FIGURE 7 | Principal component analysis (PCA) of various traits in chickpea genotypes under heat stress in a growth chamber.

Cluster II contained heat-tolerant genotypes RSG945 (29.64%), KWR108 (25.1%), and PUSA547 (30.57%). Cluster III contained the most heat-tolerant genotypes CSJ515 (28.1%), RSG888 (25.4%), PantG186 (19.7%), ICCV92944 (21.6%), and GNG1499 (29.5%), based on lower seed yield per plant reduction.

Similarly, in 2018–2019, the heat map comprised three clusters (**Figure 9**). Cluster I contained highly heat-sensitive genotypes GL15026 (76.6%), GL13001 (73.3%), ICC10685 (70.8%), DCP92-3 (77.9%), and CSG8962 (80%). Cluster II contained heat-tolerant genotypes RSG945 (34.7%), GNG1969 (38.1%), and PUSA547 (39.4%). Cluster III contained highly heat-tolerant genotypes CSJ515 (32.9%), RSG888 (36.9%), PantG186 (26.7%), ICCV92944 (26.2%), and GNG1499 (29.3%).

Identifying Heat-Tolerant Genotypes in a Controlled Environment

The heat map based on the phenotypic responses of 20 selected genotypes to HS in a growth chamber revealed three clusters based on seed yield reduction (single plant) under normal and HS conditions (**Figure 10**). Based on low reduction of seed yield per plant, five of the ten selected heat-tolerant lines—RSG945 (20.80%), PantG186 (23.2%), ICCV92944 (27.17%), RSG888 (33.67%), and CSJ315 (34.57%)—exhibited high heat tolerance and five of the ten selected heat-sensitive lines—RSG931 (76.4%), IPC13-8 (76.1%), DCP92-3 (74.58%), IPC14-9 (71.7%), and CSG8962 (68.58%)—exhibited high heat sensitivity.

DISCUSSION

Heat stress during the reproductive stage, especially pollen development and fertilization, pod set, and grain filling, significantly reduces yield in various crops, including chickpea (Awasthi et al., 2014), wheat (Yang et al., 2002), lentil (Sita et al., 2017; Bhandari et al., 2020), wheat (Bheemanahalli et al., 2019), and pea (Jiang et al., 2020; Mohapatra et al., 2020). Therefore, capturing genetic diversity for various traits of physiological

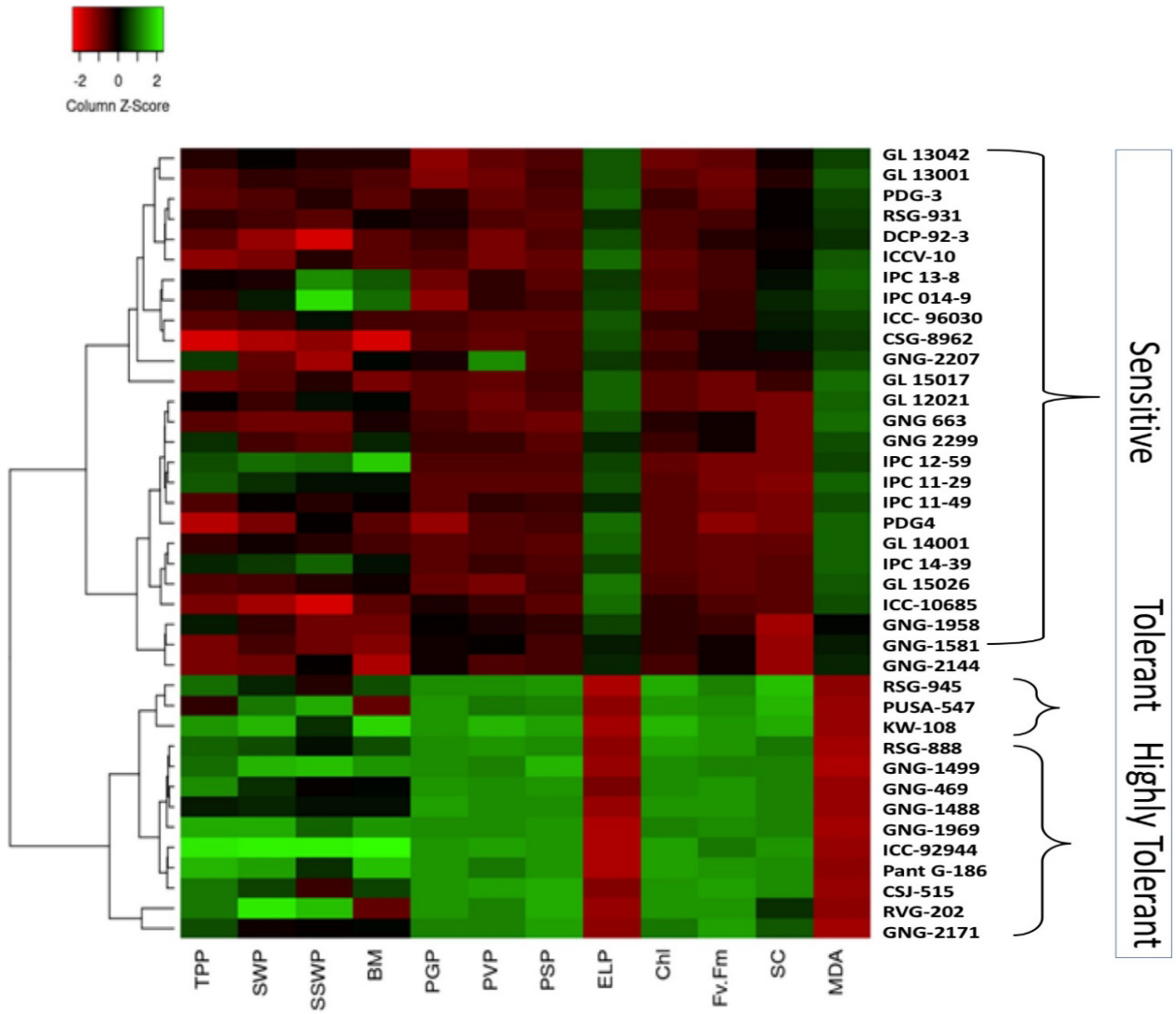

FIGURE 8 | Heat map based on the response of chickpea genotypes to heat stress in 2017–2018.

and breeding importance is a prime objective for developing heat-tolerant chickpea genotypes.

Here, we phenotyped 39 chickpea genotypes to identify sources of HS tolerance by exposing them to HS in the field and a growth chamber during heat-sensitive stages. We identified potential heat-tolerant chickpea donors with high pod set and grain yield, high chlorophyll content, PVP, PGP, photosystem II efficiency, and low MDA and EL% under HS.

High CHL content, photosystem II function, and stomatal conductance are important traits for selecting photosynthetically efficient genotypes under HS (Chaudhary et al., 2020). The heat-tolerant chickpea genotypes in the present study showed more chlorophyll content than heat-sensitive genotypes under high temperature environment of outdoor and growth chamber; these findings are similar to those reported previously in lentil plants subjected to HS (Sita et al., 2017; Bhandari et al., 2020). Previously, an average of 8% reduction in chlorophyll variable fluorescence, an important trait measuring injury to photosynthesis, was noted under HS condition, compared to normal environment, in pea (McDonald and Paulsen, 1997). Similarly, based on chlorophyll fluorescence induction traits, Petkova et al. (2007) screened 12 common bean lines for heat tolerance; "Ranit" and "Nerine" RS lines were identified to be heat tolerant on the basis of chlorophyll fluorescence. Improved functioning of stomatal conductance (gs), lower EL % and high retention of relative water content allowed in identifying 10 lentil genotypes viz., IG2507, IG3263, IG3297, and IG3312 under HS environment (Sita et al., 2017). Thus, in our study, we identified sufficient genetic variability for these traits under normal and HS conditions in the field and growth chamber for selecting heat-tolerant chickpea genotypes.

Heat stress decreases PGP and PVP in rice (Coast et al., 2016), wheat (Bheemanahalli et al., 2019), peanut (Kakani et al., 2002), sorghum (Sunoj et al., 2017), common bean (Soltani et al., 2019;

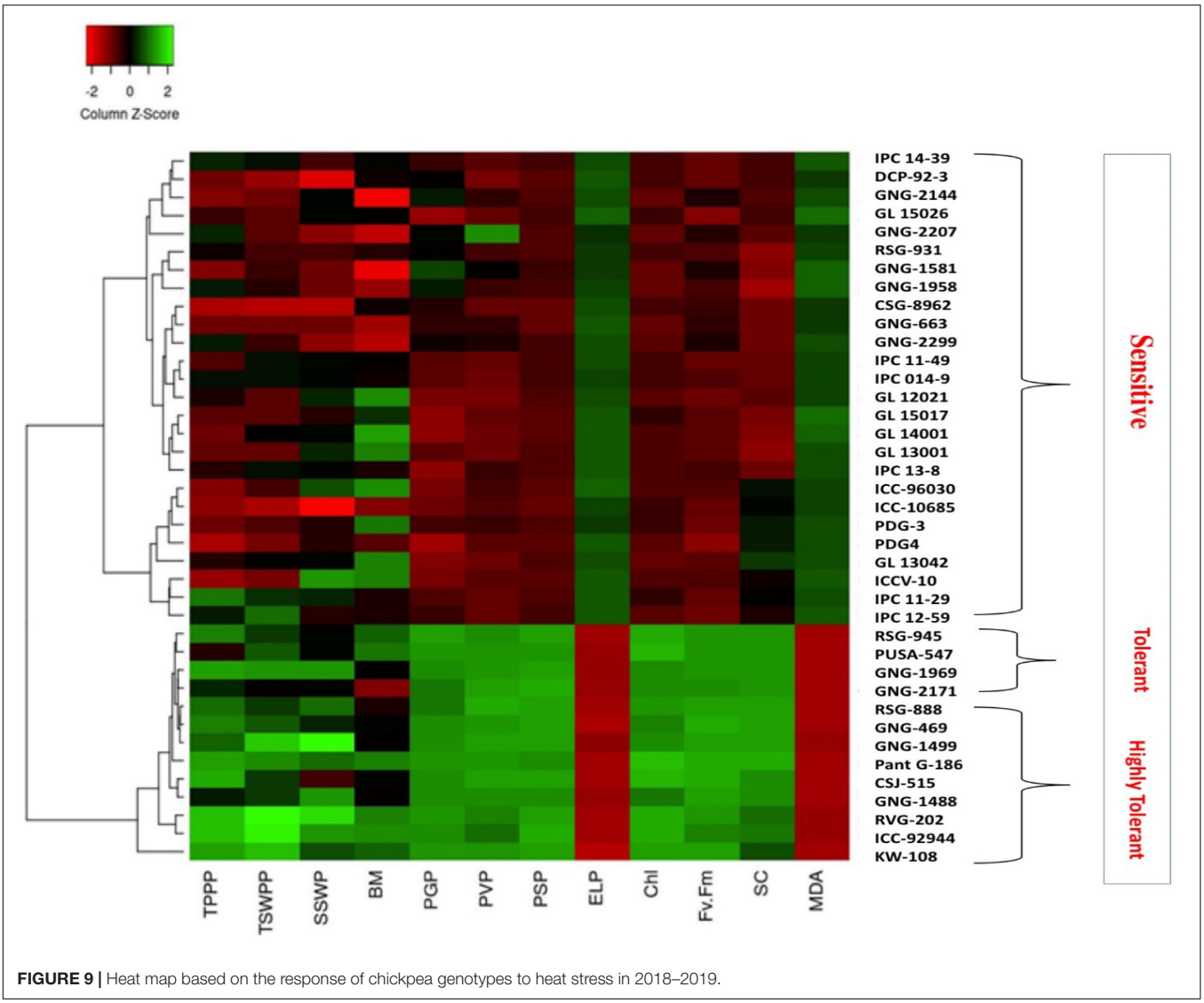

FIGURE 9 | Heat map based on the response of chickpea genotypes to heat stress in 2018–2019.

Vargas et al., 2021), and chickpea (Bhandari et al., 2020). High values of these traits indicate better reproductive function and thus high grain yield. The wide range of PGP (26.2–66.1% in 2017–2018 and 21.3–64% in 2018–2019) and PVP (24–58.7% in 2017–2018 and 23.4–55.8% in 2018–2019) under HS suggests great scope for developing heat-tolerant chickpea genotypes. Based on these two traits, GNG469 and CSJ515 genotypes exhibited higher heat tolerance than the heat-tolerant check ICCV 92944, and could be used as donor parents to improve heat tolerance in chickpea. Several researchers have used *in vitro* pollen germination to screen for heat tolerance in various crops such as peanut (Kakani et al., 2002) and cotton (Kakani et al., 2005; Song et al., 2015), mung bean (Sharma et al., 2016) and common bean (Vargas et al., 2021).

Serious losses in yield and yield-related traits (biomass, pod set, seed weight, and SYP) have been reported in various crops under HS such as winter wheat (Wheeler et al., 1996; Prasad and Djanaguiraman, 2014; Bheemanahalli et al., 2019), cowpea (Ehlers and Hall, 1998), common bean (Soltani et al., 2019), pea (Tafesse et al., 2019; Jiang et al., 2020), and lentil (Bhandari et al., 2020). HS during the reproductive stage, especially pollen development and fertilization, damaged pod and seed setting processes and thus reduced grain yield in many crops (see review by Prasad et al. (2017), for instance in common bean (Rainey and Griffiths, 2005; Vargas et al., 2021), and pea (Jiang et al., 2020). The wide range of PSP (21.7–44.9% in 2017–2018 and 22.8–45.7% in 2018–2019) under HS in the present study indicates great scope for developing chickpea genotypes involving under HS. In addition, PSP positively correlated with PVP and PGP under HS, indicating that improving these traits could lead to higher pod set% and thus improve grain yield under HS environment. Singh et al. (2015) also reported positive associations between PSP with PGP under HS in sorghum. Likewise, negative impact of HS on pollen fertility and seed setting has been reported in common bean (Soltani et al., 2019) and in lentil (Sita et al., 2017). Significant reductions in grain

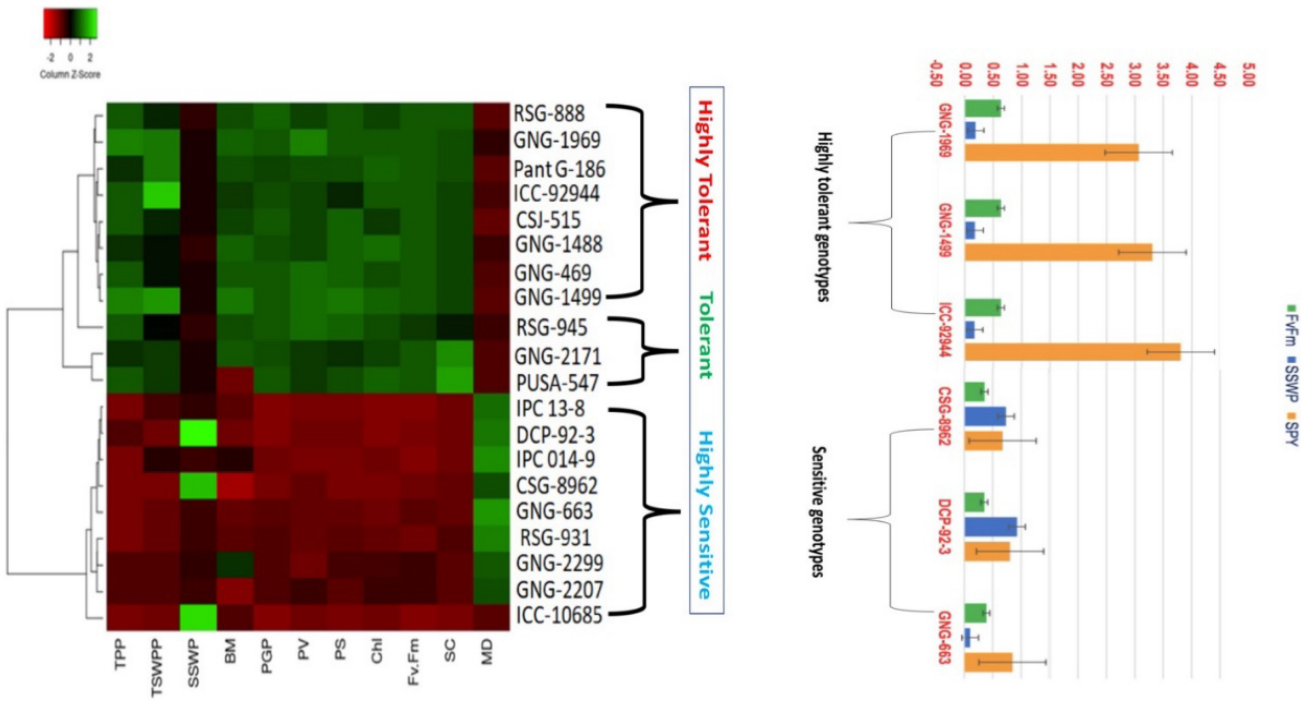

FIGURE 10 | Heat map based on the response of chickpea genotypes to heat stress in a growth chamber.

yield after HS exposure during grain filling have been reported in various crops such as wheat (Yang et al., 2002; Aziz et al., 2018), common bean (Rainey and Griffiths, 2005) including chickpea (Bhandari et al., 2020). Seed weights declined by up to 59.7% in 2017–2018 and 54.8% in 2018–2019 under HS in the field. Similar reductions (up to 50%) have been reported in wheat (Yang et al., 2002; Liu et al., 2016; Barber et al., 2017) and 37% (during the year 2016) and 26% (during the year 2017) in common bean (Vargas et al., 2021) and 16% in pea (Tafesse et al., 2019) under field condition under HS. Previously, Rainey and Griffiths (2005) also advocated reduction in seed number (83%), pod number (63%), mean seed weight (47%), and seeds pod^{-1} (73%) in common bean subjected to 33°C/30°C under greenhouse condition. In case of pea, based on high pod number, seed retention and improved seed yield under HS, genotypes "40–10," "Naparnyk," and "CDC Meadow" were found to be heat tolerant (Jiang et al., 2020). Most of the measured traits, especially PVP, PGP and yield-related traits, exhibited high heritability (**Table 2**), more so under HS than normal conditions, indicating the possibility of transferring the set traits into high-yield in heat-sensitive chickpea genotypes to improve heat tolerance and sustain yield in chickpea under HS.

Correlation studies indicated damage to membranes and oxidative stress negatively affected the yield traits suggesting reduction in these traits could be linked to improved heat tolerance, which is in agreement with previous studies in lentil and chickpea (Bhandari et al., 2020), mungbean (Sharma et al., 2016), and wheat (ElBasyoni et al., 2017). Similarly, reduced lipid peroxidation, measured as MDA, might improve heat tolerance, as reported in heat tolerant genotypes of other crops such as tomato (Zhou et al., 2019) and mungbean (Sharma et al., 2016). Chlorophyll, chlorophyll fluorescence and stomatal conductance had a positive correlation with pod number and seed yield indicating these traits could be vital in determining the heat tolerance. Some previous studies also report positive correlation of chlorophyll and chlorophyll fluorescence with heat tolerance in common bean (Petkova et al., 2007) and lentil (Sita et al., 2017). Considering this, stable leaf integrity and function in terms of photosynthesis under HS would be highly vital in improving heat tolerance in chickpea.

CONCLUSION

Genetic variability in various physiological, yield, and yield-related traits was assessed over 2 years in 39 chickpea genotypes under normal conditions and HS during reproductive and post-reproductive stages. A selected set of contrasting genotypes was validated further under control and HS conditions in a growth chamber. We found that genetic variability for pollen viability and pollen germination under HS could be used to select heat-tolerant chickpea genotypes, as the impact of HS on pollen germination and pollen development had a direct impact on pod set%, SSWP, NPP, and SYP. Moreover, yield and yield-related traits had positive and significant correlations with chlorophyll content, pollen viability%, pollen germination%, stomatal conductance, and PS II function under HS, indicating the potential to use these traits to improve heat tolerance

in chickpea. The candidate genotypes GNG469, GNG1488, GNG1499, GNG1969, GNG469, GNG1499, PantG 186, RSG 888, and CSJ515 had high PSP, NPP, and SSWP, SYP, and low decline in pollen viability and pollen germination under HS, and could be used to transfer these traits into high-yielding heat-sensitive chickpea genotypes to increase HS tolerance.

DATA AVAILABILITY STATEMENT

The original contributions presented in the study are included in the article/**Supplementary Material**; further inquiries can be directed to the corresponding author/s.

AUTHOR CONTRIBUTIONS

PD conducted the experiment. UJ helped in analysis and writing part of the manuscript. VP contributed in providing chickpea lines. KSh, SKP, and PJP helped in analysis of data. SKP helped in writing part of the manuscript. KSi and PP helped in editing the entire manuscript. HN developed the idea of this experiment. All authors contributed to the article and approved the submitted version.

ACKNOWLEDGMENTS

PD thanks CSIR-UGC, India, for providing a doctoral research fellowship. The corresponding author (HN) is thankful to DST, UGC, DBT, CSIR, India, The University of Western Australia (Australia), ICARDA (Morocco), IIPR (Kanpur, India), PAU (Ludhiana, India), and World Vegetable Center (at International Crops Research Institute for the Semi-arid tropics) for supporting the research work at various time.

SUPPLEMENTARY MATERIAL

The Supplementary Material for this article can be found online at: https://www.frontiersin.org/articles/10.3389/fpls.2022.880519/full#supplementary-material

REFERENCES

Alexander, M. P. (1969). Differential staining of aborted and non-aborted pollen. *Stain. Technol.* 44, 117–122. doi: 10.3109/10520296909063335

Awasthi, R., Kaushal, N., Vadez, V., Turner, N. C., Berger, J., Siddique, K. H., et al. (2014). Individual and combined effects of transient drought and heat stress on carbon assimilation and seed filling in chickpea. *Funct. Plant Biol.* 41, 1148–1167. doi: 10.1071/FP13340

Aziz, A., Mahmood, T., Mahmood, Z., Shazadi, K., Mujeeb-Kazi, A., and Rasheed, A. (2018). Genotypic variation and genotype × environment interaction for yield-related traits in synthetic hexaploid Wheats under a range of optimal and heat-stressed environments. *Crop Sci.* 58, 295–303. doi: 10.2135/cropsci2017.01.0035

Babicki, S., Arndt, D., Marcu, A., Liang, Y., Grant, J. R., Maciejewski, A., et al. (2016). Heatmapper: web-enabled heat mapping for all. *Nucleic Acids Res.* 44, 147–153.

Barber, H. M., Lukac, M., Simmonds, J., Semenov, M. A., and Gooding, M. J. (2017). Temporally and genetically discrete periods of wheat sensitivity to high temperature. *Front. Plant Sci.* 8:51. doi: 10.3389/fpls.2017.00051

Barnabás, B., Jäger, K., and Fehér, A. (2008). The effect of drought and heat stress on reproductive processes in cereals. *Plant Cell Environ.* 31, 11–38. doi: 10.1111/j.1365-3040.2007.01727.x

Bhandari, K., Sita, K., Sehgal, A., Bhardwaj, A., Gaur, P., Kumar, S., et al. (2020). Differential heat sensitivity of two cool-season legumes, chickpea and lentil, at the reproductive stage, is associated with responses in pollen function, photosynthetic ability and oxidative damage. *J. Agron. Crop Sci.* 206, 734–758. doi: 10.1111/jac.12433

Bheemanahalli, R., Sunoj, V. J., Saripalli, G., Prasad, P. V., Balyan, H. S., Gupta, P. K., et al. (2019). Quantifying the impact of heat stress on pollen germination, seed set, and grain filling in spring wheat. *Crop Sci.* 59, 684–696. doi: 10.2135/cropsci2018.05.0292

Bita, C., and Gerats, T. (2013). Plant tolerance to high temperature in a changing environment: scientific fundamentals and production of heat stress-tolerant crops. *Front. Plant Sci.* 4:273. doi: 10.3389/fpls.2013.00273

Brewbaker, J. L., and Kwack, B. H. (1963). The essential role of calcium ion in pollen germination and pollen tube growth. *Am. J. Bot.* 50, 859–865. doi: 10.1002/j.1537-2197.1963.tb06564.x

Canci, H., and Toker, C. (2009). Evaluation of yield criteria for drought and heat resistance in chickpea (*Cicer arietinum* L.). *J. Agron. Crop Sci.* 195, 47–54. doi: 10.1111/j.1439-037X.2008.00345.x

Chaudhary, S., Devi, P., Bhardwaj, A., Jha, U. C., Sharma, K. D., Prasad, P. V., et al. (2020). Identification and characterization of contrasting genotypes/cultivars for developing heat tolerance in agricultural crops: current status and prospects. *Front. Plant Sci.* 11:1505. doi: 10.3389/fpls.2020.587264

Coast, O., Murdoch, A. J., Ellis, R. H., Hay, F. R., and Jagadish, S. V. K. (2016). Resilience of rice (*Oryza* spp.) pollen germination and tube growth to temperature stress. *Plant Cell Environ.* 39, 26–37. doi: 10.1111/pce.12475

Devasirvatham, V., Gaur, P. M., Mallikarjuna, N., Raju, T. N., Trethowan, R. M., and Tan, D. K. (2013). Reproductive biology of chickpea response to heat stress in the field is associated with the performance in controlled environments. *Field Crops Res.* 142, 9–19. doi: 10.1016/j.fcr.2012.11.011

Ehlers, J. D., and Hall, A. E. (1998). Heat tolerance of contrasting cowpea lines in short and long days. *Field Crops Res.* 55, 11–21. doi: 10.1016/S0378-4290(97)00055-5

ElBasyoni, I., Saadalla, M., Baenziger, S., Bockelman, H., and Morsy, S. (2017). Cell membrane stability and association mapping for drought and heat tolerance in a worldwide wheat collection. *Sustainability* 9:1606. doi: 10.3390/su9091606

Gaur, P. M., Mallikarjuna, N., Knights, T., Beebe, S., Debouck, D., Mejía, A., et al. (2010). "Gene introgression in grain legumes," in *Grain Legumes: Genetic Improvement, Management And Trade*, eds S. Gupta, M. Ali, and B. B. Singh (Kanpur: Indian Society of Pulses Research and Development (IIPR)), 1–17.

Gaur, P. M., Samineni, S., Thudi, M., Tripathi, S., Sajja, S. B., Jayalakshmi, V., et al. (2019). Integrated breeding approaches for improving drought and heat adaptation in chickpea (*Cicer arietinum* L.). *Plant Breed.* 138, 389–400. doi: 10.1111/pbr.12641

Hasanuzzaman, M., Nahar, K., Alam, M., Roychowdhury, R., and Fujita, M. (2013). Physiological, biochemical, and molecular mechanisms of heat stress tolerance in plants. *Int. J. Mol. Sci.* 14, 9643–9684. doi: 10.3390/ijms14059643

Hatfield, J. L., and Prueger, J. H. (2015). Temperature extremes: effect on plant growth and development. *Weather Clim. Extremes* 10, 4–10. doi: 10.1016/j.wace.2015.08.001

Heath, R. L., and Packer, L. (1968). Photoperoxidation in isolated chloroplasts: I. Kinetics and stoichiometry of fatty acid peroxidation. *Arch. Biochem.* 125, 189–198. doi: 10.1016/0003-9861(68)90654-1

Hemantaranjan, A., Bhanu, A. N., Singh, M. N., Yadav, D. K., Patel, P. K., Singh, R., et al. (2014). Heat stress responses and thermotolerance. *Adv. Plants Agric. Res.* 1, 1–10. doi: 10.15406/apar.2014.01.00012

Jameel, S., Hameed, A., and Shah, T. M. (2021). Investigation of distinctive morpho-physio and biochemical alterations in desi chickpea at seedling stage under irrigation, heat, and combined stress. *Front. plant sci.* 12:692745. doi: 10.3389/fpls.2021.692745

Jha, U. C., Jha, R., Thakro, V., Kumar, A., Gupta, S., Nayyar, H., et al. (2021). Discerning molecular diversity and association mapping for phenological, physiological and yield traits under high temperature stress in chickpea (*Cicer arietinum* L.). *J. Genet.* 100, 1–15. doi: 10.1007/s12041-020-01254-2

Jiang, Y., Lindsay, D. L., Davis, A. R., Wang, Z., MacLean, D. E., Warkentin, T. D., et al. (2020). Impact of heat stress on pod-based yield components in field pea (*Pisum sativum* L.). *J. Agron. Crop Sci.* 206, 76–89. doi: 10.1111/jac.12365

Kakani, V. G., Prasad, P. V. V., Craufurd, P. Q., and Wheeler, T. R. (2002). Response of in vitro pollen germination and pollen tube growth of groundnut (*Arachis hypogaea* L.) genotypes to temperature. *Plant Cell Environ.* 25, 1651–1661. doi: 10.1046/j.1365-3040.2002.00943.x

Kakani, V. G., Reddy, K. R., Koti, S., Wallace, T. P., Prasad, P. V. V., Reddy, V. R., et al. (2005). Differences in in vitro pollen germination and pollen tube growth of cotton cultivars in response to high temperature. *Ann. Bot.* 96, 59–67. doi: 10.1093/aob/mci149

Kalra, N., Chakraborty, D., Sharma, A., Rai, H. K., Jolly, M., Chander, S., et al. (2008). Effect of increasing temperature on yield of some winter crops in northwest India. *Curr. Sci.* 94, 82–88.

Kaushal, N., Awasthi, R., Gupta, K., Gaur, P., Siddique, K. H., and Nayyar, H. (2013). Heat-stress-induced reproductive failures in chickpea (*Cicer arietinum*) are associated with impaired sucrose metabolism in leaves and anthers. *Funct. Plant Biol.* 40, 1334–1349. doi: 10.1071/FP13082

Krishnamurthy, L., Gaur, P. M., Basu, P. S., Chaturvedi, S. K., Tripathi, S., Vadez, V., et al. (2011). Large genetic variation for heat tolerance in the reference collection of chickpea (*Cicer arietinum* L.) germplasm. *Plant Genet. Resour.* 9, 59–69. doi: 10.1017/S1479262110000407

Liu, B., Asseng, S., Liu, L., Tang, L., Cao, W., and Zhu, Y. (2016). Testing the responses of four wheat crop models to heat stress at anthesis and grain filling. *Glob. Change Biol.* 22, 1890–1903. doi: 10.1111/gcb.13212

Lutts, S., Kinet, J. M., and Bouharmont, J. (1996). NaCl-induced senescence in leaves of rice (*Oryza sativa* L.) cultivars differing in salinity resistance. *Ann. Bot.* 78, 389–398.

McDonald, G., and Paulsen, G. (1997). High temperature effects on photosynthesis and water relations of grain legumes. *Plant Soil* 196, 47–58. doi: 10.1023/A:1004249200050

Mohapatra, C., Chand, R., Tiwari, J. K., and Singh, A. K. (2020). Effect of heat stress during flowering and pod formation in pea (*Pisum sativum* L.). *Physiol. Mol. Biol. Plants.* 26, 1119–1125. doi: 10.1007/s12298-020-00803-4

Mukherjee, S., Aadhar, S., Stone, D., and Mishra, V. (2018). Increase in extreme precipitation events under anthropogenic warming in India. *Weather Clim. Extremes* 20, 45–53. doi: 10.1016/j.wace.2018.03.005

Pareek, A., Rathi, D., Mishra, D., Chakraborty, S., and Chakraborty, N. (2019). Physiological plasticity to high temperature stress in chickpea: adaptive responses and variable tolerance. *Plant Sci.* 289:110258. doi: 10.1016/j.plantsci.2019.110258

Patterson, H. D., and Thompson, R. (1971). Recovery of inter-block information when block sizes are unequal. *Biometrika* 58, 545–554. doi: 10.2307/2334389

Petkova, V., Denev, I. D., Cholakov, D., and Porjazov, I. (2007). Field screening for heat tolerant common bean cultivars (*Phaseolus vulgaris* L.) by measuring of chlorophyll fluorescence induction parameters. *Sci. Hortic.* 111, 101–106. doi: 10.1016/j.scienta.2006.10.005

Prasad, P. V., and Djanaguiraman, M. (2014). Response of floret fertility and individual grain weight of wheat to high temperature stress: sensitive stages and thresholds for temperature and duration. *Funct. Plant Biol.* 41, 1261–1269. doi: 10.1071/FP14061

Prasad, P. V., Bheemanahalli, R., and Jagadish, S. K. (2017). Field crops and the fear of heat stress—opportunities, challenges and future directions. *Field Crops Res.* 200, 114–121. doi: 10.1016/j.fcr.2016.09.024

Rainey, K. M., and Griffiths, P. D. (2005). Differential response of common bean genotypes to high temperature. *J. Am. Soc. Hortic. Sci.* 130, 18–23. doi: 10.21273/JASHS.130.1.18

Sehgal, A., Sita, K., Siddique, K. H., Kumar, R., Bhogireddy, S., Varshney, R. K., et al. (2018). Drought or/and heat-stress effects on seed filling in food crops: impacts on functional biochemistry, seed yields, and nutritional quality. *Front. Plant Sci.* 9:1705. doi: 10.3389/fpls.2018.01705

Sharma, L., Priya, M., Bindumadhava, H., Nair, R. M., and Nayyar, H. (2016). Influence of high temperature stress on growth, phenology and yield performance of mungbean [*Vigna radiata* (L.) Wilczek] under managed growth conditions. *Sci. Hortic.* 213, 379–391. doi: 10.1016/j.scienta.2016.10.033

Singh, V., Nguyen, C. T., van Oosterom, E. J., Chapman, S. C., Jordan, D. R., and Hammer, G. L. (2015). Sorghum genotypes differ in high temperature responses for seed set. *Field Crops Res.* 171, 32–40. doi: 10.1016/j.fcr.2014.11.003

Singh, V., Nguyen, C. T., Yang, Z., Chapman, S. C., van Oosterom, E. J., and Hammer, G. L. (2016). Genotypic differences in effects of short episodes of high-temperature stress during reproductive development in sorghum. *Crop Sci.* 56, 1561–1572. doi: 10.2135/cropsci2015.09.0545

Sita, K., Sehgal, A., Kumar, J., Kumar, S., Singh, S., Siddique, K. H., et al. (2017). Identification of high-temperature tolerant lentil (*Lens culinaris* Medik.) genotypes through leaf and pollen traits. *Front. Plant Sci.* 8:744. doi: 10.3389/fpls.2017.00744

Soltani, A., Weraduwage, S. M., Sharkey, T. D., and Lowry, D. B. (2019). Elevated temperatures cause loss of seed set in common bean (*Phaseolus vulgaris* L.) potentially through the disruption of source-sink relationships. *BMC Genomics* 20:312. doi: 10.1186/s12864-019-5669-2

Song, G., Wang, M., Zeng, B., Zhang, J., Jiang, C., Hu, Q., et al. (2015). Anther response to high-temperature stress during development and pollen thermotolerance heterosis as revealed by pollen tube growth and in vitro pollen vigor analysis in upland cotton. *Planta* 241, 1271–1285. doi: 10.1007/s00425-015-2259-7

Sunoj, V. J., Somayanda, I. M., Chiluwal, A., Perumal, R., Prasad, P. V., and Jagadish, S. K. (2017). Resilience of pollen and post-flowering response in diverse sorghum genotypes exposed to heat stress under field conditions. *Crop Sci.* 57, 1658–1669. doi: 10.2135/cropsci2016.08.0706

Tafesse, E. G., Warkentin, T. D., and Bueckert, R. A. (2019). Canopy architecture and leaf type as traits of heat resistance in pea. *Field Crops Res.* 241, 107561. doi: 10.1016/j.fcr.2019.107561

Vargas, Y., Mayor-Duran, V. M., Buendia, H. F., Ruiz-Guzman, H., and Raatz, B. (2021). Physiological and genetic characterization of heat stress effects in a common bean RIL population. *PLoS One* 16:e0249859. doi: 10.1371/journal.pone.0249859

Wheeler, T. R., Batts, G. R., Ellis, R. H., Hadley, P., and Morison, J. I. L. (1996). Growth and yield of winter wheat (*Triticum aestivum*) crops in response to CO2 and temperature. *J. Agric. Sci.* 127, 37–48. doi: 10.1017/S0021859600077352

Yang, J., Sears, R. G., Gill, B. S., and Paulsen, G. M. (2002). Growth and senescence characteristics associated with tolerance of wheat-alien amphiploids to high temperature under controlled conditions. *Euphytica* 126, 185–193. doi: 10.1023/A:1016365728633

Zhou, R., Kong, L., Yu, X., Ottosen, C. O., Zhao, T., Jiang, F., et al. (2019). Oxidative damage and antioxidant mechanism in tomatoes responding to drought and heat stress. *Acta Physiol. Plant* 41, 1–11. doi: 10.1007/s11738-019-2805-1

Conflict of Interest: The authors declare that the research was conducted in the absence of any commercial or financial relationships that could be construed as a potential conflict of interest.

Publisher's Note: All claims expressed in this article are solely those of the authors and do not necessarily represent those of their affiliated organizations, or those of the publisher, the editors and the reviewers. Any product that may be evaluated in this article, or claim that may be made by its manufacturer, is not guaranteed or endorsed by the publisher.

Copyright © 2022 Devi, Jha, Prakash, Kumar, Parida, Paul, Prasad, Sharma, Siddique and Nayyar. This is an open-access article distributed under the terms of the Creative Commons Attribution License (CC BY). The use, distribution or reproduction in other forums is permitted, provided the original author(s) and the copyright owner(s) are credited and that the original publication in this journal is cited, in accordance with accepted academic practice. No use, distribution or reproduction is permitted which does not comply with these terms.

frontiers | Frontiers in Plant Science

ORIGINAL RESEARCH
published: 31 May 2022
doi: 10.3389/fpls.2022.918460

Study on the Effect of Salt Stress on Yield and Grain Quality Among Different Rice Varieties

Rui Zhang[1], Yang Wang[1], Shahid Hussain[1], Shuo Yang[1], Rongkai Li[1], Shuli Liu[1], Yinglong Chen[1], Huanhe Wei[1], Qigen Dai[1] and Hongyan Hou[2]*

[1] Jiangsu Key Laboratory of Crop Genetics and Physiology, Jiangsu Key Laboratory of Crop Cultivation and Physiology, Jiangsu Co-Innovation Center for Modern Production Technology of Grain Crops, Research Institute of Rice Industrial Engineering Technology, Key Laboratory of Saline-Alkali Soil Improvement and Utilization (Coastal Saline-Alkali Lands), Ministry of Agriculture and Rural Affairs, Yangzhou University, Yangzhou, China, [2] Yibang Agriculture Technology Development Co., Ltd., Dongying, China

Salt is one of the main factors limiting the use of mudflats. In this study, the yield, quality, and mineral content of rice seeds under salt stress were investigated. A pot experiment was conducted with Yangyugeng2, Xudao9, and Huageng5 under 0, 17.1, 25.6, and 34.2 mM NaCl of salt concentration treatments. The results showed that salt stress can significantly decrease panicle number, grain number per panicle, 1000-grain weight and yield of rice, and the panicle number was among other things the main cause of yield loss under saline conditions. When the salt concentration is less than 34.2 mM NaCl, the salt stress increases the brown rice rate and milled rice rate, thus significant increasing head milled rice rate of salt-sensitive varieties but decreasing in salt-tolerant varieties. In addition, the grain length is more sensitive than grain width to salt stress. This study also indicates that different varieties of rice exhibit different salt tolerance under salt stress, the three rice varieties in this study, in order of salt tolerance, are Xudao9, Huageng5, and Yangyugeng2. Salt stress will increase the appearance, viscosity, degree of balance, and taste value, and decrease the hardness of rice when salt concentration is less than 17.1 mM NaCl in Yangyugeng2 and Huageng5 or 25.6 mM NaCl in Xudao9. The differences in starch pasting properties among rice varieties in this study are larger than those caused by salt stress. The uptake capacity of K, Mg, P, S, and Cu ions in the seeds of different rice varieties significantly vary, and salt stress causes significant differences in the uptake capacity of K, Na, and Cu ions in rice seeds. Rice varieties with high salt tolerance can be selected for the development and utilization of mudflats, and low concentration of salt stress will increase the rice quality, all of which are meaningful to agricultural production.

Keywords: rice (*Oryza sativa* L.), salt stress, yield, grain quality, mineral elements

OPEN ACCESS

Edited by:
Raul Antonio Sperotto, Universidade do Vale do Taquari - Univates, Brazil

Reviewed by:
Shah Fahad, The University of Haripur, Pakistan
Sudhanshu Sekhar, Utkal University, India
Takashi Tanaka, Gifu University, Japan

****Correspondence:***
Qigen Dai
qgdai@yzu.edu.cn

Specialty section:
This article was submitted to Crop and Product Physiology, a section of the journal Frontiers in Plant Science

Received: *13 April 2022*
Accepted: *09 May 2022*
Published: *31 May 2022*

Citation:
Zhang R, Wang Y, Hussain S, Yang S, Li R, Liu S, Chen Y, Wei H, Dai Q and Hou H (2022) Study on the Effect of Salt Stress on Yield and Grain Quality Among Different Rice Varieties. Front. Plant Sci. 13:918460. doi: 10.3389/fpls.2022.918460

INTRODUCTION

Rice (*Oryza sativa* L.) is one of the major food sources; with the increase of population worldwide, the demand for rice will grow faster than for other crops (Krishnan et al., 2011). However, the global rice yield is deeply affected by salinity stress (Corwin, 2020; Ltaeif et al., 2021; Sangwongchai et al., 2021).

Soil salinity is one of the most common environmental stressors; about 20% of arable land and nearly half of irrigated land are being affected by salt stress in the world (Fahad et al., 2019; Dramalis et al., 2021). Saline soils are unevenly distributed throughout the world, with Oceania, Asia, America, Africa, and Europe accounting for 37.42, 33.43, 15.39, 8.43, and 5.32%, respectively (Jianfeng, 2008). In Asia, China has the largest area of saline soils. Soil salinization causes soil nutrient loss, destroys the structure of soil aggregates, and significantly affects crop growth and development (Kordrostami et al., 2017). Jiangsu Province of China has the largest coastal tidal flat that is not only an important wetland ecosystem but also one of the lands essential to agricultural production and urban development in coastal areas (Hua et al., 2017).

Under saline stress, plants have difficulty forming both firmness and hardness in the soil required for effective root systems. The low water availability causes osmotic stress and reduces efficiency in transporting nutrients such as nitrogen, phosphorus, potassium, and calcium, thereby causing nutrient deficiencies and ionic toxicity (Razzaq et al., 2020). When the electrical conductivity of irrigation water is greater than 32.8 mM NaCl, rice yield will be reduced (Eynard et al., 2005; Chen et al., 2020).

Saline soil affects both growth and yield of rice plants, and the nutrient content of rice, resulting in an imbalance of ion that affects the quality of the rice (Rao et al., 2013). Rice quality, a multi-faceted trait (Fitzgerald et al., 2009), is the result of interactions among rice genes, surrounding environment, cultivation management methods, milling conditions, and storage technologies (Han et al., 2004). The yield and quality of rice determine consumer purchasing behaviors and the ruling prices in the market (Balindong et al., 2018; Sangwongchai et al., 2021). Consumers mainly evaluate the quality of rice by its physical (milled yield, transparency, size, shape, and color) and organoleptic (cooking characteristics) properties (Fahad et al., 2019). Rice quality includes the quality of milling, appearance, cooking and eating, and nutrition (Bian et al., 2018). The appearance quality includes the shape and chalkiness of fine rice. The cooking and eating quality includes appearance, hardness, viscosity, and degree of balance; the nutritive quality includes amylose content, gel consistency, the protein content of rice (Fitzgerald et al., 2009). These characteristics are the main factors that influence the market price of rice.

Mineral elements play an important role in human health and are the main components of food (Wang et al., 2017; Razzaq et al., 2020). What people mainly consume is refined rice that is low in nutrients such as minerals and vitamins, which creates hidden hunger (micronutrient deficiencies) in developing countries where rice is a staple food (Fitzgerald et al., 2009). Micronutrient deficiencies such as copper and zinc may cause harmful effect such as hypoimmunity. Calcium is needed for proper bone growth and development, and manganese is associated with many enzymes in the body. Manganese deficiency may lead to venous sclerosis (Jiang et al., 2008).

Most of the previous literature (Menezes-Benavente et al., 2004; Nounjan et al., 2012; Senguttuvel et al., 2013) studied the effect of salt stress on the enzyme activity and gene expression of rice, but only a few researched the effect of salt stress on rice grain quality. A lot of literature (Limin, 2012; Mei et al., 2015; Thu et al., 2017) has studied the effect of salt stress on mineral element content of various organs of rice plants, but only a few studied on the mineral element content of rice seeds. In the present study, we selected Yangyugeng2, Xudao9, and Huageng5, which have been widely growing in Jiangsu Province, as the test objects. We aim to understand the effect of different salinity stress on rice grain quality and mineral element content of rice seeds.

MATERIALS AND METHODS

Experiment Materials and Experimental Designs

A pot experiment was carried out under rain shelters in the experimental field of Agricultural College of Yangzhou University, Yangzhou City, Jiangsu Province, China (119°25′E, 32°30′N) from May to November in 2019. The two-factor experiments were laid out in a completely randomized design with ten replicates, where the primary factor was salt concentration, and the secondary factor was rice varieties. The threshold value indicates the maximum salinity allowed without reducing the yield, and the threshold of rice is 32.8 mM NaCl (Das et al., 2015). The four salinity levels (0, 17.1, 25.6, and 34.2 mM NaCl) were set for this experimental study. The rice varieties used in this study were Yangyugeng2, Xudao9, and Huageng5, and these three cultivars have been widely grown in Jiangsu Province. The seeds with full-grain and the same size were selected and sterilized with prochloraz and aldimorph cartap for 3 days and rinsed with pure water three times to wash away the residues. Cleaned seeds were sown on 23 May, and the 28-day-old rice seedlings were transplanted to pots that were 27 cm high with the top and bottom diameters of 30 and 22 cm, respectively. Each pot was filled with about 15 kg of soil and planted with 4 hills, each of which was planted with four seedlings, and Each treatment has ten replicates. Before transplanting, basic fertilizers and sea salt (the main component of sea salt is sodium chloride; the ingredients are presented in **Table 1** and made by Zhejiang Blue Starfish Salt Product Co., Ltd.) were mixed with soil using a potting soil mixer.

Urea, superphosphate and potassium chloride were used as sources of nitrogen, phosphorus, and potassium, respectively. Urea (1.305 g/pot) was applied during the four growth stages, such as the pre-transplanting stage, tilling stage, panicle initiation stage and booting stage, respectively (Zhang et al., 2020). About 8.3 g/pot of superphosphate was applied as the basic fertilizer, and 1.665 g/pot potassium chloride was applied as the basic and panicle fertilizers.

Determination of Rice Yield and Yield Components

Grains per panicle is the total number of grains recorded per panicle; seed setting rate is calculated as filled grain number/total grain number (Xiong et al., 2017); the 1000-grain weight was determined by randomly selecting 200 seeds and converted to the

TABLE 1 | Q/ZLY003 type instant sea crystal produced by Zhejiang Blue Starfish Salt Products Co. Ltd. test results for each ion.

Major cation	Major cation/chlorinity ratios
Potassium ion	0.016
Magnesium ion	0.069
Sodium ion	0.570
Calcium ion	0.018
Sulfate ion	0.140

weight of 1000 seeds (Sakhare et al., 2015); rice seeds were hand-threshed, with the moisture content being adjusted to 14%, and the total seed weight per pot recorded as rice yield.

Determination of Milling Quality

A total of 500 g of grain harvested from each treatment was dried in sunshine till the grain moisture of 14% was obtained for quality analysis (Zhu et al., 2017). A 150 g rice sample passed through the rice huller twice (SY88-TH, South Korea) to obtain brown rice that would then pass through the rice polisher (LTJM-2099, made by Zhejiang Bethlehem Apparatus Co., Ltd.) to obtain milled rice. Head milled rice constituted the grain with length of 3/4 or more of the whole milled grain separated from the 30 g milled rice (Kaur et al., 2016). The computational formula of brown rice rate, milled rice rate, and head milled rice are as follows:

$$\textit{brown rice rate} = \frac{\textbf{brown rice weight}}{\textbf{150}} * \textbf{100\%}$$

$$\textit{milled rice rate} = \frac{\textbf{milled rice weight}}{\textbf{150}} * \textbf{100\%}$$

$$\textit{head milled rice rate} = \frac{\textbf{milled rice weight}}{\textbf{30}} * \textbf{milled rice rate}$$

Determination of Appearance Quality

The length, width, aspect ratio, chalkiness rate, and chalkiness degree of head milled rice were measured using a grain appearance analyzer ScanMaker i800 plus (Microtek, China) (Zhao et al., 2018).

Determination of Nutritive Quality

N concentration in rice flour was determined based on the Kjeldahl method (Hernandez-Santana et al., 2019), and the protein content was derived by multiplying the product of nitrogen content by 5.95 (Hu et al., 2020). The amylose content was determined using iodine colorimetry (Shaik et al., 2014); The gel consistency was determined based on the methods of Cagampang et al. (1973).

Determination of Cooking/Eating Quality

Rice taste analyzer (Satake, Hiroshima, Japan) was used to assess the taste value of rice grains. The taste value is a comprehensive evaluation of cooked rice and includes the appearance, hardness, viscosity, and degree of balance (Zhang et al., 2020). A sample containing 30 g of polished grains from each cultivar was placed into a stainless-steel tank, rinsed with running purified water for 30 s, drained, and reconstituted with purified water to bring the ratio of rice to water to 1:1.33. The sample was then soaked for 30 min in the tank, covered with a filter paper, and sealed with a rubber ring. The stainless-steel tank was placed into an electric rice cooker (JT783, Midea, Shunde, China), covered, steamed for 30 min, and kept warm for 10 min. The tank was taken out from the rice cooker, while gently stirring and turning over the steamed rice. Then, the tank was covered with a filter paper again and cooled for 20 min using a supporting air-cooling device. Afterward, the filter paper was replaced with the supporting steel cover to seal and cool the steamed rice at room temperature (25°C) for 90 min. An 8-g sample of steamed rice was placed into a stainless-steel ring (30-mm diameter and 9-mm height) and then pressed the rice into a cake. The rice cake was placed in a measuring tank, and the rice taste analyzer was inserted to measure appearance and taste value of the steamed rice sample. Three rice cakes were measured for each steamed rice sample, and the top and bottom surface of each cake was measured once (Zhu et al., 2021b).

Determination of Pasting Properties of Starch

The pasting properties of rice flour were determined by rapid viscosity analyzer (RVA-TecMaster, Perten, Stockholm, Sweden), according to Zhu et al. (2017). Rice flour (3 g, which moisture content of the rice flour totaled 12%; if the moisture content of rice flour was not 12%, it is necessary to increase or decrease the weight of rice flour appropriately) was weighed and placed into an RVA sample canister and 25 mL of distilled water was added; then the sample canister was transferred into the RVA for testing. The entire program cycle was 13 min. Starch samples were cycled through a heating-cooling program starting at 50°C for 1 min, then raising the temperature from 50 to 95°C at a rate of 12°C/min, holding at 95°C for 2.5 min, cooling to 50°C at 12°C/min, and ending at another hold at 50°C for 2 min. The pasting parameters were recorded for analysis (Zhu et al., 2021b). The RVA profile characteristics include such common parameters as peak viscosity, hot paste viscosity, cold paste viscosity, breakdown of secondary parameters, setback, peak time, and pasting temperature (Zhu et al., 2021a). The parameters were calculated according to the formula below (Bao, 2019):

$$\textit{breakdown} = \textit{peak viscosity} - \textit{hot paste viscosity}$$

$$\textit{setback} = \textit{cold paste viscosity} - \textit{peak viscosity}$$

Determination of Mineral Element Contents

The milled rice of Yangyugeng2, Xudao9, and Huageng5 was ground to powder and sieved through a 100-mesh sieve. A total of 0.45 g dried samples was weighed, and 5 mL HNO3 (GR) and 3 mL ultrapure water, together with 2–3 drops of hydrogen peroxide, were added; then the samples were digested in a microwave digester (MARS 5, CEM Corporation, NC, United States). After digestion, the volume was fixed at 50 mL,

filtered through a double-layer quantitative filter paper. The filtered liquid were used to measure the Cu element and ten-times dilution filtrate, which was used for testing macro element, was determined by ICP-AES (IRIS Intrepid II XSP, Thermo Scientific, MA, United States) (Dongfen et al., 2009; Domingo et al., 2016; Qing et al., 2019). The mineral elements were counted according to the following formula:

$$concentration\ of\ macro\ elements = \frac{tested\ value * 10 * 50}{1000 * weight}\ mg/g$$

$$concentration\ of\ Cu\ elements = \frac{tested\ value * 50}{weight}\ mg/kg$$

Statistical Analysis

Data were analyzed by a Two-way ANOVA to assess the effect of salinity stress on the rice yield, yield component, milling quality of rice grain, appearance quality, nutritive quality, cooking/eating quality, pasting properties of starch and mineral elemental contents of rice seeds. When the treatment means were different, the Duncan multiple range test was performed to identify significant differences at $P < 0.05$. Data arrangement and sorting were processed by Microsoft Excel 2016 and analyzed using IBM SPSS Statistics 26 software (IBM, Armonk, NY, United States), thus generating graphs using Origin 2018 (Origin Lab, Hampton, MA, United States).

RESULTS

Effect of Salt Stress on Yield and Yield Components of Rice

As indicated in **Figure 1**, salt stress had significant effect on the panicle number ($P = 0.001$), grain number per panicle ($P = 0.001$), seed setting rate ($P = 0.010$), 1000-grain weight ($P < 0.001$) and rice yield ($P < 0.001$), and it was noticeable that significant differences were also detected among rice cultivars ($P < 0.050$). There was significant interaction effect between salt treatments and rice varieties for 1000-grain weight ($P < 0.001$), but no significant interaction effect for panicle number ($P = 0.947$), grain number per panicle ($P = 0.309$), seed setting rate ($P = 0.995$), and rice yield ($P = 0.373$). The S3 treatments significantly decreased by 9.8% in the panicle number, 21.6% in the grain number per panicle, 4.4% in the 1000-grain weight, and 20% in the rice yield compared with the control (without salt treatment) in Yangyugeng2. The 1000-grain weight, rice yield and grain number per panicle of Yangyugeng2 and Huageng5 were reduced with the increasing concentration of salt by 0.8, 19.9, and 9.9% at S1 treatment and further declined as the salt concentration increased in Xudao9. The seed setting rate of Huageng5 decreased with the increasing level of salinity, while that of Yangyugeng2 and Xudao9 reduced as the concentration of salt increased by 1.88 and 2.3% at S3 treatment when the salinity level was less or equal to S2 treatment.

From the effect of salt concentration stress on yield composition, it can be seen that salt stress significantly reduced the panicle number, 1000-grain weight and yield of rice, and low concentration of salt stress increased the panicle number of Xudao9 and Huageng5, where Xudao9 reached a significant level, but Huageng5 did not. While the same salt concentration will reduce the number of spikes of Yangyugeng2 well, which indicates that the tolerance of Xudao9 to salt stress is greater than that of Huageng5 and Yangyugeng2. From the effect of salt concentration stress on the 1000-grain weight of rice seeds, the difference between rice varieties was greater than that of salt stress effect. From the effect of salt concentration stress on yield, the salt tolerance of Xudao9 was greater than that of Yangyugeng2 and Huageng5. The number of spike grains of Xudao9 and Huageng5 did not change significantly under salt concentration stress, while that of Yangyugeng2 showed a significant decrease.

Effects of Salt Stress on the Quality of Rice Milling, Appearance, and Nutrition

The results showed that salt stress significantly increased both brown rice rate and milled rice rate of rice, and variety differences had significant effect on the brown rice rate ($P < 0.001$), milled rice rate ($P < 0.001$), head milled rice rate ($P < 0.001$), and rice seed length ($P < 0.001$), width ($P < 0.001$) and aspect ratio ($P < 0.001$). It was noticeable that significant differences were also detected under salt stress except for the aspect ratio ($P = 0.280$). There was significant interaction effect between salt stress and rice varieties in terms of brown rice rate ($P < 0.001$), milled rice rate ($P < 0.001$), head milled rice rate ($P < 0.001$) and aspect ratio ($P = 0.005$), and no significant interaction effect on both length ($P = 0.130$) and width ($P = 0.248$) of rice. This study showed that the brown rice rate and milled rice rate of rice varieties significantly increased with the rising of salinity level, compared with the rates in terms of salinity level (**Figures 2A,B**). The head milled rice rate of milling quality under salt stress significantly increased in Yangyugeng2, compared with that of the control. On the contrary, the head milled rice rates of S1, S2, and S3 reduced by 2.22, 3.31, and 12.23% in Xudao9.

With the increase in salt concentration, the chalkiness rate and chalkiness degree showed an increasing and then decreasing trend under salt stress (**Figures 3A,B**), and the aspect ratio of Yangyugeng2 and Xudao9 first increased by 1.7 and 1.0% and then decreased (**Figure 2F**). The aspect ratio of Huageng5 first decreased by 1.7% and then increased (**Figure 2F**). The chalkiness rate reached its maximum in all varieties when the salt concentration was at 25.6 mM NaCl (**Figure 3A**). The chalkiness degree of Yangyugeng2 and Huageng5 gradually increased under salinity stress and reached the maximum value (21.36, 20.52) when the salt concentrations were 17.1 and 25.6 mM NaCl. However, the chalkiness degree of Xudao9 declined to the minimum value (8.36) at 17.1 mM NaCl and increased when the salt concentration was greater than 17.1 mM NaCl (**Figure 3B**).

This study indicated that significant difference among rice varieties were observed on the chalkiness rate ($P < 0.001$), chalkiness degree ($P < 0.001$), protein content ($P < 0.001$), and amylose content ($P < 0.001$), and it was noticeable that significant differences were also detected under salt stress except for the gel

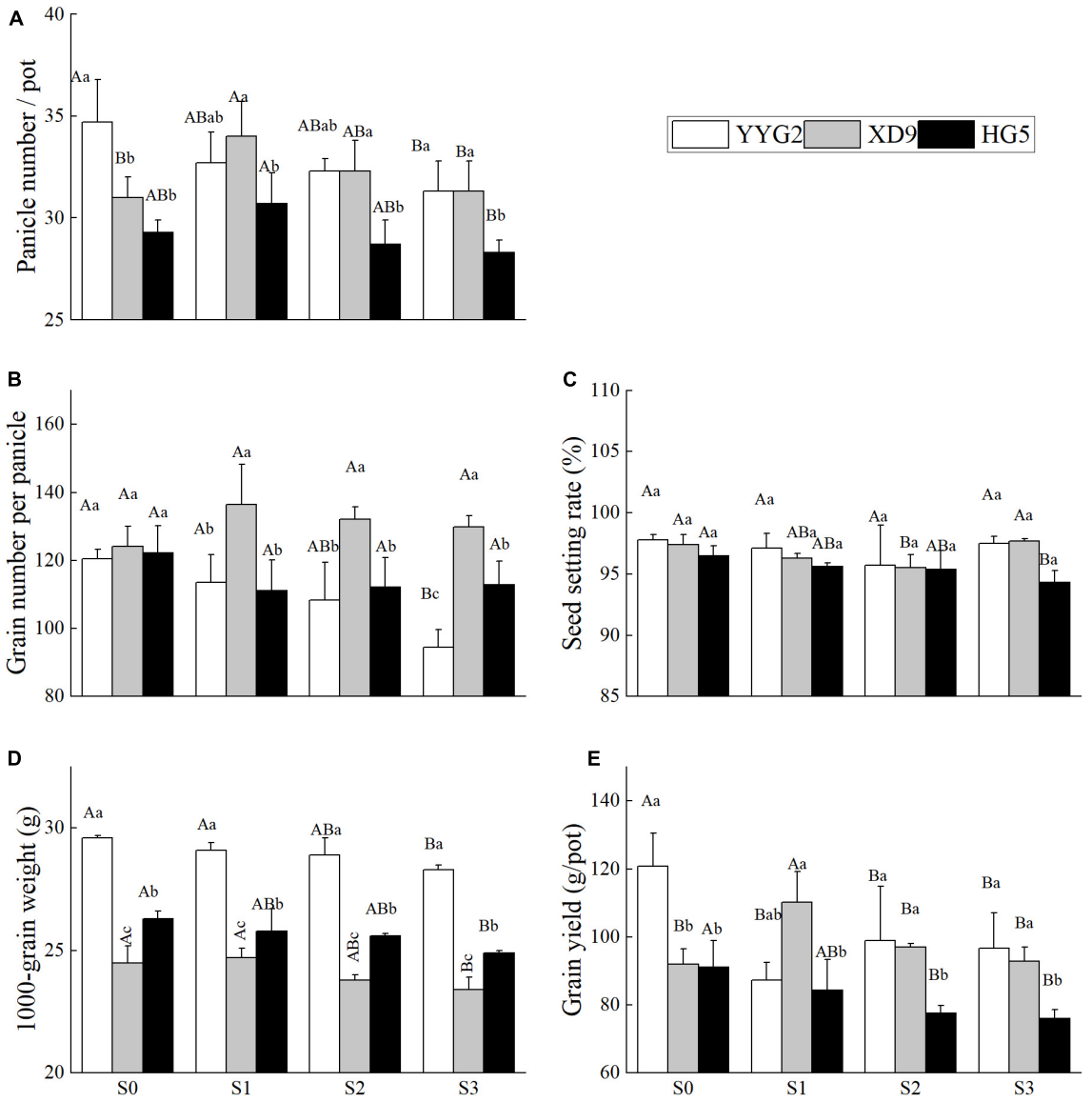

FIGURE 1 | Effect of salt stress on panicle number **(A)**, grain number per panicle **(B)**, seed setting rate **(C)**, 1000-grain weight **(D)**, and grain yield **(E)** for different rice varieties. YYG2, Yangyugeng2; XD9, Xudao9; HG5, Huageng5; V, Variety; S, Salt; S_0, S_1, S_2, and S_3 denote salt concentrations of 0, 17.1, 25.6 and 34.2 mM, respectively; In different salinity level during the same varieties, bars with the same uppercase letters are not significantly different, while within the same salt concentration in different varieties, bars with the same lowercase letters are not significantly different according to the Duncan test at $P < 0.05$.

consistency ($P = 0.323$). There was significant interaction effect between salt treatment and rice varieties in terms of chalkiness rate ($P < 0.001$), chalkiness degree ($P < 0.001$) and protein content ($P = 0.001$), and no significant interaction effect for amylose content ($P = 0.071$) and gel consistency ($P = 0.071$) of rice seeds. The nutritive quality of rice was mainly determined by protein content, amylose content and gel consistency in rice seeds. The protein content of Yangyugeng2, Xudao9, and Huageng5 was thus reduced by 1.8, 1.8, and 9.7% when the salt concentration was 17.1 mM NaCl, which showed a tendency to increase while the salinity level was greater than 17.1 mM NaCl. However, the situation of amylose content was in the opposite (**Figures 3C,D**). As salt concentration increased, a trend of first rising and then falling was seen (**Figure 3D**). With the increase of salt concentration, the gel consistency presented an overall trend of increasing first and then decreasing (**Figure 3E**).

Effect of Salt Stress on the Taste Value of Rice

As revealed in this study, the appearance, viscosity, degree of balance, and taste values of rice under salt stress showed a trend of increasing and then decreasing, and hardness exhibited a trend of decreasing and then increasing, and salt stress had significant effect on the appearance ($P = 0.005$), hardness ($P = 0.012$),

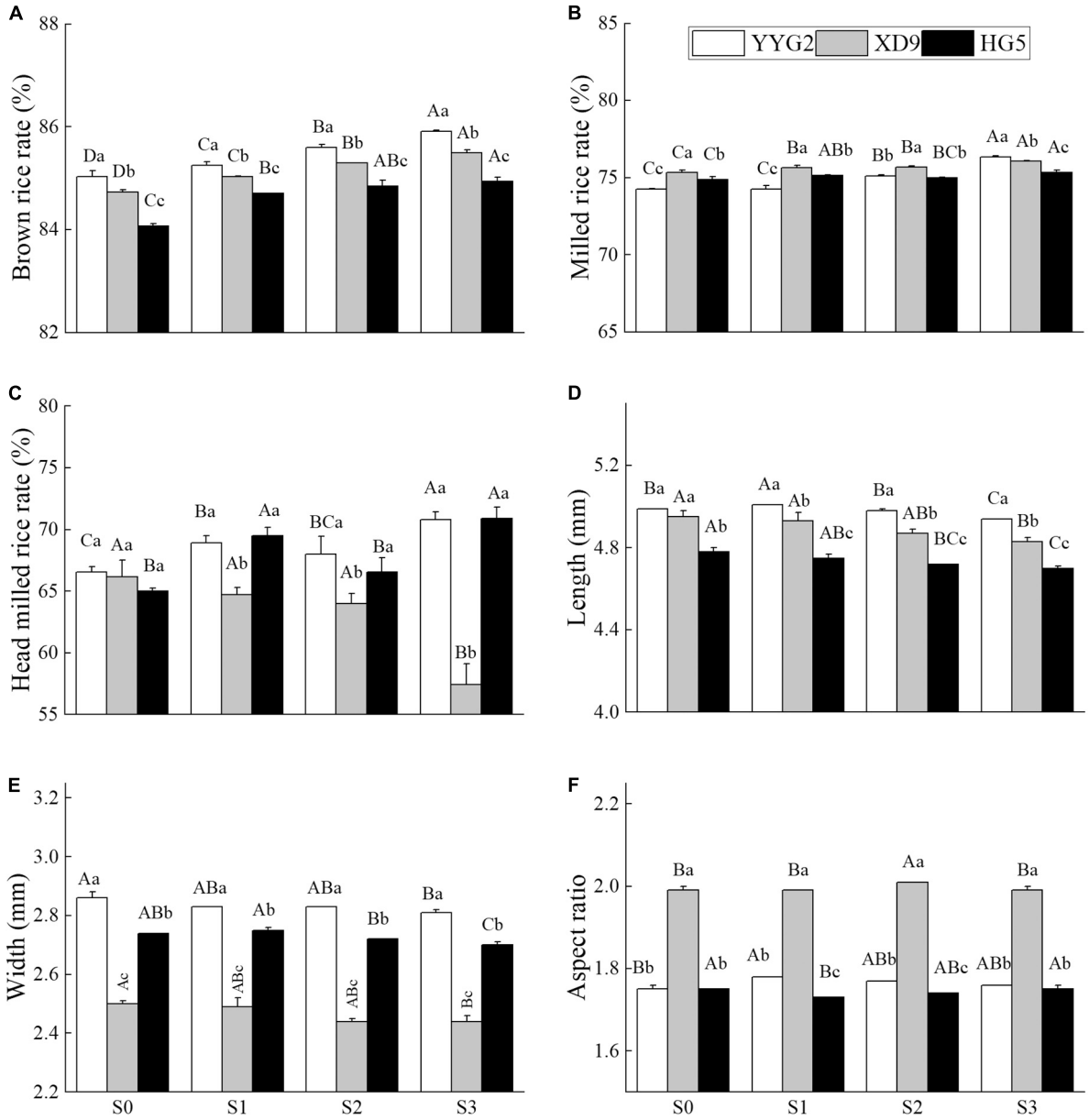

FIGURE 2 | Effect of salt stress on brown rice rate **(A)**, milled rice rate **(B)**, head milled rice rate **(C)**, length **(D)**, width **(E)**, and aspect ratio **(F)** for different rice varieties. YYG2, Yangyugeng2; XD9, Xudao9; HG5, Huageng5; V, Variety; S, Salt; S_0, S_1, S_2, and S_3 denote salt concentrations of 0, 17.1, 25.6 and 34.2 mM, respectively; In different salinity level during the same varieties, bars with the same uppercase letters are not significantly different, while within the same salt concentration in different varieties, bars with the same lowercase letters are not significantly different according to the Duncan test at $P < 0.05$.

viscosity ($p = 0.007$), degree of balance ($p = 0.006$), and taste value ($p = 0.006$). It was noticeable that significant differences in the appearance ($P < 0.001$), hardness ($P < 0.001$), viscosity ($P < 0.001$), degree of balance ($P < 0.001$), and taste value ($P < 0.001$) were also detected among rice cultivars. There was no significant interaction between salt stress and rice varieties in terms of appearance ($P = 0.132$), hardness ($P = 0.081$), viscosity ($P = 0.251$), degree of balance ($P = 0.144$), and taste value ($P = 0.160$). With the increase of salt concentration, the appearance, viscosity, degree of balance, and taste value showed a first rising and then declining trend among Yangyugeng2, Xudao9, and Huageng5. However, the three rice varieties peaked at different corresponding salt concentrations, meaning that Yangyugeng2 and Huageng5 were 17.1 mM NaCl, and Xudao9 was 25.6 mM NaCl, respectively. The result showed that the appearance, viscosity, degree of balance, and taste value increased to 4.87, 5.53, 5, and 59.87, respectively, while the salt concentration was 17.1 mM NaCl, and those of Huageng5 increased to 4.27, 3.73, 3.97, and 53.5, individually. However, the salt stress had no significant effect on the taste quality of

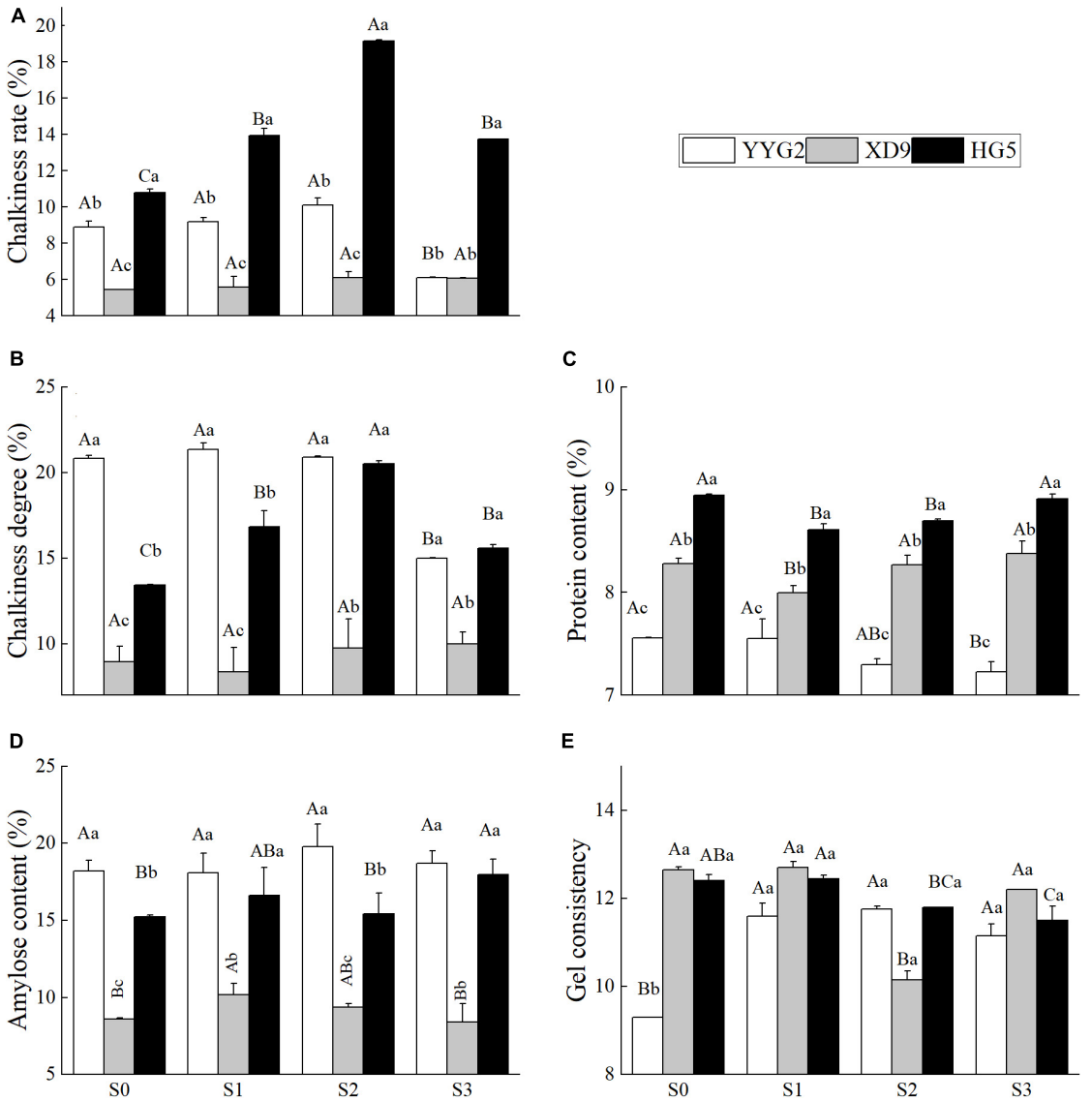

FIGURE 3 | Effect of salt stress on chalkiness rate **(A)**, chalkiness degree **(B)**, protein content **(C)**, amylose content **(D)**, gel consistency **(E)** for different rice varieties. YYG2, Yangyugeng2; XD9, Xudao9; HG5, Huageng5; V, Variety; S, Salt; S_0, S_1, S_2, and S_3 denote salt concentrations of 0, 17.1, 25.6 and 34.2 mM, respectively; In different salinity level during the same varieties, bars with the same uppercase letters are not significantly different, while within the same salt concentration in different varieties, bars with the same lowercase letters are not significantly different according to the Duncan test at $P < 0.05$.

Xudao9, whose appearance, viscosity, degree of balance, and taste value increased to the maximum value (5.9, 5.6, 5.63, and 64.03) when the salt concentration was 25.6 mM NaCl (**Figure 4**). In contrast, the hardness of Yangyugeng2 and Huageng5 decreased to the minimum value (7.43, 7.43) when the salt concentration was 17.1 mM NaCl. When the salinity level was 25.6 mM NaCl, the hardness of Xudao9 decreased to the minimum value (6.87). The effect of salt stress on appearance, viscosity, balance and taste value showed a trend of increasing and then decreasing, and the effect on hardness demonstrated a trend of decreasing and then increasing. However, the turning points were different among rice varieties. The turning point of Xudao9 was S2 treatment, while that of Huageng5 and Yangyugeng2 was S1 treatment, indicating that the salt tolerance of Huageng5 and Yangyugeng2 was lower than that of Xudao9.

Effect of Salt Stress on the Pasting Properties of Starch

The profile characteristics of RVA is a useful index to measure the cooking quality of rice. This study indicated that significant difference was observed in terms of the peak viscosity ($P < 0.001$), hot paste viscosity ($P < 0.001$), breakdown ($P < 0.001$), cold paste viscosity ($P < 0.001$), setback ($P < 0.001$), peak time ($P < 0.001$), and pasting temperature ($P = 0.002$) among rice varieties. It was noticeable that significant differences were also detected

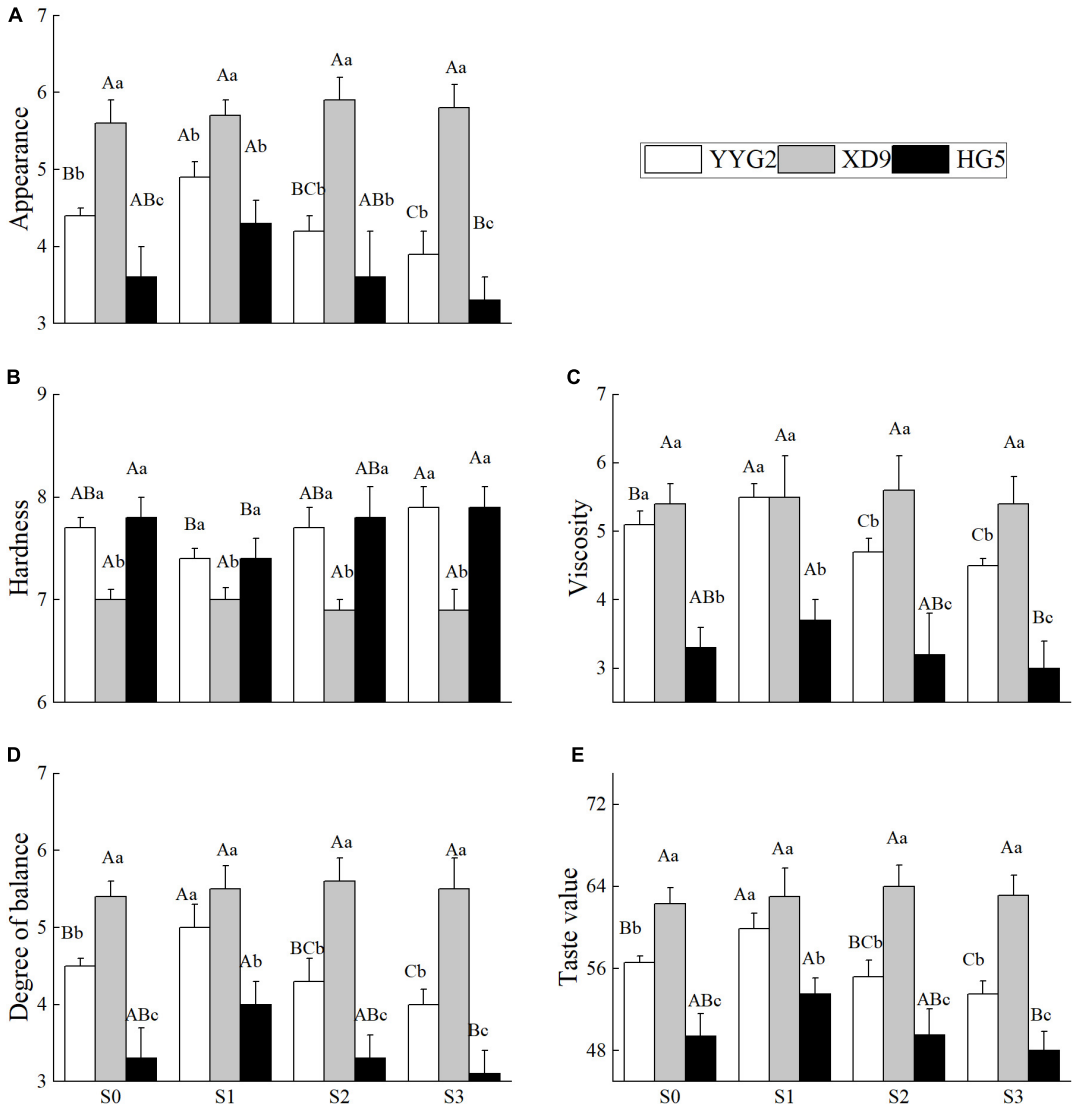

FIGURE 4 | Effect of salt stress on appearance **(A)**, hardness **(B)**, viscosity **(C)**, degree of balance **(D)**, and taste value **(E)** for different rice varieties. YYG2, Yangyugeng2; XD9, Xudao9; HG5, Huageng5; V, Variety; S, Salt; S_0, S_1, S_2, and S_3 denote salt concentrations of 0, 17.1, 25.6 and 34.2 mM, respectively; In different salinity level during the same varieties, bars with the same uppercase letters are not significantly different, while within the same salt concentration in different varieties, bars with the same lowercase letters are not significantly different according to the Duncan test at $P < 0.05$.

under salinity stress in terms of peak viscosity ($P < 0.001$), hot paste viscosity ($P = 0.044$), breakdown ($P = 0.047$), cold paste viscosity ($P < 0.001$), setback ($P = 0.011$), peak time ($P = 0.048$), and pasting temperature ($P = 0.031$). There was significant interaction effect between salt treatments and rice varieties in terms of peak viscosity ($P < 0.001$), cold paste viscosity ($P < 0.001$), and setback ($P = 0.022$) and no significant interaction effect for hot paste viscosity ($P = 0.081$), breakdown ($P = 0.879$), peak time ($P = 0.414$), and pasting temperature ($P = 0.087$). The experimental results revealed that the peak viscosity of Yangyugeng2, Xudao9, and Huageng5 increased to the maximum value (2589, 2618, and 2713) when the salt concentration was 25.6 mM NaCl and decreased to the minimum value (407.5, 831.5, and 525) when the salinity level was 17.1 mM NaCl, respectively (**Figure 5**). At the peak time, there were significant differences among rice varieties, but salinity levels were not. Furthermore, the salinity level influenced the pasting temperature when the concentration of salt was greater or equal to 25.6 mM NaCl. Salt stress increased the difference in pasting temperature among varieties, with Yangyugeng2 showing the greatest sensitivity, followed by Huageng5 and finally Xudao9 (**Figure 5G**).

Effect of Salt Stress on the Mineral Element Content of Rice Seeds

This study investigated that salt stress had significant effect on the contents of K ($P = 0.018$), Na ($P = 0.008$), and Cu ($P = 0.003$),

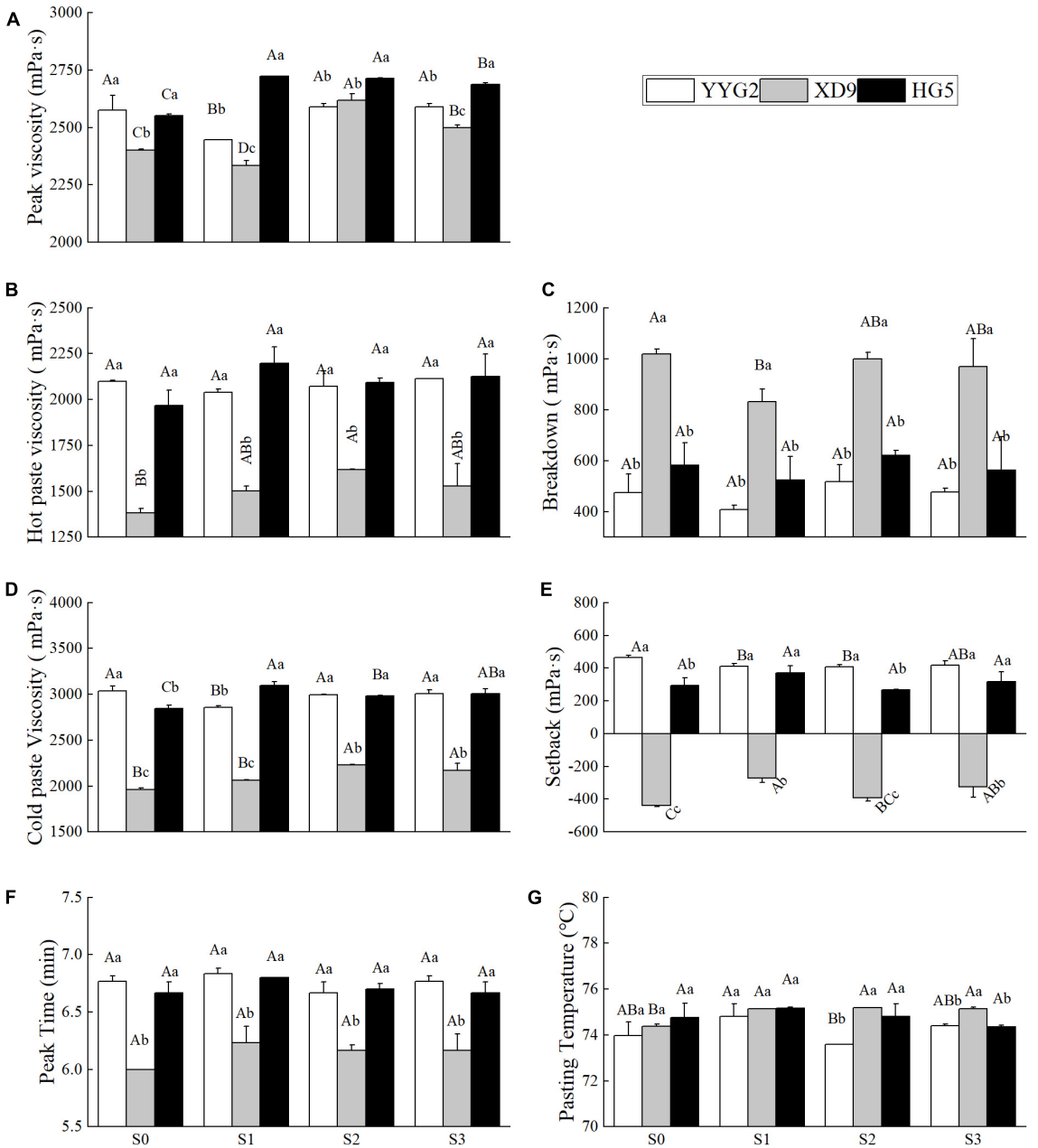

FIGURE 5 | Effects of salt stress on peak viscosity **(A)**, hot paste viscosity **(B)**, breakdown **(C)**, cold paste viscosity **(D)**, setback **(E)**, peak viscosity **(F)**, and pasting temperature **(G)** for different rice varieties. YYG2, Yangyugeng2; XD9, Xudao9; HG5, Huageng5; V, Variety; S, Salt; S_0, S_1, S_2, and S_3 denote salt concentrations of 0, 17.1, 25.6 and 34.2 mM, respectively; In different salinity level during the same varieties, bars with the same uppercase letters are not significantly different, while within the same salt concentration in different varieties, bars with the same lowercase letters are not significantly different according to the Duncan test at $P < 0.05$.

and no significant effect on the contents of S ($P = 0.700$), P ($P = 0.213$), and Mg ($P = 0.638$). And it was noticeable that significant differences were also detected among rice cultivars except for the content of Na ($P = 0.076$). There was significant interaction effect between salt treatments and rice varieties with respect to the contents of K ($P = 0.006$), Na ($P = 0.012$), and P ($P = 0.024$), and no significant interaction effect for the contents of Mg ($P = 0.247$), S ($P = 0.296$), and Cu ($P = 0.288$). In **Figure 6**, the contents of K and S in the milled rice of Yangyugeng2 were the highest (0.67, 0.38) at 17.1 mM NaCl and decreased when the salt concentration was more than 17.1 mM NaCl. The contents of K and S in head milled rice of Xudao9 were the highest (0.85, 0.39) at 25.6 mM NaCl and decreased at 34.2 mM NaCl, and the contents of K and S in head milled rice of Huageng5 increased to the maximum value (0.83, 0.40) at 34.2 mM NaCl. The P content in milled rice of Xudao9 at 34.2 mM NaCl significantly decreased

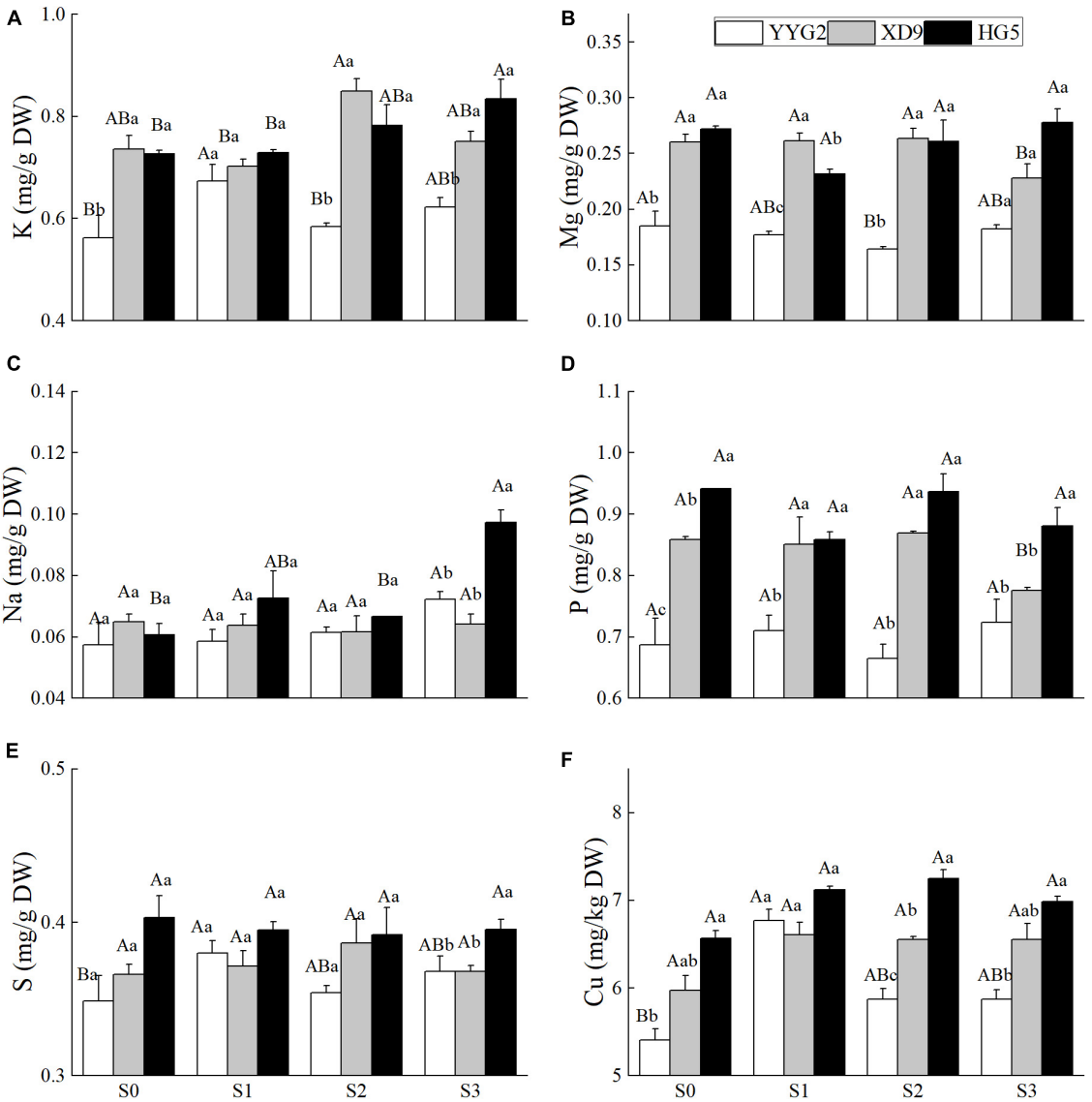

FIGURE 6 | Effect of salt stress on the K **(A)**, Mg **(B)**, Na **(C)**, P **(D)**, S **(E)**, and Cu **(F)** for different rice varieties seeds. YYG2, Yangyugeng2; XD9, Xudao9; HG5, Huageng5; S_0, S_1, S_2, and S_3 denote salt concentrations of 0, 17.1, 25.6 and 34.2 mM, respectively; In different salinity level during the same varieties, bars with the same uppercase letters are not significantly different, while within the same salt concentration in different varieties, bars with the same lowercase letters are not significantly different according to the Duncan test at $P < 0.05$.

by 9.3% compared with that under no salinity stress. A significant difference in the P content between the rice cultivars was found. Significant differences existed among varieties in terms of the Mg content in milled rice when the salt concentration was less than or equal to 25.6 mM NaCl, and no difference was observed among cultivars at 34.2 mM NaCl. The Na content in milled rice significantly increased by 66.7% at 34.2 mM NaCl, and there were significant differences among rice cultivars. The Cu content in milled rice of Yangyugeng2 and Xudao9 increased to the maximum value (6.77, 6.61) at 17.1 mM NaCl, then declined slightly when the salinity level was greater than 17.1 mM NaCl, and that of Huageng5 increased to the maximum value (7.25) at 25.6 mM NaCl.

As shown in **Figure 6**, under S3 treatment, the contents of Na, P and S accumulated in the seeds of Huageng5 were significantly higher than those in the seeds of Xudao9 and Yangyugeng2, and the contents of Cu, P, Mg, and K accumulated in the seed of Xudao9 were more than those in Yangyugeng2. The Na/K ratio of Xudao9 was lower than that of Yangyugeng2 and Huageng5, indicating that Xudao9 had the strongest salt tolerance among varieties, while the Na/K ratio of Huageng5 was slightly higher than that of Yangyugeng2. However, the absorption capacity of Huageng5 for other ions was significantly higher than that of Yangyugeng2, and other ions could mitigate the sodium ion poisoning to a certain extent, so the salt tolerance of Huageng5 was significantly stronger than that of Yangyugeng2 (**Figure 6**).

DISCUSSION

Effect of Salinity Stress on Rice Yield and Grain Quality

Rice yield is the result combining yield components that depend on the production capacity of photosynthetic materials and the functioning and distribution of assimilates. Salinity affects rice growth, which in turn affects both rice yield and quality (Turan et al., 2007; Genyou et al., 2018). The salinity stress significantly affects the yield traits of rice, such as seed setting rate, tiller number, panicle number, and paniclelength; among these contributing traits, seed setting rate is the main cause of yield loss under saline conditions (Shereen et al., 2005). However, in this study, we found that the panicle number is considered as the main factor affecting rice yield (**Figure 1**). A 12% increase in the panicle numbers of Nipponbare was reported when 20 mM NaCl was applied to at 4-weeks after transplanting (Thitisaksakul et al., 2015). In this study, the panicle number increased by 9.68 and 4.78% for Xudao9 and Huageng5, respectively, at a salt concentration of 17.1 mM NaCl, and increased by 4.19% for Xudao9 and decreased by 2.05% for Huageng5 at a salt concentration of 25.6 mM NaCl. In contrast, the panicle number of Yangyugeng2 decreased by 5.76 and 6.92% at these two salt concentrations, respectively (**Figure 1A**). This difference is closely related to the differential salt tolerance of rice varieties, as well as the timing and methods of salt stress.

Rice quality is particularly important for the health of people who eat it as a staple food (Ali et al., 2020). In comparison with the rate of the non-saline environment, the brown rice rate, milled rice rate and head milled rice rate were significantly declined at 51.3 mM NaCl (Genyou et al., 2018). This study revealed that salt stress could increase brown rice rate, milled rice rate and head milled rate when the salinity level is less than or equal to 34.2 mM NaCl. This indicated that the effect of salinity stress on the contributing quality traits of rice were related to the salinity level of in soils (**Figures 2A–C**).

Appearance quality of rice determines its capability to attract consumers, and chalkiness is the main indicator of appearance quality (Zhou et al., 2020; Ayaad et al., 2021). Seeds with high chalkiness are easily broken during milling and thus losing marketability (Sawada et al., 2016). Transparent grain with little or no chalkiness, intermediate gel consistency, intermediate amylose content and low starch content are the desired attributes of good quality rice (Rao et al., 2013). When the salt concentration was higher than 34.2 mM NaCl, the quality of milling and appearance of rice were significantly affected, and the protein contents was significantly increased (Chengke et al., 2017). The results described that the chalkiness rate and chalkiness degree of rice seed increased under the salinity stress, except for Yangyugeng2. And the chalkiness rate and degree of Yangyugeng2 declined when the salt concentration was 34.2 mM NaCl (**Figures 3A,B**). Grain length is more important than width as long grains tend to break during the milling process, and the grain aspect ratio was significantly declined in the salinity soil (Rao et al., 2013). In this study, we demonstrated that the salt stress significantly decreased the length of rice grain but increased the aspect ratio of grain seed except for Huageng5 (**Figures 2D,F**). It was reported that the application of 20 mM NaCl for 4 weeks after transplanting increased the seed length by 3.01% (Thitisaksakul et al., 2015), but in this study only Yangyugeng2 increased the seed length by 0.4% at a salt concentration of 17.1 mM NaCl (**Figure 2D**). It was also reported that salt stress (4 ds/m) did not cause any change in seed length, width and aspect ratio compared to the control group (Sangwongchai et al., 2021). It is worth noting that the duration of salt stress in this experiment was only from flowering to maturity. It can be seen that the duration of salt stress and the mode of salt application significantly affected the experimental results.

Amylose content is an important indicator of rice quality, and low-taste rice varieties with high amylose content will expand in volume during cooking, which are less likely to be tender and hard after cooling. Good-taste rice varieties with low amylose content is moist and sticky when being cooked (Juliano, 1971). Protein is the second most important ingredient after starch and the higher protein content means the better quality of rice (Chen et al., 2021). Numerous studies found that the salinity stress lower the nutritional value of rice (Yajuan et al., 2019), such as amylose content and gel consistency (Rao et al., 2013). The amylose content was significantly decreased under salt stress compared with that of no salinity level, while protein content was the opposite (Genyou et al., 2018). It was also reported that there was no significant change in the amylose and protein content of rice seeds under salt stress (4 ds/m) (Sangwongchai et al., 2021). It has further been suggested that high salt stress (EC 6–8 ds/m) increased the seed protein content, while low salt stress (EC 2.5 ds/m) decreased the seed protein content (Sangwongchai et al., 2021). In this study, the protein content of the salt-tolerant varieties showed a decreasing trend followed by an increasing trend, while the salt-sensitive varieties showed a decreasing trend. The amylose content of Xudao9 exhibited an increasing trend followed by a decreasing trend, while Huageng5 showed an increasing trend and Yangyugeng2 did not change significantly (**Figures 3C,D**). The gel consistency of salt-tolerant varieties tended to decrease and then increase, while that of salt-sensitive varieties tended to increase and then stabilization under salt stress.

The RVA spectrum of starch can better reflect the taste quality of steamed rice, but it is also affected by varieties and environmental conditions (Fan et al., 2021). The RVA curve is a characteristic that can reflect the changes in rice starch viscosity during the rapid heating and cooling of known amounts of rice flour and water (Chen et al., 2021). It has been represented that the RVA value of rice starch was closely related to the taste value of rice, with rice of good quality generally meaning high peak viscosity, high breakdown, and low setback (Genyou et al., 2018). Some scholars concluded that the setback and the pasting temperature increased significantly under 51.3 mM of salt stress, which indicated a negative effect of salt stress on the cooking and taste quality of rice (Genyou et al., 2018). It was also reported that the peak viscosity, hot paste viscosity, cold paste viscosity and breakdown of rice flour reached the maximum value under the salt environment of 17.1 mM NaCl (Dandan et al., 2020). In this study salt stress increased the peak viscosity of Xudao9 and Huageng5, and decreased the setback of Yangyugeng2, increased

the setback of Xudao9, without significant change in the setback of Huageng5. The salt stress increased the pasting temperature of Xudao9, but had no significant effect on that of Yangyugeng2 and Huageng5, which difference may be related to the salt concentrations (**Figures 5A,E,G**).

Effect of Salinity Stress on the Content of Minerals in Milled Rice

Minerals are important for maintaining human health. But as our body cannot synthesize them, people only obtain them from food (Yuanmei et al., 2016). Numerous studies have disclosed that the distribution pattern of most trace elements in rice kernels is rice bran > husk > brown rice > fine rice (Yuanmei et al., 2016). The saline stress increased the uptake of Na, K, and Mg in rice grains, but the increase in K and Mg was not significant, and the saline stress decreased the uptake of Ca, Fe, Mn, and Zn. The effect of saline stress on the Na content of brown rice and fine rice in Longdao11 was extremely prominent (Yajuan et al., 2019). Under the saline stress, Mg and Fe were significantly positively correlated, and Mg and Na were significantly negatively correlated (Yajuan et al., 2019).

This experiment demonstrated that there was a significant or extremely significant relationship among appearance quality, nutritive quality, cooking/eating quality, and pasting properties. There was no significant difference between mineral content and taste quality, mineral content and pasting properties under salinity stress.

In this study, the sodium ion uptake capacity of Huageng5 was significantly greater than that of Xudao9 and Yangyugeng2. The potassium ion uptake capacity of Huageng5 and Yangyugeng2 was significantly higher than that of Yangyugeng2. It is thus known that the uptake capacity of rice varieties depends on the uptake capacity of sodium ions and potassium ions (**Figures 6A,C**). In this study, there was a highly significant positive correlation between potassium ion content and disintegration value, and between and protein content, but a highly significant negative correlation between and setback, width and length, and between and straight chain starch content in rice flour. There was a significant negative correlation between the sodium ion content in rice flour and the length of the seeds. The accumulation of mineral content under salt stress affects the nutritional quality of rice, which in turn affects the rice palatability.

In some cases, when the salt concentration in soil was lower than 10.9 mM NaCl, there was no significant difference in rice yield between soils under or without the salinity stress. When the salt concentration was more than 10.9 mM NaCl, the rice yield and grain quality declined sharply with the increase of salt concentration (Weipu, 2014). Thus, the concentration of 10.9 mM NaCl is recommended as a critical salt concentration for saline rice production, and the salt was implemented for 10 days after transplanting (Weipu, 2014). In other cases, salt stress can increase rice yield and improve the quality of rice milling, cooking and nutrition when the salt concentration is less than or equal to 17.1 mM NaCl (**Figures 1**, **2**). Salt stress can decrease rice yield and affect rice quality when the salinity level is more than or equal to 34.2 mM NaCl (**Figures 1**, **4**). It is recommended that 17.1 mM NaCl be used as the critical salt indicator for saline rice production using salt mixing as the adding method, including sodium chloride and sodium sulfate at 2:1 with the soil before transplanting rice (Chengke et al., 2017). However, other researchers suggested 37.6 mM NaCl as a critical salt indicator for rice production in sodic saline soils. In this experiment, sodic saline soil was mixed with natural black soil in proportion to different concentrations of saline soil (Mingxia et al., 2014). In the present study, salinity stress would increase both milling quality and cooking quality of rice, without significant difference in rice yield when the salt concentration was lower than or equal to 17.1 mM NaCl (**Figures 1**, **2**, **4**). However, salt stress would significantly decrease rice yield and rice quality when the salinity level was more than 17.1 mM NaCl, which was consistent with the findings of other authors (Chengke et al., 2017). From the above discussion, the reactions of salt stress are linked to the components of salt, adding method of salt, local salt concentration and soil type.

CONCLUSION

Salt is a gift from nature and an ancient treasure for storing food. Nowadays, most of the literature elaborate on the harmful effect of salt on crops. But this study finds that the low concentration of salt has an improving effect on the quality of rice. In the future, mudflat saline land can be planted with screened salt-tolerant varieties, provided that a threshold value for these varieties can be determined to control the salt content of saline land within the threshold value, which is conducive to more rational development and utilization of saline land. This study demonstrates that panicle number is the main cause of yield loss under saline conditions, and low concentration of salt stress can increase rice yield, brown rice rate and milled rice rate of rice, and significant increases head milled rice rate of salt-sensitive varieties but decreases in salt-tolerant varieties. The brown rice rate and milled rice rate increased by 0.26–1.04 and 0.01–2.81% under salt stress. Grain length is more sensitive than grain width to salt stress, and the aspect ratio of seeds has significantly correlated with the rice variety, rather than the salt stress. Different varieties of rice exhibit different salt tolerance under salt stress; the three rice varieties in this study, in order of salt tolerance, were Xudao9, Huageng5 and Yangyugeng2. The low concentration of salt stress will increase the appearance, viscosity, degree of balance, and taste value, and decrease the hardness of rice. The differences in starch pasting properties among rice varieties in this study were larger than those caused by salt stress. The defense measures of different rice varieties vary under the salt stress: Xudao9 in a way maintains a low level of Na/K ratio; Huageng5 alleviates sodium poisoning mainly by uptaking other ions. Rice varieties selected with high salt tolerance can be selected for the development and utilization of mudflats, and the low concentration of salt treatment will increase the rice quality. More research can be conducted in the future on the mechanism of increasing rice quality in low salt concentration environment.

DATA AVAILABILITY STATEMENT

The raw data supporting the conclusions of this article will be made available by the authors, without undue reservation.

AUTHOR CONTRIBUTIONS

RZ and QD planned and designed the experiments. RZ, YW, SH, and RL performed and recorded data during the experiments. RZ, SL, and SY statistically analyzed the data and prepared the tables and graphs. RZ wrote the manuscript. YC, HW, QD, and HH approved the final manuscript after review. All authors have read and agreed to the published version of the manuscript.

FUNDING

This research was financially supported by the Jiangsu Agriculture Science and Technology Innovation Fund [CX (21) 3111], Jiangsu Province Key Research and Development Program (BE2019343), National Natural Science Foundation of China (32101817), and the Natural Science Foundation of the Jiangsu Higher Education Institutions (21KJD210001).

ACKNOWLEDGMENTS

We would like to thank Pinglei Gao for improving the manuscript.

REFERENCES

Ali, I., Ullah, S., He, L., Zhao, Q., Iqbal, A., Wei, S., et al. (2020). Combined application of biochar and nitrogen fertilizer improves rice yield, microbial activity and N-metabolism in a pot experiment. *PeerJ* 8:e10311. doi: 10.7717/peerj.10311

Ayaad, M., Han, Z., Zheng, K., Hu, G., Abo-Yousef, M., Sobeih, S. E. S., et al. (2021). Bin-based genome-wide association studies reveal superior alleles for improvement of appearance quality using a 4-way MAGIC population in rice. *J. Adv. Res.* 28, 183–194. doi: 10.1016/j.jare.2020.08.001

Balindong, J. L., Ward, R. M., Liu, L., Rose, T. J., Pallas, L. A., Ovenden, B. W., et al. (2018). Rice grain protein composition influences instrumental measures of rice cooking and eating quality. *J. Cereal Sci.* 79, 35–42. doi: 10.1016/j.jcs.2017.09.008

Bao, J. (2019). *Rice Starch*. Amsterdam: Elsevier, 55–108. doi: 10.1016/B978-0-12-811508-4.00003-4

Bian, J.-L., Xu, F.-F., Han, C., Qiu, S., Ge, J.-L., Xu, J., et al. (2018). Effects of planting methods on yield and quality of different types of japonica rice in northern Jiangsu plain, China. *J. Integr. Agric.* 17, 2624–2635. doi: 10.1016/S2095-3119(18)62141-0

Cagampang, G. B., Perez, C. M., and Juliano, B. (1973). A gel consistency test for eating quality of rice. *J. Sci Food Agric.* 24, 1589–1594. doi: 10.1002/jsfa.2740241214

Chen, F., Fang, P., Zeng, W., Ding, Y., Zhuang, Z., and Peng, Y. (2020). Comparing transcriptome expression profiles to reveal the mechanisms of salt tolerance and exogenous glycine betaine mitigation in maize seedlings. *PLoS One* 15:e0233616. doi: 10.1371/journal.pone.0233616

Chen, H., Chen, D., He, L., Wang, T., Lu, H., Yang, F., et al. (2021). Correlation of taste values with chemical compositions and Rapid Visco Analyser profiles of 36 indica rice (*Oryza sativa* L.) varieties. *Food Chem.* 349:129176. doi: 10.1016/j.foodchem.2021.129176

Chengke, L., Guoju, X., Fengju, Z., and Qian, L. (2017). Effects of different salt stresses on rice yield and quality. *J. Arid Land Resour. Environ.* 31, 137–141.

Corwin, D. L. (2020). Climate change impacts on soil salinity in agricultural areas. *Eur. J. Soil Sci.* 72, 842–862.

Dandan, X., Jun, L., Xianliang, D., Pingyang, W., Jian, T., Huanhe, W., et al. (2020). Response of quality formation of different rice varieties to salt stress. *J. Nuclear Agric. Sci.* 34, 1840–1847.

Das, P., Nutan, K. K., Singla-Pareek, S. L., and Pareek, A. (2015). Understanding salinity responses and adopting 'omics-based' approaches to generate salinity tolerant cultivars of rice. *Front. Plant Sci.* 6:712. doi: 10.3389/fpls.2015.00712

Domingo, C., Lalanne, E., Catala, M. M., Pla, E., Reig-Valiente, J. L., and Talon, M. (2016). Physiological basis and transcriptional profiling of three salt-tolerant mutant lines of rice. *Front. Plant Sci.* 7:1462. doi: 10.3389/fpls.2016.01462

Dongfen, H., Zhiqin, W., Lijun, L., and Jianchang, Y. (2009). Difference in Pb and mineral nutrient uptake and distribution between rice cultivars under the Pb stress. *Chin. J. Trop. Crops* 30, 1752–1758.

Dramalis, C., Katsantonis, D., and Koutroubas, S. D. (2021). Rice growth, assimilate translocation, and grain quality in response to salinity under Mediterranean conditions. *AIMS Agric. Food* 6, 255–272. doi: 10.3934/agrfood.2021017

Eynard, A., Lal, R., and Wiebe, K. (2005). Crop response in salt-affected soils. *J. Sustain. Agric.* 27, 5–50. doi: 10.1300/J064v27n01_03

Fahad, S., Noor, M., Adnan, M., Khan, M. A., Rahman, I. U., Alam, M., et al. (2019). "Abiotic stress and rice grain quality," in *Advances in Rice Research for Abiotic Stress Tolerance*, eds. M., Hasanuzzaman, M., Fujita, K., Nahar, and J. K., Biswas. (Amsterdam: Elsevier), 571–583. doi: 10.1016/B978-0-12-814332-2.00028-9

Fan, Y., Xiaoyuan, Z., Qiuping, L., Shuxian, L., Wu, L., Tao, Z., et al. (2021). Effects of delayed sowing and planting date on starch RVA profiles of different indica hybrid rice in the sub-suitable region of ratoon rice. *Acta Agron. Sin.* 47, 701–713. doi: 10.3724/SP.J.1006.2021.02037

Fitzgerald, M. A., Mccouch, S. R., and Hall, R. D. (2009). Not just a grain of rice: the quest for quality. *Trends Plant Sci.* 14, 133–139. doi: 10.1016/j.tplants.2008.12.004

Genyou, Z., Caijiao, Z., Xianliang, D., Jiao, Z., Zhenliang, Z., Qigeng, D., et al. (2018). Performance of yield, photosynthesis and grain quality of japonica rice cultivars under salinity stress in micro-plots. *Chin. J. Rice Sci.* 32, 146–154.

Han, Y., Xu, M., Liu, X., Yan, C., Korban, S. S., Chen, X., et al. (2004). Genes coding for starch branching enzymes are major contributors to starch viscosity characteristics in waxy rice (*Oryza sativa* L.). *Plant Sci.* 166, 357–364. doi: 10.1016/j.plantsci.2003.09.023

Hernandez-Santana, V., Diaz-Rueda, P., Diaz-Espejo, A., Raya-Sereno, M. D., Gutierrez-Gordillo, S., Montero, A., et al. (2019). Hydraulic traits emerge as relevant determinants of growth patterns in wild olive genotypes under water stress. *Front. Plant Sci.* 10:291. doi: 10.3389/fpls.2019.00291

Hu, Y., Li, L., Tian, J., Zhang, C., Wang, J., Yu, E., et al. (2020). Effects of dynamic low temperature during the grain filling stage on starch morphological structure, physicochemical properties, and eating quality of soft japonica rice. *Cereal Chem.* 97, 540–550. doi: 10.1002/cche.10268

Hua, J., Feng, Y., Jiang, Q., Bao, X., and Yin, Y. (2017). Shift of bacterial community structure along different coastal reclamation histories in Jiangsu. Eastern China. *Sci. Rep.* 7:10096. doi: 10.1038/s41598-017-10608-3

Jianfeng, Z. (2008). Discussion on ecological rehabilitation of salt-affected soils. *Res. Soil Water Conserv.* 15, 74–78.

Jiang, S. L., Wu, J. G., Thang, N. B., Feng, Y., Yang, X. E., and Shi, C. H. (2008). Genotypic variation of mineral elements contents in rice (*Oryza sativa* L.). *Eur. Food Res. Technol.* 228, 115–122. doi: 10.1007/s00217-008-0914-y

Juliano, B. O. (1971). A simplified assay for milled-rice amylose. *Cereal Sci. Today* 16, 334–340.

Kaur, P., Pal, P., Virdi, A. S., Kaur, A., Singh, N., and Mahajan, G. (2016). Protein and starch characteristics of milled rice from different cultivars affected by transplantation date. *J. Food Sci. Technol.* 53, 3186–3196. doi: 10.1007/s13197-016-2293-x

Kordrostami, M., Rabiei, B., and Hassani Kumleh, H. (2017). Biochemical, physiological and molecular evaluation of rice cultivars differing in salt tolerance at the seedling stage. *Physiol. Mol. Biol. Plants* 23, 529–544. doi: 10.1007/s12298-017-0440-0

Krishnan, P., Ramakrishnan, B., Reddy, K. R., and Reddy, V. R. (2011). High-temperature effects on rice growth, yield, and grain quality. *Adv. Agron.* 111, 87–206. doi: 10.1016/B978-0-12-387689-8.00004-7

Limin, Y. (2012). Effects of silicon on antioxidant enzymes activities and ions uptake of rice seedlings under salt stress. *J. Jilin Agric. Sci.* 37, 22–24.

Ltaeif, H. B., Sakhraoui, A., Gonzalez-Orenga, S., Landa Faz, A., Boscaiu, M., Vicente, O., et al. (2021). Responses to salinity in four plantago species from Tunisia. *Plants (Basel)* 10:1392. doi: 10.3390/plants10071392

Mei, L., Qingsong, Z., Zhaopu, L., and Shiwei, G. (2015). Effects of nitrogen forms on transport and accumulation of ions in canola *(B. napus* L.) and rice (*Oryza sativa* L.) under saline stress. *J. Plant Nutr. Fert.* 21, 181–189.

Menezes-Benavente, L., Teixeira, F. K., Alvim Kamei, C. L., and Margis-Pinheiro, M. (2004). Salt stress induces altered expression of genes encoding antioxidant enzymes in seedlings of a *Brazilian indica* rice (*Oryza sativa* L.). *Plant Sci.* 166, 323–331. doi: 10.1016/j.plantsci.2003.10.001

Mingxia, Z., Xianying, G., Xiwen, S., Feng, J., Yanqiu, G., and Shuai, W. (2014). Effect of different concentrations of saline-alkali stress on growth and yield of Rice. *J. Jilin Agric. Sci.* 39, 12–16. doi: 10.1038/s41598-020-63352-6

Nounjan, N., Nghia, P. T., and Theerakulpisut, P. (2012). Exogenous proline and trehalose promote recovery of rice seedlings from salt-stress and differentially modulate antioxidant enzymes and expression of related genes. *J. Plant Physiol.* 169, 596–604. doi: 10.1016/j.jplph.2012.01.004

Qing, Z., Yilei, J., Lianxin, Y., Yulong, W., and Yunxia, W. (2019). Impacts of elevated ozone concentration and foliar zinc application on yield, grain zinc content and bioavailability of wheat. *J. Agro Environ. Sci.* 38, 728–736.

Rao, P. S., Mishra, B., and Gupta, S. R. (2013). Effects of soil salinity and alkalinity on grain quality of tolerant, semi-tolerant and sensitive rice genotypes. *Rice Sci.* 20, 284–291. doi: 10.1016/S1672-6308(13)60136-5

Razzaq, A., Ali, A., Safdar, L. B., Zafar, M. M., Rui, Y., Shakeel, A., et al. (2020). Salt stress induces physiochemical alterations in rice grain composition and quality. *J. Food Sci.* 85, 14–20. doi: 10.1111/1750-3841.14983

Sakhare, S. D., Inamdar, A. A., and Prabhasankar, P. (2015). Roller milling process for fractionation of fenugreek seeds (*Trigonella foenumgraecum*) and characterization of milled fractions. *J. Food Sci. Technol.* 52, 2211–2219. doi: 10.1007/s13197-014-1279-9

Sangwongchai, W., Krusong, K., and Thitisaksakul, M. (2021). Salt tolerance at vegetative stage is partially associated with changes in grain quality and starch physicochemical properties of rice exposed to salinity stress at reproductive stage. *J. Sci. Food Agric.* 102, 370–382. doi: 10.1002/jsfa.11367

Sawada, H., Tsukahara, K., Kohno, Y., Suzuki, K., Nagasawa, N., and Tamaoki, M. (2016). elevated ozone deteriorates grain quality of japonica rice cv. Koshihikari, even if it does not cause yield reduction. *Rice (N Y)* 9:7. doi: 10.1186/s12284-016-0079-4

Senguttuvel, P., Vijayalakshmi, C., Thiyagarajan, K., Sritharan, R., Geetha, S., Kannanbapu, J. R., et al. (2013). Differential response of rice seedlings to salt stress in relation to antioxidant enzyme activity and membrane stability index. *Arch. Agron. Soil Sci.* 59, 1359–1371.

Shaik, S. S., Carciofi, M., Martens, H. J., Hebelstrup, K. H., and Blennow, A. (2014). Starch bioengineering affects cereal grain germination and seedling establishment. *J. Exp. Bot.* 65, 2257–2270. doi: 10.1093/jxb/eru107

Shereen, A., Mumtaz, S., Raza, S., Khan, M. A., and Solangi, S. (2005). Salinity effects on seedling growth and yield components of different inbred rice lines. *Pakistan J. Bot.* 37, 131–139.

Thitisaksakul, M., Tananuwong, K., Shoemaker, C. F., Chun, A., Tanadul, O.-U.-M., Labavitch, J. M., et al. (2015). Effects of timing and severity of salinity stress on rice (*Oryza sativa* L.) yield, grain composition, and starch functionality. *J. Agric. Food Chem.* 63, 2296–2304. doi: 10.1021/jf503948p

Thu, T. T. P., Yasui, H., and Yamakawa, T. (2017). Effects of salt stress on plant growth characteristics and mineral content in diverse rice genotypes. *Soil Sci. Plant Nutr.* 63, 264–273.

Turan, M. A., Türkmen, N., and Nilgun, T. (2007). Effect of NaCl on Stomatal Resistance and Proline, Chlorophyll, Na, Cl and K Concentrations of Lentil Plants. *J. Agron.* 6, 378–381.

Wang, G., Hu, Y., Luo, Q., Cai, R., Li, D., Chen, C., et al. (2017). Determination and analysis of mineral elements content in rice samples. *Nuclear Techn.* 40:6.

Weipu, Y. (2014). *Effect of Salt Stress Associated With Straw Returning on Yield and Quality of Rice. Master Degree*. Yangzhou: Yangzhou University.

Xiong, Q., Ma, B., Lu, X., Huang, Y. H., He, S. J., Yang, C., et al. (2017). Ethylene-inhibited jasmonic acid biosynthesis promotes Mesocotyl/Coleoptile elongation of etiolated rice seedlings. *Plant Cell* 29, 1053–1072. doi: 10.1105/tpc.16.00981

Yajuan, G., Jingpeng, L., Fu, Y., and Xin, Z. (2019). Effects of saline - alkaline stress on mineral element contents in rice husk and grain. *Soils Crops* 8, 50–59.

Yuanmei, S., Shaoming, L., Tianli, Y., and Yongmei, G. (2016). Study on mineral concentrations diversity and distribution among different rice genotypes. *Southwest China J. Agric. Sci.* 29, 1006–1011.

Zhang, X., Fu, L., Tu, Y., Zhao, H., Kuang, L., and Zhang, G. (2020).). The influence of nitrogen application level on eating quality of the two indica-japonica hybrid rice cultivars. *Plants (Basel)* 9:1663. doi: 10.3390/plants9121663

Zhao, D. S., Li, Q. F., Zhang, C. Q., Zhang, C., Yang, Q. Q., Pan, L. X., et al. (2018). GS9 acts as a transcriptional activator to regulate rice grain shape and appearance quality. *Nat. Commun.* 9:1240. doi: 10.1038/s41467-018-03616-y

Zhou, N., Wei, H., and Zhang, H. (2020). Response of milling and appearance quality of rice with good eating quality to temperature and solar radiation in lower reaches of Huai River. *Agronomy* 11:77.

Zhu, D., Zhang, H., Guo, B., Xu, K., Dai, Q., Wei, H., et al. (2017). Effects of nitrogen level on yield and quality of japonica soft super rice. *J. Integr. Agric.* 16, 1018–1027. doi: 10.1016/S2095-3119(16)61577-0

Zhu, Y., Xu, D., Chen, X., Ma, Z., Ma, H., Zhang, M., et al. (2021a). Quality characteristics of semi-glutinous japonica rice cultivated in the middle and lower reaches of the Yangtze River in China. *J. Sci. Food Agric.* doi: 10.1002/jsfa.11718

Zhu, Y., Xu, D., Ma, Z., Chen, X., Zhang, M., Zhang, C., et al. (2021b). Differences in eating quality attributes between japonica rice from the northeast region and semiglutinous japonica rice from the Yangtze River delta of China. *Foods* 10:2770. doi: 10.3390/foods10112770

Conflict of Interest: HH was employed by Yibang Agriculture Technology Development Co., Ltd.

The remaining authors declare that the research was conducted in the absence of any commercial or financial relationships that could be construed as a potential conflict of interest.

Publisher's Note: All claims expressed in this article are solely those of the authors and do not necessarily represent those of their affiliated organizations, or those of the publisher, the editors and the reviewers. Any product that may be evaluated in this article, or claim that may be made by its manufacturer, is not guaranteed or endorsed by the publisher.

Copyright © 2022 Zhang, Wang, Hussain, Yang, Li, Liu, Chen, Wei, Dai and Hou. This is an open-access article distributed under the terms of the Creative Commons Attribution License (CC BY). The use, distribution or reproduction in other forums is permitted, provided the original author(s) and the copyright owner(s) are credited and that the original publication in this journal is cited, in accordance with accepted academic practice. No use, distribution or reproduction is permitted which does not comply with these terms.

frontiers | Frontiers in Plant Science

ORIGINAL RESEARCH
published: 17 June 2022
doi: 10.3389/fpls.2022.842599

Grain Transcriptome Dynamics Induced by Heat in Commercial and Traditional Bread Wheat Genotypes

*Diana Tomás, Wanda Viegas and Manuela Silva**

LEAF – Linking Landscape, Environment, Agriculture and Food, TERRA – Laboratory for Sustainable Land Use and Ecosystem Services, Instituto Superior de Agronomia, Universidade de Lisboa, Lisbon, Portugal

High temperature (HT) events have negative impact on wheat grains yield and quality. Transcriptome profiles of wheat developing grains of commercial genotypes (Antequera and Bancal) and landraces (Ardito and Magueija) submitted to heatwave-like treatments during grain filling were evaluated. Landraces showed significantly more differentially expressed genes (DEGs) and presented more similar responses than commercial genotypes. DEGs were more associated with transcription and RNA and protein synthesis in Antequera and with metabolism alterations in Bancal and landraces. Landraces upregulated genes encoding proteins already described as HT responsive, like heat shock proteins and cupins. Apart from the genes encoding HSP, two other genes were upregulated in all genotypes, one encoding for Adenylate kinase, essential for the cellular homeostasis, and the other for ferritin, recently related with increased tolerance to several abiotic stress in Arabidopsis. Moreover, a NAC transcription factor involved in plant development, known to be a negative regulator of starch synthesis and grain yield, was found to be upregulated in both commercial varieties and downregulated in Magueija landrace. The detected diversity of molecular processes involved in heat response of commercial and traditional genotypes contribute to understand the importance of genetic diversity and relevant pathways to cope with these extreme events.

Keywords: bread wheat, commercial varieties, landraces, heatwave, grain transcriptome, RNA sequencing

OPEN ACCESS

Edited by:
Felipe Klein Ricachenevsky, Federal University of Rio Grande do Sul, Brazil

Reviewed by:
Klára Kosová, Crop Research Institute (CRI), Czechia
Manosh Kumar Biswas, University of Leicester, United Kingdom

***Correspondence:**
Manuela Silva
manuelasilva@isa.ulisboa.pt

Specialty section:
This article was submitted to Plant Abiotic Stress, a section of the journal Frontiers in Plant Science

Received: *23 December 2021*
Accepted: *16 May 2022*
Published: *17 June 2022*

Citation:
Tomás D, Viegas W and Silva M (2022) Grain Transcriptome Dynamics Induced by Heat in Commercial and Traditional Bread Wheat Genotypes. Front. Plant Sci. 13:842599. doi: 10.3389/fpls.2022.842599

INTRODUCTION

Wheat is the second most produced and consumed cereal worldwide on a daily basis (FAO©, 2019) and hexaploid bread wheat (*Triticum aestivum* L, 2n = 42) represents 90–95% of this production. However, the current growth rate of wheat production is not sufficient to cover the predicted global demand in 2050. Specifically in European countries, the stagnation of wheat yield increase is related with the progressive global warming (Brisson et al., 2010; Ray et al., 2013; Gaupp et al., 2019). The increase of mean temperature during wheat development affects grain yield and quality, due to reduction in lifecycle, pollen abortion, kernel shrinkage, and decrease in seed reserves (Asseng et al., 2014; Nuttall et al., 2018; Wang et al., 2019). The required optimum temperature for wheat anthesis and grain filling ranges from 12 to 22°C (Tewolde et al., 2006) and the overall acceleration of grain development observed under high temperature regimes is associated with the speed up of transcriptomic events (Altenbach and Kothari, 2004; Wan et al., 2008).

Transcription modulation of genes encoding heat shock proteins (HSPs) is the most studied molecular response under heat stress (Wahid et al., 2007). A recent study identified and characterized 753 HSP genes expressed in bread wheat, revealing the developmental stage and stress situation at which they are responsive (Kumar et al., 2020). HSPs transcripts were also differentially detected after 1 h and 1 d at 40°C using Wheat Genome Array profiles in seedlings of two genotypes with contrasting thermotolerances (Qin et al., 2008). The same work also detected transcription factors and genes involved in phytohormone biosynthesis/signaling, calcium and sugar signal pathways, RNA metabolism, ribosomal proteins, primary and secondary metabolisms synthesis, and biotic and abiotic stress responses. Chauhan et al. (2011) identified heat responsive genes, after 2 h of heat stress treatments (34 and 40°C), implicated in metabolites and protein synthesis in seedling shoot, flower tissues and developing grain through subtractive hybridization.

Whole transcriptome sequencing of wheat seedlings reported similar transcripts profiles after heat, drought and their combination treatments of 1 and 6 h (Liu et al., 2015). The main biological groups associated with upregulated genes were stress response, hormone stimulus response and nutrient metabolic processes, while downregulated genes were mainly enriched in photosynthesis and nutrient biosynthesis pathway. A more recent study used RNA Sequencing data obtained from developing grains of genotypes with distinct thermotolerances that underwent post anthesis heat stress for 3 days, identified different clusters of genes unique to tolerant and susceptible genotypes (Rangan et al., 2019). This work also refers that most genes uniquely expressed in tolerant genotype during heat stress are detected in both early and late grain filling reinforcing their role in heat stress response. Other work from Kino et al. (2020) compared RNA Sequencing data obtained from whole grains after post anthesis high temperature treatment (35°C during 2–12 days) against existing sequence data from individual pericarp and endosperm tissue. A significant down-regulation of pericarp genes with a known role in regulation of cell wall expansion was observed. For that reason, the authors suggested that heat treatment induces reduced expansion capability of the pericarp, which may result in a physical constraint of endosperm growth.

Several studies have shown increasing genetic erosion caused by the replacement of diverse old landraces by comparatively few and homozygous modern cultivars (Gregová et al., 1999; Caballero et al., 2001; Srinivasan et al., 2003). Landraces are dynamic populations of cultivated species lacking formal crop improvement, locally adapted and often genetically diverse [reviewed in Villa et al. (2005)]. Thus, landraces provide notable successes in crop improvement [reviewed in Dwivedi et al. (2016)] as sources of nutritional and technological quality traits and marginal environment tolerance [reviewed in Newton et al. (2010)]. They are considered extremely valuable agrobiodiversity pools in changing environmental conditions (Trethowan and Mujeeb-Kazi, 2008; Lopes et al., 2015) that may constitute a key resource facing extreme heat events like heatwaves. Heatwaves are defined by World Meteorological Organization [WMO] (2015) as five or more consecutive days of heat in which the daily maximum temperature is at least 5°C higher than the average maximum temperature. These adverse environmental events are foreseen to be increasingly frequent (Cardoso et al., 2019). The main goal of this work was to evaluate whole transcriptomic alterations induced by heatwave-like treatment during grain filling. This study was comparatively performed in two commercial varieties and two Portuguese landraces, chosen based on previous evaluations of high temperature (HT) responses regarding yield and grain composition (Tomás et al., 2020a,b,c).

MATERIALS AND METHODS

Plant Material and High Temperature Treatment

The genotypes studied in this work comprehend two bread wheat (*Triticum aestivum* L., 2n = 6× = 42, AABBDD) commercial varieties recommended to be used in Portugal (ANPOC et al., 2014), Antequera and Bancal, and two old Portuguese landraces from Vasconcellos collection, established in the 30s of the last century (Vasconcellos, 1933), Ardito and Magueija. Seeds of commercial varieties were gently supplied by ANSEME (Portugal) and seeds of traditional landraces by EAN Germplasm Bank (Oeiras, Portugal, PRT005). Twenty seeds from each genotype obtained after 2 years of controlled propagation were germinated and grown in controlled conditions–8 h of dark at 20°C and a 16 h light period divided in 6 h increasing to 25°C, 4 h at 25°C, and 6 h decreasing to 20°C. Three-week old plants were transferred individually to seven liters soil pots and maintained in greenhouse conditions.

When the first anther was observed in the first spike (anthesis), plants were transferred to growth chambers with the previously described control conditions. Ten days after anthesis (daa) subsets of ten plants (biological replicates) of each genotype were submitted to two different growth conditions for 7 days: control conditions above described or high temperature (HT) regime with a daily plateau of 40°C maximum temperature (**Supplementary Figure 1**). Immediately after the period of 4 h at maximum temperature in the last day of the treatment, two immature grains from the middle of each first spike of each plant were collected (17 daa) and stored at –80°C for posterior RNA extraction.

RNA Extraction, Library Preparation, and Sequencing

Total RNA was individually extracted from control and heat-treated immature grains using the Spectrum™ Plant Total RNA Kit (Sigma-Aldrich, Inc., Spain) and following manufacturer's instructions. For the RNA sequencing, three biological replicates were analyzed per condition and genotype, each composed of a pool of three immature grains (total 100 ng of RNA). Both library preparation and sequencing were performed and optimized by the Genomics Unit of the Instituto Gulbenkian Ciência, Oeiras. mRNA-libraries were prepared using the SMART-seq2 protocol adapted from Macaulay et al. (2016) Illumina® libraries performed used the Nextera protocol adapted

from Baym et al. (2015). The libraries quantification and quality verification were done using the Agilent Fragment Analyzer in combination with HS NGS Kit (Agilent Technologies, Santa Clara, California). Libraries were sequenced in the NextSeq500 Illumina® Sequencer using 75 SE high throughput kit (Illumina, San Diego, California) and 937302653 reads were obtained from the 24 samples.

RNA Sequencing Data Processing and Differential Gene Expression Analysis

Bioinformatic analysis from quality assessment to differential expression analysis were performed by BioData.pt. Quality control was evaluated on raw reads using FastQC (Andrews et al., 2010). Raw reads were then trimmed using fastp (Chen S. et al., 2018) to the longest continuous segment of Phred-quality (threshold of 30 or above) in order to improve overall base quality, and remove the Illumina® Smart-Seq2 adaptors from sequencing. A new quality control with FastQC was performed. The trimmed reads were mapped to *Triticum aestivum* genome[1] using hisat2 with default parameters (Kim et al., 2015). Quality control of the mapping procedure was accessed with Qualimap (Okonechnikov et al., 2016).

Read assignment to genomic features and gene expression quantification were made using featureCounts (Liao et al., 2014). Differential gene expression was tested using DESeq2 (Love et al., 2014) between transcript sets of control and HT treated samples. Manual search of gene ID and encoding products was made in Ensemble Plants BioMart (Kinsella et al., 2011).

R software (R Core Team, 2018) was used to integrate all the analysis and obtain multi-dimensional scaling analysis (MDS) plot (to show the general relationship between the samples) and hierarchical clustering of samples for all varieties and conditions represented as an heatmap and Venn diagrams (showing the relationships between the differentially expressed genes lists of all varieties and conditions).

Gene Ontology Enrichment Analysis

Gene enrichment (GO) analysis was done in AgriGOv2[2] web-based tool (Tian et al., 2017). AgriGO SEA parameter settings were as follows: Fisher test, with Bonferroni multi-test adjustment method, 0.05 significance level, five minimum mapping entries, and complete gene ontology. The GO database[3] was used to analyze GO terms enrichment of DEGs, and the Kyoto Encyclopedia of Genes and Genomes (KEGG) database[4] was used to identify the enriched metabolic pathways, as well as the enzymes involved.

RESULTS AND DISCUSSION

In this work, plants of four wheat genotypes, Antequera, Ardito, Bancal, and Magueija were submitted to HT treatment simulating a heatwave, for 1 week during grain filling stage. Transcriptome profiles of immature grains collected immediately after treatment period (17 days after anthesis) from control and treated plants were analyzed.

Traditional Genotypes Presented a More Similar High Temperature Response Than Commercial Varieties

The reference genome used to map transcripts was the IWGSC RefSeq v1.0 assembly (the first version of the reference sequence obtained from the bread wheat variety Chinese Spring). Overall, about 90% of the transcripts were mapped against the reference genome, and from these 37% mapped to multiple sites and the other 53% mapped specifically to one site in the genome. From the mapped transcripts, an average of 68% of the reads aligned to exonic regions, 29% to the intergenic regions and only 3% to intronic regions. The great percentage of transcripts mapped to intergenic domains is probably due to the incomplete genome annotation. Interestingly, commercial varieties Antequera and Bancal presented a significantly ($p < 0.05$) higher percentage (71.5%) of transcripts mapped to the exonic regions than the traditional ones Ardito and Magueija (61%). Concomitantly, the number of transcripts mapped to both intronic and intergenic regions is higher in the landraces. This may be explained by the fact that old traditional genotypes, collected in the 1930s, are more distinct from the reference genome than commercial varieties. Lastly, the results summarized in **Figure 1A** indicate that most reads (between 73 and 82%) were assigned as protein coding regions, the next most found class was non-translating–coding sequence (between 18 and 27%), and, in a very small amount ribosomal DNA (less than 3%).

Also a hierarchical clustering (**Figure 1B**) of sample-to-sample correlations revealed great intravarietal similarity between Antequera and Bancal samples, independently of the treatment, while for Ardito and Magueija, the similarities were greater between samples of the same condition (control/HT). In fact, the MDS (multi-dimensional scaling) plot grouping (**Figure 1C**) has shown that five of the six samples of each commercial varieties are closer to each other, while in landraces a clear separation between control and treatment samples was observed.

Differentially expressed genes (DEGs) between transcriptomes of immature grains from plants kept in control conditions and submitted to high temperature were considered significant with and adjusted p-value (padj) < 0.05 for all genotypes. Up and downregulated genes were obtained filtering the log2 foldchange absolute value higher than 1. For the four genotypes analyzed, a total of 10,366 DEGs were identified, 86% of them referent to Ardito and Magueija traditional genotypes, showing that they have a greater response to high temperature treatment. In a similar study done recently (Rangan et al., 2019), grain transcriptomes of three genotypes showed a higher number (more than 80%) of downregulated genes in susceptible genotypes, comparing with tolerant ones (2% of the DEGs were downregulated). Thus, the HT response of our landraces was similar to susceptible genotypes, as they present a higher number of DEGs.

[1] ftp://ftp.ensemblgenomes.org/pub/plants/release-48/fasta/triticum_aestivum/dna/Triticum_aestivum.IWGSC.dna.toplevel.fa.gz

[2] http://systemsbiology.cau.edu.cn/agriGOv2/index.php

[3] http://geneontology.org

[4] http://www.kegg.jp/kegg

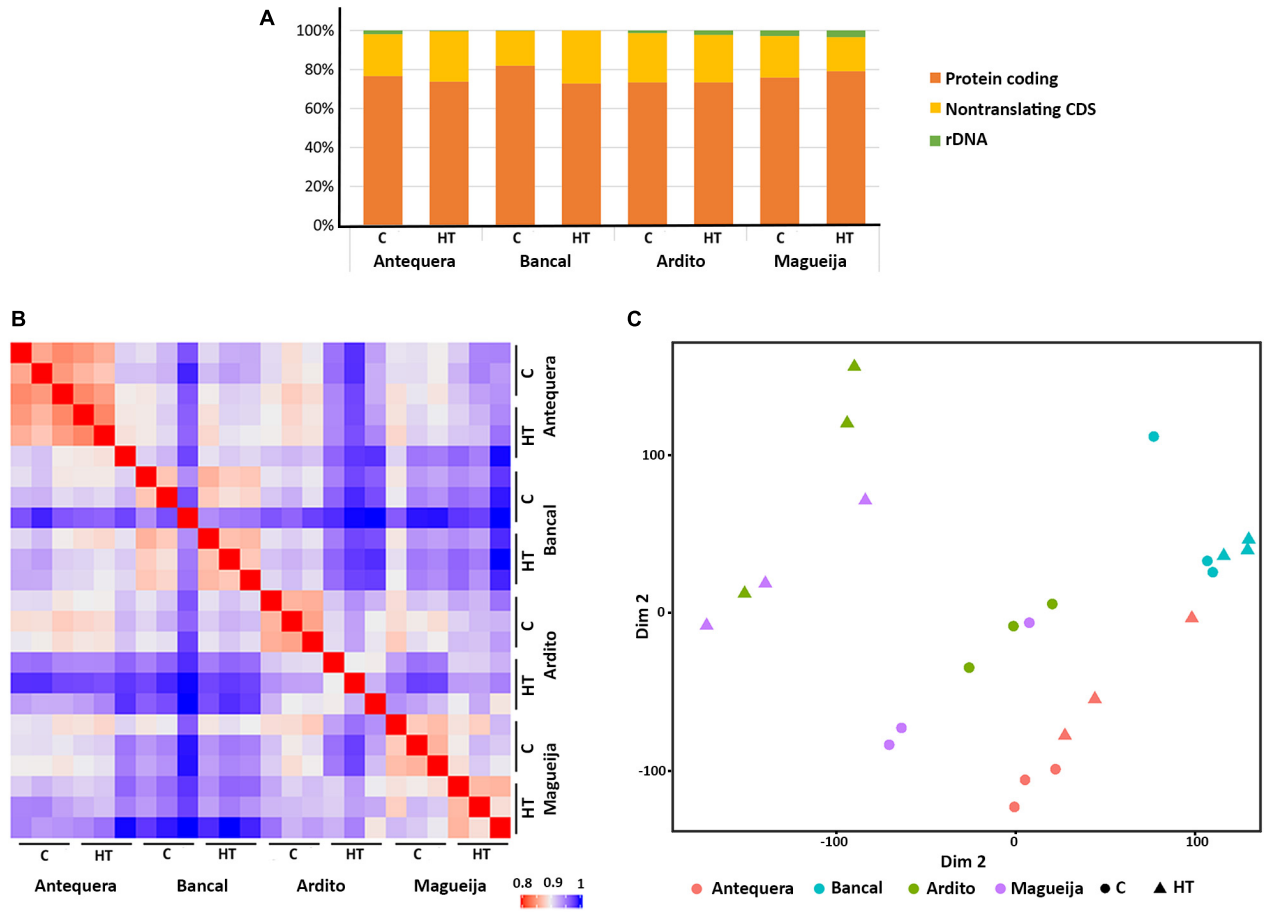

FIGURE 1 | Reads assignments by gene type and relationship between samples. **(A)** Read assignments and relative abundance of reads per type of gene. **(B)** Hierarchical clustering of sample-to-sample correlations based on Pearson correlations (right). **(C)** Multi-dimensional scaling (MDS) plot showing similarity between all samples. The comparisons were made between control (C) and high temperature (HT) reads sets of commercial varieties Antequera and Bancal and landraces Ardito and Magueija.

The number of DEGs is significantly different between all genotypes ($p < 0.05$), although these differences were less accentuated between Ardito and Magueija (**Figure 2A**). Particularizing to each genotype, the commercial variety Bancal presented the lower number of DEGs of all varieties studied, 129 in total, 69 upregulated and 60 downregulated. A ten times higher number of DEGs were identified in Antequera (1298), 339 upregulated and 959 downregulated. Considering the work above referred (Rangan et al., 2019), the higher number of DEGs detected in Antequera is in accordance with the previously reported worse heat response of this genotype in comparison to Bancal regarding grain protein content and grain yield (Tomás et al., 2020b). In Ardito, 4,375 DEGs were identified, 2,397 upregulated and 1,978 were downregulated. The genotype with greater number of DEGs (4,564) in response to high temperature treatment was Magueija, with 2,661 downregulated and 1,903 upregulated.

Our first approach was to investigate if any of A, B, and D genomes or distinct chromosomes were particularly affected by high temperature treatment, since is already documented that chromosomes 3A and 3B harbor genes involved in high temperature response [reviewed in Ni et al. (2018)]. Although, no significant differences were detected between genomes neither between chromosomes (**Supplementary Figure 2**).

The results presented in **Figure 2B** have shown that from the 1,199 upregulated genes common to more than one genotype, only six genes were common to Antequera, Bancal, Ardito, and Magueija. These six upregulated genes common to all genotypes (**Table 1**) encompassed annotated genes encoding three small heat shock proteins HSP20, one adenylate kinase, a BAG domain proteins and a ferritin. Adenylate kinase catalyzes a reversible transphosphorylation reaction that converts adenine nucleotides (ADP to ATP and AMP), and is critical for many processes in living cells (Pradet and Raymond, 1983), as, for example cellular activities maintenance during abiotic stress situations (Komatsu et al., 2014). BAG domain proteins are responsible for the modulation of chaperones activity as they bind to HSP70 proteins and promote the substrate release. Lastly, ferritin is a protein that functions in the iron storage in a soluble, non-toxic, readily available form. A recent study

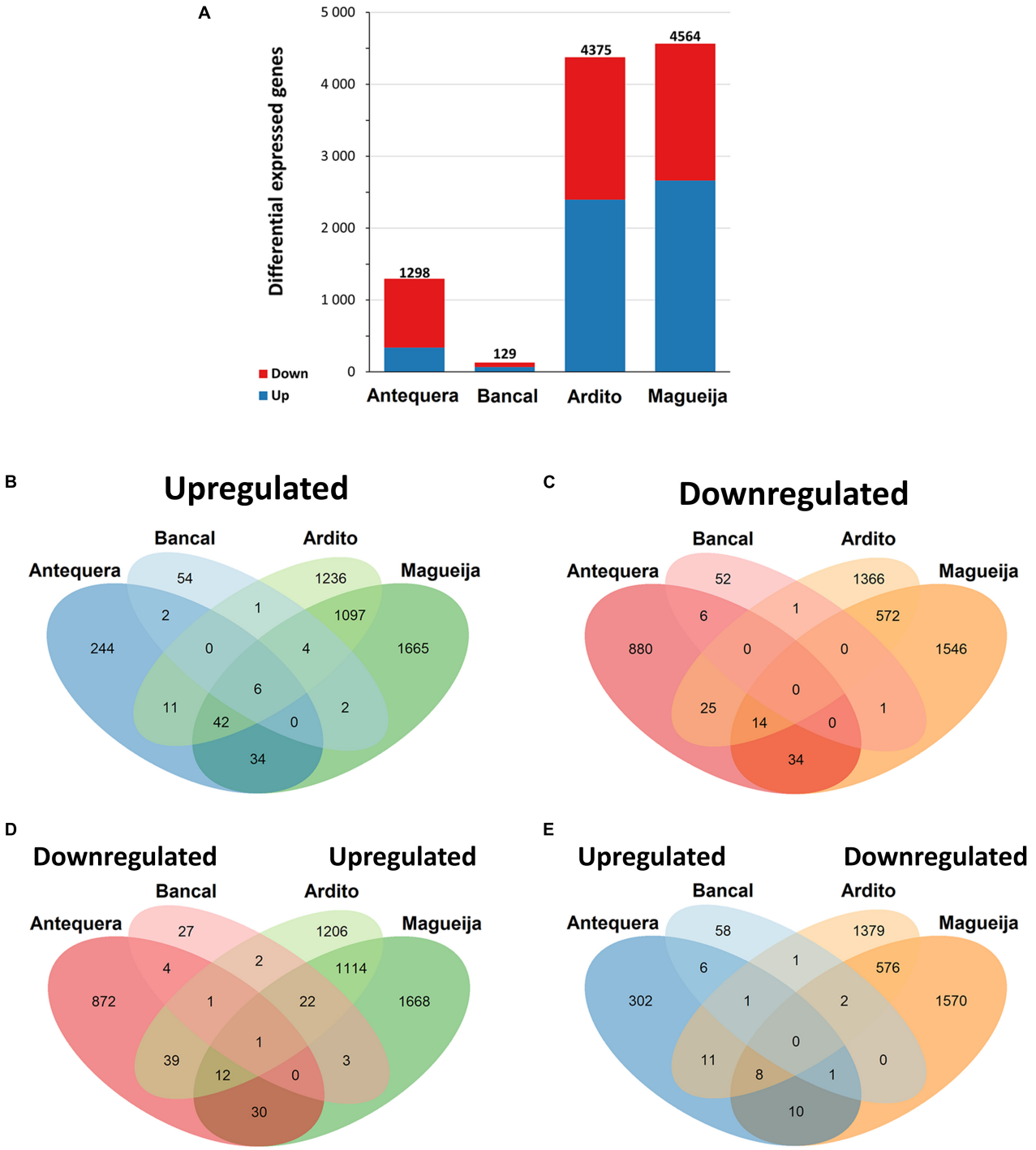

FIGURE 2 | Differentially expressed genes (DEGs). **(A)** Number of DEGs between control and high temperature treated samples of commercial varieties Antequera and Bancal and landraces Ardito and Magueija. Red and blue indicate down and upregulated genes, respectively. **(B–E)** Venn diagrams of differentially expressed genes in commercial varieties Antequera and Bancal and landraces Ardito and Magueija: **(B)** upregulated in all genotypes; **(C)** downregulated in all genotypes; **(D)** downregulated in commercial varieties and upregulated in landraces; **(E)** upregulated in commercial varieties and downregulated in landraces. Non-overlapping regions represent the number of genes exclusive to one genotype. Overlapping regions indicate the number of genes common to two, three or four genotypes.

(Zang et al., 2017) showed that the overexpression of a gene encoding a ferritin (TaFER-5B) functionally complemented the heat stress-sensitive phenotype of a ferritin-lacking mutant of Arabidopsis enhancing heat, drought, oxidative, and excess iron stress tolerance associated with the ROS scavenging, as well as leaf iron content. Thus, the present work not only identified

TABLE 1 | Upregulated genes common to all genotypes analyzed.

Gene ID	Encoded protein
TraesCS3B02G155300	Adenylate kinase
TraesCS4D02G086200	Small heat shock protein (Hsp20 family)
TraesCS4A02G092900	Small heat shock protein (Hsp20 family)
TraesCS5A02G548000	BAG domain
TraesCS4B02G089800	Small heat shock protein (Hsp20 family)
TraesCS7D02G428200	Ferritin

genes commonly modulated by HT in distant related hexaploidy wheats, but also pointed out an upregulated one that seem to be involved in HT response not only of wheat genotypes but also of dicot plants like Arabidopsis.

There is a great difference between the number of upregulated genes common to both commercial varieties and the number of these genes common to both traditional ones, as can be seen in **Figure 2B**. Only 2 of the 418 (0.48%) HT upregulated genes were common in both commercial varieties. These genes encode for a protein induced by water deficit or abscisic acid stress and ripening, and a NAC transcription factor involved in plant development (NAC019-A1). A recent work revealed that this transcription factor is known to be a negative regulator of starch synthesis, kernel weight, and kernel width in wheat developing grains (Liu et al., 2020). In fact, our previous analyses of mature grains of these genotypes subjected to HT during grain filling revealed a reduction of starch amount in both commercial varieties and an increase in both landraces (Tomás et al., 2020a,b). On the other hand, a much higher proportion of upregulated genes, 1,097 of the 5,058 (21.7%) are shared by the landrace genotypes. These genes are associated with 1,747 biological processes gene ontologies, being the most represented terms related with protein folding and metabolic process.

Concerning downregulated genes, none was commonly detected in all genotypes, and it was also observed a much higher number of genes common to both traditional landraces (572–87.6%) than between commercial varieties (6–0.92%) (**Figure 2C**). These results reinforce the already referred suggestion that traditional genotypes have a more similar response to the HT treatment than commercial ones.

Among the 110 genes downregulated in commercial genotypes and upregulated in landraces (**Figure 2D**), there were genes encoding for several HSP of different classes, related with HT response proteins involved in nitrogen metabolism and seed storage proteins, that are mainly involved in the seed quality. On the other hand, only 34 genes were upregulated in commercial varieties and downregulated in traditional genotypes (**Figure 2E**), and the gene products are very diverse, encompassing proteins involved in DNA binding, zinc finger domains, transport proteins, and several No Apical Meristem (NAM) proteins, referred before as a negative regulator of starch synthesis (Liu et al., 2020).

Looking forward to unravel if there was any HT common response related with the more affected genes, we analyzed the ten most up and downregulated genes of each genotype (**Supplementary Table 1**). It was possible to note that in the commercial varieties, upregulated genes encode for diverse products, several involved in the RNA processing. For example, pentatricopeptide-repeat-containing proteins (PPR) were encoded by these upregulated genes in both commercial genotypes. They are known to influence the expression of several organellar genes by altering RNA sequence, turnover, processing, or translation (Barkan and Small, 2014). Also PPR proteins have crucial roles in response to different abiotic stresses in rice and were found as miRNAs target genes associated with thermotolerance in wheat (Tan et al., 2014; Chen G. et al., 2018; Ravichandran et al., 2019). On the other hand, 60% of landraces upregulated genes encode for products involved in heat shock response, as heat shock proteins or heat shock factors, well-documented as high temperature responsive genes [reviewed in Kaur et al. (2019)]. One of the Magueija up regulated genes is the already identified in leaves and roots TaHsfA6f, associated with increased thermotolerance (Xue et al., 2015; Bi et al., 2020) and, to our knowledge, it is for the first time identified in developing grains. As for the downregulated genes, the only characteristic that stood out was that in Antequera 7 out of the 10 downregulated genes encode for products related with protein synthesis and regulation, which can be related with the reduction in grain protein content observed in this variety after HT treatment (Tomás et al., 2020b).

Functional Annotation and Gene Ontology Mapping of High Temperature Differentially Expressed Genes

In a more global perspective regarding each genotype response to high temperature treatment, functional annotation of DEGs of each genotype was made through the assignment of gene ontologies (GO) for biological processes, molecular functions and cellular components (**Figure 3** and **Supplementary Table 2**). **Figure 3** indicates the percentage of up and downregulated genes of each genotype, assigned to second and third levels of categories associated with each ontology. For all categories of the three ontologies the proportions of up and downregulated genes associated are very similar, being the classes with higher and lower number of genes the same in both cases for the four genotypes. This may indicate that, although the number of altered genes may be different in distinct genotypes (**Figure 3**), the functional roles in which the DEGs are involved constitute a common feature in wheat heat stress response.

In biological processes for both up and downregulated genes, the most represented categories are biological regulation (GO:0065007), cellular process (GO:0009987), metabolic process (GO:0008152), and response to stimulus (GO:0050896). It was also notorious that Bancal had a great percentage of downregulated genes assigned to several categories. For molecular functions ontology, catalytic activity and binding, mainly protein (GO:0005515) and organic cyclic compound binding (GO: 0097159) were clearly highlighted as compared with the other classes. Regarding cellular component GO, the most represented class was organelle (GO:0043226), with more

FIGURE 3 | Gene ontology percentage of up and downregulated genes in commercial varieties Antequera and Bancal and landraces Ardito and Magueija assigned to second and third levels of biological processes, molecular functions and cellular component gene ontologies. Red and blue indicate down and upregulated genes, respectively.

than 50% of the DEGs in almost all the genotypes, and the other was membrane (GO:0016020) with half of this amount.

Several GO terms were significantly represented in each genotype (**Supplementary Table 2**), except for Bancal up regulated genes, that were only significantly enriched in 16 molecular function ontologies. In total 395, 129, and 154 distinct ontologies were identified for biological processes, molecular functions and cellular components, respectively. Ardito and Magueija present a closer response as several common ontologies were significatively represented, namely some categories of response to stress, establishment of cell polarity, protein complex biogenesis, *de novo* protein folding and carbohydrate catabolism for upregulated genes and DNA metabolism, regulation of gene expression and protein complex biogenesis

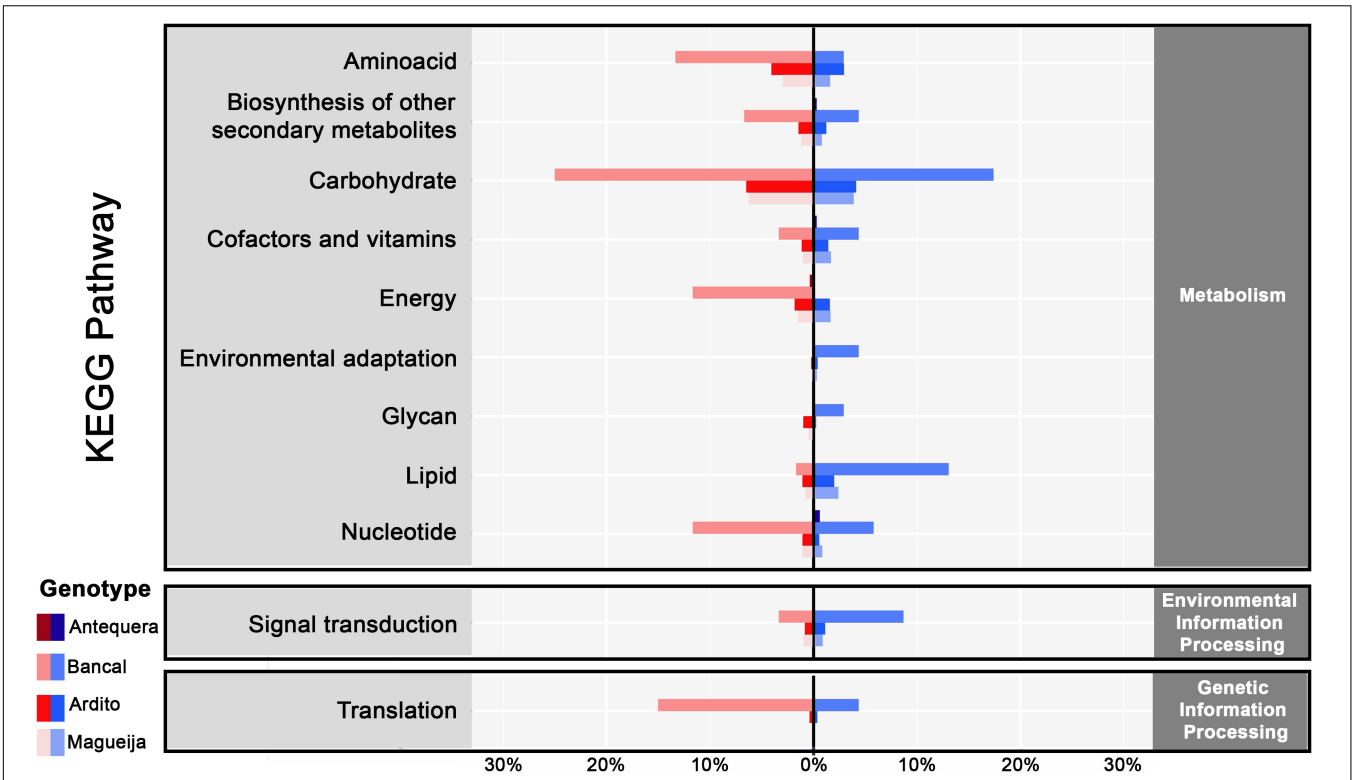

FIGURE 4 | KEGG pathways enrichment percentage of up and downregulated genes in commercial varieties Antequera and Bancal and landraces Ardito and Magueija associated with metabolic, environmental and genetic information processing pathways. Red and blue indicate down and upregulated genes, respectively.

for downregulated genes. We also found common categories in which Antequera and both landraces upregulated genes were enriched, such as protein folding, response to light and reactive oxygen species and heat acclimation biological processes and peroxisome and microbody cellular components. On the other hand, categories significantly enriched by downregulated genes common between commercial and landraces were only identified in cellular components, for instance related to nuclear lumen and thylakoid.

Particularly, from all the DEGs engaged in high temperature treatment response, 512 were assigned to response to heat category (GO:0009408), most of them presenting increased expression levels in the traditional varieties while in the commercial ones, only a small part was affected (**Supplementary Table 3**). These genes are related with other 106 biological processes, being the most represented protein folding (16%) and transcription regulation (8%), 41 cellular components with nucleus and integral component membrane being associated with a greater number of genes (14% each), and 105 molecular functions, being the most represented ATP binding (12.6%), protein binding (8.7%), and unfolded protein binding (7.3%). These classes of DEGs where also recently associated with wheat tolerance to drought during grain filling stage (Nouraei et al., 2022). Regarding unfolded protein binding, as expected, a great number of genes encode heat shock proteins (Hsp) and heat shock factors (Hsf). About 30% of the genes encode for the different Hsp20, Hsp40 (DNAJ domain), Hsp70 and Hsp90, and the great majority were upregulated in the traditional genotypes and remain unaltered or downregulated in the commercial ones. Also in the traditional genotypes, 12 genes encoding Apetala 2 proteins were identified as upregulated. Several proteins of this class were involved in grain and spike morphology, plant height, and spike emergence time determination, and play a key role in growth and development, including regulation of plant architecture and yield-related traits (Li et al., 2016; Zhao et al., 2019).

To further disclose biological functions of DEGs and determine if any pathway have a significant involvement in heat tolerance, we investigated DEGs involved in Kyoto Encyclopedia of genes and Genomes (KEGG) pathways and 749 DEGs were assigned related with 107 KEGG pathways (**Figure 4** and **Supplementary Table 4**). Antequera was the genotype with less DEGs associated with these pathways (0.5%), the traditional genotypes revealed 9% each, and Bancal was the genotype that presented the higher percentage (57%).

Analyzing the pathways associated with products encoded by downregulated genes, the ones related with carbohydrate metabolism were the most influenced in Bancal and both traditional genotypes. The only carbohydrate pathway associated with downregulated genes of all four genotypes were the Glycolysis/Gluconeogenesis pathway, although neither the genes nor the encoded enzymes were common. Although, inside this category, the majority of Bancal downregulated genes encoded for enzymes involved in pentose and glucuronate

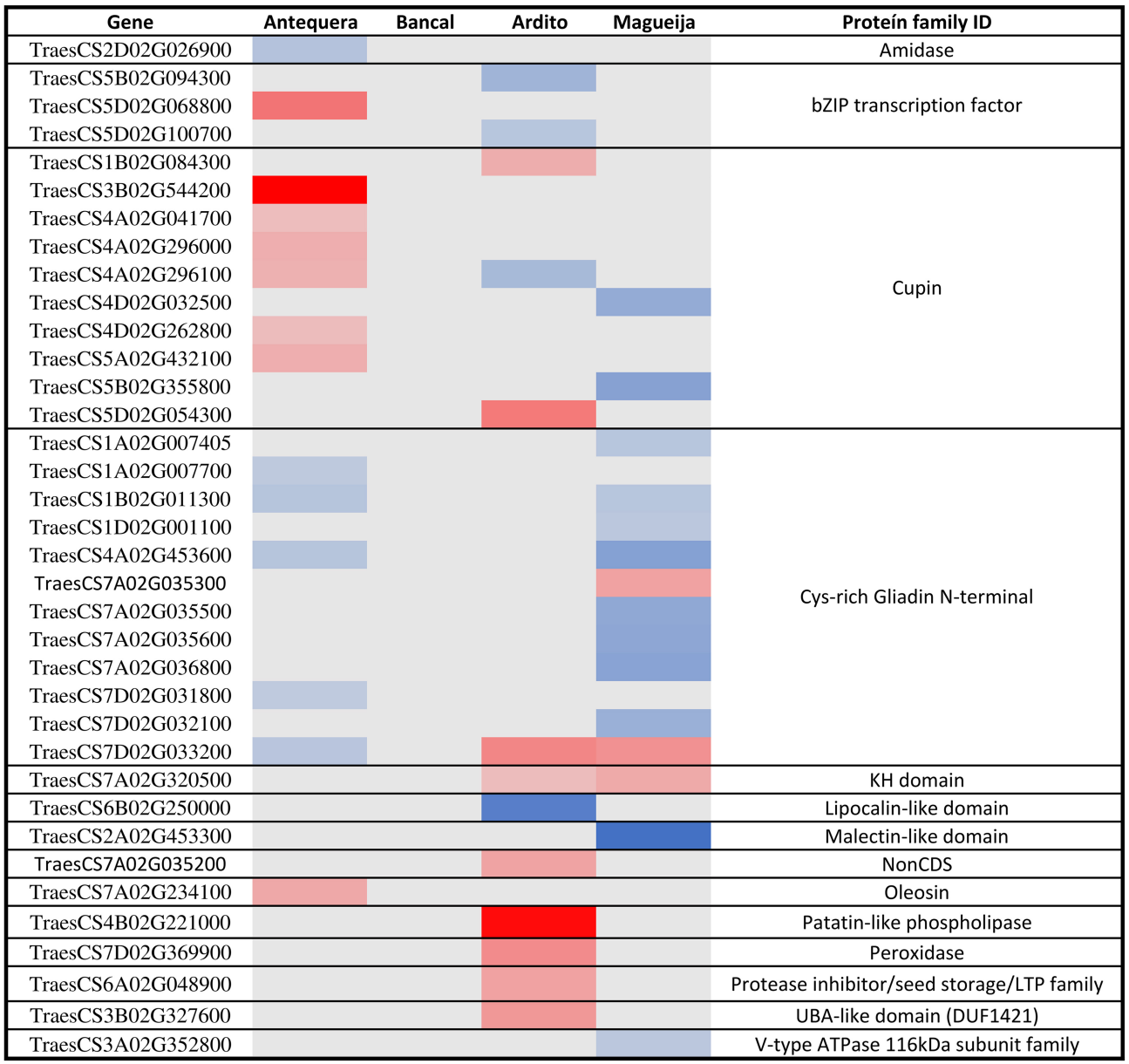

FIGURE 5 | Differentially expressed genes involved in nutrient reservoir activity ontology in commercial varieties Antequera and Bancal and landraces Ardito and Magueija. Red and blue indicate down and upregulated genes, respectively, and color intensity are related with the degree of gene expression alteration; gray represents unaltered genes.

interconversions pathway and in landraces encoded for starch and sucrose metabolism, with the majority of encoded enzymes associated with glucose synthesis. Some of the enzymes categorized in the pentose and glucuronate interconversions were pectinesterases known to be involved in cell wall remodeling that occurs during high temperature response (Wu et al., 2018). Kino et al. (2020) reported also a downregulation of genes involved in pericarp cell wall expansion due to high temperatures exposure during post anthesis, and speculate that this can be related with the reduction in grain weight observed after this stress. Our work also corroborated this suggestion since the majority of DEGs encoding pectinesterases were downregulated in landraces in which a reduction in grain weight was observed (Tomás et al., 2020a). The second most affected pathways were the ones involved in amino acid metabolism, with the majority of DEGs assigned to cysteine and methionine metabolic pathways for Bancal and both landraces. This was an unexpected result as the accumulation of this amino acid was reported in high temperature conditions (Tao et al., 2018). Again, only one pathway, the glycine, serine and threonine metabolism, was identified as being associated with downregulated genes in all the genotypes, but also again

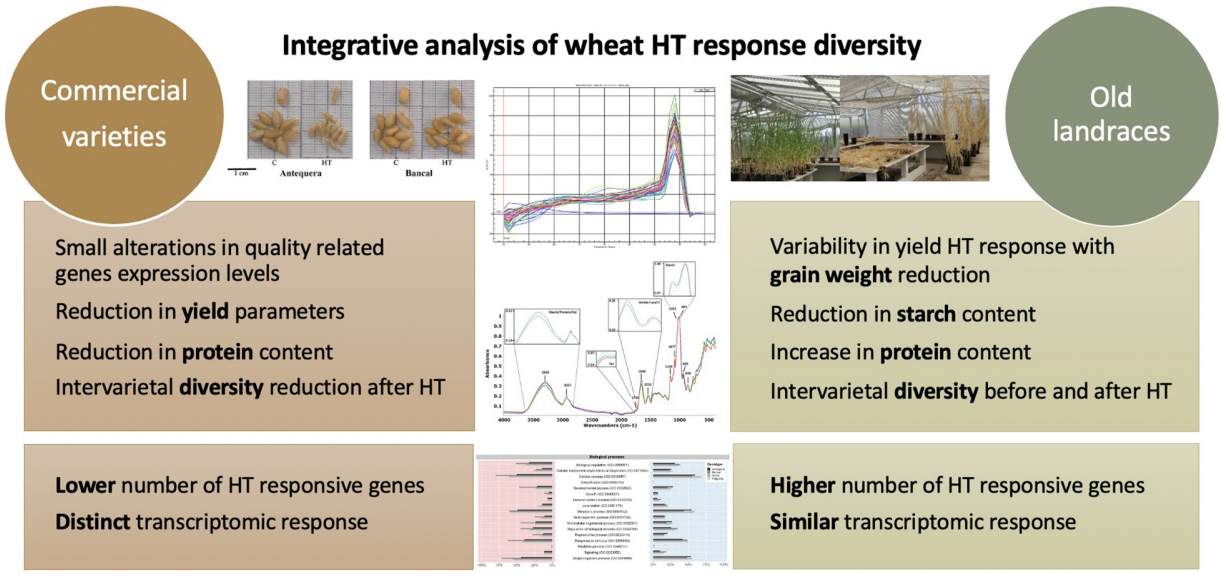

FIGURE 6 | Integrative analysis of grain yield, composition and transcriptomic analysis of the commercial varieties and the old landrace responses to heatwave at the grain-filling stage.

none of these genes was common to all the genotypes. An interesting result was the percentage of Bancal downregulated genes encoding for Aminoacyl-tRNA synthetases (nine different genes encode for six different synthases), classified in the translation pathways. This was not an expected result as several works in distinct species report an increase in different enzymes of this family in abiotic stress situations (Giritch et al., 1997; Thimm et al., 2001; Kobayashi et al., 2005; Baranašić et al., 2021). Lastly, several downregulated genes in Bancal were associated with nucleotide metabolism, more specifically with purine metabolism, and encoded for Adenosine triphosphatase (ATPase).

Upregulated genes were also associated with most of the mentioned pathways for downregulated genes. In fact, the encoded products were in some cases the same as for downregulated genes, suggesting that they include several cases of different enzyme isoforms or homologous genes with different functions, as already reported (Liu et al., 2015; Kaushik et al., 2020). Carbohydrate pathways include the greater number of associated upregulated genes for Bancal and both landraces. Particularizing, starch and sugar pathway was the most common, and glycolysis was the second. For Bancal, nucleotide metabolism was again the pathway with the higher percentage, although the encoded enzymes were involved in the dephosphorylation of ATP molecules, as well as translation pathways, in which were detected transcripts for enzymes involved in glutamate and tryptophan tRNA synthesis. Upregulated genes of Bancal and both landraces encoded also for enzymes in lipid metabolism. Specifically involved in cutin, suberine and wax biosynthesis, glycerolipid metabolism, fatty acid elongation, fatty acid biosynthesis, the latter two being related only with upregulated genes in landraces. This may indicate an alteration in lipids proportions in response to high temperature as previously reported [reviewed in Abdelrahman et al. (2020)].

High Temperature Effects in Storage Proteins Encoding Genes

Gluten is determinant for the wheat suitability to produce bread as it is a protein network that entrains air bubbles during dough fermentation. It is composed from two classes of storage proteins, glutenins, responsible for the dough strength and elasticity, and gliadins which confer extensibility and viscous properties to gluten required for dough development. Gliadin/glutenin ratio is determinant for rheological characteristics (Dhaka and Khatkar, 2015), being for that reason important to access if these proteins encoding genes' are affected by high temperature treatment. Storage proteins encoding genes are classified in the nutrient reservoir activity ontology and the expression levels of DEGs associated with this category are presented as heatmap in **Figure 5**. None of the genes presented altered expression in Bancal genotype. Additionally, about 60% of the DEGs were related with two protein families, Cupins and Gliadins.

The results obtained revealed 12 gliadin encoding genes differentially expressed, mostly upregulated in Magueija and Antequera, that may have implications in grain quality. In fact, several studies showed that an increase in gliadin fraction has a detrimental effect on the technological characteristics of wheat. Flours with higher gliadin content present weaker gluten quality and dough, with increased viscosity and stickiness (Barak et al., 2015). Additionally, Antequera and Ardito presented 6 and 2 downregulated genes encoding for Cupins, respectively, while three genes were upregulated, 1 in Ardito and 2 in Magueija. Cupins were already described as heat responsive proteins with an unusual thermostable character which facilitates their

accumulation in a number of heat-stressed organisms (Dunwell et al., 2001). A more recent work shows that these proteins are preferentially accumulated when protein synthesis components are generally decreased during heat stress, suggesting that they may provide valuable insights into improving the protein content of wheat (Wang et al., 2018). A significative reduction of protein content was previously observed in Antequera mature grains after heat stress treatment (Tomás et al., 2020b). Altogether, these results show that gliadins are more affected by high temperature treatment than glutenins in both wheat commercial varieties and landraces and reinforce the need to investigate the cupins role in heat stress response.

It must be emphasized that the expression levels of genes related with flour quality, like the ones encoding glutenins and enzymes involved in starch and puroindolines synthesis, were already evaluated through qRT-PCR (Tomás et al., 2020c), and the results obtained confirm the RNA Sequencing analysis here presented.

Overall, the results obtained in this and past works (Tomás et al., 2020a,b,c) show that high temperature treatment tend to reduce yield and quality differences observed between commercial varieties in control conditions. Conversely, differences observed between old landraces were enhanced in plants submitted to HT treatments (**Figure 6**). Characteristics like grain weight, protein content and transcription profiles of heat responsive genes on the traditional genotypes studied encourages a deeper analysis of those genotypes enclosed in Vasconcellos collection (Vasconcellos, 1933). Nevertheless, accordingly to all our analysis, the commercial variety Bancal seems to be a promising genotype to cope with high temperatures.

Several questions arise from this work, confirming that high temperature response results from a complex of physiological, cellular and molecular processes, as previously proposed (Jacott and Boden, 2020; Schaarschmidt et al., 2021). Though, several pieces are missing to compose the intricate puzzle of plant response to this abiotic stress (Jagadish et al., 2021; Khan et al., 2021). A deeper exploitation of RNA sequencing data, focusing on particular pathways, will be needed to enrich correlations between specific changes in genes expression profiles and phenotypic alterations induced by heat wave like treatments.

DATA AVAILABILITY STATEMENT

The original contributions presented in this study are publicly available and sequences data can be found here: https://www.ncbi.nlm.nih.gov/search/all/?term=PRJNA750265.

AUTHOR CONTRIBUTIONS

DT and MS: conceptualization, methodology, and validation. DT: formal analysis, investigation, visualization, and writing—original draft preparation. MS: funding acquisition and project administration. MS and WV: supervision and writing—review and editing. All authors contributed to the article and approved the submitted version.

FUNDING

DT was funded by a Fundação para a Ciência e a Tecnologia, Portugal (FCT) doctoral scholarship (SFRH/BD/93156/2013), MS by the FCT Investigator Program (IF/00834/2014), and the research work was financed by FCT research project IF/00834/2014/CP1219/CT0003, LEAF Unit (Linking Landscape, Environment, Agriculture and Food) (UID/AGR/04129/2020), and CEF Unit (Forest Research Centre, UIDB/00239/2020).

ACKNOWLEDGMENTS

We would like to thank Eng. Manuela Veloso (PRT005: EAN Germplasm Bank, Oeiras) for the landrace accessions studied in the present study. Also we would like to acknowledge the support of Ricardo Leite from Genomics Facility in Instituto Gulbenkian Ciência, on RNA sequencing design and analysis.

SUPPLEMENTARY MATERIAL

The Supplementary Material for this article can be found online at: https://www.frontiersin.org/articles/10.3389/fpls.2022.842599/full#supplementary-material

REFERENCES

Abdelrahman, M., Ishii, T., El-Sayed, M., and Tran, L. S. P. (2020). Heat sensing and lipid reprograming as a signaling switch for heat stress responses in wheat. *Plant Cell Physiol.* 61, 1399–1407. doi: 10.1093/pcp/pcaa072

Altenbach, S. B., and Kothari, K. M. (2004). Transcript profiles of genes expressed in endosperm tissue are altered by high temperature during wheat grain development. *J. Cereal Sci.* 40, 115–126. doi: 10.1016/j.jcs.2004.05.004

Andrews, S., Krueger, F., Segonds-Pichon, A., Biggins, L., Krueger, C., Wingett, S., et al. (2010). *FastQC: a Quality Control Tool for High Throughput Sequence Data*. Babraham: Babraham Institute.

ANPOC, INIAV, IpBeja, Ceres, Germen, and Cerealis (2014). *Lista de Variedade Recomendadas Sementeiras Trigo Mole*. Lisboa.

Asseng, S., Ewert, F., Martre, P., Rötter, R. P., Lobell, D. B., Cammarano, D., et al. (2014). Rising temperatures reduce global wheat production. *Nat. Clim. Change* 5, 143–147. doi: 10.1038/nclimate2470

Barak, S., Mudgil, D., and Khatkar, B. S. (2015). Biochemical and functional properties of wheat gliadins: a review. *Crit. Rev. Food Sci. Nutr.* 55, 357–368. doi: 10.1080/10408398.2012.654863

Baranašić, J., Mihalak, A., Gruiæ-Sovulj, I., Bauer, N., and Rokov-Plavec, J. (2021). Expression of genes for selected plant aminoacyl-tRNA synthetases in the abiotic stress. *Acta Bot. Croat.* 80, 35–42. doi: 10.37427/botcro-2021-010

Barkan, A., and Small, I. (2014). Pentatricopeptide repeat proteins in plants. *Annu. Rev. Plant Biol.* 65, 415–442. doi: 10.1146/annurev-arplant-050213-040159

Baym, M., Kryazhimskiy, S., Lieberman, T. D., Chung, H., Desai, M. M., and Kishony, R. (2015). Inexpensive multiplexed library preparation for megabase-sized genomes. *PLoS One* 10:e0128036. doi: 10.1371/journal.pone.0128036

Bi, H., Zhao, Y., Li, H., and Liu, W. (2020). Wheat heat shock factor TaHsfA6f increases ABA levels and enhances tolerance to multiple abiotic stresses in transgenic plants. *Int. J. Mol. Sci.* 21:3121. doi: 10.3390/IJMS21093121

Brisson, N., Gate, P., Gouache, D., Charmet, G., Oury, F. X., and Huard, F. (2010). Why are wheat yields stagnating in Europe? A comprehensive data analysis for France. *Field Crop. Res.* 119, 201–212. doi: 10.1016/j.fcr.2010.07.012

Caballero, L., Martin, L. M., and Alvarez, J. B. (2001). Allelic variation of the HMW glutenin subunits in Spanish accessions of spelt wheat (*Triticum aestivum* ssp. *spelta* L. em. Thell.). *Theor. Appl. Genet.* 103, 124–128. doi: 10.1007/s001220100565

Cardoso, R. M., Soares, P. M. M., Lima, D. C. A., and Miranda, P. M. A. (2019). Mean and extreme temperatures in a warming climate: EURO CORDEX and WRF regional climate high-resolution projections for Portugal. *Clim. Dyn.* 52, 129–157. doi: 10.1007/s00382-018-4124-4

Chauhan, H., Khurana, N., Tyagi, A. K., Khurana, J. P., and Khurana, P. (2011). Identification and characterization of high temperature stress responsive genes in bread wheat (*Triticum aestivum* L.) and their regulation at various stages of development. *Plant Mol. Biol.* 75, 35–51. doi: 10.1007/s11103-010-9702-8

Chen, G., Zou, Y., Hu, J., and Ding, Y. (2018). Genome-wide analysis of the rice PPR gene family and their expression profiles under different stress treatments. *BMC Genomics* 19:720. doi: 10.1186/s12864-018-5088-9

Chen, S., Zhou, Y., Chen, Y., and Gu, J. (2018). fastp: an ultra-fast all-in-one FASTQ preprocessor. *Bioinformatics* 34, i884–i890. doi: 10.1093/bioinformatics/bty560

Dhaka, V., and Khatkar, B. S. (2015). Effects of gliadin/glutenin and HMW-GS/LMW-GS ratio on dough rheological properties and bread-making potential of wheat varieties. *J. Food Qual.* 38, 71–82. doi: 10.1111/jfq.12122

Dunwell, J. M., Culham, A., Carter, C. E., Sosa-Aguirre, C. R., and Goodenough, P. W. (2001). Evolution of functional diversity in the cupin superfamily. *Trends Biochem. Sci.* 26, 740–746. doi: 10.1016/S0968-0004(01)01981-8

Dwivedi, S. L., Ceccarelli, S., Blair, M. W., Upadhyaya, H. D., Are, A. K., and Ortiz, R. (2016). Landrace germplasm for improving yield and abiotic stress adaptation. *Trends Plant Sci.* 21, 31–42. doi: 10.1016/j.tplants.2015.10.012

FAO© (2019). *FAOSTAT. Food Balanc. New Food Balanc*. Available online at: http://www.fao.org/faostat/en/#data/FBS (accessed April 6, 2022).

Gaupp, F., Hall, J., Mitchell, D., and Dadson, S. (2019). Increasing risks of multiple breadbasket failure under 1.5 and 2°C global warming. *Agric. Syst.* 175, 34–45. doi: 10.1016/j.agsy.2019.05.010

Giritch, A., Herbik, A., Balzer, H. J., Ganal, M., Stephan, U. W., and Bäumlein, H. (1997). A root-specific iron-regulated gene of tomato encodes a Lysyl-tRNA-synthetase-like protein. *Eur. J. Biochem.* 244, 310–317. doi: 10.1111/j.1432-1033.1997.00310.x

Gregová, E., Hermuth, J., Kraic, J., and Dotlaèil, L. (1999). Protein heterogeneity in European wheat landraces and obsolete cultivars. *Genet. Resour. Crop Evol.* 46, 521–528. doi: 10.1023/A:1008751815445

Jacott, C. N., and Boden, S. A. (2020). Feeling the heat: developmental and molecular responses of wheat and barley to high ambient temperatures. *J. Exp. Bot.* 71, 5740–5751. doi: 10.1093/JXB/ERAA326

Jagadish, S. V. K., Way, D. A., and Sharkey, T. D. (2021). Plant heat stress: concepts directing future research. *Plant Cell Environ.* 44, 1992–2005. doi: 10.1111/PCE.14050

Kaur, R., Sinha, K., and Bhunia, R. K. (2019). Can wheat survive in heat? Assembling tools towards successful development of heat stress tolerance in *Triticum aestivum* L. *Mol. Biol. Rep.* 46, 2577–2593. doi: 10.1007/s11033-019-04686-x

Kaushik, M., Rai, S., Venkadesan, S., Sinha, S. K., Mohan, S., and Mandal, P. K. (2020). Transcriptome analysis reveals important candidate genes related to nutrient reservoir, carbohydrate metabolism, and defence proteins during grain development of hexaploid bread wheat and its diploid progenitors. *Genes* 11:509. doi: 10.3390/genes11050509

Khan, A., Ahmad, M., Ahmed, M., and Iftikhar Hussain, M. (2021). Rising atmospheric temperature impact on wheat and thermotolerance strategies. *Plants* 10:43. doi: 10.3390/plants10010043

Kim, D., Langmead, B., and Salzberg, S. L. (2015). HISAT: a fast spliced aligner with low memory requirements. *Nat. Methods* 12, 357–360. doi: 10.1038/nmeth.3317

Kino, R. I., Pellny, T. K., Mitchell, R. A. C., Gonzalez-Uriarte, A., and Tosi, P. (2020). High post-anthesis temperature effects on bread wheat (*Triticum aestivum* L.) grain transcriptome during early grain-filling. *BMC Plant Biol.* 20:170. doi: 10.1186/s12870-020-02375-7

Kinsella, R. J., Kähäri, A., Haider, S., Zamora, J., Proctor, G., Spudich, G., et al. (2011). Ensembl BioMarts: a hub for data retrieval across taxonomic space. *Database* 2011:bar030. doi: 10.1093/database/bar030

Kobayashi, T., Suzuki, M., Inoue, H., Itai, R. N., Takahashi, M., Nakanishi, H., et al. (2005). Expression of iron-acquisition-related genes in iron-deficient rice is co-ordinately induced by partially conserved iron-deficiency-responsive elements. *J. Exp. Bot.* 56, 1305–1316. doi: 10.1093/jxb/eri131

Komatsu, S., Kamal, A. H. M., and Hossain, Z. (2014). Wheat proteomics: proteome modulation and abiotic stress acclimation. *Front. Plant Sci.* 5:684. doi: 10.3389/fpls.2014.00684

Kumar, A., Sharma, S., Chunduri, V., Kaur, A., Kaur, S., Malhotra, N., et al. (2020). Genome-wide identification and characterization of heat shock protein family reveals role in development and stress conditions in *Triticum aestivum* L. *Sci. Rep.* 10:7858. doi: 10.1038/s41598-020-64746-2

Li, B., Li, Q., Mao, X., Li, A., Wang, J., Chang, X., et al. (2016). Two novel AP2/EREBP transcription factor genes *TaPARG* have pleiotropic functions on plant architecture and yield-related traits in common wheat. *Front. Plant Sci.* 7:1191. doi: 10.3389/fpls.2016.01191

Liao, Y., Smyth, G. K., and Shi, W. (2014). featureCounts: an efficient general purpose program for assigning sequence reads to genomic features. *Bioinformatics* 30, 923–930. doi: 10.1093/bioinformatics/btt656

Liu, Y., Hou, J., Wang, X., Li, T., Majeed, U., Hao, C., et al. (2020). The NAC transcription factor NAC019-A1 is a negative regulator of starch synthesis in wheat developing endosperm. *J. Exp. Bot.* 71, 5794–5807. doi: 10.1093/jxb/eraa333

Liu, Z., Xin, M., Qin, J., Peng, H., Ni, Z., Yao, Y., et al. (2015). Temporal transcriptome profiling reveals expression partitioning of homeologous genes contributing to heat and drought acclimation in wheat (*Triticum aestivum* L.). *BMC Plant Biol.* 15:152. doi: 10.1186/s12870-015-0511-8

Lopes, M. S., El-Basyoni, I., Baenziger, P. S., Singh, S., Royo, C., Ozbek, K., et al. (2015). Exploiting genetic diversity from landraces in wheat breeding for adaptation to climate change. *J. Exp. Bot.* 66, 3477–3486. doi: 10.1093/jxb/erv122

Love, M. I., Huber, W., and Anders, S. (2014). Moderated estimation of fold change and dispersion for RNA-seq data with DESeq2. *Genome Biol.* 15:550. doi: 10.1186/s13059-014-0550-8

Macaulay, I. C., Teng, M. J., Haerty, W., Kumar, P., Ponting, C. P., and Voet, T. (2016). Separation and parallel sequencing of the genomes and transcriptomes of single cells using G&T-seq. *Nat. Protoc.* 11, 2081–2103. doi: 10.1038/nprot.2016.138

Newton, A. C., Akar, T., Baresel, J. P., Bebeli, P. J., Bettencourt, E., Bladenopoulos, K. V., et al. (2010). Cereal landraces for sustainable agriculture. A review. *Agron. Sustain. Dev.* 30, 237–269. doi: 10.1051/agro/2009032

Ni, Z., Li, H., Zhao, Y., Peng, H., Hu, Z., Xin, M., et al. (2018). Genetic improvement of heat tolerance in wheat: recent progress in understanding the underlying molecular mechanisms. *Crop J.* 6, 32–41. doi: 10.1016/j.cj.2017.09.005

Nouraei, S., Mia, M. S., Liu, H., Turner, N. C., and Yan, G. (2022). Transcriptome analyses of near isogenic lines reveal putative drought tolerance controlling genes in wheat. *Front. Plant Sci.* 13:857829. doi: 10.3389/FPLS.2022.857829

Nuttall, J. G., Barlow, K. M., Delahunty, A. J., Christy, B. P., and O'Leary, G. J. (2018). Acute high temperature response in wheat. *Agron. J.* 110, 1296–1308. doi: 10.2134/agronj2017.07.0392

Okonechnikov, K., Conesa, A., and García-Alcalde, F. (2016). Qualimap 2: advanced multi-sample quality control for high-throughput sequencing data. *Bioinformatics* 32, 292–294. doi: 10.1093/bioinformatics/btv566

Pradet, A., and Raymond, P. (1983). Adenine nucleotide ratios and adenylate energy charge in energy metabolism. *Annu. Rev. Plant Physiol.* 34, 199–224. doi: 10.1146/annurev.pp.34.060183.001215

Qin, D., Wu, H., Peng, H., Yao, Y., Ni, Z., Li, Z., et al. (2008). Heat stress-responsive transcriptome analysis in heat susceptible and tolerant wheat (*Triticum aestivum* L.) by using Wheat Genome Array. *BMC Genomics* 9:432. doi: 10.1186/1471-2164-9-432

R Core Team (2018). *R: A Language and Environment for Statistical Computing*. Vienna: R Foundation for Statistical Computing.

Rangan, P., Furtado, A., and Henry, R. (2019). Transcriptome profiling of wheat genotypes under heat stress during grain-filling. *J. Cereal Sci.* 91:102895. doi: 10.1016/j.jcs.2019.102895

Ravichandran, S., Ragupathy, R., Edwards, T., Domaratzki, M., and Cloutier, S. (2019). MicroRNA-guided regulation of heat stress response in wheat. *BMC Genomics* 20:488. doi: 10.1186/s12864-019-5799-6

Ray, D. K., Mueller, N. D., West, P. C., and Foley, J. A. (2013). Yield trends are insufficient to double global crop production by 2050. *PLoS One* 8:e66428. doi: 10.1371/journal.pone.0066428

Schaarschmidt, S., Lawas, L. M. F., Kopka, J., Jagadish, S. V. K., and Zuther, E. (2021). Physiological and molecular attributes contribute to high night temperature tolerance in cereals. *Plant Cell Environ.* 44, 2034–2048. doi: 10.1111/PCE.14055

Srinivasan, C. S., Thirtle, C., and Palladino, P. (2003). Winter wheat in England and Wales, 1923–1995: what do indices of genetic diversity reveal? *Plant Genet. Resour.* 1, 43–57. doi: 10.1079/pgr20031

Tan, J., Tan, Z., Wu, F., Sheng, P., Heng, Y., Wang, X., et al. (2014). A novel chloroplast-localized pentatricopeptide repeat protein involved in splicing affects chloroplast development and abiotic stress response in rice. *Mol. Plant* 7, 1329–1349. doi: 10.1093/mp/ssu054

Tao, Z., Chang, X., Wang, D., Wang, Y., Ma, S., Yang, Y., et al. (2018). Effects of sulfur fertilization and short-term high temperature on wheat grain production and wheat flour proteins. *Crop J.* 6, 413–425. doi: 10.1016/j.cj.2018.01.007

Tewolde, H., Fernandez, C. J., and Erickson, C. A. (2006). Wheat cultivars adapted to post-heading high temperature stress. *J. Agron. Crop Sci.* 120, 111–120.

Thimm, O., Essigmann, B., Kloska, S., Altmann, T., and Buckhout, T. J. (2001). Response of *Arabidopsis* to iron deficiency stress as revealed by microarray analysis. *Plant Physiol.* 127, 1030–1043. doi: 10.1104/pp.010191

Tian, T., Liu, Y., Yan, H., You, Q., Yi, X., Du, Z., et al. (2017). AgriGO v2.0: a GO analysis toolkit for the agricultural community, 2017 update. *Nucleic Acids Res.* 45, W122–W129. doi: 10.1093/nar/gkx382

Tomás, D., Coelho, L. P., Rodrigues, J. C., Viegas, W., and Silva, M. (2020a). Assessment of four Portuguese wheat landrace diversity to cope with global warming. *Front. Plant Sci.* 11:594977. doi: 10.3389/fpls.2020.594977

Tomás, D., Rodrigues, J. C., Viegas, W., and Silva, M. (2020b). Assessment of high temperature effects on grain yield and composition in bread wheat commercial varieties. *Agronomy* 10:499. doi: 10.3390/agronomy10040499

Tomás, D., Viegas, W., and Silva, M. (2020c). Effects of post-anthesis heat waves on the grain quality of seven European wheat varieties. *Agronomy* 10:268. doi: 10.3390/agronomy10020268

Trethowan, R. M., and Mujeeb-Kazi, A. (2008). Novel germplasm resources for improving environmental stress tolerance of hexaploid wheat. *Crop Sci.* 48, 1255–1265. doi: 10.2135/cropsci2007.08.0477

Vasconcellos, J. C. (1933). Trigos Portuguêses ou de há muito cultivados no País. Subsídios para o seu estudo botânico. *Bol. Agric.* 1, 1–150.

Villa, T. C. C., Maxted, N., Scholten, M., and Ford-Lloyd, B. (2005). Defining and identifying crop landraces. *Plant Genet. Resour.* 3, 373–384. doi: 10.1079/pgr200591

Wahid, A., Gelani, S., Ashraf, M., and Foolad, M. R. (2007). Heat tolerance in plants: an overview. *Environ. Exp. Bot.* 61, 199–223. doi: 10.1016/j.envexpbot.2007.05.011

Wan, Y., Poole, R. L., Huttly, A. K., Toscano-Underwood, C., Feeney, K., Welham, S., et al. (2008). Transcriptome analysis of grain development in hexaploid wheat. *BMC Genomics* 9:121. doi: 10.1186/1471-2164-9-121

Wang, P., Deng, X., and Jiang, S. (2019). Global warming, grain production and its efficiency: case study of major grain production region. *Ecol. Indic.* 105, 563–570. doi: 10.1016/j.ecolind.2018.05.022

Wang, X., Hou, L., Lu, Y., Wu, B., Gong, X., Liu, M., et al. (2018). Metabolic adaptation of wheat grains contributes to a stable filling rate under heat stress. *J. Exp. Bot.* 69, 5531–5545. doi: 10.1093/jxb/ery303

World Meteorological Organization [WMO] (2015). *Guidelines on the Definition and Monitoring of Extreme Weather and Climate Events – Draft Version - First Review by TT-DEWCE*. Available online at: www.wmo.int/pages/prog/wcp/ccl/opace/opace2/documents/DraftversionoftheGuidelinesontheDefinitionandMonitoringofExtremeWeatherandClimateEvents.pdf (accessed October 24, 2019).

Wu, H. C., Bulgakov, V. P., and Jinn, T. L. (2018). Pectin methylesterases: cell wall remodeling proteins are required for plant response to heat stress. *Front. Plant Sci.* 871:1612. doi: 10.3389/fpls.2018.01612

Xue, G.-P., Drenth, J., and McIntyre, C. L. (2015). TaHsfA6f is a transcriptional activator that regulates a suite of heat stress protection genes in wheat (*Triticum aestivum* L.) including previously unknown Hsf targets. *J. Exp. Bot.* 66, 1025–1039. doi: 10.1093/JXB/ERU462

Zang, X., Geng, X., Wang, F., Liu, Z., Zhang, L., Zhao, Y., et al. (2017). Overexpression of wheat ferritin gene TaFER-5B enhances tolerance to heat stress and other abiotic stresses associated with the ROS scavenging. *BMC Plant Biol.* 17:14. doi: 10.1186/s12870-016-0958-2

Zhao, Y., Ma, R., Xu, D., Bi, H., Xia, Z., and Peng, H. (2019). Genome-wide identification and analysis of the AP2 transcription factor gene family in wheat (*Triticum aestivum* L.). *Front. Plant Sci.* 10:1286. doi: 10.3389/fpls.2019.01286

Conflict of Interest: The authors declare that the research was conducted in the absence of any commercial or financial relationships that could be construed as a potential conflict of interest.

Publisher's Note: All claims expressed in this article are solely those of the authors and do not necessarily represent those of their affiliated organizations, or those of the publisher, the editors and the reviewers. Any product that may be evaluated in this article, or claim that may be made by its manufacturer, is not guaranteed or endorsed by the publisher.

Copyright © 2022 Tomás, Viegas and Silva. This is an open-access article distributed under the terms of the Creative Commons Attribution License (CC BY). The use, distribution or reproduction in other forums is permitted, provided the original author(s) and the copyright owner(s) are credited and that the original publication in this journal is cited, in accordance with accepted academic practice. No use, distribution or reproduction is permitted which does not comply with these terms.

frontiers | Frontiers in Plant Science

TYPE Original Research
PUBLISHED 25 August 2022
DOI 10.3389/fpls.2022.974050

Check for updates

OPEN ACCESS

EDITED BY
Raul Antonio Sperotto,
Universidade do Vale do Taquari - Univates, Brazil

REVIEWED BY
Duncan Smith,
University of Wisconsin-Madison, United States
Valmor João Bianchi,
Federal University of Pelotas, Brazil
Tom Gradziel,
University of California, Davis, United States

*CORRESPONDENCE
Carolina Álvarez-Maldini
carolina.alvarez@uoh.cl

SPECIALTY SECTION
This article was submitted to Plant Abiotic Stress, a section of the journal Frontiers in Plant Science

RECEIVED 20 June 2022
ACCEPTED 04 August 2022
PUBLISHED 25 August 2022

CITATION
Álvarez-Maldini C, Acevedo M, Estay D, Aros F, Dumroese RK, Sandoval S and Pinto M (2022) Examining physiological, water relations, and hydraulic vulnerability traits to determine anisohydric and isohydric behavior in almond (*Prunus dulcis*) cultivars: Implications for selecting agronomic cultivars under changing climate.
Front. Plant Sci. 13:974050.
doi: 10.3389/fpls.2022.974050

COPYRIGHT
© 2022 Álvarez-Maldini, Acevedo, Estay, Aros, Dumroese, Sandoval and Pinto. This is an open-access article distributed under the terms of the Creative Commons Attribution License (CC BY). The use, distribution or reproduction in other forums is permitted, provided the original author(s) and the copyright owner(s) are credited and that the original publication in this journal is cited, in accordance with accepted academic practice. No use, distribution or reproduction is permitted which does not comply with these terms.

Examining physiological, water relations, and hydraulic vulnerability traits to determine anisohydric and isohydric behavior in almond (*Prunus dulcis*) cultivars: Implications for selecting agronomic cultivars under changing climate

Carolina Álvarez-Maldini[1]*, Manuel Acevedo[2], Daniela Estay[1], Fabián Aros[1], R. Kasten Dumroese[3], Simón Sandoval[4] and Manuel Pinto[1]

[1]Instituto Ciencias Agroalimentarias Animales y Ambientales (ICA3), Campus Colchagua, Universidad de O'Higgins, San Fernando, Chile, [2]Centro Tecnológico de la Planta Forestal, Instituto Forestal, Sede Biobío, San Pedro de la Paz, Chile, [3]United States Department of Agriculture Forest Service, Rocky Mountain Research Station, Moscow, ID, United States, [4]Laboratorio de Análisis y Modelamiento de Geoinformación, Departamento de Manejo de Bosques y Medio Ambiente, Facultad de Ciencias Forestales, Universidad de Concepción, Concepción, Chile

The search for drought tolerant species or cultivars is important to address water scarcity caused by climate change in Mediterranean regions. The anisohydric–isohydric behavior concept has been widely used to describe stomatal regulation during drought, simply in terms of variation of minimal water potential (Ψ_{min}) in relation to pre-dawn water potential (Ψ_{pd}). However, its simplicity has sometimes failed to deliver consistent results in describing a complex behavior that results from the coordination of several plant functional traits. While *Prunus dulcis* (almond) is known as a drought tolerant species, little information is available regarding consistent metrics to discriminate among cultivars or the mechanisms underlying drought tolerance in almond. Here we show a sequence of plant stomatal, hydraulic, and wilting responses to drought in almonds, and the main differences between anisohydric and isohydric cultivars. In a pot desiccation experiment we observed that stomatal closure in *P. dulcis* is not driven by loss in turgor or onset of xylem cavitation, but instead, occurs early in response to decreasing Ψ_{min} that could be related to the protection of the integrity of the hydraulic system, independently of cultivar. Also, we report that anisohydric cultivars of *P. dulcis* are characterized by maximum stomatal conductance, lower water potentials for stomatal closure and turgor loss, and lower vulnerability to xylem cavitation, which are traits that correlated with metrics to discriminate

10.3389/fpls.2022.974050

anisohydric and isohydric behavior. Our results demonstrate that *P. dulcis* presents a strategy to avoid cavitation by closing stomata during the early stages of drought. Future research should also focus on below-ground hydraulic traits, which could trigger stomatal closure in almond.

KEYWORDS

drought, functional traits, xylem vulnerability to cavitation, hydroscapes, leaf water potential, stomatal conductance

Introduction

The effects of climate change, such as an increase in temperature and altered patterns of frequency, distribution, and intensity of precipitation, have been extensively characterized (Cavin et al., 2013). Areas with Mediterranean climate, such as central Chile, are especially vulnerable to climate change because more frequent and extreme drought events are expected within the next decades (Schär et al., 2004; Bambach et al., 2013; del Pozo et al., 2019). Central Chile will experience a 20% decline in precipitation by 2050 coupled with an average annual increase of 3–4°C in temperature (Hannah et al., 2013), putting at risk the feasibility of cultivation of several agronomic species. Thus, drought leading to water stress in plants is the major factor reducing agricultural productivity (Chaves et al., 2003), which is one of the main economic activities of Mediterranean central Chile. To face drought in the long term, new suitable species and cultivars with drought tolerance characteristics are being identified and considered as options for the agricultural sector. One new, drought tolerant species being considered for central Chile is almond (*Prunus dulcis* L.) (Torrecillas et al., 1996), historically cultivated in other Mediterranean regions due to its capability to withstand water stress (Marsal et al., 1997; García-Tejero et al., 2018). Morphological and structural leaf adaptations that deliver protection against excessive water loss, such as reduced leaf area and stomatal density, thicker leaf cell walls, and increased cuticle thickness have been observed in almond cultivars (Camposeo et al., 2011; Oliveira et al., 2018). Physiologically, a gradual decrease in photosynthesis and stomatal conductance with increasing water stress is a characteristic response of drought-adapted plants and it has been frequently observed in almonds (Romero et al., 2004).

At a physiological level, drought is one of the most studied stresses in plants. The primary effect of drought is the reduction in stomatal conductance to decrease water losses by transpiration and preventing drops in leaf water potential (Ψ_L), which in turn produces a reduction in carbon assimilation (Flexas et al., 2004, 2013), negatively affecting plant growth and crop production. Thus, stomatal regulation is key to control water loss and Ψ_L during water stress, but different species and cultivars have evolved other adaptive responses to limit dramatic decreases in Ψ_L, leading to the isohydric and anisohydric behavior concept (Tardieu and Simonneau, 1998). In brief, isohydric species or cultivars maintain higher Ψ_L due to stomatal closure when the soil dries, whereas anisohydric species or cultivars sustain higher stomatal conductance allowing a drop in Ψ_L with the progression of water deficit (Tardieu et al., 1996). These behaviors do not represent a simple dichotomy but rather a continuum of strategies in stomatal control. This classification in the behavior of stomata during water stress has led to the search for anisohydric species or cultivars, which could hypothetically sustain higher carbon assimilation rates during drought, and it has been extensively studied in agronomically relevant species such as *Vitis vinifera* (Schultz, 2003; Soar et al., 2006; Prieto et al., 2010). On the contrary, in almond, the identification of drought-tolerant genotypes has only been focused on physiological changes in response to specific drought treatments, or limited to a narrow range in soil water potentials (Isaakidis et al., 2004; Rouhi et al., 2007; Yadollahi et al., 2011). This does not allow characterization of the stringency of stomatal control with respect to plant water status and the proper identification of anisohydric and isohydric cultivars.

Despite this very simplified classification of stomatal regulation during drought, it has been observed that the anisohydric or isohydric behavior of cultivars, and therefore their classification, depends largely on the soil water content and its hydraulic properties. Tramontini et al. (2014) showed that water relations of *V. vinifera* (Syrah, near-anisohydric, and Cabernet Sauvignon, near-isohydric) cultivars varied significantly depending on soil hydraulic conductivity, and Hochberg et al. (2018) and Domec and Johnson (2012) indicated that the shift between anisohydric and isohydric behavior depends on soil water potential where the plants water relation parameters are measured in relation to soil properties. Regardless of such inconsistencies in the definition of the anisohydric and isohydric behavior, some methodologies have been described to isolate the effect of environmental variation. The *hydroscape*, developed by Meinzer et al. (2016), describes the stringency of stomatal regulation of Ψ_L during the drying of soil. This concept incorporates ranges of pre-dawn water potential (Ψ_{pd}) and mid-day minimum water potential (Ψ_{min}) over which stomata are effective in controlling the drop of

Ψ_L during soil desiccation until $\Psi_{pd} = \Psi_{min}$ and describes a landscape where the plant is able to sustain photosynthesis until full stomatal closure. Thus, larger hydroscapes are indicative of a higher degree of anisohydry. This methodology has been previously assessed in almond rendering consistent results with other traits related to stomatal stringency during water stress (Álvarez-Maldini et al., 2021).

Hydroscapes have also been correlated with other plant functional traits linked to anisohydric behavior. The water potential at turgor loss point (Ψ_{TLP}) is a strong predictor of an overall drought tolerance across species and biomes (Bartlett et al., 2012); a more negative Ψ_{TLP} is indicative of anisohydry and higher drought tolerance, a result initially reported by Meinzer et al. (2016) in different species. Likewise, through a meta-analysis, Fu and Meinzer (2018) found a strong correlation between the larger hydroscape areas and the lower Ψ_{TLP} values in species across different biomes. Also, Li et al. (2019) reported anisohydric *Eucalyptus* species with larger hydroscape areas were strongly linked to lower values of Ψ_{TLP}, water potential at stomatal closure (P_{gs90}), maximum stomatal conductance (gs_{max}), and leaf and stem hydraulic vulnerability to embolism (PL_{50} and P_{x50}). However, the hydroscape methodology, which has been mainly used to describe stomatal behavior of species distributed across various ecosystems, has yet to be tested broadly across a range of species and cultivars of agricultural interest and in relationship to other hydraulic and functional plant traits. Despite that Meinzer et al. (2016) and Li et al. (2019) have consistently shown a relationship between hydroscape area and traits such as Ψ_{TLP} in species from various environments, this link has yet to be proven among cultivars within a species. Given their reduced genetic variability, compared to different species adapted to distinct environments, changes in stomatal behavior and its relationship with other plant traits could be less clear. But Ψ_{TLP} and other functional traits have shown to be strong indicators of anisohydric behavior in *V. vinifera* (Tombesi et al., 2014; Albuquerque et al., 2020; Knipfer et al., 2020), which is in agreement with the multiple mechanisms that are integrated in the hydroscape that regulate plant water status and stomatal behavior.

Despite that this methodology has shown promise to properly characterize anisohydric and isohydric behavior, which in turn delivers information regarding cultivar selection, it is labor-intensive research to examine the regulation of water potential during prolonged periods of soil desiccation. Thus, correlating results from hydroscape analysis with informative functional traits such as Ψ_{TLP}, gs_{max}, or water potential at 50% loss of hydraulic conductivity (P50) would be less time-consuming and a valuable tool to help in the selection of cultivars adapted to drought prone environments. Also, identifying mechanisms and traits underlying drought resistance is essential to predict the future impacts of drought on productive species cultivated in the Mediterranean climate (Martin-StPaul et al., 2017). Considering the current need to assess almond cultivars for cultivation in central Chile, our objective was to describe anisohydric and isohydric behavior in almond cultivars. We used a pot desiccation experiment to explore dynamics of water potential, stomatal conductance, and hydroscape area toward better understanding the relationship of hydroscape area and plant functional traits.

Materials and methods

Plant material and growth conditions

The experiment was conducted between October of 2021 and February of 2022 at the experimental station in the Instituto de Ciencias Agroalimentarias Animales y Ambientales (ICA3) of the Universidad de O′Higgins, Chile (latitude: –34.61°, longitude: –70.99°, elevation: 352 m). The plant material corresponded to three cultivars of almond, Avijor (Ferragnès × Tuono), Isabelona (Blanquerna × Bella d′Aurons), and Soleta (Blanquerna × Bella d′Aurons), that were grafted onto rootpac-20 rootstocks (*Prunus besseyi* × *Prunus cerasifera*) 1 year earlier. Plants were donated by Agromillora Sur nursery (Río Claro, Maule region, Chile, latitude: –35.19°, longitude: –71.25°) in October of 2021 and transplanted into 7 L plastic pots (20 cm width × 20 cm length × 25 cm height) using a 1:1 v:v mixture of peat and perlite as substrate. An equal amount of substrate (by weight) was added to each pot (the oven-dry weight of substrate is used in Equation 1, below). The split-plot experiment had two irrigation treatments (WW and PD; whole plots) and three cultivars (Soleta, Isabelona, and Avijor; split plots). We had four blocks (each with an irrigation line) for each whole plot. Block corresponds to random effect, while cultivar and irrigation treatment are fixed effects. Each block had three experimental units (cultivars) and each experimental unit was composed by four pots with an individual plant. Thus, we employed 96 pots [2 irrigation treatments × 4 blocks × 3 cultivars × 4 pots (experimental units) of each cultivar]. Plants were irrigated daily by drip irrigation until they reached container capacity and maintained in this condition for acclimation for 1 month (November 2021) before onset of the irrigation treatments.

Irrigation treatments

After the 1-month acclimation period, the two irrigation treatments commenced. The first irrigation treatment, well-watered (WW), maintained plants at container capacity for the remainder of the experiment. For the second irrigation treatment, pot desiccation (PD), irrigation ceased allowing for a progressive decrease in substrate water content due to plant transpiration (Álvarez-Maldini et al., 2021). To ensure that water losses corresponded to plant transpiration only and

10.3389/fpls.2022.974050

not to evaporation from the substrate, the surface of each pot was covered with a plastic film, allowing only the plant stem to emerge. Pot weights were subsequently recorded at midday for the remainder of the experiment. The gravimetric substrate water content (GWC, %) was calculated according to Equation 1:

$$GWC\ (\%)\ =\ \left[\frac{(Pot - Pot_{\mathrm{dry}})}{Pot_{\mathrm{wet}} - Pot_{\mathrm{dry}}}\right] x\ 100 \qquad (1)$$

Where, *Pot* is the weight of the pot (plus substrate) at each measurement time, Pot_{dry} is the weight of the pot plus the initial, oven-dried weight of the substrate, and Pot_{wet} is the weight of the pot plus the substrate at container capacity.

Midday and pre-down water potential and pressure-volume curves

Throughout application of the irrigation treatments, pre-dawn water potential (Ψ_{pd}) and minimum mid-day water potential (Ψ_{min}) were measured at least eight times for each cultivar since the beginning of the PD treatment, procuring water potential measurements along a wide range of GWC. For leaf water potential measurements, we randomly selected two plants per experimental unit and irrigation treatment (thus, 48 plants total; 2 plants × 2 irrigation treatments × 3 cultivars × 4 replicates). One fully developed leaf from the upper third of the canopy was excised with a razor blade and Ψ_L was measured with a Scholander pressure chamber model 1505D-EXP (PMS Instruments, Albany, OR, United States) (Scholander et al., 1965). The Ψ_{pd} was measured between 06:00 and 07:00 a.m., before dawn, and Ψ_{min} was measured between 13:00 and 14:00 p.m. local time, and both parameters were measured until $\Psi_{pd} = \Psi_{min}$ was reached, which was indicative of the limits of stomatal control over plant water status.

Pressure volume (PV) curves were generated from plants of the WW treatment, for which one plant per experimental unit was randomly selected (4 plants total; 1 irrigation treatment × 3 cultivars × 1 plant of each cultivar). Leaf samples were collected before sunrise considering fully developed leaves from the upper third of the plant canopy and cut with a razor blade at the petiole and immediately stored in a sealed bag with damp paper and transported to the laboratory. Leaf PV curves were measured according to the protocol described by Tyree and Hammel (1972). Thus, leaves were allowed to slowly dehydrate under laboratory conditions, and Ψ_L and fresh mass were measured periodically with an analytical balance (Boeco model A0021E, Hamburg, Germany). The water potential at turgor loss point (Ψ_{TLP}) was identified as the inflection point of the $1/\Psi_L$ vs. relative water content (RWC) curve. Mean modulus of elasticity (ε) was estimated as the slope of turgor potential (Ψ_p) vs. RWC in the phase from full turgor to turgor loss point. Capacitance at full turgor (C_{FT}) was calculated from the slope of the linear portion from RWC and Ψ_L before the Ψ_{TLP}, normalized to saturated water content at leaf area.

Gas exchange measurements

On the same days and plants that measurements of Ψ_{pd} and Ψ_{min} were recorded, gas exchange was measured at midday with a CIRAS-3 portable photosynthesis system equipped with a CFM-3 chlorophyll fluorescence module (PP Systems, Amesbury, MA, United States). The CO_2 concentration in the leaf cuvette was adjusted to 400 ppm, the leaf temperature was maintained at 25 ± 1°C, and the PAR was set to 1,500 μmol photons m^{-2} s^{-1}. Leaves were acclimated to cuvette conditions for at least 5 min before each measurement. Then, net photosynthesis (A_N), stomatal conductance (gs), transpiration rate (E), and sub-stomatal CO_2 concentration (Ci) were measured. The instantaneous water use efficiency (iWUE) was calculated as the ratio between A_N and E. The maximum photosynthetic and stomatal conductance rates (A_{max} and gs_{max}, respectively) was considered as A_N and gs measured in plants before onset of the irrigation treatments.

Stem vulnerability to xylem cavitation

Stem vulnerability curves were constructed using the air injection method with a double ended pressure sleeve connected to a Scholander pressure chamber (model described above). We used three plants of each cultivar following the protocol of Ennajeh et al. (2010). We procured the use of branches longer than 40 cm in length to accommodate maximum vessel length to avoid an open-vessel artifact (Cochard et al., 2013). Before the stem was inserted into the pressure-sleeve, the middle portion of bark was removed with a razor blade to facilitate air entry to xylem conduits. Leaves and side branches were removed, and cuts were sealed with glue and parafilm. A flexible tube connected to a solution tank filled with distilled water was connected to the basal end of the stem. The tank was installed 60 cm in height. Then, the stems were flushed at 0.06 MPa for 45 min to remove air bubbles and the maximum conductivity of the stem was measured (K_{max}). Flow was measured gravimetrically by collecting the water from the distal end in a pre-weighed, 2-ml Eppendorf tube filled with cotton wool. Flow measurements were recorded for 2-min intervals.

After measuring K_{max}, the pressure in the chamber was progressively increased, at 5-min intervals, to 0.5, 1.0, 1.5, 2.0, 2.5, 3.0, 3.5, 4.0, 5.0, 6.0, and 7.0 MPa. Stem hydraulic conductance (K_h) was measured after slowly releasing the air and allowing the stem to equilibrate for 3-min, then flow measurements were recorded during a 2-min interval. The

percentage loss of conductivity (PLC) was calculated using Equation 2 as follows:

$$PLC\ (\%)\ =\ 100\,x\left(1-\frac{K_h}{K_{\max}}\right) \quad (2)$$

The relationship between stem hydraulic conductance and PLC was fitted with a Weibull curve using the *fitplc* package (Duursma and Choat, 2017) in the R software (version 4.2.0, R Core Team, 2022). The water potential corresponding to a 50% loss in conductivity (P50) and bootstrapped confidence intervals (CI) were calculated.

Metrics to determine anisohydric and isohydric behavior

Considering leaf water relations and gas exchange measurements described above, different metrics to assess anisohydric and isohydric behavior were calculated.

First, the slope of the relationship between Ψ_{pd} and Ψ_{min} (σ) was calculating using linear regression according to the methodology described by Martínez-Vilalta et al. (2014).

Second, the hydroscape area (hereafter, hydroscape) was measured following methodology described in Meinzer et al. (2016) and Álvarez-Maldini et al. (2021). In brief, the hydroscape is the area comprising the Ψ_{pd} vs. Ψ_{min} regression line and a 1:1 line, which is calculated according to Equation 3:

$$Hydroscape\ =\ \frac{(a\ x\ b)}{2} \quad (3)$$

Where a is the intercept of the Ψ_{pd} vs. Ψ_{min} regression line, representing the most negative Ψ_{min} when Ψ_{pd} = 0, and b is the intersection of Ψ_{pd} vs. Ψ_{min} and the 1:1 line, corresponding to the water potential at Ψ_{pd} = Ψ_{min} which indicates the limit of stomatal control to prevent further decrease in leaf water potential.

Third, the water potential at stomatal closure (Ψ_{gs90}) was calculated according to Li et al. (2019). Briefly, the stomatal conductance (gs, described in section "Gas exchange measurements") was plotted against Ψ_{min} and fitted with a weighted polynomial regression to obtain Ψ_{gs90} using the *fitplc* package from R software (version 4.2.0) (Duursma and Choat, 2017).

Statistical analysis

To assess the relationship between Ψ_{pd} and Ψ_{min}, a first-order kinetic model was fitted using PROC REG procedure (SAS Institute Inc., Cary, NC, United States) (Álvarez-Maldini et al., 2021).

Cultivar effects on A_{max}, gs_{max}, E_{max}, $iWUE_{max}$, GWC, π_o, Ψ_{TLP}, RWC_{TLP}, ε, and C_{FT} were assessed using one-way analyses of variance using generalized mixed models using procedure PROC GLIMMIX (SAS Institute Inc., Cary, NC, United States) with selection of distribution considering the Akaike Information Criteria. Differences among means were determined using a Tukey (HSD) test for multiple comparisons.

To evaluate the effect of cultivar and irrigation treatment on A_N, E, gs, iWUE, Ψ_{min} and Ψ_{pd} an ANOVA analysis was performed according to our experimental design as described above. Differences among means were determined by using a Tukey (HSD) test for multiple comparisons.

To assess the relationship between gs and Ψ_{min} during PD, a first-order kinetic model was fitted using the PROC NLIN procedure (SAS Institute Inc., Cary, NC, United States) with the Gauss-Newton method through a derivative-free algorithm. The cultivar effect was evaluated using the extra sums of squares principle (Bergerud, 1996).

Estimation and inference of regression with piecewise linear model was used to perform the analysis of the water potential (WP) curve. The model generates a linear estimate and calculates the boundaries between linear phases and corresponding slope values according to the methodology described by Muggeo (2003) and adapted by Muggeo et al. (2014) to generate models by different segments with continuous intersection point and with unequal slopes. In our analysis we generated three segments to intersection points or boundaries (Θ_1 and Θ_2). All the parameters for the model were fitted using a least-squares solver implemented in R software (R Core Team) by "*segmented*" package v1.6-0 (Muggeo, 2022).

All visualizations were made using SigmaPlot 14 (Systat Software Inc., San Jose, CA, United States).

Results

Initial plant-water relations and gas exchange among cultivars

At the end of the acclimation period and before onset of the irrigation treatments, significant differences were observed in maximum values in the gas exchange parameters of gs_{max}, E_{max}, and $iWUE_{max}$ among cultivars, while no differences were observed in A_{max} (**Table 1**). Soleta presented a significantly higher gs_{max}, followed by Isabelona, and lastly Avijor; a similar trend was observed in E_{max}, with Soleta and Isabelona reaching significantly higher values, followed by Avijor. Consistently as consequence of higher stomatal conductance, Soleta and Isabelona displayed significantly lower $iWUE_{max}$, and Avijor with significantly higher $iWUE_{max}$ (**Table 1**).

At the onset of the irrigation treatments the pot water content of Avijor, Isabelona, and Soleta was similar (102.3 ± 1.4%, 99.8 ± 4.0%, and 100.2 ± 2.1%, respectively).

TABLE 1 Mean (± standard error) values of leaf photosynthetic traits of *Prunus dulcis* cultivars measured before the imposition of the pot desiccation treatment.

Cultivar	Traits			
	A_{max} ($\mu mol\ CO_2\ m^{-2}\ s^{-1}$)	gs_{max} ($mmol\ H_2O\ m^{-2}\ s^{-1}$)	E_{max} ($mmol\ H_2O\ m^{-2}\ s^{-1}$)	$iWUE_{max}$ ($mmol\ CO_2\ mol^{-1}\ H_2O$)
Avijor	12.24 ± 0.67 ns	363.32 ± 24.14 **c**	5.18 ± 0.22 **b**	2.39 ± 0.13 **a**
Isabelona	11.24 ± 0.88 ns	517.39 ± 19.95 **b**	6.31 ± 0.13 **a**	1.82 ± 0.16 **b**
Soleta	13.22 ± 0.90 ns	623.36 ± 27.60 **a**	6.83 ± 0.17 **a**	1.97 ± 0.14 **b**

A_{max}, maximal photosynthetic rate on well-watered plants; gs_{max}, maximum stomatal conductance on well-watered plants; E_{max}, maximum transpiration rate on well-watered plants; $iWUE_{max}$, maximum water use efficiency on well-watered plants. Different letters indicate significant differences among cultivars at $p \leq 0.05$ according to Tukey test.

Hydraulic traits of cultivars

In relation to the pressure-volume curve analysis, cultivar was significant for Ψ_{TLP} (Table 2; Soleta < Avijor = Isabelona) but not for SWC, π_o, RWC_{TLP}, C_{FT}, or ε traits. We observed a trend ($p = 0.0791$) for higher πo in Soleta, followed by Isabelona, and then Avijor.

Water potential at 50% loss of conductivity (P50) showed different values among cultivars. Soleta and Isabelona had similar P50 values (–3.73 MPa and –3.80 MPa, respectively) that were lower than Avijor (–2.97 MPa) (Table 2).

Different behavior of cultivars during pot desiccation

The PD experiment lasted 50 days between December of 2021 until January of 2022. Water potential (Ψ_{min} and Ψ_{pd}) and gas exchange parameters were measured 1, 9, 15, 20, 23, 27, 35, 44, and 50 days after the beginning of the PD treatment. During the PD treatment imposition, GWC content decreased steadily, reaching pot water contents of 35.9 ± 3.7%, 31.9 ± 1.9%, and 30.7 ± 4.8% in Avijor, Isabelona, and Soleta, respectively. Pot water content in the WW treatment was 89.6 ± 5.8% in Avijor, 90.0 ± 1.3% in Isabelona, and 86.6 ± 4.8% in Soleta.

Among cultivars, all leaf water relations and gas exchange parameters were affected by the PD treatment. At conclusion of the PD treatment, A_N was significantly affected by cultivar ($p < 0.0001$), and iWUE was only affected by the PD treatment ($p = 0.0277$) with significantly lower values in stressed plants. Minimum water potential was independently affected by the irrigation treatment and cultivar, while both factors significantly interacted to affect E, gs and Ψ_{pd} (Table 3). At the end of the PD treatment and for all cultivars, Ψ_{min} decreased significantly compared with the WW treatment, reaching minimum values in Soleta followed by Avijor and by Isabelona. In all the parameters affected by the irrigation × cultivar interaction (E, gs and Ψ_{pd}), the PD treatment significantly decreased values compared to the WW treatment. In regard to gs, at the end of the PD treatment, Isabelona reached the lowest value, with higher gs in Soleta. Transpiration rate (E) was higher in Soleta in the WW treatment compared with Avijor and Isabelona, but no differences among cultivars were observed in the PD treatment (Table 3). The lowest values of Ψ_{pd} at the end of the PD treatment for Avijor, Isabelona, and Soleta were –2.93 ± 0.29, –2.39 ± 0.29, and –3.38 ± 0.12 MPa, respectively (Table 3).

Although, as previously described, the PD treatment affected leaf water potential and gas exchange parameters at the end of the experiment, the desiccation treatment influenced the behavior of stomatal conductance differently, with decreasing Ψ_{min} of each cultivar during the first stages of the desiccation treatment (Figure 1). Thus, different models were fitted for Avijor, Isabelona, and Soleta. A faster decrease in gs was observed in Avijor at higher Ψ_{min} values. On the contrary, Soleta sustained higher stomatal conductance for a longer period (at more negative Ψ_{min}) during the progression of PD, while Isabelona displayed an intermediate behavior between Soleta and Avijor (Figure 1). This pattern was similar for water potential at stomatal closure (Ψ_{gs90}) (Table 2), with Soleta and Isabelona displaying lower values of Ψ_{gs90} (–2.14 MPa and –2.25 MPa, respectively) and Avijor displaying a higher value (–1.72 MPa), although the large confidence intervals of Avijor overlapped with the Ψ_{gs90} of the other two cultivars.

Regarding the metrics of stringency of stomatal control, the slope of the linear regression fitted to the relationship of Ψ_{pd} vs. Ψ_{min} (σ) revealed that σ only ranged between 0.811 MPa MPa^{-1} in Isabelona and 0.922 MPa MPa^{-1} in Avijor (Table 2), with none of the cultivars displaying a perfect isohydric or anisohydric behavior (slopes 0 or 1, respectively).

Despite not observing perfect anisohydric or isohydric behavior, the hydroscape area ranged from 8.74 MPa^2 in Avijor to 9.223 MPa^2 in Soleta (Figure 2 and Table 2), with Isabelona displaying an intermediate value (Table 2). Thus, cultivar rankings based on hydroscape area from the more isohydric to the more anisohydric is: Isabelona, Avijor, and Soleta.

As previously demonstrated by Knipfer et al. (2020), the relationship between Ψ_{pd} and Ψ_{min} during drought is not linear, and is constituted by three phases of plant dehydration with break points between each phase that are indicative

10.3389/fpls.2022.974050

of the thresholds of stomatal closure and leaf turgor loss. Accordingly, we were able to perform the analysis of the water potential curve (WP curve) during pot desiccation for each cultivar and identify three distinct phases along the WP curve (Figure 3 and Table 4), although it displayed a different shape than the one described by Knipfer et al. (2020). According to the slope of the three phases (Table 4), a steeper decrease in water potential was observed during the first stages of the PD treatment, which continued until –0.803 MPa in Avijor, –0.334 MPa in Isabelona, and –0.997 MPa in Soleta, corresponding to the boundary between the first and second phase (Θ_1). Following Θ_1, reductions in water potential were less pronounced in the second and third phases, observed through lower slope values (β_2 and β_3) (Table 4). The boundary between the second and the third phase (Θ_2) was higher in Avijor (–1.553 MPa), Isabelona (–2.941 MPa), and Soleta (–3.513 MPa) (Figure 3).

Discussion

The anisohydric and isohydric concept has been used for several decades as a framework to describe different behaviors of plant water-relations during drought. However, this concept is not exempt from criticism due to common lack in consistency, with species or cultivars shifting from isohydric to anisohydric behavior, and vice versa (Hochberg et al., 2018). Isohydric and anisohydric behavior are simply described in terms of changes in Ψ_{min} in response to Ψ_{pd}, although it represents a whole-plant hydraulic strategy resulting from the coordination and trade-offs among different plant functional traits (Meinzer et al., 2017; Fu et al., 2019; Henry et al., 2019). Thus, using plant functional traits to predict species distribution, dynamics, and responses to environmental change has been important in physiological ecology (Adier et al., 2014), but is now rapidly gaining usefulness in the search for cultivars of interest in the agricultural industry.

TABLE 2 Values of key metrics to describe anisohydric and isohydric behavior in *Prunus dulcis* cultivars and of hydraulic traits derived from pressure volume curves (mean ± standard deviation), stem vulnerability curves (mean, CI in brackets) and leaf water potential causing 90% of stomatal closure (Ψ_{gs90}) for different almond cultivars.

Cultivar	σ (MPa MPa^{-1})	Hydroscape SWC (MPa^2)		π_o (MPa)	Ψ_{TLP} (MPa)	RWC_{TLP}	ε (MPa)	C_{FT} (mol m^{-2} MPa^{-1})	Ψ_{gs90} (MPa)	P50 (MPa)
Avijor	0.922	8.74	2.43 ± 0.28	1.52 ± 0.42	–2.01 ± 0.44 **a**	88.26 ± 1.52	12.91 ± 4.87	0.59 ± 0.09	–1.72 [1.69, 2.91]	–2.97 [2.53, 3.46]
Isabelona	0.811	8.13	2.68 ± 0.82	1.62 ± 0.25	–2.31 ± 0.13 **a**	83.08 ± 3.50	11.38 ± 5.74	0.80 ± 0.30	–2.25 [2.04, 2.53]	–3.80 [3.41, 4.28]
Soleta	0.867	9.23	2.05 ± 0.66	1.97 ± 0.24	–2.87 ± 0.17 **b**	64.22 ± 3.24	11.85 ± 2.14	0.77 ± 0.14	–2.14 [1.99, 2.33]	–3.73 [3.47, 4.02]
p-value	–	–	0.3530	0.07916	**0.0059**	0.2338	0.8885	0.3459	–	–

σ, slope of the relationship between Ψ_{pd} and Ψ_{min}; SWC, saturated water content; π_o, osmotic potential at full turgor; Ψ_{TLP}, water potential at turgor loss point; RWC_{TLP}, relative water content at turgor loss point; ε, modulus of elasticity; and C_{FT}, capacitance at full turgor. P50, water potential at 50% loss of hydraulic conductivity. Different letters within each trait indicate significant differences among means ($p \leq 0.05$). Bold values indicate significant differences between cultivars.

TABLE 3 Mean (± standard deviation) values of leaf photosynthetic traits and water potential at conclusion of the pot desiccation (PD treatment), source of variation, and *p*-values of *Prunus dulcis* cultivars subjected to PD and well-watered (WW) irrigation treatments.

	iWUE (mmol CO_2 mol^{-1} H_2O)	Ψ_{min} (MPa)	A_N (μmol CO_2 m^{-2}s^{-1})	E (mmol H_2O m^{-2}s^{-1})		gs (mmol H_2O m^{-2}s^{-1})		Ψ_{pd} (MPa)	
				WW	PD	WW	PD	WW	PD
Cultivar (C)									
Avijor	–	–2.94 ± 0.43 **ab**	8.44 ± 2.31 **a**	5.33 ± 0.15 **b**	1.14 ± 0.12 **c**	374.68 ± 19.59 **b**	51.00 ± 6.08 **cd**	–0.70 ± 0.03 **a**	–2.93 ± 0.29 **d**
Isabelona	–	–2.83 ± 0.44 **a**	6.16 ± 1.70 **b**	6.45 ± 0.18 **a**	0.95 ± 0.07 **c**	530.95 ± 27.77 **a**	41.80 ± 3.18 **d**	–1.00 ± 0.09 **b**	–2.39 ± 0.29 **c**
Soleta	–	–3.24 ± 0.49 **b**	7.26 ± 1.91 **ab**	6.30 ± 0.06 **a**	1.19 ± 0.07 **c**	531.85 ± 20.21 **a**	53.83 ± 3.53 **c**	–0.95 ± 0.05 **b**	–3.38 ± 0.12 **e**
Treatment (T)									
WW	2.06 ± 0.18 **b**	–1.83 ± 0.08 **a**	–	–	–	–	–	–	–
PD	2.18 ± 0.12 **a**	–4.18 ± 0.10 **b**	–	–	–	–	–	–	–
Source of variation									
Block	0.3920	0.3267	0.6810	0.2318		0.8034		0.2007	
C	0.3865	<**0.0001**	<**0.0001**	<0.0001		<0.0001		<0.0001	
T	**0.0277**	**0.0002**	0.0624	<0.0001		0.0370		<0.0001	
C *x* T	0.1456	0.8410	0.2343	**0.0003**		**0.0084**		<**0.0001**	

gs, stomatal conductance; Ψ_{min}, minimum midday water potential; A_N, net photosynthesis; E, transpiration rate; WUE, water use efficiency; Ψ_{pd}, pre-dawn water potential. Different letters within columns indicate statistical differences among means ($p \leq 0.05$). Bold values indicate significant differences between cultivars.

10.3389/fpls.2022.974050

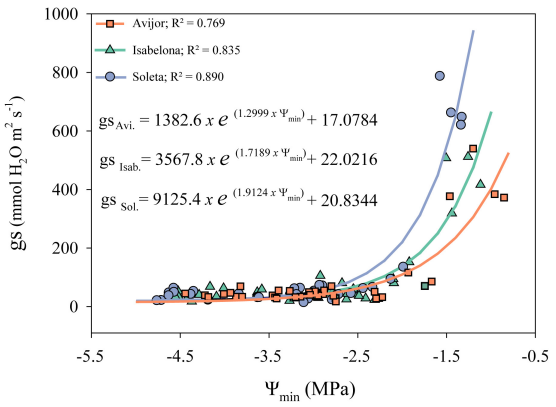

FIGURE 1
Effect of midday minimum water potential (Ψ_{min}) on stomatal conductance (gs) during the pot desiccation treatment of *Prunus dulcis* cultivars. Symbols indicate measured data and lines correspond modeled data for each cultivar. Fitted models and corresponding R^2-value for all cultivars are shown in the panel.

To fully comprehend the behavior in stomatal regulation during water stress of three almond cultivars, we assessed several metrics of anisohydric and isohydric behavior and leaf and stem functional traits for a more comprehensive framework to characterize plant response to drought (Skelton et al., 2015).

Initially, we assessed the slope of the Ψ_{min} vs. Ψ_{pd} (σ) as previously described by Martínez-Vilalta et al. (2014), but none of the cultivars displayed neither perfect isohydric nor anisohydric behavior (0 or 1 values, respectively). Although σ showed a tendency of Avijor to have a more isohydric behavior in this study, it has failed to correlate with other metrics of stomatal sensitivity in 44 species (Martínez-Vilalta and Garcia-Forner, 2017) and it has proven to be inconsistent to rank species/cultivars along a continuum of isohydric to anisohydric depending of the values of Ψ_{pd} (Poni et al., 2007; Domec and Johnson, 2012; Hochberg et al., 2018). We also used the hydroscape metric to assess the anisohydric and isohydric behavior of the three almond cultivars. According to Meinzer et al. (2016), the hydroscapes describe a water potential landscape over which plants operate before drought-induced stomatal closure, with anisohydry characterized by larger areas. Our results regarding hydroscape values are similar to the more anisohydric species reported by Meinzer et al. (2016) with 8.4 MPa^2 in *Quercus garryana*, and higher to the values reported by Li et al. (2019) in *Eucalyptus* species. Thus, according to this metric the rank of our cultivars from more isohydric to more anisohydric is Avijor, Isabelona, and Soleta. Despite the above-mentioned issues of σ, both metrics (hydroscapes and σ) ranked the cultivars equally. These consistent results could be related to the wide range in Ψ_{pd} we measured. A wide range of hydroscape areas have been reported among different species (Meinzer et al., 2016; Li et al., 2019), while in this study a lower range in area variation among cultivars (8.13 MPa^2 vs. 9.23 MPa^2) was observed. Regardless of this lower variation, cultivars also displayed differential behavior observed in stomatal responses to decreasing water availability (**Figure 1**). While Avijor had a faster decrease in stomatal conductance with decreasing Ψ_{min}, Soleta sustained higher stomatal conductance at lower values of Ψ_{min}; this points toward an isohydric behavior in Avijor and an anisohydric behavior in Soleta. This agrees with Tombesi et al. (2014) who reported stomatal closure at higher leaf and stem water potentials in a near-isohydric *V. vinifera* cultivar (Montepulciano) vs. the anisohydric cultivar (Sangiovese).

Despite reports that species with higher sensitivity to stomatal closure during leaf dehydration also have higher values of gs_{max} (Skelton et al., 2015; Henry et al., 2019), our results showed that the more anisohydric cultivar Soleta, which sustained higher gs at lower Ψ_{min}, also presented higher gs_{max}, E_{max}, and lower iWUE (**Table 1**) under conditions of high water availability. This concurs with Meinzer et al. (2017), who reported that anisohydric species have faster kinetics of stomatal opening and activation of photosynthesis with greater stomatal conductance, photosynthetic capacity, and lower iWUE, characteristic of species from dry regions that aim to maximize the utilization of unpredictable and rare precipitation events (Li et al., 2016, 2018). This trait has also been observed between anisohydric and isohydric *Vitis* cultivars (Dayer et al., 2020). These results indicate that anisohydric cultivars such as Soleta are characterized by physiological traits linked to drought tolerant species that maximize carbon gain during periods of high water availability.

As expected, the imposition of the PD experiment caused an increase in iWUE in all cultivars at the beginning of the experiment (**Supplementary Figure 1**). However, during the first 30 days of the PD treatment, the more anisohydric cultivars Soleta and Isabelona sustained higher iWUE than the isohydric-behaving Avijor (**Supplementary Figure 1**). Higher iWUE during PD in Soleta and Isabelona are explained mainly by maintenance of higher photosynthesis rates than Avijor during PD. Although it has been previously reported than isohydric cultivars are expected to present higher iWUE (Schultz, 1996; Poni et al., 2007), our results agree with Pou et al. (2012) who indicates that anisohydric *Vitis* cultivars show higher WUE due to maintenance of photosynthesis stability.

The water potential at stomatal closure (Ψ_{gs90}) is also a trait that can accurately quantify anisohydric and isohydric behavior (Skelton et al., 2015; Hochberg et al., 2018), where a more negative Ψ_{gs90} indicates that plants can sustain carbon assimilation over a wider range of leaf water potentials, which is in direct relationship with larger hydroscape areas. In agreement, we observed that the more anisohydric cultivars Soleta and Isabelona had lower Ψ_{gs90}, in contrast with the more isohydric cultivar Avijor (**Table 2**); a similar trend was also

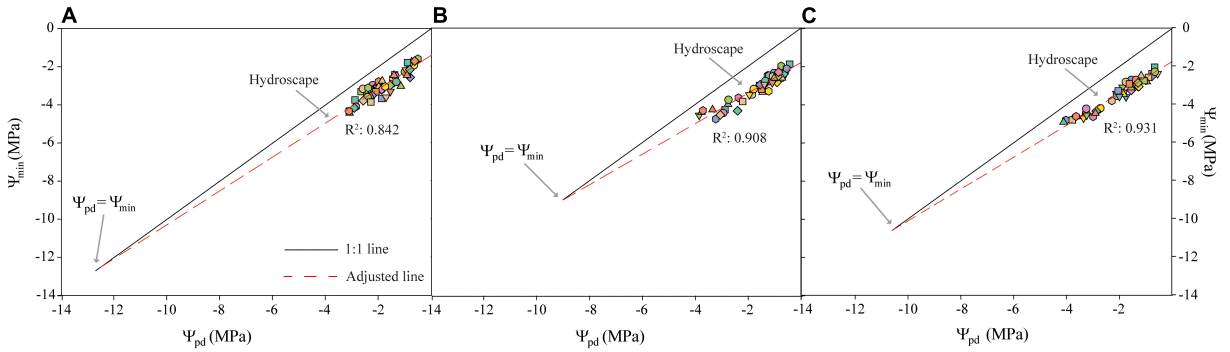

FIGURE 2
Trajectories of pre-dawn water potential (Ψ_{pd}) vs. minimum midday water potential (Ψ_{min}) during the pot desiccation treatment for the *Prunus dulcis* cultivars Avijor **(A)**, Isabelona **(B)**, and Soleta **(C)**. Solid black line represents the 1:1 line, dashed red line is the fitted linear regression of measured data. Different symbols in colors represent different individual plants measured. Hydroscape is represented by the area bounded by the regression and the 1:1 line.

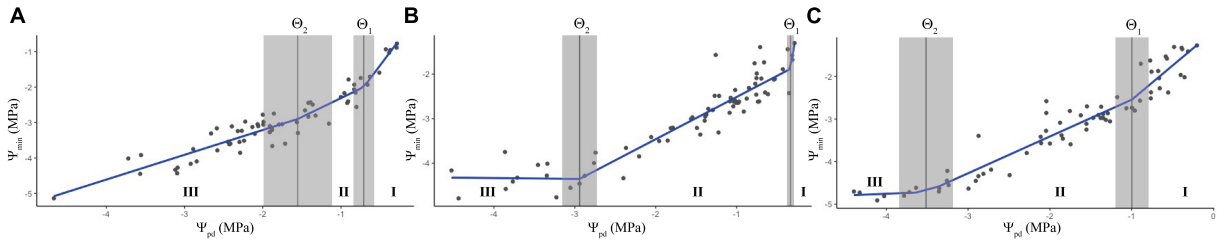

FIGURE 3
Adjustment of the piecewise linear regression (PLR) model on the relationship between pre-dawn water potential (Ψ_{pd}) and minimum mid-day water potential (Ψ_{min}) on the *Prunus dulcis* cultivars Avijor **(A)**, Isabelona **(B)**, and Soleta **(C)**. Black circles indicate data from each individual plant, blue line is the fitted model. Vertical solid lines are boundaries between phases I and II (Θ_1) and between phases II and III (Θ_2), corresponding SE values are displayed in gray lines. Model output parameters are summarized in **Table 4**.

TABLE 4 Summary of output parameters from the piecewise linear regression (PLR) model as described by Knipfer et al. (2020) used for the analysis between Ψ_{pd} and Ψ_{min} for *Prunus dulcis* cultivars.

Cultivar	Θ_1 (MPa)	Θ_2 (MPa)	β_1	β_2	β_3	RMSE	R^2
Avijor	−0.803	−1.553	2.594	1.015	0.711	0.274	0.9135
Isabelona	−0.334	−2.941	11.492	0.948	−0.018	0.319	0.8772
Soleta	−0.997	−3.513	1.610	0.865	0.078	0.305	0.9182

Θ_1, boundary between phases I and II; Θ_2, boundary between phases II and III; β_1, slope of phase I; β_2, slope of phase II; β_3, slope of phase III; R^2, fitted; and RMSE, root mean square deviation.

observed in Ψ_{TLP} values among cultivars. The water potential at turgor loss point has been widely used as an indicator of drought tolerance, as leaves with lower Ψ_{TLP} maintain open stomata, hydraulic conductance, and are able to grow under dryer conditions (Bartlett et al., 2012; Scoffoni et al., 2012; Trifilò et al., 2015). Recently, lower Ψ_{TLP} values have been positively correlated with larger hydroscapes areas, and thus anisohydry (Meinzer et al., 2016; Li et al., 2019), which supports our results regarding the contrasting anisohydric behavior of Soleta and the isohydric behavior of Avijor. Our values of Ψ_{TLP} and Ψ_{gs90} were also similar to the ones reported by Hernandez-Santana et al. (2016) in almond (−2.26 and −2.14 MPa, respectively), which are in the range of values displayed by drought-tolerant species.

Although no significant differences were observed in π_0 among cultivars (p = 0.0791) (**Table 2**), the trend in values with higher π_0 in Soleta and lower in Avijor, and the absolute lack of differences in ε, support the notion that contrast observed in Ψ_{TLP} among cultivars is mainly driven by osmotic adjustment and not by modifications of mechanical properties of the cell wall. This is consistent with a previous meta-analysis (Bartlett et al., 2012) indicating that π_0 is the main

10.3389/fpls.2022.974050

driver of Ψ_{TLP} across species, and that ε does not play a role in determining drought-tolerance. Regardless of the relationship between Ψ_{TLP} and Ψ_{gs90}, our results suggest that Ψ_{TLP} is not the main factor triggering stomatal closure because, independently of the cultivar, complete stomatal closure occurred before turgor loss ($\Psi_{gs90} > \Psi_{TLP}$). This indicates that stomatal closure is uncoupled from bulk leaf water status. Similar results were reported in anisohydric and isohydric *Vitis* cultivars (Tombesi et al., 2014) and several woody species adapted to sites with contrasting resource availability (Henry et al., 2019).

Consistent with the previously described traits, the P50 displayed that same variation among almond cultivars, with more negative values in Soleta and Isabelona than in Avijor (**Table 2**), indicating a higher vulnerability to cavitation in Avijor. Information regarding the relationship between vulnerability to cavitation and anisohydric and isohydric behavior is scarce for cultivars, but Alsina et al. (2007) reported large variability in PCL_{50} across *Vitis* cultivars (–1 to –3 MPa). Reports in different species have found a correlation between a higher xylem vulnerability to cavitation with isohydric behavior, such as in *Acer pseudoplatanus* and *Corylus avellana* (Li et al., 2016). It also has been proposed that xylem cavitation is the hydraulic signal that triggers stomatal closure in several species (Salleo et al., 2000; Nardini et al., 2001; Zufferey et al., 2011). On the contrary, the differences between Ψ_{gs90} and Ψ_{TLP} in our results showed that stomatal closure occurred before the 50% loss of xylem hydraulic conductivity in the three cultivars (Ψ_{gs90} > P50). Recent evidence also supports the notion that stomatal closure precedes xylem cavitation at community and global scales (Klein, 2014; Bartlett et al., 2016; Martin-StPaul et al., 2017) and even among cultivars (Carminati and Javaux, 2020; Dayer et al., 2020; Gambetta et al., 2020). These results indicate that the hydraulic safety margin (HSM), defined as the remainder of Ψ_{gs90} minus P_{50}, is generally positive and thus constitutes a strategy to avoid lethal embolism.

As another metric to describe the dynamics of leaf water potential during pot desiccation, we performed an analysis of the water potential curve using a piecewise linear regression according to Knipfer et al. (2018). Here, authors describe the triphasic nature of the WP curve and the prediction of the first boundary (Θ_1) between phases I and II that would correspond to the threshold at which leaf gas exchange is substantially decreased, and the second boundary (Θ_2) matching the Ψ_{TLP}. We were able to model the three phases of the WP curve and predict its corresponding boundaries and slopes (**Table 4**), but the shape of our curve diverged from the one described by Knipfer et al. (2020). Specially, a steeper decrease in water potential was observed in phase II in our cultivars while Knipfer et al. (2020) showed a minor reduction in Ψ_{min} with the continuous decrease in Ψ_{pd}. A faster dry-down in our experiment could explain the steeper reduction in Ψ_{min} during

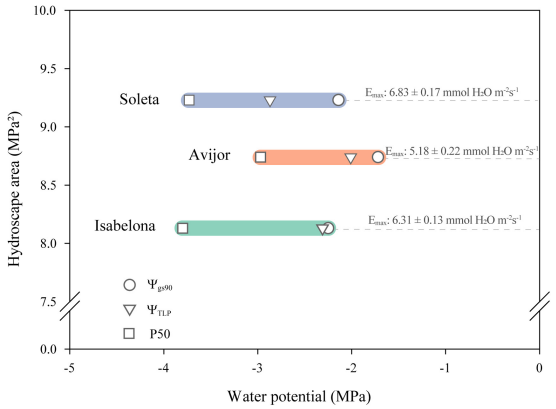

FIGURE 4
Relationships among hydroscape area and traits linked to anisohydric and isohydric behavior in the *Prunus dulcis* cultivars Avijor Isabelona, and Soleta. Ψ_{gs90}: leaf water potential causing 90% of stomatal closure, Ψ_{TLP}: water potential at turgor loss point, and P50: water potential at 50% loss of hydraulic conductivity. Values of maximum transpiration rate (E_{max}) are shown for each cultivar.

the PD treatment, indicating that factors that affect the rates of water loss and transpiration also influence dynamics of water potential. Also, the almond experiment described by Knipfer et al. (2020) was performed in 56-L potted plants, which can affect the pace of the dry-down, and thus, the dynamics of water potential, explaining the steeper decline in Ψ_{min} during phase II of our experiment. Differences in cultivar/rootstock combination could also affect the shape of the WP curve. Our predicted boundaries, Θ_1 and Θ_2, did not match stomatal closure nor Ψ_{TLP}, respectively, as indicated by Knipfer et al. (2020). It is interesting to note, however, the smaller distance between Θ_1 and Θ_2 boundaries in the isohydric Avijor (**Figure 3A**), compared to the larger distance described between the two boundaries in the more anisohydric cultivars Isabelona and Soleta (**Figures 3B,C**). Along the three phases of the WP curve, a consistent reduction in the slope of each phase was observed (**Table 4**), thus the faster reduction in Ψ_{min} occurred during the initial stages of the PD treatment until Θ_1, which could have triggered the onset of stomatal closure.

Considering all the traits described above, we observed responses to the PD treatment that suggest almond has an avoidance strategy rather than a tolerance strategy for hydraulic failure as described by Hochberg et al. (2017). First, the steep decrease in Ψ_{min} in response to decrease in Ψ_{pd} (**Figure 1**) eventually led to stomatal closure (Ψ_{gs90}) at water potentials higher than the loss of cell turgor (Ψ_{TLP}) and preceded development of cavitation in xylem conduits (P50) (**Figure 4**). This concurs with recent research stating that drought-resistant plants close their stomata at water potentials higher than that at which substantial embolism occurs (Martin-StPaul et al.,

2017). Second, we observed leaf shedding in all cultivars, especially Avijor, which further supports an avoidance strategy toward protection of perennial tissues. These responses did, however, prevent us from observing a direct measurement of $\Psi_{min} = \Psi_{pd}$. Thus, for hydroscape calculation, $\Psi_{min} = \Psi_{pd}$ was estimated by extrapolation of water potential values at the end of the PD experiment, rendering unreliable $\Psi_{min} = \Psi_{pd}$ values well beyond limits of stomatal control. Then, because the WP curves did not follow a strictly linear fit (**Table 4** and **Figure 3**), we estimated $\Psi_{min} = \Psi_{pd}$ as the intersection between a 1:1 line and the modeled piecewise regression, which yielded $\Psi_{min} = \Psi_{pd}$ values for Avijor (–6.15 MPa), Isabelona (–4.33 MPa), and Soleta (–4.83 MPa) that were closer to the observed water potential values for turgor loss and loss of hydraulic conductivity.

Despite the above-mentioned issues when calculating hydroscapes, a clear relationship was observed between hydroscape area and traits related to anisohydric behavior. Thus, Soleta cultivar with a near-anisohydric behavior displayed larger hydroscape area with lower values of Ψ_{gs90}, Ψ_{TLP}, and P50, contrary to the behavior displayed by Avijor (**Figure 4**). Thus, considering the above-mentioned traits for Soleta and Isabelona with an increased iWUE during the first stages of drought indicate, both cultivars are suitable candidates to be established under Mediterranean climate conditions of central Chile, especially in areas with restricted access to irrigation water.

Furthermore, our results regarding Soleta cultivar are in agreement with Álvarez et al. (2020) who indicated that this cultivar displayed physiological responses linked to drought tolerance when growing with its original root system (self-rooted). This result was, however, diminished when plants were grafted onto the dwarfing rootstock Rootpac-20. These results correlate with Ben Yahmed et al. (2016) that described a poor adaptation of this rootstock to Mediterranean or rain-fed conditions. Thus, considering these reports, it is important to highlight the influence of the rootstock on drought tolerance, and that the anisohydric behavior of Soleta and Isabelona cultivars may have been attenuated by the Rootpac-20 rootstock. Future work should focus on the effects of rootstock on anisohydric and isohydric behavior and consider the use of self-rooted plants for cultivation under Mediterranean conditions.

Conclusion

Our results from a pot desiccation treatment revealed that almond cultivars followed a similar response to drought: decreasing Ψ_{min} led to stomatal closure to avoid hydraulic disfunction. The different thresholds of water potentials indicate that neither turgor loss nor xylem cavitation are the hydraulic signal to induce stomatal closure, but rather that loss in soil hydraulic conductivity could be the main trigger of stomatal closure. Thus, future research regarding almond and the differences in anisohydric and isohydric behavior among its cultivars should account for below- and above-ground hydraulic traits.

Cultivars did, however, display differences in anisohydric and isohydric behavior. Anisohydric cultivars, Soleta and Isabelona, displayed larger hydroscape areas. Moreover, they presented different boundaries along the WP curve, higher gs_{max} and sustained higher stomatal conductance at lower Ψ_{min}, lower Ψ_{TLP} and vulnerability to xylem cavitation (P50), and higher iWUE than the isohydric cultivar Avijor. Because Ψ_{TLP}, P50, and gs_{max} are easily measured in well-watered plants, their assessment could be readily used to discriminate anisohydric and isohydric plants under consideration for agronomic development in Mediterranean climates without the laborious need for controlled drought experiments. Selecting plants more anisohydric in nature, such as Soleta in this research, with their ability to withstand cavitation better than their isohydric cohorts, may be preferred given expected changes in Mediterranean climates.

Data availability statement

The raw data supporting the conclusions of this article will be made available by the authors, without undue reservation.

Author contributions

CÁ-M, MP, and MA conceived and designed the experiment. CÁ-M, DE, and FA performed physiological measurements. MA and SS: contributed to data analysis. CÁ-M and RD wrote the manuscript. All authors contributed to the article and approved the submitted version.

Funding

This work was supported by the Agencia Nacional de Investigación y Desarrollo (ANID) Proyecto Fondecyt de Iniciación (no. 11200807).

Acknowledgments

We thank to Agromillora Sur S.A, especially to Natalia Torres and Cristobal Calvo, for kindly providing the plant material to conduct this investigation.

Conflict of interest

The authors declare that the research was conducted in the absence of any commercial or financial relationships that could be construed as a potential conflict of interest.

Publisher's note

All claims expressed in this article are solely those of the authors and do not necessarily represent those of their affiliated organizations, or those of the publisher, the editors and the reviewers. Any product that may be evaluated in this article, or claim that may be made by its manufacturer, is not guaranteed or endorsed by the publisher.

Supplementary material

The Supplementary Material for this article can be found online at: https://www.frontiersin.org/articles/10.3389/fpls.2022.974050/full#supplementary-material

References

Adier, P. B., Salguero-Gómez, R., Compagnoni, A., Hsu, J. S., Ray-Mukherjee, J., Mbeau-Ache, C., et al. (2014). Functional traits explain variation in plant lifehistory strategies. *Proc. Natl. Acad. Sci. U.S.A.* 111, 740–745. doi: 10.1073/PNAS.1315179111/SUPPL_FILE/PNAS.201315179SI.PDF

Albuquerque, C., Scoffoni, C., Brodersen, C. R., Buckley, T. N., Sack, L., and McElrone, A. J. (2020). Coordinated decline of leaf hydraulic and stomatal conductances under drought is not linked to leaf xylem embolism for different grapevine cultivars. *J. Exp. Bot.* 71, 7286–7300. doi: 10.1093/jxb/eraa392

Alsina, M., De Herralde, F., Aranda, X., Savé, R., and Biel, C. (2007). Water relations and vulnerability to embolism are not related: Experiments with eight grapevine cultivars. *Vitis* 46, 1–6.

Álvarez, S., Martín, H., Barajas, E., Rubio, J. A., and Vivaldi, G. A. (2020). Rootstock effects on water relations of young almond trees (cv. Soleta) when subjected to water stress and rehydration. *Water* 12:3319. doi: 10.3390/W12123319

Álvarez-Maldini, C., Acevedo, M., and Pinto, M. (2021). Hydroscapes: A useful metric for distinguishing iso-/anisohydric behavior in almond cultivars. *Plants* 10, 1–11. doi: 10.3390/plants10061249

Bambach, N., Meza, F. J., Gilabert, H., and Miranda, M. (2013). Impacts of climate change on the distribution of species and communities in the Chilean Mediterranean ecosystem. *Reg. Environ. Chang.* 13, 1245–1257. doi: 10.1007/S10113-013-0425-7/TABLES/2

Bartlett, M. K., Klein, T., Jansen, S., Choat, B., and Sack, L. (2016). The correlations and sequence of plant stomatal, hydraulic, and wilting responses to drought. *Proc. Natl. Acad. Sci. U.S.A.* 113, 13098–13103. doi: 10.1073/PNAS.1604088113/SUPPL_FILE/PNAS.1604088113.SD03.XLSX

Bartlett, M. K., Scoffoni, C., and Sack, L. (2012). The determinants of leaf turgor loss point and prediction of drought tolerance of species and biomes: A global meta-analysis. *Ecol. Lett.* 15, 393–405. doi: 10.1111/j.1461-0248.2012.01751.x

Ben Yahmed, J., Ghrab, M., and Ben Mimoun, M. (2016). Eco-physiological evaluation of different scion-rootstock combinations of almond grown in Mediterranean conditions. *Fruits* 71, 185–193. doi: 10.1051/FRUITS/2016003

Bergerud, W. A. (1996). *Introduction to logistic regression models: With worked forestry examples: biometrics information handbook no.7. Working Paper. 157.* Victoria, BC: British Columbia Ministry of Forests.

Camposeo, S., Palasciano, M., Vivaldi, G. A., and Godini, A. (2011). Effect of increasing climatic water deficit on some leaf and stomatal parameters of wild and cultivated almonds under Mediterranean conditions. *Sci. Hortic.* 127, 234–241. doi: 10.1016/j.scienta.2010.09.022

Carminati, A., and Javaux, M. (2020). Soil rather than xylem vulnerability controls stomatal response to drought. *Trends Plant Sci.* 25, 868–880. doi: 10.1016/j.tplants.2020.04.003

Cavin, L., Mountford, E. P., Peterken, G. F., and Jump, A. S. (2013). Extreme drought alters competitive dominance within and between tree species in a mixed forest stand. *Funct. Ecol.* 27, 1424–1435. doi: 10.1111/1365-2435.12126

Chaves, M. M., Maroco, J. P., and Pereira, J. S. (2003). Understanding plant responses to drought - from genes to the whole plant. *Funct. Plant Biol.* 30, 239–264. doi: 10.1071/FP02076

Cochard, H., Badel, E., Herbette, S., Delzon, S., Choat, B., and Jansen, S. (2013). Methods for measuring plant vulnerability to cavitation: A critical review. *J. Exp. Bot.* 64, 4779–4791. doi: 10.1093/jxb/ert193

Dayer, S., Herrera, J. C., Dai, Z., Burlett, R., Lamarque, L. J., Delzon, S., et al. (2020). The sequence and thresholds of leaf hydraulic traits underlying grapevine varietal differences in drought tolerance. *J. Exp. Bot.* 71, 4333–4344. doi: 10.1093/jxb/eraa186

del Pozo, A., Brunel-Saldias, N., Engler, A., Ortega-Farias, S., Acevedo-Opazo, C., Lobos, G. A., et al. (2019). Climate change impacts and adaptation strategies of agriculture in Mediterranean-Climate Regions (MCRs). *Sustainability* 11:2769. doi: 10.3390/SU11102769

Domec, J. C., and Johnson, D. M. (2012). Does homeostasis or disturbance of homeostasis in minimum leaf water potential explain the isohydric versus anisohydric behavior of *Vitis vinifera* L. cultivars? *Tree Physiol.* 32, 245–248.

Duursma, R. A., and Choat, B. (2017). fitplc - an R package to fit hydraulic vulnerability curves. *J. Plant Hydraul.* 4:e002. doi: 10.20870/jph.2017.e002

Ennajeh, M., Vadel, A. M., Cochard, H., and Khemira, H. (2010). Comparative impacts of water stress on the leaf anatomy of a drought-resistant and a drought-sensitive olive cultivar. *J. Hortic. Sci. Biotechnol.* 85, 289–294. doi: 10.1080/14620316.2010.11512670

Flexas, J., Bota, J., Cifre, J., Escalona, J. M., Galmés, J., Gulías, J., et al. (2004). Understanding down-regulation of photosynthesis under water stress: Future prospects and searching for physiological tools for irrigation management. *Ann. Appl. Biol.* 144, 273–283. doi: 10.1111/j.1744-7348.2004.tb00343.x

Flexas, J., Scoffoni, C., Gago, J., and Sack, L. (2013). Leaf mesophyll conductance and leaf hydraulic conductance: An introduction to their measurement and coordination. *J. Exp. Bot.* 64, 3965–3981. doi: 10.1093/jxb/ert319

Fu, X., and Meinzer, F. C. (2018). Metrics and proxies for stringency of regulation of plant water status (iso/anisohydry): A global data set reveals coordination and trade-offs among water transport traits. *Tree Physiol.* 39, 122–134. doi: 10.1093/treephys/tpy087

Fu, X., Meinzer, F. C., Woodruff, D. R., Liu, Y. Y., Smith, D. D., McCulloh, K. A., et al. (2019). Coordination and trade-offs between leaf and stem hydraulic traits and stomatal regulation along a spectrum of isohydry to anisohydry. *Plant Cell Environ.* 42, 2245–2258. doi: 10.1111/pce.13543

Gambetta, G. A., Herrera, J. C., Dayer, S., Feng, Q., Hochberg, U., and Castellarin, S. D. (2020). The physiology of drought stress in grapevine: Towards an integrative definition of drought tolerance. *J. Exp. Bot.* 71, 4658–4676. doi: 10.1093/jxb/eraa245

García-Tejero, I. F., Gutiérrez Gordillo, S., Souza, L., Cuadros-Tavira, S., and Durán Zuazo, V. H. (2018). Fostering sustainable water use in almond (*Prunus dulcis* Mill.) orchards in a semiarid Mediterranean environment. *Arch. Agron. Soil Sci.* 65, 164–181. doi: 10.1080/03650340.2018.1492113

Hannah, L., Roehrdanz, P. R., Ikegami, M., Shepard, A. V., Shaw, M. R., Tabor, G., et al. (2013). Climate change, wine, and conservation. *Proc. Natl. Acad. Sci. U.S.A.* 110, 6907–6912. doi: 10.1073/PNAS.1210127110/SUPPL_FILE/PNAS.201210127SI.PDF

Henry, C., John, G. P., Pan, R., Bartlett, M. K., Fletcher, L. R., Scoffoni, C., et al. (2019). A stomatal safety-efficiency trade-off constrains responses to leaf dehydration. *Nat. Commun.* 10:3398. doi: 10.1038/s41467-019-11006-1

Hernandez-Santana, V., Rodriguez-Dominguez, C. M., Fernández, J. E., and Diaz-Espejo, A. (2016). Role of leaf hydraulic conductance in the regulation of stomatal conductance in almond and olive in response to water stress. *Tree Physiol.* 36, 725–735. doi: 10.1093/treephys/tpv146

Hochberg, U., Rockwell, F. E., Holbrook, N. M., and Cochard, H. (2018). Iso/Anisohydry: A plant–environment interaction rather than a simple hydraulic trait. *Trends Plant Sci.* 23, 112–120. doi: 10.1016/j.tplants.2017.11.002

Hochberg, U., Windt, C., Ponomarenko, A., Zhang, Y.-J., Gersony, J., Rockwell, F., et al. (2017). Stomatal closure, basal leaf embolism, and shedding protect the hydraulic integrity of grape stems. *Plant physiol.* 174, 764–775. doi: 10.1104/pp.16.01816.

Isaakidis, A., Sotiropoulos, T., Almaliotis, D., Therios, I., and Stylianidis, D. (2004). Response to severe water stress of the almond (*Prunus amygdalus*) 'ferragnès' grafted on eight rootstocks. *N. Z. J. Crop Hortic. Sci.* 32, 355–362. doi: 10.1080/01140671.2004.9514316

Klein, T. (2014). The variability of stomatal sensitivity to leaf water potential across tree species indicates a continuum between isohydric and anisohydric behaviours. *Funct. Ecol.* 28, 1313–1320. doi: 10.1111/1365-2435.12289

Knipfer, T., Bambach, N., Hernandez, M. I., Bartlett, M. K., Sinclair, G., Duong, F., et al. (2020). Predicting stomatal closure and turgor loss in woody plants using predawn and midday water potential. *Plant Physiol.* 184, 881–894. doi: 10.1104/pp.20.00500

Knipfer, T., Barrios-Masias, F. H., Cuneo, I. F., Bouda, M., Albuquerque, C. P., Brodersen, C. R., et al. (2018). Variations in xylem embolism susceptibility under drought between intact saplings of three walnut species. *Tree Physiol.* 38, 1180–1192. doi: 10.1093/treephys/tpy049

Li, S., Feifel, M., Karimi, Z., Schuldt, B., Choat, B., and Jansen, S. (2016). Leaf gas exchange performance and the lethal water potential of five European species during drought. *Tree Physiol.* 36, 179–192. doi: 10.1093/TREEPHYS/TPV117

Li, X., Blackman, C. J., Choat, B., Duursma, R. A., Rymer, P. D., Medlyn, B. E., et al. (2018). Tree hydraulic traits are coordinated and strongly linked to climate-of-origin across a rainfall gradient. *Plant Cell Environ.* 41, 646–660. doi: 10.1111/pce.13129

Li, X., Blackman, C. J., Peters, J. M. R., Choat, B., Rymer, P. D., Medlyn, B. E., et al. (2019). More than iso/anisohydry: Hydroscapes integrate plant water use and drought tolerance traits in 10 eucalypt species from contrasting climates. *Funct. Ecol.* 33, 1035–1049. doi: 10.1111/1365-2435.13320

Marsal, J., Girona, J., and Mata, M. (1997). Leaf water relation parameters in almond compared to hazelnut trees during a deficit irrigation period. *J. Am. Soc. Hortic. Sci.* 122, 582–587. doi: 10.21273/JASHS.122.4.582

Martínez-Vilalta, J., and Garcia-Forner, N. (2017). Water potential regulation, stomatal behaviour and hydraulic transport under drought: deconstructing the iso/anisohydric concept. *Plant Cell Environ.* 40, 962–976. doi: 10.1111/pce.12846

Martínez-Vilalta, J., Poyatos, R., Aguadé, D., Retana, J., and Mencuccini, M. (2014). A new look at water transport regulation in plants. *New Phytol.* 204, 105–115. doi: 10.1111/NPH.12912

Martin-StPaul, N., Delzon, S., and Cochard, H. (2017). Plant resistance to drought depends on timely stomatal closure. *Ecol. Lett.* 20, 1437–1447. doi: 10.1111/ele.12851

Meinzer, F. C., Smith, D. D., Woodruff, D. R., Marias, D. E., McCulloh, K. A., Howard, A. R., et al. (2017). Stomatal kinetics and photosynthetic gas exchange along a continuum of isohydric to anisohydric regulation of plant water status. *Plant Cell Environ.* 40, 1618–1628. doi: 10.1111/pce.12970

Meinzer, F. C., Woodruff, D. R., Marias, D. E., Smith, D. D., McCulloh, K. A., Howard, A. R., et al. (2016). Mapping 'hydroscapes' along the iso- to anisohydric continuum of stomatal regulation of plant water status. *Ecol. Lett.* 19, 1343–1352. doi: 10.1111/ele.12670

Muggeo, V. M. R. (2003). Estimating regression models with unknown break-points. *Stat. Med.* 22, 3055–3071. doi: 10.1002/SIM.1545

Muggeo, V. M. R. (2022). *"segmented": Regression models with break-points/change-points (with Possibly Random Effects) estimation. R Package version 1.6-0*. Available online at: https://cran.r-project.org/web/packages/segmented/segmented.pdf

Muggeo, V. M. R., Atkins, D. C., Gallop, R. J., and Dimidjian, S. (2014). Segmented mixed models with random changepoints: a maximum likelihood approach with application to treatment for depression study. *Stat. Modell.* 14, 293–313. doi: 10.1177/1471082X13504721

Nardini, A., Tyree, M. T., and Salleo, S. (2001). Xylem cavitation in the leaf of *Prunus laurocerasus* and its impact on leaf hydraulics 1. *Plant Physiol.* 125, 1700–1709. doi: 10.1104/pp.125.4.1700

Oliveira, I., Meyer, A., Afonso, S., and Gonçalves, B. (2018). Compared leaf anatomy and water relations of commercial and traditional *Prunus dulcis* (Mill.) cultivars under rain-fed conditions. *Sci. Hortic.* 229, 226–232. doi: 10.1016/j.scienta.2017.11.015

Poni, S., Bernizzoni, F., and Civardi, S. (2007). Response of "Sangiovese" grapevines to partial root-zone drying: Gas-exchange, growth and grape composition. *Sci. Hortic.* 114, 96–103. doi: 10.1016/J.SCIENTA.2007.06.003

Pou, A., Medrano, H., Tomàs, M., Martorell, S., Ribas-Carbó, M., and Flexas, J. (2012). Anisohydric behaviour in grapevines results in better performance under moderate water stress and recovery than isohydric behaviour. *Plant Soil* 359, 335–349. doi: 10.1007/s11104-012-1206-7

Prieto, J. A., Lebon, É, and Ojeda, H. (2010). Stomatal behavior of different grapevine cultivars in response to soil water status and air water vapor pressure deficit. *OENO One* 44, 9–20. doi: 10.20870/oeno-one.2010.44.1.1459

R Core Team (2022). R: A language and environment for statistical computing. R Foundation for Statistical Computing, Vienna, Austria. https://www.R-project.org

Romero, P., Navarro, J. M., García, F., and Botía Ordaz, P. (2004). Effects of regulated deficit irrigation during the pre-harvest period on gas exchange, leaf development and crop yield of mature almond trees. *Tree Physiol.* 24, 303–312. doi: 10.1093/TREEPHYS/24.3.303

Rouhi, V., Samson, R., Lemeur, R., and Van Damme, P. (2007). Photosynthetic gas exchange characteristics in three different almond species during drought stress and subsequent recovery. *Environ. Exp. Bot.* 59, 117–129. doi: 10.1016/j.envexpbot.2005.10.001

Salleo, S., Nardini, A., Pitt, F., and Lo Gullo, M. A. (2000). Xylem cavitation and hydraulic control of stomatal conductance in Laurel (*Laurus nobilis* L.). *Plant Cell Environ.* 23, 71–79. doi: 10.1046/J.1365-3040.2000.00516.X

Schär, C., Vidale, P. L., Lüthi, D., Frei, C., Häberli, C., Liniger, M. A., et al. (2004). The role of increasing temperature variability in European summer heatwaves. *Nature* 427, 332–336. doi: 10.1038/nature02300

Scholander, P. F., Hammel, H. T., Bradstreet, E. D., and Hemmingsen, E. A. (1965). Sap pressure in vascular plants. *Science* 148, 339–346. doi: 10.1126/SCIENCE.148.3668.339

Schultz, H. R. (1996). Water relations and photosynthetic responses of two grapevine cultivars of different geographical origin during water stress. *Acta Hortic.* 427, 251–266. doi: 10.17660/ACTAHORTIC.1996.427.30

Schultz, H. R. (2003). Differences in hydraulic architecture account for near-isohydric and anisohydric behaviour of two field-grown *Vitis vinifera* L. cultivars during drought. *Plant Cell Environ.* 26, 1393–1405.

Scoffoni, C., McKown, A. D., Rawls, M., and Sack, L. (2012). Dynamics of leaf hydraulic conductance with water status: Quantification and analysis of species differences under steady state. *J. Exp. Bot.* 63, 643–658. doi: 10.1093/jxb/err270

Skelton, R. P., West, A. G., and Dawson, T. E. (2015). Predicting plant vulnerability to drought in biodiverse regions using functional traits. *Proc. Natl. Acad. Sci. U.S.A.* 112, 5744–5749. doi: 10.1073/pnas.1503376112/-/DCSupplemental.www.pnas.org/cgi//10.1073/pnas.1503376112

Soar, C. J., Speirs, J., Maffei, S. M., Penrose, A. B., McCarthy, M. G., and Loveys, B. R. (2006). Grape vine varieties Shiraz and Grenache differ in their stomatal response to VPD: Apparent links with ABA physiology and gene expression in leaf tissue. *Aust. J. Grape Wine Res.* 12, 2–12. doi: 10.1111/j.1755-0238.2006.tb00038.x

Tardieu, F., Lafarge, T., and Simonneau, T. (1996). Stomatal control by fed or endogenous xylem ABA in sunflower: Interpretation of correlations between leaf water potential and stomatal conductance in anisohydric species. *Plant Cell Environ.* 19, 75–84. doi: 10.1111/j.1365-3040.1996.tb00228.x

Tardieu, F., and Simonneau, T. (1998). Variability among species of stomatal control under fluctuating soil water status and evaporative demand: Modelling isohydric and anisohydric behaviours. *J. Exp. Bot.* 49, 419–432. doi: 10.1093/jxb/49.special_issue.419

Tombesi, S., Nardini, A., Farinelli, D., and Palliotti, A. (2014). Relationships between stomatal behavior, xylem vulnerability to cavitation and leaf water relations in two cultivars of *Vitis vinifera*. *Physiol. Plant.* 152, 453–464. doi: 10.1111/ppl.12180

Torrecillas, A., Alarcón, J. J., Domingo, R., Planes, J., and Sánchez-Blanco, M. J. (1996). Strategies for drought resistance in leaves of two almond cultivars. *Plant Sci.* 118, 135–143. doi: 10.1016/0168-9452(96)04434-2

Tramontini, S., Döring, J., Vitali, M., Ferrandino, A., Stoll, M., and Lovisolo, C. (2014). Soil water-holding capacity mediates hydraulic and hormonal signals of near-isohydric and near-anisohydric *Vitis* cultivars in potted grapevines. *Funct. Plant Biol.* 1119–1128. doi: 10.1071/FP13263

Trifilò, P., Nardini, A., Gullo, M. A. L., Barbera, P. M., Savi, T., and Raimondo, F. (2015). Diurnal changes in embolism rate in nine dry forest trees: Relationships with species-specific xylem vulnerability, hydraulic strategy and wood traits. *Tree Physiol.* 35, 694–705. doi: 10.1093/treephys/tpv049

Tyree, M. T., and Hammel, H. T. (1972). The measurement of the turgor pressure and the water relations of plants by the pressure-bomb technique. *J. Exp. Bot.* 23, 267–282. doi: 10.1093/JXB/23.1.267

Yadollahi, A., Arzani, K., Ebadi, A., Wirthensohn, M., and Karimi, S. (2011). The response of different almond genotypes to moderate and severe water stress in order to screen for drought tolerance. *Sci. Hortic.* 129, 403–413. doi: 10.1016/j.scienta.2011.04.007

Zufferey, V., Cochard, H., Ameglio, T., Spring, J. L., and Viret, O. (2011). Diurnal cycles of embolism formation and repair in petioles of grapevine (*Vitis vinifera* cv. Chasselas). *J. Exp. Bot.* 62, 3885–3894. doi: 10.1093/JXB/ERR081

frontiers | Frontiers in Plant Science

TYPE Original Research
PUBLISHED 12 October 2022
DOI 10.3389/fpls.2022.973388

Check for updates

OPEN ACCESS

EDITED BY
Felipe Klein Ricachenevsky,
Federal University of Rio Grande do Sul, Brazil

REVIEWED BY
Byju Gangadharan,
Central Tuber Crops Research Institute (ICAR), India
Natalie Laibach,
Centre for Research in Agricultural Genomics, Spanish National Research Council (CSIC), Spain

*CORRESPONDENCE
Ryo Matsumoto
r.matsumoto@cgiar.org

†PRESENT ADDRESS
Kanako Takada,
Japan International Research Center for Agricultural Sciences, Tsukuba, Ibaraki, Japan

SPECIALTY SECTION
This article was submitted to Crop and Product Physiology, a section of the journal Frontiers in Plant Science

RECEIVED 20 June 2022
ACCEPTED 14 September 2022
PUBLISHED 12 October 2022

CITATION
Matsumoto R, Asfaw A, Ishikawa H, Takada K, Shiwachi H and Asiedu R (2022) Biomass production and nutrient use efficiency in white Guinea yam (*Dioscorea rotundata* Poir.) genotypes grown under contrasting soil mineral nutrient availability. *Front. Plant Sci.* 13:973388. doi: 10.3389/fpls.2022.973388

COPYRIGHT
© 2022 Matsumoto, Asfaw, Ishikawa, Takada, Shiwachi and Asiedu. This is an open-access article distributed under the terms of the Creative Commons Attribution License (CC BY). The use, distribution or reproduction in other forums is permitted, provided the original author(s) and the copyright owner(s) are credited and that the original publication in this journal is cited, in accordance with accepted academic practice. No use, distribution or reproduction is permitted which does not comply with these terms.

Biomass production and nutrient use efficiency in white Guinea yam (*Dioscorea rotundata* Poir.) genotypes grown under contrasting soil mineral nutrient availability

Ryo Matsumoto[1*], Asrat Asfaw[1], Haruki Ishikawa[1], Kanako Takada[2†], Hironobu Shiwachi[2] and Robert Asiedu[1]

[1]International Institute of Tropical Agriculture, Ibadan, Nigeria, [2]Tokyo University of Agriculture, Tokyo, Japan

Yam (*Dioscorea* spp.) is of great importance to food security, especially in West Africa. However, the loss of soil fertility due to dwindling fallow lands with indigenous nutrient supply poses a challenge for yam cultivation. This study aimed to determine shoot and tuber biomass and nutrient use efficiency of white Guinea yam (*Dioscorea rotundata*) grown under low- and high-NPK conditions. Six white Guinea yam genotypes were used in field experiments conducted at Ibadan, Nigeria. Experiments were conducted with low soil NPK conditions with zero fertilizer input and high soil NPK conditions with mineral fertilizer input. Differences in response to soil NPK conditions, nutrient uptake, and nutrient use efficiency (apparent nutrient recovery efficiency) were observed among the tested genotypes. The genotypes TDr1499 and TDr1649, with high soil fertility susceptibility index (SFSI>1) and an increase in shoot and tuber biomass with fertilizer input, were recognized as susceptible to soil NPK conditions. There was a marked difference in apparent nutrient recovery efficiency; however, there was no varietal difference in physiological efficiency. Differences in apparent nutrient recovery efficiency among genotypes affected the fertilizer response (or susceptibility to soil NPK conditions) and the nutrient uptake. In contrast, the genotype TDr2029, with SFSI<1 and low reduction in shoot and tuber production between non-F and +F conditions, was recognized as a less susceptible genotype to soil NPK status. It was revealed that NPK fertilization did not reduce tuber dry matter content, regardless of genotype differences in susceptibility to soil NPK conditions. Hence, this could be helpful to farmers because it implies that yield can be increased without reducing tuber quality through a balanced application of soil nutrients. Our results highlight genotypic variation in sensitivity to the soil NPK availability, nutrient uptake, and nutrient use efficiency white Guinea yam. Differences in susceptibility to soil NPK conditions could be due to the genotypic variations in nutrient recovery efficiency white Guinea yam. Our findings could contribute to breeding programs for the development of

improved white Guinea yam varieties that enhance productivity in low soil fertility conditions with low and high-input farming systems.

KEYWORDS

nutrient recovery efficiency, nutrient uptake, fertilizer response, low soil fertility, West Africa, genotypic variation

Introduction

Yam (*Dioscorea* spp.) is a multispecies tuberous crop with immense potential for improving food security, especially with respect to the food and cultural systems of West Africa (Asiedu and Sartie, 2010); about 93% (66.8 million tons) of the global yam production occurs in this region (FAOSTAT, 2021). Among the species of *Dioscorea*, which vary in origin and distribution depending on tropical, subtropical, and temperate regions (Darkwa et al., 2020), white Guinea yam (*Dioscorea rotundata*) is predominantly cultivated and consumed in West Africa (Asfaw et al., 2020). The cultivation of white Guinea yam has steadily increased over the past few decades in West Africa, from 14.5 million tons in 1988 to 66.8 million tons in 2018 (FAOSTAT, 2021). The substantial increase in yam production has mainly been attributed to the expansion of the cultivation area rather than the productivity increase per unit area (FAOSTAT, 2021). The increase in yam productivity was marginal compared to that of potatoes (FAOSTAT, 2021).

In West Africa, yams are usually cultivated without chemical or organic fertilizers, often using landraces (Degras, 1993; Scott et al., 2000; Maliki et al., 2012). Traditionally, yam is the first crop after a long-term fallow because it requires fertile soils for optimum growth and yielding potential (Carsky et al., 2010). Diby et al. (2011a) reported that tuber yield was higher in fertile forest soils than in low-fertile savannah sites. It was suggested that soil fertility is crucial in yam cultivation. Similarly, Kassi et al. (2017) reported that soil organic carbon stocks contributed to the increased tuber yield, as *D. rotundata* crops harvested after *Chromoleana odorata* (green fertilizer) fallows produced the maximum yield. Consequently, yam producers perceive the decline in soil fertility as a critical constraint for yam production in areas under intensive cultivation (Lebot, 2019). Despite this, fertilizer use in Sub-Saharan Africa is generally low, partly because farmers do not recognize adequate profit opportunities with acceptable risks (Kaizzi et al., 2017).

The impact of fertilizer application on yam productivity remains unresolved due to several conflicting reports. While some studies have reported positive effects (Irving, 1956; Kpeglo et al., 1981; Lyonga, 1981; Diby et al., 2009; Diby et al., 2011c), others have reported no changes in that productivity (Kang and Wilson, 1981; Carsky et al., 2010). These discrepancies on the impact of fertilizer application on yam growth and yield could be attributed to the nutrient status of the experimental plots, as response to fertilization is affected by the soil fertility of the cultivation area. In the nutrient-poor savanna soils of Africa, the impact of fertilizer input on yam crops was positive, while it was significantly lower in the relatively fertile forest soils (Lugo et al., 1993; Diby et al., 2009; Diby et al., 2011c). Nevertheless, considering soil nutrient status, suitable fertilizer input can benefit crop yield. For example, several studies have reported that appropriate fertilizer application positively affected yam productivity in Sub-Saharan Africa (Lugo et al., 1993; Diby et al., 2009; Diby et al., 2011c; Cornet et al., 2022). Therefore, various soil management techniques are currently being developed, tested, and implemented to improve crop productivity in low-input farming systems in Africa (Kihara et al., 2020).

Matsumoto et al. (2021a) reported differential responses of white Guinea yam genotypes to available soil nutrients and identified genotypes with low soil nutrient tolerance and a high response to applied fertilizer. One of the factors for the difference in fertilizer response and tolerance to low-fertility soil among varieties is the difference in nutrient use efficiency (El-Sharkawy et al., 1998; Martí and Mills, 2002; Tamele et al., 2020). A better understanding of the physiological mechanism of fertilizer response and tolerance to low soil fertility is important for selecting and developing varieties suitable for cultivation under low fertilizer input and improving fertilizer utilization. However, there is little research on this aspect. Interspecific variation in nutrient uptake and nutrient use efficiency has been reported in *D. alata* and *D. rotundata* (Diby et al., 2011b; Hgaza et al., 2019); however, whether varietal differences exist in terms of nutrient uptake and nutrient use efficiency remains unknown. Although tuber dry matter content is a crucial characteristics highly valued by traders and consumers (Chukwu et al., 2007; Asiedu and Sartie, 2010), limited information is available regarding the effect of fertilizer on the percent dry matter content and its relationship with a fertilizer response of genotype. This study aimed to determine the biomass production and tuber dry matter content of different genotypes of white Guinea yam and their response to fertilizer input in terms of nutrient

uptake and nutrient use efficiency. Our results would contribute to the development of cultivation techniques and varieties of white Guinea yam for improved biomass production and fertilizer response.

Materials and methods

Site and soil properties

Field experiments were conducted during the 2017 and 2018 cropping seasons (April to December) in the experimental field with low soil fertility at the International Institute of Tropical Agriculture (IITA), Ibadan, Nigeria (7° 29′ N, 3° 54′ E). The low soil fertility field was induced artificially by successive planting of cassava, maize, and sorghum, without fertilizer input in IITA, Ibadan (Matsumoto et al., 2021a). To assess the soil properties in the experimental field, soil samples were collected before conducting the experiment at depths of 0–20 cm from 30 randomly selected plots. Soil pH was determined by initially suspending the soil in water (1:2.5 soil:water ratio). Exchangeable Ca^{2+}, Mg^{2+}, K^{+}, and available P were extracted according to the Mehlich-3 procedure (Mehlich, 1984). Cations were determined using an atomic absorption spectrophotometer (Accusys 211 Atomic Spectrophotometer, Buck Scientific, Connecticut, USA). P was assayed by colorimetric determination using a Genesys 10S UV-Vis spectrophotometer (Thermo Scientific, Waltham, MA, USA). Organic carbon was determined by chromic acid digestion with a spectrophotometric procedure using Genesys 10S UV-Vis spectrophotometer (Heanes, 1984). Total N was determined using the Kjeldahl method for digestion and colorimetric determination using a Technicon AAII Autoanalyzer (Seal Analytical, Wisconsin, USA) (Bremner and Mulvaney, 1982). Weather data for the experimental period were assessed using the data obtained from the Geographical Information System (GIS) unit of the IITA. Figure 1 presents the meteorological conditions during the growth period, from planting to harvest (180 days after planting) for the trials. The total precipitation and average minimum/maximum temperatures for this period were 1410.5 mm, 22.7/30.7°C in 2017, and 1526.5 mm, 22.7/30.5°C in 2018, respectively.

Plant materials and trial management

Field experiments were conducted using six genotypes of white Guinea yam. TDr1649 and TDr2484 were used in the 2017 field trial, while TDr1499, TDr1649, TDr1899, TDr2029, TDr2484, and TDr2948 were used for the 2018 trial. These genotypes are part of the mini-core collection of white Guinea yam (Pachakkil et al., 2021) maintained at the IITA. Those genotypes were selected based on the tuber yield and leaf density difference (Table 1). All the genotypes were multiplied under uniform conditions in the field at IITA headquarters during the 2016 and 2017 cropping seasons to generate high-quality planting material. Plants with symptoms of viral diseases, such as yam mosaic virus, were removed from the field during the growing period. Visually assessed clean tubers with no signs of rot or pests were used as seed tuber materials for the trials. Tubers weighing approximately 1–2 kg were cut horizontally to remove the head and tail components. The tuber centre component was cut into 50 ± 10 g pieces to obtain uniform material for planting (yam setts). Yam setts were treated with a

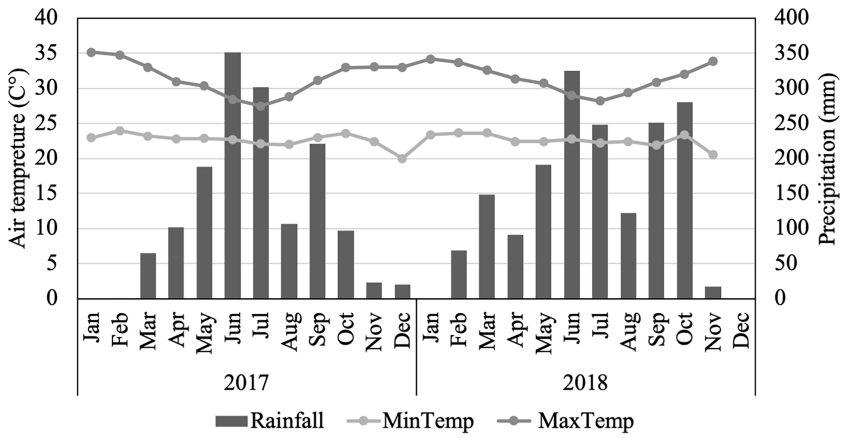

FIGURE 1
Air temperature and precipitation during the growth periods at the International Institute of Tropical Agriculture (IITA) Ibadan, Nigeria, in 2017 and 2018. Air temperature includes a black line and grey line representing maximum and minimum air temperature averages, respectively. For precipitation, data are cumulative values for every month.

10.3389/fpls.2022.973388

TABLE 1 Variation in tuber yield (g plant^{-1}) and leaf density in the white Guinea yam (*Dioscorea rotundata*) mini-core collection and the distribution of the used genotypes.

	Leaf density	Fresh tuber yield (g plant^{-1})
Mini-core collection (n=102)		
Mean	1.9	1234.9
Standard deviation	0.5	493.0
Coefficient of variance (%)	26.5	39.9
Genotype selected from mini-core collection		
TDr1499	2.7a	2726.0a
TDr1649	2.1b	2107.7ab
TDr1899	2.0b	1456.3b
TDr2029	2.0b	1401.0b
TDr2484	2.0b	2065.3ab
TDr2948	2.0b	1562.7b

The leaf density of plants was rated on a scale of 1 to 3 where 1= low, 2 = intermediate, and 3= high. Leaf density was recorded based on yam descriptors approximately 100 days after germination as the middle growth stage. Each point represents the mean of six data points. Different letters in the same column indicate significant differences ($p<0.05$) as determined by Tukey's HSD test. Data were obtained from a field evaluation at the International Institute of Tropical Agriculture (IITA) in 2014 (Pachakkil et al. (2021).

mixture of 70 g mancozeb (fungicide) and 75 mL chlorpyrifos (insecticide) dissolved in a 10 L volume of tap water for 5 min, and the setts were dried for 20 h in the shade before planting for pre-sprouting. The yam setts were planted in plastic pots (12 cm diameter × 10 cm height) filled with topsoil on 4 May 2017 and 2 May 2018. Because variation in the sprout emergence time was the main cause of variation in shoot biomass size and tuber yield within plots in yam trials (Cornet et al., 2014), seedlings that germinated simultaneously (within 14 days difference in sprout emergence date) were selected and used as experimental material in this study. Plants with uniform sprouts were transplanted into the field in a 0.5 m × 1.0 m arrangement to give 20,000 plants per hectare. A 2 m stake was provided for each plant at 30 days after planting.

The plants were transplanted into the field on a ridge approximately 40 cm high and 60 cm wide. The field experiment was laid out in a split-plot randomized block design with four replications. The main plot comprised two levels of fertilizer treatments, non-fertilized (Non-F) and fertilized (+F), while the subplot consisted of genotypes. The size of the subplot was 15 m^2. The fertilized plot (+F) received 90, 50, and 75 kg nitrogen (N), phosphorus (P), and potassium (K) per hectare, respectively. These were based on the recommendations of fertilizer amounts for low soil fertility conditions (Chude et al., 2012). In the 2017 trial, the total number of plots was 16 (two soil nutrient fertility levels × 2 genotypes × 4 replications) (detailed field design presented in Supplementary Material 1). In the 2018 trial, the total number of plots was 48 (two soil nutrient fertility levels × 6 genotypes × 4 replications) (detailed field design presented in Supplementary Material 2). Fertilizer was applied 14 days after transplanting using the side dressing method in both the 2017 and 2018 trials. To avoid fertilizer contamination, there was a 20 m distance between the non-fertilized and fertilized plots. Weeds were manually removed whenever present to maintain weed-free plots throughout the experiment.

Evaluation of shoot and tuber productivity under different soil fertility

At 180 days after planting, three plants from each subplot were selected randomly, excluding border plants in both the 2017 and 2018 trials, to analyse the effect of soil NPK conditions on shoot and tuber production. The total number of harvested samples was 12 (three plants × 4 replicates) for each genotype in both the 2017 and 2018 trials. Harvested plants were separated into leaves, stems, and tubers. Plant parts were rinsed with tap water. The total weight of fresh tuber was recorded. All leaves, stems, and a weighed sample of the tubers were dried in an oven at 80°C for three days. Dried samples were weighed to determine the total leaf and stem dry weights. The percent dry matter content of the tuber was calculated from the dry weight of the tuber sample in relation to its fresh weight. The total tuber dry weight was determined by multiplying the total fresh tuber weight by the percent dry matter content of the tuber. The percentage difference in dry shoot weight and dry tuber weight due to the difference in NPK conditions was calculated using the following formula:

$$Percentage\ difference\ (\%) = \left(\frac{\overline{xhf} - \overline{xlf}}{\overline{xhf}}\right) \times 100$$

where $\overline{xlf}$ and $\overline{xhf}$ are the mean trait values of a given genotype in non-F and +F environments, respectively.

Soil fertility susceptibility index (SFSI) was calculated using the following formula (Fischer and Maurer, 1978):

$$\textit{Soil fertility susceptibility index (SFSI)} = \left(1 - \frac{\overline{xlf}}{\overline{xhf}}\right) / \left(1 - \frac{\overline{Ylf}}{\overline{Yhf}}\right)$$

where $\overline{xlf}$ and $\overline{xhf}$ are the mean trait values of a given genotype under the non-F and +F conditions, respectively. $\overline{Ylf}$ and $\overline{Yhf}$ are the mean trait values of all genotypes under the non-F and +F conditions, respectively, and $1 - \overline{Ylf}/\overline{Yhf}$ is the soil fertility intensity index.

Nutrient uptake and use efficiency

Dried leaf and tuber samples from the 2018 trial were used to determine the nutrient content in plants. Dried leaf and tuber tissues were ground separately in a Wiley mill and passed through a ≤1 mm mesh screen. As per pre-standard methods, an NC analyser (Sumigraph NCH-22, Sumika Chemical Analysis Service Ltd., Japan) was used to determine the nitrogen content in leaf and tuber tissues (Anderson and Ingram, 1993). Ground dry plant samples (100 mg) samples were pyrolyzed with 5 mL of nitric acid, and the filtered samples were analysed to determine the P and K content in leaves and tubers using inductively coupled plasma optical emission spectrometry (ICP-OES; iCAP 6000 Series, Thermo Fisher Scientific, MA, United States). The N, P, and K uptakes by the plants was determined by adding the product of the dry weight of each plant part with the elemental concentration of each plant part. In the current study, the following fertilizer efficiency parameters were used (Craswell and Godwin, 1984):

$$\text{Apparent nutrient recovery efficiency} = (U_{tF} - U_{tN})/F \times 100$$

$$\text{Physiological efficiency} = (T_{wF} - T_{wN})/(U_{tF} - U_{tN})$$

where U_{tF} is total nutrient uptake in plants under +F condition. U_{tN} is total nutrient uptake in plants under non-F condition; F is nutrient supply (g/plant); T_{wF} is dry tuber weight under +F condition; T_{wN} is dry tuber weight under non-F condition. Apparent nutrient recovery efficiency was calculated as the efficiency of nutrient capture from soil and/or fertilizer input. Physiological efficiency was calculated as the efficiency of capturing plant nutrients in tuber yield.

Statistical analysis

Data were analysed using the linear mixed model in the lme4 package (Bates, 2010) in the R environment version 4.0.3 for statistical computing (R Core Team, 2018). To determine a significant difference between the mean values of traits obtained from non-F and +F conditions for each genotype, t-test was performed using the R package ggpubr (Kassambara, 2020). Multiple comparison analysis using Tukey's HSD test was performed to detect statistically significant differences in the obtained traits among varieties using the agricolae package (de Mendiburu, 2021). Correlation analysis among the tested parameters was determined using Pearson correlation coefficients. In all calculations, statistical significance was set at $p < 0.05$.

Results

Soil properties at the experimental sites in 2017 and 2018

The soil chemical properties of the experimental fields are presented in Table 2. Soil pH was 5.69 in 2017 and 5.98 in 2018. The organic carbon content was 0.24% and 0.39% in 2017 and 2018, respectively. No total N content change was observed between the 2017 and 2018 trials (0.04%). The available P content in 2017 (1.18 mg kg^{-1}) was lower than that in the 2018 trial (2.21 mg kg^{-1}). Exchangeable Ca and Mg in 2017 were higher than in those in the 2018 trial. Exchangeable K was 0.20 cmol[+] kg^{-1} in 2017, which was higher than that in 2018 (0.08 cmol[+] kg^{-1}).

Effect of fertilizer treatment on shoot and tuber production

The effect of fertilizer application on dry tuber weight in the 2017 trial is presented in Figure 2. Fertilizer application increased the dry tuber weight of TDr1649 plants in 2017 experimental trial. However, there was no significant difference in the dry tuber weight of TDr2484 grown between the non-F and +F conditions.

In the 2018 trial, genotype and fertilizer application interactions were significant for the dry shoot weight (Table 3 and Supplementary Material 3). Although the difference was not statistically significant, the shoot dry weight of TDr1499 was the highest among the tested genotypes. However, there was a significant difference in the dry shoot weight among the tested genotypes under +F condition, and the highest dry shoot weight was observed in TDr1499 (Table 3). The percent difference in dry shoot weight due to non-fertilizer application ranged from 14.3% (TDr2029) to 41.1% (TDr1499). SFSI for dry shoot weight ranged from 0.46 to 1.31. Among the genotypes tested under the two different fertilizer treatments, TDr1499 and TDr1649 produced significantly higher dry shoot weights in the +F condition than in the non-F state (Table 3).

Although dry tuber weight in non-F conditions ranged from 155.8 g $plant^{-1}$ (TDr1899) to 260.7 g $plant^{-1}$ (TDr2948), no significant difference was observed among the tested genotypes.

10.3389/fpls.2022.973388

TABLE 2 Soil chemical properties of the experimental site at IITA Ibadan, Nigeria.

Soil chemical properties	2017		2018	
	Mean	SD (n=6)	Mean	SD (n=6)
pH	5.69	0.21	5.98	0.04
Organic carbon (%)	0.24	0.04	0.39	0.11
Total nitrogen (%)	0.04	0.02	0.04	0.00
Available phosphorus (mg kg^{-1})	1.18	0.82	2.21	0.91
Calcium (cmol[+] kg^{-1})	2.90	0.46	0.75	0.14
Magnesium (cmol[+] kg^{-1})	0.69	0.11	0.23	0.11
Potassium (cmol[+] kg^{-1})	0.20	0.07	0.08	0.01

SD, standard deviation.

Under the +F conditions, TDr1499 had the highest dry tuber weight (489.9 g $plant^{-1}$), while TDr1899 had the lowest dry tuber weight (239.0 g $plant^{-1}$) among the tested genotypes. Genotype TDr1499 showed a 51.9% reduction in dry tuber weight in the non-F condition compared to that in the +F condition. The lowest reduction in dry tuber weight of 17.2% was recorded for the genotype TDr2029. The SFSI for dry tuber weight ranged from 0.48 to 1.44. Among the genotypes tested under the two different fertilizer conditions, TDr1499 and TDr1649 produced significantly higher dry tuber weights in the +F condition than in the non-F state (Table 3 and Supplementary Material 3).

Genotype was significant for the percent dry matter content of the tuber (Table 4). The effect of genotype and fertilizer treatment interaction on tuber percent dry matter content was not observed (Table 4). Fertilizer application did not increase the percent dry matter content of the tuber in all genotypes. Under the non-F conditions, TDr1649 (31.2%), TDr1899 (32.5%), and TDr2029 (31.0%) had a significantly higher dry matter content of tuber than TDr2428 (25.5%). TDr1649 and TDr1899 showed higher percent dry matter content of tuber than TDr1499, TDr2029, TDr2484, and TDr2048 under +F conditions (Table 4).

Nutrient uptake

Fertilizer treatment increased the N and K uptake of TDr1499 and TDr1649. The interaction between genotype and

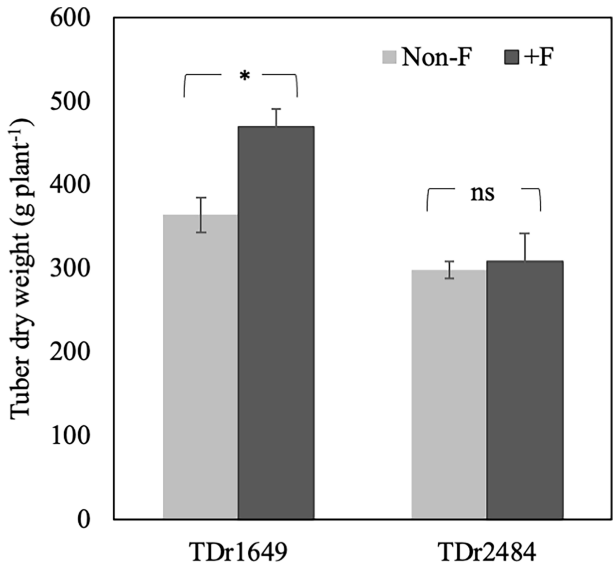

FIGURE 2
Effect of fertilizer treatment on dry tuber weight (g $plant^{-1}$) in two white Guinea yam (*Dioscorea rotundata*) genotypes in 2017. * represents a significant difference at $p< 0.05$ calculated by t-test between non-fertilized (non-F) and fertilized (+F) conditions. ns; significant difference at $p < 0.05$ calculated by t-test between non-fertilized (non-F) and fertilized (+F) conditions.

10.3389/fpls.2022.973388

TABLE 3 Effect of genotype and fertilizer treatment on the shoot and tuber weight in six white Guinea yam (*Dioscorea rotundata*) genotypes In the 2018 trial.

	Dry shoot weight (g plant^{-1})						Dry tuber weight (g plant^{-1})					
	Non-F	+F	Mean	PD	SFSI	p-value	Non-F	+F	Mean	PD	SFSI	p-value
TDr1499	76.9a	130.5a	103.7a	41.1	1.31	0.00	235.5a	489.9a	362.7a	51.9	1.44	0.00
TDr1649	64.5a	108.1ab	86.3ab	40.3	1.28	0.01	235.8a	433.3ab	334.5ab	45.6	1.26	0.01
TDr1899	45.3a	60.7c	53.0bc	25.5	0.81	0.29	155.8a	239.0d	197.4b	34.8	0.96	0.10
TDr2029	48.3a	56.4c	52.4c	14.3	0.46	0.60	260.0a	313.8bcd	286.9ab	17.2	0.48	0.41
TDr2484	48.6a	63.7c	56.2bc	23.7	0.75	0.12	200.0a	262.5cd	231.2ab	23.8	0.66	0.09
TDr2948	57.8a	78.3bc	68.1bc	26.2	0.83	0.14	260.7a	370.3bcd	315.5ab	29.6	0.82	0.08
Mean	56.9	83.0					224.6		351.5			
Type II Wald chi-square tests (Chisq)												
Genotype (G)	30.7***						69.0***					
Treatment (T)	66.2***						23.6***					
Interaction G × T	12.4*						13.0*					

Non-F, non-fertilized; +F, fertilized. PD, percent difference due to contrasting soil mineral nutrient conditions. SFSI, soil fertility susceptibility index. Different letters in the same column indicate significant difference ($p<0.05$) as determined by Tukey's HSD test. ***$p < 0.001$, *$p < 0.05$, analysed by t-test between -F and +F conditions.

fertilizer treatment was significant for P uptake ($p< 0.001$) (Table 5). The difference in genotype did not affect P uptake under non-F conditions. However, P uptake varied with genotype differences under +F conditions (Table 5). The genotypes TDr1499, TDr1649, and TDr2948 accumulated higher P than TDr1899, TDr2029, and TDr2484 under +F conditions. N uptake (g plant^{-1}) by the genotypes was 7.0 to 9.7 times higher than that of P under non-F conditions, whereas N uptake was 5.8 to 7.7 times higher than that of P under the +F conditions. Similarly, the K uptake (g plant^{-1}) was 5.7 to 9.5 times higher in the non-F condition compared to that of P, which was 4.7 to 6.3 times higher in the +F condition (Table 5).

Nutrient use efficiency parameters

Apparent nutrient recovery efficiency and physiological efficiency that already include the response to soil nutrient level were estimated considering varietal differences. Varietal difference in the apparent nutrient recovery efficiency was observed among the tested genotypes (Figure 3). Nitrogen apparent nutrient recovery efficiency ranged from 14.7 (TDr2484) to 47.7% (TDr1499). Nitrogen apparent nutrient recovery efficiency of TDr1499 was significantly higher than that of TDr1899, TDr2029, TDr2484, and TDr2948. Similar results were observed with apparent nutrient recovery efficiency for phosphorus and potassium.

TABLE 4 Effect of genotype and fertilizer treatment on percent dry matter content of tuber (%) in six white Guinea yam (*Dioscorea rotundata*) genotypes in the 2018 trial.

	Non-F	+F	p-value
TDr1499	27.8ab	28.6b	0.37
TDr1649	31.2a	34.1a	0.22
TDr1899	32.5a	33.1a	0.39
TDr2029	31.0a	29.3b	0.56
TDr2484	25.5b	27.0b	0.49
TDr2948	28.2ab	28.7b	0.51
Mean	29.37	30.13	
Type II Wald chi square tests (Chisq)			
Genotype (G)	94.2***		
Treatment (T)	0.7		
Interaction G x T	7.5		

Non-F, non-fertilized; +F, fertilized. Different letters in the same column indicate significant difference ($p<0.05$) as determined by Tukey's HSD test. p-value was calculated using t-test between -F and +F conditions. ***$p < 0.001$, analysed by t-test between -F and +F conditions.

TABLE 5 Effect of genotype and fertilizer treatment on the uptake of nitrogen, phosphorus, and potassium in six white Guinea yam (*Dioscorea rotundata*) genotypes in the 2018

	Nitrogen uptake(g plant^{-1})			Phosphorus uptake(g plant^{-1})			Potassium uptake(g plant^{-1})		
	Non-F	+F	p-value	Non-F	+F	p-value	Non-F	+F	p-value
TDr1499	2.6a	4.7a	0.00	0.3a	0.8a	0.00	2.2a	3.9a	0.01
TDr1649	2.2a	3.7ab	0.01	0.3a	0.6a	0.00	2.0a	2.8b	0.10
TDr1899	1.5a	2.3c	0.11	0.2a	0.3b	0.14	1.4a	1.9b	0.16
TDr2029	2.1a	2.9bc	0.26	0.3a	0.4b	0.12	1.7a	2.1b	0.48
TDr2484	1.9a	2.6bc	0.07	0.2a	0.4b	0.07	1.7a	2.1b	0.29
TDr2948	2.9a	3.5ab	0.43	0.3a	0.6a	0.01	2.1a	2.9ab	0.13
Mean	2.2	3.3		0.3	0.5		1.9		2.6
Type II Wald chi-square tests (Chisq)									
Genotype (G)	38.4***			66.8***			33.9***		
Treatment (T)	31.2***			87.8***			17.1***		
Interaction G x T	8.6			28.4***			9.9		

Non-F, non-fertilized; +F, fertilized. Different letters in the same column indicate significant differences difference ($p<0.05$) as determined by Tukey's HSD test. ***$p < 0.001$, analysed by t-test between -F and +F conditions.

Nitrogen physiological efficiency did not differ among the tested genotypes (p = 0.141). Similar results were observed in potassium physiological efficiency (p = 0.780). Phosphorus physiological efficiency showed high values, which ranging from 462.2 to 690.7 g plant^{-1}; however, varietal difference was not observed significantly among the tested genotypes (p = 0.208).

Correlation analysis among tested parameters (dry tuber weight and nutrient uptake)

The correlation between dry tuber weight and nutrient uptake is presented in Figure 4. The dry tuber weight and N uptake were strongly and positively correlated in the non-F and the +F groups, respectively: r = 0.83 (p = 0.04) and 0.98 (p = 0.00). A similar trend was obtained between the relationship between the P and K uptake and dry tuber weight.

Discussion

Soil fertility in Nigeria has been categorized into five levels (Chude et al., 2012). Although the critical soil nutrient levels for yam cultivation have not yet been established in West Africa, yam cultivation in soils containing< 0.1% N,< 10 mg kg^{-1} available P, and 0.15 Cmol[+] kg $^{-1}$ of exchangeable K requires external fertilizer inputs (Carsky et al., 2010). According to soil analysis performed before the experiments and previous reports by Chude et al. (2012) and Carsky et al. (2010), our experimental field in both the 2017 and 2018 trials had low soil NPK availability and could be inferred as infertile to sustain normal yam plant growth and optimize the yield

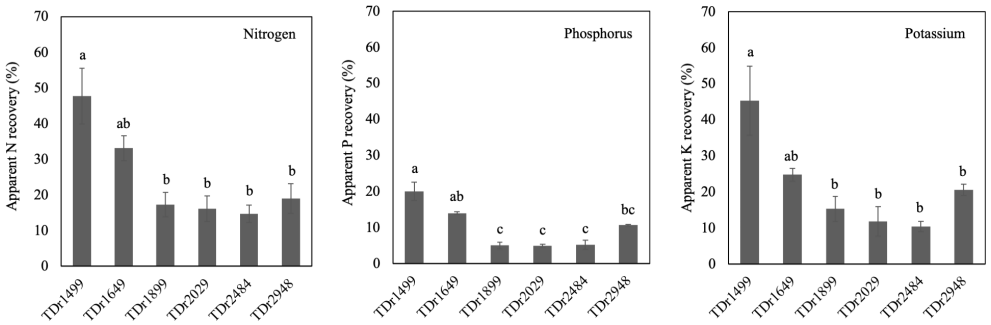

FIGURE 3
Apparent nutrient recovery efficiency of six genotypes in white Guinea yam (*Dioscorea rotundata*). Nitrogen (left box), phosphorus (centre box), and potassium physiological efficiency (right box) are shown. All values are expressed as means. Different alphabet indicates statistical significance (P< 0.05). Bars represent presents a standard error.

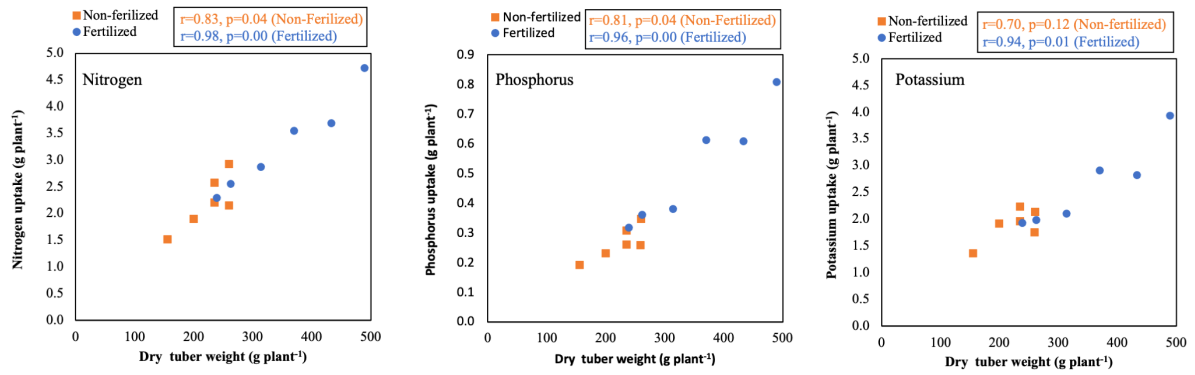

FIGURE 4
Correlation between dry tuber weight and nutrient uptake under non-fertilized and fertilized conditions in six white Guinea yam (*Dioscorea rotundata*) genotypes. Relationships for nitrogen (left box), phosphorus (centre box), and potassium (right box) uptake are shown.

(Table 2). It is, therefore, more likely to observe the positive effect of added fertilizer input in the growth and yield of yam under low soil fertility conditions. However, the fertilizer response to biomass production and tuber yield varied among the genotypes studied, suggesting that the response of soil NPK levels or fertilizer input in white Guinea yam could be genotype-specific (Figure 2, Table 3, and Supplementary Material 3).

Our results indicated differences among the white Guinea yam genotypes in the nutrient uptake (Table 5). The studied white Guinea yam genotypes absorbed N and K as primary nutrients during growth and showed an increase in tuber yield with an increase in nutrient uptake (Figure 4); this is also consistent with the results presented by Diby et al. (2011b) and Irizarry et al. (1995). The genotypes TDr1499 and TDr1649, with high response to fertilizer input, showed higher nutrient uptake than the other genotypes. In other words, the genotypes depended on the high soil fertility to exhibit high productivity. Thus, the genotypes TDr1499 and TDr1649, of Togolese origin, were responsive to fertilizer input and could be suitable candidates to maximize productivity under a high-input cultivation system.

The effect of fertilizer application on yam tuber yield is variable and sometimes conflicting (Irving, 1956; Kang and Wilson, 1981; Kpeglo et al., 1981; Lyonga, 1981; Diby et al., 2009; Carsky et al., 2010; Diby et al., 2011c). Diby et al. (2009) and Carsky et al. (2010) discussed differences in the reports on the beneficial impact of fertilizer application on yam growth and yield could be attributed to the nutrient status of the cultivation area. Dare et al., (2010, 2013, 2014) reported the potential influence of arbuscular mycorrhizal fungi that occur naturally in the yam growing areas in some of the observed variability.

This study revealed, for the first time, that there are varietal differences in the apparent recovery efficiency of white Guinea yam (Figure 3). Hgaza et al. (2019) also reported interspecific variations between the *D. alata* and *D. rotundata* genotypes in nitrogen uptake and apparent nitrogen recovery efficiency (total nitrogen uptake from fertilizer/total nitrogen rate applied × 100). Nutrient uptake in studied white Guinea yam genotypes increased with an apparent increase in nutrient recovery efficiency under +F conditions but not in physiological nutrient efficiency. This suggests the difference in nutrient recovery efficiency affected the fertilizer response or susceptibility to soil NPK condition in the white Guinea yam.

Species or cultivars with a high growth rate usually respond more favorably to fertilizer application than those with low growth rates (Mengel, 1983). Our result corroborates the findings of Mengel (1983). The fertilizer-responsive genotypes, TDr1499 and TDr1649, produced more vigorous shoot biomass than the other genotypes, which did not respond to applied fertilizer (Table 3). Therefore, the size of shoot biomass or leaf density as a morphological traits, associated with plant demand for nutrients, might be a factor contributing to varietal difference in fertilizer or soil NPK responsiveness among the tested genotypes.

Iseki et al. (2022) reported a positive correlation between shoot biomass and tuber yield and pointed out that shoot growth is important for final tuber yield. Therefore, increasing shoot growth by fertilizer application may improve tuber yield in white Guinea yam genotypes with a high response to fertilizer input. TDr1499 and TDr1649 were responsive to the fertilizer input with increased nutrient uptake, indicating that they can exhibit high productivity under high nutrient input. Productivity improvement in white Guinea yam in West Africa could be expected by combining appropriate fertilization techniques (Cornet et al., 2022) and genotypes that respond well to fertilizer under a high input system.

In contrast to TDr1499 and TDr1649, the genotypes TDr1899, TDr2029, TDr2484, and TDr2948 showed SFSI<1 and a reduction in shoot and tuber production from +F to non-F conditions (Table 3). These results indicate that these genotypes were tolerant to low soil NPK conditions or less susceptible to soil NPK status. Among the genotypes, TDr2029

was the least sensitive to soil NPK conditions. The genotypes with a high and stable yield of marketable tubers are selection targets for breeding programs for yam (Otoo et al., 2006; Asiedu and Sartie, 2010). Hence, TDr2029, of Nigerian origin, could be a potential parent to generate varieties with a stable yield and less sensitive to soil fertility conditions or the best candidate for immediate release as a new variety for the low input system in West Africa.

Likewise the tuber yield, the percent dry matter content of the tuber also varied among genotypes in white Guinea yam (Table 4). This result was consistent with Matsumoto et al. (2021b), who investigated the genotype × environment interaction on tuber quality traits on white Guinea yam. However, the application of NPK fertilizer did not affect the percent tuber dry matter content, regardless of the genotype differences in susceptibility to soil NPK conditions. This means the application of NPK increased fresh tuber yield and hence dry tuber yield without significantly influencing percent dry matter content. This is helpful to farmers because it implies that yield can be increased without reducing tuber quality by using a balanced application of soil nutrients. This is contrary to the fears expressed by some farmers that fertilizer application will reduce yam tuber quality. Our result is in line with Gizachew et al. (2022), who reported that neither organic nor mineral fertilizer application affects cassava tuber quality.

In addition to fertilizer application and soil amendments, the use of cultivars with high nutrient use efficiency and responsiveness to external nutrient supply would improve productivity in the yam cultivation system under low soil fertility conditions (Asiedu and Sartie, 2010). Breeding efforts should, therefore, focus on attributes such as high yield and high nutrient use efficiency in yams. Our results highlight the genotypic variations in white Guinea yam with respect to susceptibility to soil NPK availability, nutrient uptake, and nutrient use efficiency. The wide diversity of fertilizer response or non-susceptibility to soil NPK status might be expected in the mini-core collection of white Guinea yam, confirming the wide range of tuber yield and leaf density (Pachakkil et al., 2021). The contrasting genotypes with unique characteristics of high and less susceptibility to soil nutrient conditions provide a good opportunity for further studies to elucidate the genetic and physiological bases for and the influence of genotype × environment (including soil microbes) interactions on the differential response to these major nutrients in yam. Our findings also serve as reference for breeding new and improved varieties for low and high-input cultivation systems in West Africa.

Data availability statement

The raw data supporting the conclusions of this article will be made available by the authors, without undue reservation.

Author contributions

Conceptualization, RM; methodology and formal analysis, RM and KT; investigation and fieldwork, RM and KT; writing-original draft preparation, RM; writing-review and editing, KT, HI, HS, AA and RA; project administration, HI; funding acquisition, HI. All authors contributed to the article and approved the submitted version.

Funding

This research was supported by the Ministry of Agriculture, Forestry, and Fisheries of Japan through the "MAFF yam project".

Acknowledgments

The authors wish to thank the International Institute of Tropical Agriculture (IITA) for allowing us to use their facilities. We acknowledge the IITA staff for their support. Part of the data used in this study was generated under the project "Use of genomic information and molecular tools for yam germplasm utilization and improvement for West Africa (EDITS-Yam; 2011-2015)" of the Japan International Research Center for Agricultural Science, in collaboration with the Iwate Biotechnology Research Center and the IITA.

Conflict of interest

The authors declare that the research was conducted in the absence of any commercial or financial relationships that could be construed as a potential conflict of interest.

Publisher's note

All claims expressed in this article are solely those of the authors and do not necessarily represent those of their affiliated organizations, or those of the publisher, the editors and the reviewers. Any product that may be evaluated in this article, or claim that may be made by its manufacturer, is not guaranteed or endorsed by the publisher.

Supplementary material

The Supplementary Material for this article can be found online at: https://www.frontiersin.org/articles/10.3389/fpls.2022.973388/full#supplementary-material

References

Anderson, J. M., and Ingram, J. S. (1993). *Tropical soil biology and fertility, a handbook of methods, second edition* (UK (Oxford: CAB International. Wallingford), P. 97.

Asfaw, A., Aderonmu, D. S., Darkwa, K., De Keoyer, D., Agre, P., Abe, A., et al. (2020). Genetic parameters, prediction, and selection in a white Guinea yam early-generation breeding population using pedigree information. *Crop Sci.*, 61 1038-1051. doi: 10.1002/cs2.20382

Asiedu, R., and Sartie, A. (2010). Crops that feed the world 1. yams. yams for income and food security. *Food Secur.* 2, 305–315. doi: 10.1007/s12571-010-0085-0

Bates, D. M. (2010). *R package "lme4"*. Available at: https://cran.Rproject.org/web/packages/lme4/lme4.pdf.

Bremner, J. M., and Mulvaney, C. S. (1982). Methods of soil analysis in *American Society of agronomy*. Eds. A. L. Page, R. H. Miller and D. R. Keeny (Madison: Soil Science Society of America), 1119–1123.

Carsky, R. J., Asiedu, R., and Cornet, D. (2010). Review of soil fertility management for yam-based systems in West Africa. *Afr. J. Root Tuber Crops* 8, 1–17.

Chude, V. O., Olayiwola, S. O., Osho, A. O., and Daudu, C. K. (2012). *Fertilizer use and management practices for crops in Nigeria* Vol. 215 (Abuja: Federal Fertilizer Department, Federal Ministry of Agricultural and Rural Development).

Chukwu, G. O., Osunde, A. O., Asiedu, R., and Ogbogu, N. J. (2007). Qualities of yam tubers grown on typic paleudults: Hybrid yam and fertilizer effects. *Sci. Res. Essa.* 2 (12), 508–511.

Cornet, D., Marcos, J., Tournebize, R., and Sierra, J. (2022). Observed and modeled response of water yam (*Dioscorea alata* L.) to nitrogen supply: Consequences for nitrogen fertilizer management in the humid tropics. *Eur. J. Agron.* 138, 126536. doi: 10.1016/j.eja.2022.126536

Cornet, D., Sierra, J., Tournebize, R., and Ney, B. (2014). Yams (*Dioscorea* spp.) plant size hierarchy and yield variability: Emergence time is critical. *Eur. J. Agron.* 55, 100–107. doi: 10.1016/j.eja.2014.02.002

Craswell, E. T., and Godwin, D. C. (1984). "The efficiency of nitrogen fertilizers applied to cereals grown in different climates," in *Advances in plant nutrition*. Eds. P. B. Tinker and A. Lauchli (Vol. 1: Praeger Publishers), 1–55.

Dare, M. O., Abaidoo, R. C., Fagbola, O., and Asiedu, R. (2010). Effects of arbuscular mycorrhizal inoculation and phosphorus application on yield and nutrient uptake of yams. *Commun. Soil Sci. Plant Anal.* 41, 22,2729–2743. doi: 10.1080/00103624.2010.518264

Dare, M. O., Abaidoo, R., Fagbola, O., and Asiedu, R. (2013). Diversity of arbuscular mycorrhizal fungi in soils of yam (*Dioscorea* spp.) cropping systems in four agroecologies of Nigeria. *Arch. Agron. Soil Sci.* 59 (4), 521–531. doi: 10.1080/03650340.2011.653682

Dare, M. O., Fagbola, O., Abaidoo, R., and Asiedu, R. (2014). Evaluation of white yam (*Dioscorea rotundata*) genotypes for arbuscular mycorrhizal colonization, leaf nutrient concentrations and tuber yield under NPK fertilizer application. *J. Plant Nutr.* 37, 2014.658–673. doi: 10.1080/01904167.2013.867988

Darkwa, K., Agre, P., Olasanmi, B., Iseki, K., Matsumoto, R., Powell, A., et al. (2020). Comparative assessment of genetic diversity matrices and clustering methods in white Guinea yam (*Dioscorea rotundata*) based on morphological and molecular markers. *Sci. Rep.* 10, 13191. doi: 10.1038/s41598-020-69925-9

Degras, L. (1993). *The yam. a tropical root crop* Vol. 408 (London: Macmillan Press Ltd).

de Mendiburu, F. (2021). Agricolae: Statistical procedures for agricultural research. In: *R package version 1.4.0*. Available at: https://cran.r-project.org/web/packages/agricolae/index.html (Accessed 27 September 2021).

Diby, L. N., Hgaza, V. K., Tié, T. B., Assa, A., Carsky, R., and Girardin, O. (2011b). Mineral nutrients uptake and partitioning in *Dioscorea alata* and *Dioscorea rotundata*. *J. Appl. Biosci.* 38, 2531–2539.

Diby, N. L., Hgaza, V. K., Tie, T. B., Assa, A., Carsky, R., Girardin, O., et al. (2009). Productivity of yams (*Dioscorea* spp.) as affected by soil fertility. *J. Anim. PlantSci.* 5, 494–506.

Diby, L. N., Hgaza, V. K., Tié, T. B., Assa, A., Carsky, R., Girardin, O., et al. (2011a). How does soil fertility affect yam growth? *Acta Agr. Scand.* 61, 448–457. doi: 10.1080/09064710.2010.505578

Diby, L. N., Tie, B. T., Girardin, O., Sangakkara, R., and Frossard, E. (2011c). Growth and nutrient use efficiencies of yams (*Dioscorea* spp.) grown in two contrasting soils of West Africa. *Int. J. Agron.* 2011, 175958. doi: 10.1155/2011/175958

El-Sharkawy, M. A., López, L. F., and Tafur, M. S. (1998). Nutrient use efficiency of cassava differs with genotype architecture. *Acta Agronómica* 48, 23–32.

FAOSTAT (2021). Available at: http://www.fao.org/faostat/en/#home (Accessed 19 Jan, 2022).

Fischer, R. A., and Maurer, R. (1978). Drought resistance in spring wheat cultivars. i. grain yield responses. *Aust. J. Agric. Res.* 29, 897–912. doi: 10.1071/AR9780897

Gizachew, K. B., Eyasu, E., and Ntawuruhunga, P. (2022). "Does the application of mineral and organic fertilizer affect cassava tuber quality? An evidence from zambia". *J. Agric. Food Res.* 9, 100339. doi: 10.1016/j.jafr.2022.100339

Heanes, D. L. (1984). Determination of total organic carbon in soils by an improved chromic acid digestion and spectrophotometric procedure. *Commun. Soil Sci. Plant Anal.* 15, 1191–1213. doi: 10.1080/00103628409367551

Hgaza, K. V., Oberson, A., Kiba, I. D., Diby, L. N., Ake, S., and Frossard, E. (2019). The nitrogen nutrition of yam (*Dioscorea* spp). *J. Plant Nutr.* 43, 64–78. doi: 10.1080/01904167.2019.1659315

Irizarry, H., Goenaga, R., and Chardon, U. (1995). Nutrient uptake and dry matter yield in the 'Gunung' yam (*Dioscorea alata*) grown on an ultisol without vine support. *J. Agric. Univ. P.R.* 79, 121–130.

Irving, H. (1956). Fertilizer experiments with yams in eastern Nigeria 1947-1951. *Trop. Agric. Trinidad* 33, 67–78.

Iseki, K., Olaleye, O., and Matsumoto, R. (2022). Effect of leaf thinning on shoot growth and tuber yield of white Guinea yam. *Plant Production Sci.* 25, 1,11–1,19. doi: 10.1080/1343943X.2021.1943466

Kaizzi, K. C., Mohammed, M. B., and Nouri, M. (2017). "Fertilizer use optimization: Principles and approach," in *Fertilizer use optimization in Sub-Saharan Africa*. Eds. C. S. Wortmann and K. Sones (Nairobi, Kenya: CAB International), 9–19.

Kang, B. T., and Wilson, J. E. (1981). Effect of mound size and fertilizer on white Guinea yam (*Dioscorea rotundata*) in southern Nigeria. *Plant Soil* 61, 319–327. doi: 10.1007/BF02182013

Kassambara, A. (2020). *R packag" "ggpu"r"*. Available at: https://cran.Rproject.org/web/packages/ggpubr/ggpubr.pdf.

Kassi, S.-P. A. Y., Koné, A. W., Tondoh, J. E., and Kofi, B. Y. (2017). Chromoleana odorata fallow-cropping cycles maintain soil carbon stocks and yam yields 40 years after conversion of native- to farmland, implications for forest conservation. *Agric. Ecosyst. Environ.* 247, 298–307. doi: 10.1016/j.agee.2017.06.044

Kihara, J., Bolo, P., Kinyua, M., Nyawira, S. S., and Somer, R. (2020). Soil health and ecosystem services: Lessons from sub-Sahara Africa (SSA). *Geoderma* 370, 114342. doi: 10.1016/j.geoderma.2020.114342

Kpeglo, K. D., Obigbesan, G. O., and Wilson, J. E. (1981). "Yield and shelf life of white yam as influenced by fertilizer" in *Tropical root crops: Research strategies for the 1980s. proceedings of the first triennial root crops symposium of the international society for tropical root crops-Africa branch*. Eds. E. R. Terry, K. A. Oduro and F. Cavenes (Ottawa: International Development Research Centre).

Lebot, V. (2019). "Tropical root and tuber crops: Cassava, sweet potato, yams and aroids," in *Crop production science in horticulture series 17* (Wallingford, CT: CABI). doi: 10.1079/9781789243369.0000

Lugo, W. I. H. M., González, A., Rafols, N., and Almodóvar, C. (1993). Tillage and fertilizer rate effects on yam yields (*Dioscorea alata* L.). *J. Agric. Univ. P.R.* 77, 153–159. doi: 10.46429/jaupr.v77i3-4.4203

Lyonga, S. N. (1981). "The economics of yam cultivation in cameroon," in *Tropical root crops: Research strategies for the 1980s. in proceedings of the first triennial root crops symposium of the international society for tropical root crops-Africa branch*. Eds. E. R. Terry, K. A. Oduro and F. Cavenes (Ottawa: International Development Research Centre).

Maliki, R., Toukourou, M., Sinsin, B., and Vernier, P. (2012). Productivity of yam-based systems with herbaceous legumes and short fallows in the Guinea-Sudan transition zone of Benin. *Nutr. Cycl. Agroecosyst.* 92, 9–19. doi: 10.1007/s10705-011-9468-7

Martí, H. R., and Mills, H. A. (2002). Nitrogen and potassium nutrition affect yield, dry weight partitioning, and nutrient-use efficiency of sweet potato. *Commun. Soil Sci. Plant Anal.* 33, 1–2,287-301. doi: 10.1081/CSS-120002394

Matsumoto, R., Asfaw, A., De Koeyer, D., Muranaka, S., Yoshihashi, T., Ishikawa, H., et al. (2021b). Variation in tuber dry matter content and starch pasting properties of white Guinea yam (*Dioscorea rotundata*) genotypes grown in three agroecologies of NIGERIA. *Agronomy* 11, 1944. doi: 10.3390/agronomy11101944

Matsumoto, R., Ishikawa, H., Asfaw, A., and Asiedu, R. (2021a). Low soil nutrient tolerance and mineral fertilizer response in white Guinea yam (*Dioscorea rotundata*) genotypes. *Front. Plant Sci.* 12, 629762. doi: 10.3389/fpls.2021.629762

Mehlich, M. (1984). Mehlich 3 soil test extractant: a modification of the mehlich 2 extractant. *Commun. Soil Sci. Plant Anal.* 15, 1409–1416. doi: 10.1080/00103628409367568

Mengel, K. (1983). Responses of various crop species and cultivars to fertilizer application. *Plant Soil* 72, 305–319. doi: 10.1007/BF02181970

Otoo, E., Okonkwo, C., and Asiedu, R. (2006). Stability studies of hybrid yam (*Dioscorea rotundata* poir.) genotypes in Ghana. *J. Food Agric. Environ.* 4 (1), 234–238.

Pachakkil, B., Yamanaka, S., Girma, G., Matsumoto, R., TamiruOli, M., Bhattacharjee, R., et al. (2021). Simple sequence repeat-based mini-core collection for white Guinea yam (*Dioscorea rotundata*) germplasm. *Crop Sci.* 61 (2), 1268–1279. doi: 10.1002/csc2.20431

R Core Team (2018) *R: A language and environment for statistical computing* (Vienna, Austria: R Foundation for Statistical Computing). Available at: https://www.Rproject.org (Accessed 24 April 2020).

Scott, G. J., Rosegrant, M., and Ringler, C. (2000). "Roots and tubers for the 21st century: trends, projections and policy options," in *Food, agriculture and the environment discussion* (Washington, DC: International Food Policy Research Institute (IFPRI) and International Potato Center (CIP), 31.

Tamele, R. A., Ueno, H., Toma, Y., and Morita, N. (2020). Nitrogen recoveries and nitrogen use efficiencies of organic fertilizers with different C/N ratios in maize cultivation with low-fertile soil by 15N method. *Agriculture* 10, 272. doi: 10.3390/agriculture10070272

frontiers | Frontiers in Plant Science

TYPE Original Research
PUBLISHED 13 October 2022
DOI 10.3389/fpls.2022.880373

Check for updates

OPEN ACCESS

EDITED BY
Marco Landi,
University of Pisa, Italy

REVIEWED BY
Mohd. Kamran Khan,
Selcuk University, Turkey
Li Qian,
Tianjin University, China

*CORRESPONDENCE
Kai Zhu
zhukai72@126.com
Yanqiu Wang
wangyanqiu73@126.com

SPECIALTY SECTION
This article was submitted to Plant Abiotic Stress, a section of the journal Frontiers in Plant Science

RECEIVED 19 May 2022
ACCEPTED 21 September 2022
PUBLISHED 13 October 2022

CITATION
Zhang F, Lu F, Wang Y, Zhang Z, Wang J, Zhang K, Wu H, Zou J, Duan Y, Ke F and Zhu K (2022) Combined transcriptomic and physiological metabolomic analyses elucidate key biological pathways in the response of two sorghum genotypes to salinity stress. *Front. Plant Sci.* 13:880373. doi: 10.3389/fpls.2022.880373

COPYRIGHT
© 2022 Zhang, Lu, Wang, Zhang, Wang, Zhang, Wu, Zou, Duan, Ke and Zhu. This is an open-access article distributed under the terms of the Creative Commons Attribution License (CC BY). The use, distribution or reproduction in other forums is permitted, provided the original author(s) and the copyright owner(s) are credited and that the original publication in this journal is cited, in accordance with accepted academic practice. No use, distribution or reproduction is permitted which does not comply with these terms.

Combined transcriptomic and physiological metabolomic analyses elucidate key biological pathways in the response of two sorghum genotypes to salinity stress

Fei Zhang, Feng Lu, Yanqiu Wang*, Zhipeng Zhang, Jiaxu Wang, Kuangye Zhang, Han Wu, Jianqiu Zou, Youhou Duan, Fulai Ke and Kai Zhu*

Sorghum Breeding and Cultivation Physiology Laboratory, Sorghum Institute, Liaoning Academy of Agricultural Sciences, Shenyang, China

Sorghum is an important food crop with high salt tolerance. Therefore, studying the salt tolerance mechanism of sorghum has great significance for understanding the salt tolerance mechanism of C_4 plants. In this study, two sorghum species, *LRNK1* (salt-tolerant (ST)) and *LR2381* (salt-sensitive (SS)), were treated with 180 mM NaCl salt solution, and their physiological indicators were measured. Transcriptomic and metabolomic analyses were performed by Illumina sequencing and liquid chromatography-mass spectrometry (LC-MS) technology, respectively. The results demonstrated that the plant height, leaf area, and chlorophyll contents in *LRNK1* were significantly higher than in *LR2381*. Functional analysis of differently expressed genes (DEGs) demonstrated that plant hormone signal transduction (GO:0015473), carbohydrate catabolic processes (GO:0016052), and photosynthesis (GO:0015979) were the main pathways to respond to salt stress in sorghum. The genes of the two varieties showed different expression patterns under salt stress conditions. The metabolomic data revealed different profiles of salicylic acid and betaine between *LRNK1* and *LR2381*, which mediated the salt tolerance of sorghum. In conclusion, *LRNK1* sorghum responds to salt stress *via* a variety of biological processes, including energy reserve, the accumulation of salicylic acid and betaine, and improving the activity of salt stress-related pathways. These discoveries provide new insights into the salt tolerance mechanism of sorghum and will contribute to sorghum breeding.

KEYWORDS

sorghum, resistance, salt stress, transcriptomic, metabolomic, salicylic acid

Highlight

Transcriptomic and metabolomic data were combined to reveal the changes in genes and metabolites, which provide new insights into the salt tolerance mechanism of sorghum.

Introduction

Plant growth can be affected by various abiotic stresses such as drought, cold, heat, and high salinity conditions. To maintain adequate proliferation, plants have evolved intricate mechanisms by which they perceive external signals and respond accordingly (Rahman, 2012). A major event in stress response is the perception and transduction of stress signals through signaling components (Kumar et al., 2011), which results in the activation of numerous stress-related genes and metabolites. In *Arabidopsis* and rice plants, networks interacting during stress defenses have recently been elucidated using transcriptomic analysis (Yao et al., 2018; Chandran et al., 2019). Ionic imbalance and osmotic stress are the two major effects challenged by salt stress. These stresses result in membrane damage and enhance lipid peroxidation and the production of reactive oxygen species (ROS) (Kumar et al., 2013). The performance and mechanism of salt tolerance in plants have also been reviewed in many studies (Fahad et al., 2014; Parihar et al., 2014; Dar et al., 2015; Liang et al., 2017). Sorghum is a major food crop for millions of people worldwide and also suffers from salt stress. Food and Agriculture Organization data have demonstrated that sorghum is currently the fifth most important grain crop in the world (Zheng et al., 2011) and plays an important role in the development and evolution of dedicated energy crops. Sorghum has also evolved a series of responses to salt stress. Lacerda reported that sorghum could reduce Na^+ and Cl^- transport from the roots to the shoot and compartmentalize part of it in specific places in the stems and roots in plants treated with salt (Lacerda et al., 2001). Swami revealed changes in the protein complement of sorghum leaves under salt stress (Kumar et al., 2011). In addition, the use of exogenous components can increase the salt tolerance of sorghum, such as exogenous spermine (Chai et al., 2010), salicylic acid (Mahmood et al., 2010), abscisic acid (ABA) (Amzallag et al., 1990), and glycine betaine (Ibrahim, 2004; Agboma et al., 2008). Like other essential crops, salt stress reduces sorghum yield and production. Several articles have reviewed the physiological and biochemical responses of *sorghum* to salt stress (Almodares and Hadi, 2009; Tari et al., 2013; Anami et al., 2015; Yang et al., 2020). When *sorghum* is subjected to salt stress, cells mobilize multiple components in response. Some studies have demonstrated the stress response mechanism of salt stress in *sorghum* at the level of gene expression (Dugas et al., 2011; Fracasso et al., 2016; Yang et al., 2017), although these are insufficient. Organic solutes such as sugars, organic acids, polyols, and many nitrogen-containing compounds such as amino acids, amides, amino acids, ectoine, proteins, and quaternary ammonium compounds have been proven to play important roles in tolerating the toxicity of ions under salt stress (Ashraf and McNeilly, 2004). Meanwhile, genes also actively respond to salt stress signals, and the expression levels of some genes change dramatically in a short time to synthesize the proteins needed for stress response. Some genes are suppressed under salt stress. Biotechnological methods dedicated to planting transcriptomics analysis provide a valuable opportunity to uncover the basis of plant response to salt stress at the molecular level (Daldoul et al., 2014). The continuous advancement of technology will allow us to obtain the transcriptome expression profile in plant cells and use liquid chromatography/mass spectrometry (LC/MS) technology to identify and analyze metabolites and proteins in the plant (Fiehn, 2002). Integrative omics approaches within large-scale experiments, including genomics, transcriptomics, ionomics, proteomics, and metabolomics, can help decipher the interplay of cellular functions at different levels (Biswapriya et al., 2019). Therefore, we can reveal a series of response mechanisms triggered by cells in response to salt stress. Transcriptomics, along with metabolomics, provides a major tool for characterizing postgenomic processes (Morgenthal et al., 2006). In China, many salt-tolerant sorghum varieties have been selected after many years of breeding. *LRNK1* is a sorghum variety with high yield and salt tolerance and is an ideal plant material to study the salt tolerance mechanism of sorghum. The development of liquid chromatography-mass spectrometry (LC-MS) technology has made it possible to research such resistance in plants. With LC-MS, all nonvolatile polar metabolites, such as amino acids, can be assayed without derivatization (D'Amelia et al., 2018). In particular, short analysis times, selectivity, and almost no matrix interferences have become significant advantages for the LC-MS method when determining metabolites (Thiele et al., 2012). Natera revealed the root lipidome profile response to salt stress in barley by LC-MS (Natera et al., 2016). Kechebar found the phenolic composition changed in salt-treated Saharan trees (Karoune et al., 2017). Therefore, it is possible to use LC-MS to study the metabolite profile response to salt stress in sorghum.

In this study, we reveal changes in genes and metabolites in two extreme sorghum materials under salt stress by combining transcriptomic and metabolomic data under four treatments of salt stress and control. This study will provide technical support for the potential mining of sorghum salt tolerance and selecting salt-tolerant varieties.

Materials and methods

Plant materials

Two sorghum restorer lines, *LRNK1* (salt-tolerant (ST)) and *LR2381* (salt-sensitive, SS), were used as plant materials. While

they had different sensitivities to salt, the crop maturity period, growth rate, and phenotypic traits of the two sorghum genotypes (*Bicolor* L. Moench) were similar. *LRNK1* and *LR2381* seeds were collected from the sorghum seed resource bank in the Liaoning Academy of Agricultural Sciences with ID: 011427 and ID: 010362, respectively. After disinfection (surface-sterilized with 1% sodium hypochlorite for 5 min followed by rinsing three times with distilled water), the seeds were planted in a hydroponic beaker filled with sorghum hydroponic culture (Kimura solution, Supplementary Table S1) under artificially simulated climatic conditions: day/night temperatures of 28°C/25°C, approximately 50% relative humidity (Rh), photoperiod of 14:10 h of light (1,500 $\mu mol \cdot m^{-2} \cdot s^{-1}$)/dark in April 2019 in an artificial climate room in Liaoning Provincial Academy of Agricultural Sciences.

Salt treatment and sample collection

Sorghum plants at the six-leaf stage were used for the salt treatment experiment. For each variety, 144 plants were randomly selected and then divided into six hydroponic beakers with 24 plants in each. These six hydroponic beakers were then randomly divided into two groups: salt treatment (T) and control (C), with three hydroponic beakers in each group. For group T, both LRNK1 and LR2381 were treated with an additional 180 mM NaCl in the basic sorghum hydroponic culture, which was based on previous salt stress simulations at 60, 120, 180, and 240 mM NaCl. The two extremes of 180 mM NaCl showed significant phenotypic differences between the salt stress and control treatments. The salt-sensitive lines survived, while the salt-sensitive lines died under 240 mM NaCl simulations. In addition, the salt stress adversity simulated by 180 mM NaCl most closely matched the actual production environment. For group C, both LRNK1 and LR2381 were treated with basic sorghum hydroponic culture (no NaCl supplement). A total of four sets of samples were prepared: LRNK1-control (STC), LRNK1-salt treatment (STT), LR2381-control (SSC), and LR2381-salt treatment (SST). After 72 h of cultivation, six plant samples were randomly selected from each hydroponic beaker and the fifth leaf at tillering on each plant was sampled (18 leaves obtained in each group). These 18 leaves were pooled and divided into six parts in each group, three of which were used for RNA-seq analysis and three for metabolomic analysis. All sampled leaves were immediately placed in liquid nitrogen for 5 min, stored at −80°C, and tested within 3 to 4 weeks. The root tissue of each group was sampled to determine the physiological indicators.

After the hydroponic salt stress sampling was completed, the seedlings of the four groups of STC, STT, SSC, and SST were transplanted into prepared pots treated with the same salinity as the hydroponics for cultivation until maturity, and the sorghum growth phenotype parameter was recorded.

Determination of plant physiological indicators

The plant height and leaf area (the fifth leaf at tillering) of seedlings at the six-leaf stage with and without salt treatment were measured according to a previous report (Iqbal et al., 2010). Fresh leaves were determined by an electronic balance to obtain the fresh mass (FM) and dried at 105°C for half an hour and at 70°C for 48 h to achieve constant weight. The dry mass (DM) was recorded. Turgid mass (TM) was determined after the leaves had been immersed in distilled water for 12 h. The FM, DM, and TM of root tissues were also determined. The relative water content (RWC) of a plant tissue is expressed by RWC (%) = [(FM − DM)/(TM − DM)] * 100%. For the leaf chlorophyll content determination, the ethanol-acetone method was used as described by Zhang (1992). The same experimental protocol was repeated three times.

Total RNA extraction and sequencing

Total RNA was extracted using an RNAprep pure Plant Kit (Tiangen, Beijing, China) according to the manufacturer's instructions, and the RNA quality was evaluated by gel electrophoresis. Total RNA was reverse transcribed to cDNA by a QuantScript RT Kit (Tiangen, Beijing, China). An efficient VAHTS® mRNA-seq v2 Library Prep Kit for Illumina (Vazyme Biotech, Nanjing, China) was then used to construct the sequence libraries. All 12 mRNA libraries (six groups with three biological replicates in each group) obtained were evaluated by an Agilent 2100 Bioanalyzer (Agilent Technologies, USA) and the qRT-PCR method. Finally, all mRNA-seq libraries were sequenced on an Illumina HiSeq 4000 sequencing platform with pair-end 2 × 150 bp mode to obtain sequencing data.

mRNA sequence data processing

The sequencing data were filtered using FastQC (version 0.11.5) with default criteria. Low-quality reads and adaptor reads were removed from the raw data, and the clean data were assembled and mapped to the sorghum assembly genome (https://www.ncbi.nlm.nih.gov/genome/term=Sorghum+bicolor) using HISAT2 (version 2.1.0) (Kim et al., 2015). The value of FPKM (expected number of fragments per kb of exon per million of reads) of reads in each sample was calculated using Cufflinks (version 2.2.1) (Roberts et al., 2011). Principal component analysis (PCA) and Pearson's correlation analysis were performed based on the FPKM of reads. The differentially expressed genes (DEGs) by different comparisons were identified using DESeq2 (version 1.24.0) (Anders, 2010), with the criteria of the corrected *p*-value (padj) <0.05 by the negative binomial distribution test and $|\log_2(\text{fold change (FC)})|>0$. Genes

with log_2FC >0 and log_2FC <0 were identified as up- and downregulated DEGs, respectively. Hierarchical clustering based on the expression profiles of DEGs was presented by pheatmap (version 1.0.10). DEGs enriched into modules correlated with the phenotypes were separately subjected to the enrichment analysis for Gene Ontology (GO) and Kyoto Encyclopedia of Genes and Genomes (KEGG) pathways (Kanehisa et al., 2007). Significant GO biological processes (BP) and KEGG pathways were identified with the criterion of $p < 0.05$.

Nontargeted liquid chromatography-mass spectrometry

The chromatographic column (Accucore HILIC column; Thermo Fisher Scientific) was maintained at 40°C with an injection volume of 5 μl. The mobile phase (0.3 ml/min flow rate) consisted of 0.1% formic acid, 95% acetonitrile, and 10 mM ammonium acetate in solvent A, and 0.1% formic acid, 50% acetonitrile, and 10 mM ammonium acetate in solvent B. The gradient elution phase of solvent A was 98% for the first 1 min, decreased to 50% during 1–17 min, stabilized for 0.5 min (17.5 min), returned to 98% after 17.5–18 min, and stabilized at 98% for the last 2 min (18–20 min). A 5-min interval was set for the equilibrating instrument. All samples were analyzed using a Q Exactive (QE) HF-X mass spectrometer detector (Thermo Fisher Scientific) in positive and negative (polarity) ionization modes (spray voltage of 3.2 kV) with MS/MS data-dependent scans (mass range of 100–1500 m/z). The parameters of the electrospray ion source were set as 320°C drying gas temperature, 35 arb sheath gas flow rate, and 10 arb Aux gas flow rate. System stability and accuracy were validated using QC samples with an interval of five samples.

Nontargeted LC-MS analysis

The data were recorded using the compound discoverer (CD) software, and the parameters, including retention times and mass charge ratio of compounds, were analyzed and corrected. The relative standard deviation (RSD) and signal-to-noise (S/N) ratio were analyzed. After feature screening, candidate features (RSD >30%, S/R ratio <3, signal intensity $>10^5$) were retained and aligned against mzCloud (https://www.mzcloud.org/). QC samples were used for data normalization, and the relative expression of the metabolites was obtained and used for further analysis. The resulting three-dimensional data involving the peak number, sample name, and normalized peak area were fed into R package metaX for PCA and projections to latent structures-discriminant analysis (PLS-DA) (Wen et al., 2017). A Student's *t*-test was used to compare peak areas of three metabolites, with the threshold of variable importance in the projection (VIP) value >1, fold change (FC) ≥2 ($|log2FC| \geq 1$), and $p < 0.05$. A hierarchical clustering analysis was then performed to present the expression patterns of the differential metabolites. Subsequently, the correlations between the differential metabolites were calculated by R software (v3.1.3). Differential metabolites with significant correlations (false discovery rate, FDR <0.05) were retained and used for enrichment analysis of the KEGG pathway, with significant criteria of $padj < 0.05$.

Soluble sugars, salicylic acid, and betaine

Soluble sugars

Soluble sugar in plant leaves was determined with the methods used by Zhang (1992) with minor modifications. Plant leaves (0.25 g) were placed in a boiling water bath for 1 h. Total soluble sugar content was analyzed with the phenol-sulfuric method after hydrolysis of starch using perchloric acid.

Salicylic acid content

In total, 1.5 g of seedling leaves was placed in a grinder, and 4 ml of 80% methanol was added to grind them. PVP with 0.2 times the quality of the product was continuously ground into a homogenate. The homogenate was leached in a 4°C refrigerator for 12 h and centrifuged (10,000 r/min, 4°C, 20 min); the supernatant was transferred to a Petri dish and placed in a lighted incubator to dry. A total of 2.5 ml was added to the residue with 80% methanol and leached in a 4°C refrigerator for 12 h, followed by centrifugation. This was repeated three times. After the liquid in the petri dish dried, 2.5 ml of 100% methanol was added to dissolve the dry sample, which was placed into a centrifuge tube and centrifuged (10,000 r/min, 4°C, 10 min). The supernatant was then filtered with a 0.22-μm organic filter membrane and placed in a refrigerator at 4°C. The salicylic acid (SA) content was determined by high-performance liquid chromatography.

Betaine

The sample was predried at 105°C to a constant weight, 0.4 g of the dried sample was weighed, 50 ml of glacial acetic acid was added, and heated to dissolve. A total of 25 ml of mercuric acetate solution was added and allowed to cool, then two drops of crystal violet indicator were added and titrated with perchloric acid standard solution (0.1 mol/L) until the solution turned green. The titration result was corrected with a blank test, and high-performance liquid chromatography was used to determine the content of SA.

Statistical analysis

Differences in expression levels were investigated using a one-way analysis of variance (ANOVA). The means of the values were compared using Tukey's multiple comparison tests. A *p*-value of <0.05 was considered significant. For conjoint analysis, the correlation analysis between the top 100 DEGs and the top 50

differential metabolites was performed, and the *p*-value was calculated. KEGG enrichment analysis was then performed on these significantly related DEGs and differential metabolites. A *p*-value of <0.05 was considered significant.

Results

Effects of salt stress on plant physiological indicators

Physiological indicators showed that plant height, leaf area, and chlorophyll contents showed no significant difference between the two sorghum varieties under normal conditions (Figure 1). However, after salt treatment, these three indicators in the salt-tolerant sorghum *LRNK1* were significantly higher than in the salt-sensitive *LR2381*. In addition, RWC in *LR2381* leaves and roots had significantly lower contents than that in *LRNK1*, which revealed the serious water loss in the salt-sensitive *LR2381* due to salt stress. The morphological differences between salt-tolerant and salt-sensitive sorghum under salt stress are obvious in the seedling period, jointing period, and mature period (Table 1; Figure 1).

Illumina sequencing data summary

A total of 458.10 Mb of raw reads from the 12 libraries were generated, with an average sequencing error rate of 0.02% and an average GC content of 54.74% (Supplementary Table S2). The average data ratio of sequencing quality to Q20 and Q30 was 97.96% and 94.34%, respectively. After read mapping analysis, an average of 92.59% of reads were uniquely mapped to the sorghum genome sequence (Supplementary Table S2). PCA results showed that the biological repeat samples in each group are clustered together (Supplementary Figure S1A). Sample-to-sample correlation analysis results showed a similar result with PCA, indicating good consistency and reproducibility between biological repetitions (Supplementary Figure S1B).

DEGs between salt treatment and control group

A total of 10,771 DEGs were identified by pairwise comparison of all the groups. There were 2,354, 4,162, 719, and 1,559 upregulated DEGs and 1,863, 3,797, 1,169, and 1,576 downregulated DEGs found during the comparison of STT vs. STC, SST vs. SSC, STC vs. SSC, and STT vs. SST, respectively (Figure 2A). The expression pattern of all DEGs showed a significant distinction between different groups (Figure 2B). Venn diagram analysis results showed that there were 3,326 common DEGs between STT vs. STC and SST vs. SSC (Figure 2C).

Functional analysis of DEGs

To reveal the role of DEGs, GO and KEGG enrichment analyses were performed. GO enrichment results revealed that

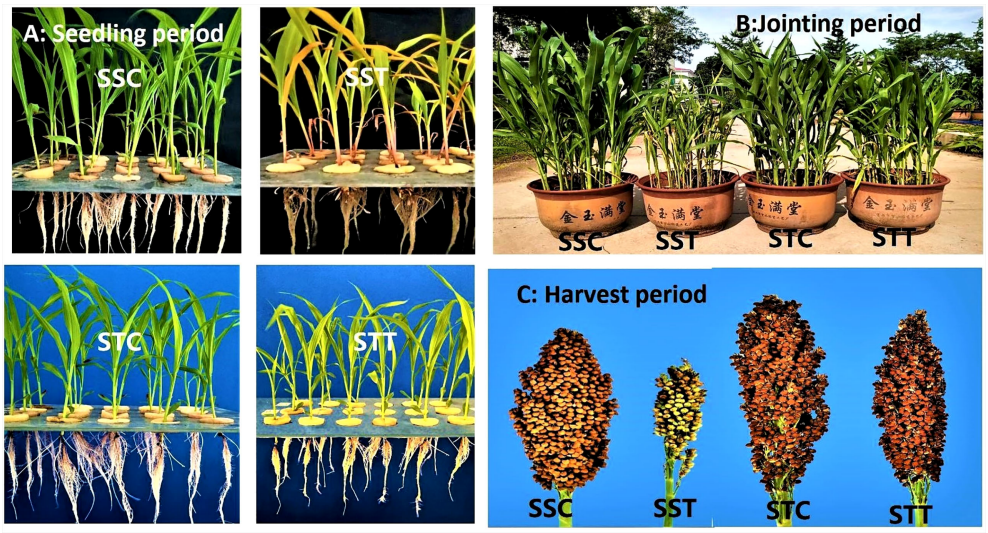

FIGURE 1
Phenotypic differences between salt-tolerant and salt-sensitive genotypes of sorghum under control and salt stress at seedling period, jointing period, and mature period **(A)** Control vs salt stress phenotypic differences at seedling period. **(B)** Control vs salt stress phenotypic differences at jointing period. **(C)** Control vs salt stress phenotypic differences at harvest period.

10.3389/fpls.2022.880373

TABLE 1 Plant physiological indicators for plant height, leaf area, leaf (FM, DM, TM, RWC), root (FM, DM, TM, RWC), and chlorophyll of salt-sensitivity (SS).

	Plant height	Leaf area	Leaf				Root				Chlorophyll
			FM	DM	TM	RWC	FM	DM	TM	RWC	
SSC	34.65 a	152.23 a	1.13 a	0.13 a	1.90 a	85.3 a	1.13 a	0.14 a	1.20 a	83.6 a	1.54 a
SST	12.86 c	46.05 c	0.02 c	0.02 b	1.71 b	74.2 b	0.15 c	0.02 b	1.01 b	71.2 b	1.12 c
STC	33.57 a	151.24 a	1.02 a	0.13 a	1.87 a	85.6 a	0.94 a	0.12 a	1.19 a	83.1 a	1.53 a
STT	20.43 b	82.79 b	0.18 b	0.07 b	1.85 a	84.7 a	0.43 b	0.06 b	1.15 a	82.7 a	1.45 b

Different lowercase letters (a–c) indicate group differences at the 0.05 level (LSD postanalyses for salt-sensitive (SS) and salt-tolerant (ST) sorghum genotypes under control (C) and salt treatment (T) groups).

11 GO terms were significantly enriched in STT vs. STC, including carbohydrate catabolic process (GO:0016052) and transmembrane transport (GO:0055085). Most of the DEGs were upregulated in the carbohydrate catabolic process, including *SbFBA* (*fructose-bisphosphate aldolase*), *SbPGK* (*phosphoglycerate kinase*), and *SbPFK* (*pyrophosphate-fructose 6-phosphate*) family members (Figure 3A). In addition, some GO processes related to DNA replication were also related based on downregulated DEGs in STT vs. STC, including DNA metabolic process (GO:0006259), mismatch repair (GO:0006298), and mismatched DNA binding (GO:0030983). *SbCAT* (*catalase*), *SbPUT* (*polyamine transporter*), *SbMSH* (*DNA mismatch repair protein*), and *SbBAT* (*amino-acid permease*) were the key differentially expressed regulators in these GO terms (Figure 3B). For the salt-sensitive species *LR2381*, 16 GO terms were enriched, most of which were related to photosynthesis, including photosynthesis (GO:0015979), photosystem II (GO:0009523), and thylakoid (GO:0009579). DEGs like *SbpsbP* (*photosystem II oxygen-evolving complex protein*), *Sbpsa* (*photosystem I assembly factor*), and *SbLHCs* (*light-harvesting complex*) played key roles in these processes (Figure 3C). KEGG results showed that biosynthesis of amino acids (sbi01230), carbon fixation in photosynthetic organisms (sbi00710), glutathione metabolism (sbi00480), and circadian rhythm–plant (sbi04712) were significantly enriched based on the DEGs in STT vs. STC, and most DEGs involved were upregulated with salt treatment. Most of the genes in the C4-dicarboxylic acid cycle (belonging to sbi00710) were active. *SbPIF* (*ATP-dependent DNA helicase*), *SbHY5* (*transcription factor HY5*), and *SbFT* (*FT-interacting protein*) in circadian rhythm–plants were upregulated. For DEGs in the glutathione metabolism, *SbNADP*$^{+}$ was downregulated and *SbGST* (*probable glutathione S-transferase*) was upregulated. As for SST vs. SSC, the upregulated DEGs were enriched in carbon fixation in photosynthetic organisms (sbi00710), plant hormone signal transduction (sbi04075), MAPK signaling pathway–plant (sbi04016), glutathione metabolism (sbi00480), and carbon metabolism (sbi01200). The downregulated DEGs were enriched in porphyrin and chlorophyll metabolism (sbi00860), photosynthesis (sbi00195), carbon metabolism (sbi01200), starch and sucrose metabolism (sbi00500), and the TCA cycle (sbi00020). DEGs in plant hormone signal transduction showed that *SbPP2C* (*probable protein phosphatase 2C*), *SbABF*, *SbIAA* (*Auxin*), *SbEIN3* (*EIN3-binding F-box protein*), and all genes related to salicylic acid (including *SbJAR1*, *SbNPR1*, and *SbTGA*) increased by salt treatment (Figure 4). Also, *SbMAP3K*

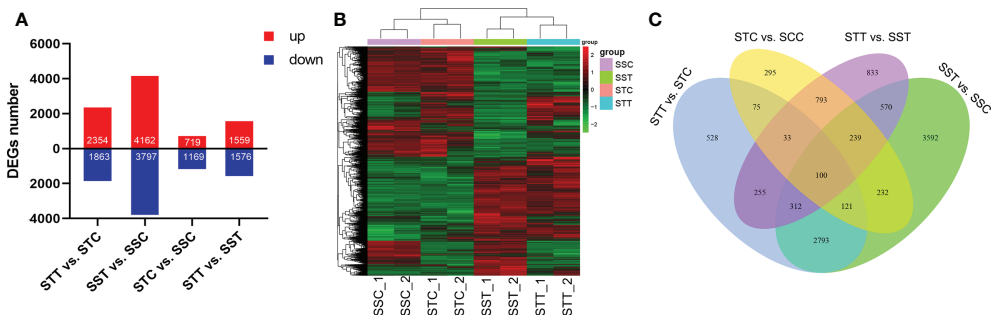

FIGURE 2
Summary of DEGs between salt treatment and control. **(A)** Number of DEGs in different comparisons. STC: LRNK1-Control, STT: LRNK1-Salt treatment, SSC: LR2381-Control, SST: LR2381-Salt treatment; **(B)** Expression heatmap of DEGs in different groups. The redder the color, the higher the expression; the greener the color, the lower the expression. **(C)** Venn diagram analysis results among different comparisons.

10.3389/fpls.2022.880373

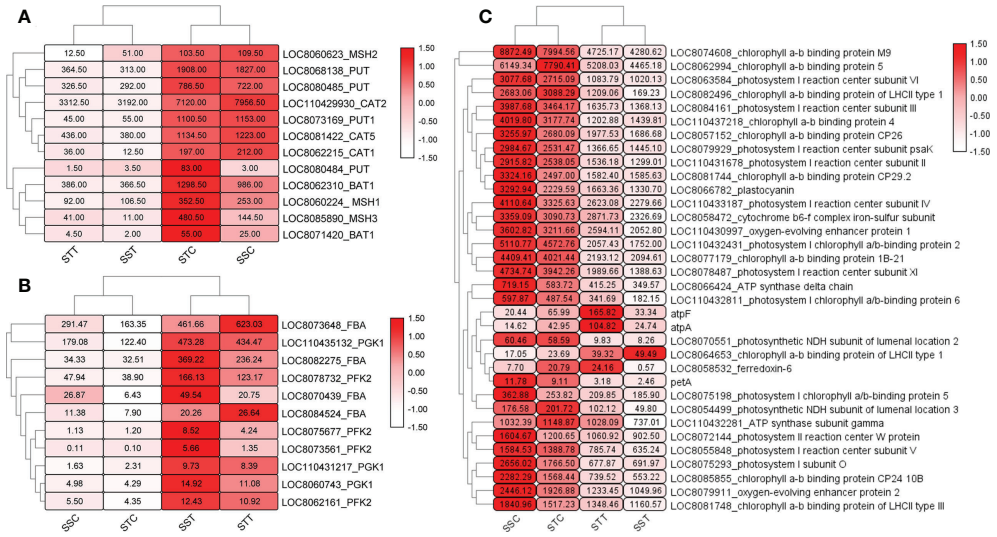

FIGURE 3
Heatmap of differently expressed genes (DEGs) in candidate pathways. The redder and larger the circle, the higher the expression. **(A)** Expression of DEGs in carbohydrate catabolic process. **(B)** Expression pattern of transcripts of SbCAT, SbPUT, SbMSH, and SbBAT. **(C)** Expression of DEGs related to photosynthesis.

responded positively to salt stress. Photosynthesis-related genes, including *SbPsa*, *SbPsb*, and *SbPet*, were downregulated by salt stress.

Summary of the LC-MS/MS metabolomics

The MS raw data (total ion current (TIC)) showed that there were 548 and 824 metabolites detected from all samples and quality controls under the negative and positive modes, respectively. PCA results showed that metabolisms differed between groups (Supplementary Figures S2A, B). XComparison analysis determined that there were 63 and 66 differential metabolites in STT vs. STC under negative and positive ion modes, respectively (Supplementary Figures S2D, E). As for SST vs. SSC, there were 40 and 46 differential metabolites under negative and positive ion modes, respectively (Supplementary Figure S2C, D).

Differential metabolites responding to salt stress

In the negative ion mode, distinct profiles of these metabolites are shown by a heatmap in these four groups (Figure 5A). In salt-tolerant *LRNK1*, 32 and 31 metabolites were up- and downregulated, respectively, after salt treatment. As for the salt-sensitive *LR2381*, salt stress mediated 31 upregulated and nine downregulated metabolites (Figure 5B). The results of the KEGG enrichment analysis showed that plant hormone signal transduction (sbi04075) was significantly enriched, which was partially regulated by salicylic acid (Com_87_neg). Aside from the two metabolites, salt stress

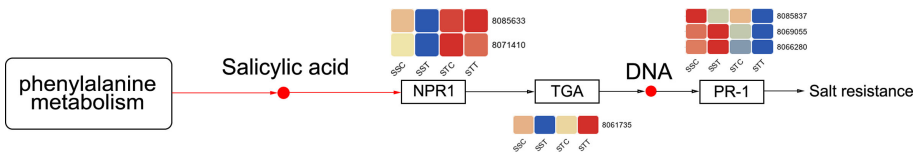

FIGURE 4
Differently expressed genes (DEGs) in the salicylic acid signal pathway. The redder the circle, the higher the expression. STC: LRNK1-Control, STT: LRNK1-Salt treatment, SSC: LR2381-Control, SST: LR2381-Salt treatment.

decreased the contents of 2-oxobutyric acid (Com_274_neg), which was involved in multiple pathways but was different in the two sorghum species. In addition, phenylalanine metabolism (map00360) and starch and sucrose metabolism (map00500) were active for energy homeostasis to cope with salt stress. Of these, five metabolites showed different profiles in STT vs. STC and SST vs. SSC (Table 2; Figure 5C), which is important.

In the positive ion mode, distinct metabolic profiling was found after salt treatment (Figure 5D). In LRNK1, 42 and 24 metabolites were up- and downregulated, respectively. In *LR2381*, salt stress mediated 37 upregulated and nine downregulated metabolites (Figure 5E). Metabolic profiling in salt-tolerant *LRNK1*, glutathione metabolism (map00480), and flavonoid biosynthesis (map00941) were significantly enriched in KEGG analysis, in which glutathione disulfide (Com_2094_pos) and gallocatechin (Com_1917_pos) act as the key regulators, respectively. As for the salt-sensitive *LR2381*, Betaine (Com_20_pos) in glycine, serine, and threonine metabolism and ABC transporters pathway were upregulated by salt stress. The expression of these three differential metabolites in different groups indicated that they were the key metabolites affected by salt stress (Table 3; Figure 5F).

Conjoint analysis of metabolomic and transcriptomic data

To better understand the relationship between DEGs and differential metabolites, integration analysis of metabolomic and transcriptomic data was performed. Association results of the KEGG pathway showed that plant hormone signal transduction (sbi04075) was active in both *LRNK1* and *LR2381*. Glutathione metabolism (sbi00480) was active in salt-tolerant *LRNK1* but not enriched in *LR2381* (Figures 6A–D). This demonstrates that plant hormone signal transduction (sbi04075) and glutathione metabolism (sbi00480) are the key pathways responding to salt stress.

Discussion

As sessile organisms, plants have developed sophisticated strategies to respond to diverse environmental stresses. Stress signals are perceived by several receptors at the cell membrane level, followed by their transduction to multiple second messengers such as abscisic acid (ABA), hydrogen peroxide (H_2O_2), and nitric oxide (NO) (Shi et al., 2014). In this study, the protective role of metabolites and gene expression patterns on the response to salt stress was revealed. A decrease in dry and fresh weights indicated that the leaves and roots of sorghum were damaged by short-term salt treatment. Relative water content is considered one of the easiest agricultural parameters that can be used to screen plants for drought and stress tolerance (Boutraa et al., 2010). The significant decrease in relative water content after salt stress in our results aligns with this view. Similar to our results, Nxele found that salinity stress could reduce water retention in sorghum plants (Nxele et al., 2017), which is a common response to salt stress. Under adverse circumstances, the chlorophyll level in the plant is a good

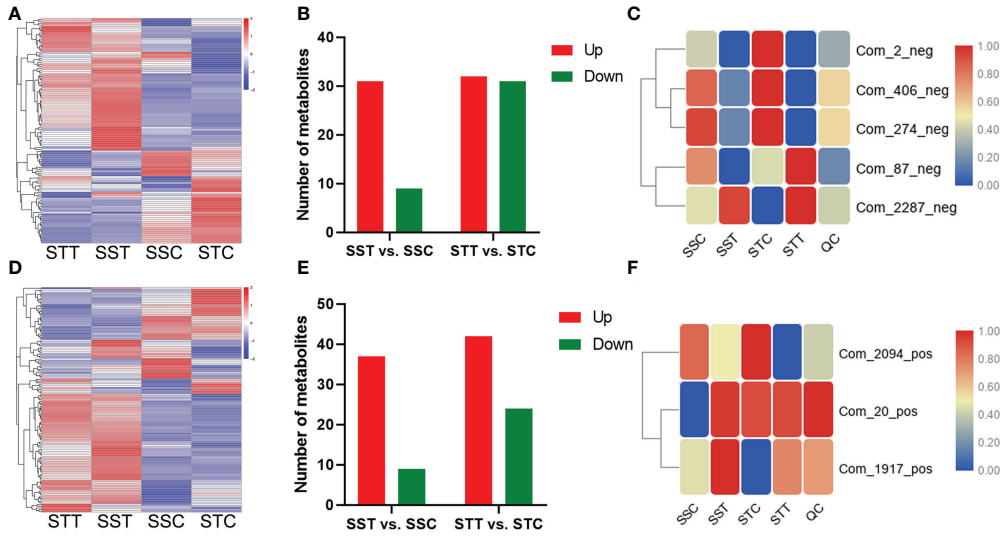

FIGURE 5
Differential metabolites respond to salt stress. **(A, D)** mean the differential metabolite content in different groups under negative and positive modes, respectively. The redder the circle, the higher the content. **(B, E)** showed the differential metabolite content in different comparisons under negative and positive modes, respectively. **(C, F)** showed the candidate metabolite profile content in different groups under negative and positive modes, respectively. The redder the circle, the higher the content.

TABLE 2 Five candidate metabolites in negative ion mode for salt-tolerant (ST) sorghum genotype under salt treatments (T).

ID	Name	Formula	Kegg_map
Com_406_neg	Uridine	$C_9H_{12}N_2O_6$	Pyrimidine metabolism/metabolic pathways
Com_2_neg	Benzoic acid	$C_7H_6O_2$	Starch and sucrose metabolism/metabolic pathways
Com_2287_neg	Trehalose 6-phosphate	$C_{12}H_{23}O_{14}P$	Glycine, serine, and threonine metabolism/cysteine and methionine metabolism/valine, leucine, and isoleucine biosynthesis/propanoate metabolism/C5-branched dibasic acid metabolism/metabolic pathways/biosynthesis of secondary metabolites/2-oxocarboxylic acid metabolism/biosynthesis of amino acids
Com_87_neg	Salicylic acid	$C_7H_6O_3$	Phenylalanine metabolism/metabolic pathways/biosynthesis of secondary metabolites/plant hormone signal transduction
Com_274_neg	2-Oxobutyric acid	$C_4H_6O_3$	Phenylalanine metabolism/metabolic pathways/biosynthesis of secondary metabolites

indicator of photosynthetic function (Xu et al., 2008; Dourado et al., 2022). It has been found that the chlorophyll level of plants decreases with aggravated salt stress (Pires et al., 2015; Rachoski et al., 2015; Dąbrowski et al., 2016). In this study, we demonstrated that the chlorophyll content in the leaves of sorghum plants was significantly decreased by salt stress, which could be affected by oxygen species (ROS) such as O^{2-} and H_2O_2 that leads to lipid peroxidation and chlorophyll destruction (Foreman et al., 2003; Rustioni et al., 2015; Dąbrowski et al., 2016). The expression of DEGs related to chlorophyll was also decreased by salt stress, which was consistent with the chlorophyll level of leaves.

The transcriptome analysis results revealed the DEGs and pathways that respond to salt stress. Two sorghum species showed differences in several biological processes. In this study, the carbohydrate catabolic process was active after salt treatment. Carbohydrates act as signaling molecules and play a role in adaptive mechanisms to stress (Hanson and Smeekens, 2009; Ramel et al., 2009). Energy provision was essential for plants to survive under abiotic stresses. To fight against abiotic stress, the upregulation of catabolism-related proteins such as phosphoglycerate kinase to activate energy-generating processes seems reasonable (Ma et al., 2017). We found that members of the *SbFBAs*, *SbPGKs*, and *SbPFKs* families increased under salt stress, indicating an active energy metabolism during salt stress. Most of the DEGs had higher expression in the salt-tolerant *LRNK1* than in the salt-sensitive *LR2381* in the control group. Under salt treatment, the expression of these genes dramatically increased in both species. The salt tolerance of sorghum plants could be related to the energy supply of carbohydrates under normal conditions.

To defend against salt stress, plant hormone signal transduction (sbi04075) was active, where the salicylic acid signal pathway showed different response patterns between the two sorghum species. As expected, the metabolite salicylic acid (Com_87_neg) showed a great difference between *LRNK1* and *LR2381*, highlighting the critical role of the salicylic acid signal pathway during salt stress. Salicylic acid is a signaling molecule known to participate in defense responses against a variety of environmental stresses (Jayakannan et al., 2015a). Previous studies have reported that salicylic acid is an important signaling phytohormone that can increase salt tolerance in plants (Borsani et al., 2001; Horváth et al., 2007; Jayakannan et al., 2015b).

Salicylic acid-mediated resistance is related to the expression of pathogenesis-related (PR) genes (Vicente and Plasencia, 2011), which is partially controlled by redox-regulated nonexpresser of pathogenesis-related 1 (NPR1) protein, a positive regulator of salicylic acid signaling acting downstream of salicylic acid (Mou et al., 2003). *NPR1* has also been shown to serve as a salicylic acid receptor (Wu et al., 2012). The overexpression of *NPR1* in many species enhances the resistance of transgenic plants to stress (Chern et al., 2001; Fitzgerald et al., 2004). In our results, transcripts of *SbNPR1* (8085633 and 8071410) were more highly expressed in *LRNK1* than in *LR2381*, and the contents of salicylic acid increased in *LRNK1* and decreased in *LR2381* after salt stress. This could lead to higher resistance in *LRNK1* sorghum.

Applying certain concentrations of salicylic acid can reduce the salt stress of many plants, including peanuts and wheat (Mahmood et al., 2010). Salicylic acid can increase the content or activity of antioxidant enzymes in plants during salt tolerance,

TABLE 3 Three candidate metabolites in positive ion mode for salt-tolerant (ST) sorghum genotypes under salt treatments (T).

ID	Name	Formula	Kegg_map
Com_2094_pos	Glutathione disulfide	cpd:C00127	Glutathione disulfide/GSSG/oxiglutatione/oxidized glutathione
Com_20_pos	Betaine	cpd:C00719	Betaine/trimethylaminoacetate/glycine betaine/*N*,*N*,*N*-trimethylglycine/**t**rimethylammonioacetate
Com_1917_pos	(+)-Gallocatechin	cpd:C12127	(+)-Gallocatechin/gallocatechol

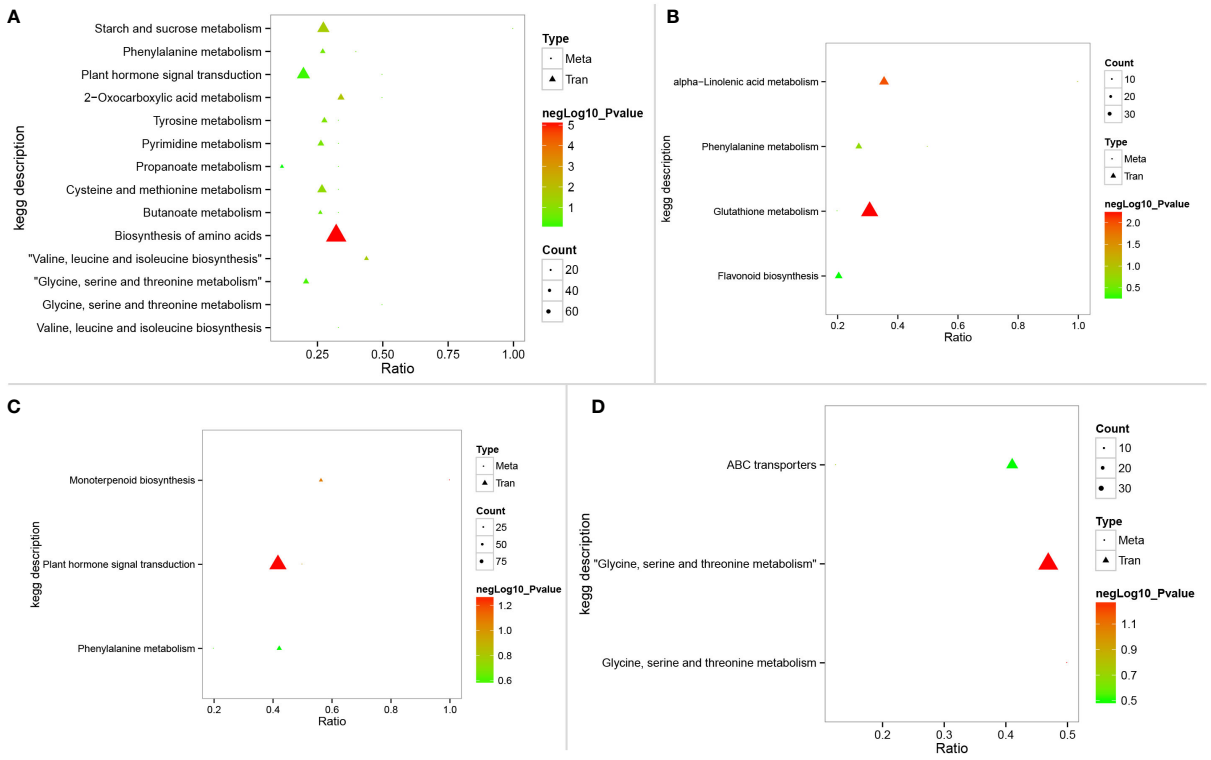

FIGURE 6
KEGG pathways enriched in integration analysis of metabolomics and transcriptomic data. **(A–D)** represent the KEGG enriched results in SST vs. SSC, STC vs. SSC, STT vs. SST, and STT vs. STC, respectively. STC: LRNK1-Control, STT: LRNK1-Salt treatment, SSC: LR2381-Control, SST: LR2381-Salt treatment.

and maintain the stability of the membrane system in plants to improve their salt tolerance of plants. The contents of hydrogen peroxide (H_2O_2) and superoxide anion radical (O^{2-}) and the harmful oxidation of lipids in plant cells could be appraised by increased malonaldehyde (MDA) content (Zhang X., 1992).

Increasing evidence has demonstrated that jasmonic acid functions in the regulation of plant responses to abiotic stresses (Qiu et al., 2014; Ding et al., 2015; Salimi et al., 2016; Aboagla et al., 2022). Although the results of metabolomics did not reflect differences in jasmonic acid between different species, transcripts of *SbJAZ* had higher expression in *LRNK1* than in *LR2381*. JAZ proteins are involved in abiotic stress tolerance mechanisms (Ye et al., 2009; Kazan, 2015; Chini et al., 2017). Enhanced stress tolerance of transgenic lines overexpressing JAZ proteins has been described in rice, cotton, and wild soybean (Ye et al., 2009; Wu et al., 2014; Zhao et al., 2016; Zhu et al., 2012). From the results, we speculated that the higher expression of *SbJAZ* promoted resistance to salt stress in *LRNK1* sorghum. The integration of metabolomic and transcriptomic results also supports this inference.

Betaine can protect plants from the adverse effects of abiotic stresses by ROS detoxification, adjusting cellular osmotica, and protecting membrane integrity (Ashraf and Foolad, 2007; Hayat et al., 2012). The overaccumulation of betaine can improve the stress resistance of wheat in a high-salt environment (Tian et al., 2016). In this study, the content of betaine (Com_20_pos) in STC (*LRNK1* without salt treatment) was significantly higher than that of SSC (*LR2381* without salt treatment). After salt treatment, the betaine in *LR2381* increased; however, due to the lack of betaine reserves before salt treatment, the *LR2381* plants suffered considerable damage under salt stress. Sufficient betaine reserves can likely help sorghum plants resist salt stress.

Conclusion

The damage of salt stress to sorghum was similar to that of other plants, including decreases in relative water content, chlorophyll, and leaf weight. The dynamic gene expression pattern responded to salt stress. As a salt-tolerant species, *LRNK1* sorghum can defend against salt stress by a variety of biological processes. According to our results, sufficient carbohydrate energy reserves under normal conditions are important for resisting salt stress, and the expression of *SbFBAs*, *SbPGKs*, and *SbPFKs* could reflect the activity of the

carbohydrate catabolic process. Importantly, the salt tolerance of sorghum was mediated by salicylic acid. Plants with higher salt tolerance have a higher salicylic acid content. Additionally, the expression of *SbNPR1*, a salicylic acid receptor, was positively correlated with salt tolerance. Similarly, betaine had been shown to respond to salt stress in sorghum, the accumulation of which under normal conditions was important for resisting salt stress. Moreover, a higher expression of *SbJAZ* promoted resistance to salt stress in *LRNK1* sorghum. The results of this research will play an important role in revealing the metabolic regulatory mechanism of sorghum salt tolerance and will contribute to sorghum breeding for salt tolerance, the efficient production of salt tolerance, and the development and utilization of saline land.

Data availability statement

The datasets presented in this study can be found in online repositories. The names of the repository/repositories and accession number(s) can be found below: NCBI [accession: PRJNA810939].

Author contributions

Lab work primarily conducted by FZ at Liaoning Agriculture Science as a PhD. FL, YW, ZZ, JW, KuZ, HW, JZ, YD, FK provided help for the manuscript preparation. KaZ provided technical guidance and advice for experiment design during the research. All authors contributed to the article and approved the submitted version.

Funding

This research was funded by the following projects: National Key R&D Program of China (2019YFD1001700), China Agriculture Research System of MOF and MARA (CARS-06), Liaoning Provincial Natural Science Foundation Project, China (2019-MS-197), Science and Technology Plan of Shenyang in 2022-Research on Sorghum Germplasm Innovation and breeding of high-quality special varieties, General Project of the Dean's Fund of Liaoning Academy of Agricultural Sciences, China (2021MS0504), and Agricultural Public Relations and Industrialization Project in Liaoning Province, China (2020JH2/10200014).

Conflict of interest

The authors declare that the research was conducted in the absence of any commercial or financial relationships that could be construed as a potential conflict of interest.

Publisher's note

All claims expressed in this article are solely those of the authors and do not necessarily represent those of their affiliated organizations, or those of the publisher, the editors and the reviewers. Any product that may be evaluated in this article, or claim that may be made by its manufacturer, is not guaranteed or endorsed by the publisher.

Supplementary material

The Supplementary Material for this article can be found online at: https://www.frontiersin.org/articles/10.3389/fpls.2022.880373/full#supplementary-material

SUPPLEMENTARY FIGURE 1
Samples correlation and PCA results based on the sequence data. **(A)** Pearson correlation between samples. **(B)** PCA results based on the sequence data.

SUPPLEMENTARY FIGURE 2
KEGG pathways enriched in integration analysis of metabolomics and transcriptomic data. **(A–D)** represent the KEGG enriched results in SST vs. SSC, STC vs. SSC, STT vs. SST, and STT vs. STC, respectively. STC: LRNK1-Control, STT: LRNK1-Salt treatment, SSC: LR2381-Control, SST: LR2381-Salt treatment.

References

Aboagla, M., Zhou, G., Nimir, N., and Adam, Y. (2022). Effect of exogenous ascorbic acid on two sorghum varieties under different types of salt stress. *Chil J. Agric. Res.* 82 (1), 10–20.

Agboma, P., Jones, M., Peltonen-Sainio, P., Rita, H., and Pehu, E. (2008). Exogenous glycinebetaine enhances grain yield of maize, sorghum and wheat grown under two supplementary watering regimes. *J. Agron. Crop Sci.* 178, 29–37. doi: 10.1111/j.1439-037X.1997.tb00348.x

Almodares, A., and Hadi, M. (2009). Production of bioethanol from sweet sorghum: A review. *Afr J. Agr Res.* 4, 772–780.

Amzallag, G., Lerner, H., and Poljakoff-Mayber, A. (1990). Exogenous ABA as a modulator of the response of sorghum to high salinity. *J. Exp. Bot.* 41, 1529–1534. doi: 10.1093/jxb/41.12.1529

Anami, S. E., Zhang, L. M., Xia, Y., Zhang, Y. M., Liu, Z. Q., and Jing, H. C. (2015). Sweet sorghum ideotypes: genetic improvement of stress tolerance. *Food Energy Secur* 4, 3–24. doi: 10.1002/fes3.54

Anders, S. (2010). Analysing RNA-seq data with the DESeq package. *Mol. Biol.* 43, 1–17.

Ashraf, M., and Foolad, M. (2007). Roles of glycine betaine and proline in improving plant abiotic stress resistance. *Environ. Exp. Bot.* 59, 206–216. doi: 10.1016/j.envexpbot.2005.12.006

Ashraf, M., and McNeilly, T. (2004). Salinity tolerance in brassica oilseeds. *Crit. Rev. Plant Sci.* 23, 157–174. doi: 10.1080/07352680490433286

Biswapriya, B. M., Carl, L., Michael, O., and Laura, A. C. (2019). Integrated omics: tools, advances and future approaches. *J. Mol. Endocrinol.* 62, 21–45. doi: 10.1530/JME-18-0055

Borsani, O., Valpuesta, V., and Botella, M. (2001). Evidence for a role of salicylic acid in the oxidative damage generated by NaCl and osmotic stress in arabidopsis seedlings. *Plant Physiol.* 126, 1024–1030. doi: 10.1104/pp.126.3.1024

Boutraa, T., Akhkha, A., Al-Shoaibi, A., and Alhejeli, A. (2010). Effect of water stress on growth and water use efficiency (WUE) of some wheat cultivars (*Triticum durum*) grown in Saudi Arabia. *J. Taibah Univ Sci.* 3, 39–48. doi: 10.1016/S1658-3655(12)60019-3

Chai, Y. Y., Jiang, C. D., Shi, L., Shi, T., and Gu, W. (2010). Effects of exogenous spermine on sweet sorghum during germination under salinity. *Biol. Plantarum* .54, 145–148. doi: 10.1007/s10535-010-0023-1

Chandran, A., Kim, J. W., Yoo, Y. H., Park, H. L., Kim, Y. J., Cho, M. H., et al. (2019). Transcriptome analysis of rice-seedling roots under soil-salt stress using RNA-seq method. *Plant Biotechnol. Rep.* 13, 567–578. doi: 10.1007/s11816-019-00550-3

Chern, M., Fitzgerald, H., Yadav, R., Canlas, P., Dong, X., and Ronald, P. (2001). Evidence for a disease-resistance pathway in rice similar to the NPR1-mediated signaling pathway in arabidopsis. *Plant J.* 27, 101–113. doi: 10.1046/j.1365-313x.2001.01070.x

Chini, A., Ben-Romdhane, W., Hassairi, A., and Aboul-Soud, M. (2017). Identification of TIFY/JAZ family genes in solanum lycopersicum and their regulation in response to abiotic stresses. *PloS One* 12, e0177381. doi: 10.1371/journal.pone.0177381

Dąbrowski, P., Baczewska-Dąbrowska, A., Pawluśkiewicz, B., Paunov, M., Aleksandrov, V., Goltsev, V., et al. (2016). Prompt chlorophyll a fluorescence as a rapid tool for diagnostic changes in PSII structure inhibited by salt stress in perennial ryegrass. *J. Photoch Photobio B.* 157, 22–31.

Daldoul, S., Ben Amar, A., Guillaumie, S., and Mliki, A. (2014). Integration of omics and system biology approaches to study grapevine (*Vitis vinifera* l.) response to salt stress: a perspective for functional genomics - a review. *J. Int. Sci. Vigne Vin.* 48, 189–200. doi: 10.20870/oeno-one.2014.48.3.1573

D'Amelia, L., Dell'Aversana, E., Woodrow, P., Ciarmiello, L. F., and Carillo, P. (2018). Metabolomics for crop improvement against salinity stress. *Genome Edi Sys Biol.* 2, 267–287.

Dar, D. T., uddin, M., Khan, M. M., Hakeem, K., and Jaleel, H. (2015). Jasmonates counter plant stress: A review. *Env. Exp. Bot.* 115, 49–57. doi: 10.1016/j.envexpbot.2015.02.010

Ding, H., Lai, J., Wu, Q., Zhang, S., Chen, L., Dai, Y.-S., et al. (2015). Jasmonate complements the function of arabidopsis lipoxygenase3 in salinity stress response. *Plant Sci.* 244, 1–7. doi: 10.1016/j.plantsci.2015.11.009

Dourado, P.R.M., de Souza, E.R., dos Santos, M.A., Monteiro, C.M.T., Monteiro, D., Paulino, M.K.S.S, et al. (2022). Stomatal regulation and osmotic adjustment in sorghum in response to salinity. *Agriculture* 12, 1–12.

Dugas, D. V., Monaco, M. K., Olson, A., Klein, R. R., Kumari, S., Ware, D., et al. (2011). Functional annotation of the transcriptome of sorghum bicolor in response to osmotic stress and abscisic acid. *BMC Genomics* .12, 514,1–51421. doi: 10.1186/1471-2164-12-514

Fahad, S., Hussain, S., Matloob, A., Khan, F., Khaliq, A., Saud, S., et al. (2014). Phytohormones and plant responses to salinity stress: a review. *Plant Growth Regul.* 75, 391–404. doi: 10.1007/s10725-014-0013-y

Fiehn, O. (2002). Metabolomics – the link between genotypes and phenotypes. *Plant Mol. Bio* 48, 155–171. doi: 10.1023/A:1013713905833

Fitzgerald, H., Chern, M., Navarre, R., and Ronald, P. (2004). Overexpression of (At) NPR1 in rice leads to a BTH- and environment-induced lesion-Mimic/Cell death phenotype. *Mol. Plant M Int.* 17, 140–151. doi: 10.1094/MPMI.2004.17.2.140

Foreman, J., Demidchik, V., Bothwell, J., Mylona, P., Miedema, H., Torres, M. A., et al. (2003). Reactive oxygen species produced by NADPH oxidase regulate plant cell growth. *Nature* 422, 442–446. doi: 10.1038/nature01485

Fracasso, A., Trindade, L. M., and Amaducci, S. (2016). Drought stress tolerance strategies revealed by RNA-seq in two sorghum genotypes with contrasting WUE. *BMC Plant Biol.* 16, 115. doi: 10.1186/s12870-016-0800-x

Hanson, J., and Smeekens, S. (2009). Sugar perception and signaling–an update. *Curr. Opin. Plant Bio.* 12, 562–567. doi: 10.1016/j.pbi.2009.07.014

Hayat, S., Hayat, Q., Alyemeni, M., Wani, D. A., Pichtel, J., and Ahmad, A. (2012). Role of proline under changing environment: A review. *Plant Signal Behav.* 7, 1456–1466. doi: 10.4161/psb.21949

Horváth, E., Szalai, G., and Janda, T. (2007). Induction of abiotic stress tolerance by salicylic acid signaling. *J. Plant Growth Regul.* 26, 290–300. doi: 10.1007/s00344-007-9017-4

Ibrahim, A. (2004). Efficacy of exogenous glycine betaine application on sorghum plants grown under salinity stress. *Acta Botan Hungar.* 46, 307–318. doi: 10.1556/ABot.46.2004.3-4.5

Iqbal, M., Khan, K., Rahman, H., and Sher, H. (2010). Detection of epistasis for plant height and leaf area per plant in maize (*Zea mays* l.) from generation means analysis. *Maydica*, 55, 33–39.

Jayakannan, M., Bose, J., Babourina, O., Rengel, Z., and Shabala, S. (2015a). Salicylic acid in plant salinity stress signalling and tolerance. *Plant Grow Regul.* 76, 25–40. doi: 10.1007/s10725-015-0028-z

Jayakannan, M., Bose, J., Babourina, O., Shabala, S., Massart, A., Poschenrieder, C., et al. (2015b). The NPR1-dependent salicylic acid signalling pathway is pivotal for enhanced salt and oxidative stress tolerance in arabidopsis. *J. Exp. Bot.* 66, 1865–1875. doi: 10.1093/jxb/eru528

Kanehisa, M., Araki, M., Goto, S., Hattori, M., Hirakawa, M., Itoh, M., et al. (2007). KEGG for linking genomes to life and the environment. *Nucl. Aci Res.* .36, 480–484. doi: 10.1093/nar/gkm882

Karoune, S., Kechebar, M., Falleh, H., Belhamra, M., Rahmoune, C., and Ksouri, R. (2017). LC-MS phenolic composition changes and antioxidant capacities of the saharan tree argania spinosa leaves under salinity. *Food Nutr. Sci.* 9, 1–11.

Kazan, K. (2015). Diverse roles of jasmonates and ethylene in abiotic stress tolerance. *Trends Plant Sci.* 20, 219–229. doi: 10.1016/j.tplants.2015.02.001

Kim, D., Langmead, B., and Salzberg, S. L. (2015). HISAT: a fast spliced aligner with low memory requirements. *Nat. Meth* 12, 357. doi: 10.1038/nmeth.3317

Kumar, A., Alam, S., Sengupta, N., and Sarina, R. (2011). Differential proteomic analysis of salt stress response in sorghum bicolor leaves. *Envir Exp. Bot.* 71, 321. doi: 10.1016/j.envexpbot.2010.12.017

Kumar, K., Kumar, M., Kim, S. R., Ryu, H., and Cho, Y. G. (2013). Insights into genomics of salt stress response in rice. *Rice* 6, 27. doi: 10.1186/1939-8433-6-27

Lacerda, C., Cambraia, J., Oliva, M., and Ruiz, H. (2001). Plant growth and solute accumulation and distribution in two sorghum genotypes, under NaCl stress. *Rev. Brasil Fisiol Veg.* 13, 107–120. doi: 10.1590/S0103-31312001000300003

Liang, W., Ma, X., Wan, P., and Liu, L. (2017). Plant salt-tolerance mechanism: A review. *Biochem. Bio Res. Communica* .495, 286–291.

Mahmood, T., Raza, S., Qasim, M., and Ashraf, M. (2010). Growth modulation and ion partitioning in salt stressed sorghum (*Sorghum bicolor* l.) by exogenous supply of salicylic acid. *Pak .J. Bot.* 42, 3047–3054.

Ma, Q., Kang, J., Long, R., Zhang, T., Xiong, J., Zhang, K., et al. (2017). Comparative proteomic analysis of alfalfa revealed new salt and drought stress-related factors involved in seed germination. *Mol. Biol. Rep.* 44, 1–10. doi: 10.1007/s11033-017-4104-5

Morgenthal, K., Weckwerth, W., and Steuer, R. (2006). Metabolomic networks in plants: Transitions from pattern recognition to biological interpretation. *Biosystems* 83, 108–117. doi: 10.1016/j.biosystems.2005.05.017

Mou, Z., Fan, W., and Dong, X. (2003). Inducers of plant systemic acquired resistance regulate NPR1 function through redox changes. *Cell* .113, 935–944. doi: 10.1016/S0092-8674(03)00429-X

Natera, S., Hill, C., Rupasinghe, T., and Roessner, U. (2016). Salt-stress induced alterations in the root lipidome of two barley genotypes with contrasting responses to salinity. *Funct. Plant Biol.* 43, 207–219. doi: 10.1071/FP15253

Nxele, X., Klein, A., and Ndimba, B. K. (2017). Drought and salinity stress alters ROS accumulation, water retention, and osmolyte content in sorghum plants. *South Afr J. Bot.* 108, 261–266. doi: 10.1016/j.sajb.2016.11.003

Parihar, P., Singh, S., Singh, D. V., and Prasad, S. (2014). Effect of salinity stress on plants and its tolerance strategies: a review. *Envir Sci. Pollut. Res.* 22, 4056–4075. doi: 10.1007/s11356-014-3739-1

Pires, I., Negrao, S., Oliveira, M., and Purugganan, M. (2015). Comprehensive phenotypic analysis of rice (oryza sativa) response to salinity stress. *Phy plantarum* 155, 43–54. doi: 10.1111/ppl.12356

Qiu, Z., Guo, J., Zhu, A., Zhang, L., and Zhang, M. (2014). Exogenous jasmonic acid can enhance tolerance of wheat seedlings to salt stress. *Ecotoxe Envsafety* 104, 202–208. doi: 10.1016/j.ecoenv.2014.03.014

Rachoski, M., Gázquez, A., Calzadilla, P. I., Bezus, R., Rodríguez, A., Ruiz, O., et al. (2015).). chlorophyll fluorescence and lipid peroxidation changes in rice somaclonal lines subjected to salt stress. *Acta Physiol. Plantarum* 37, 21–29. doi: 10.1007/s11738-015-1865-0

Rahman, A. (2012). Auxin: A regulator of cold stress response. *Physiol. Plantarum* .147, 22–31.

Ramel, F., Sulmon, C., Gouesbet, G., and Couée, I. (2009). Natural variation reveals relationships between pre-stress carbohydrate nutritional status and subsequent responses to xenobiotic and oxidative stress in arabidopsis thaliana. *Ann. Bot.* .104, 1323–1337. doi: 10.1093/aob/mcp243

Roberts, A., Trapnell, C., Donaghey, J., Rinn, J. L., and Pachter, L. (2011). Improving RNA-seq expression estimates by correcting for fragment bias. *Genome Biol.* 12, R22. doi: 10.1186/gb-2011-12-3-r22

Rustioni, L., Milani, C., Parisi, S., and Failla, O. (2015). Chlorophyll role in berry sunburn symptoms studied in different grape (*Vitis vinifera* l.) cultivars. *Scientia Horticul.* 185, 145–150. doi: 10.1016/j.scienta.2015.01.029

Salimi, F., Shekari, F., and Hamzei, J. (2016). Methyl jasmonate improves salinity resistance in German chamomile (Matricaria chamomilla l.) by increasing activity

of antioxidant enzymes. *Acta Physiol. Plantarum* 38, 1–14. doi: 10.1007/s11738-015-2023-4

Shi, H., Jiang, C., Ye, T., Tan, D. X., Reiter, R., Zhang, H., et al. (2014). Comparative physiological, metabolomic, and transcriptomic analyses reveal mechanisms of improved abiotic stress resistance in bermudagrass (*Cynodon dactylon* l.) pers. by exogenous melatonin. *J. Exp. Botany.* 66, 681–694. doi: 10.1093/jxb/eru373

Tari, I., Laskay, G., Takács, Z., and Poór, P. (2013). Response of sorghum to abiotic stresses: A review. *J. Agr Crop Sci.* 199, 264–274. doi: 10.1111/jac.12017

Thiele, B., Stein, N., Oldiges, M., and Hofmann, D. (2012). Direct analysis of underivatized amino acids in plant extracts by LC-MS-MS. *Methods Mol. Biol.* 828, 317–328. doi: 10.1007/978-1-61779-445-2_25

Tian, F., Wang, W., Liang, C., Wang, X., Wang, G., and Wang, W. (2016). Overaccumulation of glycine betaine makes the function of the thylakoid membrane better in wheat under salt stress. *Crop J.* 5, 25–36.

Vicente, M., and Plasencia, J. (2011). Salicylic acid beyond defence: Its role in plant growth and development. *J. Exp. Bot.* 62, 3321–3338. doi: 10.1093/jxb/err031

Wen, B., Mei, Z., Zeng, C., and Liu, S. (2017). MetaX: a flexible and comprehensive software for processing metabolomics data. *BMC Bioinf.* 18, 183. doi: 10.1186/s12859-017-1579-y

Wu, H., Ye, H., Yao, R., Zhang, T., and Xiong, L. (2014). OsJAZ9 acts as a transcriptional regulator in jasmonate signaling and modulates salt stress tolerance in rice. *Plant Sci.* 232, 1–12. doi: 10.1016/j.plantsci.2014.12.010

Wu, Y., Zhang, D., Chu, J., Boyle, P., Wang, Y., Brindle, I., et al. (2012). The arabidopsis NPR1 protein is a receptor for the plant defense hormone salicylic acid. *Cell Rep.* 1 (6), 639–647. doi: 10.1016/j.celrep.2012.05.008

Xu, X., Xu, H., Wang, Y., Wang, X., Qiu, Y., and Xu, B. (2008). The effect of salt stress on the chlorophyll level of the main sand-binding plants in the shelterbelt along the tarim desert highway. *Chin. Sci. Bullet* .53, 109–111. doi: 10.1007/s11434-008-6012-5

Yang, Z., Li, J.-L., Liu, L.-N., Xie, Q., and Sui, N. (2020). Photosynthetic regulation under salt stress and salt-tolerance mechanism of sweet sorghum. *Front. Plant Sci.* 10, 1722. doi: 10.3389/fpls.2019.01722

Yang, Z., Wang, Y., Wei, X., Zhao, X., Wang, B., and Sui, N. (2017). Transcription profiles of genes related to hormonal regulations under salt stress in sweet sorghum. *Plant Mol. Rep.* 35, 586–599. doi: 10.1007/s11105-017-1047-x

Yao, W., Zhao, K., Cheng, Z., Li, X., Zhou, B., and Jiang, T. (2018). Transcriptome analysis of poplar under salt stress and over-expression of transcription factor NAC57 gene confers salt tolerance in transgenic arabidopsis. *Front. Plant Sci.* 9, 1121–1131. doi: 10.3389/fpls.2018.01121

Ye, H., du, H., Tang, N., Li, X., and Xiong, L. (2009). Identification and expression profiling analysis of TIFY family genes involved in stress and phytohormone responses in rice. *Plant Mol. Biol.* . 71, 291–305. doi: 10.1007/s11103-009-9524-8

Zhang, X. (1992). *Crop physiology research method* (Beijing: Agricultural Press).

Zhao, G., Song, Y., Wang, C., Butt, H., Wang, Q., Zhang, C., et al. (2016). Genome-wide identification and functional analysis of the TIFY gene family in response to drought in cotton. *Mol. Genet. Genomic.* 291, 2173–2187. doi: 10.1007/s00438-016-1248-2

Zheng, L. Y., Guo, X. S., He, B., Sun, L., Peng, Y., Dong, S., et al. (2011). Genome-wide patterns of genetic variation in sweet and grain sorghum. *Genome Biol.* .12, 114–121. doi: 10.1186/gb-2011-12-11-r114

Zhu, D., Bai, X., Luo, X., Chen, Q., Cai, H., Ji, Y., et al. (2012). Identification of wild soybean TIFY family genes and their expression profiling analysis under bicarbonate stress. *Plant Cell Rep* 32, 263–272.

Frontiers in
Plant Science

Cultivates the science of plant biology and its applications

The most cited plant science journal, which advances our understanding of plant biology for sustainable food security, functional ecosystems and human health.

Discover the latest Research Topics

See more →

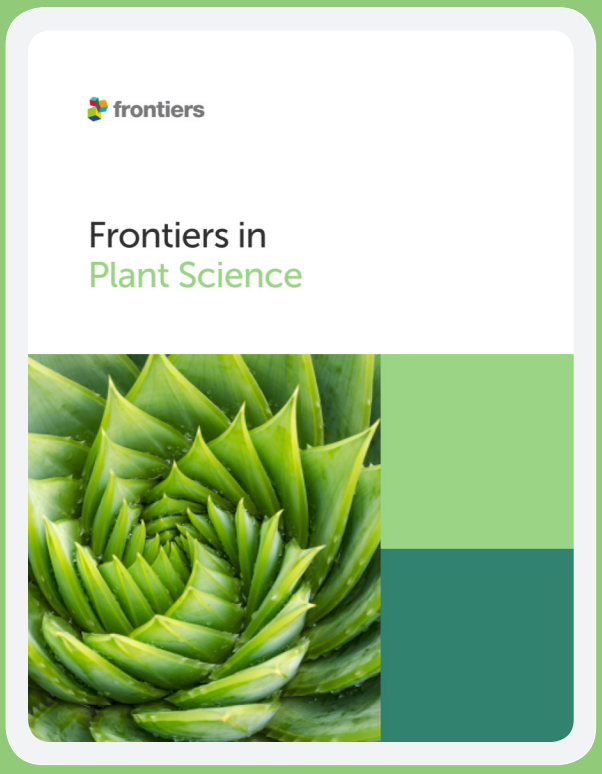

Frontiers

Avenue du Tribunal-Fédéral 34
1005 Lausanne, Switzerland
frontiersin.org

Contact us

+41 (0)21 510 17 00
frontiersin.org/about/contact